A microscopic image showing a dense cluster of cells, likely pneumococci, stained with red and blue fluorescent dyes. The red staining highlights the cell walls, while the blue staining highlights the nuclei or other internal structures. The background is dark, making the fluorescent cells stand out.

TRANSMISSION, COLONIZATION, AND MOLECULAR PATHOGENESIS OF PNEUMOCOCCUS

EDITED BY: Jorge Eugenio Vidal, Elsa Bou Ghanem, Xueqing Wu,
Kaifeng Wu, Guangchun Bai and Sven Hammerschmidt
PUBLISHED IN: *Frontiers in Cellular and Infection Microbiology*



frontiers

Frontiers eBook Copyright Statement

The copyright in the text of individual articles in this eBook is the property of their respective authors or their respective institutions or funders. The copyright in graphics and images within each article may be subject to copyright of other parties. In both cases this is subject to a license granted to Frontiers.

The compilation of articles constituting this eBook is the property of Frontiers.

Each article within this eBook, and the eBook itself, are published under the most recent version of the Creative Commons CC-BY licence.

The version current at the date of publication of this eBook is CC-BY 4.0. If the CC-BY licence is updated, the licence granted by Frontiers is automatically updated to the new version.

When exercising any right under the CC-BY licence, Frontiers must be attributed as the original publisher of the article or eBook, as applicable.

Authors have the responsibility of ensuring that any graphics or other materials which are the property of others may be included in the CC-BY licence, but this should be checked before relying on the CC-BY licence to reproduce those materials. Any copyright notices relating to those materials must be complied with.

Copyright and source acknowledgement notices may not be removed and must be displayed in any copy, derivative work or partial copy which includes the elements in question.

All copyright, and all rights therein, are protected by national and international copyright laws. The above represents a summary only. For further information please read Frontiers' Conditions for Website Use and Copyright Statement, and the applicable CC-BY licence.

ISSN 1664-8714

ISBN 978-2-83250-324-9

DOI 10.3389/978-2-83250-324-9

About Frontiers

Frontiers is more than just an open-access publisher of scholarly articles: it is a pioneering approach to the world of academia, radically improving the way scholarly research is managed. The grand vision of Frontiers is a world where all people have an equal opportunity to seek, share and generate knowledge. Frontiers provides immediate and permanent online open access to all its publications, but this alone is not enough to realize our grand goals.

Frontiers Journal Series

The Frontiers Journal Series is a multi-tier and interdisciplinary set of open-access, online journals, promising a paradigm shift from the current review, selection and dissemination processes in academic publishing. All Frontiers journals are driven by researchers for researchers; therefore, they constitute a service to the scholarly community. At the same time, the Frontiers Journal Series operates on a revolutionary invention, the tiered publishing system, initially addressing specific communities of scholars, and gradually climbing up to broader public understanding, thus serving the interests of the lay society, too.

Dedication to Quality

Each Frontiers article is a landmark of the highest quality, thanks to genuinely collaborative interactions between authors and review editors, who include some of the world's best academicians. Research must be certified by peers before entering a stream of knowledge that may eventually reach the public - and shape society; therefore, Frontiers only applies the most rigorous and unbiased reviews.

Frontiers revolutionizes research publishing by freely delivering the most outstanding research, evaluated with no bias from both the academic and social point of view. By applying the most advanced information technologies, Frontiers is catapulting scholarly publishing into a new generation.

What are Frontiers Research Topics?

Frontiers Research Topics are very popular trademarks of the Frontiers Journals Series: they are collections of at least ten articles, all centered on a particular subject. With their unique mix of varied contributions from Original Research to Review Articles, Frontiers Research Topics unify the most influential researchers, the latest key findings and historical advances in a hot research area! Find out more on how to host your own Frontiers Research Topic or contribute to one as an author by contacting the Frontiers Editorial Office: frontiersin.org/about/contact

TRANSMISSION, COLONIZATION, AND MOLECULAR PATHOGENESIS OF PNEUMOCOCCUS

Topic Editors:

Jorge Eugenio Vidal, University of Mississippi Medical Center, United States

Elsa Bou Ghanem, University at Buffalo, United States

Xueqing Wu, Zhejiang University, China

Kaifeng Wu, Zunyi Medical University Third Affiliated Hospital, China

Guangchun Bai, Albany Medical College, United States

Sven Hammerschmidt, University of Greifswald, Germany

Citation: Vidal, J. E., Ghanem, E. B., Wu, X., Wu, K., Bai, G.,
Hammerschmidt, S., eds. (2022). Transmission, Colonization, and Molecular
Pathogenesis of Pneumococcus. Lausanne: Frontiers Media SA.
doi: 10.3389/978-2-83250-324-9

Table of Contents

- 05 Editorial: Transmission, Colonization, and Molecular Pathogenesis of *Pneumococcus***
Jorge E. Vidal, Elsa N. Bou Ghanem, Xueqing Wu, Kaifeng Wu, Guangchun Bai and Sven Hammerschmidt
- 08 Rapid Increase of Oral Bacteria in Nasopharyngeal Microbiota After Antibiotic Treatment in Children With Invasive Pneumococcal Disease**
Desiree Henares, Muntsa Rocafort, Pedro Brotons, Mariona F. de Sevilla, Alex Mira, Cristian Launes, Raul Cabrera-Rubio and Carmen Muñoz-Almagro
- 20 Pneumococcal Extracellular Serine Proteases: Molecular Analysis and Impact on Colonization and Disease**
Murtadha Q. Ali, Thomas P. Kohler, Lukas Schulig, Gerhard Burchhardt and Sven Hammerschmidt
- 39 Streptococcus pneumoniae: a Plethora of Temperate Bacteriophages With a Role in Host Genome Rearrangement**
Antonio J. Martín-Galiano and Ernesto García
- 60 The Role of Minor Pilins in Assembly and Function of the Competence Pilus of Streptococcus pneumoniae**
Vitor Oliveira, Marie-Stephanie Aschtgen, Anke van Erp, Birgitta Henriques-Normark and Sandra Muschiol
- 77 Intra-Species Interactions in Streptococcus pneumoniae Biofilms**
Carina Valente, Ana R. Cruz, Adriano O. Henriques and Raquel Sá-Leão
- 91 Infant Pneumococcal Carriage in Belgium Not Affected by COVID-19 Containment Measures**
Laura Willen, Esra Ekinici, Lize Cuypers, Heidi Theeten and Stefanie Desmet
- 96 Diverse Mechanisms of Protective Anti-Pneumococcal Antibodies**
Aaron D. Gingerich and Jarrod J. Mousa
- 111 A Jack of All Trades: The Role of Pneumococcal Surface Protein A in the Pathogenesis of Streptococcus pneumoniae**
Jessica R. Lane, Muralidhar Tata, David E. Briles and Carlos J. Orihuela
- 127 Streptococcus pneumoniae and Influenza A Virus Co-Infection Induces Altered Polyubiquitination in A549 Cells**
Thomas Sura, Vanessa Gering, Clemens Cammann, Sven Hammerschmidt, Sandra Maaß, Ulrike Seifert and Dörte Becher
- 139 Extensive/Multidrug-Resistant Pneumococci Detected in Clinical Respiratory Tract Samples in Southern Sweden Are Closely Related to International Multidrug-Resistant Lineages**
Linda Yamba Yamba, Fabian Uddén, Kurt Fursted, Jonas Ahl, Hans-Christian Slotved and Kristian Riesbeck
- 150 Streptococcus pneumoniae Strains Isolated From a Single Pediatric Patient Display Distinct Phenotypes**
Hannah N. Agnew, Erin B. Brazel, Alexandra Tikhomirova, Mark van der Linden, Kimberley T. McLean, James C. Paton and Claudia Trappetti

- 166** *Increase of Macrolide-Resistance in Streptococcus pneumoniae Strains After the Introduction of the 13-Valent Pneumococcal Conjugate Vaccine in Lima, Peru*
Brayan E. Gonzales, Erik H. Mercado, Maria Pinedo-Bardales, Noemi Hinostroza, Francisco Campos, Eduardo Chaparro, Olguita Del Águila, María E. Castillo, Andrés Saenz, Isabel Reyes and Theresa J. Ochoa
- 176** *Pneumococcal Surface Proteins as Virulence Factors, Immunogens, and Conserved Vaccine Targets*
Javid Aceil and Fikri Y. Avci
- 190** *Dynamic Python-Based Method Provides Quantitative Analysis of Intercellular Junction Organization During S. pneumoniae Infection of the Respiratory Epithelium*
Devons Mo, Shuying Xu, Juan P. Rosa, Shakir Hasan and Walter Adams
- 203** *Immune Memory After Respiratory Infection With Streptococcus pneumoniae Is Revealed by in vitro Stimulation of Murine Splenocytes With Inactivated Pneumococcal Whole Cells: Evidence of Early Recall Responses by Transcriptomic Analysis*
Isabelle Franco Moscardini, Francesco Santoro, Monica Carraro, Alice Gerlini, Fabio Fiorino, Chiara Germoni, Samaneh Gholami, Elena Pettini, Donata Medaglini, Francesco Iannelli and Gianni Pozzi
- 217** *Pneumococcal BgaA Promotes Host Organ Bleeding and Coagulation in a Mouse Sepsis Model*
Moe Takemura, Masaya Yamaguchi, Momoko Kobayashi, Tomoko Sumitomo, Yujiro Hirose, Daisuke Okuzaki, Masayuki Ono, Daisuke Motooka, Kana Goto, Masanobu Nakata, Narikazu Uzawa and Shigetada Kawabata



OPEN ACCESS

EDITED AND REVIEWED BY
John S Gunn,
The Research Institute at Nationwide
Children's Hospital, United States

*CORRESPONDENCE
Jorge E. Vidal
jvidal@umc.edu

SPECIALTY SECTION
This article was submitted to
Molecular Bacterial Pathogenesis,
a section of the journal
Frontiers in Cellular and
Infection Microbiology

RECEIVED 25 August 2022
ACCEPTED 29 August 2022
PUBLISHED 13 September 2022

CITATION
Vidal JE, Bou Ghanem EN, Wu X,
Wu K, Bai G and Hammerschmidt S
(2022) Editorial: Transmission,
colonization, and molecular
pathogenesis of pneumococcus.
Front. Cell. Infect. Microbiol.
12:1028047.
doi: 10.3389/fcimb.2022.1028047

COPYRIGHT
© 2022 Vidal, Bou Ghanem, Wu, Wu,
Bai and Hammerschmidt. This is an
open-access article distributed under
the terms of the [Creative Commons
Attribution License \(CC BY\)](https://creativecommons.org/licenses/by/4.0/). The use,
distribution or reproduction in other
forums is permitted, provided the
original author(s) and the copyright
owner(s) are credited and that the
original publication in this journal is
cited, in accordance with accepted
academic practice. No use,
distribution or reproduction is
permitted which does not comply with
these terms.

Editorial: Transmission, colonization, and molecular pathogenesis of pneumococcus

Jorge E. Vidal^{1*}, Elsa N. Bou Ghanem², Xueqing Wu³,
Kaifeng Wu⁴, Guangchun Bai⁵ and Sven Hammerschmidt⁶

¹Center for Immunology and Microbial Research, Department of Cell and Molecular Biology, University of Mississippi Medical Center, Jackson, MS, United States, ²Department of Microbiology and Immunology, School of Medicine, University at Buffalo, Buffalo, NY, United States, ³Department of Infectious Diseases, Sir Run Run Shaw Hospital, Zhejiang University School of Medicine, Hangzhou, China, ⁴Department of Laboratory Medicine, The First People's Hospital of Zunyi (The Third Affiliated Hospital of Zunyi Medical University), Zunyi, China, ⁵Department of Immunology and Microbial Disease, Albany Medical College, Albany, NY, United States, ⁶Department of Molecular Genetics and Infection Biology, Interfaculty Institute for Genetics and Functional Genomics, Center for Functional Genomics of Microbes, University of Greifswald, Greifswald, Germany

KEYWORDS

Streptococcus pneumoniae, transmission, colonization, pathogenesis, invasive pneumococcal disease

Editorial on the Research Topic

Transmission, colonization, and molecular pathogenesis of pneumococcus

Streptococcus pneumoniae (Spn; pneumococcus) has been for decades a number one bacterial killer of children and older adults worldwide, but it is also a commensal of the upper respiratory tract. Although vaccination with pneumococcal conjugate vaccines has decreased the burden of invasive pneumococcal disease (IPD), mortality caused by this pathogen remains a concern worldwide. The introduction of new generations of pneumococcal vaccines is creating a niche for vaccine-escape serotypes and changes in the microbiome of the upper airways is expected to occur. Moreover, the rise of multidrug-resistant clones around the world has posed a serious threat in recent years. A comprehensive understanding of the transmission, colonization, and molecular pathogenesis of the pneumococcus is necessary to come out with improved interventions aimed to further reduce the burden of IPD. To date, more than 100 distinct pneumococcal capsular serotypes have been identified but current pneumococcal conjugate vaccines (PCV10, PCV13, PCV20), and pneumococcal polysaccharide vaccine (PPSV23) protect against up to a total of 24 different pneumococcal types. These vaccines have decreased the burden of pneumococcal disease produced by vaccine types (VT) but provide poor protection against non-vaccine serotypes (NVT) and non-encapsulated Spn (NES) strains. Additionally, the increasing prevalence of NVTs, NES and multi-drug resistant Spn strains results in more challenge for the treatment of pneumococcal infections. In this Research Topic, we have compiled a series of research articles contributing to our understanding of transmission, colonization, molecular

pathogenesis, the development of protein-based vaccines and antibiotic resistance; highlights from each study are described by the editors below.

An update on transmission in the current COVID-19 era was contributed by Willen et al.. Preventing strategies of the current COVID-19 pandemic, such as social distancing and wearing face masks, caused a reduced burden of IPD in Belgian children and the hypothesis was that transmission of pneumococci was interrupted. To gain insights into this, authors conducted a carriage surveillance in Belgium during the COVID-19 pandemic to find out that the overall pneumococcal carriage rate remained similar, comparing the data against a pre-COVID-19 period of the same children population.

Henares et al. studied the nasopharyngeal microbiota of children diagnosed with IPD and that were exposed to β -lactam antibiotics, compared to a cohort of children with IPD prior to antibiotic treatment. The authors found that antibiotic treatment increases oral bacteria and nosocomial bacterial species such as *Staphylococcus*, *Acinetobacter* and *Pseudomonas* with a transient decrease of streptococci phylogenetically related to Spn. Along the same lines, Spn forms a biofilm in the oropharynx and nasopharynx where it can interact with strains of the same species and other species. A study by Valente et al. thoroughly evaluated the interaction of phenotypically and genotypically unrelated Spn strains. As a result of intra-species interaction, their study identified four different outcomes: commensalism, competition, amensalism, and neutralism. Identifying ecological interactions in the upper airways and the molecular mechanisms of biofilm formation may guide us to future intervention studies aiming to reduce colonization by the pneumococcus.

Using pneumococcus as a model organism have provided remarkable insights to the field of genetics, but the mechanism by which Spn takes up naked and double-strand DNA is still under active investigation. In a study by Oliveira et al., authors demonstrated that the assemblage of the major pilin ComGC, the DNA receptor, is stabilized by ComGG and further identified a Glu5 residue (E5) as an essential residue to incorporate minor pilin proteins ComGD and ComGF to the major pilin subunit ComGC. Shedding light on our understanding of pneumococcal prophages, Martin-Galiano and Garcia conducted a genetic survey in >4,000 Spn genomes to identify full prophages in 43% of strains. The evolutionary relationship and putative role in pathogenesis were discussed by the authors and provide a valuable dataset to further study pneumococcal prophages.

Three review manuscripts highlight the advances on our understanding about conserved immunogenic proteins as vaccine targets. Aceil and Avci provide a thoughtful overview of multiple classes of conserved surface proteins utilized by pneumococcal strains as colonization or virulence factors. They approach the contribution of such surface proteins to colonization and IPD, and discuss data about the immune response of the human host. Then a paper by Gingerich and

Mousa reviews the most recent information about the molecular mechanism of protection of those anti-pneumococcal antibodies. The authors discuss a variety of mechanisms including opsonophagocytic activity, toxin neutralization, and inhibition of bacterial adherence. Lane et al. focus their review paper on a family of proteins collectively known as choline-binding proteins (CBPs) and in particular on PspA, one of the most abundant CBP. They summarize new developments on pathogenesis and the potential use of CBPs and PspA for the treatment and prevention of pneumococcal pneumonia.

Exciting new molecular pathogenesis insights were published in a series of manuscripts. Takemura et al. identified a novel role for the enzyme β -galactosidase (BgaA) during pneumococcal bacteremia. Authors provide experimental evidence that BgaA indirectly induces tissue damage and triggers blood clot during sepsis. A paper by Mo et al. nicely provides an automated image analysis tool to evaluate the intercellular tight junction from *in vitro* and *in vivo* experiments. This new quantitative method is such a valuable tool to investigate invasion of epithelium and endothelium, through the disruption of tight junction by Spn strains but can be utilized with other pathogens as well. Along the same lines, Sura et al. used a co-infection model with Spn and H1N1 influenza virus to investigate modifications of the proteome or ubiquitome. However, their findings point out towards minor differences in ubiquitination abundance during Spn-influenza virus co-infection.

Selection of Spn during disease evolves rapidly and help Spn to successfully adapt to the new niche. Agnew et al. isolated two clones of the same strain from blood and cerebrospinal fluid of a child with meningitis. Molecular studies identified an altered raffinose utilization between the two strains that may influence Spn clones to cause meningitis. Using transcriptome and cytokine analysis, Moscardini et al. elegantly demonstrated a “recall” adaptive and innate immune response post-Spn infection. They identified an immune response signature including genes associated to the cytokine response. Finally, Ali et al. summarized the recent advances on the contribution of extracellular serine protease to pneumococcal disease and pathogenesis. The authors focus this review on the molecular and functional analysis of such pneumococcal enzymes and update the field with recent developments regarding their immunogenicity and interaction with the human host.

Despite new generations of pneumococcal vaccines and the development and FDA-approval of new antibiotics for IPD, the isolation of pneumococcal strains with resistance to first line antibiotics is on the rise. A study set up in a high-income country, Sweden, investigated the genetic relationship between their multidrug resistant (MDR) Spn strains and MDR global Spn isolates. Investigators identified global pneumococcal sequence cluster (GPSC) 1, GPSC9 and GPSC10, with the majority of their isolates belonging to one of these GPSCs. MDR, non-vaccine strains, were identified in GPSC9 and

GPSC10 and warrants further surveillance as the burden of IPD caused by those vaccine escape strains may increase with the introduction of new generation of vaccines. Finally, [Gonzales et al.](#) investigated the burden of resistance in Peru, a low-middle income country post introduction of pneumococcal vaccines. Their stunning data revealed an increase macrolide resistance in both carriage strains and strains isolated from IPD cases in the country. Authors worry that a further increase in macrolide resistance can be observed in the years to come given that azithromycin is being empirically prescribed for COVID-19 cases worldwide.

The prevention and control of *S. pneumoniae* colonization and IPD are essential to global health. The sixteen articles published in this Research Topic have contributed to this pathogen's research from different angles e.g., pneumococcal transmission, antibiotic resistance, genomics, molecular pathology, drug innovation, and reviewing recent findings on pneumococcal colonization and proteinaceous vaccine candidates. We believe these cutting-edge research outcomes expand our knowledge on Spn transmission and molecular mechanisms of colonization and will therefore significantly contribute to pneumococcal disease prevention and further new findings in this field.

Author contributions

All authors contributed with the writing, and editing of the manuscript and approved the final version.

Acknowledgment

JEV was in part supported by grants from the National Institutes of Health (NIH; 5R21AI144571-03 and 1R21AI151571-01). The content is solely the responsibility of the authors and does not necessarily represent the official view of the NIH. The work of SH is funded by grants from the Deutsche Forschungsgemeinschaft (DFG, German Research Foundation): DFG-RTG 2719 and DFG HA 3125/5-2, the Bundesministerium für Bildung und Forschung (BMBF- Zwanzig20 -InfectControl 2020 – Project VacoME (FKZ 03ZZ0816A), Pathowiki (FKZ 03ZZ0839B) and Pneumofluidics (FKZ 01DP19007).

Conflict of interest

The authors declare that the research was conducted in the absence of any commercial or financial relationships that could be construed as a potential conflict of interest.

Publisher's note

All claims expressed in this article are solely those of the authors and do not necessarily represent those of their affiliated organizations, or those of the publisher, the editors and the reviewers. Any product that may be evaluated in this article, or claim that may be made by its manufacturer, is not guaranteed or endorsed by the publisher.



Rapid Increase of Oral Bacteria in Nasopharyngeal Microbiota After Antibiotic Treatment in Children With Invasive Pneumococcal Disease

OPEN ACCESS

Edited by:

Sven Hammerschmidt,
University of Greifswald, Germany

Reviewed by:

Anh K. Lam,
Indiana University, United States
Tiffany Zarrella,
National Institutes of Health (NIH),
United States
Markus Hilty,
University of Bern, Switzerland

*Correspondence:

Carmen Muñoz-Almagro
cma@sjdhospitalbarcelona.org;
cmunoz@uic.es

[†]These authors have contributed
equally to this work and share
senior authorship

Specialty section:

This article was submitted to
Molecular Bacterial Pathogenesis,
a section of the journal
Frontiers in Cellular and
Infection Microbiology

Received: 20 July 2021

Accepted: 10 September 2021

Published: 12 October 2021

Citation:

Henares D, Rocafor M, Brotons P,
de Sevilla MF, Mira A, Launes C,
Cabrera-Rubio R and
Muñoz-Almagro C (2021) Rapid
Increase of Oral Bacteria in
Nasopharyngeal Microbiota After
Antibiotic Treatment in Children With
Invasive Pneumococcal Disease.
Front. Cell. Infect. Microbiol. 11:744727.
doi: 10.3389/fcimb.2021.744727

Desiree Henares^{1,2}, Muntsa Rocafor^{1,2}, Pedro Brotons^{1,2,3}, Mariona F. de Sevilla^{2,4},
Alex Mira^{2,5}, Cristian Launes^{1,2,4}, Raul Cabrera-Rubio^{6,7†} and Carmen Muñoz-Almagro^{1,2,3*†}

¹ Institut de Recerca Sant Joan de Deu, Hospital Sant Joan de Deu, Barcelona, Spain, ² CIBER of Epidemiology and Public Health (CIBERESP), Instituto de Salud Carlos III, Madrid, Spain, ³ School of Medicine, Universitat Internacional de Catalunya, Barcelona, Spain, ⁴ Pediatric Department, Hospital Sant Joan de Deu, University of Barcelona, Barcelona, Spain, ⁵ Department of Health and Genomics, Center for Advanced Research in Public Health, Fundacion para el Fomento de la Investigacion Sanitaria y Biomedica de la Comunitat Valenciana (FISABIO), Valencia, Spain, ⁶ Teagasc Food Research Centre (TEAGASC), Moorepark, Fermoy, Ireland, ⁷ APC Microbiome Institute, University College Cork, Cork, Ireland

Introduction: Antibiotics are commonly prescribed to young children for treating bacterial infections such as invasive pneumococcal disease (IPD) caused by *Streptococcus pneumoniae*. Despite the obvious benefits of antibiotics, little is known about their possible side effects on children's nasopharyngeal microbiota. In other ecological niches, antibiotics have been described to perturb the balanced microbiota with short- and long-term effects on children's health. The present study aims to evaluate and compare the nasopharyngeal microbiota of children with IPD and different degree of antibiotic exposure.

Methods: We investigated differences in nasopharyngeal microbiota of two groups of children <18 years with IPD: children not exposed to antibiotics before sample collection (n=27) compared to children previously exposed (n=54). Epidemiological/clinical data were collected from subjects, and microbiota was characterized by Illumina sequencing of V3-V4 amplicons of the 16S rRNA gene.

Results: Main epidemiological/clinical factors were similar across groups. Antibiotic-exposed patients were treated during a median of 4 days (IQR: 3–6) with at least one beta-lactam (100.0%). Higher bacterial richness and diversity were found in the group exposed to antibiotics. Different streptococcal amplicon sequence variants (ASVs) were differentially abundant across groups: antibiotic use was associated to lower relative abundances of *Streptococcus* ASV2 and *Streptococcus* ASV11 (phylogenetically close to *S. pneumoniae*), and higher relative abundances of *Streptococcus* ASV3 and *Streptococcus* ASV12 (phylogenetically close to viridans group streptococci). ASVs assigned to typical bacteria from the oral cavity, including *Veillonella*, *Alloprevotella*, *Porphyromonas*, *Granulicatella*, or *Capnocytophaga*, were associated to the antibiotic-

exposed group. Common nosocomial genera such as *Staphylococcus*, *Acinetobacter*, and *Pseudomonas* were also enriched in the group exposed to antibiotics.

Conclusion: Our results point toward a reduction of *S. pneumoniae* abundance on the nasopharynx of children with IPD after antibiotic treatment and a short-term repopulation of this altered niche by oral and nosocomial bacteria. Future research studies will have to evaluate the clinical implications of these findings and if these populations would benefit from the probiotic/prebiotic administration or even from the improvement on oral hygiene practices frequently neglected among hospitalized children.

Keywords: children, nasopharyngeal microbiota, invasive pneumococcal disease (IPD), antibiotics, oral bacteria, nosocomial bacteria

INTRODUCTION

Antibiotics prescribed for treating infectious diseases save millions of lives every year, but limited information is available about their impact on the human microbiome and consequences on health. The side effects of antibiotics have been described on the gut microbiota, including transient or profound loss of specific bacterial species, reduction of microbial diversity, and loss of colonization resistance (Kim et al., 2017). In hospitalized patients, antibiotic use favors colonization by nosocomial and appearance of multidrug-resistant pathogens thus increasing the risk for healthcare-associated infections (Kim et al., 2017). Even long-term effects on children's health including obesity or diabetes have been linked to aberrant microbiomes altered by antibiotics (Boursi et al., 2015; Tai et al., 2015).

With respect to the respiratory tract, different authors have reported changes in throat, oropharynx, and lung microbiota of adult patients subjected to long-term antibiotic intake for different infections or chronic respiratory conditions (Hong et al., 2016; Wang et al., 2017; Choo et al., 2018). However, there is scarce research on the effects that occurred on children's nasopharynx, the ecological niche of the main pathogens causing disease in pediatric populations (Cleary and Clarke, 2017). Moreover, young children are subjected to a high number of short-term antibiotic prescriptions, especially for treating acute respiratory infections (Fleming-Dutra et al., 2016; Orlando et al., 2020) such as invasive pneumococcal disease (IPD).

IPD is a major cause of morbi-mortality worldwide with high incidence among children under 5 years (GBD 2016 Lower Respiratory Infections Collaborators, 2018; Wahl et al., 2018). IPD is caused by *Streptococcus pneumoniae*, a bacteria that normally colonizes the nasopharynx of children asymptomatically but can occasionally cause pneumonia, the most frequent manifestation, or other serious clinical syndromes including sepsis or meningitis (Wahl et al., 2018). Differential susceptibility to IPD might be partly explained by the nasopharyngeal microbiota, which could play a role in the transition of *S. pneumoniae* from colonization to disease states (Camelo-Castillo et al., 2019).

Management of IPD requires antibiotic treatment with varying doses, duration, and administration routes according to clinical and patient's characteristics (NICE, 2019). Since

antibiotics are crucial for appropriate treatment of IPD but also may result in perturbations of the ecological niche of *Streptococcus pneumoniae*, further insight is needed into how this disturbance is produced and what bacteria are leading the repopulation of the nasopharynx so we can counteract antibiotic-derived unwanted effects in our microbiota. Antibiotics side effects may indirectly impact children's health by causing microbiota imbalances that have been linked to pathogenesis of several respiratory infections (Bosch et al., 2017; Lanaspá et al., 2017) and chronic respiratory disorders (Hahn et al., 2018), or by rising antibiotic-resistant bacteria that have been described to persist for long time and cause infections associated to higher rates of treatment failure and mortality (Sjölund et al., 2005; Jernberg et al., 2007; Jernberg et al., 2010; Friedman et al., 2016). The present study aims to analyze and compare the nasopharyngeal microbiota of children hospitalized with IPD and different degree of exposure to antibiotics.

METHODS

Study Design, Setting, and Participants

A cross-sectional study was conducted at Sant Joan de Deu Barcelona Children's Hospital (HSJD) with children prospectively recruited from January 2014 to December 2018. The criteria for inclusion in the study were as follows: 1) <18 years of age; 2) admission to HSJD with clinical suspicion of IPD; 3) microbiological confirmation of IPD by isolation of *S. pneumoniae* and/or DNA detection of *S. pneumoniae* in any normally sterile body fluid (Camelo-Castillo et al., 2019); and 4) nasopharyngeal sample collected at any time during hospital stay for diagnostic or research purposes. Exclusion criteria were not signing informed consent or belonging to a previously defined clinical risk group for developing IPD (Gov.UK, 2020).

Patients not treated or treated only during 24 h before sample collection were considered as cases not exposed to antibiotics, while patients treated for more than 24 h prior to sample collection were considered as cases exposed to antibiotics. Different subjects were included in each group. This criterion was adopted on the basis of previous literature reporting that the sensitivity of molecular-based techniques on respiratory samples

is not affected by a relatively low time of exposition to antibiotics (Johansson et al., 2008).

Sample and Data Collection

Nasopharyngeal aspirates (NPAs) were collected and immediately frozen at -80°C until processed (Camelo-Castillo et al., 2019). Antibiotic types, administration route, and exposure time before and during hospital stay were registered for each case. Relevant epidemiological and other clinical data were recorded from each participant through the parent's interview or electronic medical record, such as delivery mode or pneumococcal vaccination status (categorized into nonvaccinated children or children ≥ 1 dose of 7-, 10-, or 13-valent pneumococcal conjugate vaccines (PCVs). Microbiological data were obtained through laboratory analyses. Pneumococcal serotypes 1, 3, 4, 5, 7F, 8, 9A, 9V, 12F, 14, 18C, and 19A were considered as serotypes with high invasive disease potential (Camelo-Castillo et al., 2019). A detailed list and description of the variables collected is included in the metadata file.

Laboratory Analyses

Bacterial DNA was extracted from NPAs by the automated system NucliSENS easyMag (BioMérieux, Marcy-l'Étoile, France). A duplex real-time PCR targeting *lytA* and *Rnase P* genes was used for pneumococcal DNA detection/quantification (Camelo-Castillo et al., 2019; CDC and Ncird). All positive *S. pneumoniae* samples were further serotyped (Selva et al., 2012). A multiplex Real-Time PCR Anyplex™ II RV16 (Seegene, Seoul, Korea) was used to detect DNA/RNA from 16 human respiratory viruses. Nasopharyngeal microbiota was characterized by 16S rRNA gene sequencing. The V3-V4 region was amplified and sequenced with Illumina MiSeq (Illumina, San Diego, California, USA) as previously described (Illumina 16S Metagenomic Sequencing Library Preparation). To control for potential contaminants, 17 negative controls were extracted, amplified, and sequenced with the samples.

Bioinformatic and Statistical Analyses

Reads were processed using the DADA2 pipeline (Callahan et al., 2016) obtaining exact amplicon sequence variants (ASVs). ASVs mapping to the human genome (GRCh38) using the Burrow-Wheeler Aligner in Deconseq v0.4.3 were filtered out (Schmieder and Edwards, 2011). Taxonomic annotation of ASVs from kingdom to genus was performed by DADA2 using the Ribosomal Database Project (RDP) training set 16. ASVs were further classified to species by an exact matching approach using function addSpecies from DADA2. Finally, Decontam R package compared prevalence of ASVs in real samples and negative controls (Davis et al., 2018), identifying contaminant ASVs that were removed from downstream analyses.

All statistical analyses were performed with R version 3.6.3. Continuous variables were described as mean and standard deviation (SD) or median and interquartile range (IQR) for parametric and nonparametric variables, respectively. Significance of continuous and normally distributed data was

assessed by t-test for group comparisons. In case of nonparametric data, Wilcoxon tests were performed. For categorical data, significance was established through chi-square test or Fisher's exact test if $\geq 25\%$ of cells presented expected frequencies ≤ 5 .

Samples were rarefied to minimum sample depth (12,601 sequences) for alpha-diversity analyses. Microbiota richness and diversity were estimated through the calculation of Chao1 and Shannon indices for each rarefied sample using the phyloseq R package (McMurdie and Holmes, 2013), and comparisons by group according to antibiotic exposure were made with linear regression analysis and accounting for confounding factors as copredictors (age, gender, seasonality, vaccination, and severity measured by ICU admission and length of hospital stay). PERMANOVA test from vegan R package (Oksanen et al., 2018) evaluated overall differences on microbiota structure according to antibiotic exposure using a Bray-Curtis matrix of relative abundance data of ASVs. In the PERMANOVA model, we also controlled for the confounding factors described above by including them as covariates. A Random Forest classification model was built in order to identify the most discriminative ASVs between subjects not exposed and exposed to antibiotics using the randomForest R package (Package 'randomForest') with default parameters and including all ASVs as explanatory variables as well as confounding variables as covariates. Random Forest is a classification algorithm evolving from the combination of many decision trees. A cross-validation is already built-in in Random Forest, since each tree in the forest has its own training and testing data; each tree uses bootstrapped samples from original data as training set and leaves one-third of data for testing, called out-of-bag (OOB) data. OOB data are used on each tree to predict the outcome, the votes for each predicted outcome from all trees are averaged, and the most voted outcome is selected as the final prediction. Therefore, the out-of-bag error predictions of the classifier were used to calculate the ROC curve and the corresponding area under the curve (AUC) as a measure of the performance of the model. Each predictor variable of the model was given an importance score (mean decrease accuracy), which measures the contribution of each feature to the performance of the model, with higher values indicating higher importance. Specifically, the MDA is the mean decrease in the accuracy over all out-of-bag cross-validated predictions when the values of the variable are randomly permuted after training compared to the original observations. The direction of the association of each quantitative feature was estimated *post hoc* with Cliff's delta test. Finally, most frequent bacterial genera with species implicated in healthcare-associated infections among infants and children were specifically selected in the study (Zingg et al., 2017), and its relative abundances were compared by group using Wilcoxon tests in order to find a possible association with antibiotics.

A phylogenetic tree was constructed containing all streptococcal-type strains from RDP database v11.5 and main streptococcal ASVs detected in our dataset. Cutadapt v1.9 trimmed V3-V4 regions for all the selected RDP streptococcal strains (Martin, 2011), and overall multiple sequence alignment was performed with MAFFT v7.4 (Katoh and Standley, 2013). FastTree inferred the phylogenetic tree according to

maximum-likelihood methods with script `make_phylogeny.py` (Price et al., 2010).

RESULTS

Characteristics of Participants

A total number of 168 cases with IPD were screened for participation in the study. Eighty-one of them met inclusion criteria, with a median age of 32 months (IQR: 18–49) and 58% were male. NPA was collected before receiving antibiotics or within the first 24 h of antibiotic intake in 27 patients (median time=0 days, IQR: 0–0.5), and were assigned to the group not exposed to antibiotics. The 54 remaining inpatients were assigned to the antibiotic-exposed group (median time between the first antibiotic intake and sample collection=4 days, IQR: 3–6). The two groups did not present significant differences either in epidemiological variables or in DNA/RNA viral detections or virulence of pneumococcus causing IPD. Clinical manifestations, days of fever before sample collection, length of hospital stay, and complications were similar among exposed and not-exposed inpatients (Table 1).

All subjects exposed to antibiotics before sample collection were treated with beta-lactam antibiotics (100.0%, n=54), and 13 received combined therapy with another antibiotic type (24.1%). Most patients were intravenously administered with antibiotics (n=50, 92.6%), except for four subjects who were exclusively orally treated prior to NPA sample collection.

Increased Richness and Diversity in the Nasopharynx of Children With IPD Exposed to Antibiotics

A total number of 4,150,123 good quality sequences were obtained from samples and negative controls. This represented a median of 51,309 sequences per sample (IQR: 38,194–73,119) and 468 sequences per negative control (IQR: 192–765) ($P<0.001$). After contaminant removal, 47,323 sequences per sample (IQR: 32,410–64,945) were kept, corresponding to 3,381 ASVs. A median number of 80 ASVs were detected per sample (IQR: 42–129). Tables S1, S2 show the main ASVs with mean relative abundances over 0.1% in each group.

For alpha diversity, higher bacterial Chao1 richness (94.8 [IQR: 57.5–137.5] vs. 44.0 [IQR: 17.7–68.0]) ($P<0.001$, $R^2 = 0.20$) and higher Shannon diversity (2.2 [IQR: 1.5–2.8] vs. 1.6 [IQR: 1.2–2.1]) ($P=0.01$, $R^2 = 0.18$) values were associated to the group exposed to antibiotics (Figures 1A, B). For the overall microbiota structure, PERMANOVA analyses further confirmed that both groups presented significant differences on their bacterial composition ($P<0.001$, $R^2 = 0.03$) Figure 1C).

Decreased Abundances of *S. pneumoniae* and Enrichment of Other Streptococci in the Nasopharynx of Children With IPD Exposed to Antibiotics

A specific pneumococcal qPCR demonstrated lower colonization rates (66.7% vs. 100%, $P=0.002$) and lower pneumococcal loads

(4.6 [IQR: 0–5.8] \log_{10} copies/ml vs. 6.3 [IQR: 5.3–6.7] \log_{10} copies/ml, $P<0.001$) in the nasopharynx of patients exposed to antibiotics vs. not exposed, without significant differences in the invasive disease potential of nasopharyngeal serotypes detected (invasive serotypes; 50.0% vs. 51.8%, $P=1.0$) or in their coverage by PCV13 vaccine (50.0% vs. 51.8%, $P=1.0$).

Analyses with 16S rRNA data not only showed lower abundance of *S. pneumoniae* associated to antibiotic use but also revealed the increase in other streptococci. Overall, a total of 373 ASVs were assigned to *Streptococcus* at the genus level representing the 31.2% of total reads in this dataset. However, 5 ASVs were the most abundant contributing to 25.6% of total reads and 82.2% of the total abundance of reads assigned to *Streptococcus* (Figure 2A). When the relative abundances of these five ASVs were compared by group, four of them were differently distributed: the group not exposed to antibiotics was enriched in *Streptococcus* ASV2 ($P=0.006$) and *Streptococcus* ASV11 ($P=0.009$), while exposed patients were enriched in *Streptococcus* ASV3 ($P<0.001$) and *Streptococcus* ASV12 ($P<0.001$) (Figure 2B). Interestingly, a streptococcal phylogenetic tree confirmed that *S. pneumoniae* type strain was most closely related to ASV2 and ASV11, while ASV3 and ASV12 were more phylogenetically close to *Streptococcus mitis/oralis/infantis* type strains (Figure S1).

Association of Antibiotic Exposure With Increased Abundance of Oral Bacteria in the Nasopharynx of Children With IPD

The results from the Random Forest model demonstrated that nasopharyngeal microbiota composition was different between both groups. The microbiota features exhibited a good discriminatory power for distinguishing inpatients not exposed to antibiotics from those exposed (AUC=0.80 (95% CI:0.69–0.92) (Figure 3A). The top 50 features with higher importance in classifying these patients, as measured by the MDA score, were plotted in Figure 3B. *Moraxella* ASV1, *Moraxella* ASV7, *Streptococcus* ASV11, and *Streptococcus* ASV2 were found among the top most important features associated to the patients not exposed to antibiotics as determined *post hoc* with Cliff's delta test. On the contrary, *Streptococcus* ASV3, *Streptococcus* ASV12, *Staphylococcus* ASV18, as well as several ASVs assigned to *Veillonella*, *Alloprevotella*, *Porphyromonas*, *Delftia*, *Capnocytophaga*, *Granulicatella*, *Neisseria*, and other genera were among the top most important features associated to antibiotic use. Most of these genera include gram-negative and anaerobic bacteria frequently found in the oral cavity (Aas et al., 2005; Mira et al., 2017; Dzidic et al., 2018). Further analyses at the genus level located *Prevotella*, *Capnocytophaga*, and *Veillonella* as the most important predictors associated to antibiotic exposure among children with IPD (Figure S2). Moreover, differential ranking analysis with Songbird also supported these findings (Figure S3).

Overrepresentation of Common Nosocomial Bacteria Among Children With IPD Exposed to Antibiotics

Staphylococcus, *Acinetobacter*, *Pseudomonas*, *Escherichia/Shigella*, *Stenotrophomonas*, *Serratia*, *Enterococcus*, *Enterobacter*, and

TABLE 1 | Epidemiological, microbiological, and clinical characteristics of the study groups.

	Not exposed (n=27)	Exposed (n=54)	P-value ^a
Epidemiological characteristics			
Age, months, median (IQR)	33 (19.0-49.5)	28.5 (18.5-48.5)	0.72
Gender, male (%)	12/27 (44.4)	35/54 (64.8)	0.13
Birth weight, grams, mean (sd) ^b	3260 (507)	3358 (444)	0.41
Gestational age, weeks, median (IQR) ^c	40 (38.2-40.4)	40.0 (39.0-40.0)	0.81
House surface per inhabitant, m ² , median (IQR) ^d	20 (18.1-28.3)	22 (16.7-28.8)	0.87
Seasonality, samples collected during viral season (%) ^e	17/27 (63.0)	31/54 (57.4)	0.81
Ethnicity, Caucasian (%)	16/24 (66.7)	34/48 (70.8)	0.92
Delivery mode, C-section (%)	6/23 (26.1)	7/42 (16.7)	0.55
Breastfeeding (%)	23/26 (88.5)	41/52 (78.8)	0.36 ^k
Breastfeeding duration, months, median (IQR) ^e	6.5 (1.6-12.0)	6.0 (1.0-9.0)	0.41
Schooled (%)	21/26 (80.8)	44/51 (86.3)	0.52 ^k
Family members under 5 years (%)	9/25 (36.0)	12/46 (26.1)	0.55
Parental smoking (%)	8/26 (30.8)	18/49 (36.7)	0.79
Basic educational level (%)	3/19 (15.8)	9/43 (20.9)	0.74 ^k
≥1 dose of Pneumococcal Conjugate Vaccine (%)	15/27 (55.5)	36/52 (69.2)	0.34
Microbiological characteristics			
Viral study			
DNA/RNA viral detection by multiplex PCR (%)	22/27 (81.5)	39/54 (72.2)	0.42 ^k
DNA/RNA viral detection >2 viruses by multiplex PCR (%)	9/27 (33.3)	15/54 (27.8)	0.79
Human rhinovirus/enterovirus (%)	16/27 (59.2)	31/53 (58.5)	1.00
Human respiratory syncytial virus (A and B) (%)	4/26 (15.4)	4/53 (7.5)	0.42 ^k
Human metapneumovirus (%)	1/27 (3.7)	2/53 (3.8)	1.00 ^k
Human coronaviruses (OC43/229E/NL63) (%)	2/27 (7.4)	2/54 (3.7)	0.60 ^k
Human parainfluenza viruses (1,2,3,4) (%)	1/27 (3.7)	6/53 (11.3)	0.41 ^k
Human influenza viruses (A and B) (%)	3/26 (11.5)	4/53 (7.5)	0.67 ^k
Human adenovirus (%)	3/27 (11.1)	8/53 (15.1)	0.74 ^k
Human bocavirus (%)	4/25 (16.0)	6/53 (11.3)	0.71 ^k
Pneumococcal study in invasive samples [#]			
Pneumococcal serotype with high invasive disease potential (%)	14/27 (51.8)	18/36 (50.0)	1.00
Pneumococcal serotype covered by PCV13 vaccination (%)	14/27 (51.8)	18/36 (50.0)	1.00
Clinical characteristics			
Time of fever before NPA collection, hours, median (IQR) ^f	120 (78-144)	128 (33-192)	0.82
Blood analytical parameters at admission			
C-Reactive Protein, mg/L, median (IQR) ^g	300 (205-324)	268 (146-335)	0.83
Procalcitonin, ng/ml, median (IQR) ^h	11.3 (6.7-17.2)	4.3 (1.2-15.1)	0.37
Hemoglobin, g/dl, median (IQR) ⁱ	10.7 (10.1-11.7)	10.8 (9.9-11.6)	0.97
Leukocytes, thousand/mm ³ , mean (SD) ^j	16.8 (8.3)	18.0 (8.9)	0.57
Clinical syndromes			
Complicated pneumonia (%)	16/27 (59.2)	29/54 (53.7)	0.81
Non-complicated pneumonia (%)	7/27 (25.9)	8/54 (14.8)	0.36
Meningitis (%)	3/27 (11.1)	5/54 (9.2)	1.00 ^k
Sepsis (%)	0/27 (0.0)	4/54 (7.4)	0.29 ^k
Bacteremia (%)	1/27 (3.7)	4/54 (7.4)	0.66 ^k
Arthritis (%)	0/27 (0.0)	4/54 (7.4)	0.29 ^k
Hospital stay and complications			
Length of Hospitalization stay, days, median (IQR)	11.0 (8.0-15.0)	10.0 (6.0-15.0)	0.69
ICU admission (%)	4/27 (14.8)	13/54 (24.1)	0.40 ^k
Respiratory support (noninvasive ventilation and/or mechanical ventilation) (%)	2/27 (7.4)	11/54 (20.4)	0.20 ^k
Thoracocentesis (%)	10/27 (37.0)	22/54 (40.7)	0.94

^aT-test and Wilcoxon test were used for parametric and nonparametric continuous variables, respectively. Chi-square test was used for categorical variables.

^bComparisons performed on 25 not exposed cases and 53 exposed cases.

^cComparisons performed on 26 not exposed cases and 53 exposed cases.

^dComparisons performed on 23 not exposed and 47 exposed cases.

^eComparisons performed on 26 not exposed cases and 50 exposed cases.

^fComparisons performed on 26 not exposed cases and 52 exposed cases.

^gComparisons performed on 26 not exposed cases and 53 exposed cases.

^hComparisons performed on 12 not exposed cases and 25 exposed cases.

ⁱComparisons performed on 25 not exposed cases and 51 exposed cases.

^jComparisons performed on 25 not exposed cases and 52 exposed cases.

^kFisher exact tests were performed for categorical variables instead of chi-square tests in case of ≥25% of cells presented expected frequencies <5.

[#]Viral season was defined as the period of time corresponding to Influenza A and VRS circulation over the basal levels according to the Surveillance Plan of ARIs in Catalonia (PIDIRAC) (<https://canalsalut.gencat.cat/ca/professionals/vigilancia-epidemiologica/pla-dinformacio-de-les-infeccions-respiratories-agudes-a-catalunya-pidirac/>) and reports from the Hospital Surveillance Network for VRS in Catalonia (Vall d'Hebrón Hospital) (<https://hospital.vallhebron.com/ca/actualitat/publicacions/informe-xarxa-de-vigilancia-hospitalaria-de-vrs>).

[#]A total of three pneumococci could not be serotyped due to low bacterial load.

SD, Standard Deviation; IQR, Interquartile Range; NPA, Nasopharyngeal aspirate.

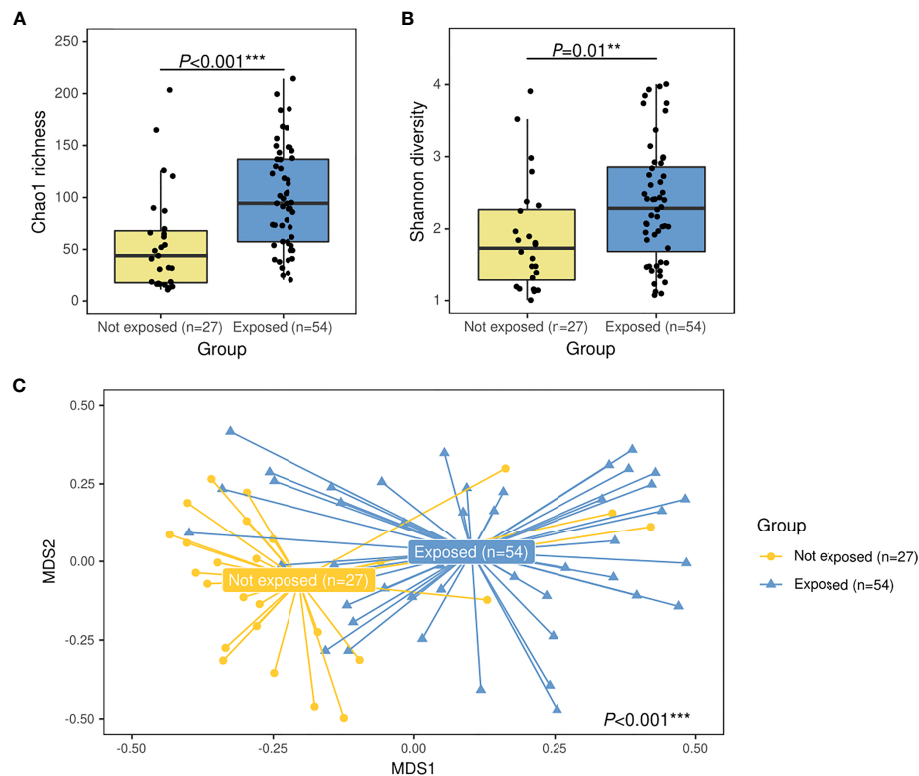


FIGURE 1 | Alpha- and beta-diversity comparisons between patients with IPD not exposed to antibiotics before sample collection (yellow) and IPD patients with previous antibiotic exposure (blue). Boxplots showing the Chao1 richness (A) and Shannon diversity indexes (B) according to antibiotic-exposure groups at the ASV level. Differences by group were assessed with simple linear regression analyses including confounding variables as copredictors (age, gender, seasonality, vaccination, ICU admission, and length of hospital stay). Three observations from the exposed group were deleted due to missing values in vaccination variable. (C) Nonmetric multidimensional scaling (NMDS) plot based on Bray–Curtis dissimilarities of nasopharyngeal microbiota composition of samples from all patients included in the study. Samples of each group are connected with their corresponding centroids using the function “ordispider” (Vegan R package). P-value corresponds to Adonis PERMANOVA test on the antibiotic- exposure group variable and including confounding variables as covariates. Significance codes: *** ≤ 0.001 ; ** ≤ 0.01 ; * ≤ 0.05 . MDS, nonmetric multidimensional scaling.

Klebsiella were found in the nasopharynx of our patients with total relative abundances of 6.2%, 0.6%, 0.5%, 0.04%, 0.03%, 0.03%, 0.01%, 0.009%, and 0.003%, respectively. However, only *Staphylococcus* ($P=0.03$), *Acinetobacter* ($P=0.02$), and *Pseudomonas* ($P=0.02$) showed significant differences with higher relative abundances in the antibiotic-exposed group (Figure 4). Of note, the antibiotic-exposed children also presented longer hospital stays prior to sample collection (median=3 days [IQR: 2–5] vs. median=0 days [IQR=0–1], $P<0.001$).

DISCUSSION

In the present study, we have demonstrated clear differences in nasopharyngeal microbiota composition of hospitalized children with IPD exposed to antibiotics compared to those not exposed.

Patients exposed to antibiotics presented richer and more diverse microbial nasopharyngeal communities in our study compared to those not exposed. This finding is in contrast to previous literature describing bacterial diversity reduction in gut

microbiota as a consequence of antibiotic intake (Kim et al., 2017) and may reflect differential effects of antibiotics across respiratory and intestinal microbiota ecosystems. Our results are in agreement with those reported in a longitudinal study by Smith et al. (2014) in adults with cystic fibrosis. This study analyzed the effects of intravenous beta-lactam antibiotics for treating exacerbations on sputum samples collected on the first day, at 3–4 days, and 8–10 days since antibiotic initiation. A transient increase in diversity at 3 days was described that normalized at days 8–10, suggesting that timing of sampling after the start of antibiotic could be key to understanding the dysbiotic effect of antibiotic exposure in the respiratory microbiota. Results from other investigations on the impact of antibiotics on respiratory microbiota are scarce and heterogeneous, mostly referring to effects observed after at least 7 days of antibiotic initiation: some studies reported decreases in bacterial community complexity (Lazarevic et al., 2013; Pittman et al., 2017; Kramná et al., 2018), while others showed no significant changes on alpha-diversity measures at all (Zhou et al., 2016; Salter et al., 2017). Other factors such as patient

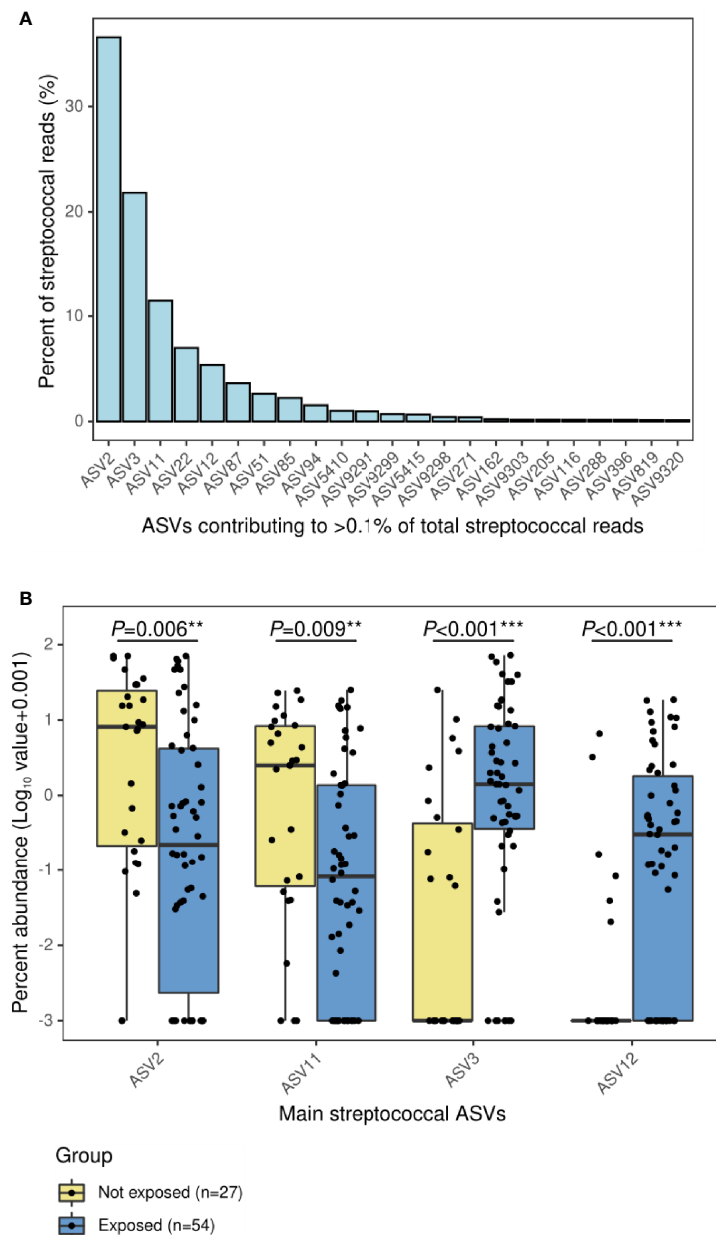


FIGURE 2 | Main ASVs assigned to *Streptococcus* in the nasopharynx of children with IPD and their relative abundance according to antibiotic-exposure groups. **(A)** Bar plot showing the ASVs with a relative contribution >0.1% to the total number of streptococcal reads. **(B)** Boxplot showing the relative abundance of main streptococcal ASVs differentially represented in antibiotic-exposure groups. Significance codes: *** ≤0.001; ** ≤0.01; * ≤0.05.

age, the specific respiratory condition analyzed, and the respiratory tract segment analyzed may explain the heterogeneity of antibiotic impacts on respiratory microbiota reported so far.

Antibiotic exposure was associated to higher relative abundance of ASVs phylogenetically close to viridans group streptococci (VGS), specifically *Streptococcus mitis/oralis/infantis* species, and anaerobic bacteria such as *Prevotella*, *Aloprevotella*, *Veillonella*, *Porphyromonas*, and *Granulicatella*. These taxa mainly corresponded to commensal bacteria more

frequently found in the oropharynx (Aas et al., 2005; Dzidic et al., 2010; Mira et al., 2017) than the nasopharynx of children (Ho Man et al., 2017; SM et al., 2018). Smith et al. (2014) also described a trend for increased relative abundances of anaerobes in sputum samples, mainly *Veillonella* and *Prevotella*, after 72 h of beta-lactam treatment. Similar effects have been observed with pneumococcal vaccination, which resulted in temporary shifts in nasopharyngeal microbiota composition with increased levels of bacterial diversity and increased relative abundances of *Prevotella*, *Veillonella*, unclassified *Bacteroidetes*, and

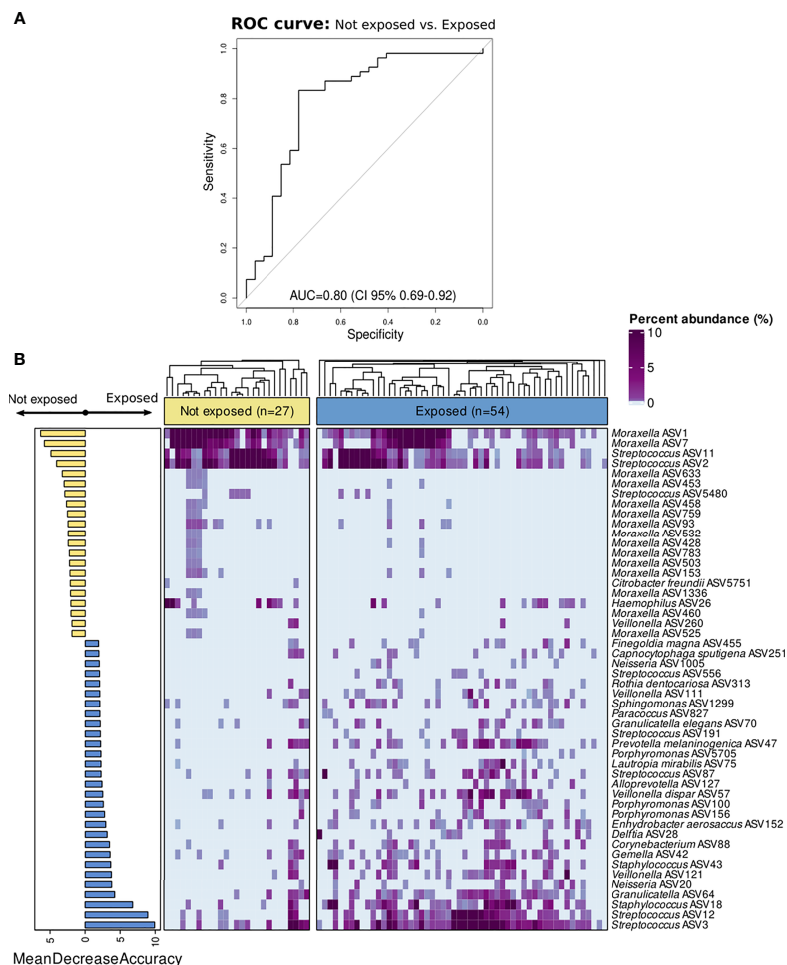


FIGURE 3 | Classification of children with IPD according to antibiotic-exposure using a Random Forest model based on nasopharyngeal microbiota composition. All ASVs as well as confounding factors (age, gender, seasonality, vaccination, ICU admission, and length of hospital stay) were included in the model. **(A)** ROC curve showing the performance of the RF model at the ASV level. **(B)** Bar plot showing top 50 most important features to class separation according to the Mean Decrease Accuracy score (confounding factors were not found among the top important features). Color-coding shows directionality of the association for each of the 50 top features to either the not exposed (yellow) or antibiotic-exposed (blue) group based on a *post hoc* analyses with Cliff's delta estimation of the effect size. In addition, a heatmap displaying relative abundance (%) of these top 50 features across samples is shown on the right. Each column represents a sample, while each row represents a different feature. In the x-axis, samples are split by group and ordered according to hierarchical clustering using a Bray–Curtis dissimilarity measure.

Leptotrichia (Biesbroek et al., 2014). Other nonpneumococcal streptococci also raised after vaccination, while pneumococcal-vaccine serotypes decreased. Despite different action mechanisms, both antibiotics and vaccination may lead to eliminating pneumococcus from nasopharynx, with probable displacement of the species detected. Our study suggests that colonizing bacteria from oropharynx may be leading the short-term repopulation of nasopharynx after antibiotic exposure. Although mainly speculative, the poor oral hygiene frequently associated to hospitalized children (Blevins, 2013) is linked to high bacterial loads and increased bacterial colonization (Fourrier et al., 1998; Bordasa et al., 2008; Barbosa et al., 2016; Carrol et al., 2020; Chhaliyil et al., 2020), which may favor the migration of bacteria from oral and dental plaque to the empty nasopharyngeal space left by pneumococcus. Other

plausible mechanisms may include the possibility that oral bacteria were already present in the nasopharynx of children with IPD in very low abundance, and such populations expanded to fully occupy the niche after antibiotic use or the new acquisition of oral bacteria *via* breathing, which may have the opportunity to colonize this niche due to the reduction of pneumococcus abundance.

The importance of these findings must be unveiled. Despite the fact that these bacteria are generally commensal microorganisms from the oropharynx (Aas et al., 2005), it has been demonstrated to be a causative role in local and disseminated infections. VGS are a common cause of bacteremia and infective endocarditis (Desai et al., 2017). Gram-negative bacteria such as *Prevotella*, *Porphyromonas*, and *Veillonella* and gram-positive cocci such as *Granulicatella* are isolated from a considerable proportion of mixed anaerobic

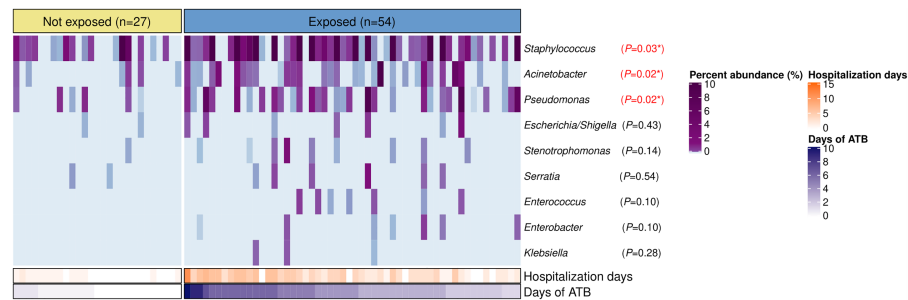


FIGURE 4 | Bacterial genera associated to nosocomial infections in the nasopharynx of patients with IPD according to antibiotic-exposure and length of hospitalization prior to sample collection. Heatmap displaying relative abundances (%) of bacterial genera with characteristic species implicated in healthcare-associated infections. Each column represents a sample, while each row a bacterial genus. Samples are split by the antibiotic-exposure group and ordered by days of antibiotic intake. Rows are sorted by total relative abundance in decreasing order. Bottom bars indicate the number of days of antibiotic exposure and days of hospitalization prior to sample collection for each patient with distinct color scales. Differences in relative abundances of these bacteria by group were assessed with Wilcoxon tests and FDR adjusted p-values are shown. Significance codes: *** ≤ 0.001 ; ** ≤ 0.01 ; * ≤ 0.05 .

infections in children (Brook, 2002). In addition, some *Prevotella* and *Porphyromonas* species have been described as important pathogens in periodontitis and inextricably linked to systemic chronic disorders as cardiovascular diseases, diabetes, and rheumatoid arthritis, through cross-reactive antibodies and increased levels of systemic inflammation (Bui et al., 2019).

A higher abundance of VGS and typical oral taxa in the nasopharynx of antibiotic-exposed cases despite active treatment could be explained by the considerable rates of resistance to beta-lactam antibiotics described in these bacteria (Nyfors et al., 2003; Desai et al., 2017; Arredondo et al., 2020), or to the biofilm mode of life of some of these species, which may restrict antibiotic penetration (Kouidhi et al., 2015). In addition, VGS constitute a reservoir of antimicrobial resistance genes that have been described to be transferred to more pathogenic organisms like *S. pneumoniae* (Jensen et al., 2015), while anaerobic gram-negative bacteria may protect penicillin-susceptible bacteria through beta-lactamase production, contributing to antibiotic failures (Brook, 2009). Worrisome is also the fact that antibiotic exposure in children with IPD and hospitalized for a median of 3 days was associated to increased abundances of *Staphylococcus*, *Pseudomonas*, and *Acinetobacter*. These genera, specially *Pseudomonas* and *Acinetobacter*, are not common respiratory commensals and are related to typical multidrug-resistant species causing nosocomial infections (Zingg et al., 2017).

Although it is probable that our findings could be transitory and a recovery of the initial stability of the nasopharyngeal microbiota is reached after antibiotic treatment ends, some changes have been described to persist for long time and for some species to become part of the commensal microbiota. Given the implication of oral bacterial species in multiple disorders and its overrepresentation in the nasopharynx of inpatients with IPD after antibiotic treatment, our study suggests that these patients could benefit from the concurrent administration of probiotics/prebiotics alongside antibiotics that may help to prevent dysbiosis and recover a balanced state of the

microbiota (Rosier et al., 2018; Lee et al., 2021). The role of the oral hygiene in preventing and recovering from such disturbances must be revealed. This practice has demonstrated to reduce colonization and density of oral pathogenic bacteria in the oropharynx as well as to reduce the risk of nosocomial infections (Bordasa et al., 2008; Amaral et al., 2009; Carrol et al., 2020; Chhaliyil et al., 2020; Vilela et al., 2015), and could be useful if the repopulation of the nasopharynx of children with IPD after antibiotic treatment is produced by the expansion of oral bacteria from the oropharynx.

This study is subject to a number of limitations. First, the small sample size may have reduced the statistical power. Nevertheless, we would like to note the valuable cohort of patients recruited in a low-prevalence area for IPD and the lack of previous studies assessing the ecological impact of antibiotics in the nasopharynx of these children. Second, its cross-sectional design only allowed identification of associations without establishing causality. Third, 16S rRNA gene sequencing studies cannot differentiate between live and death bacteria. Fourth, analyses at the species levels could not be performed because of the poor taxonomic resolution at this rank, especially for streptococcal species, possibly due to the use of short-length amplicons and the absence of respiratory tract-dedicated, thoroughly curated 16S rRNA gene databases as occurred in gut microbiota. However, we performed analyses at the ASV level that allowed the finest possible resolution by discriminating unique sequences at the single-nucleotide level. Finally, although a phylogenetic tree based on 16S rRNA gene sequences was constructed in order to identify which streptococcal strains were the most phylogenetically close to the streptococcal ASVs detected in our study, other genes may be more suitable for reliable classification of streptococcal species.

Despite these limitations, the associations described here are strong enough to encourage future longitudinal studies that confirm our findings and evaluate the relation of changes observed in nasopharyngeal communities after antibiotic use with short-term and long-term clinical outcomes. Our findings may also encourage shotgun metagenomic studies that help to

describe functional profiles and resistance patterns of nasopharyngeal communities associated to antibiotic use.

In conclusion, our results suggest a reduction of *S. pneumoniae* abundance on the nasopharynx of children with IPD after antibiotic treatment, and a short-term repopulation of this altered niche by oral and nosocomial bacteria. This emphasizes the need for understanding the clinical implications of these antibiotic-derived perturbations as well as the utility of probiotic/prebiotic administration or even oral hygiene improvement in preventing or recovering from such disturbances.

DATA AVAILABILITY STATEMENT

Raw sequence files have been deposited in the European Nucleotide Archive (ENA) at EMBL-EBI under accession number PRJEB46580. The metadata file can be found at FigShare repository (<https://figshare.com/s/b52ec8e5a72a49782b77>). The rest of data can be found in the article as supplementary files.

ETHICS STATEMENT

This research was approved by the Ethics Committee of HSJD (PIC 70-15 and PIC 137-16) and conducted in compliance with the World Medical Association's Declaration of Helsinki. All parents and/or legal guardians signed informed consent for children participating in the study.

AUTHOR CONTRIBUTIONS

Conception and study design: CM-A and RC-R. Funding: DH and CM-A. Case-control recruitment and data collection: DH, MS, and CL. Microbiological characterization: DH and AM.

REFERENCES

- Aas, J. A., Paster, B. J., Stokes, L. N., Olsen, I., and Dewhirst, F. E. (2005). Defining the Normal Bacterial Flora of the Oral Cavity. *J. Clin. Microbiol.* 43, 5721–5732. doi: 10.1128/JCM.43.11.5721-5732.2005
- Arredondo, A., Blanc, V., Mor, C., Nart, J., and León, R. (2020). Resistance to β -Lactams and Distribution of β -Lactam Resistance Genes in Subgingival Microbiota From Spanish Patients With Periodontitis. *Clin. Oral. Investig.* 24, 4639–4648. doi: 10.1007/s00784-020-03333-1
- Amaral, S. M., Cortês, A. Q., and Pires, F. R. (2009). Nosocomial Pneumonia: Importance of the Oral Environment. *J. Bras. Pneumol.* 35, 1116–1124. doi: 10.1590/S1806-37132009001100010
- Barbosa, C. G., Leme, T. D., Barbosa, A. G., Miranda, A. F., Piemonte, J. A., and Barreto, A. C. (2016). Oral Microbial Colonization in Pediatric Intensive Care Unit Patients. *J. Dent. Child. (Chic)* 83, 53–59.
- Biesbroek, G., Wang, X., Keijsers, B. J. F., Eijkemans, R. M. J., Trzciński, K., Rots, N. Y., et al (2014). Seven-Valent Pneumococcal Conjugate Vaccine and Nasopharyngeal Microbiota in Healthy Children. *Emerg. Infect. Dis.* 20, 201–210. doi: 10.3201/eid2002.131220
- Blevins, J. Y. (2013). Status of Oral Health Care in Hospitalized Children. *MCN Am. J. Matern. Nurs.* 38, 115–119. doi: 10.1097/NMC.0b013e318269daac
- Bordasa, A., McNaba, R., Staples, A. M., Bowman, J., Kanapka, J., and Bosmaa, M. P. (2008). Impact of Different Tongue Cleaning >Methods on the Bacterial

Bioinformatics analyses/statistical analyses: DH. Guidance in the analyses: MR and RC-R. Interpretation of results: DH, PB, AM, RC-R, and CM-A. Coordination: RC-R and CM-A. Writing manuscript: DH. Revising manuscript: DH, MR, PB, MS, AM, CL, RC-R, and CM-A. All authors contributed to the article and approved the submitted version.

FUNDING

This work was supported by Fondo Europeo de Desarrollo Regional (FEDER) and the Ministry of Science and Innovation, Instituto de Salud Carlos III (ISCIII) [PI16/00174 (CM-A), FI17/00248 (DH)], and Sant Joan de Deu Foundation [AFR2015 (CM-A)]. DH also received a grant from Sociedad Española de Enfermedades Infecciosas y Microbiología Clínica (SEIMC) for a research stay. The funders had no role in study design, data collection and interpretation, or the decision to submit the work for publication.

ACKNOWLEDGMENTS

We thank the Teagasc Food Research Centre, in particular Dr. Paul Cotter, for hosting a research stay of DH in his center. We also thank Amaresh Pérez-Argüello Cristina Esteva, Juan Jose Garcia-Garcia, and Daniel Penela for their contribution in taking care of patients and/or microbiological studies.

SUPPLEMENTARY MATERIAL

The Supplementary Material for this article can be found online at: <https://www.frontiersin.org/articles/10.3389/fcimb.2021.744727/full#supplementary-material>

- Load of the Tongue Dorsum. *Arch. Oral. Biol.* 53 (Suppl 1), S13–S18. doi: 10.1016/S0003-9969(08)70004-9
- Bosch, A. A. T. M., De Steenhuijsen Piters, W. A. A., Van Houten, M. A., Chu, M. L. J. N., Biesbroek, G., Kool, J., et al (2017). Maturation of the Infant Respiratory Microbiota, Environmental Drivers, and Health Consequences. *Am. J. Respir. Crit. Care Med.* 196, 1582–1590. doi: 10.1164/rccm.201703-0554OC
- Boursi, B., Mamtani, R., Haynes, K., and Yang, Y. X. (2015). The Effect of Past Antibiotic Exposure on Diabetes Risk. *Eur. J. Endocrinol.* 172, 639–648. doi: 10.1530/EJE-14-1163
- Brook, I. (2002). Anaerobic Infections in Children. *Microbes Infect.* 4, 1271–1280. doi: 10.1016/S1286-4579(02)01656-8
- Brook, I. (2009). The Role of Beta-Lactamase-Producing Bacteria in Mixed Infections. *BMC Infect. Dis.* 9, 202. doi: 10.1186/1471-2334-9-202
- Bui, F. Q., Almeida-da-Silva, C. L. C., Huynh, B., Trinh, A., Liu, J., Woodward, J., et al (2019). Association Between Periodontal Pathogens and Systemic Disease. *Biomed. J.* 42, 27–35. doi: 10.1016/j.bj.2018.12.001
- Callahan, B. J., McMurdie, P. J., Rosen, M. J., Han, A. W., Johnson, A. J. A., and Holmes, S. P. (2016). DADA2: High-Resolution Sample Inference From Illumina Amplicon Data. *Nat. Methods* 13, 581–583. doi: 10.1038/nmeth.3869
- Camelo-Castillo, A., Henares, D., Brotons, P., Galiana, A., Rodríguez, J. C., Mira, A., et al. (2019). Nasopharyngeal Microbiota in Children With Invasive Pneumococcal Disease: Identification of Bacteria With Potential Disease-

- Promoting and Protective Effects. *Front. Microbiol.* 10, 11. doi: 10.3389/fmicb.2019.00011
- Carroll, D. H., Chassagne, F., Dettweiler, M., and Quave, C. L. (2020). Antibacterial Activity of Plant Species Used for Oral Health Against *Porphyromonas Gingivalis*. *PLoS One* 15, e0239316. doi: 10.1371/JOURNAL.PONE.0239316
- CDC and Ncid Laboratory Methods for the Diagnosis of Meningitis - CHAPTER 8: Identification and Characterization of *Streptococcus Pneumoniae*. Available at: <http://www.cdc.gov/ncidod/biotech/strep/strep-doc/index.htm> (Accessed August 27, 2021).
- Chhaliyil, P., Fischer, K., Schoel, B., and Chhaliyil, P. (2020). Impact of Different Bedtime Oral Cleaning Methods on Dental-Damaging Microbiota Levels. *Dent. Hypotheses* 11, 40–46. doi: 10.4103/denthyp.denthyp_7_20
- Choo, J. M., Abell, G. C. J., Thomson, R., Morgan, L., Waterer, G., Gordon, D. L., et al (2018). Impact of Long-Term Erythromycin Therapy on the Oropharyngeal Microbiome and Resistance Gene Reservoir in Non-Cystic Fibrosis Bronchiectasis. *mSphere* 3, e00103–e00118. doi: 10.1128/msphere.00103-18
- Cleary, D. W., and Clarke, S. C. (2017). The Nasopharyngeal Microbiome. *Emerg. Top. Life Sci.* 1, 297–312. doi: 10.1042/ETLS20170041
- Davis, N. M., Proctor, D. M., Holmes, S. P., Relman, D. A., and Callahan, B. J. (2018). Simple Statistical Identification and Removal of Contaminant Sequences in Marker-Gene and Metagenomics Data. *Microbiome* 6, 226. doi: 10.1186/s40168-018-0605-2
- Desai, N., Steenbergen, J., and Katz, D. E. (2017). “Antibiotic Resistance of Non-Pneumococcal *Streptococci* and Its Clinical Impact,” in *Antimicrobial Drug Resistance* (Switzerland: Springer International Publishing), 791–810. doi: 10.1007/978-3-319-47266-9_2
- Dzidic, M., Collado, M. C., Abrahamsson, T., Artacho, A., Stensson, M., Jenmalm, M. C., et al (2018). Oral Microbiome Development During Childhood: An Ecological Succession Influenced by Postnatal Factors and Associated With Tooth Decay. *ISME J.* 12, 2292–2306. doi: 10.1038/s41396-018-0204-z
- Fleming-Dutra, K. E., Hersh, A. L., Shapiro, D. J., Bartoces, M., Enns, E. A., File, T. M., et al (2016). Prevalence of Inappropriate Antibiotic Prescriptions Among Us Ambulatory Care Visits 2010–2011. *JAMA - J. Am. Med. Assoc.* 315, 1864–1873. doi: 10.1001/jama.2016.4151
- Fourrier, F., Duvivier, B., Boutigny, H., Roussel-Delvallez, M., and Chopin, C. (1998). Colonization of Dental Plaque: A Source of Nosocomial Infections in Intensive Care Unit Patients. *Crit. Care Med.* 26, 301–308. doi: 10.1097/00003246-199802000-00032
- Friedman, N. D., Temkin, E., and Carmeli, Y. (2016). The Negative Impact of Antibiotic Resistance. *Clin. Microbiol. Infect.* 22, 416–422. doi: 10.1016/j.cmi.2015.12.002
- GBD 2016 Lower Respiratory Infections Collaborators (2018). Estimates of the Global, Regional, and National Morbidity, Mortality, and Aetiologies of Lower Respiratory Infections in 195 Countries 1990–2016: A Systematic Analysis for the Global Burden of Disease Study 2016. *Lancet Infect. Dis.* 18, 1191–1210. doi: 10.1016/S1473-3099(18)30310-4
- Gov.UK (2020). *Pneumococcal: The Green Book, Chapter 25 - GOV.UK*. Available at: <https://www.gov.uk/government/publications/pneumococcal-the-green-book-chapter-25> (Accessed August 27, 2021).
- Hahn, A., Warnken, S., Pérez-Losada, M., Freisztat, R. J., and Crandall, K. A. (2018). Microbial Diversity Within the Airway Microbiome in Chronic Pediatric Lung Diseases. *Infect. Genet. Evol.* 63, 316. doi: 10.1016/j.jmeggid.2017.12.006
- Ho Man, W., de Steenhuijsen Pijters, W. A., and Bogaert, D. (2017). The Microbiota of the Respiratory Tract: Gatekeeper to Respiratory Health. *Nat. Rev. Microbiol.* 15, 259–270. doi: 10.1038/nrmicro.2017.14
- Hong, B. Y., Maulén, N. P., Adami, A. J., Granados, H., Balcells, M. E., and Cervantes, J. (2016). Microbiome Changes During Tuberculosis and Antituberculous Therapy. *Clin. Microbiol. Rev.* 29, 915–926. doi: 10.1128/CMR.00096-15
- Illumina 16S Metagenomic Sequencing Library Preparation (15044223 B) Available at: https://support.illumina.com/content/dam/illumina-support/documents/documentation/chemistry_documentation/16s/16s-metagenomic-library-prep-guide-15044223-b.pdf (Accessed August 27, 2021).
- Jensen, A., Valdósson, O., Frimodt-Møller, N., Hollingshead, S., and Kilian, M. (2015). Commensal *Streptococci* Serve as a Reservoir for β -Lactam Resistance Genes in *Streptococcus Pneumoniae*. *Antimicrob. Agents Chemother.* 59, 3529–3540. doi: 10.1128/AAC.00429-15
- Jernberg, C., Löf, S., Edlund, C., Jansson, J. K., and Se, C. J. (2010). Long-Term Impacts of Antibiotic Exposure on the Human Intestinal Microbiota. *Microbiology* 156, 3216–3223. doi: 10.1099/mic.0.040618-0
- Jernberg, C., Löfmark, S., Edlund, C., and Jansson, J. K. (2007). Long-Term Ecological Impacts of Antibiotic Administration on the Human Intestinal Microbiota. *ISME J.* 1, 56–66. doi: 10.1038/ISMEJ.2007.3
- Johansson, N., Kalin, M., Giske, C. G., and Hedlund, J. (2008). Quantitative Detection of *Streptococcus Pneumoniae* From Sputum Samples With Real-Time Quantitative Polymerase Chain Reaction for Etiologic Diagnosis of Community-Acquired Pneumonia. *Diagn. Microbiol. Infect. Dis.* 60, 255–261. doi: 10.1016/j.diagmicrobio.2007.10.011
- Katoh, K., and Standley, D. M. (2013). MAFFT Multiple Sequence Alignment Software Version 7: Improvements in Performance and Usability. *Mol. Biol. Evol.* 30, 772–780. doi: 10.1093/molbev/mst010
- Kim, S., Covington, A., and Pamer, E. G. (2017). The Intestinal Microbiota: Antibiotics, Colonization Resistance, and Enteric Pathogens. *Immunol. Rev.* 279, 90–105. doi: 10.1111/imr.12563
- Koudih, B., Al Qurashi, Y. M. A., and Chaieb, K. (2015). Drug Resistance of Bacterial Dental Biofilm and the Potential Use of Natural Compounds as Alternative for Prevention and Treatment. *Microb. Pathog.* 80, 39–49. doi: 10.1016/j.micpath.2015.02.007
- Kramná, L., Dřevínek, P., Lin, J., Kulich, M., and Cinek, O. (2018). Changes in the Lung Bacteriome in Relation to Antipseudomonal Therapy in Children With Cystic Fibrosis. *Folia Microbiol. (Praha)* 63, 237–248. doi: 10.1007/s12223-017-0562-3
- Lanasa, M., Bassat, Q., Medeiros, M. M., and Muñoz-Almagro, C. (2017). Respiratory Microbiota and Lower Respiratory Tract Disease. *Expert Rev. Anti Infect. Ther.* 15, 703–711. doi: 10.1080/14787210.2017.1349609
- Lazarevic, V., Manzano, S., Gaia, N., Girard, M., Whiteson, K., Hibbs, J., et al (2013). Effects of Amoxicillin Treatment on the Salivary Microbiota in Children With Acute Otitis Media. *Clin. Microbiol. Infect.* 19, e335–e342. doi: 10.1111/1469-0691.12213
- Lee, C. H., Choi, Y., Seo, S. Y., Kim, S. H., Kim, I. H., Kim, S. W., et al (2021). Addition of Probiotics to Antibiotics Improves the Clinical Course of Pneumonia in Young People Without Comorbidities: A Randomized Controlled Trial. *Sci. Rep.* 11, 1–9. doi: 10.1038/s41598-020-79630-2
- Martin, M. (2011). Cutadapt Removes Adapter Sequences From High-Throughput Sequencing Reads. *EMBnet.journal* 17, 10. doi: 10.14806/ej.17.1.200
- McMurdie, P. J., and Holmes, S. (2013). Phyloseq: An R Package for Reproducible Interactive Analysis and Graphics of Microbiome Census Data. *PLoS One* 8, e61217. doi: 10.1371/journal.pone.0061217
- Mira, A., Simon-Soro, A., and Curtis, M. A. (2017). Role of Microbial Communities in the Pathogenesis of Periodontal Diseases and Caries. *J. Clin. Periodontol.* 44, S23–S38. doi: 10.1111/jcpe.12671
- NICE (2019). *Pneumonia (Community-Acquired): Antimicrobial Prescribing NICE Guideline*. Available at: www.nice.org.uk/guidance/ng138 (Accessed August 27, 2021).
- Nyfors, S., Könönen, E., Bryk, A., Syrjänen, R., and Jousimies-Somer, H. (2003). Age-Related Frequency of Penicillin Resistance of Oral Veillonella. *Diagn. Microbiol. Infect. Dis.* 46, 279–283. doi: 10.1016/S0732-8893(03)00082-8
- Oksanen, J., Blanchet, F. G., Friendly, M., Kindt, R., Legendre, P., McGlinn, D., et al (2018). *Titl Community Ecology Package*. Available at: <https://cran.r-project.org/web/packages/vegan/vegan.pdf> (Accessed August 27, 2021).
- Orlando, V., Monetti, V. M., Juste, A. M., Russo, V., Mucherino, S., Trama, U., et al (2020). Drug Utilization Pattern of Antibiotics: The Role of Age, Sex and Municipalities in Determining Variation. *Risk Manage. Healthc. Policy* 13, 63–71. doi: 10.2147/RMHP.S223042
- Package ‘randomForest’. (Available at: <https://cran.r-project.org/web/packages/randomForest/randomForest.pdf> (Accessed August 27, 2021).
- Pittman, J. E., Wylie, K. M., Akers, K., Storch, G. A., Hatch, J., Quante, J., et al (2017). Association of Antibiotics, Airway Microbiome, and Inflammation in Infants With Cystic Fibrosis. *Ann. Am. Thorac. Soc.* 14, 1548–1555. doi: 10.1513/AnnalsATS.201702-121OC

- Price, M. N., Dehal, P. S., and Arkin, A. P. (2010). FastTree 2 - Approximately Maximum-Likelihood Trees for Large Alignments. *PLoS One* 5, e9490. doi: 10.1371/journal.pone.0009490
- Rosier, B. T., Marsh, P. D., and Mira, A. (2018). Resilience of the Oral Microbiota in Health: Mechanisms That Prevent Dysbiosis. *J. Dent. Res.* 97, 371–380. doi: 10.1177/0022034517742139
- Salter, S. J., Turner, C., Watthanaworawit, W., de Goffau, M. C., Wagner, J., Parkhill, J., et al (2017). A Longitudinal Study of the Infant Nasopharyngeal Microbiota: The Effects of Age, Illness and Antibiotic Use in a Cohort of South East Asian Children. *PLoS Negl. Trop. Dis.* 11, 10. doi: 10.1371/journal.pntd.0005975
- Schmieder, R., and Edwards, R. (2011). Fast Identification and Removal of Sequence Contamination From Genomic and Metagenomic Datasets. *PLoS One* 6, e17288. doi: 10.1371/journal.pone.0017288
- Selva, L., del Amo, E., Brotons, P., and Muñoz-Almagro, C. (2012). Rapid and Easy Identification of Capsular Serotypes of Streptococcus Pneumoniae by Use of Fragment Analysis by Automated Fluorescence-Based Capillary Electrophoresis. *J. Clin. Microbiol.* 50, 3451–3457. doi: 10.1128/JCM.01368-12
- Sjölund, M., Tano, E., Blaser, M. J., Andersson, D. I., and Engstrand, L. (2005). Persistence of Resistant Staphylococcus Epidermidis After Single Course of Clarithromycin. *Emerg. Infect. Dis.* 11, 1389–1393. doi: 10.3201/EID1109.050124
- Smith, D. J., Badrick, A. C., Zakrzewski, M., Krause, L., Bell, S. C., Anderson, G. J., et al (2014). Pyrosequencing Reveals Transient Cystic Fibrosis Lung Microbiome Changes With Intravenous Antibiotics. *Eur. Respir. J.* 44, 922–930. doi: 10.1183/09031936.00203013
- Tai, N., Wong, F. S., and Wen, L. (2015). The Role of Gut Microbiota in the Development of Type 1, Type 2 Diabetes Mellitus and Obesity. *Rev. Endocr. Metab. Disord.* 16, 55–65. doi: 10.1007/s11154-015-9309-0
- Teo, S. M., Tang, H. H. F., Mok, D., Judd, L. M., Watts, S. C., Pham, K., et al (2018). Airway Microbiota Dynamics Uncover a Critical Window for Interplay of Pathogenic Bacteria and Allergy in Childhood Respiratory Disease. *Cell Host Microbe* 24, 341–352.e5. doi: 10.1016/j.chom.2018.08.005
- Vilela, M. C. N., Ferreira, G. Z., Santos, P. S. D. S., and Rezende, N. P. M. D. (2015). Oral Care and Nosocomial Pneumonia: A Systematic Review. *Einstein (São Paulo)* 13, 290–296. doi: 10.1590/S1679-45082015RW2980
- Wahl, B., O'Brien, K. L., Greenbaum, A., Majumder, A., Liu, L., Chu, Y., et al (2018). Burden of Streptococcus Pneumoniae and Haemophilus Influenzae Type B Disease in Children in the Era of Conjugate Vaccines: Global, Regional, and National Estimates for 2000–15. *Lancet Glob. Heal.* 6, e744–e757. doi: 10.1016/S2214-109X(18)30247-X
- Wang, Z. J., Chen, X. F., Zhang, Z. X., Li, Y. C., Deng, J., Tu, J., et al (2017). Effects of Anti-Helicobacter Pylori Concomitant Therapy and Probiotic Supplementation on the Throat and Gut Microbiota in Humans. *Microb. Pathog.* 109, 156–161. doi: 10.1016/j.micpath.2017.05.035
- Zhou, Y., Bacharier, L. B., Isaacson-Schmid, M., Baty, J., Schechtman, K. B., Sajol, G., et al (2016). Azithromycin Therapy During Respiratory Syncytial Virus Bronchiolitis: Upper Airway Microbiome Alterations and Subsequent Recurrent Wheeze. *J. Allergy Clin. Immunol.* 138, 1215–1219.e5. doi: 10.1016/j.jaci.2016.03.054
- Zingg, W., Hopkins, S., Gayet-Ageron, A., Holmes, A., Sharland, M., Suetens, C., et al (2017). Health-Care-Associated Infections in Neonates, Children, and Adolescents: An Analysis of Paediatric Data From the European Centre for Disease Prevention and Control Point-Prevalence Survey. *Lancet Infect. Dis.* 17, 381–389. doi: 10.1016/S1473-3099(16)30517-5

Conflict of Interest: CM-A reports grants to her organization from Pfizer outside the submitted work and personal fees from Qiagen for presentations at satellite symposiums outside the submitted work.

The remaining authors declare that the research was conducted in the absence of any commercial or financial relationships that could be construed as a potential conflict of interest.

Publisher's Note: All claims expressed in this article are solely those of the authors and do not necessarily represent those of their affiliated organizations, or those of the publisher, the editors and the reviewers. Any product that may be evaluated in this article, or claim that may be made by its manufacturer, is not guaranteed or endorsed by the publisher.

Copyright © 2021 Henares, Rocafort, Brotons, de Sevilla, Mira, Launes, Cabrera-Rubio and Muñoz-Almagro. This is an open-access article distributed under the terms of the Creative Commons Attribution License (CC BY). The use, distribution or reproduction in other forums is permitted, provided the original author(s) and the copyright owner(s) are credited and that the original publication in this journal is cited, in accordance with accepted academic practice. No use, distribution or reproduction is permitted which does not comply with these terms.



Pneumococcal Extracellular Serine Proteases: Molecular Analysis and Impact on Colonization and Disease

Murtadha Q. Ali¹, Thomas P. Kohler¹, Lukas Schulig², Gerhard Burchhardt¹ and Sven Hammerschmidt^{1*}

¹ Department of Molecular Genetics and Infection Biology, Interfaculty Institute of Genetics and Functional Genomics, Center for Functional Genomics of Microbes, University of Greifswald, Greifswald, Germany, ² Department of Pharmaceutical and Medicinal Chemistry, Institute of Pharmacy, University of Greifswald, Greifswald, Germany

OPEN ACCESS

Edited by:

Jason W. Rosch,
St. Jude Children's Research Hospital,
United States

Reviewed by:

Jens Kreth,
Oregon Health and Science University,
United States
Eric Krukonis,
University of Detroit Mercy,
United States

*Correspondence:

Sven Hammerschmidt
sven.hammerschmidt@uni-
greifswald.de

Specialty section:

This article was submitted to
Molecular Bacterial Pathogenesis,
a section of the journal
Frontiers in Cellular and
Infection Microbiology

Received: 23 August 2021

Accepted: 08 October 2021

Published: 01 November 2021

Citation:

Ali MQ, Kohler TP, Schulig L,
Burchhardt G and Hammerschmidt S
(2021) Pneumococcal
Extracellular Serine Proteases:
Molecular Analysis and Impact
on Colonization and Disease.
Front. Cell. Infect. Microbiol. 11:763152.
doi: 10.3389/fcimb.2021.763152

The pathobiont *Streptococcus pneumoniae* causes life-threatening diseases, including pneumonia, sepsis, meningitis, or non-invasive infections such as otitis media. Serine proteases are enzymes that have been emerged during evolution as one of the most abundant and functionally diverse group of proteins in eukaryotic and prokaryotic organisms. *S. pneumoniae* expresses up to four extracellular serine proteases belonging to the category of trypsin-like or subtilisin-like family proteins: HtrA, SFP, PrtA, and CbpG. These serine proteases have recently received increasing attention because of their immunogenicity and pivotal role in the interaction with host proteins. This review is summarizing and focusing on the molecular and functional analysis of pneumococcal serine proteases, thereby discussing their contribution to pathogenesis.

Keywords: *Streptococcus pneumoniae*, pneumococcal serine protease, respiratory infection, colonization, virulence factor, pathogenesis, structure

INTRODUCTION

Pneumococci (*S. pneumoniae*, the pneumococcus) are Gram-positive, facultative anaerobic bacteria, colonizing asymptotically the upper human respiratory tract (URT). Adherence to a mucosal surface of host tissues, predominantly indirectly *via* components of the extracellular matrix (ECM), is a prerequisite for establishing stable colonization (Bogaert et al., 2004). However, under certain circumstances, pneumococci disseminate from the nasopharynx to deeper tissues and the blood, leading to pneumonia and invasive diseases such as septicemia or meningitis (Song et al., 2013; Weiser et al., 2018; Bradshaw et al., 2020). Pneumococcal infections are a major cause of invasive diseases (invasive pneumococcal diseases, IPD) and death globally, especially in the most susceptible populations such as children, the elderly, and immunocompromised persons (O'Brien et al., 2009). The highest mortality is reported for children. Therefore, pneumococci are also called "The Forgotten Killer of Children," as mentioned by UNICEF and WHO (UNICEF, 2006).

Pneumococci are endowed with a plethora of virulence factors contributing to adhesion, colonization, immune evasion, and host cell damage (Ljungh et al., 1996; Kadioglu et al., 2008; Voss et al., 2012; Weiser et al., 2018; Jahn et al., 2020). The initial steps of pneumococcal pathogenesis require

an intimate, specific adherence to host structures and modulation of innate immune clearance mechanisms (Weiser et al., 2018). Pneumococcal adhesins recruit and bind to different human ECM and serum glycoproteins, including fibronectin, fibrinogen, vitronectin, thrombospondin-1, collagen, and plasmin(ogen) (Holmes et al., 2001; Bergmann et al., 2009; Voss et al., 2012; Fulde et al., 2013; Binsker et al., 2015). Striking examples are the multifunctional adhesins PspC (also referred to as CbpA), PavB, PsrP, and pilus type-1 (Rosenow et al., 1997; Pracht et al., 2005; Anderton et al., 2007; Kanwal et al., 2017). The close interaction of pneumococci with nasopharyngeal host cells is initially prevented by mucus and ciliary beating of the microvilli on the apical pole of mucosal epithelial cells (Clarke et al., 2011). However, pneumolysin inhibits ciliary beat frequency (Peter et al., 2017; Nishimoto et al., 2020), and enzymes like the pneumococcal neuraminidase NanA and hyaluronidase Hyl contribute to receptor exposure on the surface of host cells (Weiser et al., 2018). Importantly, pneumococci exhibit the ability to hijack host-derived serine protease proteolytic activities by binding plasmin(ogen), enabling ECM degradation, which facilitates colonization and dissemination of bacteria (Bergmann et al., 2005; Bergmann et al., 2013; Weiser et al., 2018). Proteases, especially serine proteases, are found in all living organisms. The intracellular and extracellular proteases are considered to be the most abundant and functional proteolytic enzymes (Page and Di Cera, 2008). These enzymes either hydrolyze peptide bonds within proteins or cleave them at their amino- or carboxyl-terminal ends (Patel, 2017). Bacterial proteases are involved in cell homeostasis, protein transport, and the structural integrity of the cell wall (Burchacka and Witkowska, 2016; Marquart, 2021). Many bacterial species express serine proteases that play a significant role in pathogenesis, such as *Bacteroides* spp., *Clostridium* spp., *Pseudomonas aeruginosa*, and *Streptococcus* spp. (Macfarlane et al., 1988; Thibodeaux et al., 2007; de Stoppelaar et al., 2013; Martínez-García et al., 2018).

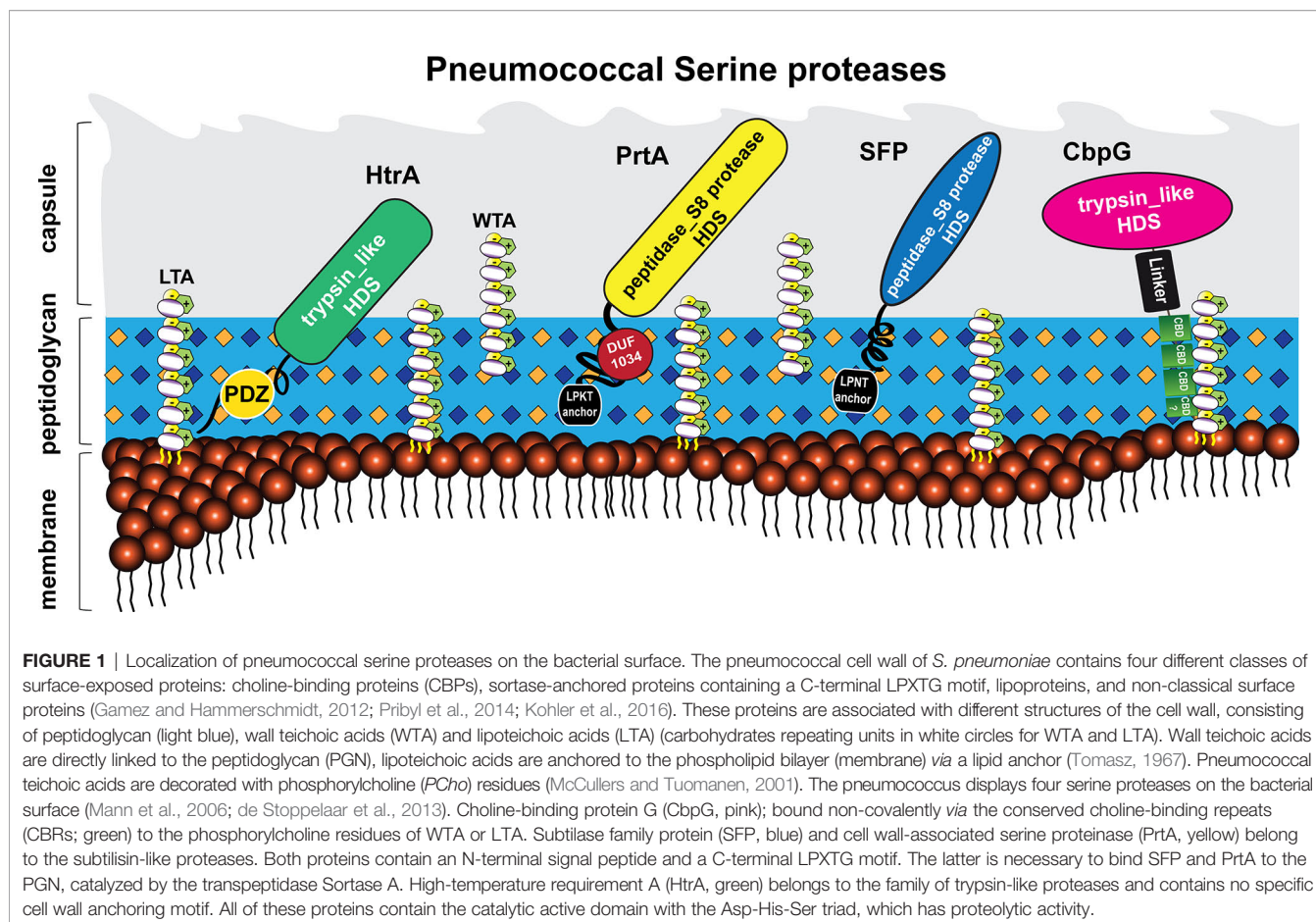
PNEUMOCOCCAL PROTEASES AND PEPTIDASES

S. pneumoniae expresses a wide range of proteases and peptidases, including cysteine proteases, zinc-metalloproteases, and serine proteases (Wani et al., 1996; Ishii et al., 2006; Marquart, 2021). More than 34 proteases in *S. pneumoniae* TIGR4 were recently reported and discussed (Kwon et al., 2011; Marquart, 2021). These proteases have different functions like involvement in the acquisition of nutrients, protein quality control, signal peptide cleavage for pre-protein secretion, and cleavage of host ECM proteins (Proctor and Manning, 1990; Marquart, 2021). It is reported that some proteases play a significant role in virulence (Collin and Olsen, 2003; Weiser et al., 2018; Kriia et al., 2020). For instance, the zinc-metalloprotease ZmpA (also known as IgA1 protease) interacts with the host immune system by cleaving IgA into inactive components, and the zinc-metalloprotease ZmpB is important for the modification of pneumococcal surface proteins (Kilian et al., 1980; Novak et al., 2000).

PNEUMOCOCCAL SURFACE PROTEINS AND EXTRACELLULAR SERINE PROTEASES

Besides in *S. pneumoniae*, serine proteases (or serine endopeptidases) have been found in many bacterial species such as *Haemophilus influenzae*, *Pseudomonas aeruginosa*, and other streptococcal species like *Streptococcus agalactiae* (group B streptococcus, GBS) (Male, 1979; Lyon and Caparon, 2004). Generally, the pneumococcus expresses different surface protein classes (Bergmann and Hammerschmidt, 2006; Pribyl et al., 2014; Kohler et al., 2016). Sortase-anchored proteins are covalently anchored to the peptidoglycan (PGN) *via* the sortase A, which cleaves a C-terminally located LPXTG motif (Bergmann and Hammerschmidt, 2006; Hammerschmidt, 2006; Nobbs et al., 2009; Löfling et al., 2011). In addition, the pneumococcal cell wall is decorated with up to 16 choline-binding proteins (CBPs), which are non-covalently bound to the phosphorylcholine of teichoic acids (Gosink et al., 2000). CBPs have been reviewed elsewhere (Maestro and Sanz, 2016). In this context, all pneumococcal serine proteases can be secreted and exposed on the pneumococcal cell surface, as shown in **Figure 1**. This extracellular localization enables a direct or indirect cleavage and inactivation of bound peptides, thereby leading to the degradation of specific substrates (Mann et al., 2006; Frolet et al., 2010). In fact, pneumococcal serine proteases are reported to play a crucial role in bacterial pathogenesis, such as adhesion, colonization, promotion of pneumococcal diseases, biofilm dispersal, and immune subversion of host cells (**Figure 4**) (Bergmann and Hammerschmidt, 2006; Moscoso et al., 2006; Mitchell and Mitchell, 2010; Voss et al., 2012; Pribyl et al., 2014; Chao et al., 2020; Ali et al., 2021).

The information on how pneumococcal serine proteases interfere with pathogenesis is crucial with respect to our understanding of pneumococci-host interactions. This review will focus on the four different pneumococcal serine proteases: HtrA, SFP, PrtA, and CbpG. These enzymes, encoded by genes of the core genome, are highly conserved and present among different pneumococcal serotypes (Bethe et al., 2001; Desa et al., 2008). The proteolytic activity is characterized by three amino acid (aa) residues, Ser-His-Asp, which form a so-called catalytic triad. The serine proteinase A (PrtA) and subtilase family protein (SFP) are cell wall-associated serine proteases of the S8 family of peptidases (Blum et al., 2021; Marquart, 2021). They are secreted and anchored covalently to the cell wall *via* the sortase A (Bethe et al., 2001; de Stoppelaar et al., 2013). PrtA contributes to host lung damage in a murine systemic infection model (de Stoppelaar et al., 2013; Mahdi et al., 2015), and in accordance, the gene encoding for PrtA is upregulated in the blood during acute pneumonia in mice (Bethe et al., 2001). In contrast, SFP may facilitate pneumococcal growth even after a lower infection dose in the lower respiratory tract (de Stoppelaar et al., 2013). The high-temperature requirement A (HtrA) serine protease is membrane-associated *via* an unknown mechanism and lacking a specific anchoring motif (Seol et al., 1991; Gasc et al., 1998; Fan et al., 2011), whereas CbpG is



non-covalently associated with the wall teichoic (WTA) and lipoteichoic acids (LTA) (Mann et al., 2006). Previous studies suggested that CbpG could be a multifunctional protease playing an important role in mucosal colonization and sepsis (Mann et al., 2006). HtrA is a heat shock protein and chaperone involved in protein quality control, cell division, colonization, and virulence (Sebert et al., 2002; Ibrahim et al., 2004a; Cassone et al., 2012).

HtrA and PrtA are upregulated in the heat-dispersed population among the genetic variants (Pettigrew et al., 2014). We recently reported that the deficiency in three out of four serine proteases of TIGR4 with only one functional gene/protein or the deficiency of all serine proteases dramatically reduces adherence and nasopharyngeal colonization (Ali et al., 2021). Interestingly, the pneumococcal serine proteases are highly conserved among all pneumococcal serotypes and immunogenic (Bethe et al., 2001; Li et al., 2016; Hsu et al., 2018; Kazemian et al., 2018). Hence, serine proteases-driven pathogenesis is opening the avenue for new targets to develop specific antimicrobials. In this regard, our review presents a comprehensive summary of our current knowledge of pneumococcal serine proteases in order to gain insight into their potential roles in pneumococcal virulence and pathogenesis at a molecular level.

BIOINFORMATICS ANALYSIS OF PNEUMOCOCCAL SERINE PROTEASES

To characterize and compare pneumococcal serine proteases on the molecular level, different database tools including PSORT db 3.0 (Yu et al., 2011), multiple sequence alignment Clustal Omega (<https://www.ebi.ac.uk/Tools/msa/clustalo/>) and pairwise sequence alignment (https://www.ebi.ac.uk/Tools/psa/emboss_water/) were used. All analyzed serine protease gene sequences (*prtA* (sp_0641), *htrA* (sp_2239), and *cbpG* (sp_0390)) of *S. pneumoniae* strain TIGR4 or D39 for *SFP* (sp_1753) were retrieved from the KEGG database (Kanehisa et al., 2006). Signal sequences were predicted using the software tool SignalP 4.0 (Emanuelsson et al., 2007; Petersen et al., 2011). Choline-binding proteins are characterized by their typical choline-binding modules (CBM) consisting of characteristic choline-binding repeats (CBRs) (Maestro and Sanz, 2016). Moreover, for the prediction of transmembrane helices, the *TMHMM Server 2.0* algorithm (Hidden Markov Model for transmembrane protein topology prediction) was applied (Krogh et al., 2001). Functional domains were predicted using Pfam (Punta et al., 2012).

The genomes of 10 clinically relevant *S. pneumoniae* strains were analyzed on DNA and protein levels with BlastN and BlastP,

respectively, for the homology analysis of pneumococcal serine proteases. The results revealed a maximum of four different serine proteases (NCBI, 2016). Comparisons on the protein level revealed high identities and similarities, indicating highly conserved sequences among the different pneumococcal strains (Table 1).

MOLECULAR CHARACTERIZATION AND STRUCTURE OF SERINE PROTEASE-LIKE/CHAPERONE HtrA

HtrA belongs to the peptidase SA clan in the S1C family and is also identical to DO subfamily protease (Pallen and Wren, 1997). More than 180 members of these proteases, including HtrA, display trypsin-like protease characteristics (Pallen and Wren, 1997; NCBI, 2016). The family of these proteases combines a catalytic domain with at least one or more C-terminal PDZ domains (Lipinska et al., 1990), which is highly conserved in both pathogenic and nonpathogenic bacteria (Seol et al., 1991; Spiess et al., 1999; Backert et al., 2018). However, the first described HtrA protease in *E. coli* is known as DegP or DO protease and localized in the periplasmic space (Lipinska et al., 1990).

Bacterial HtrA is a heat-shock-induced serine protease that displays a multifunctional role like protein quality control and bacterial survival under different stress conditions such as oxidative and heat stress (Sebert et al., 2002; Singh et al., 2018). For instance, HtrA protease in *Lactococcus* is considered as a housekeeping protease (Poquet et al., 2000), while in other bacteria, HtrA prevents the cell from the cytotoxicity of misfolded proteins by refolding or degrading them (Clausen et al., 2002; Zarzecka et al., 2019). In *E. coli*, unlike other quality control proteins such as

ClpXP, ClpAP, and HslUV, which need ATP for their chaperone function, HtrA is functional without ATP as an additional energy source (Clausen et al., 2011; Malet et al., 2012). More importantly, the function of HtrA proteins can be switched from chaperone to protease and the activity depends on the temperature (Spiess et al., 1999). The protease effect is in particular apparent at high temperatures ranging from 38–42°C, whereas the chaperon function is more pronounced at lower temperatures ranging from 30–37°C (Spiess et al., 1999).

In *S. pneumoniae*, HtrA is one of the best-studied and characterized serine proteases. High protein sequence identity (up to 100%) of the HtrA protein was detected in six different pneumococcal strains (Table 1) such as D39, Hungary 19A, serotype 19F_EF3030 and R6, indicating that HtrA is highly conserved. Therefore, it could be a desirable drug target to prevent pneumococcal diseases (Wessler et al., 2017; Xue et al., 2021). In pneumococci, HtrA is a surface-exposed serine protease, easily accessible for potential inhibitory substances or anti-infectives. HtrA is immunogenic and antibodies against HtrA are protective against invasive pneumococcal diseases (Li et al., 2016).

The molecular analysis of different HtrA serine proteases of other pathogenic bacteria *via* multiple sequence alignment (MSA) revealed a sequence similarity, especially in the functional protease and PDZ domains, as reviewed more extensively elsewhere (Backert et al., 2018; Boehm et al., 2018; Singh et al., 2018). They are widely distributed in many bacterial species such as *Escherichia coli*, *Legionella fallonii*, *Thermotoga maritima*, and *Mycobacterium tuberculosis* (Kim et al., 2003; Bai et al., 2011; Malet et al., 2012; Cortes et al., 2013; Chang, 2016; Singh et al., 2018).

Furthermore, we also analyzed the amino acid sequence of pneumococcal HtrA orthologs in other streptococci (Table 2). High sequence homologies of HtrA are present in *S. pyogenes* (group A streptococci), *S. agalactiae* (group B streptococci),

TABLE 1 | Protein sequence homology [%] of serine proteases among different selected pneumococcal strains based on protein sequences from *S. pneumoniae* TIGR4 (Tettelin et al., 2001), and D39 for SFP.

<i>S. p.</i> Strain (serotype)		gene no.	CbpG	Gene no.	HtrA	Gene no.	PrtA	gene no.	SFP
TIGR4 (4)	%ID	<i>sp_0390</i>	100.0	<i>sp_2239</i>	100.0	<i>sp_0641</i>	100.0	<i>sp_1954</i>	100.0
	%SIM		100.0		100.0		100.0		100.0
D39 (2)	%ID	<i>spd_0356</i>	99.0	<i>spd_2068</i>	100.0	<i>spd_0558</i>	95.8	<i>spd_1753</i>	100.0
	%SIM		99.5		100.0		97.8		100.0
EF3030 (19F)	%ID	<i>EF3030_01920</i>	99.6	<i>EF3030_11105</i>	99.7	<i>EF3030_03025</i>	97.5	—	—
	%SIM		99.6		100		98.7		
ST556 (19F)	%ID	<i>snd:MY_0470</i>	87.0	<i>snd:MY_2162</i>	100.0	<i>snd:MY_0688</i>	95.9	—	—
	%SIM		95.7		100.0		97.9		
ST81 (23F)	%ID	<i>spn23F03640</i>	97.8	<i>spn23F22720</i>	99.7	<i>spn23F05790</i>	97.4	<i>spn23F9760</i>	100.0
	%SIM		98.5		100.0		98.8		100.0
JJA (14)	%ID	<i>spj_0378</i>	99.3	<i>spj2269</i>	99.7	<i>spj_0592</i>	97.4	<i>spj_1948</i>	100.0
	%SIM		100.0		100.0		98.6		100.0
R6 (2)	%ID	<i>spr0349</i>	99.0	<i>spr2045</i>	100.00	<i>spr0561</i>	95.8	<i>spr1771</i>	100.0
	%SIM		99.5		100.00		97.8		100.0
G54 (19F)	%ID	<i>spg_0356</i>	100.0	<i>spg_2188</i>	98.4	<i>spg_0584</i>	96.1	—	—
	%SIM		100.0		99.0		97.8		
Hungary 19A-6 (19A)	%ID	<i>sph_0499</i>	96.8	<i>sph_2438</i>	99.5	<i>sph_0733</i>	96.2	—	—
	%SIM		96.8		100.0		98.1		
R6_CIB17 (2)	%ID	—	—	<i>E5Q10_10910</i>	100.0	—	—	<i>E5Q10_09305</i>	100.0
	%SIM		—		100.0				100.0

Analysis of the proteins were performed with tool databases BlastP (NCBI, 2016), and EMBOSS (Rice et al., 2000). Protein sequences derived from TIGR4 strain were used as reference ID, Identity; SIM, Similarity. The meaning of the bold values are % ID, Identity percentage; % SIM, Similarity percentage.

TABLE 2 | Comparison and distribution of pneumococcal serine proteases in other related bacterial species with amino acid sequence similarity and role in pathogenicity, updated from (Ali et al., 2021).

Protein (locus tag)	Protein accession no.	Bacterial species	Similarity [%]	Associated disease	Pathogenic function	Host-Targets	References
PrtA, cell wall-associated serine protease	AAK74791.1	<i>Streptococcus pneumoniae</i>	100%	CAP1, sepsis, meningitis	killing by apolactoferrin colonization adherence, pneumonia	cleaves human apolactoferrin, interact with collagen IV and plasminogen, cleavage of leader peptides from lantibiotics, possible adhesin	(Bethe et al., 2001; Mirza et al., 2011; Weiser et al., 2018; Ali et al., 2021)
PrtP (LP151), proteinase	M83946	<i>Lactobacillus paracasei</i>	35.8%	dental caries, rheumatic vascular disease, septicemia, and infective endocarditis	degrades secreted, cell-associated, and tissue-distributed and other proinflammatory chemokines	degrade proinflammatory chemokines	(von Schillde et al., 2012; Hörmannspurger et al., 2013)
PrtP (SK11), Proteinase, PIII-type	J04962, M26310	<i>Lactococcus lactis subsp. cremoris</i>	35.4%	Lactic acid bacteria (LAB), endocarditis chronic gastritis, central nervous infection	involved to adhesion and invasion, transit in the intestinal mucosa	adhesive properties, degrade alpha (S1)- and beta-caseins	(Nikolić et al., 2009; Inoue et al., 2014; Radziwill-Bienkowska et al., 2017)
PrtB, proteinase precursor	L48487	<i>Lactobacillus delbrueckii bulgaricus</i> ,	37.2%	LAB	antibacterial activity, probiotic function,	cleaves beta-casein	(Abedi et al., 2013)
PrtH, cell envelope associated proteinase	AF133727	<i>Lactobacillus helveticus</i>	36.5%	LAB	antibacterial activity,	degrades alpha and beta-caseins	(Kunji et al., 1996)
PrtS, cell envelope proteinase	AAG09771	<i>Streptococcus thermophilus</i>	35.3%	LAB	–	essential for growth	(Courtin et al., 2002)
ScpA, C5a peptidase	P15926	<i>Streptococcus pyogenes</i>	38.1%	necrotizing fasciitis, pharyngitis	facilitates the local infection	cleaves the human serum chemotaxis C5a	(Chmouryguina et al., 1996)
ScpB, C5a peptidase	U56908	<i>Streptococcus agalactiae</i>	37.5%	bacteremia, pneumonia	virulence factor, promote Fn-independent GAS invasion of human epithelial cells	inactivates C5a	(Bohnsack et al., 2000)
CbpG, choline-binding protein G	AAK74556.1	<i>Streptococcus pneumoniae</i>	100%	CAP, sepsis, meningitis	adherence, colonization virulence factor,	cell-attached form promotes adherence, extracellular form degrades fibronectin, important for mucosal and invasive disease	(Gosink et al., 2000; Mann et al., 2006; Weiser et al., 2018; Ali et al., 2021)
GEJ60330 serine proteinase	GEJ60330.1	<i>Enterococcus faecalis</i>	56%	colonizing the gastrointestinal tract and oral cavity of animals and humans	endophthalmitis, peritonitis, endocarditis, and orthopaedic	–	(Thurlow et al., 2010)
serine protease	WP_010922847.1	<i>Staphylococcus aureus</i>	40.4%	CAP, bacteremia, endocarditis, osteomyelitis	involved in the evasion of host immunity	cleaves the ECM components	(Pietrocola et al., 2017)
serine protease	NP_460444.1	<i>Salmonella enterica subsp.</i>	39.2%	foodborne diseases (Salmonellosis)	epithelial cell invasion	cleavage of E-cadherin	(Jajere, 2019)
Glu, endopeptidases	1P3C	<i>Bacillus intermedius</i>	42.2%	–	–	cleaves the peptide bond on the carboxyl end of glutamic acid	(Meijers et al., 2004)

(Continued)

TABLE 2 | Continued

Protein (locus tag)	Protein accession no.	Bacterial species	Similarity [%]	Associated disease	Pathogenic function	Host-Targets	References
SFP, subtilisin-like serine protease	ABC75782.1	<i>Streptococcus pneumoniae</i>	100%	CAP, sepsis, meningitis	facilitates bacterial growth, adherence, colonization	cleavage of leader peptides from lantibiotics	(de Stoppelaar et al., 2013; Ali et al., 2021; Marquart, 2021)
NisP, leader peptide-processing serine protease	4MZD_A	<i>Lactococcus Lactis</i>	56.6%	endocarditis infection	antibacterial lantibiotic	cleave leader peptides from lantibiotics	(Xu et al., 2014; Montalbán-López et al., 2018)
CspA, cell surface serine endopeptidase	CNG97209.1	<i>Streptococcus agalactiae</i>	38.5%	CAP, sepsis, meningitis	virulence factor, resistance to opsonophagocytosis	cleaves human fibronectin inactivates chemokines	(Harris et al., 2003; Bryan and Shelper, 2009)
HtrA (DegP) serine protease/chaperone	AAK76286.1	<i>Streptococcus pneumoniae</i>	100%	CAP, sepsis, meningitis	chaperone, heat-shock protein, protease, virulence factor, competence pathways, growth advantage in influenza A virus co-infection, adherence, colonization	quality control of secreted proteins	(Sebert et al., 2002; Ibrahim et al., 2004a; Ibrahim et al., 2004b; Cassone et al., 2012; de Stoppelaar et al., 2013; Kochan and Dawid, 2013; Sender et al., 2020; Ali et al., 2021)
	BAQ53883.1	<i>Streptococcus pyogenes</i>	71.7%	purulent diseases of the pharynx and skin	processing of extracellular virulence factors and hemolytic activity	cleavage of complement factor C5a	(Wexler et al., 1985; Lyon and Caparon, 2004)
	Q8DWP1	<i>S. agalactiae</i>	73.6%	bacteremia, pneumonia	–	–	
	VEI61035.1	<i>Streptococcus mutans</i>	72.8%	dental carries	colonization	biofilm formation	(Biswas and Biswas, 2005)
	WP_061099826.1	<i>Campylobacter jejuni</i>	52.6%	Campylobacteriosis, Guillain Barré syndrome	bacterial adhesion, transmigration, and invasion	cleavage of E-cadherin, apoptosis, and immune responses	(Zarzecka et al., 2020)
	AHC56659.1	<i>Helicobacter pylori</i>	54.5%	gastritis, ulcers symptoms	bacterial transmigration, activation of type IV secretion	cleavage of occludin, claudin-8, E-cadherin, and fibronectin	(Hoy et al., 2010; Schmidt et al., 2016; Tegtmeyer et al., 2017)
	5ZVJ_A	<i>Mycobacterium tuberculosis</i>	52.7%	tuberculosis	cell wall hydrolases	degrades a putative cell wall muramidase (Ami3)	(Wu et al., 2019)

Bold values means "Percentage identity".

S. mitis, and *S. mutans*. HtrA of *S. pyogenes* plays a significant role in cysteine protease streptococcal pyrogenic exotoxin B (SpeB) maturation and complement factor C5a cleavage (Lyon and Caparon, 2004; Cole et al., 2007). The deletion of HtrA in *S. mutans* enhanced the surface expression of several extracellular proteins such as glucan-binding protein GbpB and altered the biofilm formation (Biswas and Biswas, 2005).

Besides the impact of HtrA on pneumococcal virulence, HtrA was shown to be a multifunctional protein involved in pneumococcal growth at higher temperatures, tolerance to oxidative stress, genetic transformation, regulation of bacteriocin production, and cell division (Dawid et al., 2009; Fan et al., 2010; Tsui et al., 2011). The pneumococcal HtrA protein (**Figure 2A**) contains an amino-terminal signal peptide (31 aa), cleaved by signal peptidase I for secretion. The terminal signal peptide is

followed by a single transmembrane helix domain (aa 12-34). Thus, HtrA is found on the surface and/or secreted from *S. pneumoniae* as predicted by the presence of a putative amino-terminal signal peptide (de Stoppelaar et al., 2013; Ali et al., 2021). Additionally, HtrA contains two highly conserved unique domains, a serine protease domain and a PSD-95/Dlg/ZO-1 (PDZ) domain (de Stoppelaar et al., 2013). The trypsin-like serine protease domain has the typical triad His¹¹²-Asp¹⁵²-Ser²³⁴ (HDS) in the catalytic center, which was identified previously (de Stoppelaar et al., 2013) using Interproscan IPR009003 and IPR001940 (Zdobnov and Apweiler, 2001). Finally, the PDZ domain (abbreviation combining letters of the first three proteins discovered to share this domain, postsynaptic density protein, Drosophila discs large tumor suppressor, and zonula occludens-1) is located at the C-terminal end. HtrA in other bacterial species

Modular organization of pneumococcal serine proteases




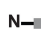


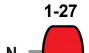






Serine proteases	N-terminal SP	Catalytic domain	Other domain architecture	TM helix	Length (amino acids)
A HtrA_sp_2239	1-32 	chymotrypsin-like serine protease 96-277 	289-375 	12-34	42 kDa 393 a.a
B CbpG_sp_0390	? 	trypsin-like serine protease 14-197 	198-206 Linker 206-207 207-265 	0	32 kDa 285 a.a
C PrtA_sp_0641	1-27 	peptidase_S8 protease like 223-764 	795-934  2099-2140 	2112-2134	240 kDa 2140 a.a
D SFP_spd_1753	1-22 	peptidase serine protease 167-461 	543-550 	552-574	64.9 kDa 579 a.a

FIGURE 2 | Schematic presentation of the modular organization in pneumococcal serine proteases. **(A)** HtrA (AAK76286.1), the signal peptide sequences (aa 1-32) are illustrated in red. The serine protease catalytic domain is shown in light green, PDZ domain is labeled in yellow. **(B)** CbpG (AAK74556.1), most likely has no signal peptide. The trypsin-like serine protease catalytic domain is shown in pink, the repeats of the choline-binding domains (CBDs) are marked in green, connected by short linker region aa 198-206. The C-terminal region aa 267-285 is probably also involved in binding to choline residues of teichoic acids. **(C)** PrtA (AAK74791.1), the signal peptide sequence aa 1-27 is depicted in red, the serine protease catalytic domain is illustrated in yellow, the DUF 1034 domain is shown in red. The C-terminal anchoring motif is labeled in yellow. **(D)** SFP (ABJ54257.1), the signal peptide sequence (1-22 aa) is shown in red, the serine protease catalytic domain is marked in blue. The length of each serine protease is given as the number of amino acids (aa). HDS, histidine, aspartate and serine; TM, transmembrane domain; SP, signal peptide sequences.

contains one or more PDZ domain(s) (Fan et al., 2011; Backert et al., 2018; Singh et al., 2018). In some situations, such as protein-protein interactions, the HtrA-PDZ domain acts as a protein folding stress sensor and controls the pyrolytic activity (Murwantoko et al., 2004; Wilken et al., 2004; Hasselblatt et al., 2007). Thus, the PDZ domains are responsible for recognizing and/or binding substrate proteins (Marquart, 2021). Fan et al. solved the pneumococcal HtrA-PDZ structure (Fan et al., 2011), which contains three α -helices and five β -strands (amino acid residues 262-386). Moreover, a comparison of the amino acid sequences of HtrA-PDZ domains in different bacterial species showed that the pneumococcal PDZ domain, which is most likely involved in the ligand recognition, has only a moderate sequence similarity and conserved secondary structure (Bohnsack et al., 2000).

The importance of HtrA in *S. pneumoniae* has been addressed in many studies. For instance, HtrA was shown to play an important role in pneumococcal competence, which is still challenging to understand due to the conflicting results. One study has shown that the HtrA protease is important for competence because the pneumococcal transformation efficiency was highly reduced in the *htrA*-mutant (Ibrahim et al., 2004b). In another study, the proteolytic activity analysis, which was performed with purified recombinant pneumococcal HtrA, revealed that HtrA cleaves the pneumococcal competence-stimulating peptide (CSP) *in vitro* (Cassone et al., 2012). Since

CSP has a significant effect on pneumococcal transformation (Pestova et al., 1996), this fact suggests that HtrA has a considerable role in pneumococcal transformation efficiency and is needed for competence. In this study it has also been shown that the deletion of *htrA* or catalytic residues did not affect natural DNA competence (Cassone et al., 2012). However, the mutation strategies and transformation settings used in these two studies were different. It can be assumed that HtrA is necessary for the transformation process after the competence machinery is turned on by CSP. If the competence genes are expressed, CSP is not needed anymore and can be degraded by HtrA. Functional CSP seems to inhibit the transformation efficiency.

The specificity of HtrA toward CSP peptide degradation is based on a phenylalanine (nonpolar) residue. The addition of denatured bovine serum albumin (BSA) inhibits the CSP peptide from being cleaved by HtrA (Cassone et al., 2012). *S. pneumoniae* expresses several proteins contributing to competence, which are highly decreased during competence followed by stabilization with the exception of ComEA and ComEC. These membrane proteins are essential for pneumococcal transformation and responsible for DNA uptake (Liu et al., 2019). While *htrA*-mutants in the previous study have shown a lower transformation efficiency (Ibrahim et al., 2004b), ComEA or ComEC degradation was not evident. This suggests that HtrA plausibly degrades these proteins at later stages of competence (Liu et al., 2019). Last but not least, the regulation of

HtrA seems to be dependent on bacterial culture conditions. It was shown that HtrA inhibits competence in a complex medium but not in a chemically defined medium (Petit et al., 2001). Overall, these findings show that HtrA acts as a competence regulator at the protein level and that environmental factors influence its regulation. Aside from the involvement of HtrA in competence, HtrA has been shown to be upregulated and controlled by the two-component regulatory system CiaRH (Sebert et al., 2002). A recent study showed that HtrA regulated by CiaRH is responsible for penicillin-binding protein 2x (PBP2x) degradation (Peters et al., 2021). In addition, HtrA is important for nasopharyngeal colonization and pneumococcal virulence (Sebert et al., 2002; de Stoppelaar et al., 2013; Ali et al., 2021).

MOLECULAR ANALYSIS OF THE SERINE PROTEASE CbpG

The human pathogen *S. pneumoniae* expresses a special class of surface-proteins known as choline-binding proteins (CBPs). A common feature of this family of proteins is that they have a modular organization and are composed of at least two domains: a functional module (FM) and a choline-binding module (CBM). CBPs are found in pneumococci or closely related species (García et al., 1988; Sanz et al., 1992; Albrich et al., 2004; Blasi et al., 2012). The repetitive sequences of the CBM associate CBPs in a non-covalent manner to the cell wall by their interaction with phosphorylcholine residues of PGN-anchored WTA and membrane-anchored LTA (Pérez-Dorado et al., 2010; Maestro and Sanz, 2016). The CBM consists of three to eighteen repetitive sequences (CBRs) of about 20 amino acids (Pérez-Dorado et al., 2012; Galán-Bartual et al., 2015; Hilleringmann et al., 2015). Apart from LytB and LytC, the CBM is located in the C-terminal part of the protein, whereas the FM is located in the N-terminal region (Pérez-Dorado et al., 2010). The number of CBPs in *S. pneumoniae* ranges from 13 to 16 proteins and is strain-dependent (Gosink et al., 2000; Maestro and Sanz, 2016). Notably, CBPs play an essential role in the integrity of the cell wall, colonization processes, and interaction with host cells (Maestro and Sanz, 2016). Pneumococcal CbpG is a member of the CBP family, which also plays a significant role in pneumococcal mucosal colonization and during sepsis (García-Bustos and Tomasz, 1987; Gosink et al., 2000). CbpG belongs to the peptidase S1, PA clan superfamily of peptidases, and is a trypsin-like serine protease (Kanz et al., 2005). The protein sequence indicates that this protein possesses a chymotrypsin-like fold and double β -barrel structure with a carboxyl-terminal choline-binding domain (NCBI, 2016; Yang et al., 2020). CbpG is considered to be a multifunctional surface-exposed serine protease with both proteolytic and adhesive functions (Gosink et al., 2000; Mann et al., 2006; Kazemian et al., 2018). These various functions of CbpG are necessary for the full virulence potential of *S. pneumoniae*. Such multifunctional proteinases can be found in many pathogenic bacterial species, and the C5a peptidase of group B streptococci (Beckmann et al., 2002; Cheng et al., 2002) and the well-characterized Pla surface protease from *Yersinia pestis* (Kukkonen and Korhonen, 2004) are striking examples.

Depending on the pneumococcal strain and serotype, there are at least two variants of CbpG produced by pneumococci. The truncated variant without CBM is shortened due to a premature stop codon after the N-terminal catalytic functional module and found in D39 (serotype 2), Hungary19A-6 (19A), R6 (2) and ST556 (19F) (Figure S1). This variant is secreted and then released into the environment. In contrast, the full-length CbpG containing a CBM is cell wall-associated (Mann et al., 2006). The modular organization of CbpG (Figure 2B) shows that the catalytic residues are present independent of expressing a full-length protein, including a CBM or a truncated version without a functional CBM. In both configurations, the proteins exhibit proteolytic activity as confirmed earlier (Mann et al., 2006). Our genome re-analysis showed a high sequence identity and similarity of CbpG among various pneumococcal serotypes indicating CbpG is highly conserved and abundant among the different pneumococcal strains (Table 1). The molecular analysis of full-length CbpG (*sp_0390*) in TIGR4 (Tettelin et al., 2001) comprises 285 aa with a molecular weight of 32 kDa, as shown in Figure 2B. According to our SignalP 4.0 analysis, a leader peptide (secretion signal peptide) is not present in all analyzed serotypes except for serotype 19F strain ST556 (Figure S1). Therefore, it is still unknown whether and how CbpG is translocated from the cytoplasm to the bacterial cell surface. The functional domain is the trypsin-like domain with 184 aa spanning from aa 14-197, containing the catalytic triad His³⁴-Asp⁸⁷-Ser¹⁵⁹ as predicted by the 3D structure analysis (Figure 3). Previous sequence analysis demonstrated 47% similarity of this domain to the S1 family of multifunctional surface-associated serine proteases (Mann et al., 2006). Furthermore, this domain is linked to the CBM by a short linker region (^{aa}Lys-Pro-Phe-Ile^{aa}) that provides flexibility to the protein and may provide stability to the catalytic domain. This catalytic functional module exhibits sequence similarities to trypsin-like serine proteases present in all CbpG variants (Gosink et al., 2000; Mann et al., 2006).

Moreover, it has been mentioned that the CBM, which is e.g., in strain TIGR4, exhibits only three choline-binding repeats (CBRs), which are located at position aa 207-265. This represents the shortest identified CBM among all choline-binding proteins. It has been proposed that at least four repeats are needed to attach the protein non-covalently to the teichoic acids of the cell wall (Yother and White, 1994). Therefore, it is still unknown if CbpG can bind to the bacterial cell surface when only three choline-binding repeats are present. In deletion studies of the CBM from the pneumococcal LytA amidase (Mellroth et al., 2014), it has been hypothesized that a higher number of CBRs leads to a higher affinity for teichoic acids of *S. pneumoniae* (Maestro and Sanz, 2016).

The CbpG amino acid sequence model was analyzed (Ali et al., 2021) and suggests that a fourth CBR at position aa 267-285 might attach CbpG to teichoic acids and allows the protein to be surface-associated. This repeat includes the aromatic residues YW and fulfills the number of aromatic residues involved in choline-binding (Waterhouse et al., 2009). The protein sequence homology of the CbpG to orthologues of other bacterial species was analyzed as well. Significant homologies of CbpG (40-56%) were found to serine proteinases of different bacterial species such as *Enterococcus faecalis*, *Staphylococcus aureus*, and *Salmonella enterica* (Table 2).

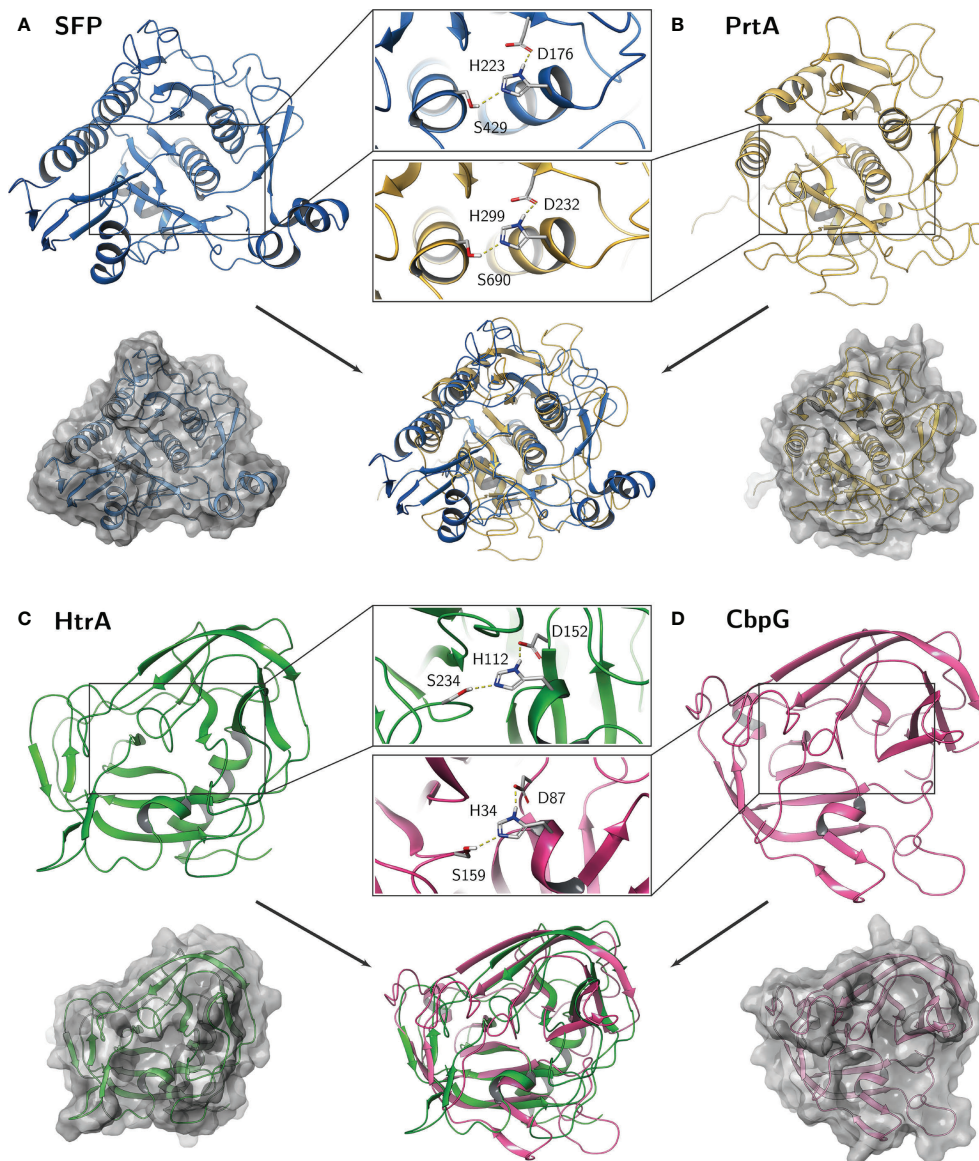


FIGURE 3 | Predicted homology models of the pneumococcal serine proteases. Catalytic residues aspartate (D), histidine (H), and serine (S) are shown as sticks in detail for **(A)** SFP, **(B)** PrtA, **(C)** HtrA, and **(D)** CbpG. The calculations were performed within the Multiple Sequence Viewer/Editor application in Maestro (Schrödinger, 2020-4).

CELL WALL-ASSOCIATED SERINE PROTEASE PrtA

The protease PrtA belongs to the family of subtilisin-like proteases (also known as subtilases), which are part of S8 family peptidases (Bethe et al., 2001; Marquart, 2021). Pneumococcal PrtA is related to serine proteases present in lactococci, cleaving the amino-terminal leader sequences from lantibiotics (Blum et al., 2021). Lantibiotics are bacteriocin peptides that are bactericidal to outcompete other bacteria (Marquart, 2021). Interestingly, both, streptococci and lactococci exhibit a wide range of endopeptidase activity (Siezen, 1999).

In pneumococci, PrtA is a major surface serine protease involved in pneumococcal virulence (Zysk et al., 2000; Bethe et al., 2001). The role of PrtA in colonization and subsequent host invasion seems to be strain-specific (Mahdi et al., 2015). The first report on pneumococcal PrtA protease highlighted the immunogenicity because of its identification using convalescent-phase serum (Zysk et al., 2000). Interestingly, a previous study showed that PrtA is a highly conserved virulence factor in pneumococci and is found in almost all strains (Bethe et al., 2001). Both *in silico* analysis and flow cytometry confirmed that PrtA is surface localized (Wizemann et al., 2001).

The first molecular characterization of PrtA was done in 2001 (Bethe et al., 2001). Bethe and co-workers (Bethe et al., 2001) showed that pneumococci produce PrtA with different molecular weights. One variant produced by pneumococci has a molecular weight of 240 kDa, whereas a truncated form has only a molecular weight of 215 kDa, which cannot be explained by signal peptide cleavage only. The same observation was also found in the related proteases PrtP proteins of *Lactobacillus paracasei* and *Lactococcus lactis* (Vos et al., 1989; Holck and Naes, 1992). The full-length PrtA (strain TIGR4 *sp.* 0641) form has a molecular weight of 240 kDa (2140 aa). The calculated mature form of PrtA has a molecular weight of 234 kDa after cleavage of the leader peptide and integration into peptidoglycan by sortase A. Furthermore, PrtA contains a typical sortase A recognition LPKTG motif spanning aa 2099–2140 followed by a hydrophobic region at the carboxy-terminus. The sortase A catalyzes covalent anchoring to the bacterial PGN (de Stoppelaar et al., 2013; Ali et al., 2021). PrtA consists of two domains, the active peptidase-S8 domain, which contains the typical catalytic triad (Asp²³²-His²⁹⁹-Ser⁶⁹⁰), spanning the region between aa 223–764 (Bethe et al., 2001; Ali et al., 2021). The second domain is a DUF-1034 (domain of unknown function), which consists of 140 amino acids and is localized between aa residues 795–934. The modular organization of PrtA is illustrated in (Figure 2C).

Of interest, the multisequence alignment of PrtA catalytic triad residues (Asp²³²-His²⁹⁹-Ser⁶⁹⁰) were highly homologous to other related bacterial species of subtilisin-like serine proteases. These catalytic triads showed a high degree of similarity and identity to the cell wall-associated proteases of *Streptococci*, *Lactococci*, and *lactobacilli* (Bethe et al., 2001; Bonifait et al., 2010).

Finally, the complete protein sequence homology to orthologues of other bacterial species was analyzed. As indicated in Table 2, PrtA shares significant similarities with other streptococcal subtilisin-like proteases. Interestingly, PrtA seems to be highly immunogenic in humans and mice; two segments of PrtA, the amino-terminal and carboxy-terminal thirds were found to be protective (Wizemann et al., 2001).

SUBTILASE FAMILY PROTEIN SFP

The SFP serine protease (known as serine peptidase) is another enzyme able to cleave leader peptides from lantibiotics (Marquart, 2021). Similar to the PrtA protease, SFP belongs to subtilisin-like/ or S8-family serine proteases. In *S. pneumoniae* D39 strain, SFP was identified as epidermin leader peptide processing serine protease EpiP (de Stoppelaar et al., 2013; Marquart, 2021).

The comparative analyses of *sfp* genes in *S. pneumoniae* strain D39 *spd_1753* (1740 nt, 579 aa), and TIGR4 *sp.* 1954 (1404 nt, 467 aa) was performed using the SYBIL database (Riley et al., 2011). The MSA analyses showed a shorter version of the *sfp* gene in TIGR4 compared to *sfp* of D39 and other strains (Figure S2). The truncation of *sfp* in strain TIGR4 is based on the deletion of one base (A) at position 1381. Instead of 8 A bases in a row, only seven are present in strain TIGR4, which was confirmed by DNA sequencing of the TIGR4 *sfp* gene. The generated frameshift leads to the premature stop at position 1404. Hence, this

truncated SFP of TIGR4 cannot be covalently anchored to the peptidoglycan. Instead, TIGR4 SFP is secreted into the extracellular environment. However, these data have to be experimentally verified.

Based on the molecular characterization of SFP (de Stoppelaar et al., 2013; Ali et al., 2021), its secretion and protease activity has been predicted. The full-length SFP has a molecular weight of 64.9 kDa and exhibits an N-terminal signal peptide (aa 1–22) and a C-terminal LPNTG anchoring motif which is thought to be functional as a target site for the sortase A and anchoring the protein to PGN (Marraffini et al., 2006). In addition, the peptidase domain spanning the aa residues 167–461 contains the catalytic triad (Asp¹⁷⁶-His²²³-Ser⁴²⁹) (Figure 2D and Figure 3A).

Furthermore, the genomic organization of the SFP locus in *S. pneumoniae* 19F and TIGR4/D39 strain is different. The *sfp* gene and six upstream and three downstream genes present in strain TIGR4 are not present in *S. pneumoniae* strain 19F EF3030 (Ali et al., 2021). Even more, the subtilisin-like protein SFP was not present in all the analyzed strains as observed by our *in silico* analysis (Table 1). Therefore, pneumococci have at least three serine proteases in the 19F_EF3030 strain (Ali et al., 2021), but probably four in most strains, such as D39 (serotype 2), TIGR4 (serotype 4), ST81 (serotype 23F), JJA (serotype 14), and R6 (serotype 2). However, the role of SFP in pneumococcal virulence is still unknown.

COMPUTER-ASSISTED 3D STRUCTURAL MODELS OF THE CATALYTIC DOMAIN OF SERINE PROTEASES

The HtrA of *E. coli* is well characterized and studied in detail for its functional role as chaperone and protease. The crystal structures of HtrA from *E. coli*, *Campylobacter jejuni* or *Thermotoga maritima* showed that the active protease at elevated temperature is composed at least as a trimer by hydrophobic interaction of the subunits (Kim et al., 2003; Zarzecka et al., 2020). By using computer-assisted analysis, we compared the catalytic center of all four serine proteases from pneumococci. The calculations were performed within the Multiple Sequence Viewer/Editor application in Maestro (Schrödinger, 2020–4) using an energy-based approach. Templates were obtained by BLAST search in the PDB database (SFP: 4MZD; PrtA: 5FAX; HtrA: 5ZVJ; CbpG: 1P3C) (Figures S3–6). As mentioned, all serine proteases have in common the typical Ser-His-Asp triad, where the histidine is polarized through hydrogen bonding by aspartate, resulting in a polarization of serine and increased nucleophilicity of the hydroxyl oxygen atom. The highly conserved arrangement and distance between these three amino acids are crucial to form the catalytic center for the cleavage of peptide bonds.

On the one hand, the comparison revealed a quite similar catalytic domain structure between HtrA and CbpG with the common double β^2 -barrel core motif adjacent to the catalytic triad. The Asp and Ser residues are localized on flexible loop structures, whereas the His residue is localized on a small helical fold (Figure 3). On the other hand, a similar subtilisin-like catalytic

domain of SFP and PrtA was observed by this modeling. Here, the overall fold consists of a dominant 7-stranded parallel β -sheet, with the catalytic Asp on the first strand (S1) and five α -helices containing Ser and His. While the core catalytic motif seems quite similar, a protease-associated domain is found within the amino acid sequence of the PrtA catalytic domain, which may mediate protein-protein interactions or substrate specificity. Due to low sequence identity, it was omitted for the homology modeling and should be further explored. Because this is only a simplified view of the active proteolytic centers of these serine proteases, there are ongoing efforts to purify the recombinant serine proteases for X-ray crystallography.

THE IMPACT OF PNEUMOCOCCAL SERINE PROTEASES ON PNEUMOCOCCAL PATHOGENESIS

S. pneumoniae are versatile pathogens that modulate the immune response and circumvent host immune defense mechanisms. The enzymatic protease activity during pneumococcal infections can contribute to the destruction of the epithelial barrier or degradation of ECM components (Ljungh et al., 1996). Next, pneumococci try to establish a more severe infection by either transmigration or/and disseminating to lungs, blood, middle ear, or the central nervous system.

Pneumococcal express various proteases and peptidases, which are involved in colonization, pneumonia, and septicemia (Marquart, 2021). In particular, pneumococcal serine proteases seem to play a role in invasive processes. In terms of specificity, substrates for serine protease are mainly the ECM component proteins, fibrin clots, cell membranes, and host immunomodulatory factors such as chemokines and cytokines (Frolet et al., 2010; Kim et al., 2010; Ruiz-Perez and Nataro, 2014).

Pneumococcal serine proteases might be involved in cleavage of adherence junctions or gap junction proteins to facilitate the pneumococcal paracellular route, which results in crossing of the epithelial barrier dissemination in the bloodstream. Recently, the impact of serine proteases on adherence, colonization, and subsequent virulence has been shown in various studies (Table 2).

The first description of various pneumococcal serine proteases along with their susceptibilities to different inhibitors was in 1991 (Courtney, 1991). Already at that time, their important role in pneumococcal pathogenesis had been reported and indicated by the degradation of host tissue components such as fibronectin, fibrinogen, elastin, laminin, and blood proteins. As has been mentioned before, pneumococcal serine proteases are virulence factors either secreted and/or bound to the bacterial cell surface. The benefit of expressing serine proteases is likely a higher efficiency in colonizing the nasopharyngeal cavity (Ali et al., 2021). To date, studies on pneumococcal serine proteases have been only marginally concentrated on their role in virulence-associated processes such as adhesion, colonization, or host defense evasion. Nevertheless, this section discusses the individual or combined

impact of pneumococcal serine proteases HtrA, CbpG, PrtA, and SFP on pneumococcal colonization and how they contribute to host-pathogen interactions.

The Extracellular HtrA Serine Protease Is Involved in Colonization and Invasive Disease

HtrA has been considered as one of the most important virulence factors associated with infectious diseases of various Gram-positive and Gram-negative bacteria. In general, HtrA protease significantly influences various functions such as bacterial fitness, adaptation to environmental stress, or enhance pneumococcal virulence (Murwantoko et al., 2004; Kochan and Dawid, 2013; Backert et al., 2018). Moreover, surface-exposed HtrA promotes nasopharyngeal colonization, whereas secreted HtrA facilitates the subsequent invasion of host tissue by degrading ECM components (Backert et al., 2018).

As mentioned above, HtrA is the best studied pneumococcal serine protease and was described for the first time 20 years ago. Subsequently, the influence of HtrA on pneumococcal pathogenesis has been addressed in several studies. For example, it has been shown that HtrA is upregulated and controlled by the two-component system (TCS) CiaRH (Sebert et al., 2002). Likewise, HtrA is considered one of the most critical serine proteases in pneumococcal virulence because HtrA degrades the competence stimulating peptides (CSPs), which impacts pneumococcal competence and late competence genes affect virulence (Ibrahim et al., 2004a; Ibrahim et al., 2004b; Cassone et al., 2012). Importantly, mice infection studies with *S. pneumoniae* D39 demonstrated that the deficiency of HtrA decreases bacterial load and inflammation in the lung after intranasal infection (de Stoppelaar et al., 2013).

Pneumococcal biofilms represent well-known pathophysiologically relevant conditions with a vital role in bacterial colonization, persistence and chronic infections (Domenech et al., 2012). In certain host compartments, pneumococci are protected against the attack of the immune system by forming sessile colonies embedded in an extracellular matrix of polysaccharides representing the biofilm. Recently, HtrA has been shown to modulate bacterial release (biofilm dispersal) from heat-induced biofilms, which were mimicking fever conditions (Chao et al., 2020).

During influenza-pneumococcal co-infections, HtrA induced the inflammation when highly expressed, thereby enhancing the bacterial load in a mouse pneumonia model (Sender et al., 2020). However, the underlying molecular mechanisms of how HtrA is implicated in colonization and invasion are not clearly understood. This raises the question of whether the HtrA protease degrades host proteins directly or do they have more complicated post-translational activities. The contribution of HtrA as chaperone or serine protease in pneumococcal attachment to epithelial cells and to deeper tissue is summarized in Figure 4A.

It is hypothesized that pneumococci can use the paracellular route to avoid intracellular killing and invade human host tissues (Iovino et al., 2016). To achieve this goal, pneumococci have to cleave proteins of adherences junction (AJ) and tight junctions (TJ) such as epithelial cadherin (E-cadherin), occludins, and

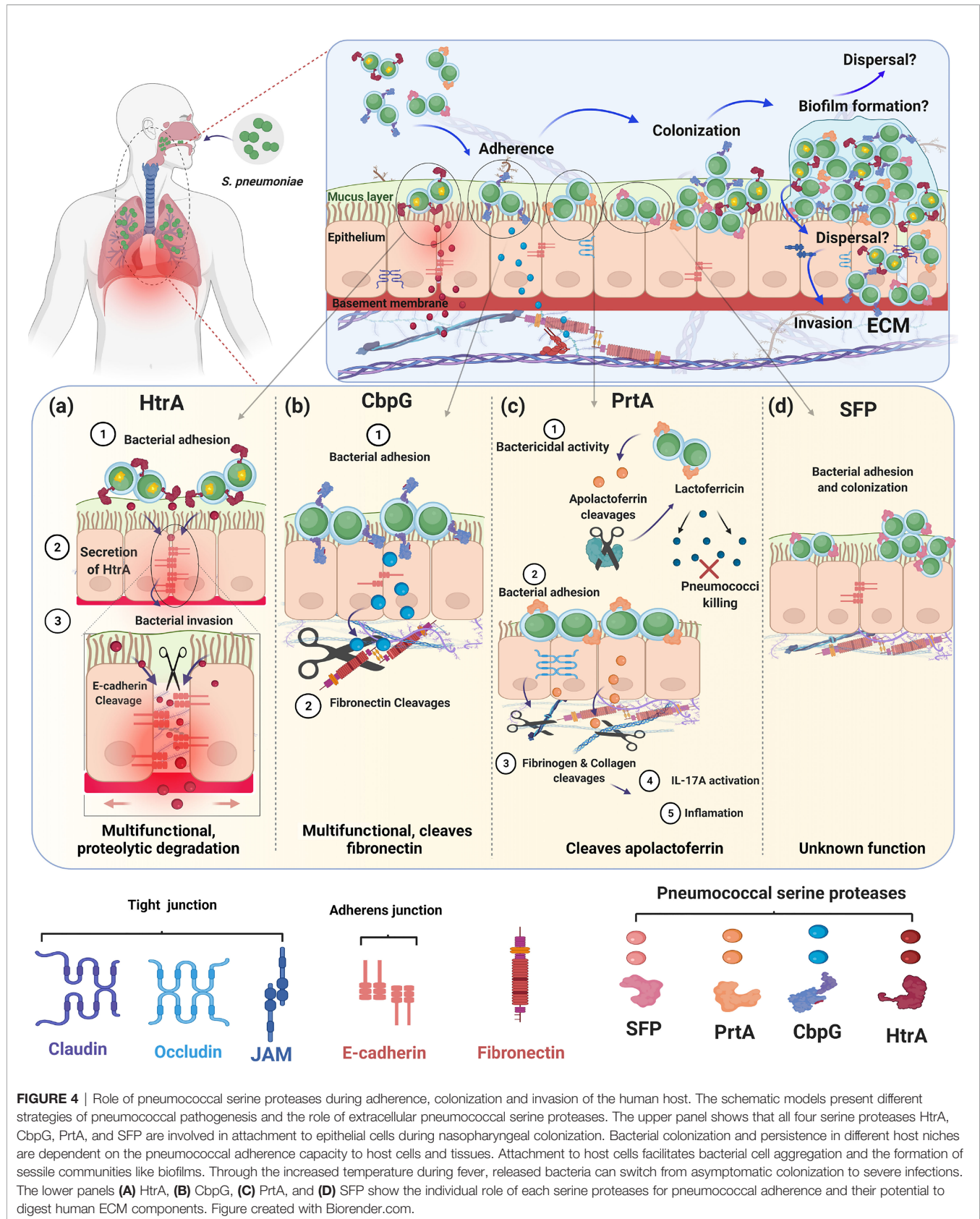


FIGURE 4 | Role of pneumococcal serine proteases during adherence, colonization and invasion of the human host. The schematic models present different strategies of pneumococcal pathogenesis and the role of extracellular pneumococcal serine proteases. The upper panel shows that all four serine proteases HtrA, CbpG, PrtA, and SFP are involved in attachment to epithelial cells during nasopharyngeal colonization. Bacterial colonization and persistence in different host niches are dependent on the pneumococcal adherence capacity to host cells and tissues. Attachment to host cells facilitates bacterial cell aggregation and the formation of sessile communities like biofilms. Through the increased temperature during fever, released bacteria can switch from asymptomatic colonization to severe infections. The lower panels (A) HtrA, (B) CbpG, (C) PrtA, and (D) SFP show the individual role of each serine proteases for pneumococcal adherence and their potential to digest human ECM components. Figure created with Biorender.com.

claudins (Devaux et al., 2019). Interestingly, stimulation of Toll-like receptors (TLRs) during pneumococcal infections down-regulate claudins, facilitating pneumococci movement across the epithelium (Clarke et al., 2011). Furthermore, in human lungs that are infected with pneumococci, a reduction of alveolar occludin, ZO-1, claudin-5, and E-cadherin, was observed (Peter et al., 2017). Besides *S. pneumoniae*, many bacterial species possess a serine protease HtrA ortholog and the impact of HtrAs on bacterial pathogenesis was reviewed recently (Backert et al., 2018). Most of the HtrAs can cleave adherence junctions, tight junctions, and ECM proteins such as fibronectin and proteoglycans, leading to a disruption of the epithelial barrier and, this mode of action is, therefore, critical for the host cell damage (Table 2).

The serine protease HtrA of *Helicobacter pylori* represents a crucial secreted virulence factor (Schmidt et al., 2016). The disruption of the gastric epithelium leads to the transmigration of *H. pylori* across the epithelium and facilitates the oncogenic CagA protein injection into host cells. Consequently, HtrA can get into the extracellular space where it cleaves cell-to-cell junction factors, such as E-cadherin, leading to a disruption of the epithelial barrier, which then enables paracellular transmigration of the bacteria (Zawilak-Pawlik et al., 2019). E-cadherin belongs to the cell adhesion molecule superfamily (CAM) and represents the target of several pathogenic bacteria, which invade the host (Hulpiau and van Roy, 2009; Devaux et al., 2019). Interestingly, E-cadherin was described as an adherence receptor for the pneumococcal surface adhesin A (PsaA), which is also acting as a substrate-binding protein for manganese (Anderton et al., 2007).

Collectively, it seems that the involvement of HtrA in bacterial pathogenesis and the enzymatic activity of HtrAs have a common origin among (pathogenic) bacteria. Considering that bacterial HtrAs show high similarities, particularly their catalytic domain, two strategies are possible and may explain the functionality of HtrA. First, the surface localization of HtrA can significantly influence adherence and colonization as has been indicated earlier (Sebert et al., 2002; Ali et al., 2021). Second, HtrA undergoes the auto-cleavage process (Jomaa et al., 2009), and due to the secretion of HtrA into the environment, HtrA can degrade host components to facilitate invasion. These activities may explain data showing that a deficiency of HtrA in *S. pneumoniae* leads to a reduced bacterial load in the blood, liver, and spleen (Ibrahim et al., 2004b; de Stoppelaar et al., 2013). So far, it is not known if the pneumococcal HtrA can degrade occludins or E-cadherin. Therefore, further analysis is needed to prove that HtrA from pneumococci also cleaves E-cadherin and to determine other substrates of HtrA.

The CbpG Serine Protease Cleaves ECM Proteins and Contributes to Adherence

Pneumococci must degrade the extracellular matrix to be able to disseminate in the host and cause invasive disease successfully. This requires the proteolytic activity of host acquired or self- proteases on the bacterial cell surface of the pneumococci. It is well known to date that several of the CBPs produced by pneumococci have multiple functions. The functions among CBPs are quite diverse, including proteolytic activity of the CbpG protein (Gosink et al.,

2000). The importance of CbpG in pneumococcal pathogenesis is demonstrated by the fact that the gene encoding CbpG is upregulated in all *in vivo* niches (Mahdi et al., 2008). As mentioned above, *in silico* analysis of clinical isolates showed that *S. pneumoniae* express either a variant with a functional CBM attaching CbpG to the cell surface or a variant without a functional CBM leading to secretion of CbpG in the host environment (Mann et al., 2006). The truncated CbpG variant is nevertheless able to degrade ECM deposited fibronectin and casein *via* its trypsin-like serine protease similarly to the other variant (Mann et al., 2006). However, a functional CBM in the C-terminal part of CbpG is needed to contribute to pneumococcal adherence and colonization.

CbpG deficient pneumococci of strain 19F_EF3030 and TIGR4 showed a significant attenuation in *in vivo* rat or mice colonization models and reduced adherence to human epithelial cells (Mann et al., 2006; Ali et al., 2021). In addition, the mortality was reduced in a septicemia infection model with infant rats (Gosink et al., 2000). These studies indicated the importance of the serine protease CbpG as a factor modulating nasopharyngeal colonization and dissemination in the blood (Gosink et al., 2000; Ali et al., 2021). Therefore, CbpG could play a role in pneumococcal transition to the blood, which may be due to its fibronectin-cleaving potential (Mann et al., 2006).

The dual functions of CbpG, cleavage of host substrates and contributing to adherence to epithelial cells correlate with a substantial defect in the colonization of the nasopharynx by a *cbpG*-mutant (Figure 4B). On the one hand, one can also speculate that the proteolytic activity of CbpG on the bacterial cell surface can modify other pneumococcal surface proteins and enable them to interact with host cell receptors or soluble host proteins. On the other hand, CbpG probably modifies the ECM and eukaryotic cell surface, thereby facilitating adhesin-receptor interactions. These are still speculations and may also account for the other proteases. However, so far, no data are yet available supporting these ideas.

Dual Role of Pneumococcal PrtA in Pneumococcal Pathogenesis

The cell wall-associated serine protease PrtA plays at least dual roles in pneumococcal infections. First, PrtA contributes to the cleavage of the human apolactoferrin to lactoferricin-like peptide, which serves as a cationic antimicrobial peptide and facilitates the killing of pneumococci (Figure 4C). This function is in a way surprising because it counteracts the virulence potential of pneumococci (Mirza et al., 2011). Second, PrtA is one of the largest pneumococcal surface proteins with a molecular weight of 240 kDa and is suggested to have adhesive functions similar to other sortase-anchored pneumococcal proteins (Frolet et al., 2010; Ali et al., 2021). A triple serine protease mutant of TIGR4 expressing only PrtA was significantly attenuated in the acute pneumonia model (Ali et al., 2021). This mutant is deficient in HtrA, and CbpG, which were shown be major virulence factors in pneumococcal pathogenesis (Mann et al., 2006; de Stoppelaar et al., 2013). In a systemic mouse infection model, mice infected with the *prtA*-mutant of strain D39 have extended survival times compared to wild-type infected mice (Bethe et al., 2001). The *prtA*-negative

strain is significantly attenuated in an intranasal mouse infection model. Thus, expression of the gene encoding PrtA is confirmed to be upregulated in the blood (Mahdi et al., 2015). In addition, by applying the experimental nasopharyngeal mouse colonization model and using strain *S. pneumoniae* 19F it was shown that PrtA is necessary for an optimal colonization (Ali et al., 2021). More important, the use of a triple knockout in 19F lacking, therefore, all serine proteases, clearly indicated that serine proteases are indispensable for pneumococcal colonization (Ali et al., 2021).

Similar to other serine proteases PrtA degrades ECM components such as collagen IV and plasminogen, which suggests that this activity fosters pneumococcal transcytosis of the mucosal barrier and spread to the bloodstream (Frolet et al., 2010; Mahdi et al., 2015). PrtA was also shown to stimulate the IL-17A response, which is a significant mediator of tissue inflammation (Hsu et al., 2018). Although the impact of PrtA on pneumococcal colonization and invasive disease as well as its substrate specificities has to be explored in greater detail, the reported data are a strong hint for the importance of PrtA during colonization, inflammation, and invasive disease. Because PrtA is highly conserved and immunogenic, it might represent a promising candidate for a proteinaceous serotype-independent multi-component vaccine.

The Unknown Functional Role of Pneumococcal Serine Protease SFP

The involvement of SFP in the pathogenesis of pneumococcal infections is still not apparent because of the minor effect of the *sfp*-mutant on virulence in experimental mouse infection models (de Stoppelaar et al., 2013).

SFP is not present in all pneumococcal strains and serotypes, as indicated in **Table 1**. However, the SFP protein shows high homology to the cell surface serine endopeptidase CspA (Bryan and Shelper, 2009), which is one of the important virulence factors for the human pathogen *Streptococcus agalactiae* (de Stoppelaar et al., 2013). Opsonophagocytosis of bacteria by host immune cells is one of the critical outcomes of classical complement activation (Harris et al., 2003). The complement component C3b deposited on the *S. agalactiae* cell surface can be cleaved by CspA, indicating the importance of CspA for immune evasion (Bryan and Shelper, 2009). So far, the impact of complement inactivation by its pneumococcal orthologue SFP is not known. In conclusion, the role of SFP for pneumococcal fitness, virulence, or immunomodulation needs further investigation and it will be interesting to identify SFP substrates.

CONCLUSION AND FUTURE PERSPECTIVES

Serine proteases in pathogenic bacteria are, in general, key virulence determinants. In pneumococci, serine proteases have a function during colonization and pneumonia. This review article covers the molecular biology of pneumococcal serine proteases and their pivotal role in pathogenesis, starting from adherence, colonization, and immune evasion. Our *in silico* analysis in

combination with hypothetical structural models revealed that the functional domains of pneumococcal serine proteases CbpG, HtrA, and PrtA, are highly conserved. The exception is SFP, which is produced only by a subset of strains. All serine proteases are secreted to the cell surface and depending on the variant, even released in the host environment. The 3D models show that the HtrA catalytic domain displays homologies to the CbpG catalytic domain, while SFP is quite similar to the catalytic domain of PrtA (**Figure 3**). Although all serine proteases have a typical catalytic triad, they might have different but also overlapping substrate specificities. The redundancy of serine proteases and probably their compensatory effect in the absence of one or more serine proteases makes it difficult to assess their individual contribution to pneumococcal fitness and virulence. Thus, all studies are in parts limited in their conclusions because of the redundancy of these serine proteases. This, in turn, leaves gaps of knowledge such as e.g., substrate specificities and host compartment specificities that have to be deciphered in experimental *in vivo* and advanced *in vitro* models. The immunogenicity of functional domains of pneumococcal serine proteases in combination with their highly conserved protein sequences fulfills one of the requirements for a protein-based serotype-independent (multi-) component vaccine. The individual potential as a vaccine candidate has, however, to be validated experimentally.

AUTHOR CONTRIBUTIONS

MA and SH conceived the concept for the review article. MA create the figures, drafted the work, and MA and GB performed the bioinformatic analyses. LS generated the 3D structural data and wrote this part. MA and SH wrote the review article, TK and GB revised it critically and gave final approval. All authors contributed to the article and approved the submitted version.

FUNDING

This study was supported by the German Academic Exchange Service (DAAD) as a grant scholarship and part of the Ph.D. thesis of MA. Funding programme/-ID: Research Grants - Doctoral Programmes in Germany, 2017/18 (57299294), ST33. This study was also supported in part by the DFG (GRK 2719). The funders had no role in study design, decision to publish, or manuscript preparation.

ACKNOWLEDGMENTS

We apologize to the authors of primary articles we have failed to cite in this review.

SUPPLEMENTARY MATERIAL

The Supplementary Material for this article can be found online at: <https://www.frontiersin.org/articles/10.3389/fcimb.2021.763152/full#supplementary-material>

REFERENCES

- Abedi, D., Feizizadeh, S., Akbari, V., and Jafarian-Dehkordi, A. (2013). *In Vitro* Anti-Bacterial and Anti-Adherence Effects of *Lactobacillus Delbrueckii* Subsp *Bulgaricus* on *Escherichia Coli*. *Res. Pharm. Sci.* 8 (4), 260–268.
- Albrich, W. C., Monnet, D. L., and Harbarth, S. (2004). Antibiotic Selection Pressure and Resistance in *Streptococcus Pneumoniae* and *Streptococcus Pyogenes*. *Emerg. Infect. Dis.* 10 (3), 514–517. doi: 10.3201/eid1003.030252
- Ali, M. Q., Kohler, T. P., Burchhardt, G., Wüst, A., Henck, N., Bolsmann, R., et al. (2021). Extracellular Pneumococcal Serine Proteases Affect Nasopharyngeal Colonization. *Front. Cell. Infect. Microbiol.* 10, 613467. doi: 10.3389/fcimb.2020.613467
- Anderton, J. M., Rajam, G., Romero-Steiner, S., Summer, S., Kowalczyk, A. P., Carlone, G. M., et al. (2007). E-Cadherin Is a Receptor for the Common Protein Pneumococcal Surface Adhesin A (PsaA) of *Streptococcus Pneumoniae*. *Microb. Pathog.* 42 (5–6), 225–236. doi: 10.1016/j.micpath.2007.02.003
- Backert, S., Bernegger, S., Skorko-Glonek, J., and Wessler, S. (2018). Extracellular HtrA Serine Proteases: An Emerging New Strategy in Bacterial Pathogenesis. *Cell Microbiol.* 20 (6), e12845. doi: 10.1111/cmi.12845
- Bai, X. C., Pan, X. J., Wang, X. J., Ye, Y. Y., Chang, L. F., Leng, D., et al. (2011). Characterization of the Structure and Function of *Escherichia Coli* DegQ as a Representative of the DegQ-Like Proteases of Bacterial HtrA Family Proteins. *Structure* 19 (9), 1328–1337. doi: 10.1016/j.str.2011.06.013
- Beckmann, C., Waggoner, J. D., Harris, T. O., Tamura, G. S., and Rubens, C. E. (2002). Identification of Novel Adhesins From Group B *Streptococci* by Use of Phage Display Reveals That C5a Peptidase Mediates Fibronectin Binding. *Infect. Immun.* 70 (6), 2869–2876. doi: 10.1128/iai.70.6.2869-2876.2002
- Bergmann, S., and Hammerschmidt, S. (2006). Versatility of Pneumococcal Surface Proteins. *Microbiology (Reading)* 152 (Pt 2), 295–303. doi: 10.1099/mic.0.28610-0
- Bergmann, S., Lang, A., Rohde, M., Agarwal, V., Rennemeier, C., Grashoff, C., et al. (2009). Integrin-Linked Kinase Is Required for Vitronectin-Mediated Internalization of *Streptococcus Pneumoniae* by Host Cells. *J. Cell Sci.* 122 (Pt 2), 256–267. doi: 10.1242/jcs.035600
- Bergmann, S., Rohde, M., Preissner, K. T., and Hammerschmidt, S. (2005). The Nine Residue Plasminogen-Binding Motif of the Pneumococcal Enolase Is the Major Cofactor of Plasmin-Mediated Degradation of Extracellular Matrix, Dissolution of Fibrin and Transmigration. *Thromb. Haemost.* 94 (2), 304–311. doi: 10.1160/th05-05-0369
- Bergmann, S., Schoenen, H., and Hammerschmidt, S. (2013). The Interaction Between Bacterial Enolase and Plasminogen Promotes Adherence of *Streptococcus Pneumoniae* to Epithelial and Endothelial Cells. *Int. J. Med. Microbiol.* 303 (8), 452–462. doi: 10.1016/j.ijmm.2013.06.002
- Bethe, G., Nau, R., Wellmer, A., Hakenbeck, R., Reinert, R. R., Heinz, H. P., et al. (2001). The Cell Wall-Associated Serine Protease PrtA: A Highly Conserved Virulence Factor of *Streptococcus Pneumoniae*. *FEMS Microbiol. Lett.* 205 (1), 99–104. doi: 10.1111/j.1574-6968.2001.tb10931.x
- Binsker, U., Kohler, T. P., Krauel, K., Kohler, S., Schwertz, H., and Hammerschmidt, S. (2015). Pneumococcal Adhesins PavB and PspC Are Important for the Interplay With Human Thrombospondin-1. *J. Biol. Chem.* 290 (23), 14542–14555. doi: 10.1074/jbc.M114.623876
- Biswas, S., and Biswas, I. (2005). Role of HtrA in Surface Protein Expression and Biofilm Formation by *Streptococcus Mutans*. *Infect. Immun.* 73 (10), 6923–6934. doi: 10.1128/IAI.73.10.6923-6934.2005
- Blasi, F., Mantero, M., Santus, P., and Tarsia, P. (2012). Understanding the Burden of Pneumococcal Disease in Adults. *Clin. Microbiol. Infect.* 18 (Suppl 5), 7–14. doi: 10.1111/j.1469-0691.2012.03937.x
- Blum, M., Chang, H. Y., Chuguransky, S., Grego, T., Kandasamy, S., Mitchell, A., et al. (2021). The InterPro Protein Families and Domains Database: 20 Years on. *Nucleic Acids Res.* 49 (D1), D344–d354. doi: 10.1093/nar/gkaa977
- Boehm, M., Simson, D., Escher, U., Schmidt, A. M., Bereswill, S., Tegtmeyer, N., et al. (2018). Function of Serine Protease HtrA in the Lifecycle of the Foodborne Pathogen *Campylobacter Jejuni*. *Eur. J. Microbiol. Immunol. (Bp)* 8 (3), 70–77. doi: 10.1556/1886.2018.00011
- Bogaert, D., De Groot, R., and Hermans, P. W. (2004). *Streptococcus Pneumoniae* Colonisation: The Key to Pneumococcal Disease. *Lancet Infect. Dis.* 4 (3), 144–154. doi: 10.1016/s1473-3099(04)00938-7
- Bohnsack, J. F., Takahashi, S., Hammitt, L., Miller, D. V., Aly, A. A., and Adderson, E. E. (2000). Genetic Polymorphisms of Group B *Streptococcus* scpB Alter Functional Activity of a Cell-Associated Peptidase That Inactivates C5a. *Infect. Immun.* 68 (9), 5018–5025. doi: 10.1128/iai.68.9.5018-5025.2000
- Bonifait, L., de la Cruz Dominguez-Punaro, M., Vaillancourt, K., Bart, C., Slater, J., Frenette, M., et al. (2010). The Cell Envelope Subtilisin-Like Proteinase Is a Virulence Determinant for *Streptococcus Suis*. *BMC Microbiol.* 10, 42. doi: 10.1186/1471-2180-10-42
- Bradshaw, J. L., Rafiqullah, I. M., Robinson, D. A., and McDaniel, L. S. (2020). Transformation of Nonencapsulated *Streptococcus Pneumoniae* During Systemic Infection. *Sci. Rep.* 10 (1), 18932. doi: 10.1038/s41598-020-75988-5
- Bryan, J. D., and Shelper, D. W. (2009). *Streptococcus Agalactiae* CspA Is a Serine Protease That Inactivates Chemokines. *J. Bacteriol.* 191 (6), 1847–1854. doi: 10.1128/JB.01124-08
- Burchacka, E., and Witkowska, D. (2016). The Role of Serine Proteases in the Pathogenesis of Bacterial Infections. *Postepy Hig. Med. Dosw. (Online)* 70 (0), 678–694. doi: 10.5604/17322693.1208011
- Cassone, M., Gagne, A. L., Spruce, L. A., Seeholzer, S. H., and Seibert, M. E. (2012). The HtrA Protease From *Streptococcus Pneumoniae* Digests Both Denatured Proteins and the Competence-Stimulating Peptide. *J. Biol. Chem.* 287 (46), 38449–38459. doi: 10.1074/jbc.M112.391482
- Chang, Z. (2016). The Function of the DegP (HtrA) Protein: Protease Versus Chaperone. *IUBMB Life* 68 (11), 904–907. doi: 10.1002/iub.1561
- Chao, Y., Bergenfelz, C., Sun, R., Han, X., Achour, A., and Hakansson, A. P. (2020). The Serine Protease HtrA Plays a Key Role in Heat-Induced Dispersal of Pneumococcal Biofilms. *Sci. Rep.* 10, 22455. doi: 10.1038/s41598-020-80233-0
- Cheng, Q., Stafslie, D., Purushothaman, S. S., and Cleary, P. (2002). The Group B *Streptococcal* C5a Peptidase Is Both a Specific Protease and an Invasin. *Infect. Immun.* 70 (5), 2408–2413. doi: 10.1128/iai.70.5.2408-2413.2002
- Chmouryguina, I., Suvorov, A., Ferrieri, P., and Cleary, P. P. (1996). Conservation of the C5a Peptidase Genes in Group A and B *Streptococci*. *Infect. Immun.* 64 (7), 2387–2390. doi: 10.1128/iai.64.7.2387-2390.1996
- Clarke, T. B., Francella, N., Huegel, A., and Weiser, J. N. (2011). Invasive Bacterial Pathogens Exploit TLR-Mediated Downregulation of Tight Junction Components to Facilitate Translocation Across the Epithelium. *Cell Host Microbe* 9 (5), 404–414. doi: 10.1016/j.chom.2011.04.012
- Clausen, T., Kaiser, M., Huber, R., and Ehrmann, M. (2011). HTRA Proteases: Regulated Proteolysis in Protein Quality Control. *Nat. Rev. Mol. Cell Biol.* 12 (3), 152–162. doi: 10.1038/nrm3065
- Clausen, T., Southan, C., and Ehrmann, M. (2002). The HtrA Family of Proteases: Implications for Protein Composition and Cell Fate. *Mol. Cell* 10 (3), 443–455. doi: 10.1016/s1097-2765(02)00658-5
- Cole, J. N., Aquilina, J. A., Hains, P. G., Henningham, A., Sriprakash, K. S., Caparon, M. G., et al. (2007). Role of Group A *Streptococcus* HtrA in the Maturation of SpeB Protease. *Proteomics* 7 (24), 4488–4498. doi: 10.1002/pmic.200700626
- Collin, M., and Olsén, A. (2003). Extracellular Enzymes With Immunomodulating Activities: Variations on a Theme in *Streptococcus Pyogenes*. *Infect. Immun.* 71 (6), 2983–2992. doi: 10.1128/iai.71.6.2983-2992.2003
- Cortes, T., Schubert, O. T., Rose, G., Arnvig, K. B., Comas, I., Aebersold, R., et al. (2013). Genome-Wide Mapping of Transcriptional Start Sites Defines an Extensive Leaderless Transcriptome in *Mycobacterium Tuberculosis*. *Cell Rep.* 5 (4), 1121–1131. doi: 10.1016/j.celrep.2013.10.031
- Courtin, P., Monnet, V., and Rul, F. (2002). Cell-Wall Proteinases PrtS and PrtB Have a Different Role in *Streptococcus Thermophilus*/*Lactobacillus Bulgaricus* Mixed Cultures in Milk. *Microbiology (Reading)* 148 (Pt 11), 3413–3421. doi: 10.1099/00221287-148-11-3413
- Courtney, H. S. (1991). Degradation of Connective Tissue Proteins by Serine Proteases From *Streptococcus Pneumoniae*. *Biochem. Biophys. Res. Commun.* 175 (3), 1023–1028. doi: 10.1016/0006-291x(91)91667-2
- Dawid, S., Seibert, M. E., and Weiser, J. N. (2009). Bacteriocin Activity of *Streptococcus Pneumoniae* Is Controlled by the Serine Protease HtrA via Posttranscriptional Regulation. *J. Bacteriol.* 191 (5), 1509–1518. doi: 10.1128/jb.01213-08
- Desa, M. N., Sekaran, S. D., Vadivelu, J., and Parasakthi, N. (2008). Distribution of CBP Genes in *Streptococcus Pneumoniae* Isolates in Relation to Vaccine

- Types, Penicillin Susceptibility and Clinical Site. *Epidemiol. Infect.* 136 (7), 940–942. doi: 10.1017/S0950268807009363
- de Stoppelaar, S. F., Bootsma, H. J., Zomer, A., Roelofs, J. J., Hermans, P. W., van 't Veer, C., et al. (2013). Streptococcus Pneumoniae Serine Protease HtrA, But Not SFP or PrtA, Is a Major Virulence Factor in Pneumonia. *PLoS One* 8 (11), e80062. doi: 10.1371/journal.pone.0080062
- Devaux, C. A., Mezouar, S., and Mege, J. L. (2019). The E-Cadherin Cleavage Associated to Pathogenic Bacteria Infections Can Favor Bacterial Invasion and Transmigration, Dysregulation of the Immune Response and Cancer Induction in Humans. *Front. Microbiol.* 10, 2598. doi: 10.3389/fmicb.2019.02598
- Domenech, M., García, E., and Moscoso, M. (2012). Biofilm Formation in Streptococcus Pneumoniae. *Microb. Biotechnol.* 5 (4), 455–465. doi: 10.1111/j.1751-7915.2011.00294.x
- Emanuelsson, O., Brunak, S., von Heijne, G., and Nielsen, H. (2007). Locating Proteins in the Cell Using TargetP, SignalP and Related Tools. *Nat. Protoc.* 2 (4), 953–971. doi: 10.1038/nprot.2007.131
- Fan, K., Zhang, J., Shang, Q., and Tu, X. (2010). 1H, 13C and 15N Resonance Assignment of the PDZ Domain of HtrA From Streptococcus Pneumoniae. *Biomol. NMR Assign.* 4 (1), 79–82. doi: 10.1007/s12104-010-9211-3
- Fan, K., Zhang, J., Zhang, X., and Tu, X. (2011). Solution Structure of HtrA PDZ Domain From Streptococcus Pneumoniae and Its Interaction With YYF-COOH Containing Peptides. *J. Struct. Biol.* 176 (1), 16–23. doi: 10.1016/j.jsb.2011.06.009
- Frolet, C., Beniazza, M., Roux, L., Gallet, B., Noirclerc-Savoye, M., Vernet, T., et al. (2010). New Adhesin Functions of Surface-Exposed Pneumococcal Proteins. *BMC Microbiol.* 10, 190. doi: 10.1186/1471-2180-10-190
- Fulde, M., Steinert, M., and Bergmann, S. (2013). Interaction of Streptococcal Plasminogen Binding Proteins With the Host Fibrinolytic System. *Front. Cell Infect. Microbiol.* 3, 85. doi: 10.3389/fcimb.2013.00085
- Galán-Bartual, S., Pérez-Dorado, I., García, P., and Hermoso, J. (2015). *Streptococcus Pneumoniae, Molecular Mechanisms of Host-Pathogen Interactions* (Amsterdam: Elsevier). doi: 10.1016/B978-0-12-410530-0.00037-5
- Gamez, G., and Hammerschmidt, S. (2012). Combat Pneumococcal Infections: Adhesins as Candidates for Protein-Based Vaccine Development. *Curr. Drug Targets* 13 (3), 323–337. doi: 10.2174/138945012799424697
- García-Bustos, J. F., and Tomasz, A. (1987). Teichoic Acid-Containing Muropeptides From Streptococcus Pneumoniae as Substrates for the Pneumococcal Autolysin. *J. Bacteriol.* 169 (2), 447–453. doi: 10.1128/jb.169.2.447-453.1987
- García, E., García, J. L., García, P., Arrarás, A., Sánchez-Puelles, J. M., and López, R. (1988). Molecular Evolution of Lytic Enzymes of Streptococcus Pneumoniae and Its Bacteriophages. *Proc. Natl. Acad. Sci. USA* 85 (3), 914–918. doi: 10.1073/pnas.85.3.914
- Gasc, A. M., Giammarinaro, P., Richter, S., and Sicard, M. (1998). Organization Around the dnaA Gene of Streptococcus Pneumoniae. *Microbiology (Reading)* 144 (Pt 2), 433–439. doi: 10.1099/00221287-144-2-433
- Gosink, K. K., Mann, E. R., Guglielmi, C., Tuomanen, E. I., and Masure, H. R. (2000). Role of Novel Choline Binding Proteins in Virulence of Streptococcus Pneumoniae. *Infect. Immun.* 68 (10), 5690–5695. doi: 10.1128/iai.68.10.5690-5695.2000
- Hammerschmidt, S. (2006). Adherence Molecules of Pathogenic Pneumococci. *Curr. Opin. Microbiol.* 9 (1), 12–20. doi: 10.1016/j.mib.2005.11.001
- Harris, T. O., Shelver, D. W., Bohnsack, J. F., and Rubens, C. E. (2003). A Novel Streptococcal Surface Protease Promotes Virulence, Resistance to Opsonophagocytosis, and Cleavage of Human Fibrinogen. *J. Clin. Invest.* 111 (1), 61–70. doi: 10.1172/jci16270
- Hasselblatt, H., Kurzbauer, R., Wilken, C., Krojer, T., Sawa, J., Kurt, J., et al. (2007). Regulation of the sigmaE Stress Response by DegS: How the PDZ Domain Keeps the Protease Inactive in the Resting State and Allows Integration of Different OMP-Derived Stress Signals Upon Folding Stress. *Genes Dev.* 21 (20), 2659–2670. doi: 10.1101/gad.445307
- Hilleringmann, M., Kohler, S., Gámez, G., and Hammerschmidt, S. (2015). “Pneumococcal Pili and Adhesins,” in *Streptococcus Pneumoniae: Molecular Mechanisms of Host-Pathogen Interactions* (Amsterdam, NL: Academic Press Is an imprint of Elsevier).
- Holck, A., and Naes, H. (1992). Cloning, Sequencing and Expression of the Gene Encoding the Cell-Envelope-Associated Proteinase From Lactobacillus Paracasei Subsp. Paracasei NCDO 151. *J. Gen. Microbiol.* 138 (7), 1353–1364. doi: 10.1099/00221287-138-7-1353
- Holmes, A. R., McNab, R., Millsap, K. W., Rohde, M., Hammerschmidt, S., Mawdsley, J. L., et al. (2001). The pavA Gene of Streptococcus Pneumoniae Encodes a Fibronectin-Binding Protein That Is Essential for Virulence. *Mol. Microbiol.* 41 (6), 1395–1408. doi: 10.1046/j.1365-2958.2001.02610.x
- Hörmannspurger, G., von Schille, M. A., and Haller, D. (2013). Lactocin as a Protective Microbial Structure in the Context of IBD. *Gut Microbes* 4 (2), 152–157. doi: 10.4161/gmic.23444
- Hoy, B., Löwer, M., Weydig, C., Carra, G., Tegtmeyer, N., Geppert, T., et al. (2010). Helicobacter Pylori HtrA Is a New Secreted Virulence Factor That Cleaves E-Cadherin to Disrupt Intercellular Adhesion. *EMBO Rep.* 11 (10), 798–804. doi: 10.1038/embor.2010.114
- Hsu, C. F., Hsiao, C. H., Tseng, S. F., Chen, J. R., Liao, Y. J., Chen, S. J., et al. (2018). PrtA Immunization Fails to Protect Against Pulmonary and Invasive Infection by Streptococcus Pneumoniae. *Respir. Res.* 19 (1), 187. doi: 10.1186/s12931-018-0895-8
- Hulpiau, P., and van Roy, F. (2009). Molecular Evolution of the Cadherin Superfamily. *Int. J. Biochem. Cell Biol.* 41 (2), 349–369. doi: 10.1016/j.biocel.2008.09.027
- Ibrahim, Y. M., Kerr, A. R., McCluskey, J., and Mitchell, T. J. (2004a). Control of Virulence by the Two-Component System CiaR/H Is Mediated via HtrA, a Major Virulence Factor of Streptococcus Pneumoniae. *J. Bacteriol.* 186 (16), 5258–5266. doi: 10.1128/JB.186.16.5258-5266.2004
- Ibrahim, Y. M., Kerr, A. R., McCluskey, J., and Mitchell, T. J. (2004b). Role of HtrA in the Virulence and Competence of Streptococcus Pneumoniae. *Infect. Immun.* 72 (6), 3584–3591. doi: 10.1128/IAI.72.6.3584-3591.2004
- Inoue, M., Saito, A., Kon, H., Uchida, H., Koyama, S., Haryu, S., et al. (2014). Subdural Empyema Due to Lactococcus Lactis Cremoris: Case Report. *Neurol. Med. Chir. (Tokyo)* 54 (4), 341–347. doi: 10.2176/nmc.cr2012-0440
- Iovino, F., Seinen, J., Henriques-Normark, B., and van Dijk, J. M. (2016). How Does Streptococcus Pneumoniae Invade the Brain? *Trends Microbiol.* 24 (4), 307–315. doi: 10.1016/j.tim.2015.12.012
- Ishii, S., Yano, T., and Hayashi, H. (2006). Expression and Characterization of the Peptidase Domain of Streptococcus Pneumoniae ComA, a Bifunctional ATP-Binding Cassette Transporter Involved in Quorum Sensing Pathway. *J. Biol. Chem.* 281 (8), 4726–4731. doi: 10.1074/jbc.M512516200
- Jahn, K., Handtke, S., Palankar, R., Weißmüller, S., Nouailles, G., Kohler, T. P., et al. (2020). Pneumolysin Induces Platelet Destruction, Not Platelet Activation, Which Can Be Prevented by Immunoglobulin Preparations *In Vitro*. *Blood Adv.* 4 (24), 6315–6326. doi: 10.1182/bloodadvances.2020002372
- Jajere, S. M. (2019). A Review of Salmonella Enterica With Particular Focus on the Pathogenicity and Virulence Factors, Host Specificity and Antimicrobial Resistance Including Multidrug Resistance. *Vet. World* 12 (4), 504–521. doi: 10.14202/vetworld.2019.504-521
- Jomaa, A., Iwanczyk, J., Tran, J., and Ortega, J. (2009). Characterization of the Autocleavage Process of the Escherichia Coli HtrA Protein: Implications for Its Physiological Role. *J. Bacteriol.* 191 (6), 1924–1932. doi: 10.1128/jb.01187-08
- Kadioglu, A., Weiser, J. N., Paton, J. C., and Andrew, P. W. (2008). The Role of Streptococcus Pneumoniae Virulence Factors in Host Respiratory Colonization and Disease. *Nat. Rev. Microbiol.* 6 (4), 288–301. doi: 10.1038/nrmicro1871
- Kanehisa, M., Goto, S., Hattori, M., Aoki-Kinoshita, K. F., Itoh, M., Kawashima, S., et al. (2006). From Genomics to Chemical Genomics: New Developments in KEGG. *Nucleic Acids Res.* 34 (Database issue), D354–D357. doi: 10.1093/nar/gkj102
- Kanwal, S., Jensch, I., Palm, G. J., Bronstrup, M., Rohde, M., Kohler, T. P., et al. (2017). Mapping the Recognition Domains of Pneumococcal Fibronectin-Binding Proteins PavA and PavB Demonstrates a Common Pattern of Molecular Interactions With Fibronectin Type III Repeats. *Mol. Microbiol.* 105 (6), 839–859. doi: 10.1111/mmi.13740
- Kanz, C., Aldebert, P., Althorpe, N., Baker, W., Baldwin, A., Bates, K., et al. (2005). The EMBL Nucleotide Sequence Database. *Nucleic Acids Res.* 33 (Database issue), D29–D33. doi: 10.1093/nar/gki098
- Kazemian, H., Afshar, D., Garcia, E., Pourmand, M. R., Jeddi-Tehrani, M., Aminharati, F., et al. (2018). CbpM and CbpG of Streptococcus Pneumoniae Elicit a High Protection in Mice Challenged With a Serotype 19F Pneumococcus. *Iran J. Allergy Asthma Immunol.* 17 (6), 574–585.

- Kilian, M., Mestecky, J., Kulhavy, R., Tomana, M., and Butler, W. T. (1980). IgA1 Proteases From Haemophilus Influenzae, Streptococcus Pneumoniae, Neisseria Meningitidis, and Streptococcus Sanguis: Comparative Immunochemical Studies. *J. Immunol.* 124 (6), 2596–2600.
- Kim, D. Y., Kim, D. R., Ha, S. C., Lokanath, N. K., Lee, C. J., Hwang, H. Y., et al. (2003). Crystal Structure of the Protease Domain of a Heat-Shock Protein HtrA From Thermotoga Maritima. *J. Biol. Chem.* 278 (8), 6543–6551. doi: 10.1074/jbc.M208148200
- Kim, D., San, B. H., Moh, S. H., Park, H., Kim, D. Y., Lee, S., et al. (2010). Structural Basis for the Substrate Specificity of PepA From Streptococcus Pneumoniae, a Dodecameric Tetrahedral Protease. *Biochem. Biophys. Res. Commun.* 391 (1), 431–436. doi: 10.1016/j.bbrc.2009.11.075
- Kochan, T. J., and Dawid, S. (2013). The HtrA Protease of Streptococcus Pneumoniae Controls Density-Dependent Stimulation of the Bacteriocin Blp Locus via Disruption of Pheromone Secretion. *J. Bacteriol.* 195 (7), 1561–1572. doi: 10.1128/JB.01964-12
- Kohler, S., Voß, F., Gómez Mejía, A., Brown, J. S., and Hammerschmidt, S. (2016). Pneumococcal Lipoproteins Involved in Bacterial Fitness, Virulence, and Immune Evasion. *FEBS Lett.* 590 (21), 3820–3839. doi: 10.1002/1873-3468.12352
- Kriaa, A., Jablaoui, A., Mkaouer, H., Akermi, N., and Maguin, E. (2020). Serine Proteases at the Cutting Edge of IBD: Focus on Gastrointestinal Inflammation. *FASEB J.* 34 (6), 7270–7282. doi: 10.1096/fj.202000031RR
- Krogh, A., Larsson, B., von Heijne, G., and Sonnhammer, E. L. (2001). Predicting Transmembrane Protein Topology With a Hidden Markov Model: Application to Complete Genomes. *J. Mol. Biol.* 305 (3), 567–580. doi: 10.1006/jmbi.2000.4315
- Kukkonen, M., and Korhonen, T. K. (2004). The OmpT Family of Enterobacterial Surface Proteases/Adhesins: From Housekeeping in Escherichia Coli to Systemic Spread of Yersinia Pestis. *Int. J. Med. Microbiol.* 294 (1), 7–14. doi: 10.1016/j.jimm.2004.01.003
- Kunji, E. R., Mierau, I., Hagting, A., Poolman, B., and Konings, W. N. (1996). The Proteolytic Systems of Lactic Acid Bacteria. *Antonie Van Leeuwenhoek* 70 (2–4), 187–221. doi: 10.1007/bf00395933
- Kwon, K., Hasseman, J., Latham, S., Grose, C., Do, Y., Fleischmann, R. D., et al. (2011). Recombinant Expression and Functional Analysis of Proteases From Streptococcus Pneumoniae, Bacillus Anthracis, and Yersinia Pestis. *BMC Biochem.* 12, 17. doi: 10.1186/1471-2091-12-17
- Li, Y., Hill, A., Beitelshees, M., Shao, S., and Lovell, J. F. (2016). Directed Vaccination Against Pneumococcal Disease. *Proc. Natl. Acad. Sci. USA* 113, 25, 6898–6903. doi: 10.1073/pnas.1603007113
- Lipinska, B., Zylicz, M., and Georgopoulos, C. (1990). The HtrA (DegP) Protein, Essential for Escherichia Coli Survival at High Temperatures, Is an Endopeptidase. *J. Bacteriol.* 172 (4), 1791–1797. doi: 10.1128/jb.172.4.1791-1797.1990
- Liu, Y., Zeng, Y., Huang, Y., Gu, L., Wang, S., Li, C., et al. (2019). HtrA-Mediated Selective Degradation of DNA Uptake Apparatus Accelerates Termination of Pneumococcal Transformation. *Mol. Microbiol.* 112 (4), 1308–1325. doi: 10.1111/mmi.14364
- Ljungh, A., Moran, A. P., and Wadström, T. (1996). Interactions of Bacterial Adhesins With Extracellular Matrix and Plasma Proteins: Pathogenic Implications and Therapeutic Possibilities. *FEMS Immunol. Med. Microbiol.* 16 (2), 117–126. doi: 10.1111/j.1574-695X.1996.tb00128.x
- Löffling, J., Vimberg, V., Battig, P., and Henriques-Normark, B. (2011). Cellular Interactions by LPxTG-Anchored Pneumococcal Adhesins and Their Streptococcal Homologues. *Cell Microbiol.* 13 (2), 186–197. doi: 10.1111/j.1462-5822.2010.01560.x
- Lyon, W. R., and Caparon, M. G. (2004). Role for Serine Protease HtrA (DegP) of Streptococcus Pyogenes in the Biogenesis of Virulence Factors SpeB and the Hemolysin Streptolysin S. *Infect. Immun.* 72 (3), 1618–1625. doi: 10.1128/iai.72.3.1618-1625.2004
- Macfarlane, G. T., Allison, C., Gibson, S. A., and Cummings, J. H. (1988). Contribution of the Microflora to Proteolysis in the Human Large Intestine. *J. Appl. Bacteriol.* 64 (1), 37–46. doi: 10.1111/j.1365-2672.1988.tb02427.x
- Maestro, B., and Sanz, J. M. (2016). Choline Binding Proteins From Streptococcus Pneumoniae: A Dual Role as Enzybiotics and Targets for the Design of New Antimicrobials. *Antibiotics (Basel)* 5 (2), 1–33. doi: 10.3390/antibiotics5020021
- Mahdi, L. K., Ogunniyi, A. D., LeMessurier, K. S., and Paton, J. C. (2008). Pneumococcal Virulence Gene Expression and Host Cytokine Profiles During Pathogenesis of Invasive Disease. *Infect. Immun.* 76 (2), 646–657. doi: 10.1128/iai.01161-07
- Mahdi, L. K., van der Hoek, M. B., Ebrahimie, E., Paton, J. C., and Ogunniyi, A. D. (2015). Characterization of Pneumococcal Genes Involved in Bloodstream Invasion in a Mouse Model. *PLoS One* 10 (11), e0141816. doi: 10.1371/journal.pone.0141816
- Male, C. J. (1979). Immunoglobulin A1 Protease Production by Haemophilus Influenzae and Streptococcus Pneumoniae. *Infect. Immun.* 26 (1), 254–261. doi: 10.1128/iai.26.1.254-261.1979
- Malet, H., Canellas, F., Sawa, J., Yan, J., Thalassinou, K., Ehrmann, M., et al. (2012). Newly Folded Substrates Inside the Molecular Cage of the HtrA Chaperone DegQ. *Nat. Struct. Mol. Biol.* 19 (2), 152–157. doi: 10.1038/nsmb.2210
- Mann, B., Orihuela, C., Antikainen, J., Gao, G., Sublett, J., Korhonen, T. K., et al. (2006). Multifunctional Role of Choline Binding Protein G in Pneumococcal Pathogenesis. *Infect. Immun.* 74 (2), 821–829. doi: 10.1128/IAI.74.2.821-829.2006
- Marquart, M. E. (2021). Pathogenicity and Virulence of Streptococcus Pneumoniae: Cutting to the Chase on Proteases. *Virulence* 12 (1), 766–787. doi: 10.1080/21505594.2021.1889812
- Marraffini, L. A., Dedent, A. C., and Schneewind, O. (2006). Sortases and the Art of Anchoring Proteins to the Envelopes of Gram-Positive Bacteria. *Microbiol. Mol. Biol. Rev.* 70 (1), 192–221. doi: 10.1128/mmbr.70.1.192-221.2006
- Martínez-García, S., Rodríguez-Martínez, S., Cancino-Díaz, M. E., and Cancino-Díaz, J. C. (2018). Extracellular Proteases of Staphylococcus Epidermidis: Roles as Virulence Factors and Their Participation in Biofilm. *Apmis* 126 (3), 177–185. doi: 10.1111/apm.12805
- McCullers, J. A., and Tuomanen, E. I. (2001). Molecular Pathogenesis of Pneumococcal Pneumonia. *Front. Biosci.* 6, D877–D889. doi: 10.2741/mccullers
- Meijers, R., Blagova, E. V., Levnikov, V. M., Rudenskaya, G. N., Chestukhina, G. G., Akimkina, T. V., et al. (2004). The Crystal Structure of Glutamyl Endopeptidase From Bacillus Intermedius Reveals a Structural Link Between Zymogen Activation and Charge Compensation. *Biochemistry* 43 (10), 2784–2791. doi: 10.1021/bi035354s
- Mellroth, P., Sandalova, T., Kikhney, A., Vilaplana, F., Hesk, D., Lee, M., et al. (2014). Structural and Functional Insights Into Peptidoglycan Access for the Lytic Amidase LytA of Streptococcus Pneumoniae. *mBio* 5 (1), e01120–e01113. doi: 10.1128/mBio.01120-13
- Mirza, S., Wilson, L., Benjamin, W. H. Jr., Novak, J., Barnes, S., Hollingshead, S. K., et al. (2011). Serine Protease PrtA From Streptococcus Pneumoniae Plays a Role in the Killing of S. Pneumoniae by Apolactoferrin. *Infect. Immun.* 79 (6), 2440–2450. doi: 10.1128/IAI.00489-10
- Mitchell, A. M., and Mitchell, T. J. (2010). Streptococcus Pneumoniae: Virulence Factors and Variation. *Clin. Microbiol. Infect.* 16 (5), 411–418. doi: 10.1111/j.1469-0691.2010.03183.x
- Montalbán-López, M., Deng, J., van Heel, A. J., and Kuipers, J. O. P. (2018). Specificity and Application of the Lantibiotic Protease NisP. *Front. Microbiol.* 9, 160. doi: 10.3389/fmicb.2018.00160
- Moscato, M., García, E., and López, R. (2006). Biofilm Formation by Streptococcus Pneumoniae: Role of Choline, Extracellular DNA, and Capsular Polysaccharide in Microbial Accretion. *J. Bacteriol.* 188 (22), 7785–7795. doi: 10.1128/jb.00673-06
- Murwantoko, Y., Yano, M., Ueta, Y., Murasaki, A., Kanda, H., Oka, C., et al. (2004). Binding of Proteins to the PDZ Domain Regulates Proteolytic Activity of HtrA1 Serine Protease. *Biochem. J.* 381 (Pt 3), 895–904. doi: 10.1042/bj20040435
- NCBI (2016). Database Resources of the National Center for Biotechnology Information. *Nucleic Acids Res.* 44 (D1), D7–19. doi: 10.1093/nar/gkv1290
- Nikolić, M., Tolínacki, M., Fira, D., Golić, N., and Topisirović, L. (2009). Variation in Specificity of the PrtP Extracellular Proteinases in Lactococcus Lactis and Lactobacillus Paracasei Subsp. Paracasei. *Folia Microbiol. (Praha)* 54 (3), 188–194. doi: 10.1007/s12223-009-0029-2
- Nishimoto, A. T., Rosch, J. W., and Tuomanen, E. I. (2020). Pneumolysin: Pathogenesis and Therapeutic Target. *Front. Microbiol.* 11, 1543. doi: 10.3389/fmicb.2020.01543
- Nobbs, A. H., Lamont, R. J., and Jenkinson, H. F. (2009). Streptococcus Adherence and Colonization. *Microbiol. Mol. Biol. Rev.* 73 (3), 407–450. doi: 10.1128/mmbr.00014-09

- Novak, R., Charpentier, E., Braun, J. S., Park, E., Murti, S., Tuomanen, E., et al. (2000). Extracellular Targeting of Choline-Binding Proteins in *Streptococcus Pneumoniae* by a Zinc Metalloprotease. *Mol. Microbiol.* 36 (2), 366–376. doi: 10.1046/j.1365-2958.2000.01854.x
- O'Brien, K. L., Wolfson, L. J., Watt, J. P., Henkle, E., Deloria-Knoll, M., McCall, N., et al. (2009). Burden of Disease Caused by *Streptococcus Pneumoniae* in Children Younger Than 5 Years: Global Estimates. *Lancet* 374 (9693), 893–902. doi: 10.1016/S0140-6736(09)61204-6
- Page, M. J., and Di Cera, E. (2008). Serine Peptidases: Classification, Structure and Function. *Cell Mol. Life Sci.* 65 (7–8), 1220–1236. doi: 10.1007/s00018-008-7565-9
- Pallen, M. J., and Wren, B. W. (1997). The HtrA Family of Serine Proteases. *Mol. Microbiol.* 26 (2), 209–221. doi: 10.1046/j.1365-2958.1997.5601928.x
- Patel, S. (2017). A Critical Review on Serine Protease: Key Immune Manipulator and Pathology Mediator. *Allergol. Immunopathol. (Madr)* 45 (6), 579–591. doi: 10.1016/j.aller.2016.10.011
- Pérez-Dorado, I., Galan-Bartual, S., and Hermoso, J. A. (2012). Pneumococcal Surface Proteins: When the Whole Is Greater Than the Sum of Its Parts. *Mol. Oral. Microbiol.* 27 (4), 221–245. doi: 10.1111/j.2041-1014.2012.00655.x
- Pérez-Dorado, I., González, A., Morales, M., Sanles, R., Striker, W., Vollmer, W., et al. (2010). Insights Into Pneumococcal Fratricide From the Crystal Structures of the Modular Killing Factor LytC. *Nat. Struct. Mol. Biol.* 17 (5), 576–581. doi: 10.1038/nsmb.1817
- Pestova, E. V., Hävarstein, L. S., and Morrison, D. A. (1996). Regulation of Competence for Genetic Transformation in *Streptococcus Pneumoniae* by an Auto-Induced Peptide Pheromone and a Two-Component Regulatory System. *Mol. Microbiol.* 21 (4), 853–862. doi: 10.1046/j.1365-2958.1996.501417.x
- Peter, A., Fatykhova, D., Kershaw, O., Gruber, A. D., Rueckert, J., Neudecker, J., et al. (2017). Localization and Pneumococcal Alteration of Junction Proteins in the Human Alveolar-Capillary Compartment. *Histochem. Cell. Biol.* 147, 6, 707–719. doi: 10.1007/s00418-017-1551-y
- Petersen, T. N., Brunak, S., von Heijne, G., and Nielsen, H. (2011). SignalP 4.0: Discriminating Signal Peptides From Transmembrane Regions. *Nat. Methods* 8 (10), 785–786. doi: 10.1038/nmeth.1701
- Peters, K., Schweizer, I., Hakenbeck, R., and Denapate, D. (2021). New Insights Into Beta-Lactam Resistance of *Streptococcus Pneumoniae*: Serine Protease HtrA Degrades Altered Penicillin-Binding Protein 2x. *Microorganisms* 9 (8). doi: 10.3390/microorganisms9081685
- Petit, C. M., Brown, J. R., Ingraham, K., Bryant, A. P., and Holmes, D. J. (2001). Lipid Modification of Prelipoproteins Is Dispensable for Growth *In Vitro* But Essential for Virulence in *Streptococcus Pneumoniae*. *FEMS Microbiol. Lett.* 200 (2), 229–233. doi: 10.1111/j.1574-6968.2001.tb10720.x
- Pettigrew, M. M., Marks, L. R., Kong, Y., Gent, J. F., Roche-Hakansson, H., and Hakansson, A. P. (2014). Dynamic Changes in the *Streptococcus Pneumoniae* Transcriptome During Transition From Biofilm Formation to Invasive Disease Upon Influenza A Virus Infection. *Infect. Immun.* 82 (11), 4607–4619. doi: 10.1128/iai.02225-14
- Pietrocola, G., Nobile, G., Rindi, S., and Speziale, P. (2017). *Staphylococcus Aureus* Manipulates Innate Immunity Through Own and Host-Expressed Proteases. *Front. Cell Infect. Microbiol.* 7, 166. doi: 10.3389/fcimb.2017.00166
- Poquet, I., Saint, V., Seznec, E., Simoes, N., Bolotin, A., and Gruss, A. (2000). HtrA Is the Unique Surface Housekeeping Protease in *Lactococcus Lactis* and Is Required for Natural Protein Processing. *Mol. Microbiol.* 35 (5), 1042–1051. doi: 10.1046/j.1365-2958.2000.01757.x
- Pracht, D., Elm, C., Gerber, J., Bergmann, S., Rohde, M., Seiler, M., et al. (2005). PavA of *Streptococcus Pneumoniae* Modulates Adherence, Invasion, and Meningeal Inflammation. *Infect. Immun.* 73 (5), 2680–2689. doi: 10.1128/iai.73.5.2680-2689.2005
- Pribyl, T., Moche, M., Dreisbach, A., Bijlsma, J. J., Saleh, M., Abdullah, M. R., et al. (2014). Influence of Impaired Lipoprotein Biogenesis on Surface and Exoproteome of *Streptococcus Pneumoniae*. *J. Proteome Res.* 13 (2), 650–667. doi: 10.1021/pr400768v
- Proctor, M., and Manning, P. J. (1990). Production of Immunoglobulin A Protease by *Streptococcus Pneumoniae* From Animals. *Infect. Immun.* 58 (9), 2733–2737. doi: 10.1128/iai.58.9.2733-2737.1990
- Punta, M., Coghill, P. C., Eberhardt, R. Y., Mistry, J., Tate, J., Boursnell, C., et al. (2012). The Pfam Protein Families Database. *Nucleic Acids Res.* 40 (Database issue), D290–D301. doi: 10.1093/nar/gkr1065
- Radziwill-Bienkowska, J. M., Robert, V., Drabot, K., Chain, F., Cherbuy, C., Langella, P., et al. (2017). Contribution of Plasmid-Encoded Peptidase S8 (PrtP) to Adhesion and Transit in the Gut of *Lactococcus Lactis* IBB477 Strain. *Appl. Microbiol. Biotechnol.* 101, 14, 5709–5721. doi: 10.1007/s00253-017-8334-1
- Rice, P., Longden, I., and Bleasby, A. (2000). EMBOS: The European Molecular Biology Open Software Suite. *Trends Genet.* 16 (6), 276–277. doi: 10.1016/s0168-9525(00)02024-2
- Riley, D. R., Angiuoli, S. V., Crabtree, J., Dunning Hotopp, J. C., and Tettelin, H. (2011). Using Sybil for Interactive Comparative Genomics of Microbes on the Web. *Bioinformatics* 28 (2), 160–166. doi: 10.1093/bioinformatics/btr652
- Rosenow, C., Ryan, P., Weiser, J. N., Johnson, S., Fontan, P., Ortqvist, A., et al. (1997). Contribution of Novel Choline-Binding Proteins to Adherence, Colonization and Immunogenicity of *Streptococcus Pneumoniae*. *Mol. Microbiol.* 25 (5), 819–829. doi: 10.1111/j.1365-2958.1997.mmi494.x
- Ruiz-Perez, F., and Nataro, J. P. (2014). Bacterial Serine Proteases Secreted by the Autotransporter Pathway: Classification, Specificity, and Role in Virulence. *Cell Mol. Life Sci.* 71 (5), 745–770. doi: 10.1007/s00018-013-1355-8
- Sanz, J. M., Diaz, E., and Garcia, J. L. (1992). Studies on the Structure and Function of the N-Terminal Domain of the Pneumococcal Murein Hydrolases. *Mol. Microbiol.* 6 (7), 921–931. doi: 10.1111/j.1365-2958.1992.tb01542.x
- Schmidt, T. P., Goetz, C., Huemer, M., Schneider, G., and Wessler, S. (2016). Calcium Binding Protects E-Cadherin From Cleavage by *Helicobacter Pylori* HtrA. *Gut Pathog.* 8 (1), 29. doi: 10.1186/s13099-016-0112-6
- Schrödinger, Release 2020-4: MacroModel, Schrödinger, LLC, New York, NY, 2020.
- Sebert, M. E., Palmer, L. M., Rosenberg, M., and Weiser, J. N. (2002). Microarray-Based Identification of HtrA, a *Streptococcus Pneumoniae* Gene That Is Regulated by the CiaRH Two-Component System and Contributes to Nasopharyngeal Colonization. *Infect. Immun.* 70 (8), 4059–4067. doi: 10.1128/iai.70.8.4059-4067.2002
- Sender, V., Hentrich, K., Pathak, A., Tan Qian Ler, A., Embaie, B. T., Lundström, S. L., et al. (2020). Capillary Leakage Provides Nutrients and Antioxidants for Rapid Pneumococcal Proliferation in Influenza-Infected Lower Airways. *Proc. Natl. Acad. Sci.* 117 (49), 31386–31397. doi: 10.1073/pnas.2012265117
- Seol, J. H., Woo, S. K., Jung, E. M., Yoo, S. J., Lee, C. S., Kim, K. J., et al. (1991). Protease Do Is Essential for Survival of *Escherichia Coli* at High Temperatures: Its Identity With the htrA Gene Product. *Biochem. Biophys. Res. Commun.* 176 (2), 730–736. doi: 10.1016/s0006-291x(05)80245-1
- Siezen, R. J. (1999). Multi-Domain, Cell-Envelope Proteinases of Lactic Acid Bacteria. *Antonie Van Leeuwenhoek* 76 (1–4), 139–155. doi: 10.1023/A:1002036906922
- Singh, K. H., Yadav, S., Kumar, D., and Biswal, B. K. (2018). The Crystal Structure of an Essential High-Temperature Requirement Protein HtrA1 (Rv1223) From *Mycobacterium Tuberculosis* Reveals Its Unique Features. *Acta Crystallogr. D Struct. Biol.* 74 (Pt 9), 906–921. doi: 10.1107/s205979831800952x
- Song, J. Y., Nahm, M. H., and Moseley, M. A. (2013). Clinical Implications of Pneumococcal Serotypes: Invasive Disease Potential, Clinical Presentations, and Antibiotic Resistance. *J. Korean Med. Sci.* 28 (1), 4–15. doi: 10.3346/jkms.2013.28.1.4
- Spies, C., Beil, A., and Ehrmann, M. (1999). A Temperature-Dependent Switch From Chaperone to Protease in a Widely Conserved Heat Shock Protein. *Cell* 97 (3), 339–347. doi: 10.1016/s0092-8674(00)80743-6
- Tegtmeier, N., Wessler, S., Necchi, V., Rohde, M., Harrer, A., Rau, T. T., et al. (2017). *Helicobacter Pylori* Employs a Unique Basolateral Type IV Secretion Mechanism for CagA Delivery. *Cell Host Microbe* 22 (4), 552–560.e555. doi: 10.1016/j.chom.2017.09.005
- Tettelin, H., Nelson, K. E., Paulsen, I. T., Eisen, J. A., Read, T. D., Peterson, S., et al. (2001). Complete Genome Sequence of a Virulent Isolate of *Streptococcus Pneumoniae*. *Science* 293 (5529), 498–506. doi: 10.1126/science.1061217
- Thibodeaux, B. A., Caballero, A. R., Marquart, M. E., Tommassen, J., and O'Callaghan, R. J. (2007). Corneal Virulence of *Pseudomonas Aeruginosa* Elastase B and Alkaline Protease Produced by *Pseudomonas Putida*. *Curr. Eye Res.* 32 (4), 373–386. doi: 10.1080/02713680701244181
- Thurlow, L. R., Thomas, V. C., Narayanan, S., Olson, S., Fleming, S. D., and Hancock, L. E. (2010). Gelatinase Contributes to the Pathogenesis of Endocarditis Caused by *Enterococcus Faecalis*. *Infect. Immun.* 78 (11), 4936–4943. doi: 10.1128/iai.01118-09

- Tomasz, A. (1967). Choline in the Cell Wall of a Bacterium: Novel Type of Polymer-Linked Choline in *Pneumococcus*. *Science* 157 (3789), 694–697. doi: 10.1126/science.157.3789.694
- Tsui, H. C., Keen, S. K., Sham, L. T., Wayne, K. J., and Winkler, M. E. (2011). Dynamic Distribution of the SecA and SecY Translocase Subunits and Septal Localization of the HtrA Surface Chaperone/Protease During *Streptococcus Pneumoniae* D39 Cell Division. *mBio* 2 (5). doi: 10.1128/mBio.00202-11
- UNICEF. (2006). *Pneumonia: The Forgotten Killer Of Children* (New York, NY, USA: United Nations Children's Emergency Fund).
- von Schillde, M. A., Hörmannspurger, G., Weiher, M., Alpert, C. A., Hahne, H., Bäuerl, C., et al. (2012). Lactocapsin Secreted by *Lactobacillus* Exerts Anti-Inflammatory Effects by Selectively Degrading Proinflammatory Chemokines. *Cell Host Microbe* 11 (4), 387–396. doi: 10.1016/j.chom.2012.02.006
- Voss, S., Gamez, G., and Hammerschmidt, S. (2012). Impact of Pneumococcal Microbial Surface Components Recognizing Adhesive Matrix Molecules on Colonization. *Mol. Oral. Microbiol.* 27 (4), 246–256. doi: 10.1111/j.2041-1014.2012.00654.x
- Vos, P., van Asseldonk, M., van Jeveren, F., Siezen, R., Simons, G., and de Vos, W. M. (1989). A Maturation Protein Is Essential for Production of Active Forms of *Lactococcus Lactis* SK11 Serine Proteinase Located in or Secreted From the Cell Envelope. *J. Bacteriol.* 171 (5), 2795–2802. doi: 10.1128/jb.171.5.2795-2802.1989
- Wani, J. H., Gilbert, J. V., Plaut, A. G., and Weiser, J. N. (1996). Identification, Cloning, and Sequencing of the Immunoglobulin A1 Protease Gene of *Streptococcus Pneumoniae*. *Infect. Immun.* 64 (10), 3967–3974. doi: 10.1128/iai.64.10.3967-3974.1996
- Waterhouse, A. M., Procter, J. B., Martin, D. M., Clamp, M., and Barton, G. J. (2009). Jalview Version 2—a Multiple Sequence Alignment Editor and Analysis Workbench. *Bioinformatics* 25 (9), 1189–1191. doi: 10.1093/bioinformatics/btp033
- Weiser, J. N., Ferreira, D. M., and Paton, J. C. (2018). *Streptococcus Pneumoniae*: Transmission, Colonization and Invasion. *Nat. Rev. Microbiol.* 16 (6), 355–367. doi: 10.1038/s41579-018-0001-8
- Wessler, S., Schneider, G., and Backert, S. (2017). Bacterial Serine Protease HtrA as a Promising New Target for Antimicrobial Therapy? *Cell Commun. Signal* 15 (1):4. doi: 10.1186/s12964-017-0162-5
- Wexler, D. E., Chenoweth, D. E., and Cleary, P. P. (1985). Mechanism of Action of the Group A Streptococcal C5a Inactivator. *Proc. Natl. Acad. Sci.* 82 (23), 8144–8148. doi: 10.1073/pnas.82.23.8144
- Wilken, C., Kitzing, K., Kurzbauer, R., Ehrmann, M., and Clausen, T. (2004). Crystal Structure of the DegS Stress Sensor: How a PDZ Domain Recognizes Misfolded Protein and Activates a Protease. *Cell* 117 (4), 483–494. doi: 10.1016/s0092-8674(04)00454-4
- Wizemann, T. M., Heinrichs, J. H., Adamou, J. E., Erwin, A. L., Kunsch, C., Choi, G. H., et al. (2001). Use of a Whole Genome Approach to Identify Vaccine Molecules Affording Protection Against *Streptococcus Pneumoniae* Infection. *Infect. Immun.* 69 (3), 1593–1598. doi: 10.1128/IAI.69.3.1593-1598.2001
- Wu, K. J., Boutte, C. C., Ioerger, T. R., and Rubin, E. J. (2019). *Mycobacterium Smegmatis* HtrA Blocks the Toxic Activity of a Putative Cell Wall Amidase. *Cell Rep.* 27 (8), 2468–2479.e2463. doi: 10.1016/j.celrep.2018.12.063
- Xue, R. Y., Liu, C., Xiao, Q. T., Sun, S., Zou, Q. M., and Li, H. B. (2021). HtrA Family Proteases of Bacterial Pathogens: Pros and Cons for Their Therapeutic Use. *Clin. Microbiol. Infect.* 559–564. doi: 10.1016/j.cmi.2020.12.017
- Xu, Y., Li, X., Li, R., Li, S., Ni, H., Wang, H., et al. (2014). Structure of the Nisin Leader Peptidase NisP Revealing a C-Terminal Autocleavage Activity. *Acta Crystallogr. D Biol. Crystallogr.* 70 (Pt 6), 1499–1505. doi: 10.1107/s1399004714004234
- Yang, M., Derbyshire, M. K., Yamashita, R. A., and Marchler-Bauer, A. (2020). NCBI's Conserved Domain Database and Tools for Protein Domain Analysis. *Curr. Protoc. Bioinform.* 69 (1), e90. doi: 10.1002/cpbi.90
- Yother, J., and White, J. M. (1994). Novel Surface Attachment Mechanism of the *Streptococcus Pneumoniae* Protein PspA. *J. Bacteriol.* 176 (10), 2976–2985. doi: 10.1128/jb.176.10.2976-2985.1994
- Yu, N. Y., Laird, M. R., Spencer, C., and Brinkman, F. S. (2011). PSORTdb—an Expanded, Auto-Updated, User-Friendly Protein Subcellular Localization Database for Bacteria and Archaea. *Nucleic Acids Res.* 39 (Database issue), D241–D244. doi: 10.1093/nar/gkq1093
- Zarzecka, U., Grinzato, A., Kandiah, E., Cysewski, D., Berto, P., Skorko-Glonek, J., et al. (2020). Functional Analysis and Cryo-Electron Microscopy of *Campylobacter Jejuni* Serine Protease HtrA. *Gut Microbes* 12 (1), 1–16. doi: 10.1080/19490976.2020.1810532
- Zarzecka, U., Harrer, A., Zawilak-Pawlik, A., Skorko-Glonek, J., and Backert, S. (2019). Chaperone Activity of Serine Protease HtrA of *Helicobacter Pylori* as a Crucial Survival Factor Under Stress Conditions. *Cell. Commun. Signal.* 17, 1, 161. doi: 10.1186/s12964-019-0481-9
- Zawilak-Pawlik, A., Zarzecka, U., Żyła-Uklejiewicz, D., Lach, J., and Strapagiel, D. (2019). Establishment of Serine Protease htrA Mutants in *Helicobacter Pylori* Is Associated With secA Mutations. *Sci. Rep.* 9, 1, 11794. doi: 10.1038/s41598-019-48030-6
- Zdobnov, E. M., and Apweiler, R. (2001). InterProScan—an Integration Platform for the Signature-Recognition Methods in InterPro. *Bioinformatics* 17 (9), 847–848. doi: 10.1093/bioinformatics/17.9.847
- Zysk, G., Bongaerts, R. J., ten Thoren, E., Bethe, G., Hakenbeck, R., and Heinz, H. P. (2000). Detection of 23 Immunogenic Pneumococcal Proteins Using Convalescent-Phase Serum. *Infect. Immun.* 68 (6), 3740–3743. doi: 10.1128/iai.68.6.3740-3743.2000

Conflict of Interest: The authors declare that the research was conducted in the absence of any commercial or financial relationships that could be construed as a potential conflict of interest.

Publisher's Note: All claims expressed in this article are solely those of the authors and do not necessarily represent those of their affiliated organizations, or those of the publisher, the editors and the reviewers. Any product that may be evaluated in this article, or claim that may be made by its manufacturer, is not guaranteed or endorsed by the publisher.

Copyright © 2021 Ali, Kohler, Schulig, Burchhardt and Hammerschmidt. This is an open-access article distributed under the terms of the Creative Commons Attribution License (CC BY). The use, distribution or reproduction in other forums is permitted, provided the original author(s) and the copyright owner(s) are credited and that the original publication in this journal is cited, in accordance with accepted academic practice. No use, distribution or reproduction is permitted which does not comply with these terms.



Streptococcus pneumoniae: a Plethora of Temperate Bacteriophages With a Role in Host Genome Rearrangement

Antonio J. Martín-Galiano¹ and Ernesto García^{2,3*}

¹ Intrahospital Infections Laboratory, National Centre for Microbiology, Instituto de Salud Carlos III (ISCIII), Majadahonda, Spain, ² Departamento de Biotecnología Microbiana y de Plantas, Centro de Investigaciones Biológicas Margarita Salas (CSIC), Madrid, Spain, ³ Centro de Investigación Biomédica en Red de Enfermedades Respiratorias (CIBERES), Madrid, Spain

OPEN ACCESS

Edited by:

Xueqing Wu,
Zhejiang University, China

Reviewed by:

Jeremy Brown,
University College London,
United Kingdom

Jorge Moura de Sousa,
Institut Pasteur, France
Yujiro Hirose,
Osaka University, Japan

*Correspondence:

Ernesto García
e.garcia@cib.csic.es

Specialty section:

This article was submitted to
Molecular Bacterial Pathogenesis,
a section of the journal
Frontiers in Cellular and
Infection Microbiology

Received: 13 September 2021

Accepted: 29 October 2021

Published: 18 November 2021

Citation:

Martín-Galiano AJ and García E (2021)
*Streptococcus pneumoniae: a
Plethora of Temperate
Bacteriophages With a Role in
Host Genome Rearrangement.*
Front. Cell. Infect. Microbiol. 11:775402.
doi: 10.3389/fcimb.2021.775402

Bacteriophages (phages) are viruses that infect bacteria. They are the most abundant biological entity on Earth (current estimates suggest there to be perhaps 10^{31} particles) and are found nearly everywhere. Temperate phages can integrate into the chromosome of their host, and prophages have been found in abundance in sequenced bacterial genomes. Prophages may modulate the virulence of their host in different ways, e.g., by the secretion of phage-encoded toxins or by mediating bacterial infectivity. Some 70% of *Streptococcus pneumoniae* (the pneumococcus)—a frequent cause of otitis media, pneumonia, bacteremia and meningitis—isolates harbor one or more prophages. In the present study, over 4000 *S. pneumoniae* genomes were examined for the presence of prophages, and nearly 90% were found to contain at least one prophage, either defective (47%) or present in full (43%). More than 7000 complete putative integrases, either of the tyrosine (6243) or serine (957) families, and 1210 full-sized endolysins (among them 1180 enzymes corresponding to 318 amino acid-long *N*-acetylmuramoyl-L-alanine amidases [LytA_{PPH}]) were found. Based on their integration site, 26 different pneumococcal prophage groups were documented. Prophages coding for tRNAs, putative virulence factors and different methyltransferases were also detected. The members of one group of diverse prophages (PPH090) were found to integrate into the 3' end of the host *lytA_{Spn}* gene encoding the major *S. pneumoniae* autolysin without disrupting it. The great similarity of the *lytA_{Spn}* and *lytA_{PPH}* genes (85–92% identity) allowed them to recombine, *via* an apparent integrase-independent mechanism, to produce different DNA rearrangements within the pneumococcal chromosome. This study provides a complete dataset that can be used to further analyze pneumococcal prophages, their evolutionary relationships, and their role in the pathogenesis of pneumococcal disease.

Keywords: *Streptococcus pneumoniae*, prophage, integrase, endolysin, lytic enzymes, tRNAs, virulence factors, genomic rearrangements

INTRODUCTION

Bacteriophages (phages) are viruses that infect bacteria. They are the most abundant biological entities on Earth — current estimates suggest there to be close to 10^{31} phage particles (Mushegian, 2020) — and can be found nearly everywhere. Temperate bacteriophages infect and kill bacteria to release phage progeny, but on occasion they may integrate into the host genome *via* site-specific recombination events, and replicate vertically. Integrated phages are stably maintained in the chromosome (i.e., as a prophage) in a state known as lysogeny (Lwoff, 1953). Campbell (1962) was the first to propose a model for the integration of λ prophage into the bacterial chromosome. This model consists of two phases: (1) the circularization of the linear phage DNA molecule injected into the cell, and (2) the linear insertion of the phage DNA into the bacterial chromosome *via* the activity of a specific integrase (Int) that catalyzes the site-specific recombination of the phage attachment site (*attP*) and bacterial attachment site (*attB*). These two sequences generally share a short stretch of identical bases (the core sequence) where this site-specific recombination occurs. After recombination, the phage genome is left integrated into the bacterial chromosome, flanked by two duplicated hybrid *att* sites: *attL* and *attR*. Under certain circumstances (prophage induction), the prophage becomes excised from the bacterial chromosome and viral replication begins *via* the lytic cycle.

Endolysins are phage-encoded enzymes capable of hydrolyzing the bacterial cell wall; they are synthesized at the end of the lytic cycle to allow the release of phage progeny. In this era of global increase in antibacterial resistance, endolysins are being tested as an alternative (or complement) to the use of antibiotics (for recent reviews see Vázquez et al., 2018; Fernández et al., 2021; Murray et al., 2021). It is well documented that, while integrated into the host genome, genes encoding Ints and endolysins are located at either end of *Streptococcus* prophages (Canchaya et al., 2003).

Prophages are often found in sequenced bacterial genomes. Indeed, nearly half of bacterial genomes appear to contain at least one prophage. The minimum doubling time is the trait most strongly correlated with lysogeny, followed by genome size and, interestingly, pathogenicity (Touchon et al., 2016).

Streptococcus pneumoniae (the pneumococcus) is a major human pathogen and a frequent cause of non-invasive diseases such as otitis, conjunctivitis and pneumonia, but also life-threatening invasive sepsis, bacteremic pneumonia, and meningitis. Pneumococcal pneumonia ranks first in terms of associated mortality among all lower respiratory tract diseases,

and is responsible for more than one million deaths every year (GBD 2016 Lower Respiratory Infections Collaborators, 2018). That prophages may contribute to bacterial virulence is well established, particularly in *Pseudomonas aeruginosa*, *Salmonella enterica*, *Escherichia coli*, *Vibrio cholerae*, *Staphylococcus* spp., and *Clostridium* spp. (Schroven et al., 2021). Prophages can alter the phenotype of their hosts at different levels, e.g., by causing them to secrete toxins, by modifying the bacterial envelope, and/or impacting bacterial infectivity and bacterial cell regulation.

High-throughput next generation sequencing techniques have now provided numerous *de novo* sequenced and assembled bacterial genomes, and over 8000 pneumococcal genomes are currently included in the NCBI Reference Sequence Database (RefSeq) database. However, while first reported in 1977 and suggested to be widespread (Bernheimer, 1977; Ramirez et al., 1999), pneumococcal prophages (PPHs) have remained relatively unexamined — that is until recently (García et al., 2005). Based on comparisons of complete prophages and their predicted encoded proteins, PPHs have been grouped into three major groups with only a small number of prophages falling outside these classes (Romero et al., 2009a; Romero et al., 2009b). More recently, pairwise comparisons of prophage sequences showed four major prophage clusters and one single prophage (Brueggemann et al., 2017). Phages belonging to the same phylogenetic group share high sequence similarity in their packaging, morphology, and lysis modules, and are typically associated with one or two main integrase types. Besides, incomplete pneumococcal prophages can be highly conserved over long periods of time and clustered into five major groups that differed from those of intact PPHs (Rezaei Javan et al., 2019).

In 2017, a pan-genome-wide association study identified PPHs as being associated with reduced pneumococcal carriage duration, although this was attributed more to the disruption caused by the integration of the phage genome and the genetic transformation competence system than to any property of the prophage itself (Lees et al., 2017). Other data have shown that a role for prophages in pneumococcal virulence and patient mortality is linked to *PblA* and/or *PblB*, two prophage-encoded proteins known to be involved in enhanced platelet activation together with higher formation of platelet-monocyte complexes (Tunjungputri et al., 2017). Prophages may naturally enter the lytic cycle, or be induced to do so *via* exposure to fluoroquinolones (López et al., 2014) (with a concomitant increase in *PblA/PblB* expression). A recent study involving patients with invasive pneumococcal disease determined that the 30-day mortality of pneumococcal meningitis was 11% in *pblB*-positive patients compared to <1% in *pblB*-negative patients, although the authors recognize that this finding does not prove causality (Cremers et al., 2019). It has also recently been suggested that incomplete PPHs and certain prophage genes may be involved in pneumococcal pathogenesis (Rezaei Javan et al., 2019). In addition, transcriptomic analyses have shown that a defective PPH may serve as a switch that controls the expression of a bacterial gene (*ychF*) located immediately downstream of the prophage *int* gene that is involved in nasopharyngeal colonization (Chen et al., 2019). A review is

Abbreviations: aa, amino acid(s); CHAP, a cysteine, histidine-dependent amidohydrolase/peptidase domain; csRNA, cia-dependent small RNA; GPSCs, Global Pneumococcal Sequence Clusters; Int, integrase; IS, insertion sequence; *lytA_{Spp}*, gene coding for the major pneumococcal autolysin; *lytA_{PPH}*, phage gene encoding a NAM-amidase of the *Amidase_2* family; NAM-amidase, N-acetylmuramoyl-L-alanine amidase; NCBI, National Center for Biotechnology Information; Mtase, DNA methyltransferase; NT, non-typeable; PMEN, Pneumococcal Molecular Epidemiology Network; PPH, pneumococcal prophage; RefSeq, NCBI Reference Sequence Database; R-M, restriction-modification; ST, sequence type.

available on the recent advances in the genomic and functional characterization of pneumococcal temperate phages, and their contribution to pneumococcal pathogenesis and genome evolution (Garriss and Henriques-Normark, 2020).

In the present study, the genomic sequences of over 4000 *S. pneumoniae* isolates from diverse lineages were examined to obtain the broadest possible picture of PPH diversity. The precise integration sites and the *att* core sequences of most of them were elucidated and used to identify the families to which a number of previously reported but incompletely studied PPHs belong. In addition, recombination between prophage and host *lytA* genes is shown to be an important source of chromosomal rearrangement in *S. pneumoniae*.

MATERIALS AND METHODS

Compilation of the Pneumococcal Genome Dataset

This study was performed using a dataset mined from the National Center for Biotechnology Information (NCBI) database (available at <https://www.ncbi.nlm.nih.gov/genome/?term=Streptococcus+pneumoniae>). The latter contains whole-genome sequences (assembled or otherwise) for more than 8500 pneumococcal genomes (last accessed January 30, 2021). Sequence types (STs) (Enright and Spratt, 1998; Jolley et al., 2018) of the strains included in the dataset were determined on the basis of whole genome sequencing data (Larsen et al., 2012).

Search for Pneumococcal Prophages

To detect PPHs, the dataset was searched, using the BLAST platform (Johnson et al., 2008), for homologs of *int*- and *lytA*_{PPH}-like genes encoding (respectively) Ints and endolysins [with respect to the latter, only *N*-acetylmuramoyl-L-alanine amidases (NAM-amidases; EC 3.5.1.28) of the *Amidase_2* family (Pfam database identifier: PF01510) (Morales et al., 2010) are currently known]. The corresponding genes/proteins of previously characterized PPHs, such as MM1 (Obregón et al., 2003a), ϕ Spn_OXC, ϕ Spn_6, and ϕ Spn_18 (Romero et al., 2009a), and others (Cámara et al., 2018). The endolysins encoded by various virulent pneumococcal phages (see below) were used as query sequences. The original and newly found genes/proteins with a coverage $\geq 90\%$ and $\geq 50\%$ identity were used in searches in an iterative manner.

Bioinformatic Analyses

Sequence comparison and alignments were performed using the BLAST platform and/or Clustal Omega package (Sievers and Higgins, 2021) running at the European Bioinformatics Institute (EMBL-EBI) website (<https://www.ebi.ac.uk>). Potential tRNAs genes were identified using ARAGORN (Laslett and Canback, 2004) and tRNAscan-SE (Schattner et al., 2005) software. Detections were recorded only when both programs coincided in the results returned. The codon usage of *S. pneumoniae* D39 was obtained from the corresponding database (Nakamura et al., 2000). Protein domains were preliminarily identified using

CDD/SPARCLE (Lu et al., 2020). PHASTER (running at <https://phaster.ca/>) was also employed to identify phage-homologous regions in bacterial genomes (Arndt et al., 2016). To ascertain equivalent detection of protein datasets, open reading frames were identified and translated from prophage sequences using Prodigal v2.6.3 (Hyatt et al., 2010). Prophage proteomes were then compared all against all through the calculation of the weighted gene repertoire relatedness (wGRR) (Pfeifer et al., 2021). Best bi-directional hits were found from hits detected by the 'easy-search' workflow of MMseqs2 (Mirdita et al., 2019) with *e*-value $< 10^{-4}$, identity $\geq 35\%$, coverage $\geq 50\%$ thresholds. Agglomerative hierarchical clustering from the resulting wGRR matrix was carried out by the *linkage* tool of the *scipy.cluster.hierarchy* python library using the 'ward' method on euclidean distances.

RESULTS

Temperate Bacteriophages Are Abundant in *S. pneumoniae*

The dataset produced contained 4003 strains, including 126 whose genomes were sequenced to complete or near-complete (chromosome) assembly level and deposited in the RefSeq database (O'Leary et al., 2016) (last accessed, October 11, 2020) (labeled in green in **Table S1**). The strains included in the dataset represent 447 different STs. Moreover, up to 50% of the strains belonged to one of 35 (out of a possible 43) Pneumococcal Molecular Epidemiology Network (PMEN) clones [including single and double locus variants (McGee et al., 2001)]. PMEN clones are resistant to one or more antibiotics in wide clinical use and dominate the population of antibiotic-resistant pneumococci. Globally susceptible clones known to be important in disease are also included in the PMEN clone dataset (<https://www.pneumogen.net/pmen/>, last accessed September 15, 2020). Further, 2557 strains in the dataset were assigned to one of the 169 Global Pneumococcal Sequence Clusters (GPSCs) and, among these strains, 1096 could be classified as belonging to one of the 35 dominant GPSCs (Gladstone et al., 2019). From a total of 46 serogroups (numbered 1–48) described to date (numbers 26 and 30 are not in use) (Lund and Henrichsen, 1978), 3573 strains belonged to one of 40 serogroups. In addition, the dataset included 4 non-encapsulated laboratory mutants and 426 non-typeable (NT) isolates (**Table S1**).

In agreement with data reported in previous studies (Ramirez et al., 1999; Brueggemann et al., 2017), PPHs were seen to be widely distributed across different *S. pneumoniae* isolates. Indeed, only 434 strains in the dataset (10.8%) (highlighted with a red background in **Table S1**) appeared to lack temperate phages. In addition, among the 126 RefSeq strains with complete (or near complete) genomes (see above), only 26 (20.6%) lacked any discernible prophage. On the basis of their Ints, more than 7000 putative PPHs (including putatively full-length and partial prophage sequences) were found in the dataset. Visual inspection of bacterial genes flanking the

prophages revealed up to 26 different integration sites (**Table 1**). PPHs were clustered into 26 groups [named from PPH005 to PPH130 (in steps of 5)] according to their purported insertion sites, and arranged in order using the genome of the non-lysogenic *S. pneumoniae* D39 (Acc. No. NC_008533.2) as a reference. It is worth noting that many more complete Ints (7234) than endolysins (1210) could be identified. In addition, the proportion of partial sequences was much higher for the endolysin genes than the Ints genes. Thus, 42% of the endolysins were found incomplete (887 incomplete out of 2097 total proteins), whereas only 7% of the Ints were apparently incomplete or partly deleted (548 out of a total of 7782) (**Table 1**). This might be because endolysin-coding genes are among those known to be difficult to assemble from short read data due to the presence of choline-binding motif clusters (Croucher et al., 2017).

In sharp contrast to the moderate number of endolysins compared to Ints in the current dataset, the number of different PPH endolysin alleles (362) was similar to that of the Int alleles (293). This strongly suggests that the PPH endolysin-coding gene

shows great genetic variability. Nevertheless, 11 PPH groups, namely 005, 020, 025, 030, 045, 055, 060, 070, 095, 110, and 115, appeared to completely lack an endolysin gene and thus were understood to represent incomplete (or defective) prophages. Taking into account the number of full Ints, these incomplete prophages correspond to nearly half (47%) of the total PPHs.

PPH Integrases

On the basis of amino acid (aa) sequence similarities and catalytic residues, site-specific Ints (recombinases) can be classified into two major families: the tyrosine or serine families (Groth and Calos, 2004). These have different structures and functional mechanisms indicating that they have evolved separately. Thus, serine Ints are usually larger than tyrosine Ints, and the aa residues important for catalysis and structure, as well as their locations, can be very different. For example, the N-terminal domain of tyrosine Ints is involved in binding the arm-type sites of *attP* and the C-terminal domains involved in catalysis, whereas in serine Ints the opposite is true (Groth and Calos, 2004; Van Duyne and Rutherford, 2013).

TABLE 1 | Number and distribution of integrases and endolysins in the pneumococcal prophages (PPHs) analyzed.

PPH group	Integrases					Endolysins			
	No. ^a	Alleles (No.)	Size (aa)	Identity (%)	Incomplete	No.	Alleles (No.)	Size (aa)	Incomplete
005	1090 (21)	34	388	>86.5	196				
010	938 (35)	35	382	>95.8	21	286	86	318	102
015	486 (25)	30	380	>96.8	265	60	32	318	457
020	40 (4)	3	388	>58.6 ^b	0				
025	1 (1)	1	388	–	0				
030	1151 (25)	17	388	>95.8	52				
035	1 (1)	1	382	–	0	1	1	318	0
040	1 (1)	1	375	–	0	1	1	318	0
045	674 (10)	16	406	>70.0 ^c	1				
050	1 (1)	1	375	–	0	1	1	318	0
055	121 (3)	6	388	>98.9	4				
060	5 (2)	2	405	>99.5	0				
065	20 (3)	3	380	>99.4	0	22 ^d	1	314	0
070	170 (11)	5	387	>98.7	0				
075	1 (1)	1	375	–	0	1	1	318	0
080	1376 (22)	61	375	>96.7	7	586	165	318	180
						1 ^e	1	288	0
085	70 (3)	8	475	>99.1	0	10	9	318	13
090	34 (5)	18	375–481	>17.3	2	6	5	318	4
095	4 (1)	1	388	–	0				
100	885 (5)	56	481	>94.3	1	220	71	318	131
105	6 (1)	4	381	>95.7	0	6 ^d	4	334	0
110	47 (1)	3	388	>99.4	0				
115	109 (4)	7	388	>98.1	1				
120	1 (1)	1	479	–	0	1 ^f	1	328	0
125	1 (1)	1	475	–	0	7	5	318	0
130	1 (1)	1	382	–	0	1	1	318	0
		(316)					(385)		
Total	7234 (189)	293 ^g			548	1210	362 ^h		887

^aFigures in parentheses correspond to the number of integrases found in 100 complete genomes (176) and 13 contigs of different isolates (13).

^bAlleles WP_001866856 and WP_033705527 are 99.7% identical.

^cAmino acid identity reached >89.1% when allele WP_050271463 was excluded from alignments.

^dLysozyme (= muramidase; EC 3.2.1.17) of the Glyco_hydro_25 (PF01183) family instead of NAM-amidase.

^ePutative NAM-amidase, but with a cysteine, histidine-dependent amidohydrolase/peptidase (CHAP; PF05257) domain.

^fPutative NAM-amidase but with a divergent Amidase_2 domain.

^gDue to allele redundancy between different PPH groups, the actual number of Int alleles is 293 rather than 315.

^hCorresponds to different prophage-encoded endolysins (357 NAM-amidases plus 5 muramidases).

Table S2 shows the complete catalog of the Ints found in this study. Excluding the prophages of the PPH090 group, which will be analyzed separately, only three Ints were found in more than one PPH group. These corresponded to the most frequent type of each group, i.e., WP_00876735 (in PPH010 and PPH130), WP_00266847 (in PPH040, PPH075, and PPH080), and WP_000704678 (in PPH055, PPH095, and PPH110). This observation agrees with the common idea that strong (albeit not absolute) specificity exists between prophage Ints and *attB/attP* sequences. For example, it has long been recognized that Int-mediated recombination occurs between *attP* of phage λ and the secondary attachment sites in the host genome, although the frequency is low (Shimada et al., 1975). In the present work, sequence identities between Ints were usually >90% within each PPH group. The PPHs contained either tyrosine or serine Ints, although PPHs with tyrosine Ints were 6.5 times more common (6243) than the latter (957) in the dataset (the Ints of PPH090 were not taken into account) (**Table 2**). Serine Ints (groups PPH085, PPH100, PPH120, and PPH125) were much more similar to each other than were the tyrosine Ints (**Table 3**). Among the tyrosine Ints, those from groups PPH010/PPH130 and PPH035 diverged greatly from the rest.

PPH Endolysins

Endolysins encoded by virulent (lytic) phages infecting *S. pneumoniae* have been extensively reviewed (López and García,

2004; García et al., 2005; Galán-Bartual et al., 2015; Maestro and Sanz, 2016; Vázquez et al., 2018). Briefly, three biochemically and structurally different peptidoglycan hydrolases of phage origin have been described so far. Two of them are choline-binding proteins: the NAM-amidase Pal (YP_004306947; 296 aa), with an *Amidase_5* domain (PF05382), and the Cpl-1 lysozyme (=muramidase) (NP_044837; 339 aa) with a *Glyco_hydro_25* (PF01183) domain. Both enzymes contain a C-terminal cell wall-binding domain composed of six choline-binding repeats (*Choline_bind_1*; PF01473). Cpl-7 (YP_009623604; 342 aa) is a choline-independent muramidase that differs from Cpl-1 in the C-terminal domain responsible for peptidoglycan binding (CW_7 repeats; PF08230). Pal is encoded by phage Dp-1, whereas Cpl-1 and Cpl-7 are the endolysins of phages Cp-1 and Cp-7, respectively. The endolysin from a recently isolated virulent podovirus very similar to Cp-1 (SOCP) (Ouennane et al., 2015) (NP_044837; 339 aa), is a muramidase 100% identical to Cpl-1. Similarly, the NAM-amidase (AQY55407; 295 aa) of the MS1 pneumococcal siphovirus (Kot et al., 2017; Silva et al., 2020) is 81% identical (89% similar) to Pal.

Taking into account that only a few virulent *S. pneumoniae*-infecting phages have been currently isolated, the diversity of their endolysins contrasts with the lytic enzymes encoded by PPHs. The latter are 318 aa-long, belong to the *Amidase_2* family (PF01510) of NAM-amidases, and contain six *Choline_bind_1*

TABLE 2 | Active site residues of PPH tyrosine and serine recombinases^a.

Name (amino acid residues)	Amino acid residue and position															
Tyrosine integrases ^b																
λ Int (356)	R212	D215	K235	H308	R311	H333	Y342									
PPH005 (388)	R220	E223	K255	H315	R318	H353	Y363									
PPH010/PPH130 (382)	R212	D215	K252	H327	R330	H353	Y362									
PPH015 (380)	R218	E221	K255	H324	R327	H350	Y360									
PPH020 (388)	R223	E226	K258	H330	R333	H356	Y366									
PPH025 (388)	R220	E223	K255	H327	R330	H353	Y363									
PPH030 (388)	R223	E226	K258	H330	R333	H356	Y366									
PPH035 (382)	R220	D223	K252	H327	R330	H353	Y362									
PPH040/PPH075/PPH080 (375)	R211	E214	K247	H320	R323	H346	Y356									
PPH045 (406)	R234	E237	K269	H349	R352	H375	Y384									
PPH050 (375)	R211	E214	K247	H320	R323	H346	Y356									
PPH055/PPH095/PPH110 (388)	R220	E223	K255	H327	R330	H353	Y363									
PPH060 (405)	R234	E237	K269	H349	R352	H375	Y384									
PPH065 (380)	R217	E219	K249	H326	R329	H352	Y362									
PPH070 (387)	R222	E235	K257	H329	R332	H355	Y365									
PPH105 (381)	R208	E211	K246	H323	R326	H349	Y359									
PPH115 (388)	R220	E223	K255	H327	R330	H353	Y363									
Serine integrases ^c																
TP901-1 Int (485)	Y8	R10	S12	Q26	V41	D47	R57	P58	D73	V77	D81	R82	L83	R85	G119	E133
PPH085 (475)	Y10	R12	S14	Q28	I43	D49	R59	P60	D75	V79	D83	R84	L85	R87	G121	E135
PPH100 (481)	Y10	R12	S14	Q28	V43	D49	R59	P60	D75	V79	D83	R84	L85	R87	G121	E135
PPH120 (479)	Y7	R9	S11	Q25	I40	D46	R56	P57	N72	V76	K80	R81	L82	R84	G118	D132
PPH125 (475)	Y10	R12	S14	Q28	I43	D49	R59	P60	D75	V79	D83	R84	L85	R87	G121	E135

^aPPH090 integrases were not included.

^bThe active site residues of the phage λ integrase (λ Int; Acc. No. P03700) have been previously described (Gibb et al., 2010). The catalytic nucleophile, Tyr342, is boldface. The accession numbers for the other tyrosine integrases studied here are: PPH005, WP_000704676; PPH010/PPH130, WP_000876735; PPH015, WP_000266841; PPH020, WP_033705527; PPH025, WP_000704686; PPH030, WP_000704664; PPH035, WP_000876736; PPH040/PPH075/PPH080, WP_000266847; PPH045, WP_000219075; PPH050, WP_061816163; PPH055/PPH095/PPH110, WP_000704678; PPH060, WP_001863308; PPH065, WP_000266851; PPH070, WP_001021836; PPH105, WP_054368747; and PPH115, WP_001866671.

^cThe active site residues of the *Lactococcus lactis* phage TP901-1 integrase (TP901-1 Int; Acc. No. CAA59475) have been previously described (Yuan et al., 2008). The catalytic nucleophile, Ser12, is boldface. The accession numbers for the other serine integrases studied are: PPH085, WP_050199652; PPH100, WP_024478469; PPH120, WP_130892475; and PPH125, WP_023396450.

TABLE 3 | Sequence similarities among tyrosine and serine integrases of PPHs ^a.

	Integrases	2	3	4	5	6	7	8	9	10	11	12	13	14	15	16
PPH group	Tyrosine integrases															
005	(1) WP_000704676	-7	-26	-145	≤-180	-143	-7	-21	-11	-21	≤-180	-7	-14	-122	-55	≤-180
010/130	(2) WP_000876735		-6	-5	-4	-3	≤-180	-3	-6	-3	-4	-10	-4	-2	-12	-5
015	(3) WP_000266841			-30	-25	-27	-5	-112	-9	-110	-25	-8	-65	-17	-26	-25
020	(4) WP_033705527				-146	≤-180	-4	-21	-16	-20	-146	-13	-18	-154	-56	-148
025	(5) WP_000704686					-144	-4	-21	-11	-21	≤-180	-6	-14	-123	-57	≤-180
030	(6) WP_000704664						-3	-25	-13	-24	-144	-12	-18	-151	-54	-146
035	(7) WP_000876736							-2	-6	-2	-4	-10	-4	NS	-12	-5
040/075/080	(8) WP_000266847								-12	≤-180	-21	-12	-63	-60	-31	-22
045	(9) WP_000219075									-11	-11	≤-180	-9	-20	-24	-10
050	(10) WP_061816163										-21	-12	-61	-19	-31	-22
055/095/110	(11) WP_000704678											-6	-14	-123	-57	≤-180
060	(12) WP_001863308												-9	-16	-24	-6
065	(13) WP_000266851													-18	-17	-21
070	(14) WP_001021836														-50	-120
105	(15) WP_054368747															-56
115	(16) WP_001866671															
	Serine integrases															
085	(1) WP_050199652	≤-170	-146	≤-180												
100	(2) WP_024478469		-179	-171												
120	(3) WP_130892475			-148												
125	(4) WP_023396450															

^aFigures correspond to Log₁₀E values calculated by pairwise alignments. NS, not significant.

repeats in the C-terminal domain (Morales et al., 2010; Morales et al., 2015). Remarkably, in addition to having the same length (957 bp), the known phage genes coding for these endolysins (*lytA_{PPH}*) are closely related (85–92% identity) to *lytA_{Spm}*, which encodes the major pneumococcal autolysin —also a NAM-amidase of the *Amidase_2* family (Morales et al., 2010). *LytA_{Spm}* is a well-known virulence factor that plays a role(s) during different steps of infection (Canvin et al., 1995; Ramos-Sevillano et al., 2015; Ramos-Sevillano et al., 2016; Corsini et al., 2021). Taking into account the strong similarities between bacterial and phage NAM-amidases, the latter may also be important in pneumococcal pathogenesis.

The current notion of an exclusive presence for *lytA*-like genes among PPHs could not be fully confirmed in the present study. As already mentioned, 1210 full-length endolysins were identified in the dataset (**Table 1** and **Table S3**). Among those, 29 proteins (≈2.5%) did not correspond to NAM-amidases of the *Amidase_2* family. There were 28 proteins homologous to the Cpl-1 lysozyme, with one containing a cysteine, histidine-dependent amidohydrolase/peptidase (CHAP) domain (PF05257) instead of an *Amidase_2* domain at the N-terminal moiety. The lysozymes were endolysins of PPH065 (22 identical proteins; WP_000739159) and PPH105 (6 proteins; 4 alleles: WP_054365577, WP_054368721, WP_054380492, and WP_054392100), which are 314 aa- and 334 aa-long respectively. Notably, all strains harboring PPH065 are members of GPSC19 and have serotype 22F (the only exception is strain 2245STDY6178828 which belongs to serotype 42) (see below).

The main differences between Cpl-1 and the PPH lysozymes detected in the present study are located in the linker region connecting the N- and the C-terminal domains. Thus, in Cpl-1, the linker (189-DDEEDDKPKTA-199) (Hermoso et al., 2003) is

longer than (and different to) that of the newly discovered endolysins (188-DDEEAKAK-195). Moreover, WP_000739159 lacks the fourth *Choline_bind_1* repeat that forms part of the C-terminal domain of the enzyme, and which is responsible for binding the enzyme to the cell wall. A detailed analysis of other PPHs (156 additional genomes, either complete or not) revealed four additional examples of 334 aa-long Cpl-1 homologs, specifically those encoded by prophages IPP16, IPP25, IPP27, and by a nameless prophage harbored by *S. pneumoniae* strain R34-3131 (**Table S4**). The latter prophage (which belongs to the PPH105 family) was already present in the dataset (**Table S1**).

The CHAP domain-containing endolysin (WP_057595562; 288 aa) found in the genome of *S. pneumoniae* strain SMRU392 (serotype 35F) is encoded by one of the PPH080 group of phages, and is identical to that of prophage 33888. The sequence of the latter was recently reported in an independent study (van Tonder et al., 2019) (**Table S4**). Since the host strain of prophage 33888 was the same as in the present study (SMRU392), and the Ints were also identical (WP_050256063), both prophages are probably the same. The WP_057595562 PPH endolysin is 63% identical (77% similar) to Skl, a proven NAM-amidase (WP_033686260; 288 aa) of an unnamed temperate phage of *Streptococcus mitis* SK137 (Llull et al., 2006). The complete genomic sequence of, presumably, the same *S. mitis* prophage (now designated as Javan331; MK448732) has recently been reported (Rezaei Javan et al., 2019). Remarkably, the existence of putative CHAP-endolysins encoded by those prophages was not mentioned in any study from other laboratories.

Among the 1181 endolysins with a predicted *Amidase_2* domain, the presence of one atypical protein was noted. This protein (WP_130892444; PPH120) is a 328 aa-long, putative NAM-amidase with a divergent *Amidase_2* domain. It is an endolysin encoded by the 36.7 kb-long prophage inserted into

PPH010_4, giving rise to PPH120 (see below). Searches for proteins very similar ($\geq 87\%$ identity) to WP_13089244 revealed several endolysins of the same length encoded by prophages of three members of the Mitis group streptococci, i.e., *Streptococcus pseudopneumoniae*, *S. mitis*, and *Streptococcus oralis*. Specifically, these prophages are 277_SPSE, 289_SPSE, and 380_SPSE (WP_049511163) from *S. pseudopneumoniae* (Roach et al., 2015), *S. mitis* strains SK564 (WP_000238871) (Kilian et al., 2014) and DD22 (WP_061864892) (Denapaité et al., 2016), *S. oralis* U-o11 (Javan367; QBX17588) (Rezaei Javan et al., 2019), and *S. oralis* subsp. *tigurinus* 859 (WP_084868230) (Diene et al., 2016). Sequence alignments also revealed the variant domain of WP_130892444 to be remarkably similar to that of the *Amidase_2* domain of LysGH15, the endolysin encoded by a myovirus phage (GH15) that infects *Staphylococcus aureus* (Gu et al., 2011). This lysin possesses a modular structure containing an N-terminal CHAP domain, a central *Amidase_2* domain, and a C-terminal SH3_5 (PF08460) bacterial-binding domain. Elucidation of the crystal structure of the *Amidase_2* domain of LysGH15 (Gu et al., 2014) revealed the aa residues involved in Zn^{2+} binding (H214, H324, and C332), catalysis (E282, and T330), as well as other important residues (W263, and N75), to be conserved in WP_130892444 at comparable positions (Figure S1). In sharp contrast, some of the equivalent residues in the NAM-amidase of *S. pneumoniae* TIGR4 (Mellroth et al., 2014; Li et al., 2015)—namely H26 and D149, as zinc ligands, and the catalytic residue H147—differed from those of WP_130892444 (and LysGH15) but were fully conserved among the widespread 318 aa-long NAM-amidases (Figure S1).

Insights Into the PPH Genomes and Identification of Their Attachment Sites

Only four *att* core sequences for PPHs were reported in studies published up until 2009 (Gindreau et al., 2000; Obregón et al., 2003b; Romero et al., 2009a), and additional core sequences have only been seldom reported in more recent papers (Cámara et al., 2018; Garriss and Henriques-Normark, 2020). To the best of our knowledge, only seven different *attB* core sequences have been previously described (Table S5). Remarkably, genome examination of many PPHs currently deposited in public databases (131 out of 158; last accessed, January 30, 2021) allow for no precise identification of the *attP* core site because most of the reported phage genomes only include the DNA region running from the first nucleotide of the *int* gene to the last one of the endolysin-coding gene (even though the definition was that of ‘complete genome’). Further, they lack the corresponding intermediate sequence where *attP* ought to be located (Table S4).

To gain insight into the sequences and locations of the integration sites of the PPHs described in the present study, a detailed analysis of all the PPHs harbored by 126 strains with near complete (chromosome assembly level) genomes was performed. The strains included in this subset represent 88 different STs, 27 PMEN clones, 66 GPSCs, and 27 different serotypes. In addition, the dataset included one non-

encapsulated laboratory mutant and four NT isolates (Table S6). As mentioned above, 100 out of 126 strains (79.4%) were lysogenic and fulfilled the above assembly requirements in the original dataset. Fifty one isolates harbored only one PPH per genome whereas 49 were polylysogenic, and one of them (strain GPSC72) contained up to five different prophages (Table S6). Taking advantage of previously determined locations of *int* genes, the genomes of these strains were examined in detail and the sequences corresponding to the *attL* and *attR* sites of 176 prophages belonging to 20 different PPH groups recorded. The sequences and locations for the remaining six groups (PPH035, PPH065, PPH090, PPH095, PPH105, and PPH110) were estimated using the partial genomes (either at the contig or scaffold assembly level) of nine additional strains included in the dataset. Prophage genomes were defined as the DNA sequence running from the first nucleotide of *attL* to the last one preceding *attR*. The *attL* sequences (obviously identical or near identical to their corresponding *attR* within each PPH group) were used as queries to map the corresponding *attB* sites on the *S. pneumoniae* D39 genome (Table 4). With the exception of PPH130, the core sequence of 24 different *attB* could be determined. As mentioned above, seven of them had been already reported, namely, PPH005, PPH010, PPH015, PPH035, PPH080, PPH085, and PPH100 (compare the data of Table 4 with those of Table S5). With the exception of PPH075, PPH125 and PPH130, in which *attB* sites appear to be located inside insertion sequences (ISs), the precise chromosomal location of the different *attB* sites could be established. Although many PPH insertion sites are located in intergenic spaces (something typical among prophages), six core attachment sites mapped within the 3' region of genes annotated for the D39 genome, and included the termination codon (TAA) of the gene where the prophage was integrated (Table 4). In addition, *attB*_{PPH035} was found to partially overlap (but apparently not interrupt) the 3' part of *ccnB* encoding csRNA2, one of the five small non-coding csRNAs (cis-dependent small RNAs) that form part of the two-component regulatory system CiaRH (Sinha et al., 2019). It should be underlined that *ccnB* is not annotated for the *S. pneumoniae* D39 genome. On the contrary, seven prophage groups potentially interrupt gene translation: 1) the core integration site of PPH010 viruses (*attB*_{PPH010}), previously reported to lie between SPD_RS00115 and SPD_RS00120 (Romero et al., 2009a) but actually located in *ccnC* coding for csRNA3 (Furi et al., 2019); 2) PPH015, which integrates into SPD_RS00125 encoding the signal recognition particle sRNA involved in membrane protein targeting (Steinberg et al., 2018); 3) PPH040, which integrates into SPD_RS01460, potentially encoding an intramembrane metalloprotease of the CAAX proteases and bacteriocin-processing enzymes (CPBP) family (Pei et al., 2011); 4) PPH050, inserted into SPD_RS01935 encoding a frameshifted choline-binding protein (CbpG) in D39 (Frolet et al., 2010); 5) a gene (SPD_RS09795) encoding UlaR [a transcriptional activator of the *ula* operon in the presence of ascorbic acid (Afzal et al., 2015)], which may be inactivated by the insertion of bacteriophages of the PPH095 group; 6) PPH100, which integrates into SPD_RS09885 encoding

TABLE 4 | Localization of *attB* sites for *S. pneumoniae* temperate prophage integration.

Prophage	<i>attB</i> (5'→3') ^a	Flanking locus tags (SPD_RS) (Product)
PPH005	2935 TTAGCACTTTATCCCTTTTGTGTGA 2960	00015 (DUF951 family protein)/00020 (redox-regulated ATPase YchF)
PPH010	24016 CTTTTTCATAATAATCTCCCT 24036 ^b	00115 (adenylosuccinate synthase)/00120 (nucleoside deaminase)
PPH015	24694 TTGTGTGCTCTTTTTTCGTGC 24715	00125 (signal recognition particle sRNA small type)
PPH020	86374 TACAACAAATGTTG TAA TATTT 86396	00445 (30S ribosomal protein S4)
PPH025	163831 ATTCCTTTACAA 163842	00880 (response regulator transcription factor)/00885 (hypothetical protein)
PPH030	179128 ATTATACTACAAAATCGGCCTTTT 179151	00970 (magnesium transporter CorA family protein)/00975 (excinuclease ABC subunit UvrA)
PPH035	231378 <u>CTTTTCATAATAATCTCCCT</u> <u>TAACTCCACCAATCAGGTGGAGTTTTT</u> AGCTCTATTTTCAGGCTTTTGGGACTATTCTAAAAATA ATTTTTCGATATTTTTCGGTATTTTTCGGATTTTGGT CGGGGAATTGGCGGGGACTTTTT 231525 ^c	01305 (GNAT family N-acetyltransferase)/01310 (type I toxin-antitoxin system Fst family toxin)
PPH040	267293 GGTCTTTTACTTGCCG 267309	01460 (CPBP family intramembrane metalloprotease)
PPH045	273279 GTAAGCATCACAAATTTAGTAAACG TAA T 273308	01495 (30S ribosomal protein S9)
PPH050	358211 AGTCAAGAACTATTT 358225	01935 (choline-binding protein CbpG; frameshifted)
PPH055	619559 CATATTATTTTGAAT 619574	03210 (DUF3165 family protein)/03215 (lactococcin 972 family bacteriocin)
PPH060	693388 AACCGATCTTAAGAAAGCTCGTAAAG 693414 ^d	03620 (hypothetical protein)/03630 (hypothetical protein)
PPH065	1006452 CTCTTAAAGACGCTGTTAAAT TAA T 1006475	05350 (HU family DNA-binding protein)
PPH070	1027141 TACAACCTTAAAAAA TAA 1027158	05425 (phosphopyruvate hydratase)
PPH075	ATGCCGATGAATTATAA	Prophage located 3' of SPD_RS06250 (cyclically-permuted mutarotase family protein)
PPH080	1415148 TTA TAAATTCATCCGC 1415162	07415 (DNA-binding protein WhiA)
PPH085	1712415 TTCCTCTACTTATCTATTCTAG 1712438	09110 (single-stranded DNA-binding protein)/09115 (SDR family NAD(P)-dependent oxidoreductase)
PPH090	1729602 TTA TTTTACTGTAATCAAGCCATCTGGCTCTACTGTGAATTCTGGC 1729647	09250 (N-acetylmuramoyl-L-alanine amidase family protein)
PPH095	1826920 CATTACGAAATATATT 1826935	09795 (transcription anti-terminator)
PPH100	1841058 ACCAACATCTCCACCAA 1841074	09885 (<i>comG</i> operon protein ComGC)
PPH105	1849319 TATGGTATAA 1849328 ^d	09920 (tRNA guanosine(34) transglycosylase Tgt)/09925 (DUF975 family protein)
PPH110	1901612 ATAA 1901615 ^e	10215 (methyltransferase domain-containing protein)/10225 (membrane protein)
PPH115	1911323 ACTTGAAATAAAGCGCATTTCTCTATA 1911349	10255 (sugar ABC transporter permease)/10265 (DUF1189 domain-containing protein)
PPH120	1933870 ATTCGTTTAAGTAATACCATAAACCTTTGTCTTTAACCAACAGTAGCCA 1933920 ^f	10405 (Choline-binding protein PcpA)
PPH125	ATGTTATTTCTCTCGTTACAAAATTACAACCTTAAAAAA TAA	Prophage located 3' of SPD_RS10665 (tRNA dihydrouridine synthase DusB). The predicted <i>attB</i> forms part of ISS <i>Spn5</i> (IS1380 family).
PPH130	Not known	Prophage located 5' of SPD_RS10885 encoding a transposase.

^aThe coordinates correspond to those in the *S. pneumoniae* D39 genome (NC_008533.2). This strain was recently renamed 'D39W' (Sinha et al., 2019) and showed some differences to another cultivar of the same strain (D39V) (Slager et al., 2018). Termination codons (TAA) are bold and underlined.

^bThis *attB* is located inside the *ccnB* gene (23,967–24,065) encoding a small non-coding *csRNA* (*cia*-dependent small RNA) named *csRNA3* (Sinha et al., 2019). This gene is not annotated for the pneumococcal D39 genome. Two additional potential *attB* sequences are present in the *S. pneumoniae* D39 genome, i.e., between SPD_RS01305 and SPD_RS01310 (231,378–231,398) (see shadowed sequence in PPH035), and between SPD_RS01320 and SPD_RS01325 (233,750–233,770).

^cThe shadowed sequence is identical to that of *attB*_{PPH010}. The part of the sequence overlapping the 3' end of the *ccnB* gene (231,331–231,427) coding for *csRNA1* (Sinha et al., 2019), is underlined. This gene is not annotated for the pneumococcal D39 genome.

^dAnother potential *attB* sequence (273,258–AACCAGTCTTAAGAAAGCTCGTAAAG–273,284) is present in the *S. pneumoniae* D39 genome, i.e., inside the SPD_RS01495 gene, encoding the 30S ribosomal protein S9.

^eIdentical sequences are present at many other positions.

^fSeven additional potential *attB* sequences are present in this gene.

ComGC, the major subunit of the competence pilus (Laurenceau et al., 2015); 7) and bacteriophages of the PPH120 group, which disrupt SPD_RS10405, i.e., the gene encoding for the PcpA choline-binding protein (Sánchez-Beato et al., 1998) (now an important component of several new protein-based, pneumococcal vaccines currently under evaluation) (Masomian et al., 2020).

Table S6 attempts to organize the different PPHs in a manner that takes into account their wide genetic diversity. For this, a

concept of 'equivalent PPH genomes' was followed, i.e., genomes that overlapped for ≥90% of their total length and showed ≥90% sequence identity were considered 'equivalent', and only one of them was used in further comparisons. **Figure S2** shows a comparison of the different PPH genomes. PPH095 and PPH110 are not depicted since, although they inserted into two different *attBs*, these PPHs were equivalent to PPH055 (see below). Due to the evident sequence variability of prophage genomes, pairwise nucleotide alignments were

initially performed only among PPHs of the same group. Several main conclusions were then drawn: 1) *int* genes were present in every prophage found, but this was not the case for endolysin-coding genes; 2) two major PPH groups were recognized, one with genome lengths ranging from ≈ 10 –20 kb on one side (e.g., PPH005 and PPH030 groups), and the other from ≈ 35 –45 kb on the other side (e.g., PPH010 and PPH080 groups); 3) major differences can still be seen among the members of a PPH group (e.g., PPH015, PPH020, PPH045 and PPH090 show large differences); 5) several PPHs with genomes of 51–92 kb appear to result from recombination events between two different prophages, e.g., i) PPH075 is the result of the insertion of an unknown defective prophage (12,227 bp) into a PPH085_5 equivalent. This defective prophage is flanked by a 33 bp-long sequence (5'-CCCTAGACTTGAAATAAAGCGCATTTCTCTATA-3') located at positions 32,873–32,905 and 45,100–45,132 of the PPH075 genome; a near-identical sequence (1,911,317-TCCTAGACTTGAAATAAAGCGCATTTCTCTATA-1,911,349) may contain part of the promoter region of SPD_RS10265 (*malA*) in the D39 genome (Nieto et al., 1997); ii) PPH080_11 appears to result from the integration of a PPH010-like prophage into a PPH080_3 equivalent; as expected, the insertion of the PPH010-like phage occurs in the sequence 5'-CTTTTTCATAATAATCTCCCT-3' at positions 2069–2089 and 32,251–32,271 of the PPH080_11 genome; iii) the insertion and rearrangement of a PPH010_4-equivalent into a previously unknown prophage gives rise to PPH120, possibly with the assistance of two ISs (*ISSpn5* and *IS1167*) and the addition of a gene cluster encoding several tRNAs. Sequence comparison revealed this prophage to be very similar (82–85% query coverage and >95% nucleotide sequence identity) to two *Streptococcus anginosus* prophages, namely Javan83 (Rezaei Javan et al., 2019) and SA01 (van der Kamp et al., 2020); interestingly, the latter two prophages appear to harbor no tRNA genes. In addition, both encode an endolysin 76% identical (88% similar) to Cpl-7 (see above), whereas, as already discussed, the new component of PPH120 codes for a peculiar 328 aa-long NAM-amidase of the *Amidase_2* family of proteins; iv) a tandem insertion of two near identical PPHs (PPH080_1A and PPH080_1B) gives rise to the 92 kb-long hybrid prophage PPH080_1AB.

Among the various prophage identification tools, we used the PHASTER program to analyze the 109 genomes included in **Table S6** (186 PPH). Up to 263 putative PPHs were predicted; 40 of them were designated as 'intact' by the program and actually corresponded to real prophages (**Table S6**). The predicted limits of the PPHs did match the real coordinates in only few cases (e.g., PPH030 from strain SP64 was almost correctly located (real: 177,043–189,925; predicted: 177,043–189,926). Unfortunately, in most instances, this was not the case. For example, in strain GPSC47 (NZ_LR216060), PPH010_9 is located between coordinates 3152 and 36,649 whereas PHASTER predicted the range 1771–42,683). Of note, the existence of PPHs of the groups 010, 015, 080, and 110 was well predicted, whereas that of those belonging to groups 020, 045 and 115 were not (**Table S7**). In our hands, the sensitivity of PHASTER (0.74) was similar to that

previously reported (Lopes de Sousa et al., 2018; Reis-Cunha et al., 2019).

Pairwise nucleotide alignments were then performed among genomes belonging to different PPH groups. In addition to equivalent PPHs (see above), a second level of similarity was allowed, i.e., those prophages with an overlap of between 80 and 89% of their genomes and showing nucleotide identities of $\geq 90\%$. **Figure 1A** shows 'equivalent' and 'very similar' genomes on white or gray backgrounds respectively. It should be underlined that equivalent prophages were distributed between different PPH groups. Thus, in addition to the equivalency between the defective prophages PPH055, PPH095, PPH110 and PPH115_2 partly mentioned above, other equivalent, putatively complete prophages of different groups were seen: 1) PPH010_2, PPH035 and PPH130; 2) PPH015_1, PPH080_8 and PPH090_3; and 3) PPH040 and PPH080_3. As expected, most of the 'very similar' category of prophages corresponded to different members of the same group, as exemplified by members of the PPH010 group such as PPH010_7–PPH010_10 and PPH010_12–PPH010_14 (**Figure 1A**). Pairwise comparison of 80 PPH sequences and a dendrogram depicted seven major prophage clusters, and three singletons (**Figure 1B**). Four of the clusters matched those described by Brueggemann et al. (2017) and one more to the defective prophages mentioned by Rezaei Javan et al. (2019) that were recognized as separate entities from full-length PPHs. The remaining PPHs (either clustered or not) correspond to previously undescribed prophages.

Other Features of Pneumococcal Prophages

Many prophages from both Gram-negative and Gram-positive bacteria integrate into tRNA genes (Williams, 2002) although this is not the case for PPHs (see above). Nevertheless, sequence analysis revealed the presence of potential tRNA genes in some PPH genomes (**Table S8**). Of note, PPH120 has nine tRNA genes located at the right end of the prophage, whereas other PPHs have these genes located closer to the middle. A search of PPH genomes reported elsewhere revealed that five previously sequenced phages (namely, IP8, IP16, IP25, IP26, and IP27) also harbor a tRNA-Ser gene, a feature not mentioned in previous reports (**Table S8**).

PblB may be an important virulence determinant in some PPHs. PblB has been described as a phage minor tail protein (a putative anti-receptor) that behaves as an adhesin mediating the galactose-specific adhesion activity of pneumococci to platelets and human lung epithelial cells *in vitro*. It is also required for nasopharyngeal and lung colonization in a mouse model of infection (Hsieh et al., 2015). The sequence diversity of PblB is notable (Brueggemann et al., 2017). Amino acid sequence alignments in the PPH dataset fully confirmed this (as shown diagrammatically in **Figure S3**), even among PPHs of the same group (e.g., in PPH010_7, in which the length of PblB was 2134 aa in strain GPSC97 but 3256 aa in GPSC25). It is also reported that the PblB encoded by the temperate phage SM1 infecting *S. mitis* (1062 aa) (Bensing et al., 2001) is very different to the protein (P15; 1987 aa) previously analyzed in the *S. pneumoniae*

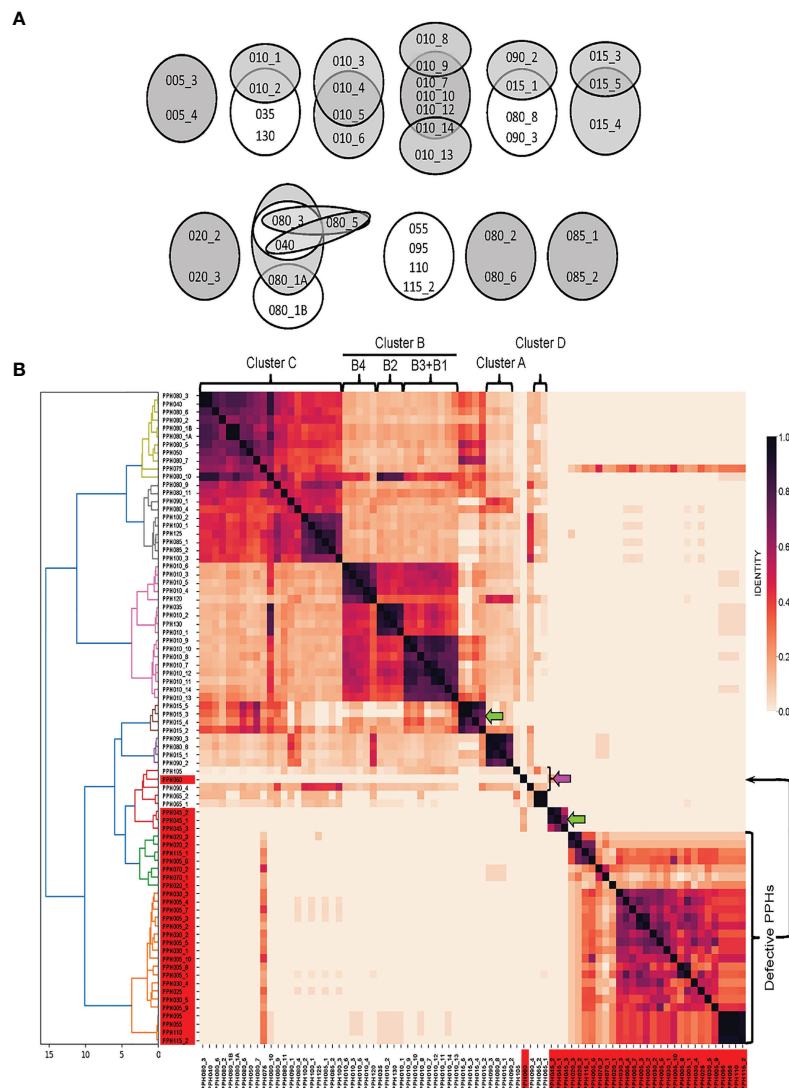


FIGURE 1 | Sequence similarities between PPHs genomes. **(A)** Venn diagrams showing equivalent or very similar pneumococcal prophages. Two PPH genomes were considered ‘equivalent’ when they overlapped for $\geq 90\%$ of their length and showed $\geq 90\%$ sequence identity (shown on a white background). When two genomes overlapped between 80 and 89% of their length, and nucleotide identities were $\geq 90\%$, the corresponding PPHs were considered as ‘very similar’. They are shown on a gray background. **(B)** wGRR similarity heatmap depicting the amino acid identity shared between pairs of prophage sequences (either full-length or defective prophages). Different colors were applied to clusters showing distance thresholds > 4 . For agglomerative hierarchical clustering, distances are shown in the X axis. The *dendrogram* and *heatmap* python tools of the *scipy.cluster.hierarchy* library were used to depict final agglomerative hierarchical clustering and heatmap plots, respectively. Green and pink arrows point to new clusters or singletons respectively. The correspondence between PPHs and the cluster organization of pneumococcal prophages previously reported (Brueggemann et al., 2017; Rezaei Javan et al., 2019) is indicated at the upper part of this panel. See **Table S4** for a proposed correlation between previously described pneumococcal prophages and PPH groups.

NTUH-P15 strain (Hsieh et al., 2015). Moreover, these two proteins differ notably from most of the PblB proteins found in the present study, particularly in their middle regions where different combinations of five different (albeit related) sequence repeats were found (**Figure S3**). PblB-like proteins were encoded by some of the phages belonging to the PPH010, PPH035, PPH040, PPH080, PPH085, and PPH100 groups. Willner et al. showed that the *S. mitis* prophage SM1 can be induced by commonly ingested substances and that the oral cavity is indeed a reservoir of *pblA* and *pblB* genes (Willner et al., 2011).

First described in the Gram-negative bacterium *Dichelobacter nodosus* (an ovine footrot pathogen), virus-associated protein E (VapE_{Dno}) has been proposed involved in virulence (Billington et al., 1996). Proteins similar to VapE have also been reported encoded by prophages of other microorganisms such as *S. aureus* (Lindsay et al., 1998), *Pseudomonas putida* (Canchaya et al., 2003), *Vibrio parahaemolyticus* (Seguritan et al., 2003), *Staphylococcus epidermidis* (Chen et al., 2013) and *Elizabethkingia anophelis* (Peng et al., 2020), although direct evidence of the involvement of VapE in virulence was provided in neither of these studies. In *S.*

pneumoniae, Romero et al. (2009a) first noted that several prophages encoded proteins similar (about 30% identity; E value = 10^{-34}) to VapE_{Dno} (also designated as *virE*). More recently, several gene products from defective prophages have been shown similar to a *Streptococcus suis* protein named VapE_{Ssu} (Rezaei Javan et al., 2019), a protein apparently unrelated in primary structure to VapE_{Dno} but which has been shown involved in virulence in a mouse model (Ji et al., 2016). The translated nucleotide dataset of PPHs was compared to both VapE_{Dno} and VapE_{Ssu} and using an E value cutoff of 10^{-20} , two sets of putative virulence-associated proteins were found (Table S9).

It is well known that bacteria have developed defense mechanisms to help them survive phage attacks. These mechanisms may interfere with the adsorption of the phage onto the cell surface, with phage genome injection, or target the foreign nucleic acid after its injection, etc. (for recent reviews see Labrie et al., 2010; Koonin et al., 2017; Rostøl and Maraffini, 2019). Phages, in turn, have evolved mechanisms to overcome restriction-modification (R-M) systems. One of these is based on the presence in phage genomes (both virulent and temperate) of orphan methyltransferase (Mtase) genes (i.e., without concomitant endonuclease-coding genes) (Murphy et al., 2013). There are three functional classes of type II DNA Mtases that function by transferring a methyl group from S-adenosyl-L-methionine to a target nucleotide base, forming either N-6-methyladenine (class I), N-4-methylcytosine (class II), or C-5-methylcytosine (class III). Our laboratory previously reported the existence of putative Mtases-encoding genes in two *S. pneumoniae* temperate phages, namely MM1 (Obregón et al., 2003a) and VO1 (Obregón et al., 2003b). Taking the Mtases of these two phages as query sequences, the complete set of PPH genomes was screened. Interestingly, more than 30 putative orphan Mtases of either the MM1 or VO1 class were detected. None of them was encoded by defective PPHs (Table S10).

PPH090, a Group of Prophages That Integrate Into the *lytA*_{Spn} Gene via an Int-Independent Mechanism

The proposed core sequence of attB_{PPH090} (46 bp-long) mapped to the 3' end of the *lytA*_{Spn} gene overlapping its termination codon (Table 4). Consequently, phage integration should not disturb *lytA* translation. In sharp contrast with other PPHs, the most striking feature of prophages of the PPH090 group is that there is no preference for a particular Int (or group of Ints) (Table S2). Specifically, different PPHs of the PPH090 group encode Ints of the tyrosine (12 entries) or serine (6 entries) families, some of which are identical to those of other prophage groups: 1) tyrosine Ints [PPH010 (WP_000876726, WP_000876733, WP_000876735, and WP_050199954), PPH015 (WP_023396066, WP_044813689, WP_050127433, WP_050203801, and WP_050221901), PPH080 (WP_000266839, WP_000266847, and WP_000266854)]; and 2) serine Ints [PPH100 (WP_024478469, WP_044812715, WP_050203932, WP_050226267, WP_050230313, and WP_050974546)]. These data strongly suggest that PPH integration into *lytA*_{Spn} does not require a specific interaction

between *attB*, *attP*, and the Int, and that some other factors may be involved—possibly recombination events between *lytA*_{Spn} and *lytA*_{PPH} (see below).

The four PPH090 genomes shown in Figure S2 encode, respectively, one of three different Ints of the tyrosine family (PPH090_1–PPH090_3) and one Int of the serine family (PPH090_4). Among them, the genome of the NT strain SMRU257 (master record NZ_CKNNY01000000) appears to be unique since, in addition to the PPH090_2 genome (39,182 bp; contig NZ_CKNNY01000002), it contains a 39,182 bp-long sequence (contig NZ_CKNNY01000010) inserted into the *ffs* gene (corresponding to SPD_RS00125 in *S. pneumoniae* D39) (Table 4). Moreover, this prophage harbors all the characteristics of a full member of the PPH015 group, including the near identical flanking *attL* and *attR* core sequences (5'-TTGTGTGCTCTTTTTCGTGC-3'). Remarkably, PPH090_2 and the 'new' PPH015 only differ at two nucleotide positions, i.e., 918 (G) and 951 (T) of the 957 bp-long *lytA*_{PPH} and *lytA*_{PPH}* genes (the asterisk indicates that the phage and bacterial *lytA* genes were probably chimeric [a hybrid] because they contain sequences of both phage and bacterial origin) (Figure S4).

The hypothesis that *lytA*_{PPH} recombines with the *lytA*_{Spn} gene and integrates into the pneumococcal genome was tested by making a detailed analysis of both the *lytA* genes and the DNA regions located between *int* and *lytA*_{Spn}*, as well as downstream of *lytA*_{PPH}*, in the integrated state (Figure 2A). Figure 2B shows the appropriateness of the hypothesis since, immediately after the termination codon of *lytA*_{PPH}*, the sequence was syntenic, i.e. shares the same genetic order, with the DNA region located 3' of *lytA*_{Spn} in a non-lysogenic strain. In fact, previous studies had already provided different kinds of evidence on the existence of recombination between these genes (Romero et al., 1990; Whatmore and Dowson, 1999; Morales et al., 2010). It has also been reported that *lytA*_{Spn} and *plyA* (the gene encoding the main pneumolysin, a cholesterol-dependent cytolysin) form part of a pathogenicity island in *S. pneumoniae*, characterized by the presence of direct repeats (ISs), phage-related genes, and/or genes potentially encoding virulence factors and mobility proteins (Ints, transposases). These findings also suggest that the *plyA*–*lytA* island is a recombination hotspot. At least eight genomic arrangements of this island have been recognized (Morales et al., 2015). During the present study, an additional arrangement that appears to be exclusive to some NT pneumococci was found (Figure 2B). It is worth mentioning that a larger protein (3628 aa residues; WP_142367134) of unknown function is encoded within the *plyA*–*lytA* island in the pneumococcal strain SMRU257.

The DNA region located immediately 3' of the corresponding *lytA*_{PPH}* gene of each of the four PPH090 was aligned with a 2 kb-long region located immediately downstream of the *lytA*_{Spn} gene of the non-lysogenic *S. pneumoniae* D39 strain (NC_008533.2; complement [1,727,602–1,729,601; the position of the last nucleotide of *lytA*_{Spn} is 1,729,602]). In agreement with the hypothesis formulated above, the four PPH090 genomes showed >96.5% nucleotide identity with the D39 genome in that region (data not shown). The PPH090 regions that run from the

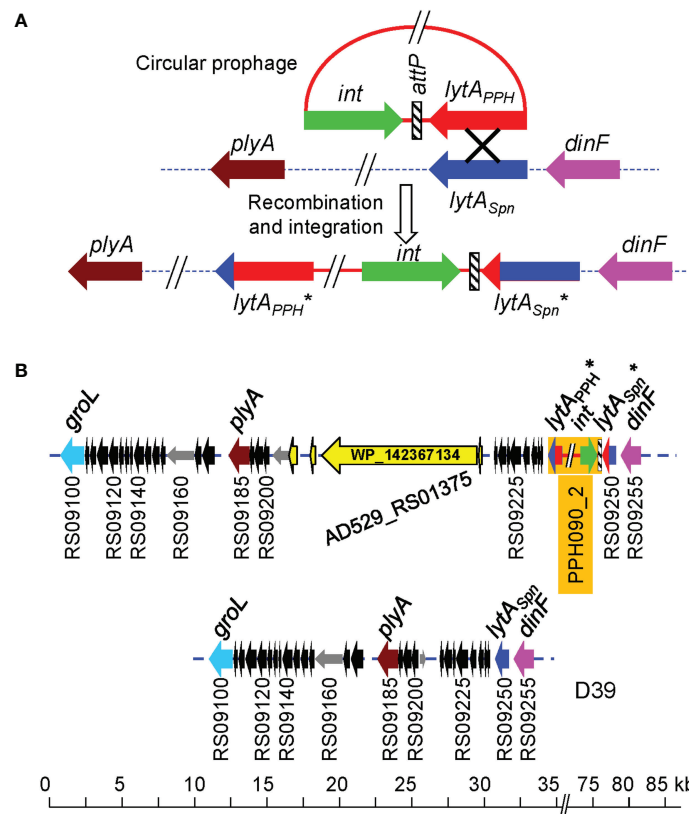


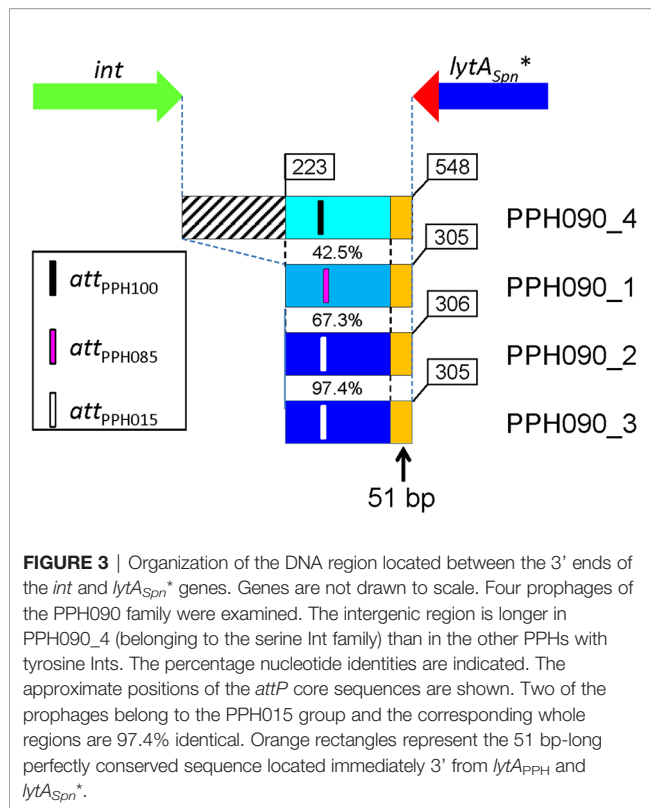
FIGURE 2 | A proposal for phage integration into the *S. pneumoniae* genome after the recombination of *lytA_{Spn}* and *lytA_{PPH}*. **(A)** The circular phage genome (red) and the pneumococcal chromosome (dotted line) are shown. Genes are drawn as arrows indicating the direction of transcription. An 'X' indicates the recombination event. The pneumococcal genes *plyA* and *dinF* that flank the *lytA_{Spn}* gene are shown for reference (Morales et al., 2015). The asterisk (*) indicates that the phage and bacterial *lytA* genes were probably chimeric because they contain sequences of both phage and bacterial origin. **(B)** Novel genomic arrangement of this *plyA*—*lytA* island in the pneumococcal strain SMRU257. The location of a gene (AD529_RS01375) encoding a large protein (3628 aa residues; WP_142367134) is shown. For comparison, the corresponding DNA region of the control D39 strain is shown at the bottom.

3' end of *int* to the 3' of *lytA_{Spn}** after integration, were also aligned (Figure 3). This region was 548 bp-long in PPH090_4 (serine Int family), and shorter (305–306 bp) in prophages with tyrosine Int-coding genes. The DNA regions corresponding to the two putative PPH015 prophages (PPH090_2 and PPH090_3) were very similar (97.7%; 298 identical nucleotides in a 305 nt overlap). The presence of a 51 bp-long sequence (5'-ATAGAAAGGAACTTCTAAATTGTTCTTTACCGCAGGCTTAGGCTTGCG-3') located immediately after the termination codon of the *lytA_{Spn}** gene and found to be conserved in all the PPHs studied (indicated by orange rectangles in Figure 3) should be noted. Among the 126 pneumococcal strains with either complete or near complete genomes, this 51 bp-long signature was absent from the 26 non-lysogenic strains (as expected), but it was found immediately downstream of the 3' end of the *lytA_{Spn}* gene among two lysogenic strains: 4041STDY6836166 (Acc. No. NZ_LS483451; positions 1,865,445–1,865,394) and GPSC72 (Acc. No. NZ_LR216049; positions 1,745,355–1,745,304). In these strains, the 51 bp-long sequence is part of a ~700 bp-long fragment that is ≥95% identical to another fragment located 3' of several

lytA_{PPH} genes, particularly those within the PPH010 group (unpublished observations). This finding indicates that those strains were once lysogenic, but that at some point, most of the prophage was lost. Interestingly, a putative transcriptional terminator is located close to the 3' end of the *lytA_{PPH}* (and *lytA_{Spn}*) genes and may function in a manner similar to that of the transcriptional terminator of the *lytA_{Spn}* gene previously determined (Díaz and García, 1990) (Figure S5).

Recombination Between Prophage and Bacterial *lytA* Genes Is a Source of Chromosomal Rearrangements in *S. pneumoniae*

PPH090-like prophages appear to be made *via* recombination of the *lytA_{PPH}* and *lytA_{Spn}* genes after the prophage is spontaneously excised from the host genome. However, recombination may also take place during the lysogenic (integrated) state of the prophage. In this instance, however, *lytA* recombination may result not in the emergence of a new PPH090 prophage but in chromosomal rearrangements. To gain insight into the recombination events that appear to occur between *lytA_{Spn}* and *lytA_{PPH}*, the



corresponding genes from the four PPH090 reported here were aligned and the position of nucleotides conserved in *lytA_{Spn}** and *lytA_{PPH}**—but not in both groups—were annotated (Figure 4A). A search for polymorphisms at those positions was then performed in all the *lytA_{Spn}* (325) and *lytA_{PPH}* (356) alleles of the dataset (Figure 4B). Few polymorphic positions appeared between positions 1 and 100 (approximately), but beyond there the average polymorphism reached 7 and 14% in the tested positions of *lytA_{Spn}** and *lytA_{PPH}** respectively. This suggests that recombination events (if any) are more frequent in the 3' than the 5' moiety of the gene. The possible significance of the notable polymorphism observed at three nucleotide positions (14 and 17 in *lytA_{PPH}*, and 282 in *lytA_{Spn}*) was not further analyzed, but the importance of the polymorphism at position 951 (very close to the 3' end of *lytA* which is located at position 957) mentioned above was studied in detail. As shown in Figure 4B, searching among the 325 *lytA_{Spn}* alleles in the resulting data showed 84 of them (154 strains) to have a 'T' instead of an 'A' nucleotide at position 951. Table S11 summarizes a systematic analysis of this region among a subset of 51 of those 84 *lytA_{Spn}* alleles (111 strains). The results indicate the existence of recombination events that produced the translocation of several DNA fragments from their original position (taking the non-lysogenic *S. pneumoniae* D39 genome as a reference) to a region located immediately downstream of the *lytA_{Spn}** gene (Figure 5). Five major rearrangement events were recorded and, in agreement with the genes found, the direct participation of PPH010 (SPD_RS00120), PPH015 (SPD_RS00130), PPH080 (SPD_RS07410), PPH085 (SPD_RS09110), or PPH100

(SPD_RS09880) was deduced. By comparing these arrangements with those of the different PPHs described in this study, the bacterial and phage *lytA* genes were seen to represent inverted repeats in arrangements A and B, and individual direct repeats in arrangements C, D, and E. A recombination event in cases A or B would likely produce a chromosomal inversion (Table S11). In addition, since the region between the *lytA* genes (the spacer) is asymmetrical around the origin of replication, a chromosomal inversion may induce changes in the relative positions of the origin and terminus of replication, as previously noted (Achaz et al., 2003). In arrangements C, D and E, a recombination event produced between repeat sequences in the same orientation on the same chromosome could result in a translocation (Hughes, 2000). A close examination of the region located immediately downstream of *lytA_{Spn}** (SPD_RS09250; depicted as gray squares in Figure 5) in 14 different strains revealed complex organizations of different length that contained prophage fragments or even putative full length prophages. For example, strain SMRU51 harbored a prophage equivalent to PPH035 (Figure 6). Of note, an additional recombination event in strain SMRU1319 (arrangement D2) produced an inversion of the genes located upstream of SPD_RS09115 and downstream of SPD_RS09110 (Table S12).

DISCUSSION

According to the data presented in this and previous studies, prophages are very common in *S. pneumoniae*: up to 90% of pneumococcal isolates may harbor temperate phages, although nearly half of them (in the present work 47%) appear to be defective and lack the genes involved in morphogenesis and lysis. These can be considered 'defective' (incomplete or remnant) PPHs that may be in a state of mutational decay (Casjens, 2003). It should be remembered that genome decay does not take place homogeneously. Previous reports have shown that, in incomplete prophages, there is an enrichment in *int* genes, whereas genes involved in phage lytic functions are preferentially lost (Bobay et al., 2014; Khan et al., 2020). Of note, some defective prophages are capable of excision from the bacterial chromosome (Chen et al., 2019). Sometimes, defective prophages are also designated as 'cryptic prophages' (Wang and Wood, 2016), although in theory this term should include only fully functional prophages that have never been induced to follow a lytic cycle (Casjens, 2003). Recently, incomplete streptococcal prophages were termed 'satellite' prophages (Rezaei Javan et al., 2019), although the characteristic dependence of true satellite prophages upon proteins produced by a helper prophage for packaging and progeny phage release was not demonstrated. A defective prophage (possibly a PPH005_1 relative) has been reported as capable of excising from the chromosome, but, as expected, it does not seem to enter the lytic cycle (Chen et al., 2019).

The present work fully confirms that the vast majority of full length PPHs harbor *lytA_{PPH}*, a gene homologous to *lytA_{Spn}* encoding a 318-aa long NAM-amidase (*Amidase_2* family)

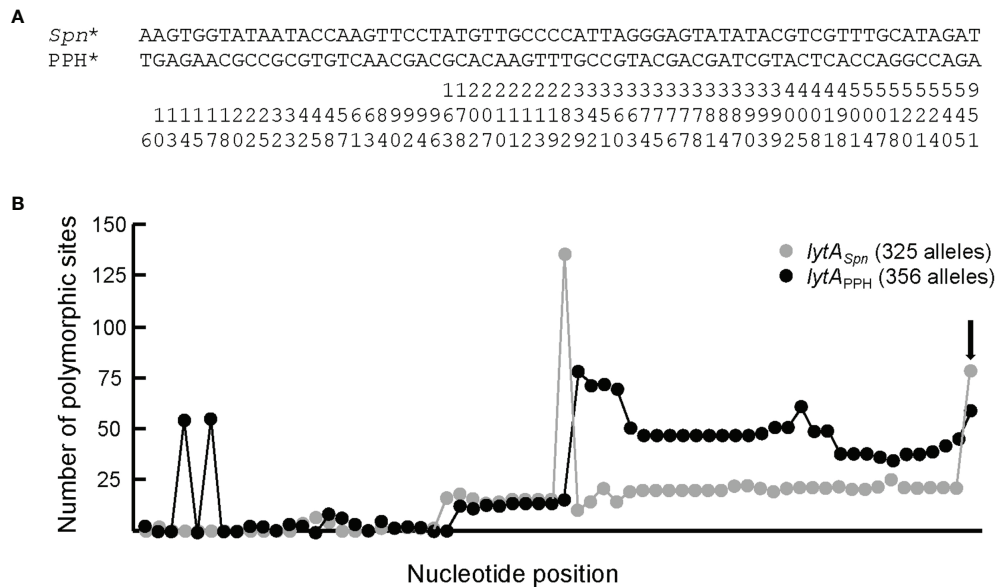


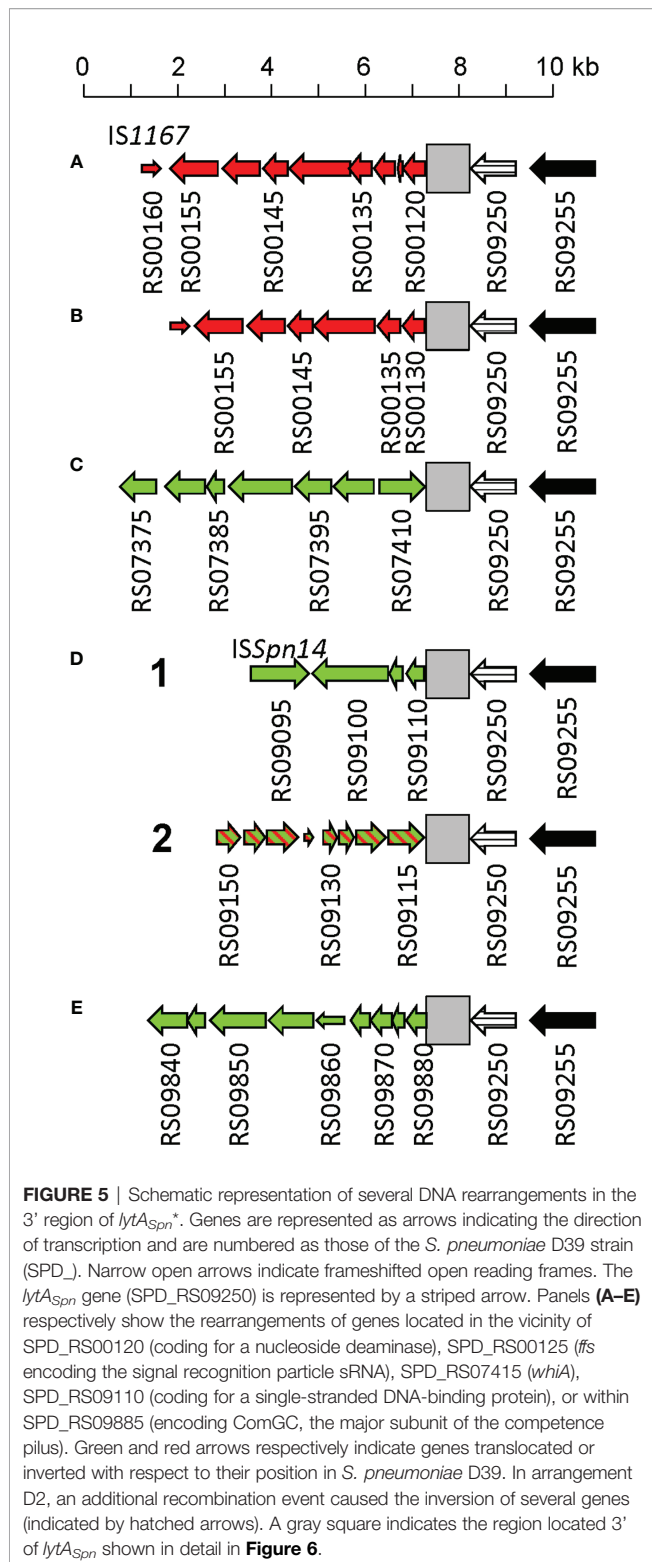
FIGURE 4 | Sequence signatures of *lytA_{Spp}*^{*} and *lytA_{PPH-090}*^{*} alleles. **(A)** Bacterial and prophage *lytA* genes of strains harboring PPH090 group phages were aligned and the positions where the bacterial (on one side) and phage (on the other) genes diverged were marked. For simplicity, the highly polymorphic region characteristic of the *lytA* gene (positions 421–480) (Morales et al., 2010) was not included in the alignment. The nucleotide positions (taking 1 as the first nucleotide of the ATG initiation codon) should be read vertically. **(B)** Distribution of polymorphic sites in bacterial and prophage alleles according to the alignment shown in panel **(A)**. The vertical arrow points to the data at the polymorphic position 951. The total length of the *lytA* gene is 957 bp.

endolysin. This clearly indicates the enhancement of phage and host fitness. A small (but significant) number of PPH endolysins (28), however, corresponded to Cpl-1-like lysozymes, and only one to a CHAP-containing enzyme. The lysozymes were the hallmark endolysins of the PPH065 and PPH105 groups. Notably, all strains harboring PPH065 were members of GPSC19 with serotype 22F (the only exception being strain 2245STDY6178828, which belongs to serotype 42). Serotype 22F is an emerging serotype (Tin Tin Htar et al., 2019) that is not included in the current 13-valent pneumococcal conjugate vaccine, although it has been incorporated into the next generation of 15- and 20-valent pneumococcal conjugate vaccines currently under evaluation (Masomian et al., 2020). All these isolates belong to clonal complex 433, which is predominant in Spain (Sempere et al., 2020). In addition, strains harboring PPH105 are of serotype 35B (sequence type 558): a single-locus variant of the PMEN Utah^{35B}-24 clone, also an emerging, multidrug-resistant serotype associated with non-vaccine serotypes (Andam et al., 2017). It has been shown that pediatric isolates of serotypes 22F form better biofilms than adult isolates (Sempere et al., 2020) and that serotype 35B pneumococci are good biofilm formers (Domenech et al., 2015). Whether this phenotype is directly related to the presence of prophages, as has been proposed (Loeffler and Fischetti, 2006; Carrolo et al., 2010; Harvey et al., 2016), remains to be determined. Previous experiments have shown that the Cpl-1 endolysin is very effective in destroying *in vitro* formed biofilms either of *S. pneumoniae*, or of the type strains of *S. pseudopneumoniae* and *S. oralis* (Domenech et al., 2011). In

addition, a recent study has shown that ClyJ-3 (an engineered chimera with a very short linker) shows improved thermal stability and has greater bactericidal activity against pneumococci, as well as reduced cytotoxicity, than does its parental enzyme (Yang et al., 2020). Since the Cpl-1-like lysozymes found in the present work also have linkers shorter than that of Cpl-1, detailed *in vitro* and *in vivo* studies of the newly discovered PPH lysozymes are warranted.

Using a subset of the database formed by complete or near complete pneumococcal genomes, up to 24 different *attB* sites were detected. Taking into account the capacity of some prophages to insert at different sites, the existence of 20 different PPH groups was disclosed. Various prophages integrate into genes encoding csRNAs. In *S. pneumoniae*, these non-coding sRNAs show a high degree of similarity to each other, and have been shown to affect pneumococcal physiology pleiotropically, e.g., they are involved in β -lactam resistance, and regulate natural competence development. The mechanism of action of csRNAs appears to be additive (Brantl and Brückner, 2014). Previous studies have also reported that prophage insertion into SPD_RS09885 interrupted competence development (Croucher et al., 2011; Croucher et al., 2014; Croucher et al., 2016) and it was found that having an intact *comGC* (also named *comYC*) gene was significantly associated with increased carriage duration (Lees et al., 2017).

A tandem prophage insertion (PPH080_1AB) was also found. This is usually interpreted as the integration of two phages that use the same *att* (in this case, 5'-TTATAATTCATCCGC-3'). The differences between the parental prophages in PPH080_1B involve



a tandem duplication of a cluster of nine genes in PPH080_1A (marked with different colors in Figure S2). Further, some rare events related to PPH insertion were also noted. PPH075, PPH080_3, and PPH120 contained *attB* sequences, which would allow another phage to be integrated into their genomes, forming a

prophage-in-prophage configuration and allowing the duplication of prophages possibly encoding medically or biologically important genes. To the best of our knowledge, this phenomenon has only previously been described in Shiga toxin-encoding prophages in *E. coli* (Nakamura et al., 2021).

Although first described in phage T4 in 1968 (Weiss et al., 1968), the role of tRNA genes in phages has been subject to debate (Bailly-Bechet et al., 2007). Viruses, which depend on the host protein expression machinery, have evolved various strategies to optimize translation, either by adapting their host codon usage to that of the host or encoding their own tRNAs. It has been noted that most phages contain only one or two tRNA genes, while a few may contain ≥ 20 (Bailly-Bechet et al., 2007). In general, temperate phages harbor fewer tRNA genes than do virulent phages. It has been suggested that tRNA acquisition may contribute to greater virulence (Bailly-Bechet et al., 2007). A more recent study of different mycobacteriophage clusters suggests that the benefits of having tRNA genes may be associated with either a better growth in their hosts (larger burst size and shorter latency) or the ability to infect more hosts (Delesalle et al., 2016). Although an increasing number of prophages are described that carry tRNA genes (Canchaya et al., 2004), their presence among *Streptococcus* prophages appears to be uncommon. In a recent analysis of 13,200 viral sequences (Morgado and Vicente, 2019), only four streptococcal phages were found to harbor tRNA genes; three were virulent [SMP from *S. suis* (Acc. No. EF116926), SP-QS1 from *S. pneumoniae* (Acc. No. HE962497), and P5652 from *Streptococcus thermophilus* (Acc. No. KY705261)], and only one was temperate [Φ ARI0746 from *S. pneumoniae* (Acc. No. KT337365)].

All the VapE_{Ssu}-like proteins were encoded by defective prophages (with the exception of PPH08_12), as previously reported (Rezaei Javan et al., 2019). Both defective and complete prophages coded for VapE_{Dno} homologs. Experimental evidence exists that the VapE_{Ssu} homolog of the defective prophage Javan757 (Acc. No. WP_000434359) is involved in virulence. Using a sepsis model, it was reported that mice infected with the wild-type pneumococcal strain had significantly greater blood and spleen bacterial counts than the isogenic Δ vapE mutant (Rezaei Javan et al., 2019). In addition, it was observed that the reduced virulence of the mutant could be explained by a significant growth delay when cultivated in serum. Further, *vapE* was upregulated only when the pneumococcal strain grew under planktonic conditions, analogous to bacteremic growth. Whether the other VapE_{Dno} homologs described here also play a significant role in pneumococcal pathogenicity warrants further investigation.

S. pneumoniae does not contain an endogenous CRISPR/Cas system; this is consistent with interference with natural transformation and thereby lateral gene transfer crucial for pneumococcal host adaptation (Bikard et al., 2012) (<https://crispr.i2bc.paris-saclay.fr/>). Among the defense mechanisms developed by bacteria to combat phage attack, R-M systems are pervasive. Their general role is to spot foreign DNA *via* base modifications and to defend the host DNA from restriction enzymes *via* Mtae activity. Recently, however, more functions for R-M systems have been described (Vasu and Nagaraja, 2013). Their activities are due to several heterogeneous proteins classified into at least four groups.

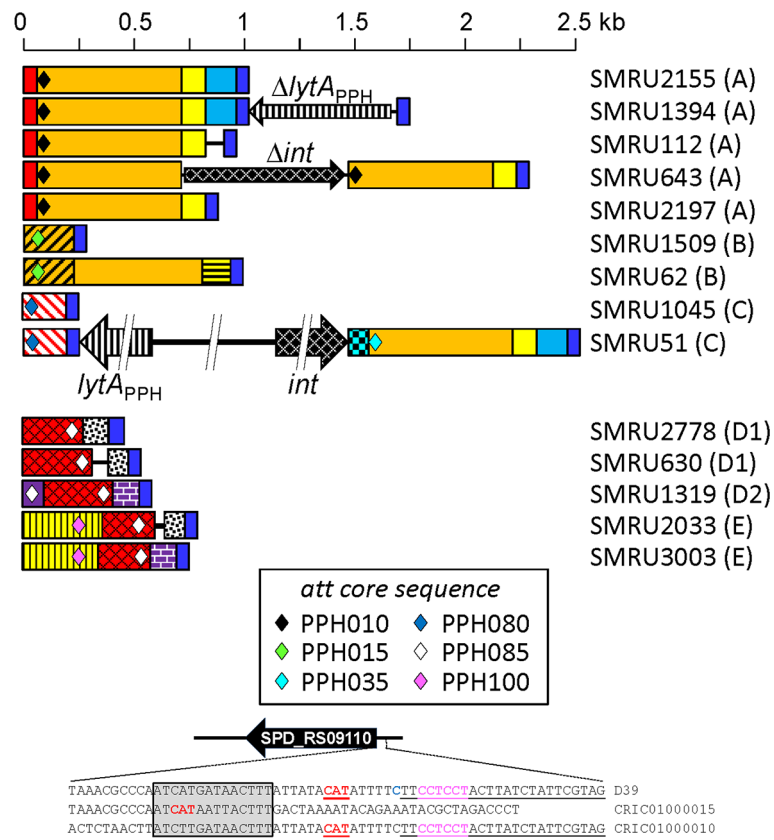


FIGURE 6 | Diagram of the region located immediately downstream of the termination codon of *lytA_{Spn}** in 14 pneumococcal strains with differently rearranged genomes. The region corresponds to that indicated with a gray square in **Figure 4**. DNA regions sharing $\geq 95\%$ nucleotide identity are shown with the same color and shadowing. The type of arrangement (A to E) is indicated in parentheses to the right of the name of each strain. The different core attachment sites are shown as diamonds. The deep blue rectangles represent the conserved 51 bp-long sequence mentioned in the text. The red rectangles correspond to the reverse complement of positions 24037–24121 of the *S. pneumoniae* D39 genome (between SPD_RS00120 encoding a nucleoside deaminase and SPD_RS00115 coding for an adenylosuccinate synthase). The purple rectangle corresponds to positions 1,712,485–1,712,386 (between SPD_RS09110 and SPD_RS09115 in the D39 chromosome). For additional information see **Tables S6** and **S8**. At the bottom, the nucleotide sequence surrounding the initiation codon of SPD_RS09110 in strains D39 and SMRU1319 (arrangement D2) is shown. The correct initiation codon is shown in red, bold font, and underlined. Another in-frame initiation codon is not underlined and apparently lacks a potential ribosome-binding site (RBS) (Acc. No. CRIC01000015). The predicted RBS of SPD_RS09110 is shown in pink lettering. The 14 bp-long repeat potentially responsible for a chromosomal inversion in strain SMRU1319 is inserted in a gray box. The *att* core sequence of PPH085 is underlined.

Most *S. pneumoniae* isolates express either the DpnI or DpnII R-M system, although a DpnIII system has also been reported (Eutsey et al., 2015). Interestingly, the virulent pneumophage Cp-1 cannot be restricted in *S. pneumoniae* because it does not contain the corresponding target sequence (5'-GATC-3') in its genome (Martín et al., 1996). The virulent pneumophage Dp-1 probably defends against host-induced DNA restriction by incorporating modified bases into it (García et al., 2005). This is consistent with a more recent report showing that resistance to Dp-1 in *S. pneumoniae* results from mutations in a single gene (SPD_RS05930) coding for a type IV restriction endonuclease (Leprohon et al., 2015). It is noteworthy that type IV restriction systems differ from other types in that the Mtase and endonuclease activities are combined in a single enzyme that requires base modification to act (Loenen and Raleigh, 2014). A phase-variable type I R-M system has also been identified in various strains of *S. pneumoniae*. This system

operates as an epigenetic switch that regulates gene expression, virulence, and phase variation (opaque versus transparent phenotype) in pneumococci (Li and Zhang, 2019). Moreover, the importance that phase-variable type I R-M systems have in the multifunctional defense against prophage SpSL1 infection in *S. pneumoniae* has been demonstrated (Furi et al., 2019).

The present study provides clear evidence of recombination events between pneumococcal and phage *lytA* homologs. Recombination is apparently independent of the phage *Int* and is facilitated by the noticeable sequence similarity between the phage and host genes ($\geq 85\%$ identity). Although uncommon, a similar process has been reported to occur between the *thyP3* and the *thyA* genes encoding the thymidylate synthase of the temperate bacteriophage $\phi 3T$ and that of the *Bacillus subtilis* host (Tucker, 1969; Stroynowski, 1981; Stout et al., 1998; Fox et al., 1999). In this case, the nucleotide sequence identity reaches 96% (Kenny et al., 1985;

Tam and Borriss, 1995). Unfortunately, whether recombination between the *B. subtilis* and the phage $\phi 3T$ genes also causes genome rearrangements, as is the case of the PPH090 group, is unknown.

The present results provide a comprehensive view of the lysogenic state of phages in *S. pneumoniae*. As in most phage genomes currently under study, the majority of the PPH genes play uncharacterized roles. There is increasing evidence that although bacteriophages do not infect eukaryotic cells, they do interact with innate immune cells via Toll-like receptors (which appears to be particularly true for temperate bacteriophages) (Cieřlik et al., 2021; Podlacha et al., 2021; Popescu et al., 2021), but the phage components involved in this are virtually unknown.

Finally, the consequences of genome rearrangements involving *lytA* genes in bacteria and phage physiology deserve to be further studied.

AUTHOR'S NOTE

This work is dedicated to our mentor and friend, Concepción Ronda, who fostered the research on pneumococcal bacteriophages in our laboratory.

DATA AVAILABILITY STATEMENT

The original contributions presented in the study are included in the article/**Supplementary Material**. Further inquiries can be directed to the corresponding author.

REFERENCES

- Achaz, G., Coissac, E., Netter, P., and Rocha, E. P. C. (2003). Associations Between Inverted Repeats and the Structural Evolution of Bacterial Genomes. *Genetics* 164, 1279–1289. doi: 10.1093/genetics/164.4.1279
- Afzal, M., Shafeeq, S., Henriques-Normark, B., and Kuipers, O. P. (2015). UlaR Activates Expression of the *Ula* Operon in *Streptococcus Pneumoniae* in the Presence of Ascorbic Acid. *Microbiology* 161, 41–49. doi: 10.1099/mic.0.083899-0
- Andam, C. P., Worby, C. J., Gierke, R., McGee, L., Pilishvili, T., and Hanage, W. P. (2017). Penicillin Resistance of Nonvaccine Type Pneumococcus Before and After PCV13 Introduction, United States. *Emerg. Infect. Dis.* 23, 1012–1015. doi: 10.3201/eid2306.161331
- Arndt, D., Grant, J. R., Marcu, A., Sajed, T., Pon, A., Liang, Y., et al (2016). PHASTER: A Better, Faster Version of the PHAST Phage Search Tool. *Nucleic Acids Res.* 44, W16–W21. doi: 10.1093/nar/gkw387
- Bailly-Bechet, M., Vergassola, M., and Rocha, E. (2007). Causes for the Intriguing Presence of tRNAs in Phages. *Genome Res.* 17, 1486–1495. doi: 10.1101/gr.6649807
- Bensing, B. A., Siboo, I. R., and Sullam, P. M. (2001). Proteins PblA and PblB of *Streptococcus Mitis*, Which Promote Binding to Human Platelets, are Encoded Within a Lysogenic Bacteriophage. *Infect. Immun.* 69, 6186–6192. doi: 10.1128/IAI.69.10.6186-6192.2001
- Bernheimer, H. P. (1977). Lysogeny in Pneumococci Freshly Isolated From Man. *Science* 195, 66–68. doi: 10.1126/science.12565
- Bikard, D., Hatoum-Aslan, A., Mucida, D., and Marraffini, L. A. (2012). CRISPR Interference can Prevent Natural Transformation and Virulence Acquisition During *In Vivo* Bacterial Infection. *Cell Host Microbe* 12, 177–186. doi: 10.1016/j.chom.2012.06.003

AUTHORS CONTRIBUTIONS

EG designed the study. AM-G and EG conducted the analyses and wrote the article. All authors contributed to the article and approved the submitted version.

ACKNOWLEDGMENTS

The help of Carmen Ascaso, who granted the infrastructure and peaceful environment required for this study to be completed, is greatly acknowledged. We thank P. García (CIB, CSIC) for carefully revising the article and suggestions. This research was supported by grants MPY 509/19 from the Instituto de Salud Carlos III (ISCIII) and SAF2017-88664-R from the Spanish Ministerio de Economía, Industria y Competitividad (MEICOM). The Centro de Investigación Biomédica en Red de Enfermedades Respiratorias (CIBERES) is an initiative of the Instituto de Salud Carlos III (ISCIII). AM-G is the recipient of a Miguel Servet contract by the ISCIII.

SUPPLEMENTARY MATERIAL

The Supplementary Material for this article can be found online at: <https://www.frontiersin.org/articles/10.3389/fcimb.2021.775402/full#supplementary-material>

- Billington, S. J., Johnston, J. L., and Rood, J. I. (1996). Virulence Regions and Virulence Factors of the Ovine Footrot Pathogen, *Dichelobacter Nodosus*. *FEMS Microbiol. Lett.* 145, 147–156. doi: 10.1111/j.1574-6968.1996.tb08570.x
- Bobay, L.-M., Touchon, M., and Rocha, E. P. C. (2014). Pervasive Domestication of Defective Prophages by Bacteria. *Proc. Natl. Acad. Sci. U.S.A.* 111, 12127–12132. doi: 10.1073/pnas.1405336111
- Brantl, S., and Brückner, R. (2014). Small Regulatory RNAs From Low-GC Gram-Positive Bacteria. *RNA Biol.* 11, 443–456. doi: 10.4161/rna.28036
- Brueggemann, A. B., Harrold, C. L., Javan, R. R., van Tonder, A. J., McDonnell, A. J., and Edwards, B. A. (2017). Pneumococcal Prophages are Diverse, But Not Without Structure or History. *Sci. Rep.* 7, 42976. doi: 10.1038/srep42976
- Cámara, J., Cubero, M., Martín-Galiano, A. J., García, E., Grau, I., Nielsen, J. B., et al (2018). Evolution of the β -Lactam-Resistant *Streptococcus Pneumoniae* PMEN3 Clone Over a 30-Year Period in Barcelona, Spain. *J. Antimicrob. Chemother.* 73, 2941–2951. doi: 10.1093/jac/dky305
- Campbell, A. M. (1962). Episomes. *Adv. Genet.* 11, 101–145. doi: 10.1016/S0065-2660(08)60286-2
- Canchaya, C., Fournous, G., and Brüssow, H. (2004). The Impact of Prophages on Bacterial Chromosomes. *Mol. Microbiol.* 53, 9–18. doi: 10.1111/j.1365-2958.2004.04113.x
- Canchaya, C., Proux, C., Fournous, G., Bruttin, A., and Brüssow, H. (2003). Prophage Genomics. *Microbiol. Mol. Biol. Rev.* 67, 238–276. doi: 10.1128/mmbr.67.2.238-276.2003
- Canvin, J. R., Marvin, A. P., Sivakumaran, M., Paton, J. C., Boulnois, G. J., Andrew, P. W., et al (1995). The Role of Pneumolysin and Autolysin in the Pathology of Pneumonia and Septicemia in Mice Infected With a Type 2 Pneumococcus. *J. Infect. Dis.* 172, 119–123. doi: 10.1093/infdis/172.1.119
- Carrolo, M., Frias, M. J., Pinto, F. R., Melo-Cristino, J., and Ramirez, M. (2010). Prophage Spontaneous Activation Promotes DNA Release Enhancing Biofilm

- Formation in *Streptococcus Pneumoniae*. *PLoS One* 5, e15678. doi: 10.1371/journal.pone.0015678
- Casjens, S. (2003). Prophages and Bacterial Genomics: What Have We Learned So Far? *Mol. Microbiol.* 49, 277–300. doi: 10.1046/j.1365-2958.2003.03580.x
- Chen, H.-J., Chang, Y.-C., Tsai, J.-C., Hung, W.-C., Lin, Y.-T., You, S.-J., et al (2013). New Structure of Phage-Related Islands Carrying *fusB* and a Virulence Gene in Fusidic Acid-Resistant *Staphylococcus Epidermidis*. *Antimicrob. Agents Chemother.* 57, 5737–5739. doi: 10.1128/AAC.01433-13
- Chen, Y.-Y., Wang, J.-T., Lin, T.-L., Gong, Y.-N., Li, T.-H., Huang, Y.-Y., et al (2019). Prophage Excision in *Streptococcus Pneumoniae* Serotype 19A ST320 Promote Colonization: Insight Into its Evolution From the Ancestral Clone Taiwan 19F-14 (ST236). *Front. Microbiol.* 10, 205. doi: 10.3389/fmicb.2019.00205
- Cieślak, M., Bagińska, N., Jończyk-Matysiak, E., Węgrzyn, A., Węgrzyn, G., and Górski, A. (2021). Temperate Bacteriophages—The Powerful Indirect Modulators of Eukaryotic Cells and Immune Functions. *Viruses* 13, 1013. doi: 10.3390/v13061013
- Corsini, B., Aguinalde, L., Ruiz, S., Domenech, M., and Yuste, J. (2021). Vaccination With LytA, LytC, or Pce of *Streptococcus Pneumoniae* Protects Against Sepsis by Inducing IgGs That Activate the Complement System. *Vaccines* 9, 186. doi: 10.3390/vaccines9020186
- Cremers, A. J. H., Mobegi, F. M., van der Gaast-de Jongh, C., van Weert, M., van Opzeeland, F. J., Vehkala, M., et al (2019). The Contribution of Genetic Variation of *Streptococcus Pneumoniae* to the Clinical Manifestation of Invasive Pneumococcal Disease. *Clin. Infect. Dis.* 68, 61–69. doi: 10.1093/cid/ciy417
- Croucher, N. J., Campo, J. J., Leb, T. Q., Liang, X., Bentley, S. D., Hanage, W. P., et al (2017). Diverse Evolutionary Patterns of Pneumococcal Antigens Identified by Pangenome-Wide Immunological Screening. *Proc. Natl. Acad. Sci. U.S.A.* 114, E357–E366. doi: 10.1073/pnas.1613937114
- Croucher, N. J., Hanage, W. P., Harris, S. R., McGee, L., van der Linden, M., de Lencastre, H., et al (2014). Variable Recombination Dynamics During the Emergence, Transmission and 'Disarming' of a Multidrug-Resistant Pneumococcal Clone. *BMC Biol.* 12, 49. doi: 10.1186/1741-7007-12-49
- Croucher, N. J., Harris, S. R., Fraser, C., Quail, M. A., Burton, J., van der Linden, M., et al (2011). Rapid Pneumococcal Evolution in Response to Clinical Interventions. *Science* 331, 430–434. doi: 10.1126/science.1198545
- Croucher, N. J., Mostowy, R., Wymant, C., Turner, P., Bentley, S. D., and Fraser, C. (2016). Horizontal DNA Transfer Mechanisms of Bacteria as Weapons of Intragenomic Conflict. *PLoS Biol.* 14, e1002394. doi: 10.1371/journal.pbio.1002394
- Delesalle, V. A., Tanke, N. T., Vill, A. C., and Krukonis, G. P. (2016). Testing Hypotheses for the Presence of tRNA Genes in Mycobacteriophage Genomes. *Bacteriophage* 6, e1219441. doi: 10.1080/21597081.2016.1219441
- Denapate, D., Rieger, M., Köndgen, S., Brückner, R., Ochigava, I., Kappeler, P., et al (2016). Highly Variable *Streptococcus Oralis* Strains are Common Among Viridans Streptococci Isolated From Primates. *mSphere* 1, e00041–e00015. doi: 10.1128/mSphere.00041-15
- Díaz, E., and García, J. L. (1990). Characterization of the Transcription Unit Encoding the Major Pneumococcal Autolysin. *Gene* 90, 157–162. doi: 10.1016/0378-1119(90)90454-y
- Diene, S. M., François, P., Zbinden, A., Entenza, J. M., and Resch, G. (2016). Comparative Genomics Analysis of *Streptococcus Tigurinus* Strains Identifies Genetic Elements Specifically and Uniquely Present in Highly Virulent Strains. *PLoS One* 11, e0160554. doi: 10.1371/journal.pone.0160554
- Domenech, M., Damián, D., Ardanuy, C., Liñares, J., Fenoll, A., and García, E. (2015). Emerging, non-PCV13 Serotypes 11A and 35B of *Streptococcus Pneumoniae* Show High Potential for Biofilm Formation *In Vitro*. *PLoS One* 10, e0125636. doi: 10.1371/journal.pone.0125636
- Domenech, M., García, E., and Moscoso, M. (2011). *In Vitro* Destruction of *Streptococcus Pneumoniae* Biofilms With Bacterial and Phage Peptidoglycan Hydrolases. *Antimicrob. Agents Chemother.* 55, 4144–4148. doi: 10.1128/aac.00492-11
- Enright, M. C., and Spratt, B. G. (1998). A Multilocus Sequence Typing Scheme for *Streptococcus Pneumoniae*: Identification of Clones Associated With Serious Invasive Disease. *Microbiology* 144, 3049–3060. doi: 10.1099/00221287-144-11-3049
- Eutsey, R. A., Powell, E., Dordel, J., Salter, S. J., Clark, T. A., Korlach, J., et al (2015). Genetic Stabilization of the Drug-Resistant PMEN1 *Pneumococcus* Lineage by its Distinctive DpnIII Restriction-Modification System. *mBio* 6, e00173. doi: 10.1128/mBio.00173-15
- Fernández, L., Cima-Cabal, M. D., Duarte, A. C., Rodríguez, A., García-Suárez, M., and García, P. (2021). Gram-Positive Pneumonia: Possibilities Offered by Phage Therapy. *Antibiotics (Basel)* 10, 1000. doi: 10.3390/antibiotics10081000
- Fox, K. M., Maley, F., Garibian, A., Changchien, L. M., and Van Roey, P. (1999). Crystal Structure of Thymidylate Synthase A From *Bacillus Subtilis*. *Protein Sci.* 8, 538–544. doi: 10.1110/ps.8.3.538
- Frolet, C., Beniazza, M., Roux, L., Gallet, B., Noirclerc-Savoye, M., Vernet, T., et al (2010). New Adhesin Functions of Surface-Exposed Pneumococcal Proteins. *BMC Microbiol.* 10, 190. doi: 10.1186/1471-2180-10-190
- Furi, L., Crawford, L. A., Rangel-Pineros, G., Manso, A. S., De Ste Croix, M., Haigh, R. D., et al (2019). Methylation Warfare: Interaction of Pneumococcal Bacteriophages With Their Host. *J. Bacteriol.* 201, e00370–e00319. doi: 10.1128/jb.00370-19
- Galán-Bartual, S., Pérez-Dorado, I., García, P., and Hermoso, J. A. (2015). "Structure and Function of Choline-Binding Proteins," in *Streptococcus Pneumoniae. Molecular Mechanisms of Host-Pathogen Interactions*. Eds. J. Brown, S. Hammerschmidt and C. Orihuela (Amsterdam: Academic Press), 207–230. doi: 10.1016/b978-0-12-410530-0.00011-9
- García, P., García, J. L., López, R., and García, E. (2005). "Pneumococcal Phages," in *Phages: Their Role in Bacterial Pathogenesis and Biotechnology*. Eds. M. K. Waldor, D. L. I. Friedman and S. Adhya (Washington, D.C.: ASM Press), 335–361. doi: 10.1128/9781555816506.ch17
- Garriss, G., and Henriques-Normark, B. (2020). Lysogeny in *Streptococcus Pneumoniae*. *Microorganisms* 8, 1546. doi: 10.3390/microorganisms8101546
- GBD 2016 Lower Respiratory Infections Collaborators (2018). Estimates of the Global, Regional, and National Morbidity, Mortality, and Aetiologies of Lower Respiratory Infections in 195 Countries 1990–2016: A Systematic Analysis for the Global Burden of Disease Study 2016. *Lancet Infect. Dis.* 18, 1191–1210. doi: 10.1016/S1473-3099(18)30310-4
- Gibb, B., Gupta, K., Ghosh, K., Sharp, R., Chen, J., and Van Duyn, G. D. (2010). Requirements for Catalysis in the Cre Recombinase Active Site. *Nucleic Acids Res.* 38, 5817–5832. doi: 10.1093/nar/gkq384
- Gindreau, E., López, R., and García, P. (2000). MM1, a Temperate Bacteriophage of the 23F Spanish/USA Multiresistant Epidemic Clone of *Streptococcus Pneumoniae*: Structural Analysis of the Site-Specific Integration System. *J. Virol.* 74, 7803–7813. doi: 10.1128/jvi.74.17.7803-7813.2000
- Gladstone, R. A., Lo, S. W., Lees, J. A., Croucher, N. J., van Tonder, A. J., Corander, J., et al (2019). International Genomic Definition of Pneumococcal Lineages, to Contextualise Disease, Antibiotic Resistance and Vaccine Impact. *EBioMedicine* 43, 338–346. doi: 10.1016/j.ebiom.2019.04.021
- Groth, A. C., and Calos, M. P. (2004). Phage Integrases: Biology and Applications. *J. Mol. Biol.* 335, 667–678. doi: 10.1016/j.jmb.2003.09.082
- Gu, J., Feng, Y., Feng, X., Sun, C., Lei, L., Ding, W., et al (2014). Structural and Biochemical Characterization Reveals LysGH15 as an Unprecedented "EF-Hand-Like" Calcium-Binding Phage Lysin. *PLoS Pathog.* 10, e1004109. doi: 10.1371/journal.ppat.1004109
- Gu, J., Xu, W., Lei, L., Huang, J., Feng, X., Sun, C., et al (2011). LysGH15, a Novel Bacteriophage Lysin, Protects a Murine Bacteremia Model Efficiently Against Lethal Methicillin-Resistant *Staphylococcus Aureus* Infection. *J. Clin. Microbiol.* 49, 111–117. doi: 10.1128/JCM.01144-10
- Harvey, R. M., Trappetti, C., Mahdi, L. K., Wang, H., McAllister, L. J., Scalvini, A., et al (2016). The Variable Region of Pneumococcal Pathogenicity Island 1 is Responsible for Unusually High Virulence of a Serotype 1 Isolate. *Infect. Immun.* 84, 822–832. doi: 10.1128/IAI.01454-15
- Hermoso, J. A., Monterroso, B., Albert, A., Galán, B., Ahrazem, O., García, P., et al (2003). Structural Basis for Selective Recognition of Pneumococcal Cell Wall by Modular Endolysin From Phage Cp-1. *Structure* 11, 1239–1249. doi: 10.1016/j.str.2003.09.005
- Hsieh, Y.-C., Lin, T.-L., Lin, C.-M., and Wang, J.-T. (2015). Identification of PblB Mediating Galactose-Specific Adhesion in a Successful *Streptococcus Pneumoniae* Clone. *Sci. Rep.* 5, 12265. doi: 10.1038/srep12265
- Hughes, D. (2000). Evaluating Genome Dynamics: The Constraints on Rearrangements Within Bacterial Genomes. *Genome Biol.* 1, REVIEWS0006. doi: 10.1186/gb-2000-1-6-reviews0006
- Hyatt, D., Chen, G.-L., LoCascio, P. F., Land, M. L., Larimer, F. W., and Hauser, L. J. (2010). Prodigal: Prokaryotic Gene Recognition and Translation Initiation

- Site Identification. *BMC Bioinformatics* 11, 119. doi: 10.1186/1471-2105-11-119
- Ji, X., Sun, Y., Liu, J., Zhu, L., Guo, X., Lang, X., et al (2016). A Novel Virulence-Associated Protein, VapE, in *Streptococcus Suis* Serotype 2. *Mol. Med. Rep.* 13, 2871–2877. doi: 10.3892/mmr.2016.4818
- Johnson, M., Zaretskaya, I., Raytselis, Y., Merezuk, Y., McGinnis, S., and Madden, T. L. (2008). NCBI BLAST: A Better Web Interface. *Nucleic Acids Res.* 36, W5–W9. doi: 10.1093/nar/gkn201
- Jolley, K. A., Bray, J. E., and Maiden, M. C. J. (2018). Open-Access Bacterial Population Genomics: BIGSdb Software, the PubMLST.org Website and Their Applications. *Wellcome Open Res.* 3, 124. doi: 10.12688/wellcomeopenres.14826.1
- Kenny, E., Atkinson, T., and Hartley, B. S. (1985). Nucleotide Sequence of the Thymidylate Synthetase Gene (*Thy3*) From the *Bacillus Subtilis* Phage ϕ 3T. *Gene* 34, 335–342. doi: 10.1016/0378-1119(85)90142-8
- Khan, A., Burmeister, A. R., and Wahl, L. M. (2020). Evolution Along the Parasitism-Mutualism Continuum Determines the Genetic Repertoire of Prophages. *PLoS Comput. Biol.* 16, e1008482. doi: 10.1371/journal.pcbi.1008482
- Kilian, M., Riley, D. R., Jensen, A., Brüggemann, H., and Tettelin, H. (2014). Parallel Evolution of *Streptococcus Pneumoniae* and *Streptococcus Mitis* to Pathogenic and Mutualistic Lifestyles. *mBio* 5, e01490–14. doi: 10.1128/mBio.01490-14
- Koonin, E. V., Makarova, K. S., and Wolf, Y. I. (2017). Evolutionary Genomics of Defense Systems in Archaea and Bacteria. *Annu. Rev. Microbiol.* 71, 233–261. doi: 10.1146/annurev-micro-090816-093830
- Kot, W., Sabri, M., Gingras, H., Ouellette, M., Tremblay, D. M., and Moineau, S. (2017). Complete Genome Sequence of *Streptococcus Pneumoniae* Virulent Phage MS1. *Genome Announc.* 5, e00333–17. doi: 10.1128/genomeA.00333-17
- Labrie, S. J., Samson, J. E., and Moineau, S. (2010). Bacteriophage Resistance Mechanisms. *Nat. Rev. Microbiol.* 8, 317–327. doi: 10.1038/nrmicro2315
- Larsen, M. V., Cosentino, S., Rasmussen, S., Friis, C., Hasman, H., Marvig, R. L., et al (2012). Multilocus Sequence Typing of Total-Genome-Sequenced Bacteria. *J. Clin. Microbiol.* 50, 1355–1361. doi: 10.1128/JCM.06094-11
- Laslett, D., and Canback, B. (2004). ARAGORN, a Program to Detect tRNA Genes and tmRNA Genes in Nucleotide Sequences. *Nucleic Acids Res.* 32, 11–16. doi: 10.1093/nar/gkh152
- Laurenceau, R., Krasteva, P. V., Diallo, A., Ouarti, S., Duchateau, M., Malosse, C., et al (2015). Conserved *Streptococcus Pneumoniae* Spirosomes Suggest a Single Type of Transformation Pilus in Competence. *PLoS Pathog.* 11, e1004835. doi: 10.1371/journal.ppat.1004835
- Lees, J. A., Croucher, N. J., Goldblatt, D., Nosten, F., Parkhill, J., Turner, C., et al (2017). Genome-Wide Identification of Lineage and Locus Specific Variation Associated With Pneumococcal Carriage Duration. *eLife* 6, e26255. doi: 10.7554/eLife.26255
- Leprohon, P., Gingras, H., Ouennane, S., Moineau, S., and Ouellette, M. (2015). A Genomic Approach to Understand Interactions Between *Streptococcus Pneumoniae* and its Bacteriophages. *BMC Genomics* 16, 972. doi: 10.1186/s12864-015-2134-8
- Li, Q., Cheng, W., Morlot, C., Bai, X.-H., Jiang, Y.-L., Wang, W., et al (2015). Full-Length Structure of the Major Autolysin LytA. *Acta Crystallogr. D Biol. Crystallogr.* 71, 1373–1381. doi: 10.1107/S1399004715007403
- Lindsay, J. A., Ruzin, A., Ross, H. F., Kurepina, N., and Novick, R. P. (1998). The Gene for Toxic Shock Toxin is Carried by a Family of Mobile Pathogenicity Islands in *Staphylococcus Aureus*. *Mol. Microbiol.* 29, 527–543. doi: 10.1046/j.1365-2958.1998.00947.x
- Li, J., and Zhang, J. R. (2019). Phase Variation of *Streptococcus Pneumoniae*. *Microbiol. Spectr.* 7. doi: 10.1128/microbiolspec.GPP3-0005-2018
- Llull, D., López, R., and García, E. (2006). Skl, a Novel Choline-Binding N-Acetylmuramoyl-L-Alanine Amidase of *Streptococcus Mitis* SK137 Containing a CHAP Domain. *FEBS Lett.* 580, 1959–1964. doi: 10.1016/j.febslet.2006.02.060
- Loeffler, J. M., and Fischetti, V. A. (2006). Lysogeny of *Streptococcus Pneumoniae* With MM1 Phage: Improved Adherence and Other Phenotypic Changes. *Infect. Immun.* 74, 4486–4495. doi: 10.1128/IAI.00020-06
- Loenen, W. A. M., and Raleigh, E. A. (2014). The Other Face of Restriction: Modification-Dependent Enzymes. *Nucleic Acids Res.* 42, 56–69. doi: 10.1093/nar/gkt747
- Lopes de Sousa, A., Maués, D., Lobato, A., Franco, E. F., Pinheiro, K., Araújo, F., et al (2018). PhageWeb – Web Interface for Rapid Identification and Characterization of Prophages in Bacterial Genomes. *Front. Genet.* 9, 644. doi: 10.3389/fgene.2018.00644
- López, E., Domenech, A., Ferrándiz, M.-J., Frias, M. J., Ardanuy, C., Ramirez, M., et al (2014). Induction of Prophages by Fluoroquinolones in *Streptococcus Pneumoniae*: Implications for Emergence of Resistance in Genetically-Related Clones. *PLoS One* 9, e94358. doi: 10.1371/journal.pone.0094358
- López, R., and García, E. (2004). Recent Trends on the Molecular Biology of Pneumococcal Capsules, Lytic Enzymes, and Bacteriophage. *FEMS Microbiol. Rev.* 28, 553–580. doi: 10.1016/j.femsre.2004.05.002
- Lund, E., and Henrichsen, J. (1978). Laboratory Diagnosis, Serology and Epidemiology of *Streptococcus Pneumoniae*. *Methods Microbiol.* 12, 241–262. doi: 10.1016/S0580-9517(08)70365-9
- Lu, S., Wang, J., Chitsaz, F., Derbyshire, M. K., Geer, R. C., Gonzales, N. R., et al (2020). CDD/SPARCLE: The Conserved Domain Database in 2020. *Nucleic Acids Res.* 48, D265–D268. doi: 10.1093/nar/gkz991
- Lwoff, A. (1953). Lysogeny. *Bacteriol. Rev.* 17, 269–337. doi: 10.1128/br.17.4.269-337.1953
- Maestro, B., and Sanz, J. M. (2016). Choline Binding Proteins From *Streptococcus Pneumoniae*: A Dual Role as Enzybiotics and Targets for the Design of New Antimicrobials. *Antibiotics (Basel)* 5, 21. doi: 10.3390/antibiotics5020021
- Martin, A. C., López, R., and García, P. (1996). Analysis of the Complete Nucleotide Sequence and Functional Organization of the Genome of *Streptococcus Pneumoniae* Bacteriophage Cp-1. *J. Virol.* 70, 3678–3687. doi: 10.1128/JVI.70.6.3678-3687.1996
- Masomian, M., Ahmad, Z., Gew, L. T., and Poh, C. L. (2020). Development of Next Generation *Streptococcus Pneumoniae* Vaccines Conferring Broad Protection. *Vaccines* 8, 132. doi: 10.3390/vaccines8010132
- McGee, L., McDougal, L., Zhou, J., Spratt, B. G., Tenover, F. C., George, R., et al (2001). Nomenclature of Major Antimicrobial-Resistant Clones of *Streptococcus Pneumoniae* Defined by the Pneumococcal Molecular Epidemiology Network. *J. Clin. Microbiol.* 39, 2565–2571. doi: 10.1128/JCM.39.7.2565-2571.2001
- Mellroth, P., Sandalova, T., Kikhney, A., Vilaplana, F., Heseck, D., Lee, M., et al (2014). Structural and Functional Insights Into Peptidoglycan Access for the Lytic Amidase LytA of *Streptococcus Pneumoniae*. *mBio* 5, e01120–e01113. doi: 10.1128/mBio.01120-13
- Mirdita, M., Steinegger, M., and Söding, J. (2019). MMseqs2 Desktop and Local Web Server App for Fast, Interactive Sequence Searches. *Bioinformatics* 35, 2856–2858. doi: 10.1093/bioinformatics/bty1057
- Morales, M., García, P., de la Campa, A. G., Liñares, J., Ardanuy, C., and García, E. (2010). Evidence of Localized Prophage-Host Recombination in the *lytA* Gene Encoding the Major Pneumococcal Autolysin. *J. Bacteriol.* 192, 2624–2632. doi: 10.1128/JB.01501-09
- Morales, M., Martín-Galiano, A. J., Domenech, M., and García, E. (2015). Insights Into the Evolutionary Relationships of LytA Autolysin and Ply Pneumolysin-Like Genes in *Streptococcus Pneumoniae* and Related Streptococci. *Genome Biol. Evol.* 7, 2747–2761. doi: 10.1093/gbe/evv178
- Morgado, S., and Vicente, A. C. (2019). Global *in-Silico* Scenario of tRNA Genes and Their Organization in Virus Genomes. *Viruses* 11, 180. doi: 10.3390/v11020180
- Murphy, J., Mahony, J., Ainsworth, S., Nauta, A., and van Sinderen, D. (2013). Bacteriophage Orphan DNA Methyltransferases: Insights From Their Bacterial Origin, Function, and Occurrence. *Appl. Environ. Microbiol.* 79, 7547–7555. doi: 10.1128/aem.02229-13
- Murray, E., Draper, L. A., Ross, R. P., and Hill, C. (2021). The Advantages and Challenges of Using Endolysins in a Clinical Setting. *Viruses* 13, 680. doi: 10.3390/v13040680
- Mushegian, A. R. (2020). Are There 10^{31} Virus Particles on Earth, or More, or Fewer? *J. Bacteriol.* 202, e00052–20. doi: 10.1128/jb.00052-20
- Nakamura, Y., Gojobori, T., and Ikemura, T. (2000). Codon Usage Tabulated From International DNA Sequence Databases: Status for the Year 2000. *Nucleic Acids Res.* 28, 292. doi: 10.1093/nar/28.1.292
- Nakamura, K., Ogura, Y., Gotoh, Y., and Hayashi, T. (2021). Prophages Integrating Into Prophages: A Mechanism to Accumulate Type III Secretion Effector Genes and Duplicate Shiga Toxin-Encoding Prophages in *Escherichia Coli*. *PLoS Pathog.* 17, e1009073. doi: 10.1371/journal.ppat.1009073

- Nieto, C., Espinosa, M., and Puyet, A. (1997). The Maltose/Maltodextrin Regulon of *Streptococcus Pneumoniae*. Differential Promoter Regulation by the Transcriptional Repressor MalR. *J. Biol. Chem.* 272, 30860–30865. doi: 10.1074/jbc.272.49.30860
- O'Leary, N. A., Wright, M. W., Brister, J. R., Ciufo, S., Haddad, D., McVeigh, R., et al (2016). Reference Sequence (RefSeq) Database at NCBI: Current Status, Taxonomic Expansion, and Functional Annotation. *Nucleic Acids Res.* 44, D733–D745. doi: 10.1093/nar/gkv1189
- Obregón, V., García, J. L., García, E., López, R., and García, P. (2003a). Genome Organization and Molecular Analysis of the Temperate Bacteriophage MM1 of *Streptococcus Pneumoniae*. *J. Bacteriol.* 185, 2362–2368. doi: 10.1128/jb.185.7.2362-2368.2003
- Obregón, V., García, P., López, R., and García, J. L. (2003b). VO1, a Temperate Bacteriophage of the Type 19A Multiresistant Epidemic 8249 Strain of *Streptococcus Pneumoniae*: Analysis of Variability of Lytic and Putative C5 Methyltransferase Genes. *Microb. Drug Resist.* 9, 7–15. doi: 10.1089/107662903764736292
- Ouennane, S., Leprohon, P., and Moineau, S. (2015). Diverse Virulent Pneumophages Infect *Streptococcus Mitis*. *PLoS One* 10, e0118807. doi: 10.1371/journal.pone.0118807
- Pei, J., Mitchell, D. A., Dixon, J. E., and Grishin, N. V. (2011). Expansion of Type II CAAX Proteases Reveals Evolutionary Origin of γ -Secretase Subunit APH-1. *J. Mol. Biol.* 410, 18–26. doi: 10.1016/j.jmb.2011.04.066
- Peng, S.-Y., Chen, L.-K., Wu, W.-J., Paramita, P., Yang, P.-W., Li, Y.-Z., et al (2020). Isolation and Characterization of a New Phage Infecting *Elizabethkingia Anophelis* and Evaluation of its Therapeutic Efficacy *In Vitro* and *In Vivo*. *Front. Microbiol.* 11, 728. doi: 10.3389/fmicb.2020.00728
- Pfeifer, E., Moura de Sousa, J. A., Touchon, M., and Rocha, E. P. C. (2021). Bacteria Have Numerous Distinctive Groups of Phage-Plasmids With Conserved Phage and Variable Plasmid Gene Repertoires. *Nucleic Acids Res.* 49, 2655–2673. doi: 10.1093/nar/gkab064
- Podlacha, M., Grabowski, Ł., Kosznik-Kawśnicka, K., Zdrojewska, K., Stasiłojć, M., Węgrzyn, G., et al (2021). Interactions of Bacteriophages With Animal and Human Organisms—Safety Issues in the Light of Phage Therapy. *Int. J. Mol. Sci.* 22, 8937. doi: 10.3390/ijms22168937
- Popescu, M., Van Belleghem, J. D., Khosravi, A., and Bollyky, P. L. (2021). Bacteriophages and the Immune System. *Annu. Rev. Virol.* 8, 67–87. doi: 10.1146/annurev-virology-091919-074551
- Ramirez, M., Severina, E., and Tomasz, A. (1999). A High Incidence of Prophage Carriage Among Natural Isolates of *Streptococcus Pneumoniae*. *J. Bacteriol.* 181, 3618–3625. doi: 10.1128/JB.181.12.3618-3625.1999
- Ramos-Sevillano, E., Urzainqui, A., Campuzano, S., Moscoso, M., González-Camacho, F., Domenech, M., et al (2015). Pleiotropic Effects of the Cell Wall Amidase LytA on *Streptococcus Pneumoniae* Sensitivity to the Host Immune Response. *Infect. Immun.* 83, 591–603. doi: 10.1128/iai.02811-14
- Ramos-Sevillano, E., Urzainqui, A., de Andrés, B., González-Tajuelo, R., Domenech, M., González-Camacho, F., et al (2016). PSG1-1 on Leukocytes is a Critical Component of the Host Immune Response Against Invasive Pneumococcal Disease. *PLoS Pathog.* 12, e1005500. doi: 10.1371/journal.ppat.1005500
- Reis-Cunha, J. L., Bartholomeu, D. C., Manson, A. L., Earl, A. M., and Cerqueira, G. C. (2019). ProphET, Prophage Estimation Tool: A Stand-Alone Prophage Sequence Prediction Tool With Self-Updating Reference Database. *PLoS One* 14, e0223364. doi: 10.1371/journal.pone.0223364
- Rezaei Javan, R., Ramos-Sevillano, E., Akter, A., Brown, J., and Brueggemann, A. B. (2019). Prophages and Satellite Prophages are Widespread in *Streptococcus* and may Play a Role in Pneumococcal Pathogenesis. *Nat. Commun.* 10, 4852. doi: 10.1038/s41467-019-12825-y
- Roach, D. J., Burton, J. N., Lee, C., Stackhouse, B., Butler-Wu, S. M., Cookson, B. T., et al (2015). A Year of Infection in the Intensive Care Unit: Prospective Whole Genome Sequencing of Bacterial Clinical Isolates Reveals Cryptic Transmissions and Novel Microbiota. *PLoS Genet.* 11, e1005413. doi: 10.1371/journal.pgen.1005413
- Romero, P., Croucher, N. J., Hiller, N. L., Hu, F. Z., Ehrlich, G. D., Bentley, S. D., et al (2009a). Comparative Genomic Analysis of Ten *Streptococcus Pneumoniae* Temperate Bacteriophages. *J. Bacteriol.* 191, 4854–4862. doi: 10.1128/jb.01272-08
- Romero, P., García, E., and Mitchell, T. J. (2009b). Development of a Prophage Typing System and Analysis of Prophage Carriage in *Streptococcus Pneumoniae*. *Appl. Environ. Microbiol.* 75, 1642–1649. doi: 10.1128/AEM.02155-08
- Romero, A., Lopez, R., and Garcia, P. (1990). Sequence of the *Streptococcus Pneumoniae* Bacteriophage HB-3 Amidase Reveals High Homology With the Major Host Autolysin. *J. Bacteriol.* 172, 5064–5070. doi: 10.1128/jb.172.9.5064-5070.1990
- Rostol, J. T., and Marraffini, L. (2019). (Ph)ighting Phages: How Bacteria Resist Their Parasites. *Cell Host Microbe* 25, 184–194. doi: 10.1016/j.chom.2019.01.009
- Sánchez-Beato, A. R., López, R., and García, J. L. (1998). Molecular Characterization of PcpA: A Novel Choline-Binding Protein of *Streptococcus Pneumoniae*. *FEMS Microbiol. Lett.* 164, 207–214. doi: 10.1016/s0378-1097(98)00206-7
- Schattner, P., Brooks, A. N., and Lowe, T. M. (2005). The tRNAscan-SE, Sscan and snoGPS Web Servers for the Detection of tRNAs and snoRNAs. *Nucleic Acids Res.* 33, W686–W689. doi: 10.1093/nar/gki366
- Schroven, K., Aertsen, A., and Lavigne, R. (2021). Bacteriophages as Drivers of Bacterial Virulence and Their Potential for Biotechnological Exploitation. *FEMS Microbiol. Rev.* 45, fuaa041. doi: 10.1093/femsre/fuaa041
- Seguritan, V., Feng, I. W., Rohwer, F., Swift, M., and Segall, A. M. (2003). Genome Sequences of Two Closely Related *Vibrio Parahaemolyticus* Phages, VP16T and VP16C. *J. Bacteriol.* 185, 6434–6447. doi: 10.1128/JB.185.21.6434-6447.2003
- Sempere, J., de Miguel, S., González-Camacho, F., Yuste, J., and Domenech, M. (2020). Clinical Relevance and Molecular Pathogenesis of the Emerging Serotypes 22F and 33F of *Streptococcus Pneumoniae* in Spain. *Front. Microbiol.* 11, 309. doi: 10.3389/fmicb.2020.00309
- Shimada, K., Weisberg, R. A., and Gottesman, M. E. (1975). Prophage Lambda at Unusual Chromosomal Locations. III. The Components of the Secondary Attachment Sites. *J. Mol. Biol.* 93, 415–429. doi: 10.1016/0022-2836(75)90237-5
- Sievers, F., and Higgins, D. G. (2021). The Clustal Omega Multiple Alignment Package. *Methods Mol. Biol.* 2231, 3–16. doi: 10.1007/978-1-0716-1036-7_1
- Silva, M. D., Oliveira, H., Faustino, A., and Sillankorva, S. (2020). Characterization of MSlys, the Endolysin of *Streptococcus Pneumoniae* Phage MS1. *Biotechnol. Rep. (Amst.)* 28, e00547. doi: 10.1016/j.btre.2020.e00547
- Sinha, D., Zimmer, K., Cameron, T. A., Rusch, D. B., Winkler, M. E., and De Lay, N. R. (2019). Redefining the Small Regulatory RNA Transcriptome in *Streptococcus Pneumoniae* Serotype 2 Strain D39. *J. Bacteriol.* 201, e00764–18. doi: 10.1128/JB.00764-18
- Slager, J., Aprianto, R., and Venning, J.-W. (2018). Deep Genome Annotation of the Opportunistic Human Pathogen *Streptococcus Pneumoniae* D39. *Nucleic Acids Res.* 46, 9971–9989. doi: 10.1093/nar/gky725
- Steinberg, R., Knüpfner, L., Origi, A., Asti, R., and Koch, H.-G. (2018). Co-Translational Protein Targeting in Bacteria. *FEMS Microbiol. Lett.* 365, fny095. doi: 10.1093/femsle/fny095
- Stout, T. J., Schellenberger, U., Santi, D. V., and Stroud, R. M. (1998). Crystal Structures of a Unique Thermal-Stable Thymidylate Synthase From *Bacillus Subtilis*. *Biochemistry* 37, 14736–14747. doi: 10.1021/bi981270l
- Stroynowski, I. T. (1981). Integration of the Bacteriophage Φ 3T-Coded Thymidylate Synthetase Gene Into the *Bacillus Subtilis* Chromosome. *J. Bacteriol.* 148, 101–108. doi: 10.1128/jb.148.1.101-108.1981
- Tam, N. H., and Borris, R. (1995). The *thyA* Gene From *Bacillus Subtilis* Exhibits Similarity With the Phage Φ 3T Thymidylate Synthase Gene. *Microbiology* 141, 291–297. doi: 10.1099/13500872-141-2-291
- Tin Tin Htar, M., Morato Martínez, J., Theilacker, C., Schmitt, H.-J., and Swerdlow, D. (2019). Serotype Evolution in Western Europe: Perspectives on Invasive Pneumococcal Diseases (IPD). *Expert Rev. Vaccines* 18, 1145–1155. doi: 10.1080/14760584.2019.1688149
- Touchon, M., Bernheim, A., and Rocha, E. P. (2016). Genetic and Life-History Traits Associated With the Distribution of Prophages in Bacteria. *ISME J.* 10, 2744–2754. doi: 10.1038/ismej.2016.47
- Tucker, R. G. (1969). Acquisition of Thymidylate Synthetase Activity by a Thymine-Requiring Mutant of *Bacillus Subtilis* Following Infection by the Temperate Phage ϕ 3. *J. Gen. Virol.* 4, 489–504. doi: 10.1099/0022-1317-4-4-489

- Tunjungputri, R. N., Mobegi, F. M., Cremers, A. J., van der Gaast-de Jongh, C. E., Ferwerda, G., Meis, J. F., et al (2017). Phage-Derived Protein Induces Increased Platelet Activation and is Associated With Mortality in Patients With Invasive Pneumococcal Disease. *mBio* 8, e01984–16. doi: 10.1128/mBio.01984-16
- van der Kamp, I., Draper, L. A., Smith, M. K., Buttner, C., Ross, R. P., and Hill, C. (2020). A New Phage Lysin Isolated From the Oral Microbiome Targeting *Streptococcus Pneumoniae*. *Pharmaceuticals (Basel)* 13, 478. doi: 10.3390/ph13120478
- Van Duyne, G. D., and Rutherford, K. (2013). Large Serine Recombinase Domain Structure and Attachment Site Binding. *Crit. Rev. Biochem. Mol. Biol.* 48, 476–491. doi: 10.3109/10409238.2013.831807
- van Tonder, A. J., Bray, J. E., Jolley, K. A., Jansen van Rensburg, M., Quirk, S. J., Haraldsson, G., et al (2019). Genomic Analyses of >3,100 Nasopharyngeal Pneumococci Revealed Significant Differences Between Pneumococci Recovered in Four Different Geographical Regions. *Front. Microbiol.* 10, 317. doi: 10.3389/fmicb.2019.00317
- Vasu, K., and Nagaraja, V. (2013). Diverse Functions of Restriction-Modification Systems in Addition to Cellular Defense. *Microbiol. Mol. Biol. Rev.* 77, 53–72. doi: 10.1128/MMBR.00044-12
- Vázquez, R., García, E., and García, P. (2018). Phage Lysins for Fighting Bacterial Respiratory Infections: A New Generation of Antimicrobials. *Front. Immunol.* 9, 2252. doi: 10.3389/fimmu.2018.02252
- Wang, X., and Wood, T. K. (2016). Cryptic Prophages as Targets for Drug Development. *Drug Resist. Updat.* 27, 30–38. doi: 10.1016/j.drug.2016.06.001
- Weiss, S. B., Hsu, W.-T., Foft, J. W., and Scherberg, N. H. (1968). Transfer RNA Coded by the T4 Bacteriophage Genome. *Proc. Natl. Acad. Sci. U.S.A.* 61, 114–121. doi: 10.1073/pnas.61.1.114
- Whatmore, A. M., and Dowson, C. G. (1999). The Autolysin-Encoding Gene (*Lyta*) of *Streptococcus Pneumoniae* Displays Restricted Allelic Variation Despite Localized Recombination Events With Genes of Pneumococcal Bacteriophage Encoding Cell Wall Lytic Enzymes. *Infect. Immun.* 67, 4551–4556. doi: 10.1128/iai.67.9.4551-4556.1999
- Williams, K. P. (2002). Integration Sites for Genetic Elements in Prokaryotic tRNA and tmRNA Genes: Sublocation Preference of Integrase Subfamilies. *Nucleic Acids Res.* 30, 866–875. doi: 10.1093/nar/30.4.866
- Willner, D., Furlan, M., Schmieder, R., Grasis, J. A., Pride, D. T., Relman, D. A., et al (2011). Metagenomic Detection of Phage-Encoded Platelet-Binding Factors in the Human Oral Cavity. *Proc. Natl. Acad. Sci. U.S.A.* 108 Suppl 1, 4547–4553. doi: 10.1073/pnas.1000089107
- Yang, H., Luo, D., Etobayeva, I., Li, X., Gong, Y., Wang, S., et al (2020). Linker Editing of Pneumococcal Lysin ClyJ Conveys Improved Bactericidal Activity. *Antimicrob. Agents Chemother.* 64, e01610–19. doi: 10.1128/aac.01610-19
- Yuan, P., Gupta, K., and Van Duyne, G. D. (2008). Tetrameric Structure of a Serine Integrase Catalytic Domain. *Structure* 16, 1275–1286. doi: 10.1016/j.str.2008.04.018

Conflict of Interest: The authors declare that the research was conducted in the absence of any commercial or financial relationships that could be construed as a potential conflict of interest.

Publisher's Note: All claims expressed in this article are solely those of the authors and do not necessarily represent those of their affiliated organizations, or those of the publisher, the editors and the reviewers. Any product that may be evaluated in this article, or claim that may be made by its manufacturer, is not guaranteed or endorsed by the publisher.

Copyright © 2021 Martín-Galiano and García. This is an open-access article distributed under the terms of the Creative Commons Attribution License (CC BY). The use, distribution or reproduction in other forums is permitted, provided the original author(s) and the copyright owner(s) are credited and that the original publication in this journal is cited, in accordance with accepted academic practice. No use, distribution or reproduction is permitted which does not comply with these terms.



The Role of Minor Pilins in Assembly and Function of the Competence Pilus of *Streptococcus pneumoniae*

Vitor Oliveira¹, Marie-Stephanie Aschtgen¹, Anke van Erp¹,
Birgitta Henriques-Normark^{1,2*†} and Sandra Muschiol^{1,2*†}

¹ Department of Microbiology, Tumor and Cell Biology, Karolinska Institutet, Stockholm, Sweden, ² Department of Clinical Microbiology, Karolinska University Hospital, Stockholm, Sweden

OPEN ACCESS

Edited by:

Sven Hammerschmidt,
University of Greifswald, Germany

Reviewed by:

George Liechti,
Uniformed Services University of the
Health Sciences, United States
Badreddine Douzi,
INRA Centre Nancy-Lorraine, France

*Correspondence:

Sandra Muschiol
sandra.muschiol@ki.se
Birgitta Henriques-Normark
birgitta.henriques@ki.se

[†]These authors have contributed
equally to this work

Specialty section:

This article was submitted to
Molecular Bacterial Pathogenesis,
a section of the journal
Frontiers in Cellular and
Infection Microbiology

Received: 03 November 2021

Accepted: 30 November 2021

Published: 22 December 2021

Citation:

Oliveira V, Aschtgen M-S,
van Erp A, Henriques-Normark B
and Muschiol S (2021) The Role
of Minor Pilins in Assembly and
Function of the Competence Pilus
of *Streptococcus pneumoniae*.
Front. Cell. Infect. Microbiol. 11:808601.
doi: 10.3389/fcimb.2021.808601

The remarkable genomic plasticity of *Streptococcus pneumoniae* largely depends on its ability to undergo natural genetic transformation. To take up extracellular DNA, *S. pneumoniae* assembles competence pili composed of the major pilin ComGC. In addition to ComGC, four minor pilins ComGD, E, F, and G are expressed during bacterial competence, but their role in pilus biogenesis and transformation is unknown. Here, using a combination of protein-protein interaction assays we show that all four proteins can directly interact with each other. Pneumococcal ComGG stabilizes the minor pilin ComGD and ComGF and can interact with and stabilize the major pilin ComGC, thus, deletion of ComGG abolishes competence pilus assembly. We further demonstrate that minor pilins are present in sheared pili fractions and find ComGF to be incorporated along the competence pilus by immunofluorescence and electron microscopy. Finally, mutants of the invariant Glu5 residue (E5), ComGD_{E5A} or ComGE_{E5A}, but not ComGF_{E5A}, were severely impaired in pilus formation and function. Together, our results suggest that ComGG, lacking E5, is essential for competence pilus assembly and function, and plays a central role in connecting the pneumococcal minor pilins to ComGC.

Keywords: competence pilus, minor pilins, natural transformation, *Streptococcus pneumoniae*, type IV pili (T4P), DNA uptake

INTRODUCTION

The transfer of genetic information among bacteria contributes to the natural diversity of prokaryotes and is a major evolutionary driving force. This phenomenon, referred to as horizontal gene transfer (HGT), can occur at high frequency between bacteria that are closely related or that coexist in the same habitat or community (Koonin et al., 2001; Beiko et al., 2005). It allows bacteria to acquire new functional traits that are important in the adaptation and survival of species and plays a role in the spread of antibiotic resistance (Vos et al., 2015; von Wintersdorff et al., 2016; Calero-Caceres et al., 2019). Transformation, one of the main mechanisms of HGT, is a widely conserved process in many bacterial species. The uptake of exogenous DNA from the surrounding environment is entirely controlled by the recipient bacteria and relies on sophisticated DNA uptake machineries often composed of bacterial surface appendages, such as type IV pili (T4P). T4P are

widespread among Gram-negative and Gram-positive bacteria and can display a wide range of functions including DNA uptake, adhesion to host cells, biofilm formation and twitching motility (Melville and Craig, 2013; Craig et al., 2019; Pelicic, 2019).

The Gram-positive respiratory pathogen *Streptococcus pneumoniae* (the pneumococcus) is naturally transformable and type IV competence pili promote initial DNA binding during the first step of transformation (Muschiol et al., 2019). These μm -long filaments are exclusively formed during bacterial competence and are essential for DNA uptake. Upon binding of extracellular DNA, the pneumococcal DNA translocation apparatus (transformasome), composed of ComEA, EndA, ComEC and ComFA, facilitates the uptake of DNA across the cellular membrane (Johnston et al., 2014). All the proteins required for competence pilus biogenesis are encoded by the *comG* operon (ComGA, B, C, D, E, F and G) and *pilD* encoded elsewhere in the genome. ComGA is an ATPase, believed to power pilus assembly, and mutants deficient in ComGA are non-transformable (Laurenceau et al., 2013). ComGB is a polytopic integral membrane protein and presumably acts as a platform for pilus assembly based on its homology with known orthologous platform proteins (Takhar et al., 2013). The remaining proteins ComGC, D, E, F and G belong to the family of pilin proteins, a conserved set of proteins found in bacteria expressing T4P and type II secretion systems (T2SSs). Pilins or pseudopilins, as they are referred to in T2SSs, are synthesized as prepilins with a characteristic N-terminal class III signal peptide, which is cleaved off by the prepilin peptidase PilD (Strom et al., 1993; Piepenbrink, 2019). Mature major and minor pilins share a similar domain structure with a conserved N-terminal and a more variable C-terminal domain and are assembled into polymeric filaments by dedicated assembly systems (Giltner et al., 2012; Berry and Pelicic, 2015). The pneumococcal pilins share the typical pilin domain structure but differ in size (86–137 aa). Their signal peptides end with a conserved Ala residue, which is recognized by the prepilin peptidase. All pneumococcal pilins, except ComGG, also contain a conserved Glu residue in position 5 after the cleavage site (E5), which was suggested to be important for fiber assembly/stabilization in other T4P and T2SSs (Strom and Lory, 1991; Aas et al., 2007; Li et al., 2012; Nivaskumar et al., 2016). The pneumococcal competence pilus is composed of the major pilin ComGC. Bacteria deficient in ComGC or expressing mutant ComGC_{E5V} lack pili and are defective in transformation (Laurenceau et al., 2013; Muschiol et al., 2017). The role of the minor pilins in competence pilus biogenesis and transformation remains poorly understood.

Minor pilins are present at lower abundance relative to the major pilin. They can be incorporated into pili at different locations and can have profound effects on pilus assembly and function. Strikingly, many Gram-negative bacteria expressing T4P or T2SSs possess a set of core minor pilins that are central components of the assembly machinery (Giltner et al., 2012; Escobar et al., 2021). In some systems additional accessory minor pilins that can be dispensable for pilus biogenesis can be involved in specific pilus associated functions such as adhesion to host cells, bacterial aggregation, and DNA uptake (Helaine et al., 2005; Helaine et al., 2007; Brissac et al., 2012; Cehovin et al., 2013; Imhaus and Dumenil, 2014; Ng et al., 2016).

Here, we investigate the role of the pneumococcal minor pilins in competence pilus biogenesis and transformation by combining genetic, biochemical, and imaging studies. Our results provide evidence that ComGD, ComGF and ComGG are found in sheared pili fractions, and we demonstrate by immunofluorescence microscopy and electron microscopy that ComGF is incorporated along the pilus filament. We also show that all minor pilins can directly interact with each other and identify ComGG as a link between the minor pilins and the major pilin ComGC.

MATERIAL AND METHODS

Bacterial Strains, Growth Conditions and Transformation

All strains used in this study are listed in **Table 1**. *S. pneumoniae* strains were grown on blood agar plates overnight at 37°C and 5% CO₂. For competence induction, plate-grown bacteria were used to inoculate Todd-Hewitt broth supplemented with 0.5% yeast extract (THY), at OD₆₂₀ = 0.05 and grown at 37°C until OD₆₂₀ = 0.15. Bacteria were then incubated at 30°C for 15 min before competence was induced by addition of competence stimulating peptide (CSP-1) at a final concentration of 100 ng/ml for 15 min. For transformation experiments, DNA (1 $\mu\text{g}/\text{ml}$) was added and transformants were selected on blood agar plates containing appropriate antibiotics, as specified. Transformability assays were performed as previously described (Muschiol et al., 2017).

Escherichia coli strains were grown at 37°C in lysogeny broth (LB) or on LB agar plates containing antibiotics (50 $\mu\text{g}/\text{ml}$ kanamycin, 100 $\mu\text{g}/\text{ml}$ ampicillin and/or 50 $\mu\text{g}/\text{ml}$ chloramphenicol), when required. *E. coli* Top 10 (Life Technologies) was used for cloning with standard techniques as described (Sambrook et al., 1989). For protein expression, *E. coli* T7 Express (NEB) was grown in Terrific Broth (TB) and LB (ratio 1:1) with appropriate antibiotics. Cultures were grown at 37°C to OD₆₀₀ = 0.5, induced with 1 mM isopropyl β -D-1 thiogalactopyranoside (IPTG) purchased from Sigma and continued to grow at room-temperature (RT), overnight (~12 h).

Generation of Mutants and Complementation Constructs

Construction of *S. pneumoniae* R6 Deletion Mutants

Pneumococcal strains were created in which *comGC*, *comGG*, *comGFG*, *comGEFG* and *comGDEFG* were deleted and replaced with a spectinomycin cassette. For this, PCR fragments flanking the upstream and downstream regions of the target genes were amplified from the *S. pneumoniae* R6 genomic DNA using Fusion Flash polymerase (Thermo Fisher Scientific). The PCR primers contained overhang sequences with BamHI and NotI restriction sites (**Table 2**). Each PCR product was digested with the respective restriction enzyme, purified and ligated to a spectinomycin cassette containing BamHI and NotI sites. The resulting fragment was PCR amplified and used to transform *S. pneumoniae* R6. Transformants were selected on blood agar

TABLE 1 | *S. pneumoniae* strains used in this study.

Strain	Description	Source/Reference
R6	R6 strain	R. Hakenbeck
R6Δ <i>comGC</i>	<i>comGC::spec</i> (Spec ^R)	This study
R6Δ <i>comGG</i>	<i>comGG::spec</i> (Spec ^R)	This study
R6Δ <i>comGFG</i>	<i>comGFG::spec</i> (Spec ^R)	This study
R6Δ <i>comGEFG</i>	<i>comGEFG::spec</i> (Spec ^R)	This study
R6Δ <i>comGDEFG</i>	<i>comGDEFG::spec</i> (Spec ^R)	This study
T4Δ <i>comG</i>	<i>comG::erm</i> (Erm ^R)	(Balaban et al., 2014)
R6Δ <i>comG</i>	<i>comG::erm</i> (Erm ^R)	This study
R6 <i>bgaA::comGD</i>	<i>bgaA::P_{comG} comGD</i> (Tet ^R)	This study
R6 <i>bgaA::comGE</i>	<i>bgaA::P_{comG} comGE</i> (Tet ^R)	This study
R6 <i>bgaA::comGF</i>	<i>bgaA::P_{comG} comGF</i> (Tet ^R)	This study
R6 <i>bgaA::comGG</i>	<i>bgaA::P_{comG} comGG</i> (Tet ^R)	This study
R6 <i>bgaA::comGDEF</i>	<i>bgaA::P_{comG} comGDEF</i> (Tet ^R)	This study
R6 <i>bgaA::comGDEFG</i>	<i>bgaA::P_{comG} comGDEFG</i> (Tet ^R)	This study
R6Δ <i>comGDEFG</i> , <i>bgaA::comGD</i>	<i>comGDEFG::spec</i> (Spec ^R), <i>bgaA::P_{comG} comGD</i> (Tet ^R)	This study
R6Δ <i>comGDEFG</i> , <i>bgaA::comGE</i>	<i>comGDEFG::spec</i> (Spec ^R), <i>bgaA::P_{comG} comGE</i> (Tet ^R)	This study
R6Δ <i>comGDEFG</i> , <i>bgaA::comGF</i>	<i>comGDEFG::spec</i> (Spec ^R), <i>bgaA::P_{comG} comGF</i> (Tet ^R)	This study
R6Δ <i>comGDEFG</i> , <i>bgaA::comGG</i>	<i>comGDEFG::spec</i> (Spec ^R), <i>bgaA::P_{comG} comGG</i> (Tet ^R)	This study
R6Δ <i>comGDEFG</i> , <i>bgaA::comGDEF</i>	<i>comGDEFG::spec</i> (Spec ^R), <i>bgaA::P_{comG} comGDEF</i> (Tet ^R)	This study
R6 <i>bgaA::comGD_{Flag}</i>	<i>bgaA::P_{comG} comGD_{Flag}</i> (Tet ^R)	This study
R6 <i>bgaA::comGE_{Flag}</i>	<i>bgaA::P_{comG} comGE_{Flag}</i> (Tet ^R)	This study
R6 <i>bgaA::comGF_{Flag}</i>	<i>bgaA::P_{comG} comGF_{Flag}</i> (Tet ^R)	This study
R6 <i>bgaA::comGG_{Flag}</i>	<i>bgaA::P_{comG} comGG_{Flag}</i> (Tet ^R)	This study
R6Δ <i>comGG</i> , <i>bgaA::comGG</i>	<i>comGG::spec</i> (Spec ^R), <i>bgaA::P_{comG} comGG</i> (Tet ^R)	This study
R6 <i>bgaA::comGCDEF</i>	<i>bgaA::P_{comG} comGCDEF</i> (Tet ^R)	This study
R6 <i>bgaA::comGCDEFG</i>	<i>bgaA::P_{comG} comGCDEFG</i> (Tet ^R)	This study
R6Δ <i>comG</i> , <i>bgaA::comGCDEF</i>	<i>comG::erm</i> (Erm ^R), <i>bgaA::comGCDEF</i> (Tet ^R)	This study
R6Δ <i>comG</i> , <i>bgaA::comGCDEFG</i>	<i>comG::erm</i> (Erm ^R), <i>bgaA::comGCDEFG</i> (Tet ^R)	This study
R6 <i>bgaA::comG</i>	<i>bgaA::comG</i> (Tet ^R)	This study
R6 <i>bgaA::comG</i> with <i>comGC_{E5A}</i>	<i>bgaA::comG</i> with <i>ComGC_{E5A}</i> (Tet ^R)	This study
R6 <i>bgaA::comG</i> with <i>comGD_{E5A}</i>	<i>bgaA::comG</i> with <i>ComGD_{E5A}</i> (Tet ^R)	This study
R6 <i>bgaA::comG</i> with <i>comGE_{E5A}</i>	<i>bgaA::comG</i> with <i>ComGE_{E5A}</i> (Tet ^R)	This study
R6 <i>bgaA::comG</i> with <i>comGF_{E5A}</i>	<i>bgaA::comG</i> with <i>ComGF_{E5A}</i> (Tet ^R)	This study
R6Δ <i>comG</i> , <i>bgaA::comG</i>	<i>comG::erm</i> (Erm ^R), <i>bgaA::comG</i> (Tet ^R)	This study
R6Δ <i>comG</i> , <i>bgaA::comG</i> with <i>comGC_{E5A}</i>	<i>comG::erm</i> (Erm ^R), <i>bgaA::comG</i> with <i>comGC_{E5A}</i> (Tet ^R)	This study
R6Δ <i>comG</i> , <i>bgaA::comG</i> with <i>comGD_{E5A}</i>	<i>comG::erm</i> (Erm ^R), <i>bgaA::comG</i> with <i>comGD_{E5A}</i> (Tet ^R)	This study
R6Δ <i>comG</i> , <i>bgaA::comG</i> with <i>comGE_{E5A}</i>	<i>comG::erm</i> (Erm ^R), <i>bgaA::comG</i> with <i>comGE_{E5A}</i> (Tet ^R)	This study
R6Δ <i>comG</i> , <i>bgaA::comG</i> with <i>comGF_{E5A}</i>	<i>comG::erm</i> (Erm ^R), <i>bgaA::comG</i> with <i>comGF_{E5A}</i> (Tet ^R)	This study

Spec^R-spectinomycin resistance, Tet^R-tetracycline resistance, Erm^R-erythromycin resistance.

plates containing spectinomycin (200 µg/ml) and confirmed by PCR and sequencing of the insertion region.

Mutant strains lacking the entire *comG* operon were produced by transformation with a PCR product containing *comG* up and downstream flanking regions fused to an erythromycin cassette amplified from T4Δ*comG* (Balaban et al., 2014) genomic DNA with primers 292-F/330-R. Clones were selected on blood agar plates containing erythromycin (1 µg/ml) and confirmed by sequencing.

Construction of Δ*comGDEFG* Mutant Strains Ectopically Expressing Minor Pilin(s) in the *bgaA* Locus

PCR and *in vivo* recombination in *E. coli* were used to generate integration vectors carrying pneumococcal minor pilin(s) for subsequent transformation into the *S. pneumoniae* strain R6. Based on the integration vector pJVW25 [kindly provided by A. Eberhardt (Eberhardt et al., 2009)], we first created a modified plasmid containing the flanking regions for integration into the *bgaA* locus but replacing the Zn²⁺ inducible promoter and *gfp* with

the sequence encoding the *comG* promoter, *comGA*, *comGB* and *comGC_{Flag}*. The respective fragment of the pJVW25 plasmid was amplified with Fusion Flash polymerase (Thermo Fisher Scientific) and primers 792-F/793-R that contained overhang sequences homologous to the *comG* promoter and the Flag tag, respectively. The insert was amplified from the *S. pneumoniae* R6 genomic DNA with primers 790-F/791-F carrying overhang sequences homologous to the pJVW25 plasmid and the Flag-tag. Insert and PCR amplified plasmid were then mixed in a 1:1 molar ratio and treated with *DpnI* for 1 h at 37°C. 1 µl of the reaction was used to transform XL10-gold competent cells (Stratagene) that combine vector and insert by homologous recombination. Clones were selected on LB plates containing ampicillin (100 µg/ml) and the plasmid was isolated using the QIAprep Spin Miniprep Kit (Qiagen) according to the manufacturer's instructions. The resulting plasmid was designated pSM828 and used as template to produce integration vectors carrying minor pilin(s) as follows: *comGD*, *comGE*, *comGF*, *comGG*, *comGDEF* and *comGDEFG*, which were PCR amplified from R6 genomic DNA using the following primers: 880-F/886-R, 906-F/907-R, 908-R/883-R,

TABLE 2 | Primers used in this study.

Name	Sequence	Description
604-F	TTGACTTGCAAGCAGAGATTATCAAG	To construct R6ΔcomGC
605-R	GCATAGGATCCTTAAAAATTTACCTCCATATTTTGATACATGGGC	To construct R6ΔcomGC
606-F	CGATTGCGGCCGCGCCTAAGAAAGTTACAGCAGATGG	To construct R6ΔcomGC
607-R	GAGGGCAAGCAGGGATTCTAAC	To construct R6ΔcomGC
372-F	GCATAGGATCCCTAATCAAAATAGTGAGGAGGAGGATATTTGAATACATAC	To amplify spectinomycin cassette
MSA62-R	CGATTGCGGCCGCTTATAATTTTTTAACTGTTATTTAAATAGTTTATAGTTAAATTACATTTTCATTAG	To amplify spectinomycin cassette
MSA37-F	GCACGCCTTCCCTTTATTGGAATC	To construct R6ΔcomGG, R6ΔcomGFG, R6ΔcomGEFG and R6ΔcomGDEFG
374-R	GCATAGGATCCCCTGCCTTAACTTTTTCTTTTCCACACGATAG	To construct R6ΔcomGG
361-R	CGATTGCGGCCGCACTAAACGAAATAAACGCTAAAAACGTCTC	To amplify spectinomycin cassette
358-F	CGATTGCGGCCGCTTATAATGCGTTGAATCCAGAATAGTCC	To construct R6ΔcomGG, R6ΔcomGFG, R6ΔcomGEFG and R6ΔcomGDEFG
336-R	CCAAATCACTTTGGATGACTTGGAC	To construct R6ΔcomGG, R6ΔcomGFG, R6ΔcomGEFG and R6ΔcomGDEFG
368-R	GCATAGGATCCGCTTAATCATTGACTTTACGATTTGC	To construct R6ΔcomGDEFG
369-R	GCATAGGATCCCCTAATTTTTGTTTCCTTAATGCGTTAATTTTTTC	To construct R6ΔcomGEFG
370-R	GCATAGGATCCCCTTATGGCTCTTTGATTGCCAAC	To construct R6ΔcomGFG
292-F	CCAGCTAAATTGATTATGGTAGACCTAG	To construct R6ΔcomG
330-R	CCACTTCCATTCCAAGTAATC	To construct R6ΔcomG
154-F	CGCTGCAGGGTTCTCCTCTACGCAGTCACCATA	To construct pSM159
139-R	CGCGATCCCTATGAATTCCTTTCTTTTCAGG	To construct pSM159, pSM200
157-F	CGCTGCAGGGTTCTCCTCTACGCAGTCACCATA	To construct pSM200
790-F	catcggtacgtcggaattctagAGAAAAGTAACTTTTGGAGTTGC	To construct pSM828, pSM850
791-R	cttatcgctgcatccttgtaacATCATTGACTTTACGATTTGCTCC	To construct pSM828
792-F	gcaactccaaaaagttactttctCTAGAATTCGCAGGTACCGATG	To construct pSM828, pSM850
793-R	gattacaaggatgacgacgataagCTACCAATTACCAGTTGGTCTGG	To construct pSM828
879-F	gctgttcttcggtgatgctccatACTTACCTCCTCACCTATACTATTC	To construct pSM990, pSM992, pSM998
885-R	taaacgcattaaggaaacaaaaaattagCTACCAATTACCAGTTGGTCTGG	To construct pSM998
905-R	CTACCAATTACCAGTTGGTCTGGTG	To construct pSM974, pSM975, pSM994
882-R	ctatcggtggaagaaagaaagtaaaCTACCAATTACCAGTTGGTCTGG	To construct pSM992
880-F	gaatagtatatggtgaggaggaagtATGGACGCATCACGGAAGAAC	To construct R6 <i>bgaA::comGD</i> R6 <i>bgaA::comGD_{Flag}</i> R6 <i>bgaA::comGDE</i> R6 <i>bgaA::comGDEFG</i>
886-R	aactggtaatggtagCTAATTTTTGTTTCCTTAATGCGTTAATTTTTTC	To construct R6 <i>bgaA::comGD</i>
906-F	tagtataggtgaggaggaagtATGAAAAATTAACGCATTAAGGAAAC	To construct R6 <i>bgaA::comGE</i> , R6 <i>bgaA::comGE_{Flag}</i>
907-R	cagaccaactggtaatggtagTTATGGCTCTTTGATTGCCAACAAAC	To construct R6 <i>bgaA::comGE</i>
908-F	tataggtgaggaggaagtTTGAGATTGAGTATTTTCTAGTGAAAAAGG	To construct R6 <i>bgaA::comGF</i> , R6 <i>bgaA::comGF_{Flag}</i>
883-R	gaccaactggtaatggtagTTAACTTTTTCTTTTCCACACGATAGATG	To construct R6 <i>bgaA::comGF</i>
910-F	agtataggtgaggaggaagtGTGTGAAAAAGAAAAAGTTAAGGCAGG	To construct R6 <i>bgaA::comGG</i> , R6 <i>bgaA::comGG_{Flag}</i>
911-R	cagaccaactggtaatggtagCTATGAATTCCTTTCTTTTCAGGCTTC	To construct R6 <i>bgaA::comGG</i> , R6 <i>bgaA::comGDEFG</i>
887-F	ttattacttatogtgccttgtaacATTTTTCTTAATGCGTTAATTTTTTC	To construct R6 <i>bgaA::comGD_{Flag}</i>
912-R	ttattacttatogtgccttgtaacTGGCTCTTTGATTGCCAACAAAC	To construct R6 <i>bgaA::comGE_{Flag}</i>
913-R	ttattacttatogtgccttgtaacACTTTTTCTTTTCCACACGATAGATGAAC	To construct R6 <i>bgaA::comGF_{Flag}</i>
914-R	ttattacttatogtgccttgtaacTGAATTCCTTTCTTTTCAGGCTTCTCTTC	To construct R6 <i>bgaA::comGG_{Flag}</i>

(Continued)

TABLE 2 | Continued

Name	Sequence	Description
904-F	ACTTACCTCCTCACCTATACTATTTCGC	To construct pSM974, pSM975, pSM994, R6 <i>bgaA::comGD_{Flag}</i> , <i>E_{Flag}</i> , <i>F_{Flag}</i> or <i>G_{Flag}</i>
831-R	gattacaaggtatgacgacgataagtaataaCTACCATACCAGTTGGTC	To construct R6 <i>bgaA::comGD_{Flag}</i> , <i>E_{Flag}</i> , <i>F_{Flag}</i> or <i>G_{Flag}</i>
546-F	GTTAAAGCTTTTACATTGGTGG C GATGTTGGTGGTCTTGCTGATTATC	To construct pSM536
547-R	GATAATCAGCAAGACCACCAACATC G CCACCAATGTAAAGCTTTAAC	To construct pSM536
548-F	GGCCTTTACCATGCTGG C AAGTCTCTTGTTTGGG	To construct pSM545
549-R	CCCAAAACCAAGAGACTT G CCAGCATGGTAAAGGCC	To construct pSM545
600-F	GGCAGTGATTTTACTGG C AGCAGTAGTCGCTCTAGCTATC	To construct pSM552
601-R	GATAGCTAGAGCGACTACTGCT G CCAGTAAATCACTGCC	To construct pSM552
608-F	GTCAAGGCTTTTACCTTGTTAG C ATCCCTGCTTGCCCTCATTGTCATCAG	To construct pSM808
609-R	CTGATGACAAATGAGGGCAAGCAGGGAT G CTAACAAGGTAAAGCCCTTGAC	To construct pSM808
808-R	cagaccaactgtaatgtagCTATGAATTCTCTTTCTTTTCAGGCTTC	To construct pSM850, pSM990,
807-R	gcctgaaaagaaagagaattcatagCTACCATACCAGTTGGTCTGG	To construct pSM850, pSM990
858-F	GATGACATTCTTAAAAAAGCTAAGGTTAAAGC	To construct pSM915, pSM913
859-R	CTACTGCTTCCAGTAAATCACTGCC	To construct pSM915, pSM913
856-F	GGCAGTGATTTTACTGGAAGCAGTAG	To construct pSM915, pSM913
857-R	GCTTTAACCTTAGCTTTTTTCAAGAATGTCATC	To construct pSM915, pSM913
845-F	ATGGACGCATCACGGAAGAAC	To construct pSM872
846-R	CGTAGAGGAGAACACCTGCC	To construct pSM872, pSM903
843-F	GGCAGGTGTTCTCCTCTACG	To construct pSM872, pSM903
844-R	GTTCTTCCGTGATGCGTCCAT	To construct pSM872
341-F	GAAAAAGGATTGGAGGTCTACCATGG	To construct pSM903
860-R	CCATGGTAGACCTCCAATCCTTTTC	To construct pSM903
413-F	CGCGGATCCGAGTCAGCTCCTCATTTTCAGAAGTTC	To construct pSM507
414-R	CGCAAGCTTTTAACTTTTTCTTTTCCACACGATAGATGAAC	To construct pSM507
415-F	CGCGGATCCGTTGAACCGACAAGTCGCC	To construct pSM429
416-R	CGCAAGCTTCTATGAATTCTTTCTTTTCAGGCTCTCTCTC	To construct pSM429
417-F	CGCCATATGGTAGAGGAACAGATTTCTTTATGGAGTTTGAAG	To construct pSM507
418-R	CGCCTCGAGCTAATTTTTGTTTCTTAATGCGTTTAATTTTCCATTTTC	To construct pSM507
419-F	CGCCATATGCAAAAAATAGGCAAGAGGAAGCAAAAATC	To construct pSM429
420-R	CGCCTCGAGTTATGGCTCTTTGATTGCCAACCACTG	To construct pSM429
49-F	CGCGGATCCACCAAGCAAAAAGAACAGTCA	To construct pSM29
2-R	CGCCTCGAGTTAATCATTGACTTTACGATTTGC	To construct pSM29
50-F	CGCGGATCCGGCTCTGTCCAGTCCACTTTTT	To construct pSM34
4-R	CGCCTCGAGCTAATTTTTGTTTCTTAATGCG	To construct pSM34, pMB13
51-F	CGCGGATCCCAAATCAAAAAATAGGCAAG	To construct pSM51
6-R	CGCCTCGAGTTATGGCTCTTTGATTGCCAACAA	To construct pSM51, pMB17
52-F	CGCGGATCCCAAGCTATGAGTCAGTCTCTCA	To construct pSM40
8-R	CGCCTCGAGTTAATTTTTCTTTTCCACACG	To construct pSM40, pMB21
53-F	CGCGGATCCTTGAACCGACAAGTCGCCACT	To construct pSM46
10-R	CGCCTCGAGCTATGAATTCTTTCTTTTTCAGG	To construct pSM46, pMB22
14-F	CGCCATATGGGCTCTGTCCAGTCCACTTTTT	To construct pMB13
15-F	CGCCATATGCAAATTCAAAAAATAGGCAAG	To construct pMB17
16-F	CGCCATATGCAAGCTATGAGTCAGTCTCTCA	To construct pMB21
17-F	CGCCATATGTTGAACCGACAAGTCGCCACT	To construct pMB22
258-F	ATTAGACCGTTCGAGTTC	To assess <i>ComGF</i> expression
259-R	CGAACCAGTTGATTGTCCT	To assess <i>ComGF</i> expression
gryA-F	GTTGCTTGGTTCAAGAAAA	To assess <i>gryA</i> expression
gryA-R	TTGCATTTGGGTCAATTTGA	To assess <i>gryA</i> expression

Overhangs are shown in lower case. Mismatched bases generating mutations are in bold.

910-F/911-R, 880-F/883-R and 880-F/911-R. The respective plasmid fragments were amplified from pSM828 using primers 879-F/885-R (*bgaA::comGD*), 904-F/905-R (*bgaA::comGE*, *bgaA::comGF* and *bgaA::comGG*), 879-F/882-R (*bgaA::comGDEF*) and 879-F/807-R (*bgaA::comGDEFG*) (Table 2). PCR amplified inserts and vectors were combined as described above. The resulting integration vectors, pSM998, pSM994, pSM975, pSM974, pSM992 and pSM990 (Table 3) were used for transformation of *S. pneumoniae* R6. Transformants were selected on blood agar plates containing tetracycline (2 µg/ml). Finally, endogenous

comGDEFG was deleted in the obtained strains (Table 1) as described earlier for the R6Δ*comGDEFG* mutant. The resulting strains lacking endogenous *comGDEFG* and expressing minor pilin(s) in the *bgaA* locus are listed in Table 1. All plasmids and strains were confirmed by PCR and DNA sequencing.

Construction of Strains Ectopically Expressing Flag-Tagged Minor Pilin(s) in the *bgaA* Locus

Using the same cloning strategy as described above, we generated strains that expressed Flag-tagged minor pilins in the *bgaA* locus.

TABLE 3 | Plasmids used in this study.

Name	Description	Source
pJW25	Integration vector	(Eberhardt et al., 2009)
pSM828	Integration vector encoding <i>comG</i> promoter (P_{comG}), <i>comGA</i> , <i>comGB</i> and <i>comGC_{Flag}</i>	This study
pSM998	Integration vector encoding P_{comG} <i>comGD</i>	This study
pSM994	Integration vector encoding P_{comG} <i>comGE</i>	This study
pSM975	Integration vector encoding P_{comG} <i>comGF</i>	This study
pSM974	Integration vector encoding P_{comG} <i>comGG</i>	This study
pSM992	Integration vector encoding P_{comG} <i>comGDEF</i>	This study
pSM990	Integration vector encoding P_{comG} <i>comGDEFG</i>	This study
pSM1021	Integration vector encoding P_{comG} <i>comGD_{Flag}</i>	This study
pSM1027	Integration vector encoding P_{comG} <i>comGE_{Flag}</i>	This study
pSM976	Integration vector encoding P_{comG} <i>comGF_{Flag}</i>	This study
pSM971	Integration vector encoding P_{comG} <i>comGG_{Flag}</i>	This study
pSM850	Integration vector encoding <i>comG</i> operon	This study
pSM526	pCR-Blunt-II-Topo encoding <i>comGCDEF</i>	This study
pSM536	pCR-Blunt-II-Topo encoding <i>comGC_{E5A}DEFG</i>	This study
pSM545	pCR-Blunt-II-Topo encoding <i>comGC_{E5A}EFG</i>	This study
pSM552	pCR-Blunt-II-Topo encoding <i>comGC_{E5A}FG</i>	This study
pSM808	pCR-Blunt-II-Topo encoding <i>comGCDEF_{E5A}G</i>	This study
pSM915	Integration vector encoding <i>comG</i> operon with <i>comGC_{E5A}</i>	This study
pSM913	Integration vector encoding <i>comG</i> operon with <i>comGD_{E5A}</i>	This study
pSM872	Integration vector encoding <i>comG</i> operon with <i>comGE_{E5A}</i>	This study
pSM903	Integration vector encoding <i>comG</i> operon with <i>comGF_{E5A}</i>	This study
pSM429	pACYCDuet-1 expressing ComGE ₂₅₋₈₆ and 6x-His ComGG ₂₁₋₁₂₈	This study
pSM507	pETDuet expressing comGD ₃₁₋₁₃₀ and 6x-His comGF ₂₄₋₁₃₇	This study
pSM29	pGEX4T1 expressing GST-ComGC ₂₅₋₉₃	This study
pSM34	pGEX4T1 expressing GST-ComGD ₂₂₋₁₃₀	This study
pSM51	pGEX4T1 expressing GST-ComGE ₂₃₋₈₆	This study
pSM40	pGEX4T1 expressing GST-ComGF ₂₁₋₁₃₇	This study
pSM46	pGEX4T1 expressing GST-ComGG ₂₁₋₁₂₈	This study
pMB13	pET21a expressing ComGD ₂₂₋₁₃₀	This study
pMB17	pET21a expressing ComGE ₂₃₋₈₆	This study
pMB21	pET21a expressing ComGF ₂₁₋₁₃₇	This study
pMB22	pET21a expressing ComGG ₂₁₋₁₂₈	This study
pKT25	BACTH vector designed to express a protein fused to the C-terminal end of T25	(Karimova et al., 1998)
pUT18C	BACTH vector designed to express a protein fused to the C-terminal end of T18	(Karimova et al., 1998)
pKT25-zip	Vector expressing the leucine zipper of GCN4 fused to T25 (control plasmid)	(Karimova et al., 1998)
pUT18C-zip	Vector expressing the leucine zipper of GCN4 fused to T18 (control plasmid)	(Karimova et al., 1998)
pKT25- <i>comGC</i>	Vector expressing T25-ComGC	(Muschiol et al., 2017)
pUT18C- <i>comGC</i>	Vector expressing T18-ComGC	(Muschiol et al., 2017)
pSM159	pKT25 expressing T25-ComGG ₂₋₁₂₈	This study
pSM200	pUT18C expressing T18-ComGG ₂₋₁₂₈	This study

In brief, *comGD*, *comGE*, *comGF* and *comGG* were amplified from R6 genomic DNA with Fusion Flash polymerase (Thermo Fisher Scientific) and the following primers: 880-F/887-R, 906-F/912-R, 908-F/913-R and 910-F/914-R (Table 2). The sequence encoding the Flag tag was added to the reverse primers. The vector was amplified from pSM828 using primers: 904-F/831-R (Table 2). The PCR amplicons for the inserts were combined with their respective PCR amplified vector and resulting plasmids pSM1021, pSM1027, pSM976 and pSM971 (Table 3) were used for transformation of *S. pneumoniae* R6. Transformants were selected on blood agar plates containing tetracycline (2 µg/ml) and confirmed by PCR and sequencing.

Construction of the R6Δ*comGG* Complemented Strain Expressing *comGG* in the *bgaA* Locus

The complemented R6Δ*comGG*, *bgaA::comGG* strain was produced in the R6 *bgaA::comGG* strain background by deletion mutagenesis as described for the construction

of *S. pneumoniae* deletion mutants. Transformants were confirmed by PCR and sequencing.

Construction of Δ*comG* Strains Ectopically Expressing the *comG* Operon and E5A Minor Pilin Variants in the *bgaA* Locus

First, an integration vector was constructed that would allow integration of the entire *comG* operon into the *bgaA* locus of the *S. pneumoniae* strain R6. For that, the *comG* operon was PCR amplified with primers 790-F/808-R from genomic R6 DNA and the vector was amplified from pJW25 with primers 792-F/807-R. Both fragments were combined as described earlier. The resulting plasmid (pSM850) was transformed into *S. pneumoniae* R6 to create R6 *bgaA::comG* and then the endogenous *comG* operon was deleted essentially as described above. R6Δ*comG*, *bgaA::comG* variants carrying a E5A point mutation in either *comGC*, *comGD*, *comGE* or *comGF* were constructed following the same approach. To introduce the point mutations, a plasmid encoding

comGC to *comGG* (pSM526) was used as template for site-directed mutagenesis with primers: 546-F/547-R (*comGC*_{E5A}), 548-F/549-R (*comGD*_{E5A}), 600-F/601-R (*comGE*_{E5A}) and 608-F/609-R (*comGF*_{E5A}). The resulting plasmids (pSM536, pSM545, pSM552 and pSM808) were then used to create integration vectors encoding *comG* with *comGC*_{E5A}, *comGD*_{E5A}, *comGE*_{E5A} or *comGF*_{E5A}, respectively. Insert and vector backbone were PCR-amplified as follows: for *comGC*_{E5A} (insert: primers 858-F/859-R on pSM536, vector: primers 856-F/857-R on pSM850), *comGD*_{E5A} (insert: primers 858-F/859-R on pSM545, vector: primers 856-F/857-R on pSM850), *comGE*_{E5A} (insert: primers 845-F/846-R on pSM552, vector: primers 843-F/844-R on pSM850) and *comGF*_{E5A} (insert: primers 341-F/846-R on pSM808, vector: primers 843-F/860-R on pSM850) and combined as described above. The resulting integration vectors pSM915, pSM913, pSM872 and pSM903 (**Table 3**) were then used for transformation of *S. pneumoniae* R6 to create R6 *bgaA::comG* with *comGC*_{E5A}, R6 *bgaA::comG* with *comGD*_{E5A}, R6 *bgaA::comG* with *comGE*_{E5A}, and R6 *bgaA::comG* with *comGF*_{E5A} (**Table 1**). In the last step, the endogenous *comG* operon was removed in these strains as described above, producing R6Δ*comG*, *bgaA::comG* with *comGC*_{E5A}, R6Δ*comG*, *bgaA::comG* with *comGD*_{E5A}, R6Δ*comG*, *bgaA::comG* with *comGE*_{E5A} and R6Δ*comG*, *bgaA::comG* with *comGF*_{E5A} (**Table 1**).

Construction of Co-Expression Plasmids for Co-Immunoprecipitation

For co-expression of the soluble domains of ComGD, ComGE, ComGF and ComGG in *E. coli*, the pACYCDuet-1 (Novagen) and the pETDuet-1 vector (Novagen) were used and plasmids were constructed as follows. The respective minor pilins were amplified by PCR from T4 genomic DNA with Fusion Flash polymerase (Thermo Fisher Scientific) and primers 417-F/418-R (*comGD*), 419-F/420-R (*comGE*), 413-F/414-R (*comGF*) and 415-F/416-R (*comGG*) (**Table 2**). The cloning is based on the T4 genome, because *comGE* is not annotated in the *S. pneumoniae* R6 strain. All PCR primer pairs contained overhang sequences with NdeI/XhoI or BamHI/HindIII restriction sites (**Table 2**). PCR products and plasmids were then digested with respective restriction enzymes and the target genes were sequentially inserted into pACYCDuet-1 and pETDuet-1 by ligation. The resulting plasmids, pSM429 encoding the soluble domain of ComGE and 6x-His tagged ComGG and pSM507 encoding the soluble domain of ComGD and 6x-His tagged ComGF (**Table 3**) were co-transformed into competent *E. coli* T7 Express for subsequent protein expression and co-immunoprecipitation.

Construction of Plasmids for Pull-Down Studies in *E. coli*

To express the soluble domain of each pilin as GST-tagged fusion or untagged protein in *E. coli*, the corresponding sequence of each pilin gene was amplified by PCR from TIGR4 (T4) genomic DNA with Fusion Flash polymerase (Thermo Fisher Scientific) and primers listed in **Table 2**. All PCR primer pairs contain overhang sequences with BamHI/XhoI or NdeI/XhoI restriction

sites. PCR products were digested with NdeI/XhoI for cloning into pGEX4T1 or BamHI/XhoI for cloning into pet21a. Vectors were cut with respective enzymes. The resulting recombinant plasmids (**Table 3**) were confirmed by sequencing and transformed into competent *E. coli* T7 Express for protein expression.

Plasmid Construction for Bacterial Two Hybrid (BACTH) Assays

Vectors expressing T25-ComGC, T18-ComGC were previously described (Muschiol et al., 2017). The gene encoding mature ComGG was PCR-amplified from *S. pneumoniae* genomic DNA using primers 154-F/139-R and 157-F/139-R (**Table 2**). PCR products were digested with PstI/BamHI and cloned into the same sites of pKT25 and pUT18C vector. All strains used for BACTH are listed in **Table 3**.

Preparation of Cell Extracts and Sheared Pili

Bacteria were grown until OD₆₂₀ = 0.15 and competence was induced as described above. Whole cell lysates were prepared from 10 ml cultures if not stated otherwise. Competent bacteria were harvested by centrifugation for 10 min at 2,700 g and 4°C. Bacterial pellets were resuspended in 100 µl of Lysis buffer containing 50 mM Tris pH 8.0 and 3% sodium dodecyl sulphate (SDS). Protein concentration was determined using a NanoDrop ND 1000 (Thermo Fisher Scientific). Samples containing 10 µg/µl total protein were resuspended in 4x NuPAGE[®] LDS Sample Buffer (Life Technologies) and used for SDS-PAGE and immunoblotting. Sheared pili were prepared from a 250 ml culture of competent bacteria. Pellet and supernatant were separated by centrifugation for 30 min at 4,000 g at 4°C. The supernatant was removed. The pellet was resuspended in 1 ml PBS containing cComplete[™] protease inhibitor cocktail (Roche) and sheared by pipetting (1 min) to release pili into the medium. This suspension was centrifuged once at 16,000 g for 10 min and the pellet was discarded. The sheared pili fraction was further centrifuged twice at 16,000 g for 5 min to remove residual bacteria.

Antibodies

Antisera against pneumococcal ComGC and ComGG has previously been described (Balaban et al., 2014). Anti-GAPDH rabbit polyclonal antibody was generously provided by P. Mellroth, MTC, Karolinska Institutet. The monoclonal anti-Flag M2 antibody was purchased from Sigma. Polyclonal anti-ComGD and anti-ComGF antiserum was produced by immunizing rabbits with a synthetic peptide, CGNGKIK RIKETKN (anti-ComGD) and CGKSSDDFRKTNAR-NH2 (anti-ComGF) (Innovagen AB). Polyclonal anti-ComGE peptide antiserum was produced against the synthetic peptide KNRQEEAKILQKEEC and affinity purified (Genscript).

SDS-PAGE and Immunoblotting

Proteins were separated in NuPAGE[™] 4-12% Bis-Tris Protein Gels (Thermo Fisher Scientific) and transferred onto PVDF membranes (Trans-Blot[®] Turbo[™] Midi PVDF Transfer Packs,

Bio-Rad) using semi-dry electrotransfer (Bio-Rad). Membranes were blocked with 5% milk in PBS containing 0.1% Tween-20 (PBST) and incubated with specific antiserum (anti-Flag 1/2000, anti-ComGC 1/2000, anti-ComGD 1/1000, anti-ComGE 1/1000, anti-ComGF 1/1000, anti-ComGG 1/1000 and anti-GAPDH 1/2000) followed by incubation with respective secondary antibodies diluted in PBST. The HRP-conjugated secondary anti-rabbit and anti-mouse antibody (GE Healthcare) and the HRP-conjugated secondary anti-goat antibody (Sigma) were used at a 1/10 000 dilution. Membranes were developed with ECL Plus™ Western Blotting Reagent (GE Healthcare) and chemiluminescence was recorded using a ChemiDoc™ XRS+ Gel Documentation System (Bio-Rad).

BACTH Assay

Plasmids encoding fusions to T25 and T18 (Table 3) were co-transformed into competent *E. coli* BTH101 (Euromedex) and selected on LB plates containing 50 µg/ml kanamycin and 100 µg/ml ampicillin. Transformants were used for BACTH assays and the functional complementation between the recombinant plasmids was determined by measuring β-galactosidase activity in liquid cultures as described previously (Muschiol et al., 2017).

RNA Extraction and Real-Time Quantitative PCR (qPCR) Analysis

S. pneumoniae strains were grown in 10 ml THY cultures, and competence was induced as described. RNA extraction was performed using the FastRNA Pro™ Blue Kit (MPBio) according to the manufacturer's instructions. After extraction, the concentration and purity of isolated RNA was determined, and 10 µg of RNA from each sample was DNase treated using the Turbo DNA-free™ Kit (Thermo Scientific). cDNA was synthesized using 1 µg of RNA and the High-Capacity cDNA Reverse Transcription Kit according to the manufacturer's protocol (Applied Biosystems™). qPCR was performed using the iTaq™ Universal SYBR® Green Supermix (Bio-Rad). Expression levels of *comGF* were assessed with primers 258-F/259-R. The specificity of each primer pair was validated by melt curve analysis of the PCR product to guarantee the absence of primer dimers and unspecific products. The mRNA expression levels were normalized to the levels of *gyrA* and the relative expression determined with the ΔΔCT method. A total of three biological replicates were included for each strain tested.

Pull-Down of GST-Tagged Proteins

All *E. coli* strains and plasmids used in this experiment are listed in Table 1 and Table 3, respectively. Protein expression was performed as described above (see, *Bacterial strains, growth conditions and transformation*). Bacteria were harvested by centrifugation and pellets were stored at -20°C. Pellets corresponding to similar amounts of protein, depending on the efficiency of protein expression, were mixed. In this way, approximately equal amounts of expressed protein were combined. Pellets were resuspended in 15 ml GST-buffer containing PBS and cComplete™ protease inhibitor cocktail (Roche) and the pellet from a culture expressing an untagged pilin was mixed with the pellet expressing a GST-tagged pilin.

Combined pellets were lysed using a Stansted cell disrupter (Homogenising Systems Limited) and spun at 20,000 g for 30 min at 4°C. Empty gravity flow columns (Bio-Rad) were filled with 0.5 ml Glutathione Sepharose™ 4 Fast Flow resin (GE Healthcare) and equilibrated with GST-buffer. Bacterial supernatant was passed over the column, followed by a washing step with 15 ml GST-buffer. Elution was performed with 0.7 ml of GST-buffer containing 10 mM L-glutathione (Sigma). Samples were analyzed by SDS-PAGE and Coomassie brilliant blue staining and immunoblotting for ComGD, ComGE and ComGG.

Immunoprecipitations

Co-Immunoprecipitation of Pneumococcal Sheared Pili

Protein A Sepharose® 4 Fast Flow (GE Healthcare) was washed three times with PBS buffer and blocked with PBS containing 5% bovine serum albumin (BSA) for 1 h at 4°C. Anti-ComGC antibodies were then bound to Protein A Sepharose, rotating for 1 h at 4°C. ComGC-coupled protein A resin was washed three times with PBS and incubated with sheared pili (200 µl, see Preparation of cell extracts and sheared pili) from *S. pneumoniae* R6 or *S. pneumoniae* R6Δ*comGC* (negative control) on a rotating wheel overnight at 4°C. After five washing steps with PBS containing cComplete™ protease inhibitor cocktail (Roche), the resin was directly resuspended in 1x NuPAGE® LDS Sample Buffer (Life Technologies) and boiled for 10 min. Samples were analyzed by SDS-PAGE and immunoblotting for ComGC, ComGD, ComGF and ComGG.

Co-Immunoprecipitation of Minor Pilins Recombinantly Expressed in *E. coli*

E. coli T7 Express competent cells were co-transformed with pSM429 and pSM507 and clones were selected on LB plates containing 100 µg/ml ampicillin and 50 µg/ml chloramphenicol. Positive clones were used for protein expression as described above. A pellet from a 250 ml culture was resuspended in 30 ml PBS containing cComplete™ protease inhibitor cocktail (Roche) and lysed using a Stansted cell disrupter (Homogenising Systems Limited). Pellet (insoluble fraction) and supernatant (soluble fraction) were separated by centrifugation at 20,000 g for 30 min at 4°C. The supernatant was filtered and incubated with Dynabeads™ Protein G (Thermo Fisher Scientific) coupled with ComGG antibodies for 1h at 4°C. Supernatant incubated with uncoupled Dynabeads™ Protein G was used as a negative control. After three washing steps with PBS containing cComplete™ protease inhibitor cocktail (Roche), the resin was directly resuspended in 1x NuPAGE® LDS Sample Buffer (Life Technologies) and boiled for 10 min. Samples were analyzed by SDS-PAGE and Coomassie brilliant blue staining and immunoblotting for ComGD, ComGE, ComGF and ComGG.

Immunofluorescence Microscopy

Bacteria were grown until OD₆₂₀ = 0.15 and competence was induced as described above. 10 ml of culture were harvested by centrifugation for 5 min at 2,700 g, 4°C. The pellet was resuspended in 5 ml PBS containing 0.5% BSA. 10 µl of this

suspension was placed on a coverslip (VWR) and air-dried. Bacteria were fixed in PBS containing 4% paraformaldehyde for 30 min and coverslips were washed three times with PBS containing 0.5% BSA. Samples were labeled with primary antibodies to ComGC, ComGD, ComGE or ComGF, diluted at 1:300, and secondary goat anti-rabbit antibody conjugated with Alexa Fluor 488 or Alexa Fluor 594 (Life technologies) or secondary rabbit anti-goat antibody conjugated with Alexa Fluor 488 (Abcam) for 1 h. Flag-tagged proteins were labeled with anti-Flag M2 monoclonal antibody (Sigma) diluted 1:300 and secondary goat anti-mouse antibody conjugated with Alexa Fluor 594 for 1 h. Coverslips were mounted onto microscope slides with Vectashield (Vector Laboratories). Samples were examined using a DV Elite microscope (Applied Precision) equipped with a scientific complementary metal-oxide-semiconductor (sCMOS) camera. Images were acquired using Softworx (Applied Precision) and analyzed in ImageJ (Schneider et al., 2012).

Transmission Electron Microscopy and Immunogold Labeling

Negative-stain electron microscopy and immunogold labeling was performed as previously described (Muschiol et al., 2017). For immunogold labelling anti-ComGF antibodies, diluted 1:100 and secondary goat anti-rabbit antibodies conjugated to 6-nm gold particles were used. Images were acquired using a Tecnai 12 Spirit Bio TWIN transmission electron microscope (FEI Company, Eindhoven, Netherlands) operated at 100 kV and a Veleta 2k x 2k camera (Olympus Soft Imaging Solutions, GmbH, Münster, Germany).

Statistical Analysis

Results are expressed, as mean \pm SD. Data were statistically analyzed using GraphPad Prism 5.04 software. Statistical analysis was done by one-way ANOVA with subsequent Dunnett's *post hoc* test (BACTH assays) or two-tailed Student's *t*-test (transformability assays) as indicated in the figure legends. Asterisks in the figures indicate groups of statistically different means (* $p \leq 0.05$, ** $p \leq 0.01$, *** $p \leq 0.001$).

RESULTS

Lack of ComGG Blocks Pilus Formation and Transformation

The *S. pneumoniae* minor pilins are encoded in the CSP (competence stimulating peptide)-inducible polycistronic *comG* operon. It consists of seven genes, encoding the ATPase ComGA, and the membrane protein ComGB, the major pilin ComGC and the four minor pilins, ComGD, ComGE, ComGF and ComGG (Figure 1A). Since all pilin genes are overlapping, we constructed a series of minor pilin deletion strains by truncating the 3' end of the *comG* operon and tested their effect on pilus formation and transformability. As shown in Figure 1B, deletion of *comGG* led to overall reduced levels of ComGC present in bacterial whole-cell lysates, while ComGC processing was not visibly affected.

The upper band corresponds to unprocessed and the lower band to processed ComGC. No ComGC was found in the sheared pilin fraction of the minor pilin mutants and the control strain deficient in ComGC (R6 Δ comGC), suggesting that competence pili are not produced in these strains. Consistent with this observation, all strains were non-transformable compared to the WT R6 strain (Figure 1C). To test whether pilus assembly and transformation can be restored in a non-transformable Δ comGDEFG strain, either single minor pilins, ComGDEF or ComGDEFG, were expressed from their native CSP-inducible promoter at the ectopic *bgaA* locus. The relative abundance of ComGC was assessed in whole-cell lysates and sheared pilin fractions by immunoblotting. As shown in Figure 1D, ComGC was detected in lower amounts in bacterial lysates of strains expressing single *comGD*, *comGE* or *comGF*, and in the strain expressing *comGDEF* compared to the WT R6 strain, suggesting that ComGC is not stable in these strains. In the complementation strain ectopically expressing *comGG* alone or *comGDEFG*, similar levels of ComGC were detected in the lysate compared to the WT strain, which indicates a stabilizing effect of ComGG on ComGC. We then assessed the presence of ComGC in the sheared pilin fraction of these strains and detected ComGC only in the complemented *comGDEFG* strain (Figure 1D), suggesting that all four minor pilins are required to restore piliation. Consistent with this result, the *comGDEFG* complemented strain was transformable to WT levels (Figure 1C), and competence pili were detectable by immunofluorescence microscopy (Figure 1E).

ComGG Can Interact With ComGC and Is Required for Stabilization of ComGD and ComGF

Because ComGG alone was able to stabilize the major pilin ComGC in a strain lacking the endogenous minor pilins (R6 Δ comGDEFG, *bgaA::comGG*), we reasoned that ComGG and ComGC likely interact directly. To test this hypothesis, we used a bacterial adenylate cyclase two-hybrid assay (Karimova et al., 1998) in which the T18 and T25 fragments of *Bordetella pertussis* adenylate cyclase (CyaA) were fused to the N-terminal end of mature ComGC and ComGG. Compared to the negative control (T25/T18), T25-ComGC/T18-ComGG and T18-ComGC/T25-ComGG showed a statistically significant increase in CyaA activity (Figure 2A), suggesting a direct interaction between these two pilins. We also tested T18 and T25 fusions for the remaining minor pilins, but these constructs were not expressed in BTH101 *E. coli* cells.

Despite its importance, ComGG alone was not sufficient to restore pilus assembly in a Δ comGDEFG mutant and only complementation with all four minor pilins could rescue the defect. We therefore reasoned that if ComGG and the other minor pilins interact directly, then their stability might be mutually dependent. To test this idea, we studied the stability of the other minor pilins in the Δ comGG deletion mutant using antisera against ComGD, ComGE, ComGF and ComGG. To verify the specificity of the antisera a strain lacking all four minor pilins was included. As can be seen in Figure 2B, the

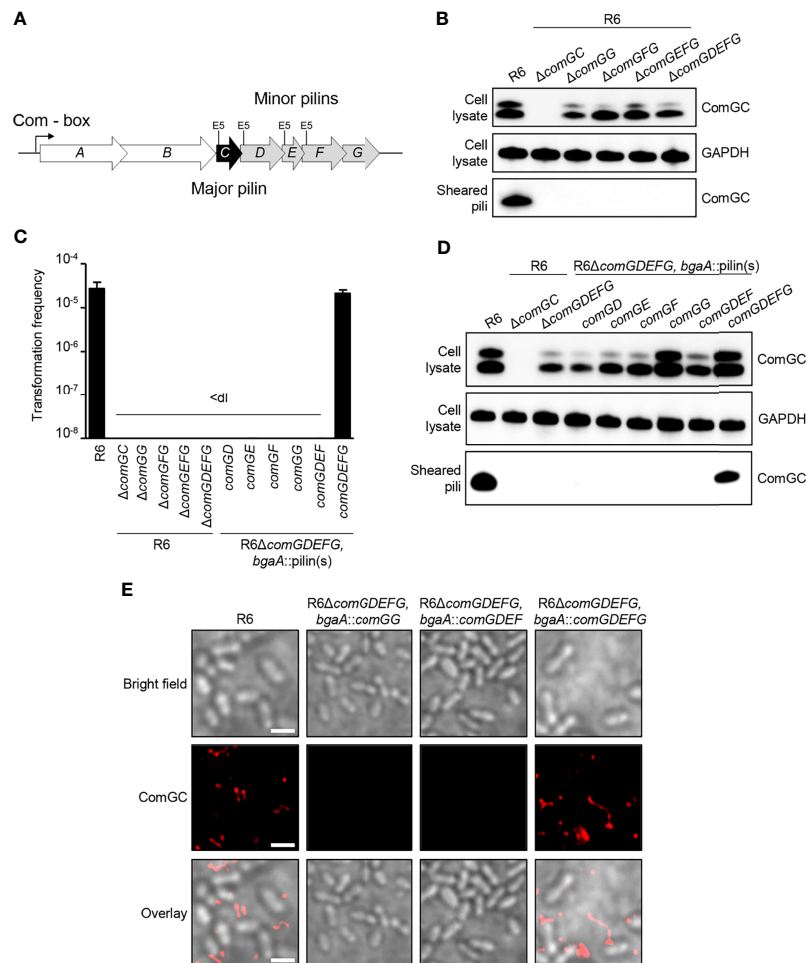


FIGURE 1 | Competence pilus assembly and transformability depends on the pneumococcal minor pilins. **(A)** Schematic representation of the *comG* operon in *S. pneumoniae* R6 strain encoding *comGA* and *comGB* (white), the major pilin gene *comGC* (black) and the minor pilin genes *comGD*, *comGE*, *comGF* and *comGG* (grey). The invariant Glu5 residue, present in all pneumococcal pilins except ComGG, is highlighted (E5). **(B)** ComGC was detected by immunoblotting in bacterial whole cell lysates and sheared pili of mutants lacking $\Delta comGC$, $\Delta comGG$, $\Delta comGFG$, $\Delta comGEFG$. The WT strain was included as a positive control and GAPDH as loading control. **(C)** Transformation frequency of WT, *comG* mutants and R6 $\Delta comGEFG$ complemented strains. The detection limit (dl) of the assay was 2.39×10^{-9} and the error bars represent the standard deviation of a minimum of three independent experiments ($n=3$). **(D)** Western blotting analysis of ComGC in bacterial whole cell lysates and sheared pili of $\Delta comGEFG$ strains expressing individual minor pilins, *comGDEF* or *comGEFG* at the ectopic *bgaA* locus. The WT strain was included as a positive control and GAPDH as loading control. **(E)** Immunofluorescence microscopy (IF) of competence-induced pili in WT R6 and R6 $\Delta comGEFG$ complemented with *comGG*, *comGDEF* or *comGEFG*. Bacteria were visualized by bright field (BF) microscopy and competence pili were labelled with antisera specific for ComGC (red). Scale bars represent 2 μm .

respective antisera detected ComGD, ComGF and ComGG in the WT strain, but not in the $\Delta comGEFG$ mutant. ComGE antisera failed to detect specific protein in pneumococcal lysates but recognized recombinant ComGE. Surprisingly, in the $\Delta comGG$ deletion mutant the levels of ComGD were strongly reduced and ComGF was entirely absent. Since we were able to detect the *comGF* transcript by qPCR in this strain (Figure 2C), the observed effect suggests that ComGG is required for the stability of the other minor pilins. In the complemented mutant with ComGG ectopically expressed under the transcriptional control of the native CSP-inducible promoter, expression of ComGD and ComGF was restored, albeit not at WT levels (Figure 2B). These results show that deletion of ComGG has a negative

impact on the stability of ComGD and ComGF, supporting evidence that the minor pilins directly interact.

Pneumococcal Minor Pilins Interact Directly

Others showed previously that minor pilins/pseudopilins can interact *via* their globular C-terminal domains (Yanez et al., 2008; Douzi et al., 2009; Cisneros et al., 2012; Mann et al., 2013). To investigate possible interactions between the pneumococcal minor pilins, we used an *in vitro* co-purification assay with affinity-tagged minor pilins in *E. coli*. The C-terminal domains of ComGC, ComGD, ComGE, ComGF and ComGG were cloned into pGEX4T1 to express them as N-terminal GST-tagged fusion

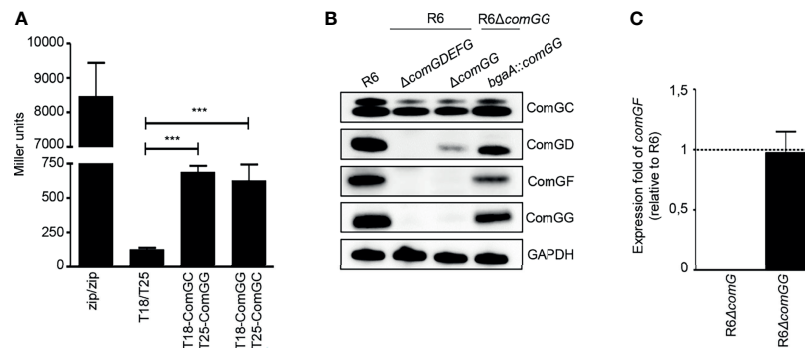


FIGURE 2 | ComGG interacts with ComGC and is required for the stability of ComGD and ComGF. **(A)** Quantification of the interaction between ComGG and ComGC by BACTH. The graph shows mean values of β -galactosidase activity expressed in Miller units for the hybrid proteins T18-ComGC/T25-ComGG and T18-ComGG/T25-ComGC. A strain expressing Zip-T18 and Zip-T25 (zip/zip), in which the hybrid proteins interact through a leucine zipper motif, was included as a positive control. *E. coli* BTH101 co-transformed with pUT18C and pKT25 empty plasmids was used as a negative control. The error bars represent the standard deviation of three independent experiments ($n=3$) with three different clones. A one-way analysis of variance test followed by Dunnett's post-test to compare each interaction pair to the negative control (T18/T25) was used for statistical analysis: $***p \leq 0.001$. **(B)** ComGC, ComGD, ComGF and ComGG were detected by immunoblotting in bacterial whole cell lysates in the WT R6 strain, a mutant lacking all minor pilins ($\Delta comGDEFG$) or $comGG$, and a complemented $\Delta comGG$ mutant strain that ectopically expressed *comGG* from the *bgaA* locus ($R6\Delta comGG$, *bgaA::comGG*). GAPDH was used as loading control. **(C)** Relative expression of *comGF* in competent $R6\Delta comG$ and $R6\Delta comGG$. The $R6\Delta comG$ operon mutant strain was included as negative control. Data was normalized to *gyrA* using the $2^{-\Delta\Delta CT}$ method and presented as the mean fold change of *comGF* relative to the WT R6 strain. Error bars represent the standard deviation of three independent experiments ($n=3$). The dotted line indicates an expression ratio of 1.

proteins or cloned into pET21a to express untagged recombinant pilins. GST-tagged and untagged proteins were expressed individually. *E. coli* pellets expressing each untagged pilin were then mixed with *E. coli* pellets expressing each GST-tagged pilin. Cells were lysed and the pilins were purified from the lysate. As control, pellets expressing each untagged pilin were mixed with pellets expressing GST alone. All purified GST-tagged pilins were detected by Coomassie Brilliant Blue staining (Figure 3A, upper gels). The GST-tagged minor pilins were slightly unstable and multiple bands that could correspond to degradation products or other contaminants were observed. We then probed the eluate fractions for ComGD, ComGE or ComGG by immunoblotting and found that all three minor pilins were pulled-down by GST-D, GST-E, GST-F and GST-G, suggesting that they could interact with each other and themselves (Figure 3A, lower gels). Untagged soluble ComGF could not be stably produced in *E. coli* and was therefore not tested in this assay. None of the minor pilin globular domains interacted detectably with GST-ComGC.

Based on these results, we hypothesized that all four minor pilins likely interact and that ComGF requires the presence of other minor pilins for its stability. To address this question, we co-expressed the C-terminal domains of ComGD, ComGE, ComGF, and ComGG in *E. coli* and performed co-immunoprecipitation with ComGG antiserum. When expressed together in *E. coli*, distinct bands in the range of 5–15 kDa corresponding to the sizes of the soluble domains of the individual minor pilins were visible in the eluate after Coomassie staining (Figure 3B), and all four minor pilins were detected by immunoblotting (Figure 3C). These data suggest that 1) ComGF is stable in the presence of ComGD, ComGE and ComGG, and 2) ComGF can either directly interact with ComGG, consistent with the pull-down results, or 3) through another minor pilin.

ComGD, ComGF and ComGG Are Present in Sheared Pili

Next, we investigated the abundance of ComGD, ComGF and ComGG in pneumococcal lysates and sheared pili fractions of the WT R6 strain by immunoblotting (Figure 4A). All three minor pilins were detected in R6 lysates but were absent in a mutant lacking *comGDEFG*. ComGD, ComGF and ComGG were also detected in sheared pili fractions with ComGG being the most abundant. As expected, the proportion of ComGD, ComGF or ComGG was much lower than the proportion of the major pilin ComGC (Figure 4A). To further examine whether ComGD, ComGF and ComGG are associated with competence pili, we performed co-immunoprecipitation on sheared pili fractions using ComGC antisera. All three minor pilins tested were found in sheared pili of CSP-induced cultures, suggesting that they are part of the pilus, and were absent in non-induced cultures, and in a strain lacking ComGC (Figure 4B). Minor amounts of ComGC were detectable in the CSP induced no antibody condition, probably due to unspecific binding to Protein A sepharose.

ComGF Is Incorporated Throughout the Competence Pilus

Because ComGD, ComGF and ComGG were detected in sheared pili fractions, we also performed immunofluorescence microscopy to examine the localization of these minor pilins. While we failed to detect any signal in competent WT bacteria stained with ComGD or ComGG antisera, specific ComGF signal was detected in competent bacteria stained with ComGF antisera (Figure 5A). To confirm that the ComGF signal is associated with the competence pilus, we performed immunogold electron microscopy with ComGF antisera and observed labeling of

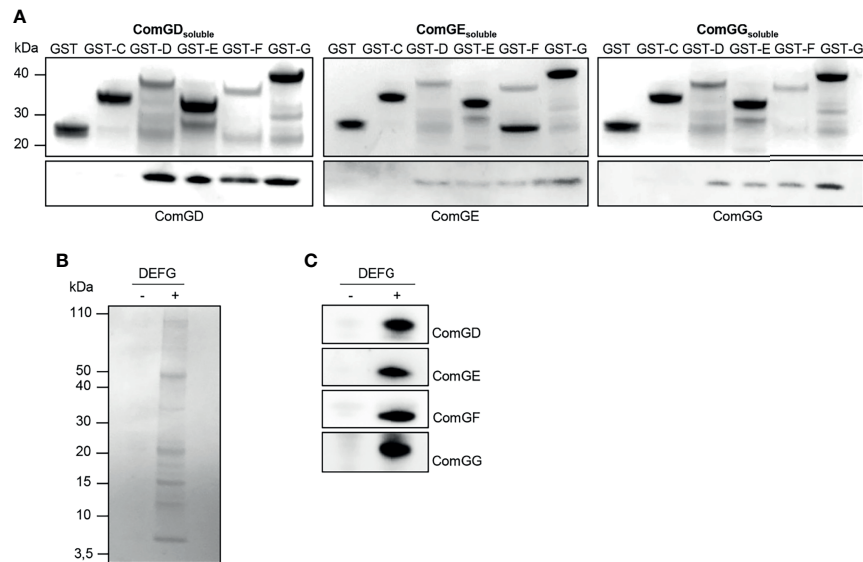


FIGURE 3 | Soluble domains of pneumococcal minor pilins interact directly. **(A)** Untagged (ComGD_{soluble}, ComGE_{soluble} or ComGG_{soluble}) or GST-tagged C-terminal, soluble domains of the pneumococcal pilins (GST-C, GST-D, GST-E, GST-F or GST-G) were expressed individually in *E. coli*. Pellets expressing untagged protein were mixed with pellets expressing GST-tagged pilins, lysed in a high-pressure cell disrupter and the supernatants were applied to GSH Sepharose Fast Flow affinity resin. *E. coli* expressing only GST was included as a negative control. Elution fractions were separated by SDS-PAGE and the upper gel part was stained with Coomassie brilliant blue and the lower gel part was immunoblotted with antisera specific for ComGD, ComGE or ComGG. **(B, C)** Co-immunoprecipitation (IP) of minor pilins co-expressed in *E. coli*. The bacterial pellet from cells co-expressing the soluble domains of ComGD, ComGE, ComGF and ComGG was lysed, centrifuged and the supernatant was immunoprecipitated using anti-ComGG antibodies coupled to Protein G Dynabeads™ (+). Uncoupled beads (-) were included as a negative control. IP samples were separated by SDS-PAGE followed by **(B)** Coomassie brilliant blue staining and **(C)** immunoblotting with antibodies against ComGD, ComGE, ComGF and ComGG.

ComGF sporadically throughout the competence pilus, indicating that the minor pilin ComGF may be incorporated into the pilus filament (**Figure 5B**).

To further investigate the possible localization of ComGD, ComGE and ComGG, strains expressing a Flag-tagged minor pilin were generated. Direct insertion of the sequence encoding the Flag tag in the *comG* operon was not possible because all minor pilins are overlapping. For that reason, an additional copy

of *comGD*, *comGE*, *comGF* or *comGG* encoding a C-terminal Flag-tag was integrated ectopically at the *bgaA* locus under the control of the native CSP-inducible promoter. Expression of the Flag-tagged minor pilins was confirmed by immunoblotting using anti-Flag antibodies (**Figure 5C**), and the transformation frequency of these strains was similar to WT levels (**Figure 5D**). Consistent with the electron microscopy results, ComGF, detected with mouse anti-Flag antibodies, co-localized with the

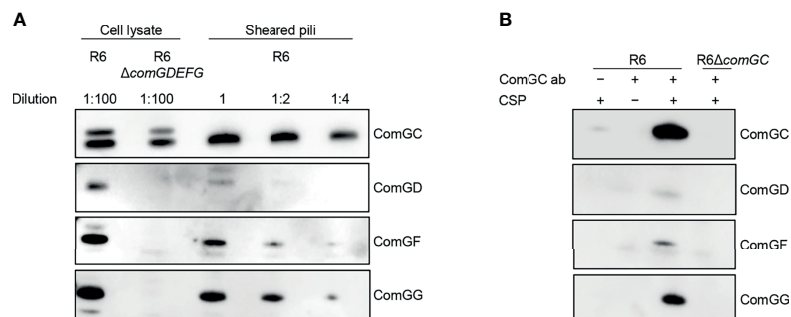


FIGURE 4 | Localization of ComGD, ComGF and ComGG. **(A)** Whole-cell lysate (diluted 1:100) and the sheared fraction (2-fold serial dilutions as indicated) from WT R6 were analysed by immunoblotting with antisera specific for ComGC, ComGD, ComGF and ComGG. The lysate from a strain lacking all four minor pilins (R6 $\Delta comGDEFG$) was included as a negative control and indicates the specificity of detection. **(B)** Co-immunoprecipitation of sheared pili from WT R6 strain using anti-ComGC antibodies (ComGC ab). As negative controls a non-induced culture (-CSP), a no antibody control (-ComGC ab) and a strain lacking the major pilin (R6 $\Delta comGC$) were included. IP samples were probed for the presence of ComGC, ComGD, ComGF and ComGG by immunoblotting.

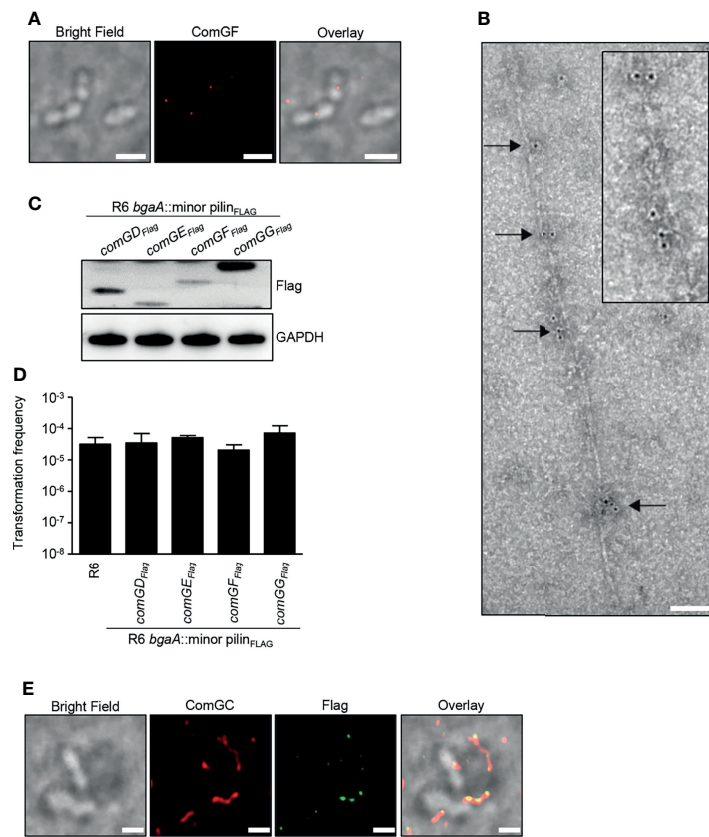


FIGURE 5 | Visualization of the minor pilin ComGF. **(A)** BF and IF microscopy of competent WT R6 bacteria stained with anti-ComGF antibodies (red). Scale bars represent 2 μ m. **(B)** Immunogold electron microscopy of competent WT R6 bacteria. Electron micrographs were stained with anti-ComGF antibodies and secondary antibodies conjugated to 6-nm gold particles. Black arrows indicate gold particles incorporated throughout the pilus filament. The inset (black box) shows an enlargement of the immunogold-labelled pilus. Scale bar represents 100 nm. **(C)** Bacterial whole cell lysates of R6 strains encoding an extra copy of C-terminal Flag-tagged *comGD*, *comGE*, *comGF* or *comGG* in the *bgaA* locus were analysed by immunoblotting using Flag-antiserum. GAPDH was used as loading control. **(D)** Transformation frequency of WT R6 and R6 strains encoding an extra copy of C-terminal Flag-tagged minor pilins. The error bars represent the standard deviation of a minimum of three independent experiments ($n=3$). **(E)** Co-localization of ComGF_{Flag} and ComGC visualized by IF microscopy. Competent bacteria ectopically expressing Flag-tagged ComGF (R6 *bgaA::comGF_{Flag}*) were labelled with primary antibodies specific for ComGC (red) and anti-Flag antibodies (green). Bacteria were visualized by BF microscopy. Scale bars correspond to 1 μ m.

competence pilus stained with rabbit anti-ComGC serum (Figure 5E). In contrast, ComGD-Flag, ComGE-Flag or ComGG-Flag could not be detected despite repeated attempts.

ComGD_{E5A} and ComGE_{E5A} Affect Competence Pilus Formation and Function

A conserved feature among type IV pilins is the invariant E5 residue in position 5 after the prepilin cleavage site, and substitution of E5 in the major pilin ComGC by valine abolishes competence pilus assembly and function (Laurenceau et al., 2013). To gain insight into the role of the E5 residue present in ComGD, ComGE and ComGF, we generated E5 variants in these minor pilins and tested their ability to assemble pili and to take up DNA. Given the difficulties of directly manipulating the native *comG* operon, we reintroduced the *comG* operon including its promoter ectopically at the *bgaA* locus using a modified version of the integration vector pJVW25, and subsequently deleted the native operon. Before we

constructed similar integration vectors with minor pilin E5 mutations, we verified that our control strain expressing *comG* ectopically in *bgaA*, and deficient in its native *comG* operon (R6 Δ *comG*, *bgaA::comG*), was functional. Indeed, using immunofluorescence microscopy, we were able to detect pili on the surface of competent R6 Δ *comG*, *bgaA::comG* bacteria (Figure 6A) and more importantly, this strain was transformable (Figure 6C). Encouraged by these results, E5A substitutions were constructed in *comGD*, *comGE* and *comGF* and the strains were tested for their ability to produce pili. ComGC was detected in similar amounts in whole-cell lysates of all mutant strains carrying E5A, the *comG* control strain and the WT R6 strain (Figure 6B). Consistent with previous findings for ComGC_{E5V} (Laurenceau et al., 2013), ComGC was absent in sheared pili in a ComGC_{E5A} strain (Figure 6B). The levels of ComGC in the sheared pili fractions of the strains with E5A substitution in the minor pilins showed varying amounts of ComGC compared to the control strain and were overall reduced in the ComGD_{E5A}

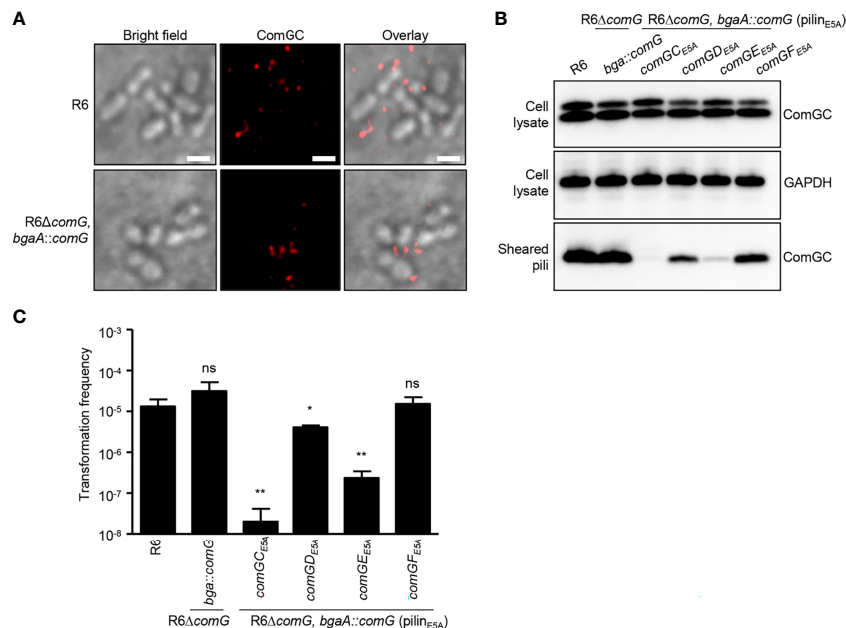


FIGURE 6 | E5A mutations affect minor pilin function of ComGD and ComGE. **(A)** Visualization of competence-induced pili in WT R6 and R6Δ*comG*, *bgaA::comG* complemented strain by IF microscopy. Bacteria were visualized by bright field microscopy and competence pili were labelled with antibodies specific for ComGC (red). Scale bars represent 2 μm. **(B)** ComGC was detected by immunoblotting in bacterial whole cell lysates and sheared pili of E5A mutant strains (*comGC_{E5A}*, *comGD_{E5A}*, *comGE_{E5A}* or *comGF_{E5A}*). The WT R6 strain and the complemented mutant strain in which the native *comG* operon was expressed ectopically (R6Δ*comG*, *bgaA::comG*) were included as positive controls. GAPDH was used as a loading control. **(C)** Transformation frequency of WT R6 strain, R6Δ*comG*, *bgaA::comG* complemented mutant and E5A mutant strains. The error bar represents the standard deviation of a minimum of three independent experiments. A t-test was used for statistical analysis: * $p \leq 0.05$ and ** $p \leq 0.01$, ns, no significant difference ($C_{E5A} p = 0.0043$; $D_{E5A} p = 0.0237$ and $E_{E5A} p = 0.0047$).

and ComGE_{E5A} strain (**Figure 6B**). Surprisingly, pilus formation in the presence of the ComGE_{E5A} variant was nearly abolished, suggesting a dominant negative effect of this amino acid substitution. The transformation frequency of those strains correlated well with the amount of ComGC present in sheared pili, and the ComGD_{E5A} and ComGE_{E5A} strain had significantly reduced transformation rates. These results reveal that E5 is necessary for two of the three minor pilins in which it is conserved, and suggests that ComGD, and especially ComGE, rely more heavily on their N-terminal α -helix interactions.

DISCUSSION

The pneumococcal competence pilus belongs to the T4P family and is essential for DNA uptake of this pathogen. The major pilin ComGC forms the backbone of the competence pilus, however, the contribution of the minor pilins, ComGD, ComGE, ComGF and ComGG in pilus biogenesis and function remained unclear.

In the present study, we show that mutant strains deficient in ComGDEFG, ComGEFG, ComGFG and ComGG are non-piliated and non-transformable. This suggests that ComGG is essential for pilus assembly, and that the minor pilin(s) ComGD, ComGDE and ComGDEF are not sufficient for piliation. Moreover, neither individual minor pilins, nor ComGDEF

were able to restore piliation in a Δ*comGDEFG* background, and functional competence pili were only assembled in presence of all minor pilins. *Bacillus subtilis* expresses a homologous *comG* operon and consistent with our findings, all minor pilins in *B. subtilis* are required for pilus assembly and transformation (Chung and Dubnau, 1998; Chen et al., 2006). Strikingly, also T2SSs contain five pilins (one major and four minor pseudopilins), and all minor pseudopilins are required for efficient Pula secretion by the *Klebsiella oxytoca* T2SS (Possot et al., 2000). The finding that all minor pilins are required for competence pilus assembly suggests that they are interdependent and that their translation must be tightly orchestrated to form a stable and functional complex. Studies in *E. coli* that demonstrate a link between the operon gene order and efficient co-translational assembly of protein complexes, would support this assumption (Shieh et al., 2015; Wells et al., 2016). Thus, deletion of any of the minor pilin genes would hamper the formation of a stable minor pilin complex and thereby abolish competence pilus formation. Interestingly, in *P. aeruginosa* it was shown that a specific stoichiometric ratio among the minor pilins was important for pilus function, and loss or overexpression of minor pilins impaired the twitching motility (Giltner et al., 2010).

A main finding in this study is that all four minor pilins can directly interact with each other and likely form a minor pilin

complex. It is important to note that we used the soluble domains of the pneumococcal minor pilins to test putative interactions and therefore might have missed other interactions involving the hydrophobic domains. The observation that the soluble domain of ComGC did not interact with soluble ComGG, whereas fulllength ComGC and ComGG interacted in the BACTH assay, confirmed this assessment. In line with our results, others reported that the soluble domain of the major pilin in *B. subtilis* (ComGC) and in *Pseudomonas aeruginosa* (XcpT) did not interact with minor pilins lacking the hydrophobic domain (Douzi et al., 2009; Mann et al., 2013).

Another important finding is the intriguing role of ComGG. Our results showed that fulllength ComGG and ComGC directly interact, further supported by two observations: (I) all deletion mutants lacking ComGG showed reduced levels of the major pilin ComGC and (II) ComGG alone is able to stabilize ComGC when ectopically expressed in a strain lacking all four minor pilins. Several examples of minor subunits that provide a link to the major subunit have been identified both in T4P and T2SS biogenesis. In *P. aeruginosa* it was proposed that the minor pilin complex PilVWXE together with the large, non-pilin PilY1, form an assembly initiation complex, while FimU couples this complex to the major pilin subunit PilA (Nguyen et al., 2015). In contrast to ComGG, FimU is incorporated into pili in the absence of the other minor pilins (Nguyen et al., 2015). The structure of FimU strongly resembles the minor pseudopilin GspH in *E. coli*, and the GspH pseudopilin homolog in *P. aeruginosa*, XcpU, was proposed to link the pseudopilin XcpVWX complex to the major pseudopilin XcpT (Douzi et al., 2009; Nguyen et al., 2015). In the *Klebsiella* T2SS, the minor pilin PulH, a XcpU homologue, links the priming complex composed of PulI, PulJ and PulK to the major pseudopilin PulG (Cisneros et al., 2012).

ComGG is also important for the stabilization of the other minor pilins, and in a ComGG deficient strain, no ComGF and less ComGD was detected. Similar observations on mutually dependent minor pilins have been reported in other bacteria (Winther-Larsen et al., 2005; Mann et al., 2013). Intriguingly, ComGG is the last minor pilin in the *comG* operon and the only pneumococcal minor pilin that lacks the conserved E5 residue. It was previously speculated that ComGG could form the competence pilus tip (Piepenbrink and Sundberg, 2016). This was based on the observation that E5 is involved in interactions with the N-terminus of the previously incorporated pilin into the growing pseudopilus fiber, and hence would be dispensable for the first pilin subunit integrated into the pilus (Korotkov et al., 2012). *E. coli* GspK is an example of such a protein and was shown to form a trimeric complex with GspI and GspJ, presumably at the tip of the pseudopilus (Korotkov and Hol, 2008). We find ComGD, ComGF and ComGG in the sheared pili fraction of competent *S. pneumoniae* and by co-immunoprecipitation of sheared pili. However, we were not able to detect ComGG by immunofluorescence microscopy or electron microscopy in the competence pilus. This could simply be due to its low abundance, especially if there is only one of each per pilus. It could also reflect variability in antibody affinities for the different pilins or different accessibilities of epitopes for

staining, hence does not rule out the potential localization of ComGG at the pilus tip.

Notably, our immunofluorescence and electron microscopy data suggest that ComGF is incorporated throughout the competence pilus, which has also been demonstrated for minor pilins in *P. aeruginosa* and *Clostridium difficile* T4P (Giltner et al., 2010; Piepenbrink et al., 2015). Since ComGF was not stable in the absence of ComGG nor the other minor pilins, it is tempting to speculate that the entire minor pilin complex becomes incorporated into the pilus. It could also mean that ComGF has additional pilus-related functions besides its role in the minor pilin complex and becomes stabilized differently when built into the ComGC fiber. Because the minor pilin mutant expressing ComGF_{E5A} was not impaired in pilus formation and function, interactions with ComGF are presumably E5-independent. In contrast, competent bacteria expressing ComGD_{E5A} or ComGE_{E5A} variants showed reduced levels of ComGC in the sheared pili fraction and reduced transformation frequencies compared to the WT R6 strain, revealing a critical role for E5 in ComGD and ComGE in competence pilus biogenesis.

Minor pseudopilins in Gram-negative bacteria have been proposed as initiators and terminators of pseudopilus assembly. In the “initiator” scenario, pseudopilus assembly takes place beneath the minor pseudopilin complex, which would consequently end up at the tip of the pilus forming a cap (Korotkov et al., 2012). Alternatively, the minor pseudopilin complex remains in the inner-membrane and integrates major pseudopilin subunits from the base, thereby controlling/terminating pseudopilus elongation (Douzi et al., 2009). A more dynamic role for PilY1 and the minor pilins in *Myxococcus xanthus* was recently reported. In this model, PilY1 and the minor pilins form a priming complex to initiate T4P extension. The complex locates at the tip of the pilus and at the same time functions as terminator of pilus retraction (Treuner-Lange et al., 2020). It is interesting to consider whether the pneumococcal minor pilins may have a similar function since the competence pilus was recently shown to be a dynamic structure that is able to retract for efficient DNA uptake (Lam et al., 2021).

Because all pneumococcal minor pilins are required for pilus formation and given their ability to interact with each other, we propose that the pneumococcal minor pilins form a complex and that ComGG couples this complex to the major pilin ComGC. Based on our results, the function of the pneumococcal minor pilin complex appears to be primarily related to initiation of competence pilus assembly and/or elongation. The precise interaction network and the molecular events leading to the formation of such a putative minor pilin complex and its localization will require further studies.

DATA AVAILABILITY STATEMENT

The original contributions presented in the study are included in the article/supplementary material, further inquiries can be directed to the corresponding authors.

AUTHOR CONTRIBUTIONS

VO, SM and BHN designed the study. VO, MSA, AvE, and SM performed the experiments. VO, SM, and BHN wrote the manuscript. All authors contributed to writing. All authors contributed to the article and approved the submitted version.

REFERENCES

- Aas, F. E., Winther-Larsen, H. C., Wolfgang, M., Frye, S., Lovold, C., Roos, N., et al. (2007). Substitutions in the N-Terminal Alpha Helical Spine of Neisseria Gonorrhoeae Pili Affect Type IV Pilus Assembly, Dynamics and Associated Functions. *Mol. Microbiol.* 63, 69–85. doi: 10.1111/j.1365-2958.2006.05482.x
- Balaban, M., Battig, P., Muschiol, S., Tirier, S. M., Wartha, F., Normark, S., et al. (2014). Secretion of a Pneumococcal Type II Secretion System Pilus Correlates With DNA Uptake During Transformation. *Proc. Natl. Acad. Sci. U.S.A.* 111, E758–E765. doi: 10.1073/pnas.1313860111
- Beiko, R. G., Harlow, T. J., and Ragan, M. A. (2005). Highways of Gene Sharing in Prokaryotes. *Proc. Natl. Acad. Sci. U.S.A.* 102, 14332–14337. doi: 10.1073/pnas.0504068102
- Berry, J. L., and Pelicic, V. (2015). Exceptionally Widespread Nanomachines Composed of Type IV Pilins: The Prokaryotic Swiss Army Knives. *FEMS Microbiol. Rev.* 39, 134–154. doi: 10.1093/femsre/fuu001
- Brissac, T., Mikaty, G., Dumenil, G., Coureuil, M., and Nassif, X. (2012). The Meningococcal Minor Pilin Pilx Is Responsible for Type IV Pilus Conformational Changes Associated With Signaling to Endothelial Cells. *Infect. Immun.* 80, 3297–3306. doi: 10.1128/IAI.00369-12
- Calero-Caceres, W., Ye, M., and Balcazar, J. L. (2019). Bacteriophages as Environmental Reservoirs of Antibiotic Resistance. *Trends Microbiol.* 27, 570–577. doi: 10.1016/j.tim.2019.02.008
- Cehovin, A., Simpson, P. J., McDowell, M. A., Brown, D. R., Noschese, R., Pallett, M., et al. (2013). Specific DNA Recognition Mediated by A Type IV Pilin. *Proc. Natl. Acad. Sci. U.S.A.* 110, 3065–3070. doi: 10.1073/pnas.1218832110
- Chen, I., Provvedi, R., and Dubnau, D. (2006). A Macromolecular Complex Formed by A Pilin-Like Protein In Competent Bacillus Subtilis. *J. Biol. Chem.* 281, 21720–21727. doi: 10.1074/jbc.M604071200
- Chung, Y. S., and Dubnau, D. (1998). All Seven Comg Open Reading Frames Are Required for DNA Binding During Transformation of Competent Bacillus Subtilis. *J. Bacteriol.* 180, 41–45. doi: 10.1128/JB.180.1.41-45.1998
- Cisneros, D. A., Bond, P. J., Pugsley, A. P., Campos, M., and Francetic, O. (2012). Minor Pseudopilin Self-Assembly Primes Type II Secretion Pseudopilus Elongation. *EMBO J.* 31, 1041–1053. doi: 10.1038/emboj.2011.454
- Craig, L., Forest, K. T., and Maier, B. (2019). Type IV Pili: Dynamics, Biophysics and Functional Consequences. *Nat. Rev. Microbiol.* 17, 429–440. doi: 10.1038/s41579-019-0195-4
- Douzi, B., Durand, E., Bernard, C., Alphonse, S., Cambillau, C., Filloux, A., et al. (2009). The XcpV/GspI Pseudopilin Has a Central Role In the Assembly of a Quaternary Complex Within the T2SS Pseudopilus. *J. Biol. Chem.* 284, 34580–34589. doi: 10.1074/jbc.M109.042366
- Eberhardt, A., Wu, L. J., Errington, J., Vollmer, W., and Veening, J. W. (2009). Cellular Localization of Choline-Utilization Proteins In Streptococcus Pneumoniae Using Novel Fluorescent Reporter Systems. *Mol. Microbiol.* 74, 395–408. doi: 10.1111/j.1365-2958.2009.06872.x
- Escobar, C. A., Douzi, B., Ball, G., Barbat, B., Alphonse, S., Quinton, L., et al. (2021). Structural Interactions Define Assembly Adapter Function of a Type II Secretion System Pseudopilin. *Structure* 29, 1116–1127.e1118. doi: 10.1016/j.str.2021.05.015
- Giltner, C. L., Habash, M., and Burrows, L. L. (2010). Pseudomonas Aeruginosa Minor Pilins Are Incorporated Into Type IV Pili. *J. Mol. Biol.* 398, 444–461. doi: 10.1016/j.jmb.2010.03.028
- Giltner, C. L., Nguyen, Y., and Burrows, L. L. (2012). Type IV Pilin Proteins: Versatile Molecular Modules. *Microbiol. Mol. Biol. Rev.* 76, 740–772. doi: 10.1128/MMBR.00035-12
- Helaine, S., Carbonnelle, E., Prouvensier, L., Beretti, J. L., Nassif, X., and Pelicic, V. (2005). PilX, A Pilus-Associated Protein Essential for Bacterial Aggregation, Is a Key to Pilus-Facilitated Attachment of Neisseria Meningitidis to Human Cells. *Mol. Microbiol.* 55, 65–77. doi: 10.1111/j.1365-2958.2004.04372.x
- Helaine, S., Dyer, D. H., Nassif, X., Pelicic, V., and Forest, K. T. (2007). 3D Structure/Function Analysis of Pilx Reveals How Minor Pilins Can Modulate the Virulence Properties of Type IV Pili. *Proc. Natl. Acad. Sci. U.S.A.* 104, 15888–15893. doi: 10.1073/pnas.0707581104
- Imhaus, A. F., and Dumenil, G. (2014). The Number of Neisseria Meningitidis Type IV Pili Determines Host Cell Interaction. *EMBO J.* 33, 1767–1783. doi: 10.15252/embj.201488031
- Johnston, C., Martin, B., Fichant, G., Polard, P., and Claverys, J. P. (2014). Bacterial Transformation: Distribution, Shared Mechanisms and Divergent Control. *Nat. Rev. Microbiol.* 12, 181–196. doi: 10.1038/nrmicro3199
- Karimova, G., Pidoux, J., Ullmann, A., and Ladant, D. (1998). A Bacterial Two-Hybrid System Based on a Reconstituted Signal Transduction Pathway. *Proc. Natl. Acad. Sci. U.S.A.* 95, 5752–5756. doi: 10.1073/pnas.95.10.5752
- Koonin, E. V., Makarova, K. S., and Aravind, L. (2001). Horizontal Gene Transfer in Prokaryotes: Quantification and Classification. *Annu. Rev. Microbiol.* 55, 709–742. doi: 10.1146/annurev.micro.55.1.709
- Korotkov, K. V., and Hol, W. G. (2008). Structure of the GspK-GspI-GspJ Complex from the Enterotoxigenic Escherichia Coli Type 2 Secretion System. *Nat. Struct. Mol. Biol.* 15, 462–468. doi: 10.1038/nsmb.1426
- Korotkov, K. V., Sandkvist, M., and Hol, W. G. (2012). The Type II Secretion System: Biogenesis, Molecular Architecture and Mechanism. *Nat. Rev. Microbiol.* 10, 336–351. doi: 10.1038/nrmicro2762
- Lam, T., Ellison, C. K., Eddington, D. T., Brun, Y. V., Dalia, A. B., and Morrison, D. A. (2021). Competence Pili In Streptococcus Pneumoniae Are Highly Dynamic Structures That Retract to Promote DNA Uptake. *Mol. Microbiol.* 116(2), 381–396. doi: 10.1111/mmi.14718
- Laurenceau, R., Pehau-Arnaud, G., Baconnais, S., Gault, J., Malosse, C., Dujancourt, A., et al. (2013). A Type IV Pilus Mediates DNA Binding During Natural Transformation In Streptococcus Pneumoniae. *PLoS Pathog.* 9, e1003473. doi: 10.1371/journal.ppat.1003473
- Li, J., Egelman, E. H., and Craig, L. (2012). Structure of the Vibrio Cholerae Type IVb Pilus and Stability Comparison with the Neisseria Gonorrhoeae Type IVa Pilus. *J. Mol. Biol.* 418, 47–64. doi: 10.1016/j.jmb.2012.02.017
- Mann, J. M., Carabetta, V. J., Cristea, I. M., and Dubnau, D. (2013). Complex Formation and Processing of the Minor Transformation Pilins of Bacillus Subtilis. *Mol. Microbiol.* 90, 1201–1215. doi: 10.1111/mmi.12425
- Melville, S., and Craig, L. (2013). A Type IV Pili In Gram-Positive Bacteria. *Microbiol. Mol. Biol. Rev.* 77, 323–341. doi: 10.1128/MMBR.00063-12
- Muschiol, S., Aschtgen, M. S., Nannapaneni, P., and Henriques-Normark, B. (2019). Gram-Positive Type IV Pili and Competence. *Microbiol. Spectr.* 7(1), 1–6. doi: 10.1128/microbiolspec.PSIB-0011-2018
- Muschiol, S., Erendsson, S., Aschtgen, M. S., Oliveira, V., Schmieder, P., de Lichtenberg, C., et al. (2017). Structure of the Competence Pilus Major Pilin Comgc in Streptococcus Pneumoniae. *J. Biol. Chem.* 292(34), 14134–14146. doi: 10.1074/jbc.M117.787671
- Ng, D., Harn, T., Altindal, T., Kolappan, S., Marles, J. M., Lala, R., et al. (2016). The Vibrio Cholerae Minor Pilin TcpB Initiates Assembly and Retraction of the Toxin-Coregulated Pilus. *PLoS Pathog.* 12(12), e1006109. doi: 10.1371/journal.ppat.1006109
- Nguyen, Y., Sugiman-Marangos, S., Harvey, H., Bell, S. D., Charlton, C. L., Junop, M. S., et al. (2015). Pseudomonas Aeruginosa Minor Pilins Prime Type IVa Pilus Assembly and Promote Surface Display of the Pili1 Adhesin. *J. Biol. Chem.* 290, 601–611. doi: 10.1074/jbc.M114.616904
- Nivaskumar, M., Santos-Moreno, J., Malosse, C., Nadeau, N., Chamot-Rooke, J., Tran Van Nhieu, G., et al. (2016). Pseudopilin Residue E5 Is Essential For Recruitment by the Type 2 Secretion System Assembly Platform. *Mol. Microbiol.* 101, 924–941. doi: 10.1111/mmi.13432

ACKNOWLEDGMENTS

This work was supported by grants from the Swedish Research Council, Stockholm County Council, the Swedish Foundation for Strategic research (SSF), and the Knut and Alice Wallenberg Foundation.

- Pelcic, V. (2019). Monoderm Bacteria: The New Frontier for Type IV Pilus Biology. *Mol. Microbiol.* 112, 1674–1683. doi: 10.1111/mmi.14397
- Piepenbrink, K. H. (2019). DNA Uptake by Type IV Filaments. *Front. Mol. Biosci.* 6, 1. doi: 10.3389/fmolb.2019.00001
- Piepenbrink, K. H., Maldarelli, G. A., Martinez de la Pena, C. F., Dingle, T. C., Mulvey, G. L., Lee, A., et al. (2015). Structural and Evolutionary Analyses Show Unique Stabilization Strategies in the Type IV Pili of *Clostridium Difficile*. *Structure* 23, 385–396. doi: 10.1016/j.str.2014.11.018
- Piepenbrink, K. H., and Sundberg, E. J. (2016). Motility and Adhesion Through Type IV Pili In Gram-Positive Bacteria. *Biochem. Soc. Trans.* 44, 1659–1666. doi: 10.1042/BST20160221
- Possot, O. M., Vignon, G., Bomchil, N., Ebel, F., and Pugsley, A. P. (2000). Multiple Interactions Between Pullulanase Secretion Components Involved In Stabilization and Cytoplasmic Membrane Association of PulE. *J. Bacteriol.* 182, 2142–2152. doi: 10.1128/JB.182.8.2142-2152.2000
- Sambrook, J., Fritsch, E. F., and Maniatis, T. (1989). *Molecular Cloning: A Laboratory Manual*. (Cold Spring Harbor, NY: Cold Spring Harbor Laboratory).
- Schneider, C. A., Rasband, W. S., and Eliceiri, K. W. (2012). NIH Image to ImageJ: 25 Years of Image Analysis. *Nat. Methods* 9, 671–675. doi: 10.1038/nmeth.2089
- Shieh, Y. W., Minguez, P., Bork, P., Auburger, J. J., Guilbride, D. L., Kramer, G., et al. (2015). Operon Structure and Cotranslational Subunit Association Direct Protein Assembly In Bacteria. *Science* 350, 678–680. doi: 10.1126/science.aac8171
- Strom, M. S., and Lory, S. (1991). Amino Acid Substitutions In Pilin of *Pseudomonas Aeruginosa*. Effect on Leader Peptide Cleavage, Amino-Terminal Methylation, and Pilus Assembly. *J. Biol. Chem.* 266, 1656–1664. doi: 10.1016/S0021-9258(18)52345-0
- Strom, M. S., Nunn, D. N., and Lory, S. (1993). A Single Bifunctional Enzyme, Pild, Catalyzes Cleavage and N-Methylation of Proteins Belonging to the Type IV Pilin Family. *Proc. Natl. Acad. Sci. U.S.A.* 90, 2404–2408. doi: 10.1073/pnas.90.6.2404
- Takhar, H. K., Kemp, K., Kim, M., Howell, P. L., and Burrows, L. L. (2013). The Platform Protein Is Essential for Type IV Pilus Biogenesis. *J. Biol. Chem.* 288, 9721–9728. doi: 10.1074/jbc.M113.453506
- Treuner-Lange, A., Chang, Y. W., Glatzer, T., Herfurth, M., Lindow, S., Chreifi, G., et al. (2020). PilY1 and Minor Pilins Form a Complex Priming the Type IVa Pilus In *Myxococcus Xanthus*. *Nat. Commun.* 11(1), 5054. doi: 10.1038/s41467-020-18803-z
- von Wintersdorff, C. J., Penders, J., van Niekerk, J. M., Mills, N. D., Majumder, S., van Alphen, L. B., et al. (2016). Dissemination of Antimicrobial Resistance in Microbial Ecosystems through Horizontal Gene Transfer. *Front. Microbiol.* 7, 173. doi: 10.3389/fmicb.2016.00173
- Vos, M., Hesselman, M. C., Te Beek, T. A., van Passel, M. W. J., and Eyre-Walker, A. (2015). Rates of Lateral Gene Transfer in Prokaryotes: High but Why? *Trends Microbiol.* 23, 598–605. doi: 10.1016/j.tim.2015.07.006
- Wells, J. N., Bergendahl, L. T., and Marsh, J. A. (2016). Operon Gene Order Is Optimized for Ordered Protein Complex Assembly. *Cell Rep.* 14(4), 679–685. doi: 10.1016/j.celrep.2015.12.085
- Winther-Larsen, H. C., Wolfgang, M., Dunham, S., van Putten, J. P., Dorward, D., Lovold, C., et al. (2005). A Conserved Set of Pilin-Like Molecules Controls Type IV Pilus Dynamics and Organelle-Associated Functions In *Neisseria Gonorrhoeae*. *Mol. Microbiol.* 56, 903–917. doi: 10.1111/j.1365-2958.2005.04591.x
- Yanez, M. E., Korotkov, K. V., Abendroth, J., and Hol, W. G. (2008). The Crystal Structure of a Binary Complex of Two Pseudopilins: Epsi And Epsj From The Type 2 Secretion System of *Vibrio Vulnificus*. *J. Mol. Biol.* 375, 471–486. doi: 10.1016/j.jmb.2007.10.035

Conflict of Interest: The authors declare that the research was conducted in the absence of any commercial or financial relationships that could be construed as a potential conflict of interest.

Publisher's Note: All claims expressed in this article are solely those of the authors and do not necessarily represent those of their affiliated organizations, or those of the publisher, the editors and the reviewers. Any product that may be evaluated in this article, or claim that may be made by its manufacturer, is not guaranteed or endorsed by the publisher.

Copyright © 2021 Oliveira, Aschtgen, van Erp, Henriques-Normark and Muschiol. This is an open-access article distributed under the terms of the Creative Commons Attribution License (CC BY). The use, distribution or reproduction in other forums is permitted, provided the original author(s) and the copyright owner(s) are credited and that the original publication in this journal is cited, in accordance with accepted academic practice. No use, distribution or reproduction is permitted which does not comply with these terms.



Intra-Species Interactions in *Streptococcus pneumoniae* Biofilms

Carina Valente^{1‡}, Ana R. Cruz^{1†‡}, Adriano O. Henriques² and Raquel Sá-Leão^{1*}

¹ Laboratory of Molecular Microbiology of Human Pathogens, Instituto de Tecnologia Química e Biológica António Xavier, Universidade Nova de Lisboa, Oeiras, Portugal, ² Laboratory of Microbial Development, Instituto de Tecnologia Química e Biológica António Xavier, Oeiras, Portugal

OPEN ACCESS

Edited by:

Guangchun Bai,
Albany Medical College, United States

Reviewed by:

Muhammad Ammar Zafar,
Wake Forest School of Medicine,
United States

Masaya Yamaguchi,
Osaka University, Japan
Lance Edward Keller,
University of Mississippi Medical
Center, United States

*Correspondence:

Raquel Sá-Leão
rsaleao@itqb.unl.pt

†Present address:

Ana R. Cruz Laboratory of Host-
Microbiota Interaction, Institut Necker
Enfants Malades, Paris, France

‡These authors have contributed
equally to this work and
share first authorship

Specialty section:

This article was submitted to
Molecular Bacterial Pathogenesis,
a section of the journal
Frontiers in Cellular and
Infection Microbiology

Received: 27 October 2021

Accepted: 14 December 2021

Published: 05 January 2022

Citation:

Valente C, Cruz AR, Henriques AO and
Sá-Leão R (2022) Intra-Species
Interactions in *Streptococcus*
pneumoniae Biofilms.
Front. Cell. Infect. Microbiol. 11:803286.
doi: 10.3389/fcimb.2021.803286

Streptococcus pneumoniae is a human pathogen responsible for high morbidity and mortality worldwide. Disease is incidental and is preceded by asymptomatic nasopharyngeal colonization in the form of biofilms. Simultaneous colonization by multiple pneumococcal strains is frequent but remains poorly characterized. Previous studies, using mostly laboratory strains, showed that pneumococcal strains can reciprocally affect each other's colonization ability. Here, we aimed at developing a strategy to investigate pneumococcal intra-species interactions occurring in biofilms. A 72h abiotic biofilm model mimicking long-term colonization was applied to study eight pneumococcal strains encompassing 6 capsular types and 7 multilocus sequence types. Strains were labeled with GFP or RFP, generating two fluorescent variants for each. Intra-species interactions were evaluated in dual-strain biofilms (1:1 ratio) using flow cytometry. Confocal microscopy was used to image representative biofilms. Twenty-eight dual-strain combinations were tested. Interactions of commensalism, competition, amensalism and neutralism were identified. The outcome of an interaction was independent of the capsular and sequence type of the strains involved. Confocal imaging of biofilms confirmed the positive, negative and neutral effects that pneumococci can exert on each other. In conclusion, we developed an experimental approach that successfully discriminates pneumococcal strains growing in mixed biofilms, which enables the identification of intra-species interactions. Several types of interactions occur among pneumococci. These observations are a starting point to study the mechanisms underlying those interactions.

Keywords: biofilms, co-colonization, colonization, multiple carriage, competition, intraspecies interactions, *Streptococcus pneumoniae*

INTRODUCTION

Streptococcus pneumoniae is an important bacterial pathogen associated with high morbidity and mortality worldwide (GBD, 2018). Nevertheless, disease is a rare event compared with the frequency of asymptomatic nasopharyngeal colonization (Weiser et al., 2018).

Nasopharyngeal colonization is particularly frequent in young children (Gray et al., 1980), where multiple pneumococcal strains can simultaneously colonize the same host, a phenomenon known as multiple serotype carriage or co-colonization (Turner et al., 2011; Valente et al., 2012; Wyllie et al.,

2014; Kamng'ona et al., 2015; Kandasamy et al., 2015; Valente et al., 2016b). Co-colonization is frequent, reaching up to 40% or 50%, depending on the geographical setting and the methodology used for its detection (Turner et al., 2011; Valente et al., 2012; Wyllie et al., 2014; Kamng'ona et al., 2015; Kandasamy et al., 2015; Valente et al., 2016b).

During colonization, pneumococci form biofilms that confer protection from the host and enable horizontal gene transfer, the main evolutionary mechanism of this species (Barnes et al., 1995; Hiller et al., 2010; Wei and Havarstein, 2012).

Several lines of evidence indicate that intra-species competition (*i.e.*, competition between pneumococcal strains) occurs during co-colonization and has a determinant role in shaping its epidemiology and population structure. For example, the dominance of a limited subset of capsular types (typically 5–6 types) in carriage, when several are known to circulate in a population, is a clear indication that strains have different competitive abilities to colonize (Hausdorff et al., 2005). Introduction of pneumococcal conjugate vaccines worldwide also indicates that, following serotype replacement, the population structure of pneumococci is reshaped due to expansion of a limited number of non-vaccine types in carriage and disease (Moore et al., 2015; Waight et al., 2015; Azarian et al., 2020). In addition, using a mouse model of colonization, Lipsitch and co-workers showed that the presence of a resident pneumococcal strain could affect colonization by a second (challenger) strain (Lipsitch et al., 2000).

The mechanisms mediating pneumococcal intra-species competition have been addressed in a few subsequent studies. Trzciński et al. tested clinical isolates and isogenic variants of six capsular types in a mouse model of multiple-serotype carriage and observed that the competitive ability of a strain to colonize depends strongly, but not exclusively, on the composition of its polysaccharide capsule (Trzciński et al., 2015). Apart from the capsule, the *blp* (bacteriocin-like peptide) locus and the competence system were also implicated in competitive interactions. Dawid et al., used a 19A clinical isolate and its *blp* bacteriocin deleted derivative, to demonstrate that the *blp* locus promotes intra-species competition, both *in vitro* (using overlay assays) and *in vivo* (using a murine model of colonization) (Dawid et al., 2007). In a follow-up study, Wholey et al. observed a cross-stimulation between the *blp* and competence systems with implications for intra-species interactions (Wholey et al., 2016). Moreover, in dual-strain biofilms, bacteriocin producing pneumococci, not only had a competitive advantage over non-producers, but also increased DNA exchange through natural transformation (Wholey et al., 2016). Using an infant mouse model of colonization, Shen et al. showed that the competitive advantage of a resident strain is quorum sensing-dependent and is mediated by the late-competence activated fratricide effectors CbpD and CibAB (Shen et al., 2019). Finally, Wu et al. tested three clinical isolates, of serotypes 6B, 19F and 23F, in an eight-hour dual-strain biofilm model and showed that strain 19F was outcompeted by strains 6B and 23F through a contact-dependent unknown mechanism (Wu et al., 2017).

While other types of interactions, beyond competition, are theoretically possible among pneumococci, they have remained

mostly undescribed. One exception are the studies of Trzciński et al. and Wu et al., who described strain combinations where co-existence was observed suggesting a neutral interaction (Trzciński et al., 2015; Wu et al., 2017). In addition, while using isogenic laboratory strains (D39 wt and D39 *pspA/pspC* null mutant) to study natural transformation in multi-strain biofilms, Marks and co-authors found that mixed populations of pneumococci may increase the adaptive potential of less fit strains (Marks et al., 2012), suggesting that commensalism may occur between pneumococci.

Despite significant advances on the study of pneumococcal co-colonization during the last two decades, progress has been hampered by methodological constraints associated with the need to quantitatively distinguish cells of different strains when in mixed-strain experimental conditions. While it is recognized that there is significant within strain genetic diversity in pneumococci, the number of strains being used in such studies has been limited and has mainly relied on the use of laboratory strains and its derivatives.

In this study, we developed a strategy to study pneumococci in multi-strain biofilms and applied it to a diverse set of strains which included natural isolates obtained from samples collected from colonized human subjects. We show that various types of intra-species interactions, including commensalism, do occur and can be quantitatively characterized.

MATERIALS AND METHODS

Study Collection

The study collection consisted of 12 strains previously isolated from nasopharyngeal samples of healthy children in which co-colonization was detected (Sá-Leão et al., 2009; Valente et al., 2012; Nunes et al., 2016; Valente et al., 2016a; Valente et al., 2016b; Félix et al., 2021) and two laboratory strains, D39 and TIGR4, commonly used in pneumococcal studies worldwide. Epidemiological relevance of selected strains and their serotypes and genotypes are indicated in **Tables 1, 2**. Four strains were non-encapsulated and were designated as non-typable (NT).

Fluorescent Labelling of *S. pneumoniae* Strains

Each strain was labelled with GFP or RFP generating two fluorescently labelled strains. Constructs *P_{hlpA}-hlpA-gfp-Cam^r* (for GFP-labelling) and *P_{hlpA}-hlpA-hlpA-rfp-Cam^r* (for RFP-labelling), kindly provided by Jan-Willem Veening, were used (Kjos et al., 2015). These constructs bear a translational fusion of the histone-like protein A gene (*hlpA*) to GFP or RFP, where the fusion proteins are produced under the control of the *hlpA* promoter; the constructs also carry a transcriptional fusion to a chloramphenicol resistance gene. Constructs were first integrated by allelic replacement in the genome of *S. pneumoniae* D39 (laboratory strain) generating strains D39_GFP and D39_RFP. DNA was extracted from either D39_GFP or D39_RFP and

TABLE 1 | Rationale for selection of *S. pneumoniae* strains based on epidemiological relevance.

Serotype	PCV13 serotype	Observations	References
3	Yes	High invasive disease potential Increasing in PCV13 era	(Sá-Leão et al., 2011; Horácio et al., 2016)
15A	No	Increasing in carriage in PCV13 era	(Félix et al., 2021)
19A	Yes	Highly prevalent in carriage and disease before the introduction of PCV13	(Isturiz et al., 2017)
19F	Yes	Remains in carriage in PCV13 era	(Nunes et al., 2016; Félix et al., 2021)
22F; 33F	No	Increasing in carriage in PCV13 era Important cause of invasive pneumococcal disease Targeted by upcoming PCV15 and PCV20 vaccines	(Moore et al., 2015; Félix et al., 2021)
NT	No	Non-encapsulated Very frequent in colonization Frequently detected in co-colonization Associated with multidrug resistance Associated to conjunctivitis outbreaks	(Marks et al., 2012; Valentino et al., 2014; Valente et al., 2016b)

PCV13, PCV15 and PCV20 correspond to 13-valent, 15-valent and 20-valent pneumococcal conjugate vaccines. NT - non-typeable.

amplified by PCR using primers previously described (Kjos et al., 2015). PCR products were purified with Exo-SAP and used for transformation of other strains.

Two transformation protocols, in liquid medium and in biofilms, were used. For transformation in liquid medium cells were grown in C+Y (pH 7.4) (Junges et al., 2017) to an optical density of 0.5 at 600nm (OD₆₀₀), diluted at a 1:100 ratio and grown until an OD_{600nm} of 0.1 was reached; at this time, 100ng/mL of CSP1 (NH₂-EMRLSKFFRDFILQRKK-COOH) or CSP2 (NH₂-EMRISRIILDFLRLKK-COOH) (Mimotopes, Australia) and 400ng/mL of DNA were added. The mixture was incubated for 3h at 37°C.

For clinical isolates which did not yield transformants using the conditions described above, transformation in biofilms was attempted. Cells were grown in C+Y (pH 7.4) (Junges et al., 2017) to an OD₆₀₀ of 0.5, diluted at a 1:100 ratio, grown until an OD₆₀₀ of 0.2 and transferred to 24-well plates (Costar, Corning), in a final volume of 2mL per well. Plates were incubated for 4h at 34°C in a 5% CO₂ atmosphere to promote biofilm formation (Wei and Havarstein, 2012). The supernatant was carefully aspirated to remove planktonic bacteria and replaced with 2mL of fresh medium supplemented with 0.5µg/mL of DNA and the

appropriate CSP at a final concentration of either 100ng/mL or 1000ng/mL.

In both protocols transformants were selected on TSA blood plates supplemented with 4µg/mL chloramphenicol. For selected clones, the presence of the fusion constructs at the *hlpA* locus was first verified by PCR.

Fluorescence Microscopy

For selected clones resulting from the integration of the *P_{hlpA}-hlpA-gfp* or *P_{hlpA}-hlpA-hlpA-rfp* fusions, production of GFP or RFP was assessed by fluorescence microscopy. Two mL of exponential phase culture were centrifuged at 5900g for 10min and pellets were resuspended in PBS. Cell suspensions were mounted on a slide covered with a thin layer of 1.7% agarose. Images were acquired on a Leica DM 6000B fluorescence microscope controlled by MetaMorph V5.8 software through a 100X 1.4 NA oil immersion objective and captured with an Andor iXon 885 EMCCD camera. Filters for image acquisition were set for contrast phase optics, TX2 (excitation: 560/40nm; emission: 645/75nm), and FITC (excitation: 480/40nm; emission: 527/30nm). Exposure times were 50ms for contrast phase, 3000ms for TX2, and 500ms for FITC.

TABLE 2 | Bacterial strains initially chosen for the study of intra-species interactions.

Strain	Serotype	MLST ¹	Observation ²	Reference
D39	2	595	selected	(Avery et al., 1944)
TIGR4	4	205	selected	(Tettelin et al., 2001)
2099	3	260	–	(Nunes et al., 2016)
7632	15A	8322	selected	(Nunes et al., 2016)
5262.1	19A	276	–	(Sá-Leão et al., 2009)
5902	19A	63	–	(Simões et al., 2011)
1990	19F	177	selected	(Nunes et al., 2016)
5756	22F	433	selected	(Sá-Leão et al., 2009)
8046	22F	9161	–	(Nunes et al., 2016)
8276	33F	717	–	(Félix et al., 2021)
5262.2	NT	344	–	(Sá-Leão et al., 2009)
5435	NT	344	selected	(Sá-Leão et al., 2009)
7031	NT	344	selected	(Nunes et al., 2016)
6209	NT	4583	selected	(Simões et al., 2011)

MLST, multilocus sequence typing; NT, non-typeable (non-encapsulated). ¹STs mainly associated with colonization isolates (www.pubmlst.org).

²Strains tested in dual-strain biofilms are indicated as “selected”. Other strains did not meet one or more validation criteria and were excluded.

Biofilm Growth Medium for the Study of Intra-Species Interactions

Strains were grown in a modified version of the chemically defined medium described by van de Rijn and Kessler, herein named mCDM, in which the final concentration of cysteine-HCl was increased to 0.8mg/mL (instead of 0.5mg/mL), choline chloride was added at a final concentration of 1mg/mL, except when otherwise indicated. The carbon source was galactose (10mg/mL) instead of glucose (the complete recipe of mCDM is given in **Table S1**). Cysteine promotes faster bacterial growth as it can act as a radical scavenger and as an additional amino-acid source. Choline is a nutritional requirement for pneumococcal growth and was added at a concentration of 1mg/mL to promote better growth (Rane and Subbarow, 1940; Tomasz, 1967). Galactose was chosen as it is the most abundant sugar in the human nasopharynx (Blanchette et al., 2016). All experiments were carried out in 24-well plates (Costar, Corning) and the cultures incubated at 34°C (Keck et al., 2000) in a 5% CO₂-enriched atmosphere.

In Vitro Biofilm Model

An in-house developed abiotic biofilm model mimicking long term-colonization was used. Strains were first grown in mCDM in planktonic growth conditions until mid-exponential phase. A 1:500 dilution of each strain of interest, corresponding to 10⁵ cells in 2.5mL of mCDM, was transferred to 24-well plates and incubated at 34°C in 5% CO₂ for 72 hours. At 24h and 48h, 2.0mL of spent medium were carefully removed and 2.0mL of pre-warmed fresh medium was added avoiding disturbance of the biofilm attached to the bottom of the well. At 72h, biofilms were resuspended in 300μL of PBS and either serially diluted for colony forming units (CFU) counts or sonicated to separate aggregates prior to flow cytometry analysis (described below). Sonication was done in a Bioruptor UCD-300 apparatus with an ultrasonic wave frequency of 20KHz (12 cycles of 10s at high intensity with 30s break between pulses).

Single-Strain and Dual-Strain Biofilm

To evaluate interactions between strains, dual-strain biofilms were grown in a 1:1 ratio in the conditions described above. To allow for strain discrimination, dual-strain biofilm experiments used one GFP-labelled strain and one RFP-labelled strain. As a control, each pair of strains was also tested with the reverse fluorescent markers. For comparative analysis, single-strain biofilms of the same strain variants were obtained in parallel. For all experiments three biological replicates were done and each included three technical replicates.

Flow Cytometry for Assessment of Cell Counts and Cell Density in Single-Strain and Dual-Strain Biofilm

Cell counts of single- and dual-strain biofilms were obtained by flow cytometry as a proxy for cell viability. Biofilms disrupted by sonication (see above) were diluted in an appropriate volume of PBS to achieve a rate of 500 events/s. Cell counts were obtained in a Bio-Rad S3e Cell Sorter controlled by the ProSort software v1.6 using the following parameters: nozzle size of 100microns,

lasers of 488nm and 561nm, and filters FL1 (525/30nm) and FL3 (615/25nm) for data collection of GFP- and RFP-labelled cells, respectively. Flow cytometry conditions were set as: FSC 311V, SSC 240V, FL1 811V and FL3 335V. As the detection limit of the Bio-Rad S3e Cell Sorter is above the expression levels of RFP-labelled cells, these were detected as non-labelled in the FL1 filter.

For each pair of strains tested in dual-strain biofilm, the corresponding single-strain biofilms were first analyzed. Cells in single biofilms were counted (about 30000 events). Cells of the RFP-labelled strain were used to establish a “red region” in the FL1 Area log plot. Similarly, cells of the GFP-labelled strain were used to establish a “green region” in the same FL1 Area log plot. Potential overlap between these two regions was investigated and, when occurring, the relative proportion of GFP-labelled cells present in the “red region” was determined. For dual-strain biofilms, the relative proportion of the RFP-labelled and GFP-labelled strains was estimated by counting 30000 events and determining how many occurred in the red or green regions. When appropriate, a correction (based on the single-strain biofilm results) was applied. Finally, to estimate the cell density for each strain in single and dual-strain biofilms, total cell counts in 50μL were obtained.

Identification of Intra-Species Interactions

To investigate whether intra-species interactions occurred in the dual-strain biofilm experiments results obtained for a given pair of strains were combined in order to increase statistical power. For each strain, total cell counts obtained in single-strain biofilms (GFP- plus RFP-labelled variant cells) were compared to the total cell counts obtained for that strain in dual-strain biofilms. Interactions were considered to occur when statistically significant differences were observed ($p < 0.05$). Upon detection of an interaction, a ratio between the geometric means of cell counts in dual- and single-strain biofilms was calculated. Negative interactions were defined by ratios < 1 and positive interactions were defined by ratios > 1 .

Confocal Microscopy for Biofilm Imaging

Biofilms were grown in 24-well microscope slides suitable for confocal microscopy (IBIDI, Germany) as described above. Z-sections were acquired at 0.81μm intervals on a Zeiss LSM 880 point scanning confocal microscope using the Airyscan detector, a 20x plan-apochromat 0.8 NA objective (Zeiss) and the 488nm and 561nm laser lines. The Zeiss Zen 3.0 (black edition) software was used to control the microscope, adjust spectral detection for the emission of GFP and RFP and to process the Airyscan raw images.

Colorimetric Quantification of Biofilm Biomass Through Crystal Violet Staining

Single- and dual-strain biofilms were grown for 72h as described. At hour 72, supernatants were removed and biofilms were imaged before and after crystal violet staining. For staining, 50μL of crystal violet (CV, 1% w/v) were added to each well and incubated at room temperature for 30 min. CV was removed by inversion, the plates were allowed to air-dry for 10 min and the biofilms were washed twice with 500μL of PBS. Biofilms were

imaged on a Zeiss Axio Zoom.V16 stereo microscope equipped with a Zeiss Axiocam 503 mono CCD camera and controlled with the Zen 2.1 software (blue edition), using the 1X 0.25NA objective and bright field optics. CV was solubilized by addition of 1mL of 95% ethanol and incubation with agitation until no stained culture was observed at the bottom of the well. Absorbance at 595nm was measured with a Tecan Infinite F200 plate reader. Absorbance was measured for three biofilms per strain or combination of strains.

Statistical Analysis

GraphPad Prism 7.0 (GraphPad Software Inc., La Jolla, California, USA) was used for all statistical analyses. The Kruskal-Wallis test corrected for FDR with the Benjamini and Hochberg method was used for comparisons between three groups. The Mann-Whitney U test was used for comparisons between two groups. The Mann-Whitney U test corrected for FDR with the Benjamini and Hochberg method was used for the remaining comparisons.

RESULTS

Fluorescence Labelling of Epidemiologically Relevant *S. pneumoniae* Strains

We were able to successfully obtain GFP- and RFP-labelled variants of 14 pneumococcal strains of nine serotypes (serotypes 2, 3, 4, 15A, 19A, 19F, 22F, 33F, and NT) and 12 genetic backgrounds (STs 63, 177, 205, 260, 276, 344, 433, 595, 717, 4583, 8322, and 9161) (Table S2). Fluorescence microscopy allowed confirmation of GFP or RFP expression in all cells of the population for each fluorescent variant (Figures 1A, S1). The exceptions to this scenario were the RFP-labelled variant of strain 5262.1-19A and the GFP-labelled variant of strain 2099-3 in which fluorescence was noted in a small fraction of the population only (Figure S1, see, for example, cells marked with arrow).

We were unable, however, to transform eight other strains initially selected to be included in the study. These strains had the serotype-ST combinations 1-228, 11A-408, 15A-63, 19F-309, 33F-717, 35B-198, NT-3097, and NT-6996. Transformation of these strains was attempted multiple times using planktonic and biofilm conditions. Possibly, the laboratory conditions may have been inadequate to induce competence in these strains or the strains might have defects in genes essential for competence (Lee and Morrison, 1999; Croucher et al., 2011). Other studies have also reported difficulties in transforming non-laboratory strains (Joloba et al., 2010; Evans and Rozen, 2013).

Cell Viability and Population Homogeneity of *S. pneumoniae* GFP- and RFP-Labelled Variants

In preparation for dual-strain biofilm experiments mixing GFP- and RFP-labelled strains, we investigated, for each labelled variant, the cell viability and the homogeneity of the fluorescence signal in 72h biofilms.

Single strain biofilms were prepared and cell viability (CFU/mL) of the WT (unlabelled) strain and the corresponding GFP- or RFP-labelled variants was compared. Strains displayed different abilities to grow in biofilm, with mean CFU counts at 72h ranging between 10^5 and 10^{11} CFU/mL ($p < 0.001$, Kruskal-Wallis test with Benjamini and Hochberg correction for False Discovery Rate). For most triplets (9 of 14) no significant differences were observed (Figures 1B, S1). One triplet (corresponding to WT strain 5756) showed significant differences in the viability of labelled variants (GFP vs RFP), but no significant differences between each variant and the WT (Figure 1B). The other four triplets (corresponding to WT strains 2099, 5262.2, 5902, and 8046) showed significant differences in cell viability (in at least one variant when compared to the WT strain) and were excluded from further analyses (Figure S1).

We then wanted to identify GFP and RFP variants yielding homogenous (narrow single peaks) and non-overlapping profiles, an essential requirement to enable cell counts of two populations of the same species by flow cytometry. With that in mind, the distribution of the fluorescence signal in the population was investigated by flow cytometry, for each strain variant (GFP or RFP), after growth of single-strain biofilms. For most variants, biofilm cells produced a homogenous signal (Figures 1C, S1). For two strains (5262.1 and 8276), however, high heterogeneity was observed for both the GFP and RFP signals (Figure S1). As this would compromise the capacity to distinguish mixed GFP- and RFP-producing cultures, these variants were excluded.

In summary, we selected GFP- and RFP- variants of eight strains to be used in dual-strain biofilm experiments.

Dual-Strain Biofilm Experiments

The eight strains remaining in the study were grown in dual-strain biofilms in which one strain was labelled with GFP and the other with RFP (for example, strain A-GFP was grown together with strain B-RFP), for a total of 28 combinations. As controls, the reverse labelling combination was also tested in a dual-strain biofilm (A-RFP together with B-GFP), and single-strain biofilms of all variants were also examined (A-GFP, A-RFP, B-GFP, and B-RFP) (Figure 2). In all cases, cell counts for each strain were measured at 72h by flow cytometry.

For most combinations (21 out of 28), no significant differences in cell counts were observed when the isogenic GFP- and RFP-variants of a given strain were compared in the same experimental condition (Figures S2A–D). In seven combinations significant variations were observed in at least one comparison, in which case the assays were excluded from further analyses (Figure S2E).

In total, twenty-one combinations of dual-strain biofilms were validated for the investigation of intra-species interactions. These included strains of serotypes 2, 4, 15A, 19F, 22F, and NT of six distinct MLST profiles (Table 2 and Figure S2).

Identification of Intra-Species Interactions

To identify intra-species interactions, cell counts of each strain grown in dual-strain biofilm were compared to those obtained in a single-strain biofilm experiment run in parallel. Among the 21

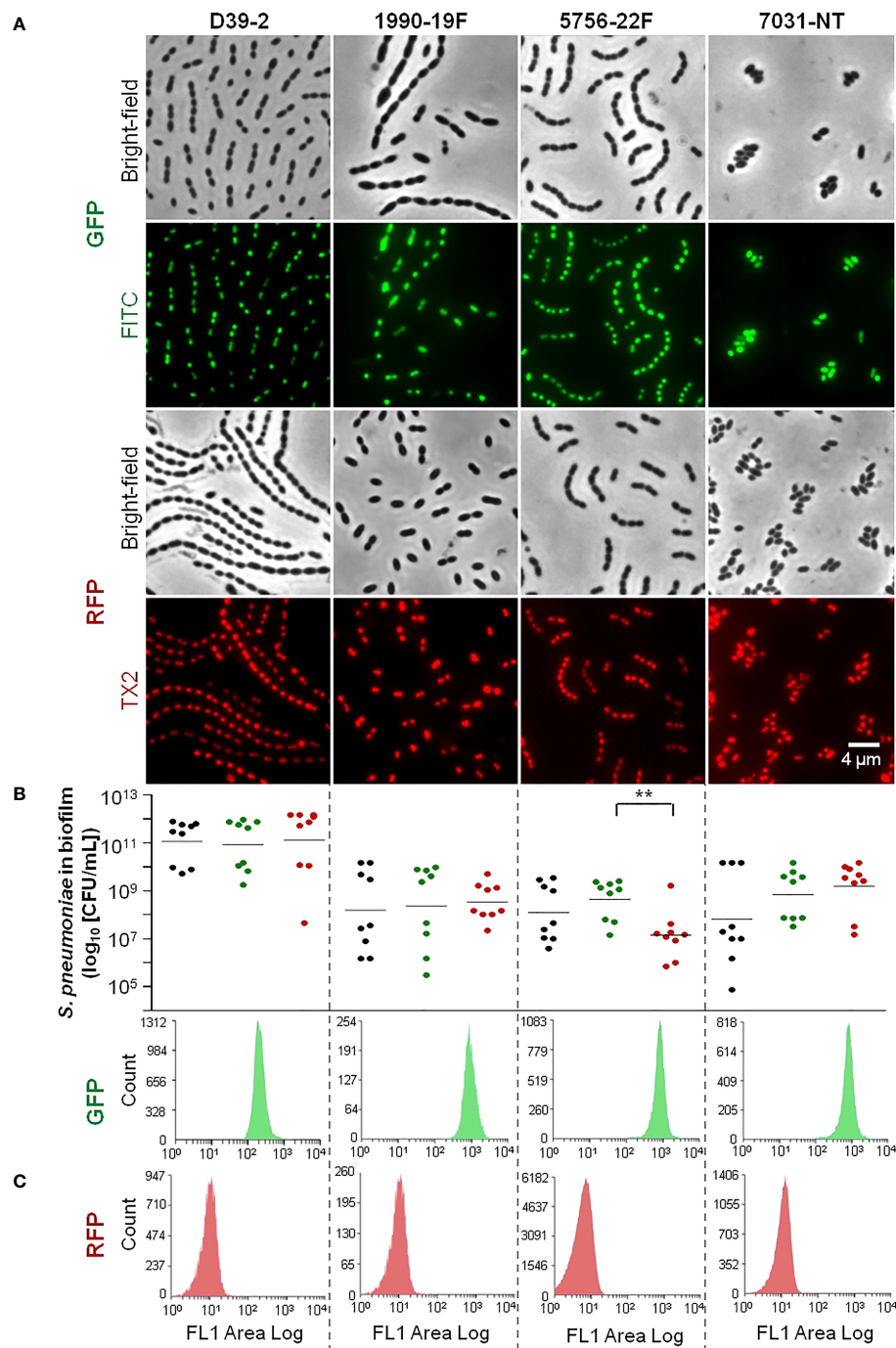
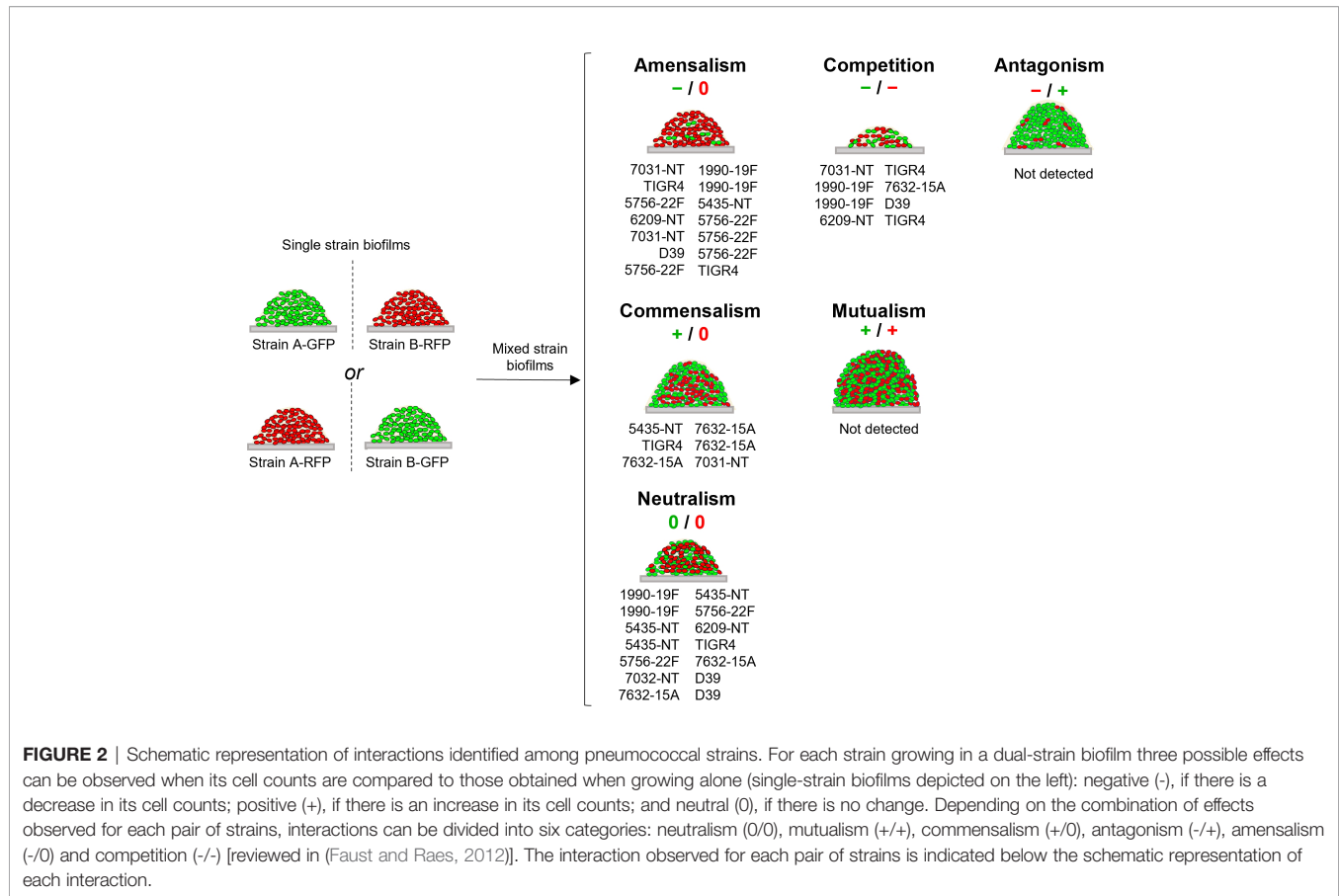


FIGURE 1 | Representative fluorescently labelled strains used in the study (remaining strains are shown in **Figure S1**). Strains' reference and serotype are indicated on top of panel **(A)**. **(A)** Imaging of GFP and RFP-labelled strains by fluorescence microscopy. GFP- and RFP-labelled strains were grown until exponential phase and imaged by fluorescence microscopy with filters for contrast phase optics, FITC and TX2. **(B)** Viability of wild-type and fluorescently labelled variants in the biofilm model. Each WT strain and its correspondent GFP- and RFP-labelled variants were grown under biofilm-promoting conditions (see the *Materials and Methods* section), after which viability (CFU/mL) was determined. Black, green and red dots indicate WT, GFP- and RFP-labelled cells, respectively. three independent experiments, each with an intra-experiment triplicate. ****** $p < 0.01$ (Kruskal Wallis test with Benjamini and Hochberg correction for FDR). **(C)** Flow cytometry analysis of fluorescent variants in biofilm model. Biofilm formation was induced as described in **(B)**. After 72h biofilms were resuspended and sonicated and cell counts were obtained by flow cytometry. Representative histograms are shown.



combinations of dual-strain biofilms tested, interactions of commensalism (n=3), competition (n=4), amensalism (n=7) and neutralism (n=7) were detected (Table 3 and Figure 2, S2).

Importantly, we found that the outcome of an interaction is independent of the capsular and sequence types of the strains involved. An example that illustrates this observation is the interaction of strain 7632-15A (ST8322) with strains 5435-NT and 7031-NT (both ST344). In the first case (7632-15A and 5435-NT) the NT strain is benefited by the presence of the 15A strain, whereas in the second case (7632-15A and 7031-NT) it is the 15A strain that is benefited by the presence of the NT strain.

Imaging of Intra-Species Interactions Occurring in Dual-Strain Biofilms

Dual-strain biofilms representative of interactions of commensalism, competition, and amensalism were selected for confocal microscopy. Imaging of single- and dual-strain biofilms produced by strains 5435-NT and 7632-15A confirmed the commensality identified between these two strains by flow cytometry (Figure 3A). In particular, we confirmed that strain 5435-NT increased in biofilm depth (z-axis, proxy to biofilm biomass) when in co-culture with strain 7632-15A (Figure 3A and Table S3).

Similarly, the competitive interaction observed by flow cytometry for strains 7031-NT and TIGR4 was also detected in the confocal microscopy images (Figure 3B). A decrease in

biofilm depth was noted for both strains when grown in dual-strain biofilms as compared to their growth in single-strain biofilm (Figure 3B and Table S3).

Finally, the amensalism identified between strains 1990-19F and 7031-NT by flow cytometry (Figure 3C) was also observed by confocal microscopy imaging of these two strains when grown in single- and dual-strain biofilms. The significant decrease in cell counts (quantified by flow cytometry) of strain 7031-NT when growing in the presence of strain 1990-19F, translated into a major reduction of the biofilm produced by this strain when in co-culture with the 19F strain. In fact, the total biofilm biomass of the dual-strain biofilms of this pair was found to be mostly attributable to the growth of the 19F strain (Figure 3C and Table S3).

The same representative pairs were also imaged before and after crystal violet staining (Figure S3A) and the total biofilm biomass was quantified (Figure S3B). The biomass quantified following crystal violet staining correlated with the biomass results obtained using CLSM.

Imaging of Intra-Species Interactions Occurring in Dual-Strain Biofilms Grown in Different Concentrations of Choline

To rule out possible effects of the choline concentration used in our mCDM (1mg/mL) on the activity of choline-binding proteins – important for pneumococcal growth in biofilm and

TABLE 3 | Dual-strain combinations tested for intra-species interactions.

Strains tested	Cell counts in dual biofilm ^a (GM dual)	Cell counts in single biofilm ^a (GM single)	GM dual ^b	Net result ^c	Type of interaction
			GM single		
5435-NT and 7632-15A					
5435-NT	5.37x10 ⁷	4.28x10 ⁵	1.25x10 ²	↑	Commensalism
7632-15A	2.05x10 ⁸	8.10x10 ⁸	Ns	=	
7632-15A and TIGR4					
7632-15A	4.44x10 ⁶	7.26x10 ⁶	Ns	=	“
TIGR4	9.54x10 ⁵	2.06x10 ⁵	4.64x10 ⁰	↑	
7031-NT and 7632-15A					
7031-NT	1.13x10 ⁷	1.86x10 ⁵	ns	=	“
7632-15A	2.97x10 ⁸	1.07x10 ⁸	2.77x10 ⁰	↑	
7031-NT and TIGR4					
7031-NT	3.08x10 ⁴	1.03x10 ⁶	3.00x10 ⁻²	↓	Competition
TIGR4	5.51x10 ⁴	2.73x10 ⁵	2.02x10 ⁻¹	↓	
1990-19F and 7632-15A					
1990-19F	6.87x10 ⁴	1.12x10 ⁶	6.12x10 ⁻²	↓	“
7632-15A	2.84x10 ⁶	7.00x10 ⁶	4.06x10 ⁻¹	↓	
1990-19F and D39					
1990-19F	2.92x10 ⁵	1.21x10 ⁶	2.41x10 ⁻¹	↓	“
D39	1.83x10 ⁴	2.53x10 ⁵	7.22x10 ⁻²	↓	
6209-NT and TIGR4					
6209-NT	1.66x10 ⁵	3.46x10 ⁶	4.80x10 ⁻²	↓	“
TIGR4	5.07x10 ⁵	4.49x10 ⁶	1.13x10 ⁻¹	↓	
1990-19F and 7031-NT					
1990-19F	2.23x10 ⁶	2.29x10 ⁶	ns	=	Amensalism
7031-NT	1.18x10 ⁴	2.66x10 ⁷	4.44x10 ⁻⁴	↓	
1990-19F and TIGR4					
1990-19F	1.24x10 ⁵	2.98x10 ⁵	ns	=	“
TIGR4	1.99x10 ⁴	2.10x10 ⁵	9.47x10 ⁻²	↓	
5435-NT and 5756-22F					
5435-NT	7.05x10 ⁶	8.23x10 ⁶	ns	=	“
5756-22F	4.68x10 ⁷	8.94x10 ⁷	5.23x10 ⁻¹	↓	
5756-22F and 6209-NT					
5756-22F	1.46x10 ⁷	2.03x10 ⁷	ns	=	“
6209-NT	1.39x10 ⁶	4.78x10 ⁶	2.92x10 ⁻¹	↓	
5756-22F and 7031-NT					
5756-22F	1.84x10 ⁷	1.25x10 ⁷	ns	=	“
7031-NT	1.56x10 ⁶	1.30x10 ⁷	1.20x10 ⁻¹	↓	
5756-22F and D39					
5756-22F	5.46x10 ⁵	9.62x10 ⁵	ns	=	“
D39	4.61x10 ⁵	1.07x10 ⁶	4.31x10 ⁻¹	↓	
5756-22F and TIGR4					
5756-22F	3.60x10 ⁴	1.44x10 ⁶	2.49x10 ⁻²	↓	“
TIGR4	1.57x10 ⁵	2.28x10 ⁵	ns	=	
1990-19F and 5435-NT					
1990-19F	2.49x10 ⁵	5.77x10 ⁵	ns	=	Neutralism
5435-NT	8.41x10 ⁴	9.92x10 ⁴	ns	=	
1990-19F and 5756-22F					
1990-19F	7.80x10 ⁵	1.77x10 ⁶	ns	=	“
5756-22F	4.33x10 ⁵	5.84x10 ⁵	ns	=	
5435-NT and 6209-NT					
5435-NT	1.13x10 ⁵	4.83x10 ⁵	ns	=	“
6209-NT	6.88x10 ⁶	7.96x10 ⁶	ns	=	
5435-NT and TIGR4					
5435-NT	7.62x10 ⁴	1.27x10 ⁵	ns	=	“
TIGR4	7.40x10 ⁴	6.79x10 ⁵	ns	=	
5756-22F and 7632-15A					
5756-22F	4.84x10 ⁶	3.55x10 ⁶	ns	=	“
7632-15A	3.89x10 ⁷	1.74x10 ⁷	ns	=	
7031-NT and D39					
7031-NT	3.57x10 ⁵	2.79x10 ⁶	ns	=	“
D39	7.61x10 ⁵	1.62x10 ⁶	ns	=	

(Continued)

TABLE 3 | Continued

Strains tested	Cell counts in dual biofilm ^a (GM dual)	Cell counts in single biofilm ^a (GM single)	GM dual ^b	Net result ^c	Type of interaction
			GM single		
7632-15A and D39					
7632-15A	2.25x10 ⁶	6.16x10 ⁶	ns	=	“
D39	7.58x10 ⁵	3.05x10 ⁵	ns	=	

^aCell counts, as a proxy of cell viability, were obtained by flow cytometry. Values indicate the geometric mean of 18 biological replicates (nine with GFP-labelling and nine with RFP-labelling) obtained for each strain in each condition (single-strain or dual-strain biofilm). The detailed results obtained for biological replica are presented in **Figure 3** and **Figure S2**.

^bThe ratio between the geometric mean of cell counts of each strain in dual- and single-strain biofilms was calculated as a proxy of the strength of intra-species interaction. Results are only indicated when statistically significant differences were obtained following comparisons of the cell counts in dual- vs single-strain biofilms.

^c↑ strain benefits (i.e., cell counts increase) from growing in the presence of the other strain; ↓ strain is harmed (i.e., cell counts decrease) when growing in the presence of the other strain; = strain is not affected by the presence of the other strain.
ns, not significant.

for fratricide (Moscoso et al., 2006; Perez-Dorado et al., 2010) -, single- and dual-strain biofilms representative of the interactions identified were grown in low (4μg/mL) and high (20mg/mL) concentrations of choline chloride.

At a lower concentration of choline (4μg/mL) there was lower biofilm growth, both in single- and dual-strain biofilms. Still, the interactions previously observed were maintained (**Figure S4**). By contrast, the increase of choline chloride to 20mg/mL severely hampered the ability of strains to grow in biofilm (in agreement with previous studies focusing on the importance of CBPs to biofilm development) (Moscoso et al., 2006). This lack of growth in biofilm prevented us to draw conclusions on the effect of this high concentration of choline in the interactions detected (**Figure S5**). Taken together, the results showed that the concentration of choline chloride used in our mCDM promotes better biofilm growth and has no impact on the interactions observed.

DISCUSSION

Multiple strains of pneumococci often coexist in the upper respiratory tract (Turner et al., 2011; Valente et al., 2012; Kamng'ona et al., 2015; Kandasamy et al., 2015; Valente et al., 2016b). The intra-species interactions resulting from this co-existence, however, have not been actively investigated. We developed a strategy to study such interactions and applied it to a diverse collection of *S. pneumoniae* strains.

We tested eight pneumococcal strains in pairs in a three-day long abiotic biofilm model. We found that, depending on the combination, strains could be positively affected, negatively affected or unaffected by the presence of other strain. Four types of interactions were observed: commensalism (14%), competition (19%), amensalism (33%), and neutralism (33%).

All positive interactions were of commensalism. To the best of our knowledge, this is the first report describing commensalism between naturally-occurring, colonizing strains of *S. pneumoniae*. We observed that strains of diverse backgrounds were positively affected, i.e. produced a better biofilm, in the presence of other strain.

Positive interactions between strains of the same species were identified before (Selak et al., 2016). Selak et al. showed that natural isolates of bifidobacteria obtained from intestinal

biopsies cooperated for the degradation of complex carbohydrates. This resulted in cross-feeding and co-existence of strains with different metabolic profiles enabling colonization of diverse areas of the intestinal lumen (Selak et al., 2016). Since nutrient diffusion within biofilms is diminished (Stewart, 2003), it seems possible that the positive interactions identified in our study result, at least in part, from a mechanism of cross-feeding of metabolic by-products or nutrients resulting from cell lysis. Another possibility is that cooperation is occurring through the production of molecules that enable scavenging of otherwise unavailable nutrients or that degrade specific metabolites. We are conducting additional studies to address these possibilities.

Negative interactions were due to competition or amensalism. Both types of interactions were observed before in pneumococci. Pneumococcal colonization studies in children have repeatedly reported that, at any time, only a few serotypes account for most of the isolates, suggesting strain competition for niche occupancy affecting population structure and epidemiology (Félix et al., 2021). Biofilm studies and experiments with animal models have also unravelled these types of interactions and have explored some of the biological mechanisms governing them (Lipsitch et al., 2000; Dawid et al., 2007; Trzciński et al., 2015; Shen et al., 2019). Examples of such mechanisms include bacteriocin secretion (Dawid et al., 2007; Maricic et al., 2016) and exclusion of a newcomer by a resident strain *via* competence-mediated fratricide (Shen et al., 2019). Mechanisms of passive competition, where one strain is indirectly affected by the presence of another, could also have a role in the negative interactions identified in our study. Differences in colonization ability attributable to the capsular type metabolic cost and associated cell surface charge (Lipsitch et al., 2000; Trzciński et al., 2015), in growth rates, or in tolerance to metabolic products or niche components, for example, could be involved.

Neutral interactions were detected in one third of the combinations tested indicating that either pneumococcal strains frequently co-exist without affecting each other (neutralism), or that those effects could not be detected with the system used. Neutral interactions among bacteria are not frequently described. Nevertheless, a recent study reported dominance of neutral interactions among actinobacteria in the soil ecosystem (Yan et al., 2021), particularly in oligotrophic conditions, i.e., in nutrient poor conditions that resulted from

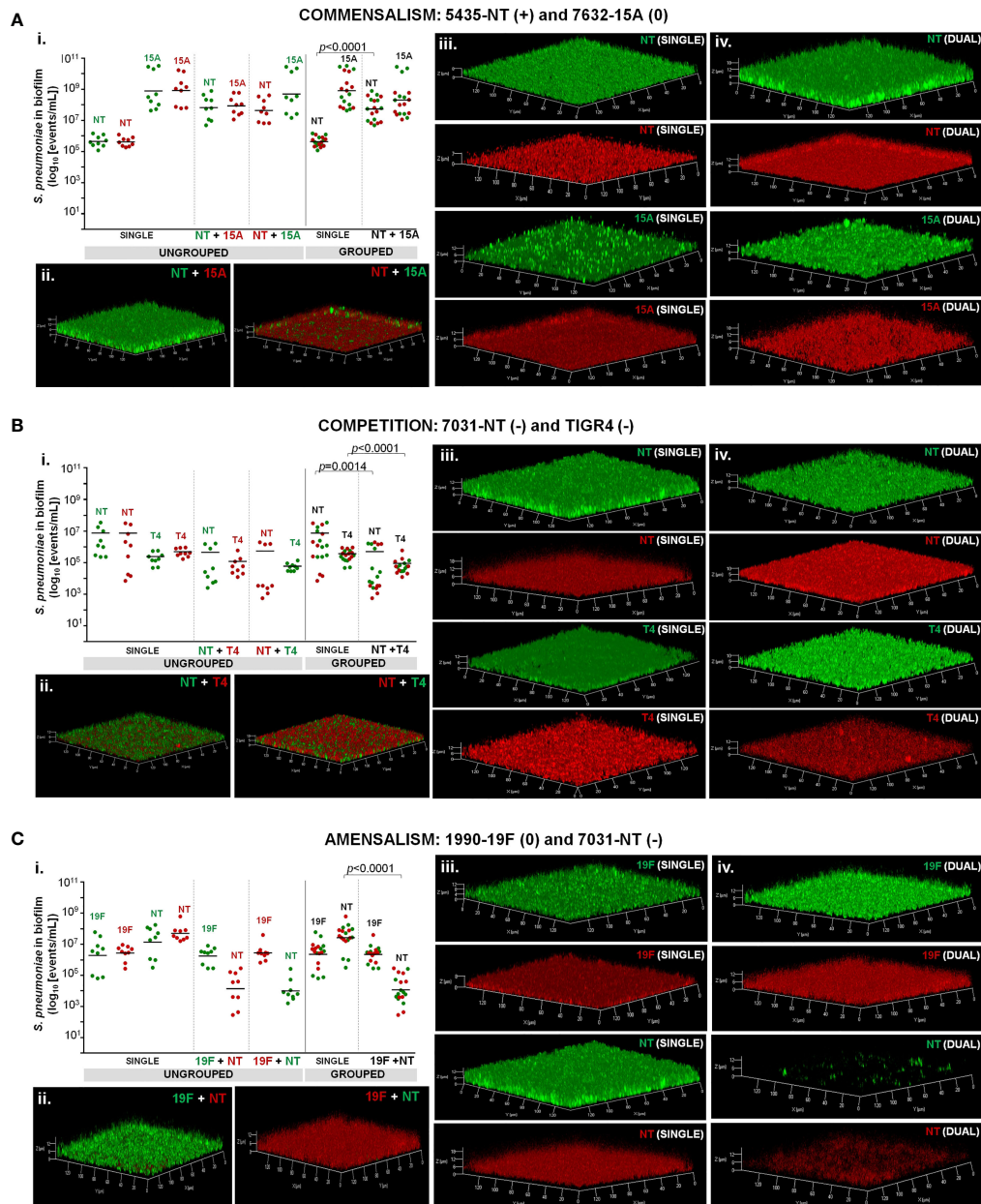


FIGURE 3 | Dual-strain combinations representative of commensalism (A), competition (B), and amensalism (C). Strains were tested in dual-strain biofilms (one GFP- and one RFP-labelled strain) in a 1:1 ratio. Reverse labelling combinations were also tested as controls. For comparative analysis, single-strain biofilms were grown in parallel. Intra-species interactions were considered to occur when statistically significant differences between a given strain in single and dual-strain biofilms were observed ($p < 0.05$), Mann-Whitney U test corrected with Benjamini and Hochberg method for FDR. (i.) Cell counts. Cell counts of strains in single- and dual-strain biofilms were obtained by flow cytometry, events/mL were calculated and compared. For each strain, one out of three possible outcomes was determined when grown in the presence of another: positive (+), if there was a beneficial effect; neutral (0), if there was no effect; and negative (-) if there was harm. Black bars indicate geometric means. Green and red dots correspond to GFP- and RFP-labelled cells, respectively. Graphics represent the ungrouped and grouped analyses for each pair using data from three independent experiments, each with an intra-experiment triplicate. (ii.) Imaging of dual-strain biofilms. (iii.) Imaging of single strain biofilms. (iv.) Single-channel images of dual-strain biofilms. All CLSM images are transparent projections of 3D reconstructions from z-sections acquired at 0.81 μm intervals on a Zeiss LSM 880 point scanning confocal microscope using the Airyscan detector, a 20x plan-apochromat 0.8 NA objective (Zeiss) and the 488 nm and 561 nm laser lines.

metabolic overlap between species. Given the large array of metabolic profiles identified among pneumococcal strains (Watkins et al., 2015), it seems possible that our strains have different nutritional requirements; this possibility, however, was not addressed in the present study. It is also possible that intra-species interactions may occur at a local level, with no impact on the total cells that form the biofilm (Kim et al., 2014). As populations of cells are being studied as a whole, such interactions would also have been missed with our approach.

Our study has some limitations. Firstly, our experimental approach was based on an *in vitro* system that does not take into consideration the effect that host- or microbiota-associated factors might have on pneumococcal intra-species interactions. In addition, our strains were inoculated in equal proportions and at the same time point. These are important limitations as, in natural colonization, pneumococcal strains co-occurring in the same host often are present at different proportions and may have been acquired in different occasions (Valente et al., 2012; Valente et al., 2016b). This approach prevented us from detecting positive or negative interactions that are dependent on relative cell-density and time of strains' exposure. An example where this scenario would be relevant is the competition model proposed by Shen and co-authors, in which earlier activation of the competence regulon, and hence the production of the fratricide effectors CbpD and CibAB, conferred an advantage to the resident strain (occupying a niche) in the presence of a newcomer (Shen et al., 2019).

Secondly, some GFP- and RFP- labelled variants showed significant differences in cell viability compared to the parental strain; others had significant heterogeneity in the fluorescence signal. These limitations prevented the use of some strains with our experimental approach. Both fluorescent constructs used in this study were expressed under the control of the *hlpA* promoter. Kjos et al. showed that for the laboratory strain D39, *hlpA-gfp* and *hlpA-rfp* fusions did not affect cell viability nor growth rate in liquid medium, were expressed throughout the cell cycle, and that fluorescence intensity remained high and stable with low cell-to-cell variation, as assessed by fluorescence microscopy (Kjos et al., 2015). Variation in the fluorescence signal, however, was not tested under biofilm-forming conditions, nor inspected for other strains or evaluated by flow cytometry. Possibly, the heterogeneity observed in our strains derives from natural variability previously described for isogenic strains (reviewed in (Jørgensen et al., 2013)), from the existence of a sub-population of cells that are either dying or dead but still retaining cell integrity (biofilms include many dead cells (Bayles, 2007)), or a combination of both. These limitations led to the exclusion of various strains limiting the magnitude of potential findings.

Thirdly, we observed heterogeneity within replicated biofilm experiments, which even though expected, hampered analyses of some dual-strain specific combinations. Marks et al. have shown that biofilms grown on an epithelial cell layer have increased reproducibility and lead to higher biofilm yields compared to biofilms obtained in abiotic conditions (Marks et al., 2012). In our optimized abiotic system, we have successfully obtained

yields comparable to the ones described by Marks et al. The inclusion of an epithelial cell layer, albeit possibly increasing reproducibility, would increase the complexity of the analysis and would hinder accurate distinction and quantification of pneumococcal strains by flow cytometry.

In any event, the use of several strains led us to make two important observations: (i) the outcome of an interaction is independent of capsular and sequence type; (ii) a given strain, when grown in the presence of another, may be benefited, harmed or not affected, depending on the strain it is interacting with.

Overall, we were able to develop a strategy that enables identification of different types of intra-species interactions in biofilms and successfully applied it to a diverse collection of pneumococcal isolates. We validated the use of flow cytometry for direct quantification of bacteria within the biofilm, as opposed to more traditional methods, such as bacterial cell counts on selective media. Our approach enables discrimination between strains of the same serotype, genotype and antibiotype, overcoming a limitation of strategies previously described (Wu et al., 2017). Representative interactions were further confirmed through a qualitative approach based on CLSM, *i.e.*, we were able to visualize positive, negative and neutral effects that *S. pneumoniae* strains may exert on each other and these were in agreement with the results obtained using flow cytometry. Furthermore, this approach could be adapted to other species and to more complex systems through the optimization of fluorescent constructs and the selection of other fluorescent reporters. In fact, a comparable strategy has recently been applied to visualize oral streptococcal species using integrative and replicative plasmids with strong promoters fused to fluorescent reporters (Shields et al., 2019).

In conclusion, we provide novel evidence that a panoply of intra-species interactions occur between naturally colonizing pneumococcal isolates and these are independent of serotype and genotype. These observations are a starting point to study the mechanisms underlying those interactions. Such studies will add to the growing body of knowledge regarding how the upper respiratory tract microbiota is shaped and adapts to changes triggered by the use of vaccines and antibiotics allowing the design of alternative strategies to modulate this ecosystem as a way to prevent infection.

DATA AVAILABILITY STATEMENT

The original contributions presented in the study are included in the article/**Supplementary Material**. Further inquiries can be directed to the corresponding author.

AUTHOR CONTRIBUTIONS

The study was designed by CV and RS-L. Data acquisition, analysis and interpretation were performed by CV, AC, AH, and

RS-L. The manuscript was drafted by CV, AC, and RS-L and critically revised by all authors. All authors contributed to the article and approved the submitted version.

FUNDING

This work was supported by project PTDC/BIA-MIC/30703/2017 from Fundação para a Ciência e a Tecnologia (FCT), Portugal; LISBOA-01-0145-FEDER-007660 (Microbiologia Molecular, Estrutural e Celular, funded by FEDER through COMPETE2020 – Programa Operacional Competitividade e Internacionalização); and LISBOA-01-0145-FEDER-016417 (ONEIDA co-funded by Fundos Europeus Estruturais e de Investimento, Programa Operacional Regional Lisboa 2020 and Fundação para a Ciência e a Tecnologia (FCT)). CV was supported by post-doctoral fellowship from FCT SFRH/BPD/115280/2016. The funders had no role in the design of the study, collection, analysis, and interpretation of data, writing of the manuscript or in the decision to submit the manuscript for

publication. The work was partially supported by PPBI - Portuguese Platform of BioImaging (PPBI-POCI-01-0145-FEDER-022122) co-funded by national funds from OE - “Orçamento de Estado” and by European funds from FEDER - “Fundo Europeu de Desenvolvimento Regional”.

ACKNOWLEDGMENTS

The authors are grateful to Jan-Willem Veening for providing the fluorescent constructs for strain-labelling and to Ana Cristina Paulo for help with the statistical analysis.

SUPPLEMENTARY MATERIAL

The Supplementary Material for this article can be found online at: <https://www.frontiersin.org/articles/10.3389/fcimb.2021.803286/full#supplementary-material>

REFERENCES

- Avery, O. T., Macleod, C. M., and McCarty, M. (1944). Studies on the Chemical Nature of the Substance Inducing Transformation of Pneumococcal Types: Induction of Transformation by a Desoxyribonucleic Acid Fraction Isolated From *Pneumococcus* Type Iii. *J. Exp. Med.* 79, 137–158. doi: 10.1084/jem.79.2.137
- Azarian, T., Martinez, P. P., Arnold, B. J., Qiu, X., Grant, L. R., Corander, J., et al. (2020). Frequency-Dependent Selection can Forecast Evolution in *Streptococcus Pneumoniae*. *PLoS Biol.* 18, e3000878. doi: 10.1371/journal.pbio.3000878
- Barnes, D. M., Whittier, S., Gilligan, P. H., Soares, S., Tomasz, A., and Henderson, F. W. (1995). Transmission of Multidrug-Resistant Serotype 23F *Streptococcus Pneumoniae* in Group Day Care: Evidence Suggesting Capsular Transformation of the Resistant Strain *In Vivo*. *J. Infect. Dis.* 171, 890–896. doi: 10.1093/infdis/171.4.890
- Bayles, K. W. (2007). The Biological Role of Death and Lysis in Biofilm Development. *Nat. Rev. Microbiol.* 5, 721–726. doi: 10.1038/nrmicro1743
- Blanchette, K. A., Shenoy, A. T., Milner, J. 2nd, Gilley, R. P., McClure, E., Hinojosa, C. A., et al. (2016). Neuraminidase A-Exposed Galactose Promotes *Streptococcus Pneumoniae* Biofilm Formation During Colonization. *Infect. Immun.* 84, 2922–2932. doi: 10.1128/IAI.00277-16
- Croucher, N. J., Harris, S. R., Fraser, C., Quail, M. A., Burton, J., van der Linden, M., et al. (2011). Rapid Pneumococcal Evolution in Response to Clinical Interventions. *Science* 331, 430–434. doi: 10.1126/science.1198545
- Dawid, S., Roche, A. M., and Weiser, J. N. (2007). The Blp Bacteriocins of *Streptococcus Pneumoniae* Mediate Intraspecies Competition Both *In Vitro* and *In Vivo*. *Infect. Immun.* 75, 443–451. doi: 10.1128/IAI.01775-05
- Evans, B. A., and Rozen, D. E. (2013). Significant Variation in Transformation Frequency in *Streptococcus Pneumoniae*. *ISME J.* 7, 791–799. doi: 10.1038/ismej.2012.170
- Faust, K., and Raes, J. (2012). Microbial Interactions: From Networks to Models. *Nat. Rev. Microbiol.* 10, 538–550. doi: 10.1038/nrmicro2832
- Félix, S., Handem, S., Nunes, S., Paulo, A. C., Candeias, C., Valente, C., et al. (2021). Impact of Private Use of the 13-Valent Pneumococcal Conjugate Vaccine (PCV13) on Pneumococcal Carriage Among Portuguese Children Living in Urban and Rural Regions. *Vaccine* 39, 4524–4533. doi: 10.1016/j.vaccine.2021.06.035
- GBD (2018). Estimates of the Global, Regional, and National Morbidity, Mortality, and Aetiologies of Lower Respiratory Infections in 195 Countries 1990–2016: A Systematic Analysis for the Global Burden of Disease Study 2016. *Lancet Infect. Dis.* 18, 1191–1210. doi: 10.1016/S1473-3099(18)30310-4
- Gray, B. M., Converse, G. M. 3rd, and Dillon, H. C. Jr. (1980). Epidemiologic Studies of *Streptococcus Pneumoniae* in Infants: Acquisition, Carriage, and Infection During the First 24 Months of Life. *J. Infect. Dis.* 142, 923–933. doi: 10.1093/infdis/142.6.923
- Hausdorff, W. P., Feikin, D. R., and Klugman, K. P. (2005). Epidemiological Differences Among Pneumococcal Serotypes. *Lancet Infect. Dis.* 5, 83–93. doi: 10.1016/S1473-3099(05)70083-9
- Hiller, N. L., Ahmed, A., Powell, E., Martin, D. P., Eutsey, R., Earl, J., et al. (2010). Generation of Genic Diversity Among *Streptococcus Pneumoniae* Strains via Horizontal Gene Transfer During a Chronic Polyclonal Pediatric Infection. *PLoS Pathog.* 6, e1001108. doi: 10.1371/journal.ppat.1001108
- Horácio, A. N., Silva-Costa, C., Lopes, J. P., Ramirez, M., and Melo-Cristino, J. (2016). Serotype 3 Remains the Leading Cause of Invasive Pneumococcal Disease in Adults in Portugal, (2012–2014) Despite Continued Reductions in Other 13-Valent Conjugate Vaccine Serotypes. *Front. Microbiol.* 7, 1616. doi: 10.3389/fmicb.2016.01616
- Isturiz, R., Sings, H. L., Hilton, B., Arguedas, A., Reinert, R. R., and Jodar, L. (2017). *Streptococcus Pneumoniae* Serotype 19A: Worldwide Epidemiology. *Expert Rev. Vaccines* 16, 1007–1027. doi: 10.1080/14760584.2017.1362339
- Jørgensen, M. G., Van Raaphorst, R., and Veening, J. (2013). “Noise and Stochasticity in Gene Expression: A Pathogenic Fate Determinant,” in *Methods in Microbiology*. Eds. C. Harwood and A. Wipat (London, UK: Academic Press), 157–175.
- Joloba, M. L., Kidenya, B. R., Kateete, D. P., Katabazi, F. A., Muwanguzi, J. K., Asiimwe, B. B., et al. (2010). Comparison of Transformation Frequencies Among Selected *Streptococcus Pneumoniae* Serotypes. *Int. J. Antimicrob. Agents* 36, 124–128. doi: 10.1016/j.ijantimicag.2010.03.024
- Junges, R., Salvadori, G., Shekhar, S., Amdal, H. A., Periseleris, J. N., Chen, T., et al. (2017). A Quorum-Sensing System That Regulates *Streptococcus Pneumoniae* Biofilm Formation and Surface Polysaccharide Production. *MSphere* 2, e00324–e00317. doi: 10.1128/mSphere.00324-17
- Kamng’ona, A. W., Hinds, J., Bar-Zeev, N., Gould, K. A., Chaguza, C., Msefula, C., et al. (2015). High Multiple Carriage and Emergence of *Streptococcus Pneumoniae* Vaccine Serotype Variants in Malawian Children. *BMC Infect. Dis.* 15, 234. doi: 10.1186/s12879-015-0980-2
- Kandasamy, R., Gurung, M., Thapa, A., Ndimah, S., Adhikari, N., Murdoch, D. R., et al. (2015). Multi-Serotype Pneumococcal Nasopharyngeal Carriage Prevalence in Vaccine Naïve Nepalese Children, Assessed Using Molecular Serotyping. *PLoS One* 10, e0114286. doi: 10.1371/journal.pone.0114286
- Keck, T., Leiacker, R., Heinrich, A., Kuhnemann, S., and Rettinger, G. (2000). Humidity and Temperature Profile in the Nasal Cavity. *Rhinology* 38, 167–171.
- Kim, W., Racimo, F., Schluter, J., Levy, S. B., and Foster, K. R. (2014). Importance of Positioning for Microbial Evolution. *Proc. Natl. Acad. Sci. USA* 111, E1639–E1647. doi: 10.1073/pnas.1323632111

- Kjos, M., Aprianto, R., Fernandes, V. E., Andrew, P. W., Van Strijp, J. A., Nijland, R., et al. (2015). Bright Fluorescent *Streptococcus Pneumoniae* for Live-Cell Imaging of Host-Pathogen Interactions. *J. Bacteriol.* 197, 807–818. doi: 10.1128/JB.02221-14
- Lee, M. S., and Morrison, D. A. (1999). Identification of a New Regulator in *Streptococcus Pneumoniae* Linking Quorum Sensing to Competence for Genetic Transformation. *J. Bacteriol.* 181, 5004–5016. doi: 10.1128/JB.181.16.5004-5016.1999
- Lipsitch, M., Dykes, J. K., Johnson, S. E., Ades, E. W., King, J., Briles, D. E., et al. (2000). Competition Among *Streptococcus Pneumoniae* for Intranasal Colonization in a Mouse Model. *Vaccine* 18, 2895–2901. doi: 10.1016/S0264-410X(00)00046-3
- Maricic, N., Anderson, E. S., Oipari, A. E., Yu, E. A., and Dawid, S. (2016). Characterization of a Multi-peptide Lantibiotic Locus in *Streptococcus Pneumoniae*. *MBio* 7, e01656–e01615. doi: 10.1128/mBio.01656-15
- Marks, L. R., Reddinger, R. M., and Hakansson, A. P. (2012). High Levels of Genetic Recombination During Nasopharyngeal Carriage and Biofilm Formation in *Streptococcus Pneumoniae*. *MBio* 3, e00200–e00212. doi: 10.1128/mBio.00200-12
- Moore, M. R., Link-Gelles, R., Schaffner, W., Lynfield, R., Lexau, C., Bennett, N. M., et al. (2015). Effect of Use of 13-Valent Pneumococcal Conjugate Vaccine in Children on Invasive Pneumococcal Disease in Children and Adults in the USA: Analysis of Multisite, Population-Based Surveillance. *Lancet Infect. Dis.* 15, 301–309. doi: 10.1016/S1473-3099(14)71081-3
- Moscoso, M., Garcia, E., and Lopez, R. (2006). Biofilm Formation by *Streptococcus Pneumoniae*: Role of Choline, Extracellular DNA, and Capsular Polysaccharide in Microbial Accretion. *J. Bacteriol.* 188, 7785–7795. doi: 10.1128/JB.00673-06
- Nunes, S., Felix, S., Valente, C., Simões, A. S., Tavares, D. A., Almeida, S. T., et al. (2016). The Impact of Private Use of PCV7 in 2009 and 2010 on Serotypes and Antimicrobial Resistance of *Streptococcus Pneumoniae* Carried by Young Children in Portugal: Comparison With Data Obtained Since 1996 Generating a 15-Year Study Prior to PCV13 Introduction. *Vaccine* 34, 1648–1656. doi: 10.1016/j.vaccine.2016.02.045
- Perez-Dorado, I., Gonzalez, A., Morales, M., Sanles, R., Striker, W., Vollmer, W., et al. (2010). Insights Into Pneumococcal Fratricide From the Crystal Structures of the Modular Killing Factor LytC. *Nat. Struct. Mol. Biol.* 17, 576–U572. doi: 10.1038/nsmb.1817
- Rane, L., and Subbarow, Y. (1940). Nutritional Requirements of the *Pneumococcus*: I. Growth Factors for Types I, II, V, VII, VIII. *J. Bacteriol.* 40, 695–704. doi: 10.1128/jb.40.5.695-704.1940
- Sá-Leão, R., Nunes, S., Brito-Avô, A., Frazão, N., Simões, A. S., Crisóstomo, M. I., et al. (2009). Changes in Pneumococcal Serotypes and Antibiotypes Carried by Vaccinated and Unvaccinated Day-Care Centre Attendees in Portugal, a Country With Widespread Use of the Seven-Valent Pneumococcal Conjugate Vaccine. *Clin. Microbiol. Infect.* 15, 1002–1007. doi: 10.1111/j.1469-0691.2009.02775.x
- Sá-Leão, R., Pinto, F., Aguiar, S., Nunes, S., Carriço, J. A., Frazão, N., et al. (2011). Analysis of Invasiveness of Pneumococcal Serotypes and Clones Circulating in Portugal Before Widespread Use of Conjugate Vaccines Reveals Heterogeneous Behavior of Clones Expressing the Same Serotype. *J. Clin. Microbiol.* 49, 1369–1375. doi: 10.1128/JCM.01763-10
- Selak, M., Riviere, A., Moens, F., Van Den Abbeele, P., Geirnaert, A., Rogelj, I., et al. (2016). Inulin-Type Fructan Fermentation by Bifidobacteria Depends on the Strain Rather Than the Species and Region in the Human Intestine. *Appl. Microbiol. Biotechnol.* 100, 4097–4107. doi: 10.1007/s00253-016-7351-9
- Shen, P., Lees, J. A., Bee, G. C. W., Brown, S. P., and Weiser, J. N. (2019). Pneumococcal Quorum Sensing Drives an Asymmetric Owner-Intruder Competitive Strategy During Carriage via the Competence Regulon. *Nat. Microbiol.* 4, 198–208. doi: 10.1038/s41564-018-0314-4
- Shields, R. C., Kaspar, J. R., Lee, K., Underhill, S. A. M., and Burne, R. A. (2019). Fluorescence Tools Adapted for Real-Time Monitoring of the Behaviors of *Streptococcus* Species. *Appl. Environ. Microbiol.* 85, e00620–e00619. doi: 10.1128/AEM.00620-19
- Simões, A. S., Pereira, L., Nunes, S., Brito-Avô, A., De Lencastre, H., and Sá-Leão, R. (2011). Clonal Evolution Leading to Maintenance of Antibiotic Resistance Rates Among Colonizing *Pneumococci* in the PCV7 Era in Portugal. *J. Clin. Microbiol.* 49, 2810–2817. doi: 10.1128/JCM.00517-11
- Stewart, P. S. (2003). Diffusion in Biofilms. *J. Bacteriol.* 185, 1485–1491. doi: 10.1128/JB.185.5.1485-1491.2003
- Tettelin, H., Nelson, K. E., Paulsen, I. T., Eisen, J. A., Read, T. D., Peterson, S., et al. (2001). Complete Genome Sequence of a Virulent Isolate of *Streptococcus Pneumoniae*. *Science* 293, 498–506. doi: 10.1126/science.1061217
- Tomasz, A. (1967). Choline in the Cell Wall of a Bacterium: Novel Type of Polymer-Linked Choline in *Pneumococcus*. *Science* 157, 694–697. doi: 10.1126/science.157.3789.694
- Trzciński, K., Li, Y., Weinberger, D. M., Thompson, C. M., Cordy, D., Bessolo, A., et al. (2015). Effect of Serotype on Pneumococcal Competition in a Mouse Colonization Model. *MBio* 6, e00902–e00915. doi: 10.1128/mBio.00902-15
- Turner, P., Hinds, J., Turner, C., Jankhot, A., Gould, K., Bentley, S., et al. (2011). Improved Detection of Nasopharyngeal Co-Colonization by Multiple Pneumococcal Serotypes Using Latex Agglutination or Molecular Serotyping by Microarray. *J. Clin. Microbiol.* 49, 1784–1789. doi: 10.1128/JCM.00157-11
- Valente, C., Dawid, S., Pinto, F. R., Hinds, J., Simões, A. S., Gould, K. A., et al. (2016a). The *Blp* Locus of *Streptococcus Pneumoniae* Plays a Limited Role in the Selection of Which Strains can Co-Colonize the Human Nasopharynx. *Appl. Environ. Microbiol.* 82, 5206–5215. doi: 10.1128/AEM.01048-16
- Valente, C., Hinds, J., Gould, K. A., Pinto, F. R., De Lencastre, H., and Sá-Leão, R. (2016b). Impact of the 13-Valent Pneumococcal Conjugate Vaccine on *Streptococcus Pneumoniae* Multiple Serotype Carriage. *Vaccine* 34, 4072–4078. doi: 10.1016/j.vaccine.2016.06.017
- Valente, C., Hinds, J., Pinto, F., Brugger, S. D., Gould, K., Mühlemann, K., et al. (2012). Decrease in Pneumococcal Co-Colonization Following Vaccination With the Seven-Valent Pneumococcal Conjugate Vaccine. *PloS One* 7, e30235. doi: 10.1371/journal.pone.0030235
- Valentino, M. D., McGuire, A. M., Rosch, J. W., Bispo, P. J., Burnham, C., Sanfilippo, C. M., et al. (2014). Unencapsulated *Streptococcus Pneumoniae* From Conjunctivitis Encode Variant Traits and Belong to a Distinct Phylogenetic Cluster. *Nat. Commun.* 5, 5411. doi: 10.1038/ncomms6411
- Waight, P. A., Andrews, N. J., Ladhani, S. N., Sheppard, C. L., Slack, M. P., and Miller, E. (2015). Effect of the 13-Valent Pneumococcal Conjugate Vaccine on Invasive Pneumococcal Disease in England and Wales 4 Years After its Introduction: An Observational Cohort Study. *Lancet Infect. Dis.* 15, 535–543. doi: 10.1016/S1473-3099(15)70044-7
- Watkins, E. R., Penman, B. S., Lourenço, J., Buckee, C. O., Maiden, M. C., and Gupta, S. (2015). Vaccination Drives Changes in Metabolic and Virulence Profiles of *Streptococcus Pneumoniae*. *PloS Pathog.* 11, e1005034. doi: 10.1371/journal.ppat.1005034
- Wei, H., and Havarstein, L. S. (2012). Fratricide is Essential for Efficient Gene Transfer Between *Pneumococci* in Biofilms. *Appl. Environ. Microbiol.* 78, 5897–5905. doi: 10.1128/AEM.01343-12
- Weiser, J. N., Ferreira, D. M., and Paton, J. C. (2018). *Streptococcus Pneumoniae*: Transmission, Colonization and Invasion. *Nat. Rev. Microbiol.* 16, 355–367. doi: 10.1038/s41579-018-0001-8
- Wholey, W. Y., Kochan, T. J., Storck, D. N., and Dawid, S. (2016). Coordinated Bacteriocin Expression and Competence in *Streptococcus Pneumoniae* Contributes to Genetic Adaptation Through Neighbor Predation. *PloS Pathog.* 12, e1005413. doi: 10.1371/journal.ppat.1005413
- Wu, X., Jacobs, N. T., Bozio, C., Palm, P., Lattar, S. M., Hanke, C. R., et al. (2017). Competitive Dominance Within Biofilm Consortia Regulates the Relative Distribution of *Pneumococcal* Nasopharyngeal Density. *Appl. Environ. Microbiol.* 83, e00953–e00917. doi: 10.1128/AEM.00953-17
- Wyllie, A. L., Chu, M. L., Schellens, M. H., Van Engelsdorp Gastelaars, J., Jansen, M. D., van der Ende, A., et al. (2014). *Streptococcus Pneumoniae* in Saliva of Dutch Primary School Children. *PloS One* 9, e102045. doi: 10.1371/journal.pone.0102045
- Yan, B. F., Liu, N., Liu, M. H., Du, X. Y., Shang, F., and Huang, Y. (2021). Soil Actinobacteria Tend to Have Neutral Interactions With Other Co-Occurring Microorganisms, Especially Under Oligotrophic Conditions. *Environ. Microbiol.* 23, 4126–4140. doi: 10.1111/1462-2920.15483

Conflict of Interest: The authors declare that the research was conducted in the absence of any commercial or financial relationships that could be construed as a potential conflict of interest.

Publisher's Note: All claims expressed in this article are solely those of the authors and do not necessarily represent those of their affiliated organizations, or those of the publisher, the editors and the reviewers. Any product that may be evaluated in

this article, or claim that may be made by its manufacturer, is not guaranteed or endorsed by the publisher.

Copyright © 2022 Valente, Cruz, Henriques and Sá-Leão. This is an open-access article distributed under the terms of the Creative Commons Attribution License

(CC BY). The use, distribution or reproduction in other forums is permitted, provided the original author(s) and the copyright owner(s) are credited and that the original publication in this journal is cited, in accordance with accepted academic practice. No use, distribution or reproduction is permitted which does not comply with these terms.



Infant Pneumococcal Carriage in Belgium Not Affected by COVID-19 Containment Measures

Laura Willen^{1*}, Esra Ekinici¹, Lize Cuyper², Heidi Theeten¹ and Stefanie Desmet^{2,3}

¹ Centre for the Evaluation of Vaccination, Vaccine and Infectious Disease Institute, University of Antwerp, Wilrijk, Belgium,

² Department of Laboratory Medicine, National Reference Centre for Pneumococci, University Hospitals Leuven,

Leuven, Belgium, ³ Laboratory of Clinical Bacteriology and Mycology, Department of Microbiology, Immunology and Transplantation, Katholieke Universiteit Leuven, Leuven, Belgium

OPEN ACCESS

Edited by:

Xueqing Wu,
Zhejiang University, China

Reviewed by:

Qiucheng Shi,
Zhejiang University, China
Abraham Moller,
National Institutes of Health (NIH),
United States

*Correspondence:

Laura Willen
laura.willen@uantwerpen.be

Specialty section:

This article was submitted to
Molecular Bacterial Pathogenesis,
a section of the journal
Frontiers in Cellular and
Infection Microbiology

Received: 30 November 2021

Accepted: 30 December 2021

Published: 17 January 2022

Citation:

Willen L, Ekinici E, Cuyper L,
Theeten H and Desmet S (2022)
Infant Pneumococcal Carriage
in Belgium Not Affected by
COVID-19 Containment Measures.
Front. Cell. Infect. Microbiol. 11:825427.
doi: 10.3389/fcimb.2021.825427

Streptococcus pneumoniae is an important and frequently carried respiratory pathogen that has the potential to cause serious invasive diseases, such as pneumonia, meningitis, and sepsis. Young children and older adults are among the most vulnerable to developing serious disease. With the arrival of the COVID-19 pandemic and the concomitant restrictive measures, invasive disease cases caused by respiratory bacterial species, including pneumococci, decreased substantially. Notably, the stringency of the containment measures as well as the visible reduction in the movement of people appeared to coincide with the drop in invasive disease cases. One could argue that wearing protective masks and adhering to social distancing guidelines to halt the spread of the SARS-CoV-2 virus, also led to a reduction in the person-to-person transmission of respiratory bacterial species. Although plausible, this conjecture is challenged by novel data obtained from our nasopharyngeal carriage study which is performed yearly in healthy daycare center attending children. A sustained and high pneumococcal carriage rate was observed amid periods of stringent restrictive measures. This finding prompts us to revisit the connection between nasopharyngeal colonization and invasion and invites us to look closer at the nasopharyngeal microbiome as a whole.

Keywords: *Streptococcus pneumoniae*, nasopharyngeal carriage, invasive pneumococcal disease, COVID-19, containment measures

INTRODUCTION

Streptococcus pneumoniae is part of the commensal flora of the upper respiratory tract and colonizes, together with several other bacterial species, the nasopharyngeal niche. Even though its residency in the nasopharynx typically goes unnoticed, when natural immunological barriers are crossed, respiratory or even systemic disease ensues. Pneumococcal colonization is, thus, imperative for disease to occur and is responsible for the horizontal spread of the different pneumococcal serotypes within the community. Close contact between individuals, and therefore crowded places, adds to the spread of pneumococci (Bogaert et al., 2004). Young children are particularly known to frequently possess pneumococci, even more so when attending daycare centers, and especially so during the drier and colder months when its spread is more likely to coincide with respiratory viral infections (Numminen et al., 2015).

Pneumococcal conjugate vaccines (PCV) were developed to prevent (invasive) pneumococcal disease caused by the, at the time, most invasive serotypes. In countries with a high vaccine uptake, this has led to decreases in both carriage and cases of invasive pneumococcal disease (IPD) caused by the vaccine serotypes (Cohen et al., 2015; Vissers et al., 2018; Wouters et al., 2020; National Reference Centre for invasive *S. pneumoniae*, 2021). However, the nasopharyngeal niche is a complex and highly dynamic environment with high turnovers of colonizing species and serotypes. Vaccinating against the most invasive pneumococci, thus, results in their replacement by other serotypes in the nasopharyngeal niche (Bogaert et al., 2004). Evidently, monitoring the distribution of the different pneumococcal serotypes within populations is essential to inform vaccination policy and direct future vaccine development. As a result, many countries worldwide have performed nasopharyngeal carriage studies, some of which are still ongoing (Cohen et al., 2015; Vissers et al., 2018; Wagner et al., 2019; Wouters et al., 2020). In Belgium, our group has been monitoring asymptomatic pneumococcal carriage in daycare attending children (aged between 6-30 months old) every winter since 2016, with carriage rates fluctuating between 68 and 74% (Wouters et al., 2020) (unpublished data).

In response to the outbreak of the COVID-19 pandemic in early 2020, countries worldwide laid down a range of restrictive measures to contain the further spread of the SARS-CoV-2 virus. This has led to the discontinuation of several pneumococcal monitoring studies in many countries. Also, in Belgium, this appeared challenging. However, with great effort comes great reward: despite the many restrictions imposed on the Belgian people, monitoring nasopharyngeal carriage was not interrupted and the target number of recruited children was obtained. More importantly, high sustained carriage rates were measured during this period. The importance of our findings was revealed when the Invasive Respiratory Infection Surveillance (IRIS) Initiative published international surveillance data of invasive bacterial diseases in *The Lancet Digital Health* (Brueggemann et al., 2021). They confirmed the much-anticipated impact of country-wide lockdowns on the incidence of invasive disease caused by the three most common respiratory pathogens *S. pneumoniae*, *Haemophilus influenzae*, and *Neisseria meningitidis*. Significant and sustained reductions were observed, based on surveillance data from 37 laboratories from 26 countries worldwide, that appeared to coincide with the stringency of COVID-19 containment measures (measured using the Oxford COVID-19 Government Response Tracker) and with changes in the movement of people (measured using Google COVID-19 Community Mobility Reports).

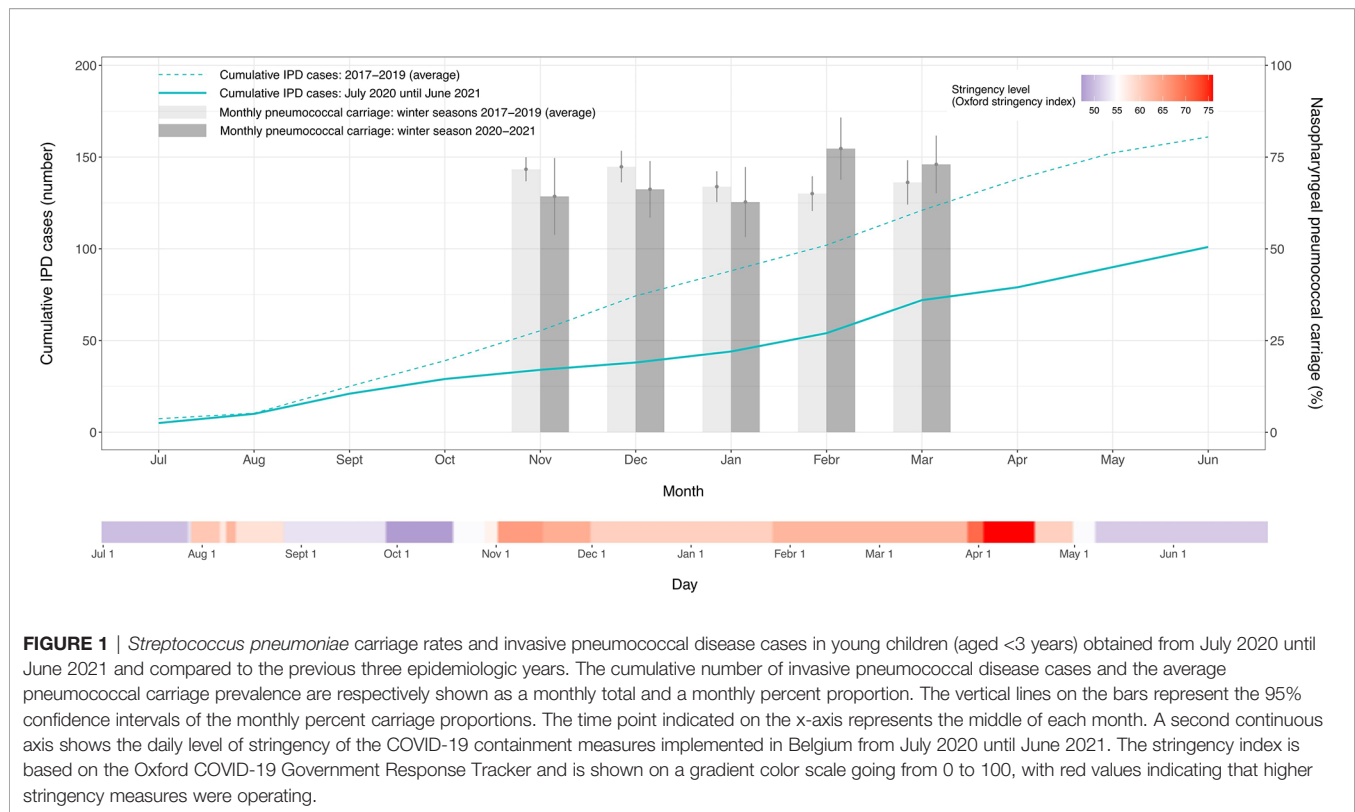
THE BELGIAN SITUATION: STRINGENT MEASURES, BUT HIGH PNEUMOCOCCAL CARRIAGE RATES

In Belgium, the government announced a lockdown on March 18, 2020, thereby ordering the closing of shops, and enacting

stay-at-home orders and travel restrictions. This resulted in a drastic reduction in movement as indicated by corresponding mobility data (Sciensano, 2021). A gradual relaxation of the containment measures from May 2020 led to a worsening COVID-19 epidemiologic situation and, consequently, new restrictions were gradually implemented from early October 2020 until late April 2021 (Oxford stringency index > 55) (Figure 1). Analogous to the observations made by IRIS, also this second period of restrictive measures in Belgium – corresponding to the winter of the epidemiologic year 2020-2021 – was characterized by a reduction in IPD cases of 42% in young Belgian children (aged <3 years) when compared to previous non-COVID epidemiologic years (2017-2019). As a result, the pronounced seasonality typical for IPD did not manifest itself in the winter of 2020-2021 (Figure 1).

These reductions in disease incidence could be explained by an interruption in person-to-person bacterial respiratory transmission (Brueggemann et al., 2021). While plausible, high pneumococcal carriage rates recorded during the same period seem to suggest otherwise. In the winter of 2020-2021, we did not detect a significant change in overall *S. pneumoniae* carriage proportion (67.43%) compared to the average of the previous three years (69.07%) ($X^2 = 0.56$, $P=0.46$) (Figure 1). The observed discordance between IPD cases and carriage prevalence in the same age group may, thus, point to a more complex situation and possible interspecies interactions in the nasopharyngeal microbiome.

Even though bacterial colonization is a necessary precursor for invasive disease, it does not imply the occurrence of disease per se, nor do we understand all the interspecies interactions or host factors that should coalesce for the bacteria to become invasive. Altered transmission of other species inhabiting the nasopharyngeal microbiome could also have contributed to the reduced IPD cases (Bogaert et al., 2004). Viral respiratory infections are known to be associated with IPDs (Weiser et al., 2018; Berry et al., 2020). Therefore, a more fitting hypothesis, and previously raised by Smith et al. (Smith and Opatowski, 2021), is that the COVID-19 containment measures reduced the overall respiratory viral circulation, which could have eventually impacted the incidence of IPD in children. It is thought that the inflammatory conditions in the upper respiratory tract following a respiratory viral infection both favor the presence and transmission of *S. pneumoniae*, and increase its likelihood of penetrating host tissues (Weiser et al., 2018). However, recent work revealed that while influenza-like illnesses (ILIs) indeed increase the pneumococcal invasion risk, it does not increase their transmission or acquisition risk (Domenech de Cellès et al., 2019). Consequently, interventions targeting ILIs were predicted not to have a marked indirect effect on pneumococcal carriage – a prediction confirmed by the sustained high carriage rates observed in our study. Importantly, we did not assess pneumococcal carriage density, a precursor of IPD, and known to be elevated in individuals with ILIs (Brotons et al., 2017; Miellet et al., 2021). Possibly also SARS-CoV-2 co-infections could have impacted pneumococcal carriage rates (Howard, 2021);



however, in our study, none of the tested children (746/907, 82%) was positive for SARS-CoV-2 (unpublished data).

SCRUTINIZING THE RELATIONSHIP BETWEEN PNEUMOCOCCAL CARRIAGE, TRANSMISSION, AND INVASION: WHAT ELSE TO CONSIDER?

It can, however, not be ruled out that along with a decrease in the co-circulating viral population, also a reduced frequency of within- and between-age contacts in the overall pediatric population has impacted IPD development (Domenech de Cellès et al., 2019). Both pneumococci and respiratory viruses, including SARS-CoV-2, can be transmitted from person-to-person *via* respiratory secretions through direct physical contact or directly through the air *via* large respiratory droplets (Weiser et al., 2018; Leung, 2021). Airborne transmission, on the other hand, is likely more important for the transmission of respiratory viruses/SARS-CoV-2 than for pneumococci. However, it should not be dismissed as a possible transmission route for the latter: a study on ferrets living in cages three meters apart from each other did observe transmission of pneumococci between them (McCullers et al., 2010). Lastly, just like respiratory viruses and SARS-CoV-2, pneumococci can also be transmitted indirectly *via* contact with contaminated surfaces or objects (fomites), with the duration of their survival in the environment depending on the situation, going from several

hours in nutrient-poor conditions to a couple of days in e.g. saliva or biofilms (Marks et al., 2014; Hamaguchi et al., 2017; Marzoli et al., 2021; Morimura et al., 2021). Notably, in daycare settings, pneumococci were seen to survive for hours and could be cultured from environmental surfaces, including toys (Marks et al., 2014). Given the parallel routes of transmission of both pneumococci and respiratory viruses, restrictions that were primarily aimed at reducing transmission of SARS-CoV-2 might, thus, also have affected pneumococcal transmission in the overall pediatric population. Importantly, during the country's first lockdown (March–May 2020), Belgian daycare centers remained open but were only occupied for 50%. Since we do not have carriage data of this period or its aftermath, we cannot tell if transmission between children declined following reduced contacts. On the other hand, in the winter of 2020–2021, the number of children attending daycare was in line with previous years, and essentially little restrictions were imposed, likely adding to the sustained high carriage rates. Adding to this, and if we want to understand the epidemiology of the pneumococcus entirely, it is paramount to also define (yearly) pneumococcal carriage rates in Belgian children who do not attend daycare centers [i.e. 40% of the Belgian children, (OECD, 2021)].

Of course, the carriage prevalence reported here only depicts the situation in Belgian daycares, a high transmission setting in which changes in the overall pneumococcal carriage might be hard to discern. Given the marked differences in the capacity of specific *S. pneumoniae* serotypes and clones to cause invasive disease (Brueggemann et al., 2003), individual serotype carriage

proportions should be disentangled to better understand how such an overall high carriage rate relates to the observed drop in IPD cases. In Belgium specifically, serotype distributions might have shifted given the country's switch in PCV recommendation in September 2019, one year prior to our study. That year, PCV13 replaced PCV10, extending children's protection to an additional three serotypes. Of note, the impact of an earlier switch in the Belgian PCV program in 2016 – from PCV13 to PCV10 – was only detectable two years after its implementation (Wouters et al., 2020). Likely a similar interval is needed to detect the impact of the second switch. More so, IPD surveillance in Belgium indicated that in 2020 the same proportion of serotype 19A strains (43.8%) were responsible for IPD in children <2 years of age compared to that in 2019 (39.4%) (National Reference Centre for invasive *S. pneumoniae*, 2021). Nonetheless, shifts in the distribution of circulating serotypes and in the multilocus sequence types of pneumococcal serotype 19A following the 2019-switch in PCV recommendation are being investigated, and could be instructive for even better understanding how overall high carriage rates relate to the observed drop in IPD cases. A relation that could, in fact, be an amalgam of all players discussed here, including (but not limited to) respiratory viruses, serotype replacements, and reduced contacts.

CONCLUSION

The sustained high asymptomatic carriage patterns observed in our study reveal that IPD incidence does not solely depend on pneumococcal carriage rates, and that likely many more factors are at play. Our finding, thus, puts the relationship between high pneumococcal carriage rate and invasive disease into perspective and sheds a light on the potential role of the co-circulating viral populations when it comes to IPD incidence in young children. Evidently, we should not narrow down on a single component cause, nor should we devalue the importance of person-to-person bacterial respiratory transmission. When unraveling the epidemiology of the pneumococcus many factors need to be considered. We believe that our results and insights presented here will be able to assist further pneumococcal research.

REFERENCES

- Berry, I., Tuite, A. R., Salomon, A., Drews, S., Harris, A. D., Hatchette, T., et al. (2020). Association of Influenza Activity and Environmental Conditions With the Risk of Invasive Pneumococcal Disease. *JAMA Netw. Open* 3, 1–11. doi: 10.1001/jamanetworkopen.2020.10167
- Bogaert, D., De Groot, R., and Hermans, P. W. M. (2004). *Streptococcus pneumoniae* Colonisation: The Key to Pneumococcal Disease. *Lancet Infect. Dis.* 4, 144–154. doi: 10.1016/S1473-3099(04)00938-7
- Brotons, P., Bassat, Q., Lanaspá, M., Henares, D., Perez-Arguuello, A., Madrid, L., et al. (2017). Nasopharyngeal Bacterial Load as a Marker for Rapid and Easy Diagnosis of Invasive Pneumococcal Disease in Children From Mozambique. *PLoS One* 12, e0184762. doi: 10.1371/journal.pone.0184762
- Brueggemann, A. B., Griffiths, D. T., Meats, E., Peto, T., Crook, D. W., and Spratt, B. G. (2003). Clonal Relationships Between Invasive and Carriage *Streptococcus*

Especially so since results like these are scarce, considering most countries were not able to continue monitoring nasopharyngeal carriage during the COVID-19 pandemic.

DATA AVAILABILITY STATEMENT

The raw data supporting the conclusions of this article will be made available by the authors, without undue reservation.

ETHICS STATEMENT

The studies involving human participants were reviewed and approved by Comité voor Medische Ethiek, University Hospital Antwerp, Edegem (Belgium). Written informed consent to participate in this study was provided by the participants' legal guardian/next of kin.

AUTHOR CONTRIBUTIONS

HT acquired funding, conceptualized, and supervised the study. LW, EE, LC, and SD analyzed and verified the underlying data. LW wrote the first draft of the manuscript and visualized the data. All authors reviewed and edited the manuscript, had full access to all the data in the study and had final responsibility for the decision to submit for publication.

FUNDING

UZ Leuven, as the national reference center for pneumococci, is supported by Sciensano, which is gratefully acknowledged. SD and HT received an investigator-initiated research grant from Pfizer. The study is also supported by a research grant from Research Foundation Flanders (FWO Research Grant 1150017N, Antigoon ID 33341). The funders had no role in the study design, the collection, analysis, and interpretation of data, the writing of the report, or in the decision to publish.

- pneumoniae* and Serotype- and Clone-Specific Differences in Invasive Disease Potential. *J. Infect. Dis.* 187, 1424–1432. doi: 10.1086/374624
- Brueggemann, A. B., Jansen van Rensburg, M. J., Shaw, D., McCarthy, N. D., Jolley, K. A., Maiden, M. C. J., et al. (2021). Changes in the Incidence of Invasive Disease Due to *Streptococcus pneumoniae*, *Haemophilus influenzae*, and *Neisseria meningitidis* During the COVID-19 Pandemic in 26 Countries and Territories in the Invasive Respiratory Infection Surveillance Initiative: A Prospective Analysis of Surveillance Data. *Lancet Digit. Heal.* 3, e360–e370. doi: 10.1016/S2589-7500(21)00077-7
- Cohen, R., Varon, E., Doit, C., Schlemmer, C., Romain, O., Thollot, F., et al. (2015). A 13-Year Survey of Pneumococcal Nasopharyngeal Carriage in Children With Acute Otitis Media Following PCV7 and PCV13 Implementation. *Vaccine* 33, 5118–5126. doi: 10.1016/j.vaccine.2015.08.010
- Domenech de Cellès, M., Arduin, H., Lévy-Bruhl, D., Georges, S., Souty, C., Guillemot, D., et al. (2019). Unraveling the Seasonal Epidemiology of

- Pneumococcus. *Proc. Natl. Acad. Sci.* 116, 1802–1807. doi: 10.1073/pnas.1812388116
- Hamaguchi, S., Ammar Zafar, M., Cammer, M., and Weiser, J. N. (2017). Capsule Prolongs Survival of *Streptococcus pneumoniae* During Starvation. *Infect. Immun.* 86, e00802–e00817. doi: 10.1128/IAI.00802-17
- Howard, L. M. (2021). Is There an Association Between Severe Acute Respiratory Syndrome Coronavirus 2 (SARS-CoV-2) and *Streptococcus pneumoniae*? *Clin. Infect. Dis.* 72, E76–E78. doi: 10.1093/cid/ciaa1812
- Leung, N. H. L. (2021). Transmissibility and Transmission of Respiratory Viruses. *Nat. Rev. Microbiol.* 19, 528–545. doi: 10.1038/s41579-021-00535-6
- Marks, L. R., Reddinger, R. M., and Hakansson, A. P. (2014). Biofilm Formation Enhances Fomite Survival of *Streptococcus pneumoniae* and *Streptococcus pyogenes*. *Infect. Immun.* 82, 1141–1146. doi: 10.1128/IAI.01310-13
- Marzoli, F., Bortolami, A., Pezzuto, A., Mazzetto, E., Piro, R., Terregino, C., et al. (2021). A Systematic Review of Human Coronaviruses Survival on Environmental Surfaces. *Sci. Total Environ.* 778:146191. doi: 10.1016/j.scitotenv.2021.146191
- McCullers, J. A., McAuley, J. L., Browall, S., Iverson, A. R., Boyd, K. L., and Normark, B. H. (2010). Influenza Enhances Susceptibility to Natural Acquisition of and Disease Due to *Streptococcus pneumoniae* in Ferrets. *J. Infect. Dis.* 202, 1287–1295. doi: 10.1086/656333
- Miellet, W. R., van Veldhuizen, J., Nicolaie, M. A., Mariman, R., Bootsma, H. J., Bosch, T., et al. (2021). Influenza-Like Illness Exacerbates Pneumococcal Carriage in Older Adults. *Clin. Infect. Dis.* 73 (9), e2680–e2689. doi: 10.1093/cid/ciaa1551
- Morimura, A., Hamaguchi, S., Akeda, Y., and Tomono, K. (2021). Mechanisms Underlying Pneumococcal Transmission and Factors Influencing Host-Pneumococcus Interaction: A Review. *Front. Cell. Infect. Microbiol.* 11:639450. doi: 10.3389/fcimb.2021.639450
- National Reference Centre for invasive *S. pneumoniae* (2021). *Report National Reference Centre Streptococcus pneumoniae 2020* (Leuven, Belgium): Sciensano. Available at: [https://nrchm.wiv-isp.be/nl/ref_centra_lab/streptococcus_pneumoniae_invasive/Rapporten/Rapport Streptococcus pneumoniae 2020.pdf](https://nrchm.wiv-isp.be/nl/ref_centra_lab/streptococcus_pneumoniae_invasive/Rapporten/Rapport%20Streptococcus%20pneumoniae%2020.pdf).
- Numminen, E., Chewapreecha, C., Turner, C., Goldblatt, D., Nosten, F., Bentley, S. D., et al. (2015). Climate Induces Seasonality in Pneumococcal Transmission. *Sci. Rep.* 5, 1–15. doi: 10.1038/srep11344
- OECD (2021) *OECD Family Database - PF3.2: Enrolment in Childcare and Pre-School*. Available at: https://www.oecd.org/els/soc/PF3_2_Enrolment_childcare_preschool.pdf.
- Sciensano (2021) *COVID-19 Wekelijks Epidemiologisch Bulletin (23 Juli 2021)*. Available at: <https://www.info-coronavirus.be/nl/>.
- Smith, D. R. M., and Opatowski, L. (2021). COVID-19 Containment Measures and Incidence of Invasive Bacterial Disease. *Lancet Digit. Heal.* 3, e331–e332. doi: 10.1016/S2589-7500(21)00085-6
- Vissers, M., Wijmenga-Monsuur, A. J., Knol, M. J., Badoux, P., Van Houten, M. A., van der Ende, A., et al. (2018). Increased Carriage of non-Vaccine Serotypes With Low Invasive Disease Potential Four Years After Switching to the 10-Valent Pneumococcal Conjugate Vaccine in The Netherlands. *PloS One* 13, 1–15. doi: 10.1371/journal.pone.0194823
- Wagner, B. G., Althouse, B. M., Givon-Lavi, N., Hu, H., and Dagan, R. (2019). Stable Dynamics of Pneumococcal Carriage Over a Decade in the Pre-PCV Era. *Vaccine* 37, 5625–5629. doi: 10.1016/j.vaccine.2019.07.077
- Weiser, J. N., Ferreira, D. M., and Paton, J. C. (2018). *Streptococcus pneumoniae*: Transmission, Colonization and Invasion. *Nat. Rev. Microbiol.* 16, 355–367. doi: 10.1038/s41579-018-0001-8
- Wouters, I., Desmet, S., Van Heirstraeten, L., Herzog, S. A., Beutels, P., Verhaegen, J., et al. (2020). How Nasopharyngeal Pneumococcal Carriage Evolved During and After a PCV13-To-PCV10 Vaccination Programme Switch in Belgium 2016 to 2018. *Euro. Surveill.* 25, pii=1900303. doi: 10.2807/1560-7917.ES.2020.25.5.1900303

Conflict of Interest: SD and HT received an investigator-initiated research grant from Pfizer.

The remaining authors declare that the research was conducted in the absence of any commercial or financial relationships that could be construed as a potential conflict of interest.

Publisher's Note: All claims expressed in this article are solely those of the authors and do not necessarily represent those of their affiliated organizations, or those of the publisher, the editors and the reviewers. Any product that may be evaluated in this article, or claim that may be made by its manufacturer, is not guaranteed or endorsed by the publisher.

Copyright © 2022 Willen, Ekinci, Cuypers, Theeten and Desmet. This is an open-access article distributed under the terms of the Creative Commons Attribution License (CC BY). The use, distribution or reproduction in other forums is permitted, provided the original author(s) and the copyright owner(s) are credited and that the original publication in this journal is cited, in accordance with accepted academic practice. No use, distribution or reproduction is permitted which does not comply with these terms.



Diverse Mechanisms of Protective Anti-Pneumococcal Antibodies

Aaron D. Gingerich¹ and Jarrod J. Mousa^{1,2,3*}

¹ Center for Vaccines and Immunology, College of Veterinary Medicine, University of Georgia, Athens, GA, United States,

² Department of Infectious Diseases, College of Veterinary Medicine, University of Georgia, Athens, GA, United States,

³ Department of Biochemistry and Molecular Biology, Franklin College of Arts and Sciences, University of Georgia, Athens, GA, United States

OPEN ACCESS

Edited by:

Kaifeng Wu,
Zunyi Medical University Third Affiliated
Hospital, China

Reviewed by:

Xue Mei Zhang,
Chongqing Medical University, China
Jorge Eugenio Vidal,
University of Mississippi Medical
Center, United States

*Correspondence:

Jarrod J. Mousa
jarrod.mousa@uga.edu

Specialty section:

This article was submitted to
Molecular Bacterial Pathogenesis,
a section of the journal
Frontiers in Cellular and
Infection Microbiology

Received: 29 November 2021

Accepted: 11 January 2022

Published: 28 January 2022

Citation:

Gingerich AD and Mousa JJ (2022)
Diverse Mechanisms of Protective
Anti-Pneumococcal Antibodies.
Front. Cell. Infect. Microbiol. 12:824788.
doi: 10.3389/fcimb.2022.824788

The gram-positive bacterium *Streptococcus pneumoniae* is a leading cause of pneumonia, otitis media, septicemia, and meningitis in children and adults. Current prevention and treatment efforts are primarily pneumococcal conjugate vaccines that target the bacterial capsule polysaccharide, as well as antibiotics for pathogen clearance. While these methods have been enormously effective at disease prevention and treatment, there has been an emergence of non-vaccine serotypes, termed serotype replacement, and increasing antibiotic resistance among these serotypes. To combat *S. pneumoniae*, the immune system must deploy an arsenal of antimicrobial functions. However, *S. pneumoniae* has evolved a repertoire of evasion techniques and is able to modulate the host immune system. Antibodies are a key component of pneumococcal immunity, targeting both the capsule polysaccharide and protein antigens on the surface of the bacterium. These antibodies have been shown to play a variety of roles including increasing opsonophagocytic activity, enzymatic and toxin neutralization, reducing bacterial adherence, and altering bacterial gene expression. In this review, we describe targets of anti-pneumococcal antibodies and describe antibody functions and effectiveness against *S. pneumoniae*.

Keywords: *Streptococcus pneumoniae*, monoclonal antibody, opsonophagocytic, immune evasion, pneumococcal vaccination

INTRODUCTION

Streptococcus pneumoniae is a gram-positive opportunistic bacterial pathogen that colonizes the upper respiratory tract, and is a leading cause of bacterial infections worldwide (Weiser et al., 2018), (Denny and Loda, 1986). Bacterial colonization is a precursor to pneumococcal disease, which can manifest as otitis media, pneumonia, septicemia and meningitis. *S. pneumoniae* is found in up to 27-65% of children and <10% of adults in a commensal carriage state (Yahiaoui et al., 2016). In 2000, it was estimated that *S. pneumoniae* was responsible for over 800,000 deaths in children annually (O'Brien et al., 2009). Due to the continued high burden of disease despite an effective vaccine, *S. pneumoniae* was designated a priority pathogen by the World Health Organization in 2017 (WHO, 2017). Multiple colonization events in the lifetime of an individual result in serum antibody responses to the capsular polysaccharide (CPS) (Weinberger et al., 2008) and protein antigens (McCool et al., 2002; Zhang et al., 2006; Prevaes et al., 2012; Turner et al., 2013). The CPS is a critical virulence factor for *S. pneumoniae*

survival during invasive disease, and the CPS can inhibit the innate immune response *via* inhibition of phagocytosis, preventing recognition of the bacteria by host receptors, and evasion of neutrophil extracellular traps (Hyams et al., 2010). Each pneumococcal serotype, of which 100 serotypes have been identified, has a distinct CPS that varies in its biochemical and antigenic structure (Ganaie et al., 2020). The most effective preventative measure against pneumococcal infection is vaccination with either a 23-valent pneumococcal polysaccharide vaccine (PPSV23) or a multivalent pneumococcal conjugate vaccine (PCV7, PCV10, PCV13, PCV15, or PCV20). While the CPS is the primary antigen in both vaccines, the CPS antigens in PCV-based vaccines are linked to a carrier protein to induce T-dependent antibody responses leveraging the hapten-carrier effect. However, due to the limited serotypes included in PCVs, protection is incomplete, and this has caused an increase of non-vaccine serotypes in carriage and disease (Klugman, 2009; von Gottberg et al., 2014). Nonencapsulated strains of *S. pneumoniae* are also able to colonize the nasopharyngeal tract and are not affected by current vaccines (Keller et al., 2016). These strains have unique surface proteins that allow for colonization and virulence in the absence of the CPS (Keller et al., 2016).

In light of limited serotype coverage, increasing prevalence of non-vaccine serotypes, and increasing antibiotic resistance among non-vaccine serotypes, conserved protein antigens and other molecules have also been studied as potential vaccine candidates, as these would presumably induce broadly reactive antibodies that would be effective against a greater number of serotypes than CPS-based vaccines (Daniels et al., 2016). Multiple antigens have been tested in animal models and clinical trials, including the toxin pneumolysin (Ply) (Kamtchoua et al., 2013; Odutola et al., 2017; Hammitt et al., 2019), pneumococcal surface protein A (PspA) (Briles et al., 2000b; Nabors et al., 2000; Frey et al., 2013), pneumococcal surface adhesin A (PsaA) (Wang et al., 2010; Moffitt and Malley, 2016), pneumococcal choline binding protein A (PcpA) (Glover et al., 2008; Verhoeven et al., 2014; Xu et al., 2017), pneumococcal histidine triad protein (PhtD) (Denoël et al., 2011b; Kaur et al., 2014; André et al., 2021), Phosphorycholine (PC) (Trolle et al., 2000; Tanaka et al., 2007), Neuraminidase (Nan) (Janesch et al., 2018) and choline binding proteins (CbpA, CbpG) (Mann et al., 2006; Hernani et al., 2011; Ricci et al., 2011). Antibodies are a key component of pneumococcal immunity, and their mechanisms of action are important to understand for vaccine design efforts (Figure 1 and Table 1). Here we review anti-pneumococcal antibodies, including antibody targets and known mechanisms of action.

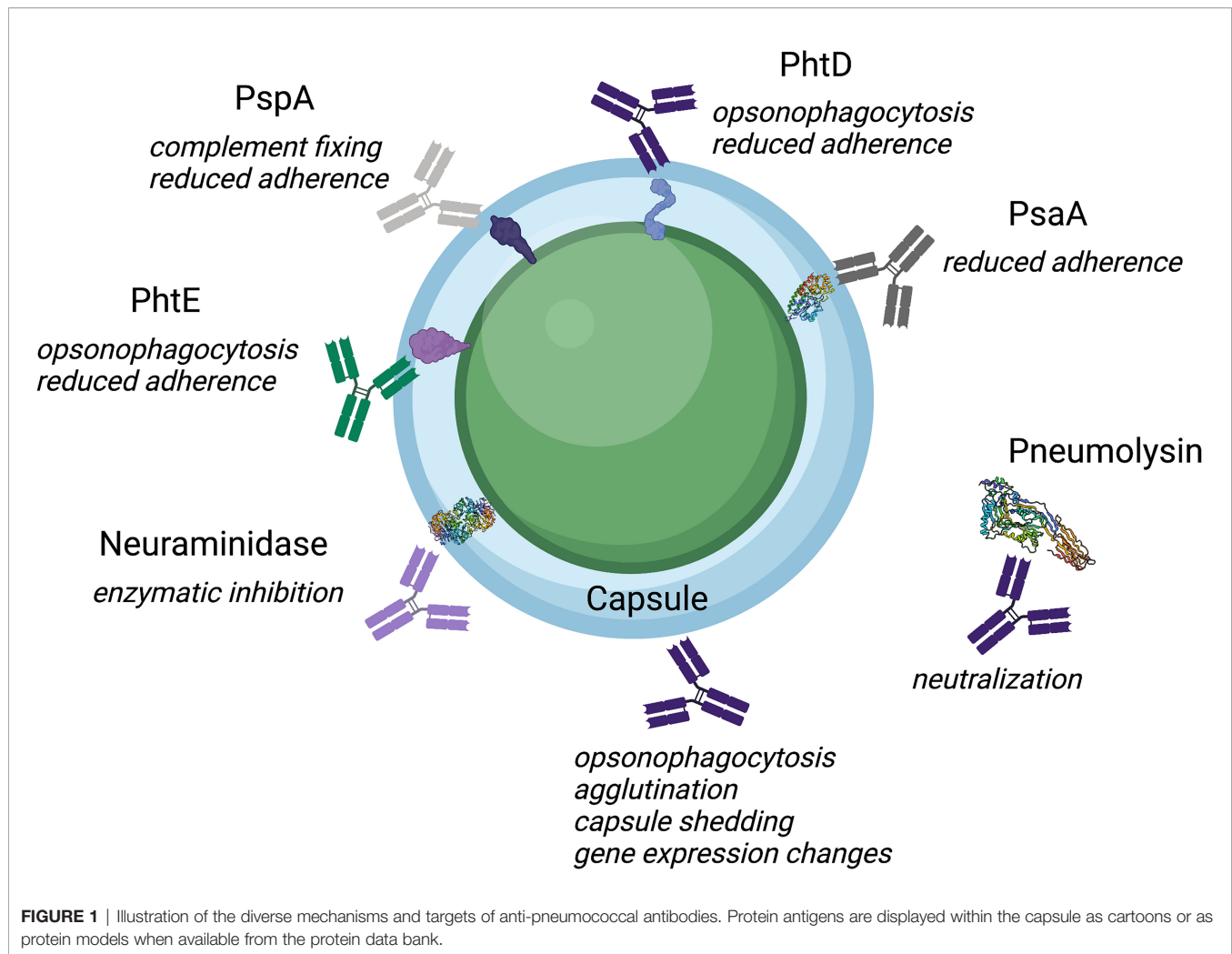
Antibodies to the Pneumococcal Capsular Polysaccharide

One of the most important virulence factors of *S. pneumoniae* is the CPS, which encases the bacterium and is the defining antigen for serotype identification. Currently, 100 distinct capsule serotype structures have been identified, with at least 30 serotypes being responsible for invasive pneumococcal disease (Luck et al., 2020). The CPS is typically negatively charged, which

allows the bacteria to avoid mucous entrapment and enables colonization of the nasopharynx (Magee and Yother, 2001; Nelson et al., 2007; Li et al., 2013). As the CPS encases the bacterium, it protects deeper antigenic structures, and inhibits the binding of immunoglobulins, complement components, and C-reactive protein (Weiser et al., 2018). The CPS also reduces opsonization with C3b/iC3b, thereby impairing the receptors of phagocytic cells from interacting with antibody Fc regions (Abeyta et al., 2003; Hyams et al., 2010). It has been hypothesized that the CPS also protects bacteria from entrapment by neutrophil extracellular traps (Wartha et al., 2007). Due to the vital importance of the CPS to bacterial survival and virulence, it has long been a therapeutic target. PPSV23 and PCV vaccines have been approved for use in humans and have been widely effective. However, there has been a rise in the incidence of nonvaccine serotypes, and serotypes 3 and 19A have also persisted despite vaccination efforts (Wantuch and Avci, 2018; Linley et al., 2019).

A key function of CPS targeting vaccines is to elicit antibodies that have opsonophagocytic activity, which has been well defined to be a predictor of protection (Poehling et al., 2006; Ekström et al., 2007; Goldblatt et al., 2010; Prymula et al., 2011; Dagan et al., 2013; Lee et al., 2014) (Figure 2). Indeed, *in vitro* opsonophagocytic assays are the gold standard for measuring antibody-mediated immunity (Romero-Steiner et al., 1997; Song et al., 2013; Toh et al., 2021). In addition, antibody agglutination activity is a correlate of protection (Bull, 1915), as the establishment of colonization by *S. pneumoniae* is a critical first step in disease pathogenesis, and antibody agglutinating activity inhibits colonization (Bogaert et al., 2004; Simell et al., 2012) (Figure 2). For example, CPS-specific antibodies from nasal washes of vaccinated individuals are important for protection against colonization (Mitsi et al., 2017), and human mAbs targeting the CPS can have both opsonophagocytic and agglutination activity *in vitro* (Babb et al., 2021).

While a majority of described antibodies targeting the CPS rely on increasing opsonophagocytic and agglutinating activity to offer protection, nonopsonic antibodies to the pneumococcal CPS can also offer protection. The first study to discover this phenomenon found that a mouse IgG₁, mAb 1E2, targeting the serotype 3 CPS was unable to opsonize and kill bacteria *in vitro* yet was protective *in vivo* (Tian et al., 2009). In several follow up studies, mAb 1E2 was shown to alter the expression of over 50 genes (Doyle et al., 2021), which included genes involved in quorum sensing and increased fratricide (*Yano* et al., 2011). Upon interaction with mAb 1E2, iron uptake (*piuB* gene) was increased, sensitivity to oxidative stress (*dpr* gene) was amplified, and rapid capsule shedding was observed (Doyle et al., 2021) (Figure 2). mAb 1E2 also reduces colonization in mice (Doyle and Pirofski, 2016). A mechanistic study on mAb 1E2 revealed that neutrophils were not needed for its protective efficacy (Tian et al., 2009), but macrophages were required (Sarah et al., 2012). These studies demonstrate that anti-CPS antibody functions beyond opsonophagocytic and agglutination activity can protect against pneumococcal disease, and such functions may be important to consider in current and future vaccines.



Serotype specific IgG targeting the CPS is sufficient to protect against the homologous serotype, and additional antibody isotypes beyond IgG can offer protection. Serotype 8 specific mAbs NAD (an IgA) and D11 (an IgM) have been examined *in vitro*, and NAD was shown to increase complement deposition (**Figure 2**) whereas D11 was not, and neither NAD nor D11 promoted significant neutrophil mediated killing in an opsonophagocytic assay (Burns et al., 2003). In the presence of bacteria, complement, and D11 or NAD, a decrease in IL-8 secretion by neutrophils was observed (Burns et al., 2003). Both the D11 and NAD antibodies were found to be protective against infection in the mouse model (Burns et al., 2003). Additional studies with D11 revealed treated mice had significantly less IFN- γ , MIP-2, IL-12, MCP-1/JE, and TNF- α compared to control mice (Burns et al., 2005). mAb A7, a serotype 3-specific IgM, induced a decrease in keratinocyte-derived chemokine, IL-6 and macrophage inflammatory protein-2 in mAb treated mice, similar to levels seen in penicillin treated mice (Fabrizio et al., 2007). Together these studies demonstrate that the connection between antibody-mediated protection and immunomodulation plays a key role in protection *in vivo* and should be further explored.

Antibodies to Pneumococcal Proteins

Pneumococcal Surface Protein A

While vaccine-induced CPS-specific antibodies can protect against colonization with vaccine-included serotypes, natural colonization leads the induction of both CPS-specific antibodies and anti-protein antibodies (Wilson et al., 2017). Pneumococcal surface protein A (PspA) is one of the most prevalent antigens on the surface of *S. pneumoniae* and plays a major role in protective immunity (Khan and Jan, 2017). PspA aids the bacteria in evading the bactericidal activity of neutrophil extracellular traps (Martinez et al., 2019), inhibits complement (Tu et al., 1999; Ren et al., 2004; Ren et al., 2012) by reducing the amount of C3 that is deposited on the bacteria (Mukerji et al., 2012), and binds lactoferrin, which likely blocks the active site of apolactoferrin responsible for bacterial killing (Shaper et al., 2004; Bitsakis et al., 2012; Mirza et al., 2016). PspA is classified into 3 families with 6 clades based on sequence similarities in the variable N-terminal α -helical region (Hollingshead et al., 2000). Numerous studies have demonstrated the protective effects of PspA-based vaccines, which lead to increased survival and decreased bacterial

TABLE 1 | Antigens evaluated in clinical trials and animal models.

Antigen	Antigen function	Antibody function	Tested as Vaccine?	Species tested	Vaccine status	Protection	Antibody Therapy	Protection	
Capsular polysaccharide	Inhibition of phagocytosis	Opsonophagocytosis	Yes	Murine	FDA approved	Yes	Yes	Yes	Burns et al., 2003; Burns et al., 2005; Fabrizio et al., 2007; Tian et al., 2009; Yano et al., 2011; Sarah et al., 2012; Doyle and Pirofski, 2016; Keller et al., 2016; Mitsi et al., 2017; Babb et al., 2021; Doyle et al., 2021
	Blocking host receptors	Agglutination		Human					
Phosphorylcholine	Evasion of NETs	Capsule shedding	Yes	Murine	Murine model	Yes	Yes	Yes	Wallick et al., 1983; Briles et al., 1992; Fischer et al., 1995; Trolle et al., 2000; Tanaka et al., 2007
	Bacterial adherence	Gene expression							
PspA	Inhibition of complement deposition	Increase C3 deposition	Yes	Murine	Phase 1	Protection not yet assessed in humans.	Yes	Yes	Wu et al., 1997; Briles et al., 2000b; Briles et al., 2000c; Nabors et al., 2000; Ferreira et al., 2006b; Daniels et al., 2010; Bitsakis et al., 2012; Frey et al., 2013; Piao et al., 2014; Nagano et al., 2018; Nakahashi-Ouchida et al., 2021
	Binding of lactoferrin	Inhibition of lactoferrin binding		Human					
PsaA	Evasion of NETs	Enhancing NETs	Yes	Murine	Phase 1	Yes, in animal models	ND	ND	Talkington et al., 1996; Briles et al., 2000a; Miyaji et al., 2001; Romero-Steiner et al., 2003; Oliveira et al., 2006; Pimenta et al., 2006; Romero-Steiner et al., 2006; Wang et al., 2010
	ABC transporter of Zn ²⁺ and Mn ²⁺	Reduced adherence		Human					
PhtD	Attachment to epithelial cells	Protection against oxidative stress	Yes	Murine	Phase 1/2	Yes, in animal models. Did not reduce colonization or otitis media in humans	Yes	Yes	Wizemann et al., 2001; Denoël et al., 2011a; Denoël et al., 2011b; Godfroid et al., 2011; Bologa et al., 2012; Khan and Pichichero, 2012; Seiberling et al., 2012; Plumptre et al., 2013b; Ravinder et al., 2014; Berglund et al., 2014; Leroux-Roels et al., 2014; Odutola et al., 2017; Papastamatiou et al., 2018; Visan et al., 2018; Hammitt et al., 2019; André et al., 2020; Huang et al., 2021
	Inhibition of complement deposition	Increase C3 deposition		Macaque					
Neuraminidase	Zn ²⁺ acquisition	Reduced adherence	No	ND	ND	ND	Yes	No	Janesch et al., 2018
	Adherence to epithelial cells	Opsonophagocytosis		Human					
Pneumolysin	Promotes biofilm formation	Enzymatic inhibition	Yes	ND	ND	ND	Yes	No	Janesch et al., 2018
	Cytotoxic activity	Neutralization		Human					
Pneumolysin	Inhibition of complement deposition	Neutralization	Yes	Murine	Phase 1/2	Yes in animal models. Did not reduce colonization or otitis	Yes	Yes	García-Suárez et al., 2004; Ferreira et al., 2006a; Sanders et al., 2010; Lu et al., 2014; Mann et al., 2014; Hermand et al., 2017; Odutola et al., 2017; Hammitt et al., 2019; Petukhova
	Biofilm formation	Neutralization		Macaque					

(Continued)

TABLE 1 | Continued

Antigen	Antigen function	Antibody function	Tested as Vaccine?	Species tested	Vaccine status	Protection	Antibody Therapy	Protection	
CbpG	Cleavage of casein and fibronectin	Opsonophagocytosis	Yes	Murine	Murine model	media in humans Yes	Yes	Yes	et al., 2020; Thanawastien et al., 2021 Mann et al., 2006; Kazemian et al., 2018
PcpA	Adherence to epithelial cells	Increase C3 deposition Reduced adherence Opsonophagocytosis	Yes	Murine Human	Phase 1	Protection not yet assessed in humans. Yes, in animal models	Yes	Yes	Glover et al., 2008; Verhoeven et al., 2014; Brooks et al., 2015; Ochs et al., 2016; Xu et al., 2017; Visan et al., 2018
PspC/CbpA	Adherence to epithelial cells Binding complement factor H, C4BP, and vitronectin	Increase C3 deposition Block fH binding Opsonophagocytosis	Yes	Murine	Murine model	Protective against certain serotypes	Yes	Protective when used with other antibodies	Cao et al., 2007; Lu et al., 2008; Ferreira et al., 2009; Hernani et al., 2011; Ricci et al., 2011; Mann et al., 2014; Chen et al., 2015

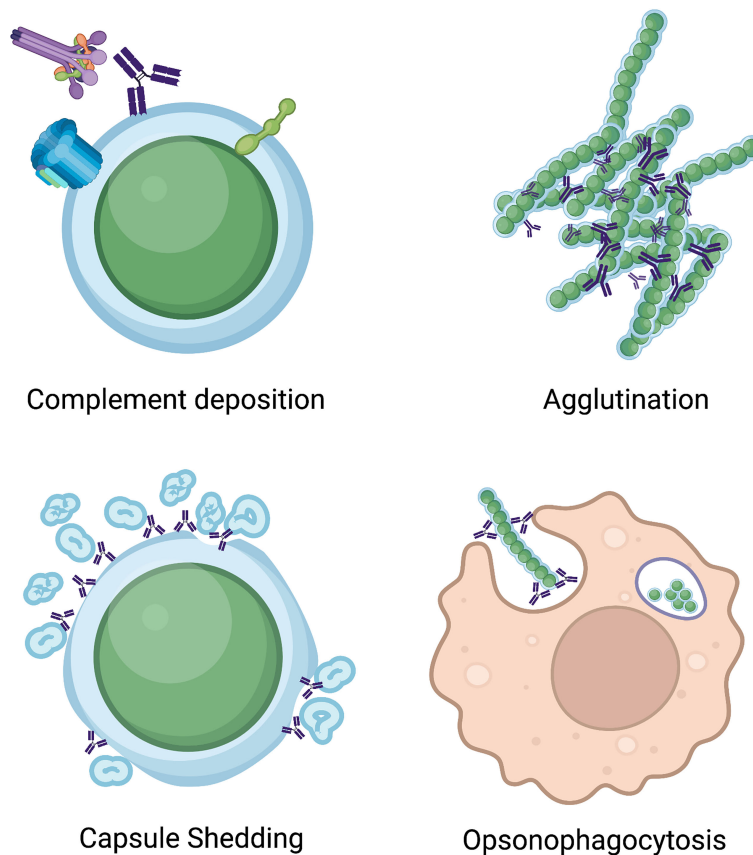


FIGURE 2 | Illustration of mechanisms of anti-pneumococcal antibodies. Antibodies binding pneumococcal antigens can increase complement deposition, leading to formation of the membrane attack complex, induce bacterial agglutination, cause capsule shedding, and increase opsonophagocytic activity of phagocytic cells.

burden in animal models (Wu et al., 1997; Briles et al., 2000c; Ferreira et al., 2006b; Daniels et al., 2010; Piao et al., 2014; Nagano et al., 2018; Nakahashi-Ouchida et al., 2021). It has also been demonstrated that antibodies targeting PspA can have their function enhanced *via* targeting activating FcγRI with fusion proteins consisting of PspA and IgG2a Fc, which then is able to enhance PspA-specific immune responses (Wiedinger et al., 2020). Another study demonstrated that by fusing a humanized single-chain antibody component (in which the variable domain binds to FcγRI) to PspA, protection could be achieved in the absence of adjuvant (Bitsaktsis et al., 2012). This vaccine could be enhanced further by adding an additional FcγRI binding moiety to the vaccine mentioned above (Kumar et al., 2020). PspA vaccines have advanced to human clinical trials and demonstrated safety and robust antibody responses (Briles et al., 2000b; Nabors et al., 2000; Frey et al., 2013), however, concerns exist about using full length PspA due to its sequence homology with human cardiac myosin (Ginsburg et al., 2012).

Vaccine derived antibodies targeting PspA mainly function by increasing complement C3 deposition leading to increased phagocytosis. Passive immunization with an anti-PspA mAb XiR278 protected mice from infection at 10x the LD₅₀ when given before or shortly after pneumococcal infection (Swiatlo et al., 2003). Another study generated broadly reactive anti-PspA mouse mAbs, one of which, mAb 140H1, bound to 98% of the 48 strains tested, which encompasses the clinically relevant PspA clades 1-5 (Kristian et al., 2016). mAb 140H1 was shown to be protective in *in vivo* mouse sepsis and pneumonia models, including 24 hrs after intranasal infection (Kristian et al., 2016). This study also demonstrated that mAb 140H1 and others were able to increase C3 deposition on the surface of bacteria and increase bacterial killing in opsonophagocytic killing assays. This suggests that the complement deposition induced by these anti-PspA mAbs facilitates phagocytic uptake and killing by neutrophils (Kristian et al., 2016). In support of this observation, increased C3 deposition on the surface of bacteria *via* anti-PspA mAb binding has been demonstrated in numerous studies (Ren et al., 2004; Ren et al., 2012; Bitsaktsis et al., 2012; Goulart et al., 2013; Khan et al., 2015; Genschmer et al., 2019; Wiedinger et al., 2020). Additional functions for anti-PspA mAbs include inhibition of lactoferrin by anti-PspA mAbs (Bitsaktsis et al., 2012), and enhanced trapping and killing of *S. pneumoniae* by neutrophil extracellular traps (Martinez et al., 2019).

Pneumococcal Surface Adhesin A

The pneumococcal surface adhesin A (PsaA) is a multifunctional surface exposed lipoprotein that is found in all known serotypes (Sampson et al., 1997). PsaA is an ABC transporter binding protein that is capable of transporting Zn²⁺ and Mn²⁺ (Dintilhac et al., 1997; Lawrence et al., 1998; Jakubovics and Jenkinson, 2001; W et al., 2004). PsaA can also facilitate attachment to host cells (Sampson et al., 1994; Novak et al., 2000; Romero-Steiner et al., 2003; McAllister et al., 2004; Romero-Steiner et al., 2006) and protect against oxidative stress (Tseng et al., 2002). The binding receptor for PsaA is E-cadherin, the cell-cell junction protein found in respiratory epithelial cells (Anderton et al.,

2007). PsaA employs multiple effects on host cells including cytoplasmic foaming, excessive vacuolation, and nuclear structure changes leading to colonization and internalization of the bacteria (Anderton et al., 2007). It was recently discovered that PsaA interacts with human Annexin A2 (ANXA2) (Hu et al., 2021). Immunization studies with recombinant PsaA showed a significant reduction in recovery time against pneumococcal carriage (Briles et al., 2000a; Miyaji et al., 2001; Oliveira et al., 2006; Pimenta et al., 2006; Wang et al., 2010). However when used in a systemic challenge model those protective effects were either minimal (Talkington et al., 1996) or not significant (Wang et al., 2010). Anti-PsaA antibodies can reduce the ability of *Streptococcus pneumoniae* to bind to Detroit 562 cells (pharyngeal epithelial cells) *in vitro* (Romero-Steiner et al., 2003; Romero-Steiner et al., 2006).

Pneumococcal Histidine Triad Proteins

The pneumococcal histidine triad proteins are a group of four proteins (PhtA, PhtB, PhtD, PhtE) that are present on the surface of *S. pneumoniae* (Adamou et al., 2001). PhtD is the most conserved of the group with 91-98% identity across strains isolated from cases of invasive disease (Yun et al., 2015). While the function of PhtD is not fully understood, it is important for attachment to respiratory epithelial cells *in vitro* (Khan and Pichichero, 2012; Plumptre et al., 2013a; Kallio et al., 2014). Additionally, PhtD has been shown *in vitro* to aid in Zn²⁺ acquisition and ultimately bacterial homeostasis as Zn²⁺ is a vital nutrient (Ogunniyi et al., 2009; Eijkelkamp et al., 2016). PhtD can also reduce complement deposition *via* Factor H (FH) (Ogunniyi et al., 2009). Several studies have demonstrated that immunization with PhtD or other Pht antigens elicits antibodies that protect against sepsis, pneumonia, and reduced colonization in animal models (Wizemann et al., 2001; Denoël et al., 2011a; Denoël et al., 2011b; Godfroid et al., 2011; Plumptre et al., 2013b; Ravinder et al., 2014; Papastamatiou et al., 2018; André et al., 2020). In a non-human primate model, vaccination with a combined PhtD/pneumolysin formulation was protective against lethal challenge (Denoël et al., 2011b). PhtD-based vaccine candidates have advanced to clinical trials, and several trials have demonstrated that immunization with PhtD was well tolerated and immunogenic (Bologa et al., 2012; Khan and Pichichero, 2012; Seiberling et al., 2012; Berglund et al., 2014; Leroux-Roels et al., 2014; Hammitt et al., 2019). However in a clinical trial in 6-12 month old infants, vaccination with PhtD/dPly/PCV13 did not show an increase in vaccine efficacy against acute otitis media compared to the standard PCV13 vaccine (Hammitt et al., 2019). In an additional study, a PHiD-CV/dPly/PhtD vaccine containing a 10-valent polysaccharide conjugate (10VT) combined with pneumolysin toxoid and pneumococcal histidine triad protein D was immunogenic but no improvement in pneumococcal carriage in infants was seen regardless of dose or schedule (Odutola et al., 2017). Vaccine induced PhtD antibodies were shown to increase complement C3b deposition on the bacterial surface and increase phagocytosis.

Antibodies targeting PhtD have demonstrated protection in preclinical animal models. Anti-PhtD polyclonal antibodies are

able to reduce colonization (Ravinder et al., 2014) and protect against lethal sepsis (Brookes et al., 2015) in a passive transfer mouse model. The use of anti-PhtD mAbs has also been explored. Human anti-PhtD mAbs are protective against both sepsis and pneumonia models of infection in mice when given prior to infection (Huang et al., 2021). Additionally, administration of an anti-PhtD mAb (PhtD3) 24 hours post infection was able to rescue mice from infection (Huang et al., 2021). An *in vivo* mechanism for anti-PhtD antibodies has not been fully elucidated, however, a recent study demonstrated that when depleting complement *via* cobra venom factor the protective effect of anti-PhtD antibodies was lost (Visan et al., 2018). Furthermore, depletion of macrophages but not neutrophils also resulted in loss of protection (Visan et al., 2018). The mechanism of anti-PhtD antibodies has been tested *in vitro* where it was observed that antibodies are able to inhibit bacterial attachment to epithelial cells (Kallio et al., 2014; Kaur et al., 2014), promote complement deposition (André et al., 2021) (Visan et al., 2018), and increase bacterial phagocytosis (Visan et al., 2018; Malekan et al., 2020; André et al., 2021; Huang et al., 2021).

Neuraminidase

S. pneumoniae utilizes neuraminidases for sugar acquisition, and these neuraminidases are a key virulence factor of which three have been described: NanA, NanB and NanC (Cámara et al., 1994; Berry et al., 1996; Xu et al., 2011; Hammond et al., 2021). These neuraminidases cleave terminal sialic acids providing essential nutrients (King et al., 2006; Burnaugh et al., 2008), interfere with C3 deposition (Dalia et al., 2010), promote biofilm formation (Parker et al., 2009), and are required for adherence and invasion of brain endothelial cells (Uchiyama et al., 2009). Due to the multitude of essential functions for *S. pneumoniae* these neuraminidases provide an attractive target for therapeutic antibodies. Utilizing an *in vitro* assay with differentiated airway epithelial cells, it was shown that anti-neuraminidase mAbs can preserve the terminal epithelial sugar composition during *S. pneumoniae* infection leading to a 10-20 fold decrease in bacterial growth compared to control mAbs (Janesch et al., 2018). Similar effects were seen in an *in vivo* mouse model, where anti-neuraminidase mAbs led to a reduction in desialylation of the airways (Janesch et al., 2018). However, in an acute murine pneumonia treatment with the anti-neuraminidase mAbs there was no effect on survival, lung burden, or host inflammatory responses (Janesch et al., 2018). While anti-neuraminidase mAbs exert an inhibitory effect on the neuraminidases, this does not lead to a positive effect on mortality or bacterial burden in a murine model of acute pneumonia (Janesch et al., 2018).

Pneumolysin

The virulence factor pneumolysin (Ply) is a cholesterol-dependent cytolysin that plays an essential role in pneumococcal disease. Pneumolysin lacks a secretory signal and is localized in the cytoplasm or the cell wall, and is released during autolysis and bacterial growth (García-Suárez et al., 2007; Price and Camilli, 2009). Pneumolysin exhibits a

wide range of effects, including cytotoxic activity (Steinfert et al., 1989; Rubins et al., 1992; Rayner et al., 1995) to host cells, increasing bacterial penetration (Ring et al., 1998; Zysk et al., 2001), increasing inflammation (Feldman et al., 1991; Cockeran et al., 2001; Yoo et al., 2010; Subramanian et al., 2019), blocking complement (Paton et al., 1984; Mitchell et al., 1991; Rubins et al., 1995; Alcantara et al., 2001), and being a vital factor in biofilm formation and pneumococcal transmission (Shak et al., 2013; Marks et al., 2014; Zafar et al., 2017). Due to its conserved nature between strains and serotypes (Han and Zhang, 2019), (Kancierski and Möllby, 1987) pneumolysin has been well studied as a therapeutic target. Numerous studies investigating antibodies targeting Ply have demonstrated their protective efficacy. Ply renders platelets nonfunctional and inhibits platelet-thrombus formation in whole blood, and an *in vitro* study demonstrated that anti-Ply antibodies are able to neutralize Ply and rescue platelet function (Jahn et al., 2020). Murine derived anti-pneumolysin mAbs were able to neutralize its cytolytic activity and inhibit binding of pneumolysin to cholesterol (Kucinskaite-Kodze et al., 2020). In a recent study, anti-pneumolysin human polyclonal antibodies did not decrease adherence of TIGR4 to A549 cells *in vitro*, however, in an *in vivo* murine model, passive transfer of anti-pneumolysin antibodies did show a significant decrease in colonization of TIGR4 (Kaur et al., 2014). Biofilm formation plays a key role in pneumococcal colonization and Ply is important for biofilm formation, independent of its cytolytic activity (Shak et al., 2013). High serum levels of anti-Ply antibodies have been correlated to delayed colonization in infants (Holmlund et al., 2006; Francis et al., 2009), and low anti-Ply antibodies may be a predisposing factor in developing pneumococcal pneumonia (Huo et al., 2004). Inactive Ply mutants are able to induce antibodies that neutralize Ply *via* an *in vitro* anti-hemolytic assay (Kamtchoua et al., 2013). Several studies have demonstrated that immunization with Ply generates anti-pneumolysin antibodies that are protective (Sanders et al., 2010; Lu et al., 2014; Mann et al., 2014; Hermand et al., 2017; Petukhova et al., 2020; Thanawastien et al., 2021). The direct use of anti-pneumolysin mAbs was protective when administered intravenously in a lethal intranasal model of infection in mice (García-Suárez et al., 2004). However, a recent study showed that using a DNA vaccine vector, low levels of anti-pneumolysin antibodies were generated that were not protective in a septic challenge model in mice (Ferreira et al., 2006a). In human clinical trials, anti-pneumolysin antibodies derived from vaccination are able to neutralize pneumolysin (Kamtchoua et al., 2013) but no differences were seen in colonization, bacterial load, or clearance due to the vaccine compared to controls (Odutola et al., 2017; Hammitt et al., 2019). While antibodies targeting Ply have been shown to function through the neutralization of its cytolytic activity, antibody inhibition of other Ply functions such as adherence, complement blocking, and biofilm formation have not been demonstrated.

Choline Binding Proteins

The virulence factor CbpG is an adhesin with putative serine protease activity in both colonization and sepsis (Galán-Bartual

et al., 2015). The protease portion of CbpG is able to cleave casein and fibronectin, and enzymatic activity is able to remain intact regardless of being surface bound or secreted (Mann et al., 2006). Another closely related antigen, CbpM, was demonstrated to bind to fibronectin facilitating *S. pneumoniae* attachment to epithelial cells (Afshar et al., 2016). Vaccination with recombinant CbpG induces antibodies that are able to confer protection against colonization to a limited degree and provide robust protection against systemic infection (Mann et al., 2006). In another study, mice immunized with CbpG or CbpM and challenged *via* intraperitoneal injection had a significant increase in protection and clearance of bacteria as early as 48 hours post infection (Kazemian et al., 2018). Serum containing anti-CbpG and anti-CbpM antibodies from the aforementioned study were also found to increase neutrophil mediated opsonophagocytosis (Kazemian et al., 2018). Finally, a passive transfer model using anti-CbpG and anti-CbpM antibodies in mice demonstrated a protective effect against *S. pneumoniae* challenge although not as robust as that seen in immunization studies with the antigens (Kazemian et al., 2018). Currently, antibodies targeting CbpG and CbpM have been shown to increase neutrophil mediated opsonophagocytosis, but other functions of these antibodies need to be further elucidated.

PcpA is another member of the choline binding protein family that is under the control of the manganese-dependent regulator *psaR*, and high concentrations of Mn suppress expression (Johnston et al., 2006). Immunization with PcpA elicits antibody responses that provide protection against lung and systemic infections (Glover et al., 2008; Verhoeven et al., 2014; Xu et al., 2017), but do not protect against colonization in the nasopharynx (Sánchez-Beato et al., 1998). In phase I human trials PcpA was used in a trivalent recombinant vaccine containing PhtD, PlyD1 and PcpA, the vaccine demonstrated immunogenicity with an increase in antibody concentration, however protection was not assessed (Brooks et al., 2015). Passive transfer of human anti-PcpA polyclonal antibodies in a murine challenge model were able to mediate protection (Ochs et al., 2016). The adherence effect of PcpA on the surface of bacteria was successfully blocked by utilizing Fab fragments targeting PcpA, which blocked adherence of *S. pneumoniae* to human epithelial cells *in vitro* (Khan et al., 2012). Macrophages but not neutrophils were required for anti-PcpA antibody protective efficacy in a passive transfer model (Visan et al., 2018). Additionally, anti-PcpA antibodies are able to enhance complement C3b deposition (Visan et al., 2018), increase phagocytosis and block adherence of the bacteria.

CbpA/PspC is involved in the adhesion and colonization of the nasopharynx and in the binding of pIgR (Kerr et al., 2006; Orihuela et al., 2009). PspC is important in the recruitment and binding of complement factor H (Dave et al., 2001; Hammerschmidt et al., 2007; Ricci et al., 2011), evading complement by binding of C4BP (Dieudonné-Vatran et al., 2009; Haleem et al., 2019), and prevention of terminal complement complex mediated lysis by binding vitronectin (Voss et al., 2013; Kohler et al., 2015). Due to its role in

virulence on multiple fronts, it is a key immunogenic target, however, while it is present in all clinically relevant serotypes, it is quite variable making it a difficult target for vaccination efforts (Brooks-Walter et al., 1999; Iannelli et al., 2002; Georgieva et al., 2018). This high degree of variability has led to mixed results when PspC has been used for immunization. Studies have demonstrated that immunization with PspC alone (Hernani et al., 2011; Ricci et al., 2011) or a multivalent approach with other pneumococcal antigens PspA and/or Ply are protective (Cao et al., 2007; Mann et al., 2014; Chen et al., 2015). However, other studies have shown that immunization with PspC is not protective (Lu et al., 2008; Ferreira et al., 2009; Ricci et al., 2011). These different results are likely due to the high variability of PspC between different serotypes. Passive immunization with anti-PspC antibodies has demonstrated protection (Mann et al., 2014), however, once again mixed results have been seen where passive immunization with anti-PspC antibodies alone were not protective but showed a protective and synergistic effect once administered with anti-PspA and anti-ClpB antibodies (Cao et al., 2007). PspC antibodies can increase complement deposition (Ricci et al., 2011), interfere with fH binding (Ricci et al., 2011; Glennie et al., 2016) and promote opsonophagocytic killing of *S. pneumoniae* (Ricci et al., 2011; Georgieva et al., 2018) *in vitro*.

Other Antigens Phosphorylcholine

S. pneumoniae contains phosphorylcholine (PC) also known as ChoP, a structural component that is linked to bacterial adherence *via* the platelet activating factor receptor (PAF-R) (Cundell et al., 1995; Iuchi et al., 2019). Several key virulence proteins such as the CBPs and PspA are attached to the cell wall *via* PC (Rosenow et al., 1997). PC-dependent binding to the epithelial receptor asialo-GM1 has also been demonstrated (Sundberg-Kövamees et al., 1996). PC expression is essential to the bacteria as mutant bacteria that do not express PC are unable to colonize the upper respiratory tract in mice and are less virulent in murine sepsis models (Kharat and Tomasz, 2006). The C-reactive protein (CRP) recognizes PC and initiates the classical complement pathway increasing phagocytosis of *S. pneumoniae* (Mold et al., 1982). Due to PC's important role in adherence and association with key proteins, it offers a promising therapeutic target. Early on in the field it was demonstrated that anti-PC antibodies in normal mouse serum provide protection against intravenous pneumococcal challenge (Briles et al., 1981). Anti-PC mAbs were also found to be protective against several different serotypes in a murine infection model (Briles et al., 1992). One study demonstrated that pretreating *S. pneumoniae* with an anti-PC mAb reduced the adherence of *S. pneumoniae* with high levels of PC but not low levels of PC in both *in vitro* and *in vivo* models (Iuchi et al., 2019). Several studies have concluded that immunization with PC elicits anti-PC antibodies that are able to enhance clearance of *S. pneumoniae* and provide protection against pneumococcal infection (Wallick et al., 1983; Fischer et al., 1995; Trolle et al., 2000; Tanaka et al., 2007).

CONCLUSION

This review has discussed the important role of anti-pneumococcal antibodies in protection against pneumococcal infections. While currently approved vaccines only target the pneumococcal capsule of the bacteria *via* immunization, more recent studies have demonstrated the potential of targeting conserved antigens that help bacteria evade the immune system. The antimicrobial effects of anti-pneumococcal antibodies are wide ranging and impressive, and include an increase in complement deposition, enhanced opsonophagocytic activity, amplified NET and lactoferrin mediated killing, interference with attachment and penetration of host cells, neutralization of cytotoxic proteins, and modulation of the inflammatory response. A greater understanding of how anti-pneumococcal antibodies function is crucial. Studies to date have demonstrated that optimal antibody responses are unlikely to target one antigen but multiple antigens with different functions essential to *S. pneumoniae* fitness and/or survival. This synergistic approach may be our most

successful path against an ever-evolving pathogen. The emergence of non-vaccine serotype and associated antibiotic resistance of pneumococcal isolates illustrates the need for vaccines that are capable of eliciting antibodies with greater serotype coverage and/or mAb treatments targeting conserved surface exposed antigens.

AUTHOR CONTRIBUTIONS

AG and JM wrote and revised the manuscript. All authors contributed to the article and approved the submitted manuscript.

FUNDING

American Lung Association Innovation Award (JJM) K01OD026569 (JJM).

REFERENCES

- Abeyta, M., Hardy, G. G., and Yother, J. (2003). Genetic Alteration of Capsule Type But Not PspA Type Affects Accessibility of Surface-Bound Complement and Surface Antigens of *Streptococcus Pneumoniae*. *Infect. Immun.* 71, 218–225. doi: 10.1128/IAI.71.1.218-225.2003
- Adamou, J. E., Heinrichs, J. H., Erwin, A. L., Walsh, W., Gayle, T., Dormitzer, M., et al. (2001). Identification and Characterization of a Novel Family of Pneumococcal Proteins That Are Protective Against Sepsis. *Infect. Immun.* 69, 949–958. doi: 10.1128/IAI.69.2.949-958.2001
- Afshar, D., Pourmand, M. R., Jeddi-Tehrani, M., Saboor Yaraghi, A. A., Azarsa, M., and Shokri, F. (2016). Fibrinogen and Fibronectin Binding Activity and Immunogenic Nature of Choline Binding Protein M. *Iran. J. Public Health* 45, 1610–1617.
- Alcantara, R. B., Preheim, L. C., and Gentry-Nielsen, M. J. (2001). Pneumolysin-Induced Complement Depletion During Experimental Pneumococcal Bacteremia. *Infect. Immun.* 69, 3569–3575. doi: 10.1128/IAI.69.6.3569-3575.2001
- Anderton, J. M., Rajam, G., Romero-Steiner, S., Summer, S., Kowalczyk, A. P., Carlone, G. M., et al. (2007). E-Cadherin is a Receptor for the Common Protein Pneumococcal Surface Adhesin A (PsaA) of *Streptococcus Pneumoniae*. *Microb. Pathog.* 42, 225–236. doi: 10.1016/j.micpath.2007.02.003
- André, G. O., Assoni, L., Rodriguez, D., Leite, L. C. C., Dos Santos, T. E. P., Ferraz, L. F. C., et al. (2020). Immunization With PhtD Truncated Fragments Reduces Nasopharyngeal Colonization by *Streptococcus Pneumoniae*. *Vaccine* 38, 4146–4153. doi: 10.1016/j.vaccine.2020.04.050
- André, G. O., Borges, M. T., Assoni, L., Ferraz, L. F. C., Sakshi, P., Adamson, P., et al. (2021). Protective Role of PhtD and its Amino and Carboxyl Fragments Against Pneumococcal Sepsis. *Vaccine* 39, 3626–3632. doi: 10.1016/j.vaccine.2021.04.068
- Babb, R., Doyle, C. R., and Pirofski, L.-A. (2021). Isolation and Characterization of Human Monoclonal Antibodies to Pneumococcal Capsular Polysaccharide 3. *Microbiol. Spectr.* 9, e0144621. doi: 10.1128/Spectrum.01446-21
- Berglund, J., Vink, P., Tavares Da Silva, F., Lestrade, P., and Boutriau, D. (2014). Safety, Immunogenicity, and Antibody Persistence Following an Investigational *Streptococcus Pneumoniae* and *Haemophilus Influenzae* Triple-Protein Vaccine in a Phase 1 Randomized Controlled Study in Healthy Adults. *Clin. Vaccine Immunol.* 21, 56–65. doi: 10.1128/VI.00430-13
- Berry, A. M., Lock, R. A., and Paton, J. C. (1996). Cloning and Characterization of NanB, a Second *Streptococcus Pneumoniae* Neuraminidase Gene, and Purification of the NanB Enzyme From Recombinant *Escherichia Coli*. *J. Bacteriol.* 178, 4854–4860. doi: 10.1128/jb.178.16.4854-4860.1996
- Bitsaktsis, C., Iglesias, B. V., Li, Y., Colino, J., Snapper, C. M., Hollingshead, S. K., et al. (2012). Mucosal Immunization With an Unadjuvanted Vaccine That Targets *Streptococcus Pneumoniae* PspA to Human Fcγ Receptor Type I Protects Against Pneumococcal Infection Through Complement- and Lactoferrin-Mediated Bactericidal Activity. *Infect. Immun.* 80, 1166–1180. doi: 10.1128/IAI.05511-11
- Bogaert, D., De Groot, R., and Hermans, P. W. M. (2004). *Streptococcus Pneumoniae* Colonisation: The Key to Pneumococcal Disease. *Lancet Infect. Dis.* 4, 144–154. doi: 10.1016/S1473-3099(04)00938-7
- Bologa, M., Kamtchoua, T., Hopfer, R., Sheng, X., Hicks, B., Bixler, G., et al. (2012). Safety and Immunogenicity of Pneumococcal Protein Vaccine Candidates: Monovalent Choline-Binding Protein A (PcpA) Vaccine and Bivalent PcpA-Pneumococcal Histidine Triad Protein D Vaccine. *Vaccine* 30, 7461–7468. doi: 10.1016/j.vaccine.2012.10.076
- Briles, D. E., Ades, E., Paton, J. C., Sampson, J. S., Carlone, G. M., Huebner, R. C., et al. (2000a). Intranasal Immunization of Mice With a Mixture of the Pneumococcal Proteins PsaA and PspA is Highly Protective Against Nasopharyngeal Carriage of *Streptococcus Pneumoniae*. *Infect. Immun.* 68, 796–800. doi: 10.1128/IAI.68.2.796-800.2000
- Briles, D. E., Forman, C., and Crain, M. (1992). Mouse Antibody to Phosphocholine can Protect Mice From Infection With Mouse-Virulent Human Isolates of *Streptococcus Pneumoniae*. *Infect. Immun.* 60, 1957–1962. doi: 10.1128/iai.60.5.1957-1962.1992
- Briles, D. E., Hollingshead, S. K., King, J., Swift, A., Braun, P. A., Park, M. K., et al. (2000b). Immunization of Humans With Recombinant Pneumococcal Surface Protein A (Rpspa) Elicits Antibodies That Passively Protect Mice From Fatal Infection With *Streptococcus Pneumoniae* Bearing Heterologous PspA. *J. Infect. Dis.* 182, 1694–1701. doi: 10.1086/317602
- Briles, D. E., Hollingshead, S. K., Nabors, G. S., Paton, J. C., and Brooks-Walter, A. (2000c). The Potential for Using Protein Vaccines to Protect Against Otitis Media Caused by *Streptococcus Pneumoniae*. *Vaccine* 19 Suppl1, S87–S95. doi: 10.1016/s0264-410x(00)00285-1
- Briles, D. E., Nahm, M., Schroer, K., Davie, J., Baker, P., Kearney, J., et al. (1981). Antiphosphocholine Antibodies Found in Normal Mouse Serum are Protective Against Intravenous Infection With Type 3 *Streptococcus Pneumoniae*. *J. Exp. Med.* 153, 694–705. doi: 10.1084/jem.153.3.694
- Brookes, R. H., Ming, M., Williams, K., Hopfer, R., Gurunathan, S., Gallichan, S., et al. (2015). Passive Protection of Mice Against *Streptococcus Pneumoniae* Challenge by Naturally Occurring and Vaccine-Induced Human Anti-PhtD Antibodies. *Hum. Vaccin. Immunother.* 11, 1836–1839. doi: 10.1080/21645515.2015.1039210
- Brooks, W. A., Chang, L.-J., Sheng, X., and Hopfer, R. (2015). Safety and Immunogenicity of a Trivalent Recombinant PcpA, PhtD, and PlyDI

- Pneumococcal Protein Vaccine in Adults, Toddlers, and Infants: A Phase I Randomized Controlled Study. *Vaccine* 33, 4610–4617. doi: 10.1016/j.vaccine.2015.06.078
- Brooks-Walter, A., Briles, D. E., and Hollingshead, S. K. (1999). The *pspC* Gene of *Streptococcus Pneumoniae* Encodes a Polymorphic Protein, PspC, Which Elicits Cross-Reactive Antibodies to PspA and Provides Immunity to Pneumococcal Bacteremia. *Infect. Immun.* 67, 6533–6542. doi: 10.1128/IAI.67.12.6533-6542.1999
- Bull, C. G. (1915). The Mechanism of the Curative Action Of Antipneumococcus Serum. *J. Exp. Med.* 22, 457–464. doi: 10.1084/jem.22.4.457
- Burnaugh, A. M., Frantz, L. J., and King, S. J. (2008). Growth of *Streptococcus Pneumoniae* on Human Glycoconjugates is Dependent Upon the Sequential Activity of Bacterial Exoglycosidases. *J. Bacteriol.* 190, 221–230. doi: 10.1128/JB.01251-07
- Burns, T., Abadi, M., and Pirofski, L.-A. (2005). Modulation of the Lung Inflammatory Response to Serotype 8 Pneumococcal Infection by A Human Immunoglobulin M Monoclonal Antibody to Serotype 8 Capsular Polysaccharide. *Infect. Immun.* 73, 4530–4538. doi: 10.1128/IAI.73.8.4530-4538.2005
- Burns, T., Zhong, Z., Steinitz, M., and Pirofski, L. (2003). Modulation of Polymorphonuclear Cell Interleukin-8 Secretion by Human Monoclonal Antibodies to Type 8 Pneumococcal Capsular Polysaccharide. *Infect. Immun.* 71, 6775–6783. doi: 10.1128/IAI.71.12.6775-6783.2003
- Cámara, M., Boulnois, G. J., Andrew, P. W., and Mitchell, T. J. (1994). A Neuraminidase From *Streptococcus Pneumoniae* has the Features of a Surface Protein. *Infect. Immun.* 62, 3688–3695. doi: 10.1128/iai.62.9.3688-3695.1994
- Cao, J., Chen, D., Xu, W., Chen, T., Xu, S., Luo, J., et al. (2007). Enhanced Protection Against Pneumococcal Infection Elicited by Immunization With the Combination of PspA, PspC, and ClpP. *Vaccine* 25, 4996–5005. doi: 10.1016/j.vaccine.2007.04.069
- Chen, A., Mann, B., Gao, G., Heath, R., King, J., Maisonneuve, J., et al. (2015). Multivalent Pneumococcal Protein Vaccines Comprising Pneumolysin With Epitopes/Fragments of CbpA and/or PspA Elicit Strong and Broad Protection. *Clin. Vaccine Immunol.* 22, 1079–1089. doi: 10.1128/ CVI.00293-15
- Cockeran, R., Steel, H. C., Mitchell, T. J., Feldman, C., and Anderson, R. (2001). Pneumolysin Potentiates Production of Prostaglandin E(2) and Leukotriene B (4) by Human Neutrophils. *Infect. Immun.* 69, 3494–3496. doi: 10.1128/IAI.69.5.3494-3496.2001
- Cundell, D. R., Gerard, N. P., Gerard, C., Idanpaan-Heikkilä, I., and Tuomanen, E. I. (1995). *Streptococcus Pneumoniae* Anchor to Activated Human Cells by the Receptor for Platelet-Activating Factor. *Nature* 377, 435–438. doi: 10.1038/377435a0
- Dagan, R., Patterson, S., Juergens, C., Greenberg, D., Givon-Lavi, N., Porat, N., et al. (2013). Comparative Immunogenicity and Efficacy of 13-Valent and 7-Valent Pneumococcal Conjugate Vaccines in Reducing Nasopharyngeal Colonization: A Randomized Double-Blind Trial. *Clin. Infect. Dis.* 57, 952–962. doi: 10.1093/cid/cit428
- Dalia, A. B., Standish, A. J., and Weiser, J. N. (2010). Three Surface Exoglycosidases From *Streptococcus Pneumoniae*, NanA, BgaA, and StrH, Promote Resistance to Opsonophagocytic Killing by Human Neutrophils. *Infect. Immun.* 78, 2108–2116. doi: 10.1128/IAI.01125-09
- Daniels, C. C., Coan, P., King, J., Hale, J., Benton, K. A., Briles, D. E., et al. (2010). The Proline-Rich Region of Pneumococcal Surface Proteins A and C Contains Surface-Accessible Epitopes Common to All Pneumococci and Elicits Antibody-Mediated Protection Against Sepsis. *Infect. Immun.* 78, 2163–2172. doi: 10.1128/IAI.01199-09
- Daniels, C. C., Rogers, P. D., and Shelton, C. M. (2016). A Review of Pneumococcal Vaccines: Current Polysaccharide Vaccine Recommendations and Future Protein Antigens. *J. Pediatr. Pharmacol. Ther.* 21, 27–35. doi: 10.5863/1551-6776-21.1.27
- Dave, S., Brooks-Walter, A., Pangburn, M. K., and McDaniel, L. S. (2001). PspC, a Pneumococcal Surface Protein, Binds Human Factor H. *Infect. Immun.* 69, 3435–3437. doi: 10.1128/IAI.69.5.3435-3437.2001
- Denny, F. W., and Loda, F. A. (1986). Acute Respiratory Infections are the Leading Cause of Death in Children in Developing Countries. *Am. J. Trop. Med. Hyg.* 35, 1–2. doi: 10.4269/ajtmh.1986.35.1
- Denoël, P., Godfroid, F., Hermand, P., Verlant, V., and Poolman, J. (2011a). Combined Protective Effects of Anti-PhtD and Anti-Pneumococcal Polysaccharides. *Vaccine* 29, 6451–6453. doi: 10.1016/j.vaccine.2011.01.085
- Denoël, P., Philipp, M. T., Doyle, L., Martin, D., Carletti, G., and Poolman, J. T. (2011b). A Protein-Based Pneumococcal Vaccine Protects Rhesus Macaques From Pneumonia After Experimental Infection With *Streptococcus Pneumoniae*. *Vaccine* 29, 5495–5501. doi: 10.1016/j.vaccine.2011.05.051
- Dieudonné-Vatran, A., Krentz, S., Blom, A. M., Meri, S., Henriques-Normark, B., Riesbeck, K., et al. (2009). Clinical Isolates of *Streptococcus Pneumoniae* Bind the Complement Inhibitor C4b-Binding Protein in a PspC Allele-Dependent Fashion. *J. Immunol.* 182, 7865–7877. doi: 10.4049/jimmunol.0802376
- Dintilhac, A., Alloing, G., Granadel, C., and Claverys, J. P. (1997). Competence and Virulence of *Streptococcus Pneumoniae*: *Adc* and *PsaA* Mutants Exhibit a Requirement for Zn and Mn Resulting From Inactivation of Putative ABC Metal Permeases. *Mol. Microbiol.* 25, 727–739. doi: 10.1046/j.1365-2958.1997.5111879.x
- Doyle, C. R., and Pirofski, L. (2016). Reduction of *Streptococcus Pneumoniae* Colonization and Dissemination by a Nonopsonic Capsular Polysaccharide Antibody. *MBio* 7, e02260-15. doi: 10.1128/mBio.02260-15
- Doyle, C. R., Moon, J.-Y., Daily, J. P., Wang, T., and Pirofski, L.-a (2021). A Capsular Polysaccharide-Specific Antibody Alters *Streptococcus Pneumoniae* Gene Expression During Nasopharyngeal Colonization of Mice. *Infect. Immun.* 86, e00300-18. doi: 10.1128/IAI.00300-18
- Eijkelkamp, B. A., Pederick, V. G., Plumtre, C. D., Harvey, R. M., Hughes, C. E., Paton, J. C., et al. (2016). The First Histidine Triad Motif of PhtD Is Critical for Zinc Homeostasis in *Streptococcus Pneumoniae*. *Infect. Immun.* 84, 407–415. doi: 10.1128/IAI.01082-15
- Ekström, N., Våkeväinen, M., Verho, J., Kilpi, T., and Käyhty, H. (2007). Functional Antibodies Elicited by Two Heptavalent Pneumococcal Conjugate Vaccines in The Finnish Otitis Media Vaccine Trial. *Infect. Immun.* 75, 1794–1800. doi: 10.1128/IAI.01673-06
- Fabrizio, K., Groner, A., Boes, M., and Pirofski, L. (2007). A Human Monoclonal Immunoglobulin M Reduces Bacteremia and Inflammation in a Mouse Model of Systemic Pneumococcal Infection. *Clin. Vaccine Immunol.* 14, 382–390. doi: 10.1128/ CVI.00374-06
- Feldman, C., Munro, N. C., Jeffery, P. K., Mitchell, T. J., Andrew, P. W., Boulnois, G. J., et al. (1991). Pneumolysin Induces the Salient Histologic Features of Pneumococcal Infection in the Rat Lung In Vivo. *Am. J. Respir. Cell Mol. Biol.* 5, 416–423. doi: 10.1165/ajrcmb/5.5.416
- Ferreira, D. M., Arêas, A. P. M., Darrieux, M., Leite, L. C. C., and Miyaji, E. N. (2006a). DNA Vaccines Based on Genetically Detoxified Derivatives of Pneumolysin Fail to Protect Mice Against Challenge With *Streptococcus Pneumoniae*. *FEMS Immunol. Med. Microbiol.* 46, 291–297. doi: 10.1111/j.1574-695X.2006.00040.x
- Ferreira, D. M., Darrieux, M., Silva, D. A., Leite, L. C. C., Ferreira, J. M. C. J., Ho, P. L., et al. (2009). Characterization of Protective Mucosal and Systemic Immune Responses Elicited by Pneumococcal Surface Protein PspA and PspC Nasal Vaccines Against a Respiratory Pneumococcal Challenge in Mice. *Clin. Vaccine Immunol.* 16, 636–645. doi: 10.1128/ CVI.00395-08
- Ferreira, D. M., Miyaji, E. N., Oliveira, M. L. S., Darrieux, M., Arêas, A. P. M., Ho, P. L., et al. (2006b). DNA Vaccines Expressing Pneumococcal Surface Protein A (PspA) Elicit Protection Levels Comparable to Recombinant Protein. *J. Med. Microbiol.* 55, 375–378. doi: 10.1099/jmm.0.46217-0
- Fischer, R. T., Longo, D. L., and Kenny, J. J. (1995). A Novel Phosphocholine Antigen Protects Both Normal and X-Linked Immune Deficient Mice Against *Streptococcus Pneumoniae*. Comparison of the 6-O-Phosphocholine Hydroxyhexanoate-Conjugate With Other Phosphocholine-Containing Vaccines. *J. Immunol.* 154, 3373–3382.
- Francis, J. P., Richmond, P. C., Pomat, W. S., Michael, A., Keno, H., Phuanukoonnon, S., et al. (2009). Maternal Antibodies to Pneumolysin But Not to Pneumococcal Surface Protein A Delay Early Pneumococcal Carriage in High-Risk Papua New Guinean Infants. *Clin. Vaccine Immunol.* 16, 1633–1638. doi: 10.1128/ CVI.00247-09
- Frey, S. E., Lottenbach, K. R., Hill, H., Blevins, T. P., Yu, Y., Zhang, Y., et al. (2013). A Phase I, Dose-Escalation Trial in Adults of Three Recombinant Attenuated *Salmonella Typhi* Vaccine Vectors Producing *Streptococcus Pneumoniae* Surface Protein Antigen PspA. *Vaccine* 31, 4874–4880. doi: 10.1016/j.vaccine.2013.07.049

- Galán-Bartual, S., Pérez-Dorado, I., García, P., and Hermoso, J. A. (2015). "Chapter 11 - Structure and Function of Choline-Binding Proteins," In: *Streptococcus Pneumoniae Molecular Mechanisms of Host-Pathogen Interactions*. Eds. J. Brown, S. Hammerschmidt and C. B. T.-S. P. Orihuela (Amsterdam: Academic Press), 207–230. doi: 10.1016/B978-0-12-410530-0.00011-9
- Ganaie, F., Saad, J. S., McGee, L., van Tonder, A. J., Bentley, S. D., Lo, S. W., et al. (2020). A New Pneumococcal Capsule Type, 10D, is the 100th Serotype and Has a Large Cps Fragment From an Oral Streptococcus. *MBio* 11. doi: 10.1128/mBio.00937-20
- García-Suárez, M., del, M., Cima-Cabal, M. D., Flórez, N., García, P., Cernuda-Cernuda, R., et al. (2004). Protection Against Pneumococcal Pneumonia in Mice by Monoclonal Antibodies to Pneumolysin. *Infect. Immun.* 72, 4534–4540. doi: 10.1128/IAI.72.8.4534-4540.2004
- García-Suárez, M. D. M., Flórez, N., Astudillo, A., Vázquez, F., Villaverde, R., Fabrizio, K., et al. (2007). The Role of Pneumolysin in Mediating Lung Damage in a Lethal Pneumococcal Pneumonia Murine Model. *Respir. Res.* 8, 3. doi: 10.1186/1465-9921-8-3
- Genschmer, K. R., Vadesilho, C. F. M., McDaniel, L. S., Park, S.-S., Hale, Y., Miyaji, E. N., et al. (2019). The Modified Surface Killing Assay Distinguishes Between Protective and Nonprotective Antibodies to PspA. *mSphere* 4, e00589–19. doi: 10.1128/mSphere.00589-19
- Georgieva, M., Kagedan, L., Lu, Y.-J., Thompson, C. M., and Lipsitch, M. (2018). Antigenic Variation in Streptococcus Pneumoniae PspC Promotes Immune Escape in the Presence of Variant-Specific Immunity. *MBio* 9, e00264–18. doi: 10.1128/mBio.00264-18
- Ginsburg, A. S., Nahm, M. H., Khambaty, F. M., and Alderson, M. R. (2012). Issues and Challenges in the Development of Pneumococcal Protein Vaccines. *Expert Rev. Vaccines* 11, 279–285. doi: 10.1586/erv.12.5
- Glennie, S., Gritzfeld, J. F., Pennington, S. H., Garner-Jones, M., Coombes, N., Hopkins, M. J., et al. (2016). Modulation of Nasopharyngeal Innate Defenses by Viral Coinfection Predisposes Individuals to Experimental Pneumococcal Carriage. *Mucosal Immunol.* 9, 56–67. doi: 10.1038/mi.2015.35
- Glover, D. T., Hollingshead, S. K., and Briles, D. E. (2008). Streptococcus Pneumoniae Surface Protein PcpA Elicits Protection Against Lung Infection and Fatal Sepsis. *Infect. Immun.* 76, 2767–2776. doi: 10.1128/IAI.01126-07
- Godfroid, F., Hermand, P., Verlant, V., Denoël, P., and Poolman, J. T. (2011). Preclinical Evaluation of the Pht Proteins as Potential Cross-Protective Pneumococcal Vaccine Antigens. *Infect. Immun.* 79, 238–245. doi: 10.1128/IAI.00378-10
- Goldblatt, D., Southern, J., Ashton, L., Andrews, N., Woodgate, S., Burbidge, P., et al. (2010). Immunogenicity of a Reduced Schedule of Pneumococcal Conjugate Vaccine in Healthy Infants and Correlates of Protection for Serotype 6B in the United Kingdom. *Pediatr. Infect. Dis. J.* 29, 401–405. doi: 10.1097/INF.0b013e3181c67f04
- Goulart, C., da Silva, T. R., Rodriguez, D., Politano, W. R., Leite, L. C. C., and Darrieux, M. (2013). Characterization of Protective Immune Responses Induced by Pneumococcal Surface Protein A in Fusion With Pneumolysin Derivatives. *PLoS One* 8, e59605. doi: 10.1371/journal.pone.0059605
- Haleem, K. S., Ali, Y. M., Yesilkaya, H., Kohler, T., Hammerschmidt, S., Andrew, P. W., et al. (2019). The Pneumococcal Surface Proteins PspA and PspC Sequester Host C4-Binding Protein To Inactivate Complement C4b on the Bacterial Surface. *Infect. Immun.* 87, e00742–18. doi: 10.1128/IAI.00742-18
- Hammerschmidt, S., Agarwal, V., Kunert, A., Haelbich, S., Skerka, C., and Zipfel, P. F. (2007). The Host Immune Regulator Factor H Interacts via Two Contact Sites With the PspC Protein of Streptococcus Pneumoniae and Mediates Adhesion to Host Epithelial Cells. *J. Immunol.* 178, 5848–5858. doi: 10.4049/jimmunol.178.9.5848
- Hammit, L. L., Campbell, J. C., Borys, D., Weatherholtz, R. C., Reid, R., Goklish, N., et al. (2019). Efficacy, Safety and Immunogenicity of a Pneumococcal Protein-Based Vaccine Co-Administered With 13-Valent Pneumococcal Conjugate Vaccine Against Acute Otitis Media in Young Children: A Phase IIb Randomized Study. *Vaccine* 37, 7482–7492. doi: 10.1016/j.vaccine.2019.09.076
- Hammond, A. J., Binsker, U., Aggarwal, S. D., Ortigoza, M. B., Loomis, C., and Weiser, J. N. (2021). Neuraminidase B Controls Neuraminidase A-Dependent Mucus Production and Evasion. *PLoS Pathog.* 17, e1009158. doi: 10.1371/journal.ppat.1009158
- Han, C., and Zhang, M. (2019). Genetic Diversity and Antigenicity Analysis of Streptococcus Pneumoniae Pneumolysin Isolated From Children With Pneumococcal Infection. *Int. J. Infect. Dis.* 86, 57–64. doi: 10.1016/j.ijid.2019.06.025
- Hermant, P., Vandercammen, A., Mertens, E., Di Paolo, E., Verlant, V., Denoël, P., et al. (2017). Preclinical Evaluation of a Chemically Detoxified Pneumolysin as Pneumococcal Vaccine Antigen. *Hum. Vaccin. Immunother.* 13, 220–228. doi: 10.1080/21645515.2016.1234553
- Hernani, M., de, L., Ferreira, P. C. D., Ferreira, D. M., Miyaji, E. N., Ho, P. L., et al. (2011). AndNasal Immunization of Mice With Lactobacillus Casei Expressing the Pneumococcal Surface Protein C Primes the Immune System and Decreases Pneumococcal Nasopharyngeal Colonization in Mice. *FEMS Immunol. Med. Microbiol.* 62, 263–272. doi: 10.1111/j.1574-695X.2011.00809.x
- Hollingshead, S. K., Becker, R., and Briles, D. E. (2000). Diversity of PspA: Mosaic Genes and Evidence for Past Recombination in Streptococcus Pneumoniae. *Infect. Immun.* 68, 5889–5900. doi: 10.1128/IAI.68.10.5889-5900.2000
- Holmlund, E., Quianbao, B., Ollgren, J., Nohynek, H., and Käyhty, H. (2006). Development of Natural Antibodies to Pneumococcal Surface Protein A, Pneumococcal Surface Adhesin A and Pneumolysin in Filipino Pregnant Women and Their Infants in Relation to Pneumococcal Carriage. *Vaccine* 24, 57–65. doi: 10.1016/j.vaccine.2005.07.055
- Huang, J., Gingerich, A. D., Royer, F., Paschall, A. V., Pena-Briseno, A., Avci, F. Y., et al. (2021). Broadly Reactive Human Monoclonal Antibodies Targeting the Pneumococcal Histidine Triad Protein Protect Against Fatal Pneumococcal Infection. *Infect. Immun.* 89, e00747–20. doi: 10.1128/IAI.00747-20
- Huo, Z., Spencer, O., Miles, J., Johnson, J., Holliman, R., Sheldon, J., et al. (2004). Antibody Response to Pneumolysin and to Pneumococcal Capsular Polysaccharide in Healthy Individuals and Streptococcus Pneumoniae Infected Patients. *Vaccine* 22, 1157–1161. doi: 10.1016/j.vaccine.2003.09.025
- Hu, Y., Park, N., Seo, K. S., Park, J. Y., Somaratne, R. P., Olivier, A. K., et al. (2021). Pneumococcal Surface Adhesion A Protein (PsaA) Interacts With Human Annexin A2 on Airway Epithelial Cells. *Virulence* 12, 1841–1854. doi: 10.1080/21505594.2021.1947176
- Hyams, C., Camberlein, E., Cohen, J. M., Bax, K., and Brown, J. S. (2010). The Streptococcus Pneumoniae Capsule Inhibits Complement Activity and Neutrophil Phagocytosis by Multiple Mechanisms. *Infect. Immun.* 78, 704–715. doi: 10.1128/IAI.00881-09
- Iannelli, F., Oggioni, M. R., and Pozzi, G. (2002). Allelic Variation in the Highly Polymorphic Locus pspC of Streptococcus Pneumoniae. *Gene* 284, 63–71. doi: 10.1016/S0378-1119(01)00896-4
- Iuchi, H., Otori, J., Kyutoku, T., Ito, K., and Kurono, Y. (2019). Role of Phosphorylcholine in Streptococcus Pneumoniae and Nontypeable Haemophilus Influenzae Adherence to Epithelial Cells. *Auris. Nasus. Larynx.* 46, 513–519. doi: 10.1016/j.anl.2018.11.003
- Jahn, K., Handtke, S., Palankar, R., Weißmüller, S., Nouailles, G., Kohler, T. P., et al. (2020). Pneumolysin Induces Platelet Destruction, Not Platelet Activation, Which can be Prevented by Immunoglobulin Preparations In Vitro. *Blood Adv.* 4, 6315–6326. doi: 10.1182/bloodadvances.2020002372
- Jakubovics, N. S., and Jenkinson, H. F. (2001). Out of the Iron Age: New Insights Into the Critical Role of Manganese Homeostasis in Bacteria. *Microbiology* 147, 1709–1718. doi: 10.1099/00221287-147-7-1709
- Janesch, P., Rouha, H., Badarau, A., Stulik, L., Mirkina, I., Caccamo, M., et al. (2018). Assessing the Function of Pneumococcal Neuraminidases NanA, NanB and NanC in In Vitro and In Vivo Lung Infection Models Using Monoclonal Antibodies. *Virulence* 9, 1521–1538. doi: 10.1080/21505594.2018.1520545
- Johnston, J. W., Briles, D. E., Myers, L. E., and Hollingshead, S. K. (2006). Mn2+-Dependent Regulation of Multiple Genes in Streptococcus Pneumoniae Through PsaR and the Resultant Impact on Virulence. *Infect. Immun.* 74, 1171–1180. doi: 10.1128/IAI.74.2.1171-1180.2006
- Kallio, A., Sepponen, K., Hermant, P., Denoël, P., Godfroid, F., and Melin, M. (2014). Role of Pht Proteins in Attachment of Streptococcus Pneumoniae to Respiratory Epithelial Cells. *Infect. Immun.* 82, 1683–1691. doi: 10.1128/IAI.00699-13
- Kamtchoua, T., Bologa, M., Hopfer, R., Neveu, D., Hu, B., Sheng, X., et al. (2013). Safety and Immunogenicity of the Pneumococcal Pneumolysin Derivative PlyD1 in a Single-Antigen Protein Vaccine Candidate in Adults. *Vaccine* 31, 327–333. doi: 10.1016/j.vaccine.2012.11.005

- Kanclerski, K., and Möllby, R. (1987). Production and Purification of Streptococcus Pneumoniae Hemolysin (Pneumolysin). *J. Clin. Microbiol.* 25, 222–225. doi: 10.1128/jcm.25.2.222-225.1987
- Kaur, R., Surendran, N., Ochs, M., and Pichichero, M. E. (2014). Human Antibodies to PhtD, PcpA, and Ply Reduce Adherence to Human Lung Epithelial Cells and Murine Nasopharyngeal Colonization by Streptococcus Pneumoniae. *Infect. Immun.* 82, 5069–5075. doi: 10.1128/IAI.02124-14
- Kazemian, H., Afshar, D., Garcia, E., Pourmand, M. R., Jeddi-Tehrani, M., Aminharati, F., et al. (2018). CbpM and CbpG of Streptococcus Pneumoniae Elicit a High Protection in Mice Challenged With a Serotype 19f Pneumococcus. *Iran. J. Allergy Asthma. Immunol.* 17, 574–585.
- Keller, L. E., Robinson, D. A., and McDaniel, L. S. (2016). Nonencapsulated Streptococcus Pneumoniae: Emergence and Pathogenesis. *MBio* 7, e01792. doi: 10.1128/mBio.01792-15
- Kerr, A. R., Paterson, G. K., McCluskey, J., Iannelli, F., Oggioni, M. R., Pozzi, G., et al. (2006). The Contribution of PspC to Pneumococcal Virulence Varies Between Strains and is Accomplished by Both Complement Evasion and Complement-Independent Mechanisms. *Infect. Immun.* 74, 5319–5324. doi: 10.1128/IAI.00543-06
- Khan, N., and Jan, A. T. (2017). Towards Identifying Protective B-Cell Epitopes: The PspA Story. *Front. Microbiol.* 8. doi: 10.3389/fmicb.2017.00742
- Khan, M. N., and Pichichero, M. E. (2012). Vaccine Candidates PhtD and PhtE of Streptococcus Pneumoniae are Adhesins That Elicit Functional Antibodies in Humans. *Vaccine* 30, 2900–2907. doi: 10.1016/j.vaccine.2012.02.023
- Khan, N., Qadri, R. A., and Sehgal, D. (2015). Correlation Between In Vitro Complement Deposition and Passive Mouse Protection of Anti-Pneumococcal Surface Protein A Monoclonal Antibodies. *Clin. Vaccine Immunol.* 22, 99–107. doi: 10.1128/CI.00001-14
- Khan, M. N., Sharma, S. K., Filkins, L. M., and Pichichero, M. E. (2012). PcpA of Streptococcus Pneumoniae Mediates Adherence to Nasopharyngeal and Lung Epithelial Cells and Elicits Functional Antibodies in Humans. *Microbes Infect.* 14, 1102–1110. doi: 10.1016/j.micinf.2012.06.007
- Kharat, A. S., and Tomasz, A. (2006). Drastic Reduction in the Virulence of Streptococcus Pneumoniae Expressing Type 2 Capsular Polysaccharide But Lacking Choline Residues in the Cell Wall. *Mol. Microbiol.* 60, 93–107. doi: 10.1111/j.1365-2958.2006.05082.x
- King, S. J., Hippe, K. R., and Weiser, J. N. (2006). Deglycosylation of Human Glycoconjugates by the Sequential Activities of Exoglycosidases Expressed by Streptococcus Pneumoniae. *Mol. Microbiol.* 59, 961–974. doi: 10.1111/j.1365-2958.2005.04984.x
- Klugman, K. P. (2009). The Significance of Serotype Replacement for Pneumococcal Disease and Antibiotic Resistance. *Adv. Exp. Med. Biol.* 634, 121–128. doi: 10.1007/978-0-387-79838-7_11
- Kohler, S., Hallström, T., Singh, B., Riesbeck, K., Spartà, G., Zipfel, P. F., et al. (2015). Binding of Vitronectin and Factor H to Hic Contributes to Immune Evasion of Streptococcus Pneumoniae Serotype 3. *Thromb. Haemost.* 113, 125–142. doi: 10.1160/TH14-06-0561
- Kristian, S. A., Ota, T., Bubeck, S. S., Cho, R., Groff, B. C., Kubota, T., et al. (2016). Generation and Improvement of Effector Function of a Novel Broadly Reactive and Protective Monoclonal Antibody Against Pneumococcal Surface Protein A of Streptococcus Pneumoniae. *PLoS One* 11, e0154616. doi: 10.1371/journal.pone.0154616
- Kucinskaite-Kodze, I., Simanavicius, M., Dapkunas, J., Pleckaityte, M., and Zvirbliene, A. (2020). Mapping of Recognition Sites of Monoclonal Antibodies Responsible for the Inhibition of Pneumolysin Functional Activity. *Biomol* 10. doi: 10.3390/biom10071009
- Kumar, S., Sunagar, R., and Gosselin, E. J. (2020). Preclinical Efficacy of a Trivalent Human FcγRI-Targeted Adjuvant-Free Subunit Mucosal Vaccine Against Pulmonary Pneumococcal Infection. *Vaccines* 8, 193. doi: 10.3390/vaccines8020193
- Lawrence, M. C., Pilling, P. A., Epa, V. C., Berry, A. M., Ogunniyi, A. D., and Paton, J. C. (1998). The Crystal Structure of Pneumococcal Surface Antigen PsaA Reveals a Metal-Binding Site and a Novel Structure for a Putative ABC-Type Binding Protein. *Structure* 6, 1553–1561. doi: 10.1016/s0969-2126(98)00153-1
- Lee, H., Choi, E. H., and Lee, H. J. (2014). Efficacy and Effectiveness of Extended-Valency Pneumococcal Conjugate Vaccines. *Korean. J. Pediatr.* 57, 55–66. doi: 10.3345/kjp.2014.57.2.55
- Leroux-Roels, G., Maes, C., De Boever, F., Traskine, M., Rüggeberg, J. U., and Borys, D. (2014). Safety, Reactogenicity and Immunogenicity of a Novel Pneumococcal Protein-Based Vaccine in Adults: A Phase I/II Randomized Clinical Study. *Vaccine* 32, 6838–6846. doi: 10.1016/j.vaccine.2014.02.052
- Linley, E., Bell, A., Gritzfeld, J. F., and Borrow, R. (2019). Should Pneumococcal Serotype 3 Be Included in Serotype-Specific Immunoassays? *Vaccines* 7, 4. doi: 10.3390/vaccines7010004
- Li, Y., Weinberger, D. M., Thompson, C. M., Trzciński, K., and Lipsitch, M. (2013). Surface Charge of Streptococcus Pneumoniae Predicts Serotype Distribution. *Infect. Immun.* 81, 4519–4524. doi: 10.1128/IAI.00724-13
- Luck, J. N., Tettelin, H., and Orihuela, C. J. (2020). Sugar-Coated Killer: Serotype 3 Pneumococcal Disease. *Front. Cell. Infect. Microbiol.* 10. doi: 10.3389/fcimb.2020.613287
- Lu, L., Ma, Z., Jokiranta, T. S., Whitney, A. R., DeLeo, F. R., and Zhang, J.-R. (2008). Species-Specific Interaction of Streptococcus Pneumoniae With Human Complement Factor H. *J. Immunol.* 181, 7138–7146. doi: 10.4049/jimmunol.181.10.7138
- Lu, J., Sun, T., Hou, H., Xu, M., Gu, T., Dong, Y., et al. (2014). Detoxified Pneumolysin Derivative Plym2 Directly Protects Against Pneumococcal Infection via Induction of Inflammatory Cytokines. *Immunol. Invest.* 43, 717–726. doi: 10.3109/08820139.2014.930478
- Magee, A. D., and Yother, J. (2001). Requirement for Capsule in Colonization by Streptococcus Pneumoniae. *Infect. Immun.* 69, 3755–3761. doi: 10.1128/IAI.69.6.3755-3761.2001
- Malekan, M., Siadat, S. D., Aghasadehgi, M., Shahrokhi, N., Afrough, P., Behrouzi, A., et al. (2020). Evaluation of Protective Immunity Responses Against Pneumococcal PhtD and its C-Terminal in Combination With Outer-Membrane Vesicles as Adjuvants. *J. Med. Microbiol.* 69, 465–477. doi: 10.1099/jmm.0.001103
- Mann, B., Orihuela, C., Antikainen, J., Gao, G., Sublett, J., Korhonen, T. K., et al. (2006). Multifunctional Role of Choline Binding Protein G in Pneumococcal Pathogenesis. *Infect. Immun.* 74, 821–829. doi: 10.1128/IAI.74.2.821-829.2006
- Mann, B., Thornton, J., Heath, R., Wade, K. R., Tweten, R. K., Gao, G., et al. (2014). Broadly Protective Protein-Based Pneumococcal Vaccine Composed of Pneumolysin Toxoid-CbpA Peptide Recombinant Fusion Protein. *J. Infect. Dis.* 209, 1116–1125. doi: 10.1093/infdis/jit502
- Marks, L. R., Reddinger, R. M., and Hakansson, A. P. (2014). Biofilm Formation Enhances Fomite Survival of Streptococcus Pneumoniae and Streptococcus Pyogenes. *Infect. Immun.* 82, 1141–1146. doi: 10.1128/IAI.01310-13
- Martinez, P. J., Farhan, A., Mustafa, M., Javadi, N., Darkoh, C., Garrido-Sanabria, E., et al. (2019). PspA Facilitates Evasion of Pneumococci From Bactericidal Activity of Neutrophil Extracellular Traps (NETs). *Microb. Pathog.* 136, 103653. doi: 10.1016/j.micpath.2019.103653
- McAllister, L. J., Tseng, H., Ogunniyi, A. D., Jennings, M. P., McEwan, A. G., and Paton, J. C. (2004). AndMolecular Analysis of the Psa Permease Complex of Streptococcus Pneumoniae. *Mol. Microbiol.* 53, 889–901. doi: 10.1111/j.1365-2958.2004.04164.x
- McCool, T. L., Cate, T. R., Moy, G., and Weiser, J. N. (2002). The Immune Response to Pneumococcal Proteins During Experimental Human Carriage. *J. Exp. Med.* 195, 359–365. doi: 10.1084/jem.20011576
- Mirza, S., Benjamin, W. H. J., Coan, P. A., Hwang, S.-A., Winslett, A.-K., Yother, J., et al. (2016). The Effects of Differences in pspA Alleles and Capsular Types on the Resistance of Streptococcus Pneumoniae to Killing by Apolactoferrin. *Microb. Pathog.* 99, 209–219. doi: 10.1016/j.micpath.2016.08.029
- Mitchell, T. J., Andrew, P. W., Saunders, F. K., Smith, A. N., and Boulnois, G. J. (1991). Complement Activation and Antibody Binding by Pneumolysin via a Region of the Toxin Homologous to a Human Acute-Phase Protein. *Mol. Microbiol.* 5, 1883–1888. doi: 10.1111/j.1365-2958.1991.tb00812.x
- Mitsi, E., Roche, A. M., Reiné, J., Zangari, T., Owugha, J. T., Pennington, S. H., et al. (2017). Agglutination by Anti-Capsular Polysaccharide Antibody is Associated With Protection Against Experimental Human Pneumococcal Carriage. *Mucosal Immunol.* 10, 385–394. doi: 10.1038/mi.2016.71
- Miyaji, E. N., Dias, W. O., Gamberini, M., Gebara, V. C. B. C., Schenkman, R. P. F., Wild, J., et al. (2001). PsaA (Pneumococcal Surface Adhesin A) and PspA (Pneumococcal Surface Protein A) DNA Vaccines Induce Humoral and Cellular Immune Responses Against Streptococcus Pneumoniae. *Vaccine* 20, 805–812. doi: 10.1016/S0264-410X(01)00395-4
- Moffitt, K., and Malley, R. (2016). Rationale and Prospects for Novel Pneumococcal Vaccines. *Hum. Vaccin. Immunother.* 12, 383–392. doi: 10.1080/21645515.2015.1087625

- Mold, C., Du Clos, T. W., Nakayama, S., Edwards, K. M., and Gewurz, H. (1982). C-Reactive Protein Reactivity With Complement and Effects on Phagocytosis. *Ann. N. Y. Acad. Sci.* 389, 251–262. doi: 10.1111/j.1749-6632.1982.tb22141.x
- Mukerji, R., Mirza, S., Roche, A. M., Widener, R. W., Croney, C. M., Rhee, D.-K., et al. (2012). Pneumococcal Surface Protein A Inhibits Complement Deposition on the Pneumococcal Surface by Competing With the Binding of C-Reactive Protein to Cell-Surface Phosphocholine. *J. Immunol.* 189, 5327–5335. doi: 10.4049/jimmunol.1201967
- Nabors, G. S., Braun, P. A., Herrmann, D. J., Heise, M. L., Pyle, D. J., Gravenstein, S., et al. (2000). Immunization of Healthy Adults With a Single Recombinant Pneumococcal Surface Protein A (PspA) Variant Stimulates Broadly Cross-Reactive Antibodies to Heterologous PspA Molecules. *Vaccine* 18, 1743–1754. doi: 10.1016/s0264-410x(99)00530-7
- Nagano, H., Kawabata, M., Sugita, G., Tsuruhara, A., Ohori, J., Jimura, T., et al. (2018). Transcutaneous Immunization With Pneumococcal Surface Protein A in Mice. *Laryngoscope* 128, E91–E96. doi: 10.1002/lary.26971
- Nakashishi-Ouchida, R., Uchida, Y., Yuki, Y., Katakai, Y., Yamanoue, T., Ogawa, H., et al. (2021). A Nanogel-Based Trivalent PspA Nasal Vaccine Protects Macaques From Intratracheal Challenge With Pneumococci. *Vaccine* 39, 3353–3364. doi: 10.1016/j.vaccine.2021.04.069
- Nelson, A. L., Roche, A. M., Gould, J. M., Chim, K., Ratner, A. J., and Weiser, J. N. (2007). Capsule Enhances Pneumococcal Colonization by Limiting Mucus-Mediated Clearance. *Infect. Immun.* 75, 83–90. doi: 10.1128/IAI.01475-06
- Novak, R., Tuomanen, E., and Charpentier, E. (2000). The Mystery of psaA and Penicillin Tolerance in *Streptococcus pneumoniae*: MicroCorrespondence. *Mol. Microbiol.* 36, 1505–1506. doi: 10.1046/j.1365-2958.2000.01959.x
- O'Brien, K. L., Wolfson, L. J., Watt, J. P., Henkle, E., Deloria-Knoll, M., McCall, N., et al. (2009). Burden of Disease Caused by *Streptococcus pneumoniae* in Children Younger Than 5 Years: Global Estimates. *Lancet (London, England)*. 374, 893–902. doi: 10.1016/S0140-6736(09)61204-6
- Ochs, M. M., Williams, K., Sheung, A., Lheritier, P., Visan, L., Rouleau, N., et al. (2016). A Bivalent Pneumococcal Histidine Triad Protein D-Choline-Binding Protein A Vaccine Elicits Functional Antibodies That Passively Protect Mice From *Streptococcus pneumoniae* Challenge. *Hum. Vaccin. Immunother.* 12, 2946–2952. doi: 10.1080/21645515.2016.1202389
- Odutola, A., Ota, M. O. C., Antonio, M., Ogundare, E. O., Saidu, Y., Foster-Nyarko, E., et al. (2017). Efficacy of a Novel, Protein-Based Pneumococcal Vaccine Against Nasopharyngeal Carriage of *Streptococcus pneumoniae* in Infants: A Phase 2, Randomized, Controlled, Observer-Blind Study. *Vaccine* 35, 2531–2542. doi: 10.1016/j.vaccine.2017.03.071
- Ogunniyi, A. D., Grabowicz, M., Mahdi, L. K., Cook, J., Gordon, D. L., Sadlon, T. A., et al. (2009). Pneumococcal Histidine Triad Proteins are Regulated by the Zn²⁺-Dependent Repressor AdcR and Inhibit Complement Deposition Through the Recruitment of Complement Factor H. *FASEB J.* 23, 731–738. doi: 10.1096/fj.08-119537
- Oliveira, M. L. S., Arêas, A. P. M., Campos, I. B., Monedero, V., Perez-Martínez, G., Miyaji, E. N., et al. (2006). Induction of Systemic and Mucosal Immune Response and Decrease in *Streptococcus pneumoniae* Colonization by Nasal Inoculation of Mice With Recombinant Lactic Acid Bacteria Expressing Pneumococcal Surface Antigen A. *Microbes Infect.* 8, 1016–1024. doi: 10.1016/j.micinf.2005.10.020
- Orihuela, C. J., Mahdavi, J., Thornton, J., Mann, B., Wooldridge, K. G., Abouseada, N., et al. (2009). Laminin Receptor Initiates Bacterial Contact With the Blood Brain Barrier in Experimental Meningitis Models. *J. Clin. Invest.* 119, 1638–1646. doi: 10.1172/JCI36759
- Papastamatiou, T., Routsias, J. G., Koutsou, O., Dotsika, E., Tsakris, A., and Spoulou, V. (2018). Evaluation of Protective Efficacy of Selected Immunodominant B-Cell Epitopes Within Virulent Surface Proteins of *Streptococcus pneumoniae*. *Infect. Immun.* 86, e00673–17. doi: 10.1128/IAI.00673-17
- Parker, D., Soong, G., Planet, P., Brower, J., Ratner, A. J., and Prince, A. (2009). The NanA Neuraminidase of *Streptococcus pneumoniae* is Involved in Biofilm Formation. *Infect. Immun.* 77, 3722–3730. doi: 10.1128/IAI.00228-09
- Paton, J. C., Rowan-Kelly, B., and Ferrante, A. (1984). Activation of Human Complement by the Pneumococcal Toxin Pneumolysin. *Infect. Immun.* 43, 1085–1087. doi: 10.1128/iai.43.3.1085-1087.1984
- Petukhova, E. S., Vorobyev, D. S., Sidorov, A. V., Semenova, I. B., Volokh, Y. V., Leonova, A. Y., et al. (2020). Immunization With Recombinant Pneumolysin Induces the Production of Antibodies and Protects Mice in a Model of Systemic Infection Caused by *Streptococcus pneumoniae*. *Bull. Exp. Biol. Med.* 168, 485–487. doi: 10.1007/s10517-020-04736-6
- Piao, Z., Akeda, Y., Takeuchi, D., Ishii, K. J., Ubukata, K., Briles, D. E., et al. (2014). Protective Properties of a Fusion Pneumococcal Surface Protein A (PspA) Vaccine Against Pneumococcal Challenge by Five Different PspA Clades in Mice. *Vaccine* 32, 5607–5613. doi: 10.1016/j.vaccine.2014.07.108
- Pimenta, F. C., Miyaji, E. N., Arêas, A. P. M., Oliveira, M. L. S., De Andrade, A., Ho, P. L., et al. (2006). Intranasal Immunization With the Cholera Toxin B Subunit-Pneumococcal Surface Antigen A Fusion Protein Induces Protection Against Colonization With *Streptococcus pneumoniae* and has Negligible Impact on the Nasopharyngeal and Oral Microbiota of Mice. *Infect. Immun.* 74, 4939–4944. doi: 10.1128/IAI.00134-06
- Plumptre, C. D., Ogunniyi, A. D., and Paton, J. C. (2013a). Surface Association of Pht Proteins of *Streptococcus pneumoniae*. *Infect. Immun.* 81, 3644–3651. doi: 10.1128/IAI.00562-13
- Plumptre, C. D., Ogunniyi, A. D., and Paton, J. C. (2013b). Vaccination Against *Streptococcus pneumoniae* Using Truncated Derivatives of Polyhistidine Triad Protein D. *PLoS One* 8, e78916. doi: 10.1371/journal.pone.0078916
- Poehling, K. A., Talbot, T. R., Griffin, M. R., Craig, A. S., Whitney, C. G., Zell, E., et al. (2006). Invasive Pneumococcal Disease Among Infants Before and After Introduction of Pneumococcal Conjugate Vaccine. *JAMA* 295, 1668–1674. doi: 10.1001/jama.295.14.1668
- Prevaes, S. M. P. J., van Wamel, W. J. B., de Vogel, C. P., Veenhoven, R. H., van Gils, E. J. M., and van Belkum, A. (2012). Nasopharyngeal Colonization Elicits Antibody Responses to Staphylococcal and Pneumococcal Proteins That Are Not Associated With a Reduced Risk of Subsequent Carriage. *Infect. Immun.* 80 (6), 2186–2193. doi: 10.1128/IAI.00037-12
- Price, K. E., and Camilli, A. (2009). Pneumolysin Localizes to the Cell Wall of *Streptococcus pneumoniae*. *J. Bacteriol.* 191, 2163–2168. doi: 10.1128/JB.01489-08
- Prymula, R., Hanovcova, I., Splino, M., Kriz, P., Motlova, J., Lebedova, V., et al. (2011). Impact of the 10-Valent Pneumococcal non-Typeable Haemophilus Influenzae Protein D Conjugate Vaccine (PHiD-CV) on Bacterial Nasopharyngeal Carriage. *Vaccine* 29, 1959–1967. doi: 10.1016/j.vaccine.2010.12.086
- Ravinder, K., Naveen, S., Martina, O., E, P. M., and A, M. B. (2014). Human Antibodies to PhtD, PcpA, and Ply Reduce Adherence to Human Lung Epithelial Cells and Murine Nasopharyngeal Colonization by *Streptococcus pneumoniae*. *Infect. Immun.* 82, 5069–5075. doi: 10.1128/IAI.02124-14
- Rayner, C. F., Jackson, A. D., Rutman, A., Dewar, A., Mitchell, T. J., Andrew, P. W., et al. (1995). Interaction of Pneumolysin-Sufficient and -Deficient Isogenic Variants of *Streptococcus pneumoniae* With Human Respiratory Mucosa. *Infect. Immun.* 63, 442–447. doi: 10.1128/iai.63.2.442-447.1995
- Ren, B., Li, J., Genschmer, K., Hollingshead, S. K., and Briles, D. E. (2012). The Absence of PspA or Presence of Antibody to PspA Facilitates the Complement-Dependent Phagocytosis of Pneumococci *In Vitro*. *Clin. Vaccine Immunol.* 19, 1574–1582. doi: 10.1128/CI.00393-12
- Ren, B., Szalai, A. J., Hollingshead, S. K., and Briles, D. E. (2004). Effects of PspA and Antibodies to PspA on Activation and Deposition of Complement on The Pneumococcal Surface. *Infect. Immun.* 72, 114–122. doi: 10.1128/IAI.72.1.114-122.2004
- Ricci, S., Janulczyk, R., Gerlini, A., Braione, V., Colomba, L., Iannelli, F., et al. (2011). The Factor H-Binding Fragment of PspC as a Vaccine Antigen for the Induction of Protective Humoral Immunity Against Experimental Pneumococcal Sepsis. *Vaccine* 29, 8241–8249. doi: 10.1016/j.vaccine.2011.08.119
- Ring, A., Weiser, J. N., and Tuomanen, E. I. (1998). Pneumococcal Trafficking Across the Blood-Brain Barrier. Molecular Analysis of a Novel Bidirectional Pathway. *J. Clin. Invest.* 102, 347–360. doi: 10.1172/JCI2406
- Romero-Steiner, S., Caba, J., Rajam, G., Langley, T., Floyd, A., Johnson, S. E., et al. (2006). Adherence of Recombinant Pneumococcal Surface Adhesin A (Rpsaa)-Coated Particles to Human Nasopharyngeal Epithelial Cells for the Evaluation of Anti-PsaA Functional Antibodies. *Vaccine* 24, 3224–3231. doi: 10.1016/j.vaccine.2006.01.042
- Romero-Steiner, S., Libutti, D., Pais, L. B., Dykes, J., Anderson, P., Whitin, J. C., et al. (1997). Standardization of an Opsonophagocytic Assay for the Measurement of Functional Antibody Activity Against *Streptococcus*

- Pneumoniae Using Differentiated HL-60 Cells. *Clin. Diagn. Lab. Immunol.* 4, 415–422. doi: 10.1128/cdli.4.4.415-422.1997
- Romero-Steiner, S., Pilishvili, T., Sampson, J. S., Johnson, S. E., Stinson, A., Carlone, G. M., et al. (2003). Inhibition of Pneumococcal Adherence to Human Nasopharyngeal Epithelial Cells by Anti-PsaA Antibodies. *Clin. Diagn. Lab. Immunol.* 10, 246–251. doi: 10.1128/cdli.10.2.246-251.2003
- Rosenow, C., Ryan, P., Weiser, J. N., Johnson, S., Fontan, P., Ortqvist, A., et al. (1997). Contribution of Novel Choline-Binding Proteins to Adherence, Colonization and Immunogenicity of *Streptococcus Pneumoniae*. *Mol. Microbiol.* 25, 819–829. doi: 10.1111/j.1365-2958.1997.mmi494.x
- Rubins, J. B., Charboneau, D., Paton, J. C., Mitchell, T. J., Andrew, P. W., and Janoff, E. N. (1995). Dual Function of Pneumolysin in the Early Pathogenesis of Murine Pneumococcal Pneumonia. *J. Clin. Invest.* 95, 142–150. doi: 10.1172/JCI117631
- Rubins, J. B., Duane, P. G., Charboneau, D., and Janoff, E. N. (1992). Toxicity of Pneumolysin to Pulmonary Endothelial Cells *In Vitro*. *Infect. Immun.* 60, 1740–1746. doi: 10.1128/iai.60.5.1740-1746.1992
- Sampson, J. S., Furlow, Z., Whitney, A. M., Williams, D., Facklam, R., and Carlone, G. M. (1997). Limited Diversity of *Streptococcus Pneumoniae* psaA Among Pneumococcal Vaccine Serotypes. *Infect. Immun.* 65, 1967–1971. doi: 10.1128/iai.65.5.1967-1971.1997
- Sampson, J. S., O'Connor, S. P., Stinson, A. R., Tharpe, J. A., and Russell, H. (1994). Cloning and Nucleotide Sequence Analysis of PsaA, the *Streptococcus Pneumoniae* Gene Encoding a 37-Kilodalton Protein Homologous to Previously Reported *Streptococcus* Sp. Adhesins. *Infect. Immun.* 62, 319–324. doi: 10.1128/iai.62.1.319-324.1994
- Sánchez-Beato, A. R., López, R., and García, J. L. (1998). Molecular Characterization of PcpA: A Novel Choline-Binding Protein of *Streptococcus Pneumoniae*. *FEMS Microbiol. Lett.* 164, 207–214. doi: 10.1111/j.1574-6968.1998.tb13087.x
- Sanders, M. E., Norcross, E. W., Moore, Q. C. 3rd, Fratkin, J., Thompson, H., and Marquart, M. E. (2010). Immunization With Pneumolysin Protects Against Both Retinal and Global Damage Caused by *Streptococcus Pneumoniae* Endophthalmitis. *J. Ocul. Pharmacol. Ther.* 26, 571–577. doi: 10.1089/jop.2010.0077
- Sarah, W., Haijun, T., Nico van, R., Liise-anne, P., and N, W. J. (2012). A Serotype 3 Pneumococcal Capsular Polysaccharide-Specific Monoclonal Antibody Requires Fcγ Receptor III and Macrophages To Mediate Protection Against Pneumococcal Pneumonia in Mice. *Infect. Immun.* 80, 1314–1322. doi: 10.1128/IAI.06081-11
- Seiberling, M., Bologa, M., Brookes, R., Ochs, M., Go, K., Neveu, D., et al. (2012). Safety and Immunogenicity of a Pneumococcal Histidine Triad Protein D Vaccine Candidate in Adults. *Vaccine* 30, 7455–7460. doi: 10.1016/j.vaccine.2012.10.080
- Shak, J. R., Ludewick, H. P., Howery, K. E., Sakai, F., Yi, H., Harvey, R. M., et al. (2013). Novel Role for the *Streptococcus Pneumoniae* Toxin Pneumolysin in the Assembly of Biofilms. *MBio* 4, e00655-13. doi: 10.1128/mBio.00655-13
- Shaper, M., Hollingshead, S. K., Benjamin, W. H. J., and Briles, D. E. (2004). PspA Protects *Streptococcus Pneumoniae* From Killing by Apolactoferrin, and Antibody To PspA Enhances Killing of Pneumococci by Apolactoferrin [Corrected]. *Infect. Immun.* 72, 5031–5040. doi: 10.1128/IAI.72.9.5031-5040.2004
- Simell, B., Auranen, K., Käyhty, H., Goldblatt, D., Dagan, R., and O'Brien, K. L. (2012). The Fundamental Link Between Pneumococcal Carriage and Disease. *Expert Rev. Vaccines* 11, 841–855. doi: 10.1586/erv.12.53
- Song, J. Y., Moseley, M. A., Burton, R. L., and Nahm, M. H. (2013). Pneumococcal Vaccine and Opsonic Pneumococcal Antibody. *J. Infect. Chemother.* 19, 412–425. doi: 10.1007/s10156-013-0601-1
- Steinfurt, C., Wilson, R., Mitchell, T., Feldman, C., Rutman, A., Todd, H., et al. (1989). Effect of *Streptococcus Pneumoniae* on Human Respiratory Epithelium. *Vitro. Infect. Immun.* 57, 2006–2013. doi: 10.1128/iai.57.7.2006-2013.1989
- Subramanian, K., Neill, D. R., Malak, H. A., Spelmink, L., Khandaker, S., Dalla Libera Marchiori, G., et al. (2019). Pneumolysin Binds to the Mannose Receptor C Type 1 (MRC-1) Leading to Anti-Inflammatory Responses and Enhanced Pneumococcal Survival. *Nat. Microbiol.* 4, 62–70. doi: 10.1038/s41564-018-0280-x
- Sundberg-Kövamees, M., Holme, T., and Sjögren, A. (1996). Interaction of the C-Polysaccharide of *Streptococcus Pneumoniae* With the Receptor Asialo-GM1. *Microb. Pathog.* 21, 223–234. doi: 10.1006/mpat.1996.0057
- Swiatlo, E., King, J., Nabors, G. S., Mathews, B., and Briles, D. E. (2003). Pneumococcal Surface Protein A Is Expressed *In Vivo*, and Antibodies to PspA Are Effective for Therapy in a Murine Model of Pneumococcal Sepsis. *Infect. Immun.* 71, 7149–7153. doi: 10.1128/IAI.71.12.7149-7153.2003
- Talkington, D. F., Brown, B. G., Tharpe, J. A., Koenig, A., and Russell, H. (1996). Protection of Mice Against Fatal Pneumococcal Challenge by Immunization With Pneumococcal Surface Adhesin A (PsaA). *Microb. Pathog.* 21, 17–22. doi: 10.1006/mpat.1996.0038
- Tanaka, N., Fukuyama, S., Fukuiwa, T., Kawabata, M., Sagara, Y., Ito, H., et al. (2007). Intranasal Immunization With Phosphorylcholine Induces Antigen Specific Mucosal and Systemic Immune Responses in Mice. *Vaccine* 25, 2680–2687. doi: 10.1016/j.vaccine.2006.10.014
- Thanawastien, A., Joyce, K. E., Cartee, R. T., Haines, L. A., Pelton, S. I., Tweten, R. K., et al. (2021). Preclinical *In Vitro* and *In Vivo* Profile of a Highly-Attenuated, Broadly Efficacious Pneumolysin Genetic Toxoid. *Vaccine* 39, 1652–1660. doi: 10.1016/j.vaccine.2020.04.064
- Tian, H., Weber, S., Thorkildson, P., Kozel, T. R., and Pirofski, L.-A. (2009). Efficacy of Opsonic and Nonopsonic Serotype 3 Pneumococcal Capsular Polysaccharide-Specific Monoclonal Antibodies Against Intranasal Challenge With *Streptococcus Pneumoniae* in Mice. *Infect. Immun.* 77, 1502–1513. doi: 10.1128/IAI.01075-08
- Toh, Z. Q., Higgins, R. A., Mazarakis, N., Abbott, E., Nathanielsz, J., Balloch, A., et al. (2021). Evaluating Functional Immunity Following Encapsulated Bacterial Infection and Vaccination. *Vaccines* 9, 667. doi: 10.3390/vaccines9060677
- Trolle, S., Chachaty, E., Kassir-Chikhani, N., Wang, C., Fattal, E., Couvreur, P., et al. (2000). Intranasal Immunization With Protein-Linked Phosphorylcholine Protects Mice Against a Lethal Intranasal Challenge With *Streptococcus Pneumoniae*. *Vaccine* 18, 2991–2998. doi: 10.1016/S0264-410X(00)00089-X
- Tseng, H.-J., McEwan, A. G., Paton, J. C., and Jennings, M. P. (2002). Virulence of *Streptococcus Pneumoniae*: PsaA Mutants are Hypersensitive to Oxidative Stress. *Infect. Immun.* 70, 1635–1639. doi: 10.1128/IAI.70.3.1635-1639.2002
- Tu, A. H., Fulgham, R. L., McCrory, M. A., Briles, D. E., and Szalai, A. J. (1999). Pneumococcal Surface Protein A Inhibits Complement Activation by *Streptococcus Pneumoniae*. *Infect. Immun.* 67, 4720–4724. doi: 10.1128/IAI.67.9.4720-4724.1999
- Turner, P., Turner, C., Green, N., Ashton, L., Lwe, E., Jankhot, A., et al. (2013). Serum Antibody Responses to Pneumococcal Colonization in the First 2 Years of Life: Results From an SE Asian Longitudinal Cohort Study. *Clin. Microbiol. Infect.* 19, E551–E558. doi: 10.1111/1469-0691.12286
- Uchiyama, S., Carlin, A. F., Khosravi, A., Weiman, S., Banerjee, A., Quach, D., et al. (2009). The Surface-Anchored NanA Protein Promotes Pneumococcal Brain Endothelial Cell Invasion. *J. Exp. Med.* 206, 1845–1852. doi: 10.1084/jem.20090386
- Verhoeven, D., Xu, Q., and Pichichero, M. E. (2014). Vaccination With a *Streptococcus Pneumoniae* Trivalent Recombinant PcpA, PhtD and PlyD1 Protein Vaccine Candidate Protects Against Lethal Pneumonia in an Infant Murine Model. *Vaccine* 32, 3205–3210. doi: 10.1016/j.vaccine.2014.04.004
- Visan, L., Rouleau, N., Proust, E., Peyrot, L., Donadieu, A., and Ochs, M. (2018). Antibodies to PcpA and PhtD Protect Mice Against *Streptococcus Pneumoniae* by a Macrophage- and Complement-Dependent Mechanism. *Hum. Vaccin. Immunother.* 14, 489–494. doi: 10.1080/21645515.2017.1403698
- von Gottberg, A., de Gouveia, L., Tempia, S., Quan, V., Meiring, S., von Mollendorf, C., et al. (2014). Effects of Vaccination on Invasive Pneumococcal Disease in South Africa. *N. Engl. J. Med.* 371, 1889–1899. doi: 10.1056/NEJMoa1401914
- Voss, S., Hallström, T., Saleh, M., Burchhardt, G., Pribyl, T., Singh, B., et al. (2013). The Choline-Binding Protein PspC of *Streptococcus Pneumoniae* Interacts With the C-Terminal Heparin-Binding Domain of Vitronectin. *J. Biol. Chem.* 288, 15614–15627. doi: 10.1074/jbc.M112.443507
- Wallick, S., Clafin, J. L., and Briles, D. E. (1983). Resistance to *Streptococcus Pneumoniae* Is Induced by a Phosphocholine-Protein Conjugate. *J. Immunol.* 130, 2871–2875.

- Wang, S., Li, Y., Shi, H., Scarpellini, G., Torres-Escobar, A., Roland, K. L., et al. (2010). Immune Responses to Recombinant Pneumococcal PsaA Antigen Delivered by a Live Attenuated Salmonella Vaccine. *Infect. Immun.* 78, 3258–3271. doi: 10.1128/IAI.00176-10
- Wantuch, P. L., and Avci, F. Y. (2018). Current Status and Future Directions of Invasive Pneumococcal Diseases and Prophylactic Approaches to Control Them. *Hum. Vaccin. Immunother.* 14, 2303–2309. doi: 10.1080/21645515.2018.1470726
- Wartha, F., Beiter, K., Albiger, B., Fernebro, J., Zychlinsky, A., Normark, S., et al. (2007). Capsule and D-Alanylated Lipoteichoic Acids Protect Streptococcus Pneumoniae Against Neutrophil Extracellular Traps. *Cell. Microbiol.* 9, 1162–1171. doi: 10.1111/j.1462-5822.2006.00857.x
- Weinberger, D. M., Dagan, R., Givon-Lavi, N., Regev-Yochay, G., Malley, R., and Lipsitch, M. (2008). Epidemiologic Evidence for Serotype-Specific Acquired Immunity to Pneumococcal Carriage. *J. Infect. Dis.* 197, 1511–1518. doi: 10.1086/587941
- Weiser, J. N., Ferreira, D. M., and Paton, J. C. (2018). Streptococcus Pneumoniae: Transmission, Colonization and Invasion. *Nat. Rev. Microbiol.* 16, 355–367. doi: 10.1038/s41579-018-0001-8
- W, J. J., E, M. L., M, O. M., H, B. W., E, B. D., and K, H. S. (2004). Lipoprotein PsaA in Virulence of Streptococcus Pneumoniae: Surface Accessibility and Role in Protection From Superoxide. *Infect. Immun.* 72, 5858–5867. doi: 10.1128/IAI.72.10.5858-5867.2004
- WHO (2017). *WHO Publishes List of Bacteria for Which New Antibiotics are Urgently Needed* (Geneva: Media Cent).
- Wiedinger, K., McCauley, J., and Bitsakis, C. (2020). Isotype-Specific Outcomes in Fc Gamma Receptor Targeting of PspA Using Fusion Proteins as a Vaccination Strategy Against Streptococcus Pneumoniae Infection. *Vaccine* 38, 5634–5646. doi: 10.1016/j.vaccine.2020.06.067
- Wilson, R., Cohen, J. M., Reglinski, M., Jose, R. J., Chan, W. Y., Marshall, H., et al. (2017). Naturally Acquired Human Immunity to Pneumococcus Is Dependent on Antibody to Protein Antigens. *PLoS Pathog.* 13, e1006137. doi: 10.1371/journal.ppat.1006137
- Wizemann, T. M., Heinrichs, J. H., Adamou, J. E., Erwin, A. L., Kunsch, C., Choi, G. H., et al. (2001). Use of a Whole Genome Approach to Identify Vaccine Molecules Affording Protection Against Streptococcus Pneumoniae Infection. *Infect. Immun.* 69, 1593–1598. doi: 10.1128/IAI.69.3.1593-1598.2001
- Wu, H. Y., Nahm, M. H., Guo, Y., Russell, M. W., and Briles, D. E. (1997). Intranasal Immunization of Mice With PspA (Pneumococcal Surface Protein A) can Prevent Intranasal Carriage, Pulmonary Infection, and Sepsis With Streptococcus Pneumoniae. *J. Infect. Dis.* 175, 839–846. doi: 10.1086/513980
- Xu, G., Kiefel, M. J., Wilson, J. C., Andrew, P. W., Oggioni, M. R., and Taylor, G. L. (2011). Three Streptococcus Pneumoniae Sialidases: Three Different Products. *J. Am. Chem. Soc.* 133, 1718–1721. doi: 10.1021/ja110733q
- Xu, Q., Pryharski, K., and Pichichero, M. E. (2017). Trivalent Pneumococcal Protein Vaccine Protects Against Experimental Acute Otitis Media Caused by Streptococcus Pneumoniae in an Infant Murine Model. *Vaccine* 35, 337–344. doi: 10.1016/j.vaccine.2016.11.046
- Yahiaoui, R. Y., den Heijer, C. D., van Bijnen, E. M., Paget, W. J., Pringle, M., Goossens, H., et al. (2016). Prevalence and Antibiotic Resistance of Commensal Streptococcus Pneumoniae in Nine European Countries. *Future Microbiol.* 11, 737–744. doi: 10.2217/fmb-2015-0011
- Yano, M., Gohil, S., Coleman, J. R., Manix, C., and Pirofski, L. (2011). Antibodies to Streptococcus Pneumoniae Capsular Polysaccharide Enhance Pneumococcal Quorum Sensing. *MBio* 2, e00176–11. doi: 10.1128/mBio.00176-11
- Yoo, I.-H., Shin, H.-S., Kim, Y.-J., Kim, H.-B., Jin, S., and Ha, U.-H. (2010). Role of Pneumococcal Pneumolysin in the Induction of an Inflammatory Response in Human Epithelial Cells. *FEMS Immunol. Med. Microbiol.* 60, 28–35. doi: 10.1111/j.1574-695X.2010.00699.x
- Yun, K. W., Lee, H., Choi, E. H., and Lee, H. J. (2015). Diversity of Pneumolysin and Pneumococcal Histidine Triad Protein D of Streptococcus Pneumoniae Isolated From Invasive Diseases in Korean Children. *PLoS One* 10, e0134055. doi: 10.1371/journal.pone.0134055
- Zafar, M. A., Wang, Y., Hamaguchi, S., and Weiser, J. N. (2017). Host-To-Host Transmission of Streptococcus Pneumoniae Is Driven by Its Inflammatory Toxin, Pneumolysin. *Cell Host Microbe* 21, 73–83. doi: 10.1016/j.chom.2016.12.005
- Zhang, Q., Bernatoniene, J., Bagrade, L., Pollard, A. J., Mitchell, T. J., Paton, J. C., et al. (2006). Serum and Mucosal Antibody Responses to Pneumococcal Protein Antigens in Children: Relationships With Carriage Status. *Eur. J. Immunol.* 36, 46–57. doi: 10.1002/eji.200535101
- Zysk, G., Schneider-Wald, B. K., Hwang, J. H., Bejo, L., Kim, K. S., Mitchell, T. J., et al. (2001). Pneumolysin is the Main Inducer of Cytotoxicity to Brain Microvascular Endothelial Cells Caused by Streptococcus Pneumoniae. *Infect. Immun.* 69, 845–852. doi: 10.1128/IAI.69.2.845-852.2001

Conflict of Interest: AG and JM have applied for a provisional patent application covering human monoclonal antibody sequences for prevention and treatment of pneumococcal infection.

The remaining authors declare that the research was conducted in the absence of any commercial or financial relationships that could be construed as a potential conflict of interest.

Publisher's Note: All claims expressed in this article are solely those of the authors and do not necessarily represent those of their affiliated organizations, or those of the publisher, the editors and the reviewers. Any product that may be evaluated in this article, or claim that may be made by its manufacturer, is not guaranteed or endorsed by the publisher.

Copyright © 2022 Gingerich and Mousa. This is an open-access article distributed under the terms of the Creative Commons Attribution License (CC BY). The use, distribution or reproduction in other forums is permitted, provided the original author(s) and the copyright owner(s) are credited and that the original publication in this journal is cited, in accordance with accepted academic practice. No use, distribution or reproduction is permitted which does not comply with these terms.



A Jack of All Trades: The Role of Pneumococcal Surface Protein A in the Pathogenesis of *Streptococcus pneumoniae*

Jessica R. Lane, Muralidhar Tata, David E. Briles and Carlos J. Orihuela*

Department of Microbiology, The University of Alabama at Birmingham, Birmingham, AL, United States

OPEN ACCESS

Edited by:

Jorge Eugenio Vidal,
University of Mississippi Medical
Center, United States

Reviewed by:

Ed Swiatlo,
Southeast Louisiana Veterans Health
Care System, United States
Masaya Yamaguchi,
Osaka University, Japan

*Correspondence:

Carlos J. Orihuela
corihuel@uab.edu

Specialty section:

This article was submitted to
Molecular Bacterial Pathogenesis,
a section of the journal
Frontiers in Cellular and
Infection Microbiology

Received: 30 November 2021

Accepted: 10 January 2022

Published: 02 February 2022

Citation:

Lane JR, Tata M, Briles DE and
Orihuela CJ (2022) A Jack of All
Trades: The Role of Pneumococcal
Surface Protein A in the Pathogenesis
of *Streptococcus pneumoniae*.
Front. Cell. Infect. Microbiol. 12:826264.
doi: 10.3389/fcimb.2022.826264

Streptococcus pneumoniae (*Spn*), or the pneumococcus, is a Gram-positive bacterium that colonizes the upper airway. *Spn* is an opportunistic pathogen capable of life-threatening disease should it become established in the lungs, gain access to the bloodstream, or disseminate to vital organs including the central nervous system. *Spn* is encapsulated, allowing it to avoid phagocytosis, and current preventative measures against infection include polyvalent vaccines composed of capsular polysaccharide corresponding to its most prevalent serotypes. The pneumococcus also has a plethora of surface components that allow the bacteria to adhere to host cells, facilitate the evasion of the immune system, and obtain vital nutrients; one family of these are the choline-binding proteins (CBPs). Pneumococcal surface protein A (PspA) is one of the most abundant CBPs and confers protection against the host by inhibiting recognition by C-reactive protein and neutralizing the antimicrobial peptide lactoferricin. Recently our group has identified two new roles for PspA: binding to dying host cells via host-cell bound glyceraldehyde 3-phosphate dehydrogenase and co-opting of host lactate dehydrogenase to enhance lactate availability. These properties have been shown to influence *Spn* localization and enhance virulence in the lower airway, respectively. Herein, we review the impact of CBPs, and in particular PspA, on pneumococcal pathogenesis. We discuss the potential and limitations of using PspA as a conserved vaccine antigen in a conjugate vaccine formulation. PspA is a vital component of the pneumococcal virulence arsenal – therefore, understanding the molecular aspects of this protein is essential in understanding pneumococcal pathogenesis and utilizing PspA as a target for treating or preventing pneumococcal pneumonia.

Keywords: *Streptococcus pneumoniae*, choline-binding proteins, pneumococcal surface protein A (PspA), pathogenesis, vaccine

INTRODUCTION

Streptococcus pneumoniae (*Spn*), or the pneumococcus, is a Gram-positive bacterium that colonizes the nasopharynx. From the nasopharynx, *Spn* can disseminate to normally sterile sites to cause opportunistic infections. These sites include the middle ear, where *Spn* causes otitis media (Bluestone et al., 1992). *Spn* can also be aspirated into the lower respiratory tract to cause pneumonia. These infections typically occur in infants, those who are immunocompromised, or in the elderly (Brooks and Mias, 2018). In approximately 30% of individuals with pneumonia, *Spn* gains access to the bloodstream and the ensuing bacteremia can result in sepsis and disseminated organ damage (Askim et al., 2016; Asner et al., 2019). Within the bloodstream, pneumococci encounter the blood-brain barrier and in rare cases can cross this endothelial cell barrier to cause meningitis (Ring et al., 1998; Thigpen et al., 2011). It is important to consider that *Spn* is primarily an asymptomatic commensal and severe infections are uncommon among otherwise healthy adults. Clinical epidemiological studies show that most affected individuals had at least one or more underlying conditions placing them at higher risk of infection (Bogaert et al., 2004). Pneumococcal infections, even among those who are susceptible, are commonly preceded by prior viral exposure (O'Brien et al., 2000; Jansen et al., 2008). Viral infections, particularly influenza, have been shown to prime mucosal epithelial cells for bacterial binding, enhance carbohydrate and protein levels in airway secretions, and disarm or deflect the immune system. These events enhance the susceptibility of the lower airway for bacterial establishment and, once pneumonia develops, can accelerate the progression towards invasive disease (Hament et al., 1999; Diavatopoulos et al., 2010; Loughran et al., 2019; Van Der Poll and Opal, 2009).

In 2018, the Centers for Disease Control and Prevention reported that pneumococcal pneumonia resulted in 150,000 individuals being hospitalized in the United States, while pneumococcal bacteremia and meningitis caused 3,500 deaths (Centers for Disease Control and Prevention, 2018). Across the globe, pneumococcal burden was estimated to be 26.7 incidences per 1,000 people causing over one million deaths (Global Burden of Disease Lower Respiratory Infections Collaborators, 2018). Multiple vaccines are currently licensed to protect against *Spn* disease and all are composed of capsular polysaccharide from *Spn*'s most prevalent serotypes (Scott et al., 2021). Since the introduction of a 7-valent conjugate vaccine in 2000, followed by the 13-valent version in 2010, invasive pneumococcal disease (IPD) in children <5 years has drastically decreased by as much 93% in the United States (Centers for Disease Control and Prevention, 2018). In adults, there has been an overall reduction of IPD incidence from 16 to 8 cases per 100,000 (Centers for Disease Control and Prevention, 2018). However, the threat of vaccine escape, serotype 3 for which the vaccine has poor efficacy, and remnant disease caused by non-vaccine serotypes, has kept efforts to improve on these vaccines a top priority (Scott et al., 2021). Along such lines and in 2021, 15- and 20-valent conjugate vaccines were approved, and these will most likely further lower pneumonia rates in the near future (Hurley

et al., 2020). Despite the tremendous success of the conjugate vaccines, *Spn* remains a leading cause of community-acquired pneumonia and invasive disease (Global Burden of Disease Lower Respiratory Infections Collaborators, 2018).

Spn has several virulence factors that aid its survival within the host, one of these being its capsular polysaccharide which protects it from phagocytosis by immune cells (Hyams et al., 2010). Another being the toxin pneumolysin, which forms pores in the membranes of host cells resulting in ion dysregulation and, at higher concentrations, cell death by apoptosis or necroptosis (Hirst et al., 2004; González-Juarbe et al., 2015). Pneumococcal pneumonia is characterized by a strong inflammatory response in the airway that results in lung consolidation and loss of gas exchange. Pneumolysin, in addition to killing cells and causing the release of alarmins, activates the classical complement cascade (Mitchell and Dalziel, 2014). Lipoteichoic (LTA) and cell wall teichoic acid (WTA) associated with the pneumococcus are Toll-like receptor 1/2 ligands and therefore are also inflammatory (Draing et al., 2006). Phosphorylcholine (PC) residues that are present on LTA and WTA mimic the molecular structure of host platelet-activating factor and bind to platelet-activating factor receptor (PAFr) (Cundell et al., 1995). This activates host cells, resulting in chemokine production, and the PC residues on the surface of the bacterium are targeted by C-reactive protein, which activates complement and exacerbates inflammation (Pepys and Hirschfield, 2003). The pneumococcus is generally protected by its capsule from killing by infiltrated immune cells until the host develops capsule-specific antibody, which then effectively opsonizes the bacterium for phagocytosis.

Clinical isolates of *Spn* vary considerably in their genetic content, as much as 10-15% between strains, and carry between 10-16 choline-binding proteins (CBP) (Hiller et al., 2007; Gisch et al., 2013). With exception to serotype 1 (Cornick et al., 2017), the majority of *Spn* produce pneumococcal surface protein A (PspA), a 65 to 99-kDa CBP that protects the bacteria from C-reactive protein-mediated activation of complement and from killing by lactoferricin, a cationic antimicrobial peptide (Hammerschmidt et al., 1999; Tu et al., 1999). Recent findings from our group describe two new functions for PspA, as an adhesin and means to co-opt host metabolic enzymes for its benefit (Park et al., 2021a; Park et al., 2021b). Indeed, this protein acts as a "Jack of All Trades." In this review, we will summarize how PC and CBPs contribute to pneumococcal pathogenesis and the role PspA plays during infection. At conclusion, we will discuss how our new understanding of PspA virulence provides insight into *Spn* pathogenesis and the implications towards new treatments and potentially improved vaccines.

Phosphorylcholine on the Pneumococcal Surface

Pneumococcal cell wall is located outside the cell membrane and underneath the capsular polysaccharide layer of *Spn*. It is composed of peptidoglycan chains cross-linked to each other with interlaced teichoic acid (Galán-Bartual et al., 2015). The cell wall also acts as an anchor point for capsule types that rely on the

Wxy/Wzy-dependent synthesis pathway (Geno et al., 2015). PC is a small amino alcohol that is essential for eukaryotic cell growth but also commonly found on the surface of bacterial pathogens (García et al., 1998; Harnett and Harnett, 1999). Choline is not synthesized by *Spn*, yet the bacteria is dependent on it for growth or one of its structural analogues, such as ethanolamine (Galán-Bartual et al., 2015). The *lic* operon in *Spn* encodes the transporters and enzymes necessary for the uptake and conversion of environmental choline into PC, eventually incorporating it into either LTA or WTA (Zhang et al., 1999).

LTA and WTA are composed of four to eight repeating units of ribitol 5-phosphate, *N*-acetyl-D-galactosaminyl (GalNAc), 2-acetamido-4-amino-2,4,6-trideoxy-D-galactose (AATGal), and D-glucose (Behr et al., 1992; Jennings et al., 1980). The number of PC residues on the pneumococcal surface varies between strains and can also be influenced by phase-variation (Weiser et al., 1994; Kim and Weiser, 1998). PC on the surface of the pneumococcus functions as a mimetic of platelet-activating factor and thereby binds PAFr on host cells (Cundell et al., 1995; Ring et al., 1998). Its binding by pneumococcal PC results in MAPK activation as well as recruitment of β -arrestin and clathrin to the receptor base for its internalization (Ishii and Shimizu, 2000; Radin et al., 2005; Stafforini, 2009; Asmat et al., 2014). Subsequently, clathrin-mediated endocytosis occurs with uptake of the receptor-bound bacteria into an endosome. Thus, PC plays a vital role in pneumococcal adhesion and the invasion of non-immune cells. Its lowered expression has been shown to result in decreased levels of colonization of the upper airway in a murine model of infection (Kharat and Tomasz, 2006).

PC on the surface of microorganisms is an important target for the host response. C-reactive protein (CRP), which is made by the liver in response to IL-6, binds to PC activating the complement cascade (Volanakis and Kaplan, 1971; Thompson et al., 1999). Classical complement proteins such as C1q, C4, and C2 recognize and bind to PC-bound CRP with subsequent activation of the cascade and opsonization of the bacterial surface (Rupprecht et al., 2007). Additionally, an anti-phosphorylcholine (anti-PC) IgM autoantibody is produced by CD5⁺ B-cells that provides another layer of host defense against *Spn* or other PC-bearing pathogens (Briles et al., 1981). Notably, anti-PC antibodies are ubiquitous in human sera with up to 10% of total IgM being reactive to PC (Su et al., 2006; Chou et al., 2008).

CHOLINE-BINDING PROTEINS

CBPs generally consist of three major domains: a leader peptide, a variable biologically functional domain sometimes followed by a proline-rich domain (PRD), and a conserved choline-binding domain (Bergmann and Hammerschmidt, 2006). The majority of CBPs contain a choline-binding domain at the C-terminal end with some exceptions such as LytB and LytC, where the domain is present at the N-terminus, while for CbpL it is present in the central region of the protein (Bergmann and Hammerschmidt, 2006). The choline-binding domain is modular with a variable

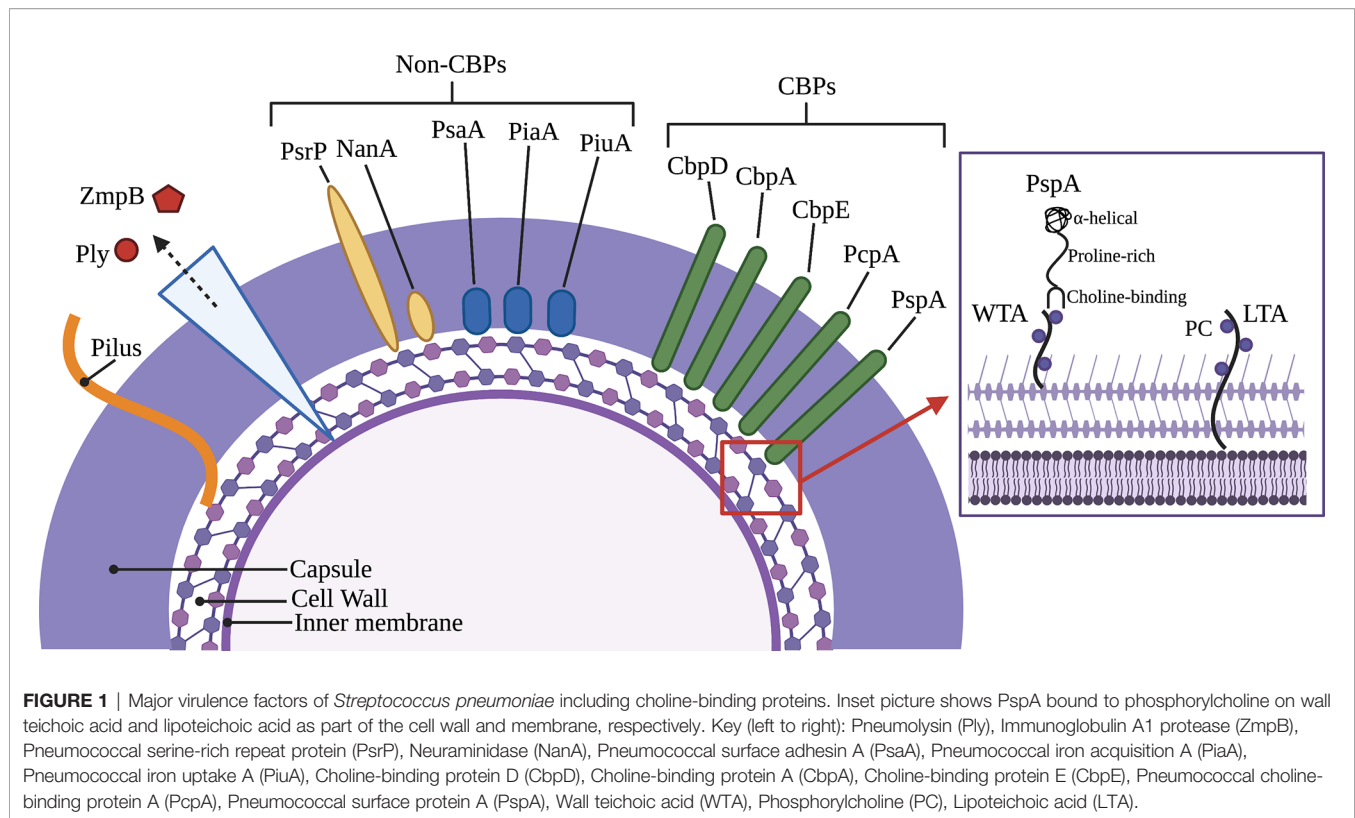
number of repeating units consisting of a ~20 amino acid-sequence, i.e., choline-binding motifs. Only four to five choline-binding motifs are required for interaction with PC on LTA or WTA to occur and for the CBP to become docked onto the pneumococcal surface (Yother and White, 1994). The majority of *Spn* strains carry two PC residues per repeating unit of AATGal and GalNAc on LTA or WTA and these are linked *via* a phosphodiester bond to the O6 molecule of GalNAc (Vollmer et al., 2019). Choline-binding motifs are spaced so that the choline-binding domain becomes interlaced with the repeating PC residues.

Most strains of *Spn* encode more than 10 CBPs in their genome (Hakenbeck et al., 2009). Among those best characterized are the cell wall hydrolytic enzymes LytA, LytB, and LytC, the pneumococcal surface protein A (PspA), pneumococcal choline-binding protein A (PcpA), and the choline-binding proteins CbpA and CbpC (**Figure 1**) (Hakenbeck et al., 2009). For a complete list of pneumococcal CBPs and their function during colonization and pathogenesis see **Table 1**. Unfortunately, the nomenclature of CBPs becomes complicated as proteins have more than one name and related proteins have similar names and abbreviations. For instance, choline-binding protein A (CbpA) and pneumococcal surface protein C (PspC) are the same protein (Rosenow et al., 1997; Gosink et al., 2000). Herein, we will discuss PspA and CbpA, and will use these names to maintain distinction.

Structure and Variability of PspA

PspA is an abundant surface-exposed virulence factor. It is found in nearly all clinical isolates of *Spn*, but not in other *Streptococci* (Crain et al., 1990). Transcriptomic studies suggest it is expressed across all anatomical host sites and organs during infection (D'Mello et al., 2020). Based on the sequence variations among strains and differences in reactivity with antibodies, it is now recognized that PspA proteins are mosaics. The size of mature PspA ranges from 65 to 99 kDa across various strains consisting of the three major domains: the N-terminal alpha-helical, the proline-rich, and the C-terminal choline-binding (**Figure 2**).

The N-terminal region of PspA is 280-380 amino acids (aa) long, immunogenic, and highly variable. It is composed of an antiparallel coiled-coil alpha-helical charged domain (α HD) in an elongated rod-like shape. The charge on the α HD is significantly polarized being electropositive at the C-terminal end and electronegative at the N-terminal end (Lamani et al., 2000). This polarization helps the interaction between PspA and the negatively charged capsule while also decreasing the antibacterial phagocytic activity (Nomura and Nagayama, 1995). The C-terminal 100 aa's of α HD consist of a clade-defining region (CDR) which is the basis for the classification of PspA into 3 families (Hollingshead et al., 2000). Each family is divided into clades, with Family 1 comprised of clade 1 and 2; Family 2 comprised of clades 3, 4 and 5; and Family 3 comprised of the rarer clade 6. Primary amino acid sequences within the same clade exhibit $\geq 90\%$ identity compared to only $\leq 55\%$ identity across different families. The first 100 N-terminal aa's and the last 100 C-terminal aa's of the α HD can also elicit a protective antibody response against *Spn* (McDaniel et al., 1994;



Roche et al., 2003; Vadesilho et al., 2014) and for this reason are thought to be highly variable between strains. Even though there is significant cross-reactivity of antibodies against different families of PspA, protection is not always guaranteed across different families, an important consideration for its inclusion in any future vaccine formulations.

The PRD domain consists of repeats of a 6-7 aa motif and can occur several times in any sequence with their diversity well-characterized by Mukerji et al. (2018). Based on the primary amino acid sequence of PspA in 123 pneumococcal isolates, PRD has been divided into three distinct groups. A common motif that is present in many PRD is PAPAPAPA; in some cases, this motif is truncated or interrupted by other amino acids or overlap with other motifs. Another short amino acid motif present in PRD sequences is PKPEQP, occurring in 96% of Group 1 and 73% of Group 3 strains, while it is absent in Group 2 (Mukerji et al., 2018). There are also other differences in motif patterns, for example, in Group 3 the repetition of motifs occurs less frequently and are more dispersed across the PRD, while in Group 1 only a few of the motifs were repetitive, QPAPA or PAPA. Another distinguishing feature of Group 3 PRD-domains in relation to other groups is the presence of a 22 aa non-proline block (NPB) "QQAEDYARRSEEEYNRLTQQ". The NPB is highly conserved, however, a significant single amino acid polymorphism was observed within the NPB immediately preceding "QQQ". There were other significant variations observed in the flanking regions of NPB (Mukerji et al., 2018), however the biological significance of these variations is unknown. Both the NPB and the PKPEQP motifs of PRD

elicited an immune response and provided protection in mice from a fatal pneumococcal infection caused by isolates that carried a version of PspA with these motifs (Daniels et al., 2010). Notably, the PRD motif is not exclusive to PspA and is also found in CbpA (Rosenow et al., 1997). CbpA, like PspA, has N-terminal alpha-helical domains with the PRD motif positioned between these and the CBD (Luo et al., 2005).

Due to its surface exposure and the fact that antibodies against PspA help eradicate the bacteria, PspA is under considerable immunological pressure. Accordingly, the presence of mosaic gene structure and diversity in PspA sequences across various *Spn* are indicative of intraspecies horizontal gene transfer and genetic recombination. These derivatives, in turn, are positively selected within the host as they are a means to evade the adaptive immune response against PspA. Notably, the conserved nature of PspA's repeat motifs imply a direction of evolution where these motifs not only provide antigenic variability, but also confer functions to PspA that impact its virulence. One clear example of this is the NPB (detailed below).

ESTABLISHED ROLES FOR PSPA IN PNEUMOCOCCAL VIRULENCE

PspA was discovered by McDaniel et al. as a result of studies that identified a monoclonal antibody against *Spn* that was not specific against its capsule but was protective against bacterial challenge (McDaniel et al., 1984). The antigen was subsequently

TABLE 1 | Choline-binding proteins of *Streptococcus pneumoniae*.

Name	Abbreviation	Function
Autolysin A	LytA	<i>N</i> -acetylmuramoyl-L-alanine amidase; fratricide; capsule shedding; lysis-mediated release of pneumolysin (Tomasz and Westphal, 1971; Mitchell et al., 1997; Kietzman et al., 2016)
Autolysin B	LytB	Separation of daughter cells via <i>N</i> -acetylglucosamine (García et al., 1999; Gosink et al., 2000)
Autolysin C	LytC	Lysozyme; fratricide; binds extracellular DNA to facilitate biofilm formation (Gosink et al., 2000; Eldholm et al., 2009)
Choline-binding protein A	CbpA (also PspC)	Binds laminin receptor; binds polymeric immunoglobulin receptor; mediates bacterial uptake and translocation across epithelial and endothelial layers; binds C3, binds serum factor H (Zhang et al., 2000; Duthy et al., 2002; Orihuela et al., 2004b; Orihuela et al., 2009; Brown et al., 2014)
Choline-binding protein D	CbpD	Competence-mediated fratricide (Gosink et al., 2000; Eldholm et al., 2009)
Choline-binding protein E (also phosphorylcholine esterase)	CbpE (also Pce)	Curates PC residues on pneumococcal surface (Gosink et al., 2000; Hermoso et al., 2005)
Choline-binding protein F	CbpF	Immunity protein protects against autolysis by LytC (Molina et al., 2009)
Choline-binding protein G	CbpG	Serine protease; adhesin (Gosink et al., 2000; Mann et al., 2006)
Choline-binding protein I	CbpI	Adhesin; immune evasion (García et al., 1988; Frolet et al., 2010)
Choline-binding protein J	CbpJ	Adhesin; immune evasion (Frolet et al., 2010; Yamaguchi et al., 2019)
Choline-binding protein K	CbpK	Adhesin (Gosink et al., 2000; Tettelin et al., 2001)
Choline-binding protein L	CbpL	Invasion; immune evasion (Frolet et al., 2010; Gutiérrez-Fernández et al., 2016)
Choline-binding protein M	CbpM	Adhesin; immune evasion (Frolet et al., 2010; Afshar et al., 2016)
Pneumococcal surface protein A	PspA	Blocks C-reactive protein; binds lactoferricin; binds GAPDH; binds LDH (McDaniel et al., 1984; McDaniel et al., 1986; McDaniel et al., 1987; Shaper et al., 2004; Mukerji et al., 2012; Park et al., 2021a; Park et al., 2021b)
Pneumococcal choline-binding protein A	PcpA	Adhesin; aggregation (Sánchez-Beato et al., 1998)

recognized as being a surface protein, opening the possibility of protein-based vaccines against the pneumococcus. Subsequent studies by McDaniel and others showed that PspA was required for pneumococcal virulence and that PspA was a CBP. Further studies over the next decade by McDaniel along with Briles and Yother introduced details about the complexity of PspA and established its critical role in pneumococcal pathogenesis and virulence (McDaniel et al., 1987; Briles et al., 1988; Crain et al., 1990; Yother and Briles, 1992; Yother and White, 1994; Briles et al., 1996).

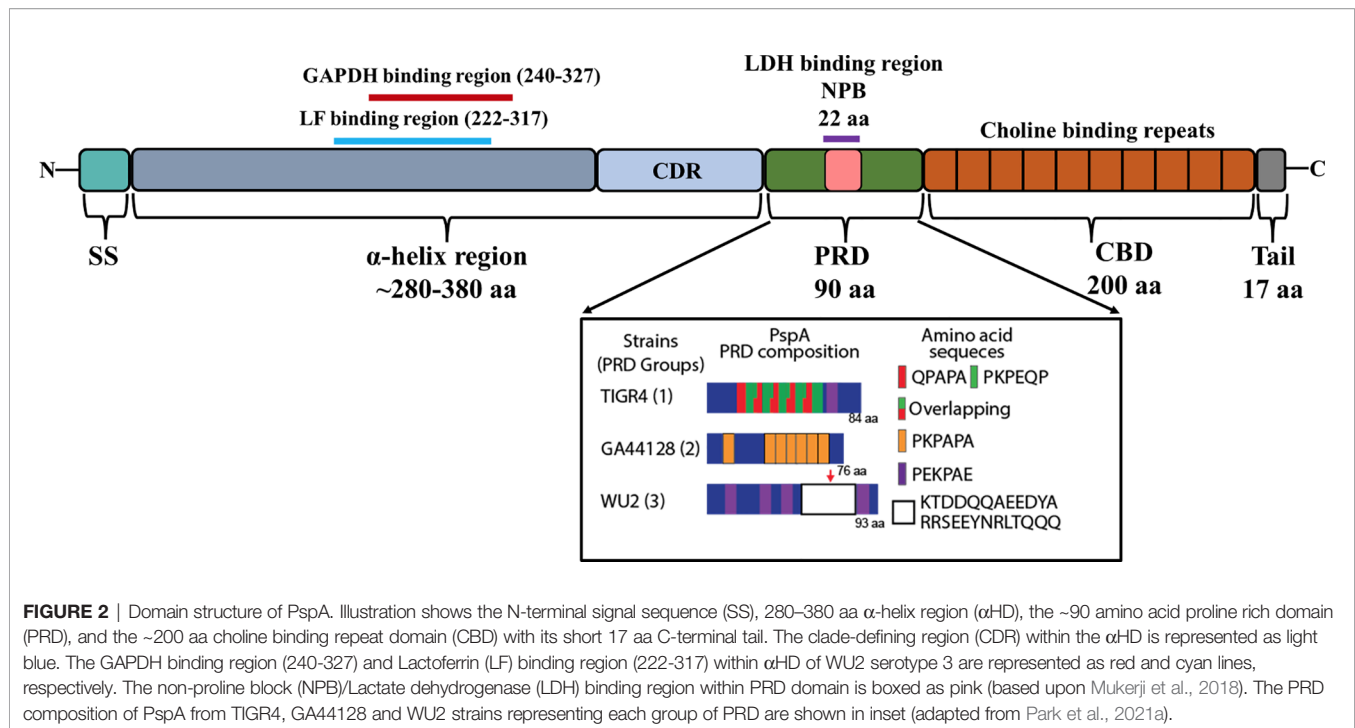
PspA Regulation

The gene encoding PspA is in the chromosome and not part of a polycistronic operon. Upstream of *pspA* in strain TIGR4 is a 289 bp intergenic region that presumably regulates its expression (Tettelin et al., 2001; Ribeiro et al., 2012). Two-component signal transduction systems (TCSTS) function to sense environmental cues and regulate pneumococcal gene expression (Gómez-Mejía et al., 2018). It has been reported that *pspA* expression is positively regulated via the VicRK TCSTS and that the phosphorylated VicR (YycF) response regulator increases its binding upstream of the gene (Ng et al., 2005). The binding of VicR-P protected these regions from digestion by DNase I, suggesting enhanced transcription regulation of PspA (Ng et al., 2005). Additionally, there is a second TCSTS in *Spn* that regulates PspA called RR/HK06, which also regulates CbpA (Standish et al., 2007). *pspA* expression was repressed when the response regulator RR06 was phosphorylated and overexpressed (Standish et al., 2007). A recent report by Im et al. also showed *pspA* gene expression is influenced by carbon-catabolite repression and nutrient availability (Im et al., 2021). Altogether, one can infer that the regulation of *pspA* is multifaceted and complex.

Importantly, there have been numerous reports that show *pspA* expression is responsive to the host environment (Gupta et al., 2009; Ogunniyi et al., 2002; Orihuela et al., 2004a; Lemessurier et al., 2006). Current efforts to characterize *in vivo* PspA gene expression include dual species RNA-seq of infected organs from mice using multiple bacterial strains (D'Mello et al., 2020). Using *Spn* serotypes 2, 4, and 6A, our group found that *pspA* was one of the 100 most highly expressed genes overall and that this high level of expression was shared across all anatomical sites of infection including the nasopharynx, lungs, blood, heart, and kidneys (D'Mello et al., 2020). Viral infections can enhance dispersal of pneumococci from biofilms under different conditions, such as during a fever. Interestingly, increased expression of *pspA* was observed when pneumococci were exposed to influenza A virus (IAV). This occurred when pneumococci were grown either planktonically or as a biofilm (Pettigrew et al., 2014). Expression of *pspA* was also observed to be increased in pneumococci that had recently dispersed from a biofilm versus those growing as a biofilm (Pettigrew et al., 2014).

Complement Evasion

Complement is an enzymatic, self-amplifying cascade that involves the deposition of opsonizing proteins on the surface of bacteria that facilitate their recognition and uptake by phagocytes along with the release of chemotactic and activating factors that attract and recruit immune cells to the site of infection. Complement culminates in the formation of the membrane-attack complex (MAC) which has bactericidal effects, although the thick Gram-positive cell wall of the pneumococcus is resistant to this process (Loughran et al., 2019). Regarding the classical cascade, immunoglobulins such as IgA, IgG, and IgM recognize and bind to specific moieties on the bacterial surface (Andre et al., 2017). Recognition is to antigens



previously seen by the host during prior infection episodes or to components where naturally occurring antibody is generated, for example PC within WTA (Winkelstein and Tomasz, 1978). Regarding the alternative cascade, degradation of serum protein C3 results in the generation of C3a and C3b. C3b recognizes teichoic acid and binds to bacterial surface components initiating activation of the pathway (Hummell et al., 1981; Andre et al., 2017). The complement cascade can be blocked by serum Factor H, which the pneumococcus binds to via CbpA, which in turn binds Factor I and degrades C3b (Hyams et al., 2013). Other ways to activate complement are certain serum proteins, such as lectins, which act through the classical and lectin cascades. One of which is aforementioned CRP (Thompson et al., 1999). Many excellent reviews on the complement cascade and other serum factors that mediate host-defense are available (Ehrnthaller et al., 2011; Merle et al., 2015b; Merle et al., 2015a).

Studies by Ren et al., have shown that PspA inhibits complement deposition on *Spn* and this feature is vital for *Spn* virulence (Ren et al., 2004). PspA, due to its being one of the most abundant CBPs, competes with CRP for the recognition of PC residues on the pneumococcal cell surface (Mukerji et al., 2012). Isogenic deficient mutants of PspA were observed to elicit greater activation of the classical complement cascade with increased deposition of C1q and C3b proteins on the bacterial surface compared to wildtype *Spn* (Li et al., 2007). Consistent with this, it has been shown by multiple investigators that PspA-deficient pneumococci are cleared more quickly from the bloodstream and are bound to a greater extent by complement, whether initiated by the alternative or classical cascade, when compared to wildtype bacteria (Tu et al., 1999; Ren et al., 2004; Mukerji et al., 2012). PspA is also able to inhibit immune adherence, where complement-bound bacteria become

attached to erythrocytes and are subsequently targeted by macrophages for clearance (Li et al., 2007). By reducing the effectiveness of the complement pathways, PspA reduces the clearance of *Spn* during infection and accordingly enhances pneumococcal virulence.

Lactoferricin Inhibition

Human lactoferrin (hLF) is an iron-binding globular glycoprotein ~80 kDa present in mucosal secretions with a high affinity for ferric (Fe^{3+}) iron (Hammerschmidt et al., 1999). Lactoferrin can be divided between an iron-bound “closed” hololactoferrin and the iron-free “open” apolactoferrin (Baker and Baker, 2005). Apolactoferrin is capable of bacteriostatic activity through iron-chelation which binds up any free exogenous iron thereby inhibiting the use of the metal by bacteria. Apolactoferrin is also capable of direct bactericidal activity *via* its breakdown and the formation of a small peptide called lactoferricin. This peptide has a large concentration of positively charged residues, similar to other cationic antimicrobial peptides, and serves to destabilize the negatively charged bacterial cell membrane (Shaper et al., 2004). Lactoferricin also interrupts the interactions between bacterial-sequestered cations, such as Ca^{2+} and Mg^{2+} , and the lipoteichoic acids in Gram-positive bacteria, leading to the de-stability and increased permeability of the cell membrane (Baker and Baker, 2005).

The α HD of PspA contains a lactoferrin-binding region within aa residues 168–288 (Håkansson et al., 2001). This region serves to protect the bacterium from lactoferricin-mediated killing (Pérez-Dorado et al., 2012; Shaper et al., 2004). PspA showed comparably stronger affinity towards human lactoferrin compared to that from other species

(Hammerschmidt et al., 1999). Håkansson et al. also reported that the ability of *Spn* to bind lactoferrin was entirely dependent on PspA. PspA versions belonging to Family 1 and Family 2 both bound to lactoferrin as demonstrated using PspA deficient pneumococci (Håkansson et al., 2001). The conservation of this trait, despite PspA's considerable variability, highlights its importance. Accordingly, Andre et al. showed that antibodies that blocked PspA's interaction with lactoferrin enhanced bacterial killing (André et al., 2015).

NEWLY DISCOVERED FUNCTIONS OF PSPA

Recent publications by our group have identified new facets of *Spn* virulence involving PspA and its ability to utilize the complex host environment to its advantage. Continued elucidation of how PspA enhances pneumococcal pathogenesis will provide key information and direction towards the development of novel therapeutic or prophylactic strategies.

Host Lactate Utilization

During pneumococcal colonization and pneumonia, host molecules that are normally intracellular are released as a result of pneumolysin-mediated necroptosis of host cells (Labbé and Saleh, 2008; Gonzalez-Juarbe et al., 2018). These include molecules that *Spn* directly co-opts to its advantage (Van Der Sluijs et al., 2004). One newly appreciated factor is the host enzyme lactate dehydrogenase (LDH); a tetrameric protein abundant in mammalian cells composed of combinations of LDH-A and LDH-B. LDH-A converts pyruvate to lactate to generate NAD⁺ from available NADH while LDH-B acts in the reverse (Burgner and Ray, 1984). We have recently shown that *Spn* binds to host LDH-A during lung infection (**Figure 5**) (Park et al., 2021b). When mice were challenged with *Spn* that had incubated with mouse LDH-A, there was a 10-fold increase in bacterial titers collected from the lungs and an increase in bacteremia within a period of 24 hours post-infection (Park et al., 2021b). The binding site of PspA to LDH-A was determined to be the conserved 22-amino NPB that is sometimes found within the PRD (Park et al., 2021b). *Spn* that do not contain the NPB fragment within their version of PspA were unable to bind to LDH-A and did not benefit from co-incubation prior to mouse challenge. NPB is also found in some versions of CbpA and *Spn* having the NPB only in CbpA also benefitted from LDH co-incubation (Park et al., 2021b). Notably, it was determined that the enzymatic activity of LDH-A was crucial for enhancement of pneumococcal virulence. Mice challenged with *Spn* incubated with an enzymatically inactive version of LDH-A did not become hyper-virulent. Moreover, incubation of *Spn* with lactate was sufficient to confer the same effect as mixture with LDH-A. These results suggest that the NPB of PRD on PspA or CbpA co-opts host LDH-A with lactate potentially serving as a virulence-amplifying nutrient.

Adhesion to Dying Host Cells

Recent findings indicate that PspA can also function as an adhesin (**Figure 3**). This property of PspA is novel as it only

mediates binding to dying host cells (Park et al., 2021a). Following mammalian programmed cell death, including both necroptosis and apoptosis, the inner membrane of the host cell undergoes a process where phosphatidylserine residues are flipped outward. These residues serve as “eat me” signals to macrophages who take up the cells but also are bound by free host glyceraldehyde 3-phosphate dehydrogenase (GAPDH) (Fadok et al., 1992; Martin et al., 1995). Using pull-down assays and liquid chromatography/mass spectrometry (LC-MS), it was discovered that PspA binds to mammalian GAPDH, specifically by the amino acids 230-281 in the α HD (Park et al., 2021a). It was subsequently shown that PspA uses GAPDH to adhere to dying lung cells during infection, which impacted the bacterium's localization within the airway thereby enhancing pneumococcal virulence during pneumonia (Park et al., 2021a). *Spn* in particular seemed to take advantage of this trait during co-infection with IAV, which sensitized cells to pneumolysin-mediated necroptosis (Gonzalez-Juarbe et al., 2020), and a condition which enhances *pspA* expression (Park et al., 2021a). It is noteworthy that the identified GAPDH-binding motif on PspA overlaps with the lactoferrin-binding domain. What is more, GAPDH binds to both apo- and holo-lactoferrin by which the host cell either egresses or acquires iron, respectively (Sheokand et al., 2014; Chauhan et al., 2015). Given the importance of lactoferrin binding, this overlap in PspA's domains raises the possibility that *Spn* uses GAPDH as a bait to acquire iron from lactoferrin, or GAPDH may serve as a sink for lactoferrin bound to PspA thereby preventing its cleavage to lactoferricin. These vital questions require further investigation.

Other Interactions

In our studies that identified PspA as having affinity to lactate dehydrogenase and GAPDH, it was observed that PspA also had affinity to numerous other host proteins (Park et al., 2021a; Park et al., 2021b). Among these was the filamentous protein vimentin, which has been implicated as a key ligand for group B Streptococci and *E. coli* with regard to their ability to gain access to the central nervous system (Deng et al., 2019). Other host molecules include keratin (types I-III), pyruvate kinase, alpha-enolase, and beta-tubulin (Park et al., 2021a; Park et al., 2021b). Multiple interactions between pneumococcal surface proteins and the host is a common feature. For example, CbpA specifically binds to laminin receptor, polymeric immunoglobulin receptor, C3, and serum Factor H (Smith and Hostetter, 2000; Lu et al., 2003; Lu et al., 2006; Orihuela et al., 2009). These multiple roles reveal the efficiency of the bacterium, the highly versatile nature of the α HD of PspA and CbpA, and suggest our understanding of PspA's interactions is most likely incomplete.

POTENTIAL OF PSPA AS A VACCINE ANTIGEN

Several epidemiological studies were conducted across different countries to evaluate the distribution of PspA families among

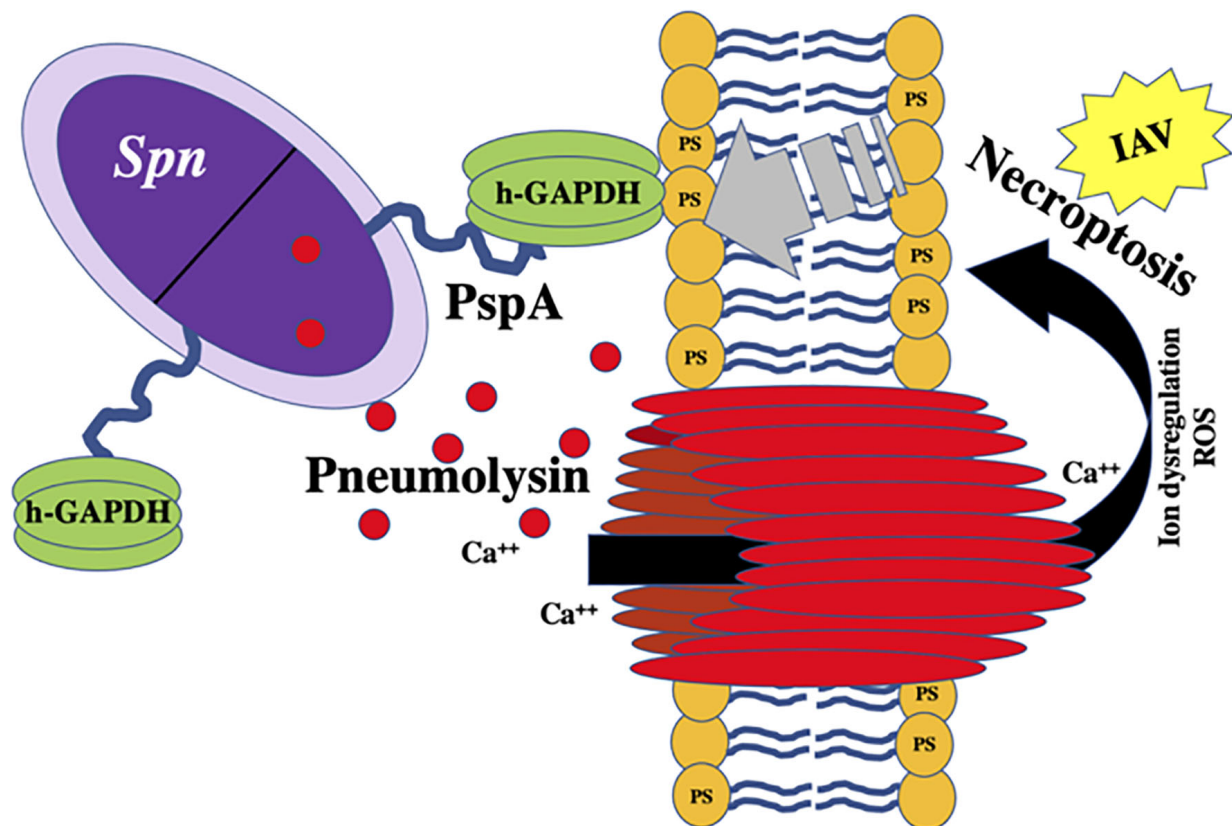


FIGURE 3 | Proposed model of PspA-mediated binding to host-derived GAPDH on necroptotic cells. hGAPDH binds to dying cells via phosphatidylserine (PS) residues flipped from the inner to outer membrane during programmed cell death. Host cell death during *Spn* infection is primarily due to pneumolysin-mediated necroptosis. PspA binds to hGAPDH during this process. New data indicates that sensitivity of lung cells to pneumolysin-mediated necroptosis is drastically exacerbated by concomitant influenza A virus (IAV) infection (Gonzalez-Juarbe et al., 2020).

different isolates. On average, 43.6% of isolates belonged to family 1, 53.5% of isolates belonged to family 2, 0.2% of isolates belong to family 3, and the rest are non-typable. Although there are differences in the proportions of the distribution of PspA families in different populations in the world, the vast majority are composed predominantly of families 1 and 2 (Table 2 and Figure 4). Pneumococcal isolates from pediatric patients, including from middle ear fluid or nasopharyngeal secretions, reveal that the majority of PspA proteins fall into either family 2 or family 1 (Vela Coral et al., 2001; Mollerach et al., 2004; Melin et al., 2008; Jiang et al., 2021). While in adults over 50 years of age, differences in the PspA family distribution show that the majority (> 50–55%) of PspA proteins are in family 2 (Hollingshead et al., 2006). In meningitis isolates from Germany, PspA proteins were evenly distributed over families 1 and 2 with clades 1 and 3 (Heeg et al., 2007). Recent studies in Japan reported that >55% of isolates from adults over the age of 15 years old are in PspA family 1 and >55% isolates from pediatric patients under the age of 16 years are in PspA family 2 (Kawaguchiya et al., 2018; Chang et al., 2021). Additionally, epidemiological surveillance in Brazil conducted during 1977–2002 revealed 50.5% of the isolates

belonged to family 1, 43.2% were members of family 2, and 6.3% were not classified. Across all studies, Family 3 was consistently the least common version of PspA. Its greatest reported prevalence came from one Japanese study that showed 3.2% of pneumococcal isolates from the upper respiratory tract belonged to Family 3 (Hotomi et al., 2013). In all, it is evident that were PspA to be used as a vaccine antigen versions must be used that provide protection against both family 1 and 2 while also considering that family 3 or other unclassifiable versions of PspA have the potential to emerge thereafter.

The α HD of PspA has several properties that make it attractive as a vaccine protein candidate including high expression of the protein at important anatomical sites for colonization and transmission (D'Mello et al., 2020), immunogenicity and cross-reactivity of elicited antibodies (Nabors et al., 2000), accessibility for antibody binding at the cell surface (Vadesilho et al., 2014; Scott et al., 2021), and demonstrated protection in animal models of severe infection (Hollingshead et al., 2000; Miyaji et al., 2015). The PRD of PspA has also been shown to elicit an antibody response and protection against *Spn* infection (Mukerji et al., 2018).

TABLE 2 | Distribution of PspA families across different countries.

Country	Number of Isolates	Family 1	Family 2	Family 3	Non-typable	Year of Isolates	Source of Isolates	Reference
China	81	29.6	69.1	1	0	2014-2018	Pediatric patients with the median age of patients being 1.08 (0.79–3.20)	Jiang et al., 2021
Japan	1,939	55.5	43.50	0.3	0.2	2014–2019	Adult over the age of 15 years old	Chang et al., 2021
Japan	678	42.3	56.6	0.6	0	June–November 2016	Pediatric outpatients under the age of 16 years (median age 2.0 years; mean \pm SD, 2.9 \pm 2.4 years)	Kawaguchiya et al., 2018
Korea	185	30.8	68.6	0.5	0	1991-2016	Children <18 years of age	Yun et al., 2017
Japan	251	44.6	49.4	3.2	1.6	January and May 2003	Upper respiratory tract infections in patients from 0 to 68 years old	Hotomi et al., 2013
China	171	29.90	70.1	0	0	2006-2008	Children <14 years of age	Qian et al., 2012
Spain	112	39.3	59.8	0	0.3	1997 -2007	Healthy children carriers and patients with invasive disease	Rolo et al., 2009
Finland	81	48.1	48.1	0	1.23	1994-1997	Nasopharyngeal carriers from children < 2 years of age	Melin et al., 2008
Finland	154	50.6	44.8	0	3.8	1994-1997	Acute otitis media from children < 2 years of age	Melin et al., 2008
Germany	40	50	50	0	0	1997-2003	Pneumococcal meningitis from children < 16 years of age	Heeg et al., 2007
Japan	141	55.3	41.1	0	3.5	2003-2004	Patients over 15 years old diagnosed with community acquired pneumonia	Ito et al., 2007
Poland	156	37.8	57.7	0	4.5	1997 -2002	Meningitis patients among different age groups	Sadowy et al., 2006
Brazil	183.0	35.5	44.3	0	20.2	2000-2001	Nasopharyngeal isolates from children < 5 years of age	Pimenta et al., 2006
France	215	24.2	74.0	0	0.5	1995-2002	Isolates from adults over 50 years of age collected in seven countries	Hollingshead et al., 2006
Canada	148	37.2	61.5	0	0.0	1995-2002	Isolates from adults over 50 years of age collected in seven countries	Hollingshead et al., 2006
Spain	150	38.0	60.0	0	1.3	1995-2002	Isolates from adults over 50 years of age collected in seven countries	Hollingshead et al., 2006
Sweden	67	41.8	58.2	0	0.0	1995-2002	Isolates from adults over 50 years of age collected in seven countries	Hollingshead et al., 2006
USA	930	41.0	58.0	0	0.4	1995-2002	Isolates from adults over 50 years of age collected in seven countries	Hollingshead et al., 2006
UK	237	50.6	49.4	0	0.0	1995-2002	Isolates from adults over 50 years of age collected in seven countries	Hollingshead et al., 2006
Australia	100	54.0	46.0	0	0.0	1995-2002	Isolates from adults over 50 years of age collected in seven countries	Hollingshead et al., 2006
Brazil	366	50.5	43.2	0	6.3	1977–2002	Epidemiological surveillance	Brandileone et al., 2004
Argentina	149	54.4	41.6	0	4.0	1993-2000	Isolates from children < 6 years of age	Mollerach et al., 2004
Colombia	40	62.5	35	0	1	1994-1998	Isolates from children <5 years of age	Vela Coral et al., 2001

Notably, and as we continue to identify subdomains of PspA that have independent biological roles, this information can be used to select versions of PspA which are not only cross-protective as result of opsonization, but also because they are capable of neutralizing the biological activities of PspA. For example, antibodies that prevent PspA interactions with lactoferrin/GAPDH or lactate dehydrogenase, have the potential to alter bacterial resistance to host killing, its localization in the airway, and nutrient acquisition, respectively.

In addition to PspA, multiple other pneumococcal surface proteins have been studied as potential vaccine candidates (Miyaji et al., 2015; Masomian et al., 2020; Scott et al., 2021). One promising option are multivalent protein vaccines. These combine multiple antigens to increase antigen delivery and

induce broader protection in the host. Candidate proteins worthy of consideration for protection against *Spn* include a pneumolysin toxoid, CbpA, and the pneumococcal histidine triad protein D (PhtD) among others (Chen et al., 2015; Scott et al., 2021). PspA in combination with pneumolysin is in particular intriguing given the importance of induced cell death on PspA binding and cell death-mediated accessibility to host-derived lactate dehydrogenase. Along such lines, it has been shown that these two proteins are synergic in regard to the protection they incur in mice when used together (Briles et al., 2000).

The major concerns regarding the use of PspA in a pneumococcal vaccine stem from the lack of cross-reactivity between all the clades. Antibody against clades 1 and 2

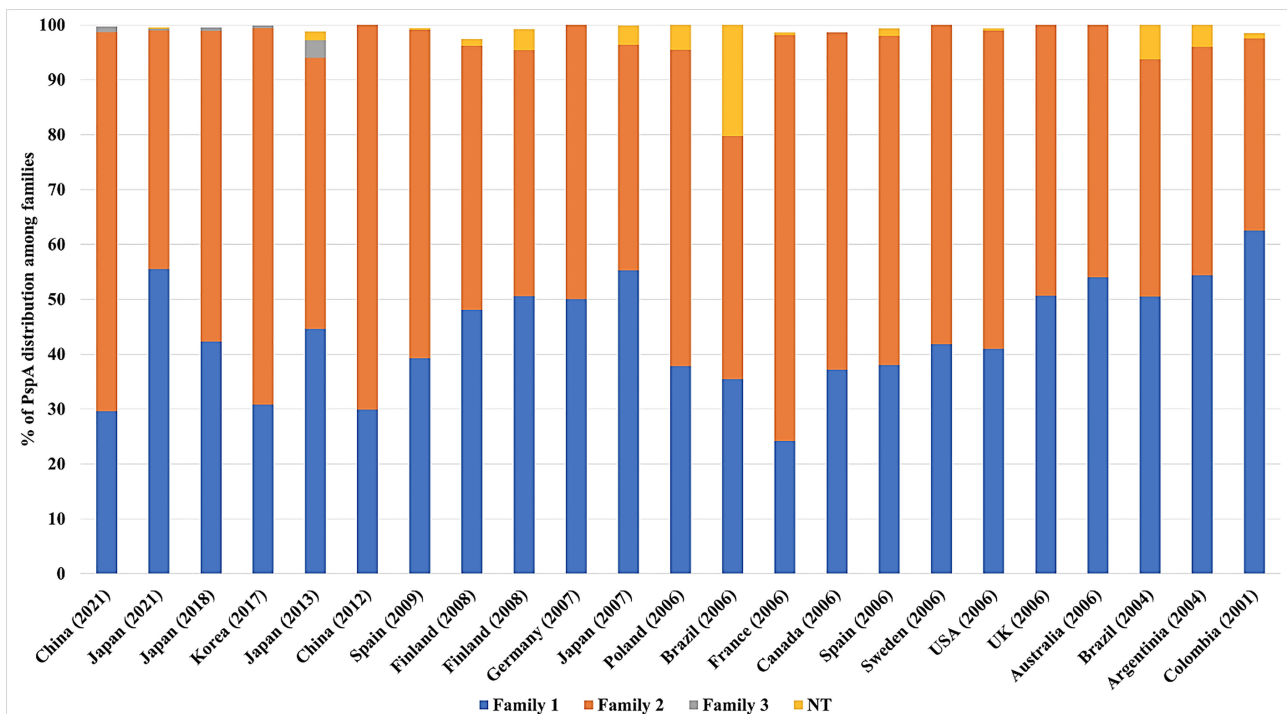


FIGURE 4 | Distribution of PspA families across several countries. The proportion of PspA family 1 (blue), 2 (orange), 3 (grey), and non-typable (NT-Yellow) from each study is represented as percentage (%). The origin of *Spn* and the number of isolates from each study are detailed in **Table 2** along with the corresponding reference. For some studies, not all *Spn* strains examined carried the gene for PspA. In these instances the % distribution of PspA is less than 100%.

are cross protective, however, cross protection is reduced with consideration to clades 3, 4, and 5 (Sempere et al., 2021). This concern overlaps the mosaic nature of PspA with regard to its ability to evade the host immune response and indicates that to avoid “PspA replacement” or emergence of a non-typable PspA version, any multi-valent PspA vaccine should be developed that covers conserved regions under both positive and negative pressure by the host (Yamaguchi et al., 2019). The risk of this can also be diminished by including more than one protein in any vaccine formulation, such as pneumolysin (Sempere et al., 2021). Another concern was raised when it was found that PspA has low sequence homology with human cardiac myosin, which may elicit the production of autoantibodies against cardiac tissue leading to inflammation and tissue damage along with autoimmune disease (Ginsburg et al., 2012). To avoid this risk, antigen design can purposely exclude the region of PspA with the low myosin homology.

PspA vaccine clinical trials are ongoing. Recently, a phase I clinical trial was completed with a recombinant PspA oral vaccine developed using three different avirulent strains of *Salmonella typhi* (RASV) each expressing PspA (ClinicalTrials.gov Identifier: NCT01033409). A similar study showed promising results in mice using an oral attenuated RASV-expressing PspA vaccine (Seo et al., 2012). The future of pneumococcal vaccine design may rely less on using the capsule polysaccharides as antigenic targets and more on bacterial

surface proteins such as PspA for broader and sustained protection with less risk of serotype escape.

CONCLUSION

Spn continues to be a leading cause of respiratory diseases such as community-acquired pneumonia with transmission rates high amongst substantial portions of the population. Current treatment options against pneumococcal infections rely on antibiotics, which are dwindling due to the spread of resistance, whereas prophylactic options are centered on the polysaccharide-based vaccines, with serotype escape beginning to impact overall efficacy. *Spn* has virulence factors that allow it to invade, colonize, and infect its host and these have been studied extensively over the years. Surface proteins on *Spn* such as PspA have garnered renewed interest as potential vaccine candidates due to its presence on nearly all clinical isolates along with high expression across different anatomical sites in the host. Reports have shown promising results in animal models of *Spn* infection where immunization against PspA protects against severe disease and enhances clearance of the bacteria *via* opsonophagocytosis. Vaccine designs using PspA will have to consider low homology with cardiac myosin to avoid undue inflammation or activation of autoantibodies. Other CBPs are also in consideration, highlighting the move

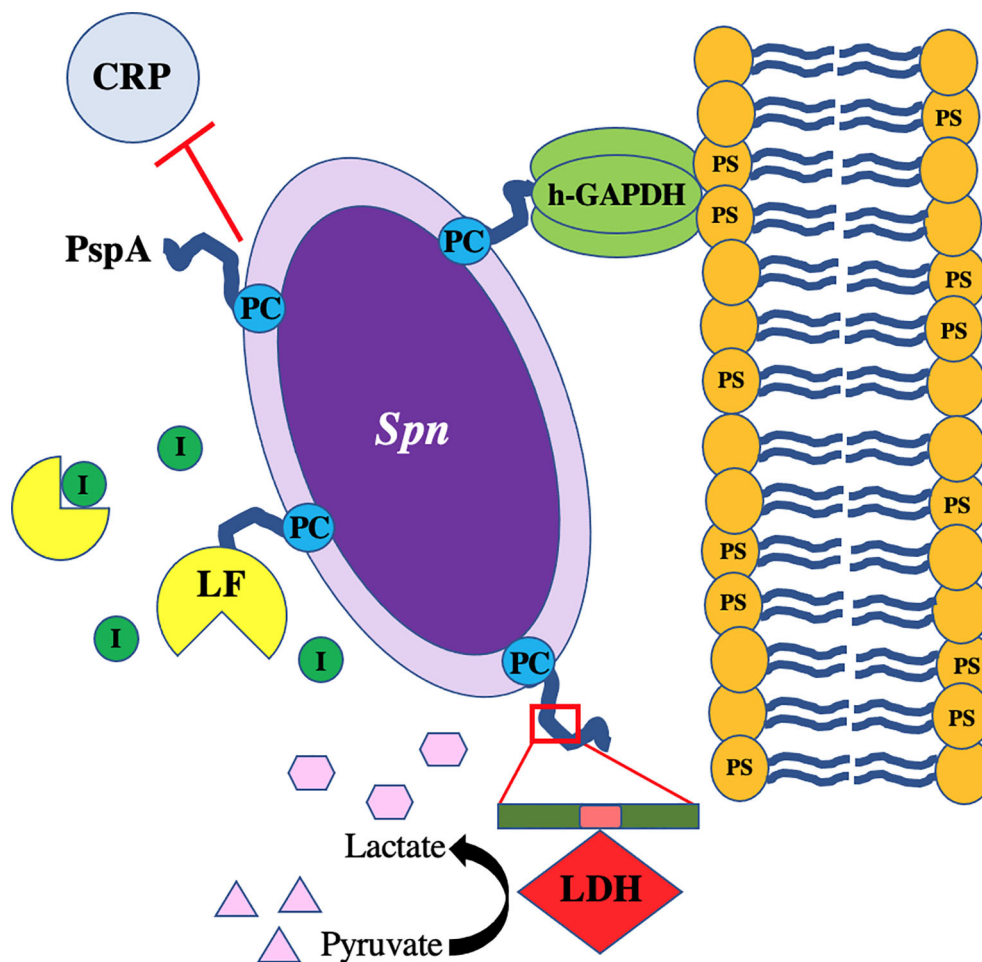


FIGURE 5 | PspA interacts with *Streptococcus pneumoniae* as a “Jack of All Trades.” The pneumococcus with PspA (in blue) extending beyond the capsule which blocks the binding of C-reactive protein (CRP) to phosphorylcholine (PC) on the bacterial surface and acts as an adhesin by binding to host GAPDH. *Spn* co-opts host lactate dehydrogenase (LDH) bound to the non-proline block (in pink) of the proline-rich domain (in green) on PspA and uses converted lactate as a nutrient in poor environmental conditions. PspA on the surface of the pneumococcus also binds to lactoferrin (LF) to protect the bacterium from killing by lactoferricin.

away from dependence on capsule-based antibody recognition by the host and more towards protein-based formulations. New information regarding PspA virulence and its ability to act as a “Jack of all Trades” have improved our understanding of this complex protein and help guide future research questions (Figure 5). As such, continued studies into the molecular mechanisms of PspA during pneumococcal dissemination and infection will be necessary to fully elucidate the vital role this virulence factor plays in *Spn* pathogenesis and possible targeting for development of novel therapies.

REFERENCES

Afshar, D., Pourmand, M. R., Jeddi-Tehrani, M., Saboor Yaraghi, A. A., Azarsa, M., and Shokri, F. (2016). Fibrinogen and Fibronectin Binding Activity and Immunogenic Nature of Choline Binding Protein M. *Iran J. Public Health* 45, 1610–1617.

AUTHOR CONTRIBUTIONS

JL wrote the first draft of the paper. JL, MT, DB and CO contributed to the subsequent writing, editing, and direction of the paper. All authors approved the submitted version.

FUNDING

CO receives support from NIH grants AI156898, AI148368, AI114800, and AI146149.

Andre, G. O., Converso, T. R., Politano, W. R., Ferraz, L. F. C., Ribeiro, M. L., Leite, L. C. C., et al. (2017). Role of *Streptococcus pneumoniae* Proteins in Evasion of Complement-Mediated Immunity. *Front. Microbiol.* 8. doi: 10.3389/fmicb.2017.00224

André, G. O., Politano, W. R., Mirza, S., Converso, T. R., Ferraz, L. F. C., Leite, L. C. C., et al. (2015). Combined Effects of Lactoferrin and Lysozyme on

- Streptococcus pneumoniae* Killing. *Microbial. Pathog.* 89, 7–17. doi: 10.1016/j.micpath.2015.08.008
- Askim, Å., Mehl, A., Paulsen, J., Dewan, A. T., Vestreim, D. F., Åsvold, B. O., et al. (2016). Epidemiology and Outcome of Sepsis in Adult Patients With *Streptococcus pneumoniae* Infection in a Norwegian County 1993–2011: An Observational Study. *BMC Infect. Dis.* 16, 223. doi: 10.1186/s12879-016-1553-8
- Asmat, T. M., Agarwal, V., Saleh, M., and Hammerschmidt, S. (2014). Endocytosis of *Streptococcus pneumoniae* via the Polymeric Immunoglobulin Receptor of Epithelial Cells Relies on Clathrin and Caveolin Dependent Mechanisms. *Int. J. Med. Microbiol.* 304, 1233–1246. doi: 10.1016/j.ijmm.2014.10.001
- Asner, S. A., Agyeman, P. K. A., Gradoux, E., Posfay-Barbe, K. M., Heininger, U., Giannoni, E., et al. (2019). Burden of *Streptococcus pneumoniae* Sepsis in Children After Introduction of Pneumococcal Conjugate Vaccines: A Prospective Population-Based Cohort Study. *Clin. Infect. Dis.* 69, 1574–1580. doi: 10.1093/cid/ciy1139
- Baker, E. N., and Baker, H. M. (2005). Lactoferrin. *Cell. Mol. Life Sci.* 62, 2531. doi: 10.1007/s00018-005-5368-9
- Behr, T., Fischer, W., Peter-Katalinić, J., and Egge, H. (1992). The Structure of Pneumococcal Lipoteichoic Acid. *Eur. J. Biochem.* 207, 1063–1075. doi: 10.1111/j.1432-1033.1992.tb17143.x
- Bergmann, S., and Hammerschmidt, S. (2006). Versatility of Pneumococcal Surface Proteins. *Microbiology* 152, 295–303. doi: 10.1099/mic.0.28610-0
- Bluestone, C. D., Stephenson, J. S., and Martin, L. M. (1992). Ten-Year Review of Otitis Media Pathogens. *Pediatr. Infect. Dis. J.* 11, S7–11. doi: 10.1097/00006454-199208001-00002
- Bogaert, D., De Groot, R., and Hermans, P. W. M. (2004). *Streptococcus pneumoniae* Colonisation: The Key to Pneumococcal Disease. *Lancet Infect. Dis.* 4, 144–154. doi: 10.1016/S1473-3099(04)00938-7
- Brandileone, M. C., Andrade, A. L., Teles, E. M., Zanella, R. C., Yara, T. I., Di Fabio, J. L., et al. (2004). Typing of Pneumococcal Surface Protein A (PspA) in *Streptococcus pneumoniae* Isolated During Epidemiological Surveillance in Brazil: Towards Novel Pneumococcal Protein Vaccines. *Vaccine* 22, 3890–3896. doi: 10.1016/j.vaccine.2004.04.009
- Briles, D. E., Ades, E., Paton, J. C., Sampson, J. S., Carlone, G. M., Huebner, R. C., et al. (2000). Intranasal Immunization of Mice With a Mixture of the Pneumococcal Proteins PsaA and PspA is Highly Protective Against Nasopharyngeal Carriage of *Streptococcus pneumoniae*. *Infect. Immun.* 68, 796–800. doi: 10.1128/IAI68.2.796-800.2000
- Briles, D. E., Latham Clafflin, J., Schroer, K., and Forman, C. (1981). Mouse IgG3 Antibodies are Highly Protective Against Infection With *Streptococcus pneumoniae*. *Nature* 294, 88–90. doi: 10.1038/294088a0
- Briles, D. E., Tart, R. C., Wu, H.-Y., Ralph, B. A., Russell, M. W., and Mcdaniel, L. S. (1996). Systemic and Mucosal Protective Immunity to Pneumococcal Surface Protein A. *Ann. New York Acad. Sci.* 797, 118–126. doi: 10.1111/j.1749-6632.1996.tb52954.x
- Briles, D. E., Yother, J., and Mcdaniel, L. S. (1988). Role of Pneumococcal Surface Protein A in the Virulence of *Streptococcus pneumoniae*. *Rev. Infect. Dis.* 10 Suppl2, S372–S374. doi: 10.1093/cid/10.Supplement_2.S372
- Brooks, L. R. K., and Mias, G. I. (2018). *Streptococcus pneumoniae*'s Virulence and Host Immunity: Aging, Diagnostics, and Prevention. *Front. Immunol.* 9. doi: 10.3389/fimmu.2018.01366
- Brown, A. O., Mann, B., Gao, G., Hankins, J. S., Humann, J., Giardina, J., et al. (2014). *Streptococcus pneumoniae* Translocates Into the Myocardium and Forms Unique Microlesions That Disrupt Cardiac Function. *PLoS Pathog.* 10, e1004383. doi: 10.1371/journal.ppat.1004383
- Burgner, J. W., and Ray, W. J. (1984). On the Origin of the Lactate Dehydrogenase Induced Rate Effect. *Biochemistry* 23, 3636–3648. doi: 10.1021/bi00311a010
- Centers for Disease Control and Prevention (2018). Active Bacterial Core Surveillance Report Emerging Infections Program Network. *Streptococcus pneumoniae*.
- Chang, B., Kinjo, Y., Morita, M., Tamura, K., Watanabe, H., Tanabe, Y., et al. (2021). Distribution and Variation of Serotypes and Pneumococcal Surface Protein A Clades of *Streptococcus pneumoniae* Strains Isolated From Adult Patients With Invasive Pneumococcal Disease in Japan. *Front. Cell Infect. Microbiol.* 11, 617573. doi: 10.3389/fcimb.2021.617573
- Chauhan, A. S., Rawat, P., Malhotra, H., Sheokand, N., Kumar, M., Patidar, A., et al. (2015). Secreted Multifunctional Glyceraldehyde-3-Phosphate Dehydrogenase Sequesters Lactoferrin and Iron Into Cells via a non-Canonical Pathway. *Sci. Rep.* 5, 18465. doi: 10.1038/srep18465
- Chen, A., Mann, B., Gao, G., Heath, R., King, J., Maissonneuve, J., et al. (2015). Multivalent Pneumococcal Protein Vaccines Comprising Pneumolysin With Epitopes/Fragments of CbpA and/or PspA Elicit Strong and Broad Protection. *Clin. Vaccine Immunol.* 22, 1079–1089. doi: 10.1128/CVI.00293-15
- Chou, M.-Y., Hartvigsen, K., Hansen, L. F., Fogelstrand, L., Shaw, P. X., Boullier, A., et al. (2008). Oxidation-Specific Epitopes are Important Targets of Innate Immunity. *J. Internal Med.* 263, 479–488. doi: 10.1111/j.1365-2796.2008.01968.x
- Cornick, J. E., Tastan Bishop, Ö., Yalcin, F., Kiran, A. M., Kumwenda, B., Chaguza, C., et al. (2017). The Global Distribution and Diversity of Protein Vaccine Candidate Antigens in the Highly Virulent *Streptococcus pneumoniae* Serotype 1. *Vaccine* 35, 972–980. doi: 10.1016/j.vaccine.2016.12.037
- Crain, M. J., Waltman, W. D., Turner, J. S., Yother, J., Talkington, D. F., Mcdaniel, L. S., et al. (1990). Pneumococcal Surface Protein A (PspA) is Serologically Highly Variable and is Expressed by All Clinically Important Capsular Serotypes of *Streptococcus pneumoniae*. *Infect. Immun.* 58, 3293–3299. doi: 10.1128/iai.58.10.3293-3299.1990
- Cundell, D. R., Gerard, N. P., Gerard, C., Idanpaan-Heikkilä, I., and Tuomanen, E. I. (1995). *Streptococcus pneumoniae* Anchor to Activated Human Cells by the Receptor for Platelet-Activating Factor. *Nature* 377, 435–438. doi: 10.1038/377435a0
- D'Mello, A., Riegler, A. N., Martínez, E., Beno, S. M., Ricketts, T. D., Foxman, E. F., et al. (2020). An In Vivo Atlas of Host-Pathogen Transcriptomes During *Streptococcus pneumoniae* Colonization and Disease. *Proc. Natl. Acad. Sci. U.S.A.* 117, 33507–33518. doi: 10.1073/pnas.2010428117
- Daniels, C. C., Coan, P., King, J., Hale, J., Benton, K. A., Briles, D. E., et al. (2010). The Proline-Rich Region of Pneumococcal Surface Proteins A and C Contains Surface-Accessible Epitopes Common to All Pneumococci and Elicits Antibody-Mediated Protection Against Sepsis. *Infect. Immun.* 78, 2163–2172. doi: 10.1128/IAI.01199-09
- Deng, L., Spencer, B. L., Holmes, J. A., Mu, R., Rego, S., Weston, T. A., et al. (2019). The Group B Streptococcal Surface Antigen I/II Protein, BspC, Interacts With Host Vimentin to Promote Adherence to Brain Endothelium and Inflammation During the Pathogenesis of Meningitis. *PLoS Pathog.* 15, e1007848. doi: 10.1371/journal.ppat.1007848
- Diavatopoulos, D. A., Short, K. R., Price, J. T., Wilksch, J. J., Brown, L. E., Briles, D. E., et al. (2010). Influenza A Virus Facilitates *Streptococcus pneumoniae* Transmission and Disease. *FASEB J.* 24, 1789–1798. doi: 10.1096/fj.09-146779
- Draing, C., Pfizenmaier, M., Zummo, S., Mancuso, G., Geyer, A., Hartung, T., et al. (2006). Comparison of Lipoteichoic Acid From Different Serotypes of *Streptococcus pneumoniae*. *J. Biol. Chem.* 281, 33849–33859. doi: 10.1074/jbc.M602676200
- Duthy, T. G., Ormsby, R. J., Giannakis, E., Ogunniyi, A. D., Stroehrer, U. H., Paton, J. C., et al. (2002). The Human Complement Regulator Factor H Binds Pneumococcal Surface Protein PspC via Short Consensus Repeats 13 to 15. *Infect. Immun.* 70, 5604–5611. doi: 10.1128/IAI.70.10.5604-5611.2002
- Ehrnthaller, C., Ignatius, A., Gebhard, F., and Huber-Lang, M. (2011). New Insights of an Old Defense System: Structure, Function, and Clinical Relevance of the Complement System. *Mol. Med.* 17, 317–329. doi: 10.2119/molmed.2010.00149
- Eldholm, V., Johnsborg, O., Haugen, K., Ohnstad, H. S., and Håvarstein, L. S. (2009). Fratricide in *Streptococcus pneumoniae*: Contributions and Role of the Cell Wall Hydrolases CbpD, LytA and LytC. *Microbiology* 155, 2223–2234. doi: 10.1099/mic.0.026328-0
- Fadok, V. A., Voelker, D. R., Campbell, P. A., Cohen, J. J., Bratton, D. L., and Henson, P. M. (1992). Exposure of Phosphatidylserine on the Surface of Apoptotic Lymphocytes Triggers Specific Recognition and Removal by Macrophages. *J. Immunol.* 148, 2207–2216.
- Frolet, C., Beniazza, M., Roux, L., Gallet, B., Noirclerc-Savoye, M., Vernet, T., et al. (2010). New Adhesin Functions of Surface-Exposed Pneumococcal Proteins. *BMC Microbiol.* 10, 190. doi: 10.1186/1471-2180-10-190
- Galán-Bartual, S., Pérez-Dorado, I., García, P., and Hermoso, J. A. (2015). "Chapter 11 - Structure and Function of Choline-Binding Proteins," in *Streptococcus pneumoniae*. Eds. J. Brown, S. Hammerschmidt and C. Orihuela (Amsterdam: Academic Press), 207–230.

- García, E., García, J. L., García, P., Arrarás, A., Sánchez-Puelles, J. M., and López, R. (1988). Molecular Evolution of Lytic Enzymes of *Streptococcus pneumoniae* and its Bacteriophages. *Proc. Natl. Acad. Sci. U.S.A.* 85, 914–918. doi: 10.1073/pnas.85.5.914
- García, P., González, M. P., García, E., López, R., and García, J. L. (1999). LytB, a Novel Pneumococcal Murein Hydrolase Essential for Cell Separation. *Mol. Microbiol.* 31, 1275–1281. doi: 10.1046/j.1365-2958.1999.01238.x
- García, J. L., Sánchez-Beato, A. R., Medrano, F. J., and López, R. (1998). Versatility of Choline-Binding Domain. *Microb. Drug Resist.* 4, 25–36. doi: 10.1089/mdr.1998.4.25
- Geno, K. A., Gilbert, G. L., Song, J. Y., Skovsted, I. C., Klugman, K. P., Jones, C., et al. (2015). Pneumococcal Capsules and Their Types: Past, Present, and Future. *Clin. Microbiol. Rev.* 28, 871–899. doi: 10.1128/CMR.00024-15
- Ginsburg, A. S., Nahm, M. H., Khambaty, F. M., and Alderson, M. R. (2012). Issues and Challenges in the Development of Pneumococcal Protein Vaccines. *Expert Rev. Vaccines* 11, 279–285. doi: 10.1586/erv.12.5
- Gisch, N., Kohler, T., Ulmer, A. J., Muthing, J., Pribyl, T., Fischer, K., et al. (2013). Structural Reevaluation of *Streptococcus pneumoniae* Lipoteichoic Acid and New Insights Into Its Immunostimulatory Potency. *J. Biol. Chem.* 288, 15654–15667. doi: 10.1074/jbc.M112.446963
- Global Burden of Disease Lower Respiratory Infections Collaborators (2018). Estimates of the Global, Regional, and National Morbidity, Mortality, and Aetiologies of Lower Respiratory Infections in 195 Countries 1990–2016: A Systematic Analysis for the Global Burden of Disease Study 2016. *Lancet Infect. Dis.* 18, 1191–1210. doi: 10.1016/S1473-3099(18)30310-4
- Gómez-Mejía, A., Gámez, G., and Hammerschmidt, S. (2018). *Streptococcus pneumoniae* Two-Component Regulatory Systems: The Interplay of the Pneumococcus With its Environment. *Int. J. Med. Microbiol.* 308, 722–737. doi: 10.1016/j.ijmm.2017.11.012
- Gonzalez-Juarbe, N., Bradley, K. M., Riegler, A. N., Reyes, L. F., Brissac, T., Park, S.-S., et al. (2018). Bacterial Pore-Forming Toxins Promote the Activation of Caspases in Parallel to Necroptosis to Enhance Alarmin Release and Inflammation During Pneumonia. *Sci. Rep.* 8, 5846. doi: 10.1038/s41598-018-24210-8
- González-Juarbe, N., Gilley, R. P., Hinojosa, C. A., Bradley, K. M., Kamei, A., Gao, G., et al. (2015). Pore-Forming Toxins Induce Macrophage Necroptosis During Acute Bacterial Pneumonia. *PLoS Pathog.* 11, e1005337–e1005337. doi: 10.1371/journal.ppat.1005337
- Gonzalez-Juarbe, N., Riegler, A. N., Jureka, A. S., Gilley, R. P., Brand, J. D., Trombley, J. E., et al. (2020). Influenza-Induced Oxidative Stress Sensitizes Lung Cells to Bacterial-Toxin-Mediated Necroptosis. *Cell Rep.* 32 (8), 1–12. doi: 10.1016/j.celrep.2020.108062
- Gosink, K. K., Mann, E. R., Guglielmo, C., Tuomanen, E. I., and Masure, H. R. (2000). Role of Novel Choline Binding Proteins in Virulence of *Streptococcus pneumoniae*. *Infect. Immun.* 68, 5690–5695. doi: 10.1128/IAI.68.10.5690-5695.2000
- Gupta, R., Shah, P., and Swiatlo, E. (2009). Differential Gene Expression in *Streptococcus pneumoniae* in Response to Various Iron Sources. *Microbial. Pathog.* 47, 101–109. doi: 10.1016/j.micpath.2009.05.003
- Gutiérrez-Fernández, J., Saleh, M., Alcorlo, M., Gómez-Mejía, A., Pantoja-Uceda, D., Treviño, M. A., et al. (2016). Modular Architecture and Unique Teichoic Acid Recognition Features of Choline-Binding Protein L (CbpL) Contributing to Pneumococcal Pathogenesis. *Sci. Rep.* 6, 38094. doi: 10.1038/srep38094
- Håkansson, A., Roche, H., Mirza, S., Mcdaniel, L. S., Brooks-Walter, A., and Briles, D. E. (2001). Characterization of Binding of Human Lactoferrin to Pneumococcal Surface Protein A. *Infect. Immun.* 69, 3372–3381. doi: 10.1128/IAI.69.5.3372-3381.2001
- Hakenbeck, R., Madhour, A., Denapaite, D., and Brückner, R. (2009). Versatility of Choline Metabolism and Choline-Binding Proteins in *Streptococcus pneumoniae* and Commensal Streptococci. *FEMS Microbiol. Rev.* 33, 572–586. doi: 10.1111/j.1574-6976.2009.00172.x
- Hament, J.-M., Kimpen, J. L. L., Fleer, A., and Wolfs, T. F. W. (1999). Respiratory Viral Infection Predisposing for Bacterial Disease: A Concise Review. *FEMS Immunol. Med. Microbiol.* 26, 189–195. doi: 10.1111/j.1574-695X.1999.tb01389.x
- Hammerschmidt, S., Bethge, G., Remane, P. H., and Chhatwal, G. S. (1999). Identification of Pneumococcal Surface Protein A as a Lactoferrin-Binding Protein of *Streptococcus pneumoniae*. *Infect. Immun.* 67, 1683–1687. doi: 10.1128/IAI.67.4.1683-1687.1999
- Harnett, W., and Harnett, M. M. (1999). Phosphorylcholine: Friend or Foe of the Immune System? *Immunol. Today* 20, 125–129. doi: 10.1016/S0167-5699(98)01419-4
- Heeg, C., Franken, C., van der Linden, M., Al-Lahham, A., and Reinert, R. R. (2007). Genetic Diversity of Pneumococcal Surface Protein A of *Streptococcus pneumoniae* Meningitis in German Children. *Vaccine* 25, 1030–1035. doi: 10.1016/j.vaccine.2006.09.061
- Hermoso, J. A., Lagartera, L., González, A., Stelter, M., García, P., Martínez-Ripoll, M., et al. (2005). Insights Into Pneumococcal Pathogenesis From the Crystal Structure of the Modular Teichoic Acid Phosphorylcholine Esterase Pce. *Nat. Struct. Mol. Biol.* 12, 533–538. doi: 10.1038/nsmb940
- Hiller, N. L., Janto, B., Hogg, J. S., Boissy, R., Yu, S., Powell, E., et al. (2007). Comparative Genomic Analyses of Seventeen *Streptococcus pneumoniae* Strains: Insights Into the Pneumococcal Supragenome. *J. Bacteriol.* 189, 8186–8195. doi: 10.1128/JB.00690-07
- Hirst, R. A., Kadioglu, A., O'callaghan, C., and Andrew, P. W. (2004). The Role of Pneumolysin in Pneumococcal Pneumonia and Meningitis. *Clin. Exp. Immunol.* 138, 195–201. doi: 10.1111/j.1365-2249.2004.02611.x
- Hollingshead, S. K., Baril, L., Ferro, S., King, J., Coan, P., Briles, D. E., et al. (2006). Pneumococcal Surface Protein A (PspA) Family Distribution Among Clinical Isolates From Adults Over 50 Years of Age Collected in Seven Countries. *J. Med. Microbiol.* 55, 215–221. doi: 10.1099/jmm.0.46268-0
- Hollingshead, S. K., Becker, R., and Briles, D. E. (2000). Diversity of PspA: Mosaic Genes and Evidence for Past Recombination in *Streptococcus pneumoniae*. *Infect. Immun.* 68, 5889–5900. doi: 10.1128/IAI.68.10.5889-5900.2000
- Hotomi, M., Togawa, A., Kono, M., Ikeda, Y., Takei, S., Hollingshead, S. K., et al. (2013). PspA Family Distribution, Antimicrobial Resistance and Serotype of *Streptococcus pneumoniae* Isolated From Upper Respiratory Tract Infections in Japan. *PLoS One* 8, e58124. doi: 10.1371/journal.pone.0058124
- Hummell, D. S., Berninger, R. W., Tomasz, A., and Winkelstein, J. A. (1981). The Fixation of C3b to Pneumococcal Cell Wall Polymers as a Result of Activation of the Alternative Complement Pathway. *J. Immunol.* 127, 1287–1289.
- Hurley, D., Griffin, C., Young, M. Jr., Scott, D. A., Pride, M. W., Scully, I. L., et al. (2020). Safety, Tolerability, and Immunogenicity of a 20-Valent Pneumococcal Conjugate Vaccine (PCV20) in Adults 60 to 64 Years of Age. *Clin. Infect. Dis.* 73, e1489–e1497. doi: 10.1093/cid/ciaa1045
- Hyams, C., Trzcinski, K., Camberlein, E., Weinberger, D. M., Chimalapati, S., Noursadeghi, M., et al. (2013). *Streptococcus pneumoniae* Capsular Serotype Invasiveness Correlates With the Degree of Factor H Binding and Opsonization With C3b/Ic3b. *Infect. Immun.* 81, 354–363. doi: 10.1128/IAI.00862-12
- Hyams, C., Yuste, J., Bax, K., Camberlein, E., Weiser, J. N., and Brown, J. S. (2010). *Streptococcus pneumoniae* Resistance to Complement-Mediated Immunity Is Dependent on the Capsular Serotype. *Infect. Immun.* 78, 716–725. doi: 10.1128/IAI.01056-09
- Im, H., Kruckow, K. L., D'mello, A., Ganaie, F., Martinez, E., Luck, J. N., et al. (2021). Anatomical Site-Specific Carbohydrate Availability Impacts *Streptococcus pneumoniae* Virulence and Fitness During Colonization and Disease. *Infect. Immun.* 89, 10045121. doi: 10.1128/IAI.00451-21
- Ishii, S., and Shimizu, T. (2000). Platelet-Activating Factor (PAF) Receptor and Genetically Engineered PAF Receptor Mutant Mice. *Prog. Lipid Res.* 39, 41–82. doi: 10.1016/S0163-7827(99)00016-8
- Ito, Y., Osawa, M., Isozumi, R., Imai, S., Ito, I., Hirai, T., et al. (2007). Pneumococcal Surface Protein A Family Types of *Streptococcus pneumoniae* From Community-Acquired Pneumonia Patients in Japan. *Eur. J. Clin. Microbiol. Infect. Dis.* 26, 739–742. doi: 10.1007/s10096-007-0364-7
- Jansen, A. G. S. C., Sanders, E. A. M., van der Ende, A., Van Loon, A. M., Hoes, A. W., and Hak, E. (2008). Invasive Pneumococcal and Meningococcal Disease: Association With Influenza Virus and Respiratory Syncytial Virus Activity? *Epidemiol. Infect.* 136, 1448–1454. doi: 10.1017/S0950268807000271
- Jennings, H. J., Lugowski, C., and Young, N. M. (1980). Structure of the Complex Polysaccharide C-Substance From *Streptococcus pneumoniae* Type 1. *Biochemistry* 19, 4712–4719. doi: 10.1021/bi00561a026
- Jiang, H., Meng, Q., Liu, X., Chen, H., Zhu, C., and Chen, Y. (2021). PspA Diversity, Serotype Distribution and Antimicrobial Resistance of Invasive

- Pneumococcal Isolates From Paediatric Patients in Shenzhen, China. *Infect. Drug Resist.* 14, 49–58. doi: 10.2147/IDR.S286187
- Kawaguchiya, M., Urushibara, N., Aung, M. S., Morimoto, S., Ito, M., Kudo, K., et al. (2018). Genetic Diversity of Pneumococcal Surface Protein A (PspA) in Paediatric Isolates of non-Conjugate Vaccine Serotypes in Japan. *J. Med. Microbiol.* 67, 1130–1138. doi: 10.1099/jmm.0.000775
- Kharat, A. S., and Tomasz, A. (2006). Drastic Reduction in the Virulence of *Streptococcus pneumoniae* Expressing Type 2 Capsular Polysaccharide But Lacking Choline Residues in the Cell Wall. *Mol. Microbiol.* 60, 93–107. doi: 10.1111/j.1365-2958.2006.05082.x
- Kietzman, C. C., Gao, G., Mann, B., Myers, L., and Tuomanen, E. I. (2016). Dynamic Capsule Restructuring by the Main Pneumococcal Autolysin LytA in Response to the Epithelium. *Nat. Commun.* 7, 10859–10859. doi: 10.1038/ncomms10859
- Kim, J. O., and Weiser, J. N. (1998). Association of Intrastrain Phase Variation in Quantity of Capsular Polysaccharide and Teichoic Acid With the Virulence of *Streptococcus pneumoniae*. *J. Infect. Dis.* 177, 368–377. doi: 10.1086/514205
- Labbe, K., and Saleh, M. (2008). Cell Death in the Host Response to Infection. *Cell Death Differ.* 15, 1339–1349. doi: 10.1038/cdd.2008.91
- Lamani, E., Mcpherson, D. T., Hollingshead, S. K., and Jedrzejewski, M. J. (2000). Production, Characterization, and Crystallization of Truncated Forms of Pneumococcal Surface Protein A From *Escherichia Coli*. *Protein Expr. Purif.* 20, 379–388. doi: 10.1006/prep.2000.1320
- Lemessurier, K. S., Ogunniyi, A. D., and Paton, J. C. (2006). Differential Expression of Key Pneumococcal Virulence Genes In Vivo. *Microbiology* 152, 305–311. doi: 10.1099/mic.0.28438-0
- Li, J., Glover, D. T., Szalai, A. J., Hollingshead, S. K., and Briles, D. E. (2007). PspA and PspC Minimize Immune Adherence and Transfer of Pneumococci From Erythrocytes to Macrophages Through Their Effects on Complement Activation. *Infect. Immun.* 75, 5877–5885. doi: 10.1128/IAI.00839-07
- Loughran, A. J., Orihuela, C. J., Tuomanen, E. I., Fischetti, V. A., Novick, R. P., Ferretti, J. J., et al. (2019). *Streptococcus pneumoniae*: Invasion and Inflammation. *Microbiol. Spectr.* 7, 7.2.15. doi: 10.1128/9781683670131.ch20
- Lu, L., Lamm, M. E., Li, H., Cortes, B., and Zhang, J. R. (2003). The Human Polymeric Immunoglobulin Receptor Binds to *Streptococcus pneumoniae* via Domains 3 and 4. *J. Biol. Chem.* 278, 48178–48187. doi: 10.1074/jbc.M306906200
- Lu, L., Ma, Y., and Zhang, J. R. (2006). *Streptococcus pneumoniae* Recruits Complement Factor H Through the Amino Terminus of CbpA. *J. Biol. Chem.* 281, 15464–15474. doi: 10.1074/jbc.M602404200
- Luo, R., Mann, B., Lewis, W. S., Rowe, A., Heath, R., Stewart, M. L., et al. (2005). Solution Structure of Choline Binding Protein A, the Major Adhesin of *Streptococcus pneumoniae*. *EMBO J.* 24, 34–43. doi: 10.1038/sj.emboj.7600490
- Mann, B., Orihuela, C., Antikainen, J., Gao, G., Sublett, J., Korhonen, T. K., et al. (2006). Multifunctional Role of Choline Binding Protein G in Pneumococcal Pathogenesis. *Infect. Immun.* 74, 821–829. doi: 10.1128/IAI.74.2.821-829.2006
- Martin, S. J., Reutelingersperger, C. P., McGahon, A. J., Rader, J. A., Van Schie, R. C., Lafate, D. M., et al. (1995). Early Redistribution of Plasma Membrane Phosphatidylserine is a General Feature of Apoptosis Regardless of the Initiating Stimulus: Inhibition by Overexpression of Bcl-2 and Abl. *J. Exp. Med.* 182, 1545–1556. doi: 10.1084/jem.182.5.1545
- Masomian, M., Ahmad, Z., Ti Gew, L., and Poh, C. L. (2020). Development of Next Generation *Streptococcus pneumoniae* Vaccines Conferring Broad Protection. *Vaccines* 8, 132. doi: 10.3390/vaccines8010132
- McDaniel, L. S., Ralph, B. A., McDaniel, D. O., and Briles, D. E. (1994). Localization of Protection-Eliciting Epitopes on PspA of *Streptococcus pneumoniae* Between Amino Acid Residues 192 and 260. *Microb. Pathog.* 17, 323–337. doi: 10.1006/mpat.1994.1078
- McDaniel, L. S., Scott, G., Kearney, J. F., and Briles, D. E. (1984). Monoclonal Antibodies Against Protease-Sensitive Pneumococcal Antigens can Protect Mice From Fatal Infection With *Streptococcus pneumoniae*. *J. Exp. Med.* 160, 386–397. doi: 10.1084/jem.160.2.386
- McDaniel, L. S., Scott, G., Widenhofer, K., Carroll, J. M., and Briles, D. E. (1986). Analysis of a Surface Protein of *Streptococcus pneumoniae* Recognised by Protective Monoclonal Antibodies. *Microb. Pathog.* 1, 519–531. doi: 10.1016/0882-4010(86)90038-0
- McDaniel, L. S., Yother, J., Vijayakumar, M., McGarry, L., Guild, W. R., and Briles, D. E. (1987). Use of Insertional Inactivation to Facilitate Studies of Biological Properties of Pneumococcal Surface Protein A (PspA). *J. Exp. Med.* 165, 381–394. doi: 10.1084/jem.165.2.381
- Melin, M. M., Hollingshead, S. K., Briles, D. E., Hanage, W. P., Lahdenkari, M., Kajjalainen, T., et al. (2008). Distribution of Pneumococcal Surface Protein A Families 1 and 2 Among *Streptococcus pneumoniae* Isolates From Children in Finland Who had Acute Otitis Media or Were Nasopharyngeal Carriers. *Clin. Vaccine Immunol.* 15, 1555–1563. doi: 10.1128/CVI.00177-08
- Merle, N. S., Church, S. E., Fremeaux-Bacchi, V., and Roumenina, L. T. (2015a). Complement System Part I – Molecular Mechanisms of Activation and Regulation. *Front. Immunol.* 6. doi: 10.3389/fimmu.2015.00262
- Merle, N. S., Noe, R., Halbwachs-Mecarelli, L., Fremeaux-Bacchi, V., and Roumenina, L. T. (2015b). Complement System Part II: Role in Immunity. *Front. Immunol.* 6. doi: 10.3389/fimmu.2015.00257
- Mitchell, T. J., Alexander, J. E., Morgan, P. J., and Andrew, P. W. (1997). Molecular Analysis of Virulence Factors of *Streptococcus pneumoniae*. *J. Appl. Microbiol.* 83, 62S–71S. doi: 10.1046/j.1365-2672.83.s1.7.x
- Mitchell, T. J., and Dalziel, C. E. (2014). “The Biology of Pneumolysin,” in *MACPF/CDC Proteins - Agents of Defence, Attack and Invasion*. Eds. G. Anderluh and R. Gilbert (Dordrecht: Springer Netherlands), 145–160.
- Miyaji, E. N., Vadesilho, C. F. M., Oliveira, M. L. S., Zelanis, A., Briles, D. E., Ho, P. L., et al. (2015). Evaluation of a Vaccine Formulation Against *Streptococcus pneumoniae* Based on Choline-Binding Proteins. *Clin. Vaccine Immunol.* 22, 213–220. doi: 10.1128/CVI.00692-14
- Molina, R., González, A., Stelter, M., Pérez-Dorado, I., Kahn, R., Morales, M., et al. (2009). Crystal Structure of CbpF, a Bifunctional Choline-Binding Protein and Autolysis Regulator From *Streptococcus pneumoniae*. *EMBO Rep.* 10, 246–251. doi: 10.1038/embor.2008.245
- Mollerach, M., Regueira, M., Bonofiglio, L., Callejo, R., Pace, J., Di Fabio, J. L., et al. (2004). Invasive *Streptococcus pneumoniae* Isolates From Argentinian Children: Serotypes, Families of Pneumococcal Surface Protein A (PspA) and Genetic Diversity. *Epidemiol. Infect.* 132, 177–184. doi: 10.1017/S0950268803001626
- Mukerji, R., Hendrickson, C., Genschmer, K. R., Park, S.-S., Bouchet, V., Goldstein, R., et al. (2018). The Diversity of the Proline-Rich Domain of Pneumococcal Surface Protein A (PspA): Potential Relevance to a Broad-Spectrum Vaccine. *Vaccine* 36, 6834–6843. doi: 10.1016/j.vaccine.2018.08.045
- Mukerji, R., Mirza, S., Roche, A. M., Widener, R. W., Croney, C. M., Rhee, D.-K., et al. (2012). Pneumococcal Surface Protein A Inhibits Complement Deposition on the Pneumococcal Surface by Competing With the Binding of C-Reactive Protein to Cell-Surface Phosphocholine. *J. Immunol.* 189, 5327–5335. doi: 10.4049/jimmunol.1201967
- Nabors, G. S., Braun, P. A., Herrmann, D. J., Heise, M. L., Pyle, D. J., Gravenstein, S., et al. (2000). Immunization of Healthy Adults With a Single Recombinant Pneumococcal Surface Protein A (PspA) Variant Stimulates Broadly Cross-Reactive Antibodies to Heterologous PspA Molecules. *Vaccine* 18, 1743–1754. doi: 10.1016/S0264-410X(99)00530-7
- Ng, W.-L., Tsui, H.-C. T., and Winkler, M. E. (2005). Regulation of the pspA Virulence Factor and Essential pcsB Murein Biosynthetic Genes by the Phosphorylated VicR (YycF) Response Regulator in *Streptococcus pneumoniae*. *J. Bacteriol.* 187, 7444–7459. doi: 10.1128/JB.187.21.7444-7459.2005
- Nomura, S., and Nagayama, A. (1995). Mechanism of Enhancement of Bactericidal Activity of Phagocytes Against *Klebsiella pneumoniae* Treated With Subminimal Inhibitory Concentrations of Cefodizime. *Chemotherapy* 41, 267–275. doi: 10.1159/000239355
- O'Brien, K. L., Walters, M. I., Sellman, J., Quinlisk, P., Regnery, H., Schwartz, B., et al. (2000). Severe Pneumococcal Pneumonia in Previously Healthy Children: The Role of Preceding Influenza Infection. *Clin. Infect. Dis.* 30, 784–789. doi: 10.1086/313772
- Ogunniyi, A. D., Giammarinaro, P., and Paton, J. C. (2002). The Genes Encoding Virulence-Associated Proteins and the Capsule of *Streptococcus pneumoniae* are Upregulated and Differentially Expressed In Vivo. *Microbiology* 148, 2045–2053. doi: 10.1099/00221287-148-7-2045
- Orihuela, C. J., Gao, G., Francis, K. P., Yu, J., and Tuomanen, E. I. (2004b). Tissue-Specific Contributions of Pneumococcal Virulence Factors to Pathogenesis. *J. Infect. Dis.* 190, 1661–1669. doi: 10.1086/424596
- Orihuela, C. J., Mahdavi, J., Thornton, J., Mann, B., Wooldridge, K. G., Abouseada, N., et al. (2009). Laminin Receptor Initiates Bacterial Contact With the Blood

- Brain Barrier in Experimental Meningitis Models. *J. Clin. Invest.* 119, 1638–1646. doi: 10.1172/JCI36759
- Orihuela, C. J., Radin, J. N., Sublett, J. E., Gao, G., Kaushal, D., and Tuomanen, E. I. (2004a). Microarray Analysis of Pneumococcal Gene Expression During Invasive Disease. *Infect. Immun.* 72, 5582–5596. doi: 10.1128/IAI.72.10.5582-5596.2004
- Park, S.-S., Gonzalez-Juarbe, N., Martínez, E., Hale, J. Y., Lin, Y.-H., Huffines, J. T., et al. (2021a). *Streptococcus pneumoniae* Binds to Host Lactate Dehydrogenase via PspA and PspC To Enhance Virulence. *mBio* 12 (3), 1–13, e00673–e00621. doi: 10.1128/mBio.00673-21
- Park, S.-S., Gonzalez-Juarbe, N., Riegler, A. N., Im, H., Hale, Y., Platt, M. P., et al. (2021b). *Streptococcus pneumoniae* Binds to Host GAPDH on Dying Lung Epithelial Cells Worsening Secondary Infection Following Influenza. *Cell Rep.* 35. doi: 10.1016/j.celrep.2021.109267
- Pepys, M. B., and Hirschfield, G. M. (2003). C-Reactive Protein: A Critical Update. *J. Clin. Invest.* 111, 1805–1812. doi: 10.1172/JCI200318921
- Pérez-Dorado, I., Galan-Bartual, S., and Hermoso, J. A. (2012). Pneumococcal Surface Proteins: When the Whole is Greater Than the Sum of its Parts. *Mol. Oral. Microbiol.* 27, 221–245. doi: 10.1111/j.2041-1014.2012.00655.x
- Pettigrew, M. M., Marks, L. R., Kong, Y., Gent, J. F., Roche-Hakansson, H., Hakansson, A. P., et al. (2014). Dynamic Changes in the *Streptococcus pneumoniae* Transcriptome During Transition From Biofilm Formation to Invasive Disease Upon Influenza A Virus Infection. *Infect. Immun.* 82, 4607–4619. doi: 10.1128/IAI.02225-14
- Pimenta, F. C., Ribeiro-Dias, F., Brandileone, M. C., Miyaji, E. N., Leite, L. C., and Sgambatti De Andrade, A. L. (2006). Genetic Diversity of PspA Types Among Nasopharyngeal Isolates Collected During an Ongoing Surveillance Study of Children in Brazil. *J. Clin. Microbiol.* 44, 2838–2843. doi: 10.1128/JCM.00156-06
- Qian, J., Yao, K., Xue, L., Xie, G., Zheng, Y., Wang, C., et al. (2012). Diversity of Pneumococcal Surface Protein A (PspA) and Relation to Sequence Typing in *Streptococcus pneumoniae* Causing Invasive Disease in Chinese Children. *Eur. J. Clin. Microbiol. Infect. Dis.* 31, 217–223. doi: 10.1007/s10096-011-1296-9
- Radin, J. N., Orihuela, C. J., Murrti, G., Guglielmo, C., Murray, P. J., and Tuomanen, E. I. (2005). Arrestin 1 Participates in Platelet-Activating Factor Receptor-Mediated Endocytosis of *Streptococcus pneumoniae*. *Infect. Immun.* 73, 7827–7835. doi: 10.1128/IAI.73.12.7827-7835.2005
- Ren, B., Szalai, A. J., Hollingshead, S. K., and Briles, D. E. (2004). Effects of PspA and Antibodies to PspA on Activation and Deposition of Complement on the Pneumococcal Surface. *Infect. Immun.* 72, 114–122. doi: 10.1128/IAI.72.1.114-122.2004
- Ribeiro, F. J., Przybylski, D., Yin, S., Sharpe, T., Gnerre, S., Abouelleil, A., et al. (2012). Finished Bacterial Genomes From Shotgun Sequence Data. *Genome Res.* 22, 2270–2277. doi: 10.1101/gr.141515.112
- Ring, A., Weiser, J. N., and Tuomanen, E. I. (1998). Pneumococcal Trafficking Across the Blood-Brain Barrier. Molecular Analysis of a Novel Bidirectional Pathway. *J. Clin. Invest.* 102, 347–360. doi: 10.1172/JCI2406
- Roche, H., Håkansson, A., Hollingshead, S. K., and Briles, D. E. (2003). Regions of PspA/EF3296 Best Able to Elicit Protection Against *Streptococcus pneumoniae* in a Murine Infection Model. *Infect. Immun.* 71, 1033–1041. doi: 10.1128/IAI.71.3.1033-1041.2003
- Rolo, D., Ardanuy, C., Fleites, A., Martín, R., and Liñares, J. (2009). Diversity of Pneumococcal Surface Protein A (PspA) Among Prevalent Clones in Spain. *BMC Microbiol.* 9, 80. doi: 10.1186/1471-2180-9-80
- Rosenow, C., Ryan, P., Weiser, J. N., Johnson, S., Fontan, P., Ortqvist, A., et al. (1997). Contribution of Novel Choline-Binding Proteins to Adherence, Colonization and Immunogenicity of *Streptococcus pneumoniae*. *Mol. Microbiol.* 25, 819–829. doi: 10.1111/j.1365-2958.1997.mmi494.x
- Rupprecht, T. A., Angele, B., Klein, M., Heesemann, J., Pfister, H.-W., Botto, M., et al. (2007). Complement C1q and C3 Are Critical for the Innate Immune Response to *Streptococcus pneumoniae* in the Central Nervous System. *J. Immunol.* 178, 1861–1869. doi: 10.4049/jimmunol.178.3.1861
- Sadowy, E., Skoczynska, A., Fielt, J., Gniadkowski, M., and Hryniewicz, W. (2006). Multilocus Sequence Types, Serotypes, and Variants of the Surface Antigen PspA in *Streptococcus pneumoniae* Isolates From Meningitis Patients in Poland. *Clin. Vaccine Immunol.* 13, 139–144. doi: 10.1128/CI.13.1.139-144.2006
- Sánchez-Beato, A. R., López, R., and García, J. L. (1998). Molecular Characterization of PcpA: A Novel Choline-Binding Protein of *Streptococcus pneumoniae*. *FEMS Microbiol. Lett.* 164, 207–214. doi: 10.1111/j.1574-6968.1998.tb13087.x
- Scott, N. R., Mann, B., Tuomanen, E. I., and Orihuela, C. J. (2021). Multi-Valent Protein Hybrid Pneumococcal Vaccines: A Strategy for the Next Generation of Vaccines. *Vaccines* 9, 209. doi: 10.3390/vaccines9030209
- Sempere, J., Llamós, M., Del Río Menéndez, L., López Ruiz, B., Domenech, M., and González-Camacho, F. (2021). Pneumococcal Choline-Binding Proteins Involved in Virulence as Vaccine Candidates. *Vaccines* 9, 181. doi: 10.3390/vaccines9020181
- Seo, S.-U., Kim, J.-J., Yang, H., Kwon, H.-J., Yang, J.-Y., Curtiss Iii, R., et al. (2012). Effective Protection Against Secondary Pneumococcal Pneumonia by Oral Vaccination With Attenuated Salmonella Delivering PspA Antigen in Mice. *Vaccine* 30, 6816–6823. doi: 10.1016/j.vaccine.2012.09.015
- Shaper, M., Hollingshead, S. K., Benjamin, W. H., and Briles, D. E. (2004). PspA Protects *Streptococcus pneumoniae* From Killing by Apolactoferrin, and Antibody to PspA Enhances Killing of Pneumococci by Apolactoferrin. *Infect. Immun.* 72, 5031–5040. doi: 10.1128/IAI.72.9.5031-5040.2004
- Sheokand, N., Malhotra, H., Kumar, S., Tillu, V. A., Chauhan, A. S., Raje, C. I., et al. (2014). Moonlighting Cell-Surface GAPDH Recruits Apotransferrin to Effect Iron Egress From Mammalian Cells. *J. Cell Sci.* 127, 4279–4291. doi: 10.1242/jcs.154005
- Smith, B. L., and Hostetter, M. K. (2000). C3 as Substrate for Adhesion of *Streptococcus pneumoniae*. *J. Infect. Dis.* 182, 497–508. doi: 10.1086/315722
- Stafforini, D. M. (2009). Biology of Platelet-Activating Factor Acetylhydrolase (PAF-AH, Lipoprotein Associated Phospholipase A2). *Cardiovasc. Drugs Ther.* 23, 73–83. doi: 10.1007/s10557-008-6133-8
- Standish, A. J., Stroehrer, U. H., and Paton, J. C. (2007). The Pneumococcal Two-Component Signal Transduction System RR/HK06 Regulates CbpA and PspA by Two Distinct Mechanisms. *J. Bacteriol.* 189, 5591–5600. doi: 10.1128/JB.00335-07
- Su, J., Georgiades, A., Wu, R., Thulin, T., De Faire, U., and Frostegård, J. (2006). Antibodies of IgM Subclass to Phosphorylcholine and Oxidized LDL are Protective Factors for Atherosclerosis in Patients With Hypertension. *Atherosclerosis* 188, 160–166. doi: 10.1016/j.atherosclerosis.2005.10.017
- Tettelin, H., Nelson, K. E., Paulsen, I. T., Eisen, J. A., Read, T. D., Peterson, S., et al. (2001). Complete Genome Sequence of a Virulent Isolate of *Streptococcus pneumoniae*. *Science* 293, 498–506. doi: 10.1126/science.1061217
- Thigpen, M. C., Whitney, C. G., Messonnier, N. E., Zell, E. R., Lynfield, R., Hadler, J. L., et al. (2011). Bacterial Meningitis in the United States 1998–2007. *New Engl. J. Med.* 364, 2016–2025. doi: 10.1056/NEJMoa1005384
- Thompson, D., Pepys, M. B., and Wood, S. P. (1999). The Physiological Structure of Human C-Reactive Protein and its Complex With Phosphocholine. *Structure* 7, 169–177. doi: 10.1016/S0969-2126(99)80023-9
- Tomasz, A., and Westphal, M. (1971). Abnormal Autolytic Enzyme in a Pneumococcus With Altered Teichoic Acid Composition. *Proc. Natl. Acad. Sci. U. S. A.* 68, 2627–2630. doi: 10.1073/pnas.68.11.2627
- Tu, A.-H. T., Fulgham, R. L., Mccrory, M. A., Briles, D. E., and Szalai, A. J. (1999). Pneumococcal Surface Protein A Inhibits Complement Activation by *Streptococcus pneumoniae*. *Infect. Immun.* 67, 4720–4724. doi: 10.1128/IAI.67.9.4720-4724.1999
- Vadesilho, C. F. M., Ferreira, D. M., Gordon, S. B., Briles, D. E., Moreno, A. T., Oliveira, M. L. S., et al. (2014). Mapping of Epitopes Recognized by Antibodies Induced by Immunization of Mice With PspA and PspC. *Clin. Vaccine Immunol.* 21, 940–948. doi: 10.1128/CI.00239-14
- Van Der Poll, T., and Opal, S. M. (2009). Pathogenesis, Treatment, and Prevention of Pneumococcal Pneumonia. *Lancet* 374, 1543–1556. doi: 10.1016/S0140-6736(09)61114-4
- Van Der Sluis, K. F., Van Elden, L. J. R., Nijhuis, M., Schuurman, R., Pater, J. M., Florquin, S., et al. (2004). IL-10 Is an Important Mediator of the Enhanced Susceptibility to Pneumococcal Pneumonia After Influenza Infection. *J. Immunol.* 172, 7603–7609. doi: 10.4049/jimmunol.172.12.7603
- Vela Coral, M. C., Fonseca, N., Castañeda, E., Di Fabio, J. L., Hollingshead, S. K., and Briles, D. E. (2001). Pneumococcal Surface Protein A of Invasive *Streptococcus pneumoniae* Isolates From Colombian Children. *Emerg. Infect. Dis.* 7, 832–836. doi: 10.3201/eid0705.017510
- Volanakis, J. E., and Kaplan, M. H. (1971). Specificity of C-Reactive Protein for Choline Phosphate Residues of Pneumococcal C-Polysaccharide. *Proc. Soc. Exp. Biol. Med.* 136, 612–614. doi: 10.3181/00379727-136-35323

- Vollmer, W., Massidda, O., Tomasz, A., Fischetti, V. A., Novick, R. P., Ferretti, J. J., et al. (2019). The Cell Wall of *Streptococcus pneumoniae*. *Microbiol. Spectr.* 7, 7.3.19. doi: 10.1128/microbiolspec.GPP3-0018-2018
- Weiser, J. N., Austrian, R., Sreenivasan, P. K., and Masure, H. R. (1994). Phase Variation in Pneumococcal Opacity: Relationship Between Colonial Morphology and Nasopharyngeal Colonization. *Infect. Immun.* 62, 2582–2589. doi: 10.1128/iai.62.6.2582-2589.1994
- Winkelstein, J. A., and Tomasz, A. (1978). Activation of the Alternative Complement Pathway by Pneumococcal Cell Wall Teichoic Acid. *J. Immunol.* 120, 174–178.
- Yamaguchi, M., Goto, K., Hirose, Y., Yamaguchi, Y., Sumitomo, T., Nakata, M., et al. (2019). Identification of Evolutionarily Conserved Virulence Factor by Selective Pressure Analysis of *Streptococcus pneumoniae*. *Commun. Biol.* 2, 96. doi: 10.1038/s42003-019-0340-7
- Yother, J., and Briles, D. E. (1992). Structural Properties and Evolutionary Relationships of PspA, a Surface Protein of *Streptococcus pneumoniae*, as Revealed by Sequence Analysis. *J. Bacteriol.* 174, 601–609. doi: 10.1128/jb.174.2.601-609.1992
- Yother, J., and White, J. M. (1994). Novel Surface Attachment Mechanism of the *Streptococcus pneumoniae* Protein PspA. *J. Bacteriol.* 176, 2976–2985. doi: 10.1128/jb.176.10.2976-2985.1994
- Yun, K. W., Choi, E. H., and Lee, H. J. (2017). Genetic Diversity of Pneumococcal Surface Protein A in Invasive Pneumococcal Isolates From Korean Children 1991–2016. *PLoS One* 12, e0183968. doi: 10.1371/journal.pone.0183968
- Zhang, J.-R., Idanpaan-Heikkilä, I., Fischer, W., and Tuomanen, E. I. (1999). Pneumococcal Licd2 Gene is Involved in Phosphorylcholine Metabolism. *Mol. Microbiol.* 31, 1477–1488. doi: 10.1046/j.1365-2958.1999.01291.x
- Zhang, J. R., Mostov, K. E., Lamm, M. E., Nanno, M., Shimida, S., Ohwaki, M., et al. (2000). The Polymeric Immunoglobulin Receptor Translocates Pneumococci Across Human Nasopharyngeal Epithelial Cells. *Cell* 102, 827–837. doi: 10.1016/S0092-8674(00)00071-4

Conflict of Interest: The authors declare that the research was conducted in the absence of any commercial or financial relationships that could be construed as a potential conflict of interest.

Publisher's Note: All claims expressed in this article are solely those of the authors and do not necessarily represent those of their affiliated organizations, or those of the publisher, the editors and the reviewers. Any product that may be evaluated in this article, or claim that may be made by its manufacturer, is not guaranteed or endorsed by the publisher.

Copyright © 2022 Lane, Tata, Briles and Orihuela. This is an open-access article distributed under the terms of the Creative Commons Attribution License (CC BY). The use, distribution or reproduction in other forums is permitted, provided the original author(s) and the copyright owner(s) are credited and that the original publication in this journal is cited, in accordance with accepted academic practice. No use, distribution or reproduction is permitted which does not comply with these terms.



Streptococcus pneumoniae and Influenza A Virus Co-Infection Induces Altered Polyubiquitination in A549 Cells

Thomas Sura¹, Vanessa Gering², Clemens Cammann², Sven Hammerschmidt³, Sandra Maaß¹, Ulrike Seifert² and Dörte Becher^{1*}

¹ Department of Microbial Proteomics, Institute of Microbiology, University of Greifswald, Greifswald, Germany, ² Friedrich Loeffler-Institute of Medical Microbiology-Virology, University Medicine Greifswald, Greifswald, Germany, ³ Department of Molecular Genetics and Infection Biology, Interfaculty Institute for Genetics and Functional Genomics, University of Greifswald, Greifswald, Germany

OPEN ACCESS

Edited by:

Jason W. Rosch,
St. Jude Children's Research Hospital,
United States

Reviewed by:

Hannah Rowe,
Oregon State University, United States
Tomoko Sumitomo,
Osaka University, Japan

*Correspondence:

Dörte Becher
dbecher@uni-greifswald.de

Specialty section:

This article was submitted to
Molecular Bacterial Pathogenesis,
a section of the journal
Frontiers in Cellular and
Infection Microbiology

Received: 18 November 2021

Accepted: 25 January 2022

Published: 24 February 2022

Citation:

Sura T, Gering V, Cammann C, Hammerschmidt S, Maaß S, Seifert U and Becher D (2022) Streptococcus pneumoniae and Influenza A Virus Co-Infection Induces Altered Polyubiquitination in A549 Cells. Front. Cell. Infect. Microbiol. 12:817532. doi: 10.3389/fcimb.2022.817532

Epithelial cells are an important line of defense within the lung. Disruption of the epithelial barrier by pathogens enables the systemic dissemination of bacteria or viruses within the host leading to severe diseases with fatal outcomes. Thus, the lung epithelium can be damaged by seasonal and pandemic influenza A viruses. Influenza A virus infection induced dysregulation of the immune system is beneficial for the dissemination of bacteria to the lower respiratory tract, causing bacterial and viral co-infection. Host cells regulate protein homeostasis and the response to different perturbances, for instance provoked by infections, by post translational modification of proteins. Aside from protein phosphorylation, ubiquitination of proteins is an essential regulatory tool in virtually every cellular process such as protein homeostasis, host immune response, cell morphology, and in clearing of cytosolic pathogens. Here, we analyzed the proteome and ubiquitinome of A549 alveolar lung epithelial cells in response to infection by either *Streptococcus pneumoniae* D39Δcps or influenza A virus H1N1 as well as bacterial and viral co-infection. Pneumococcal infection induced alterations in the ubiquitination of proteins involved in the organization of the actin cytoskeleton and Rho GTPases, but had minor effects on the abundance of host proteins. H1N1 infection results in an anti-viral state of A549 cells. Finally, co-infection resembled the imprints of both infecting pathogens with a minor increase in the observed alterations in protein and ubiquitination abundance.

Keywords: co-infection, ubiquitin, influenza A virus, *Streptococcus pneumoniae* D39, A549

INTRODUCTION

Respiratory tract infections are among the most prevalent causes of death worldwide (Roth et al., 2018). These infections are mainly caused by influenza A virus (IAV), *Streptococcus pneumoniae* and other pathogens (Aliberti and Kaye, 2013; Troeger et al., 2019). Infections with IAV can cause dissemination of bacteria to the lower respiratory tract allowing viral and bacterial co-infection (Ruuskanen and Järvinen, 2014; Self et al., 2017). Thus, viral and bacterial co-infection is related to

increased mortality compared to single infections (Palacios et al., 2009; Hammerschmidt, 2016; Cawcutt and Kalil, 2017). Recently, it has been shown that co-infection occurs in seasonal and pandemic IAV infection in more than 30% of all cases (Brundage, 2006; Morens et al., 2008). The Gram-positive bacterium *S. pneumoniae* is mainly associated as secondary infection in IAV infected patients (Palacios et al., 2009). Influenza A virus infection can cause disruption of the epithelial barrier and impaired immune response causing bacterial spreading and reduced bacterial killing (Siemens et al., 2017). In the lung, epithelial cells act as an important line of defense and are involved in pathogen sensing and initiation of the host immune response (Vareille et al., 2011; Hiemstra et al., 2015). Among others, posttranslational modifications of proteins, like protein phosphorylation and ubiquitination, regulate processes within the host cell. Proteins can be modified with various types of ubiquitination like monoubiquitination and polyubiquitination. Ubiquitin, a protein of 76 amino acids, is covalently linked to the ϵ -amine group of lysine residues in target proteins and thus, regulates their stability, localization or interaction properties. The function of ubiquitination depends on the length and linkage type of the ubiquitin chain. Furthermore, ubiquitin is involved in the regulation of immunity and clearance of intracellular pathogens (Bhat and Greer, 2011; Zinngrebe et al., 2014; Hu and Sun, 2016). It was demonstrated previously that bacterial and viral pathogens are able to manipulate the ubiquitin proteasome system (UPS) to evade the host defense. Moreover, host ubiquitin is misused by influenza A viruses to facilitate particle uncoating and transport within the host cell (Rudnicka and Yamauchi, 2016; Yamauchi, 2020). Here, we infected type 2 lung epithelial cells (A549) with a pandemic IAV, with *S. pneumoniae* D39 Δ cps, and conducted viral and bacterial co-infection to elaborate the effects of these infections on protein abundance and on protein ubiquitination. We enriched for K48 and K63 polyubiquitinated proteins, because these ubiquitin chains are the most dominant within the lung tissue, and applied label free LC-MS/MS based quantification. The results of this study contribute to the understanding of the ubiquitin mediated regulatory processes during viral and bacterial co-infection.

MATERIALS AND METHODS

Bacterial and Viral Strains

Streptococcus pneumoniae D39 Δ cps, a non-encapsulated mutant of D39 was described earlier (Saleh et al., 2013).

The pandemic influenza A/H1N1 virus [A/Germany-BY/74/2009(H1N1)] was kindly provided by the Institute of Immunology (FLI, Federal Research Institute for Animal Health) (Greifswald-Insel Riems, Germany).

Cell Culture and Infections

A549 alveolar type 2 lung epithelial cells (ATCC CCL-185) were cultured in T75 flasks in RPMI medium (Invitrogen)

supplemented with 10% fetal calf serum (FCS) at 37°C in 5% CO₂ atmosphere. For infection experiments, cells were seeded into T75 flasks and grown to 80-90% confluence. 2 h before all infections the medium of A549 cells was exchanged by RPMI without FCS.

Bacteria were grown at 37°C in Todd Hewitt broth supplemented with 0.5% yeast extract (THY) to mid-exponential phase (OD₆₀₀ of 0.35-0.40). Pneumococci were washed and resuspended in PBS prior to infection. A549 cells were infected with *S. pneumoniae* D39 Δ cps at a MOI of 15 and were harvested 6 h post infection.

For viral infections, A549 cells were infected at a MOI of 5. After 2 h the medium was replaced by RPMI supplemented with 10% FCS and cells were harvested 24 hours post infection. Viral replication was confirmed *via* qRT-PCR (**Supplementary Figure S1**).

For co-infections, A549 cells were infected with IAV followed by bacterial infection. Cells were infected with IAV at a MOI of 5. After 2 h the medium was replaced by RPMI supplemented with 10% FCS and infected cells were cultured for additional 20 h at 37°C in 5% CO₂ atmosphere. Then, 2 h before bacterial infection, media was changed to RPMI without FCS. Hereafter, A549 cells were infected with *S. pneumoniae* D39 Δ cps (MOI 15) for 6 h.

At the end of the infection period cells were washed with PBS and cells were detached using trypsin and counted. Cell counts were determined by light microscopic quantification of cell viability. Cells were stained with 0.4% (v/v) trypan blue under serum-free conditions and visually examined.

All experiments were performed in triplicates (n=3).

Interleukin ELISA

ELISA plates (Human IL-6/IL-8 Max Deluxe Set [BioLegend]) were coated with capture antibody and incubated for 16-18 h at 4°C. Plates were washed (PBS + 0.5% Tween-20). Hereafter, plates were blocked with blocking solution for 1 h with shaking at 200 rpm. Furthermore, standard series were prepared (IL-8: 1000 pg/ml – 15.6 pg/ml, IL-6: 500 pg/ml – 7.8 pg/ml). Non-specific bindings were blocked, blocking solution was removed and plates were washed. Standards and cell culture medium samples were added to the plates and incubated for 2 h with shaking. After the plates were washed, they were incubated with the detection antibody for 1 h. The detection antibody solution was removed and plates were washed. Avidin-HRP solution was added and incubated for 30 min with shaking. Avidin-HRP solution was removed and plates were washed. TMB substrate solution was added and incubated for 15 min in the dark. Stop solution (2 N H₂SO₄) was added and absorbance was measured at 450 nm and 570 nm within 15 min.

Protein Extraction

Protein extraction was performed as described elsewhere (Sura et al., 2021). Briefly, harvested cells were resuspended in 1 ml lysis buffer (50 mM Tris HCl [pH 7.5], 0.15 M NaCl, 1 mM EDTA, 1% NP 40, 10% glycerol, 1x cComplete Protease Inhibitor Cocktail [Roche], 1 mM PMSF, 10 mM N-ethylmaleimide, 20 μ M MG132), sonicated to shear DNA and cleared by

centrifugation. Protein concentration of the samples was determined by the BCA assay.

Selective Enrichment of K48 and K63 Ubiquitinated Proteins

Lysates containing 500 µg of total protein were transferred into new tubes and filled to 300 µl with lysis buffer. To reduce unspecific binding of proteins to magnetic beads, 10 µl of magnetic control beads (LifeSensors) have been added to the samples and were incubated in an overhead shaker for 1 h at 10 rpm and 4°C. Afterwards, supernatants were transferred into new tubes. For the enrichment of K48 ubiquitinated proteins, 40 µl of K48 magnetic TUBE HF (LifeSensors), washed with Tris-buffered saline with Tween20 (TBS-T), were added, followed by an incubation for 3 h at 10 rpm and 4°C. To enrich K63 polyubiquitinated proteins, 700 µl water and K63 Flag-TUBE (LifeSensors) with a final concentration of 50 nM were added to the precleared sample and incubated for 2 h at 10 rpm and 4°C. Subsequently, 8 µl of magnetic anti-Flag beads were added and samples were incubated for additional 2 h. The unbound fraction of both enrichments was removed and the beads were washed three times with 500 µl TBS-T. To elute the enriched proteins, beads were resuspended in 25 µl SDS buffer (5% SDS; 50 mM TEAB; 5 mM TCEP) and incubated at 65°C for 45 min with 300 rpm shaking. Finally, the supernatants were transferred into new tubes.

Proteolytic Digest

Extracted and enriched ubiquitinated proteins were digested by suspension trapping on micro S Traps (Protifi) as described elsewhere (Sura et al., 2021). Briefly, lysates containing 30 µg protein were transferred into new tubes and disulfide bonds were reduced by adding TCEP. Thiol groups were alkylated by adding iodoacetamide for proteome samples or chloroacetamide for ubiquitinome samples. Proteins were digested by adding 25 µl digestion buffer (50 mM TEAB) containing 1.2 µg trypsin for proteome samples and 600 ng trypsin (Promega) for ubiquitin enriched samples followed by an incubation for 3 h at 47°C. Peptides were subsequently eluted with 40 µl 50 mM TEAB; 0.1% acetic acid; 60% ACN in 0.1% acetic acid. All eluted fractions of a sample were pooled and dried in a vacuum concentrator. Dried peptides were stored at -80°C

Peptide Fractionation

Peptides generated from crude protein extracts were fractionated by off-line high pH reversed phase chromatography as described elsewhere (Sura et al., 2021).

LC-MS/MS Analysis

The peptide composition of the generated samples was analyzed by LC-MS/MS with an EASY-nLC 1000 (Thermo Fisher Scientific) coupled to a QExactive mass spectrometer (Thermo Fisher Scientific). Peptides were loaded onto in-house packed fused silica columns of 20 cm length and an inner diameter of 75 µm, filled with ReproSil Pur 120 C18-AQ 1.9 µm (Dr. Maisch). Peptides were subsequently eluted by a non-linear binary gradient of 165 min from 2% to 99% solvent B (0.1% acetic

acid in acetonitrile) in solvent A (0.1% acetic acid). Detailed information on the gradient and LC setup can be found in **Supplementary Table S1**. MS/MS data for the proteome and the K48 ubiquitin chain enriched samples were acquired as previously described (Sura et al., 2021). For the K63 ubiquitin chain enriched samples the mass spectrometer was operated in DDA mode. The survey scan was acquired from 300–1650 m/z with a resolution of 70,000 at 200 m/z. The 10 most abundant ions were selected for fragmentation *via* HCD with a normalized collision energy of NCE 27. The AGC target was set to 1E5 with an underfill ratio of 10% and a maximum injection time of 180 ms. MS/MS spectra were acquired in centroid mode with a resolution of 17,500 at 200 m/z. Ions with unassigned charge states as well as charge 1 and higher than 6 were excluded from fragmentation. Dynamic exclusion was set to 30 s and lock mass correction was enabled. Detailed information on the MS/MS acquisition parameters for all datasets are provided in **Supplementary Tables S2 and S3**.

Database Search

Datasets of enriched polyubiquitinated and total proteome samples were processed separately. Raw data were searched with MaxQuant (version 1.6.17.0) (Cox and Mann, 2008; Cox et al., 2014) against the UniProt databases for human (July 2019, UP000005640, 20,416 entries), Influenza A virus (A/Germany-BY/74/2009(H1N1)) (December 2017, UP000153067, 10 entries) and for *S. pneumoniae* D39 (September 2020, UP000001452, 1,915 entries). The maximum number of allowed missed cleavages was 2 and precursor mass tolerance was set to 4.5 ppm. Carbamidomethylation (C) was set as a fixed modification, oxidation (M) and acetylation (protein N-termini) were set as variable modifications for both datasets. GlyGly (K) was set as an additional variable modification for K48 and K63 ubiquitin chain enriched samples. Proteins were identified with at least two unique peptides, and peptide-spectrum match (PSM) and protein false discovery rate (FDR) were set to 0.01. Match between runs was applied and protein abundances were calculated by the MaxLFQ algorithm. A detailed table of applied parameters for database searching can be found in **Supplementary Tables S4 and S5**.

Data Analysis

Identified protein groups were analyzed with Perseus (version 1.6.15.0) (Tyanova et al., 2016; Tyanova and Cox, 2018). Only identified by site and reverse hits, as well as potential contaminations were removed. To assess differentially expressed proteins, a two tailed *t* test was applied for proteins with “LFQ intensity” values in three out of three replicates of the compared groups. Proteins were considered as differentially expressed with a *p* value < 0.05 and a fold change > 1.5. Quantification results and summary statistics can be found in **Supplementary Table S6**. Functional annotation enrichment of proteins with significantly changed abundance was performed with the Database for Annotation, Visualization and Integrated Discovery (DAVID v6.8) (Da Huang et al., 2009a; Da Huang et al., 2009b) and Reactome (Jassal et al., 2020). Protein interaction networks were created with STRING (v11.0)

(Szkarczyk et al., 2019). Data were visualized using Inkscape (version 0.92.2) and RStudio (version 1.3.1073) with the packages ggplot2 (version 3.3.5), dplyr (version 1.0.6), EnhancedVolcano (version 1.4.0), splitstackshape (version 1.4.8), shadowtext (version 0.0.8) and ggpubr (version 0.4.0). Data variance was assessed by calculation of CVs from proteins with quantitative values in all three replicates (**Supplementary Figure S2**).

RESULTS

To investigate the effect of bacterial or viral mono-infections and bacto-viral co-infections we infected A549 cells at a MOI that does not kill the majority of the A549 cells within the analyzed time frame. Also, we aimed to explore, whether the co-infection will be more severe to A549 cells than the infections with a single pathogen. Therefore, we analyzed the proteome and ubiquitinome of mono- and co-infected A549 cells.

Cell Count and Interleukin Secretion

A549 cells were grown to 80%-90% confluence. Hereafter, cells were challenged either with the influenza A virus H1N1, *S. pneumoniae* D39Δcps, or both pathogens in a viral bacterial co-infection. After 24 h of viral infection the A549 cell count significantly increased by more than 25% (**Supplementary Figure S3**). This indicates that IAV propagation does not interfere with A549 proliferation within the observed time frame. In contrast, a 25% reduced cell count was observed after 6 h of *S. pneumoniae* infection. After co-infection the number of cells did not change compared to the uninfected control.

Cell culture supernatants of each infection were used to determine the levels of secreted immune modulating effectors. The average (n=3) level of IL-6 and IL-8 was increased after *S. pneumoniae* infection and bacto-viral co-infection (**Supplementary Figure S4**), but not after single viral infection. In detail, there is a difference in IL-6 and IL-8 levels when comparing the bacterial single infection or the co-infection with the corresponding mock infection. In contrast, there is no difference between the single H1N1 infection and the associated mock infection. Therefore, the H1N1 infection does not lead to an increased interleukin production.

Differentially Abundant Proteins in Proteome and Ubiquitinome

For all experiments, the PSM FDR and the protein FDR have been set to 0.01. Proteins were considered as significantly changed in abundance, when they were quantified in all three replicates of the compared groups with a fold change greater than 1.5 and a *p*-value below 0.05. This, in total, resulted in the identification of more than 90,000 peptides, enabling quantification of more than 5,800 proteins for the proteome data set. In the proteome of A549 cells 74, 37 and 107 proteins were found to be significantly changed in abundance upon H1N1 infection, *S. pneumoniae* infection, and co-infection, respectively (**Figure 1A**). H1N1 infection induced the accumulation

of various proteins, whereas the *S. pneumoniae* infection mainly led to decreasing protein abundances. Moreover, different sets of proteins were effected by viral or bacterial infection. This is also reflected by the low overlap between these infections (**Figure 1B**).

After enrichment of polyubiquitinated proteins we were able to identify more than 34,000 and 9,800 peptides, from the K48 and K63 enriched samples, respectively. This enabled the quantification of more than 2,800 proteins after K48 enrichment and more than 850 proteins in the K63 enriched data set (**Figure 1A**). In contrast to the proteome and K63 polyubiquitin enriched data sets, *S. pneumoniae* infection induced more changes than H1N1 infection in the K48 polyubiquitin enriched data set. Comparison of the proteins, which were differentially expressed upon viral and bacterial infection, revealed only a limited number of shared proteins between the single infections (**Figures 1A, C, D**). To elaborate whether altered abundance detected for proteins in the polyubiquitin enriched data sets originates from alterations in protein abundance in general, we examined the overlap of proteins that were detected with altered abundance in those data sets (**Supplementary Figure S5**). Whereas upon pneumococcal infection three proteins were detected with differential expression in the proteome and K48 enriched samples, 18 and 15 proteins were differentially expressed in the proteome and K48 enriched data set upon viral and co-infection, respectively (**Supplementary Figure S5**). This indicates that in most cases altered abundance in polyubiquitin enriched samples is independent of variations in the abundance of the respective proteins. Hence, differential abundance in polyubiquitin enriched data sets is caused by changing polyubiquitination incidence rather than by changing protein abundance. Volcano plots and MA plots, comparing the different conditions are shown in **Supplementary Figures S6–S8**.

Functional Analysis of Proteins Differentially Expressed in the Total Proteome Samples

To get detailed insights into the processes driving the cellular response to the infecting pathogens, we used the Database for Annotation, Visualization and Integrated Discovery (DAVID) to perform annotation enrichment on proteins with significantly changed abundance.

Infecting A549 cells with H1N1 significantly altered the abundance of 74 proteins within the proteome samples. The abundance of 63 proteins was increased and decreased for eleven proteins. Functional annotation enrichment revealed that *type I interferon*, *ISG* and other terms, which represent a response to viruses, were mainly enriched within proteins of increased abundance (**Figure 2A**). No terms have been enriched from proteins with reduced abundance (**Figure 2A**).

In the proteome of *S. pneumoniae* infected A549 cells only 37 proteins were detected with significantly altered abundance, among them we detected ten with increased abundance and 27 with decreased abundance. Here, the terms *oxidation-reduction process* (*p*-value = 0.00022) and *regulation of translation* (*p*-value =

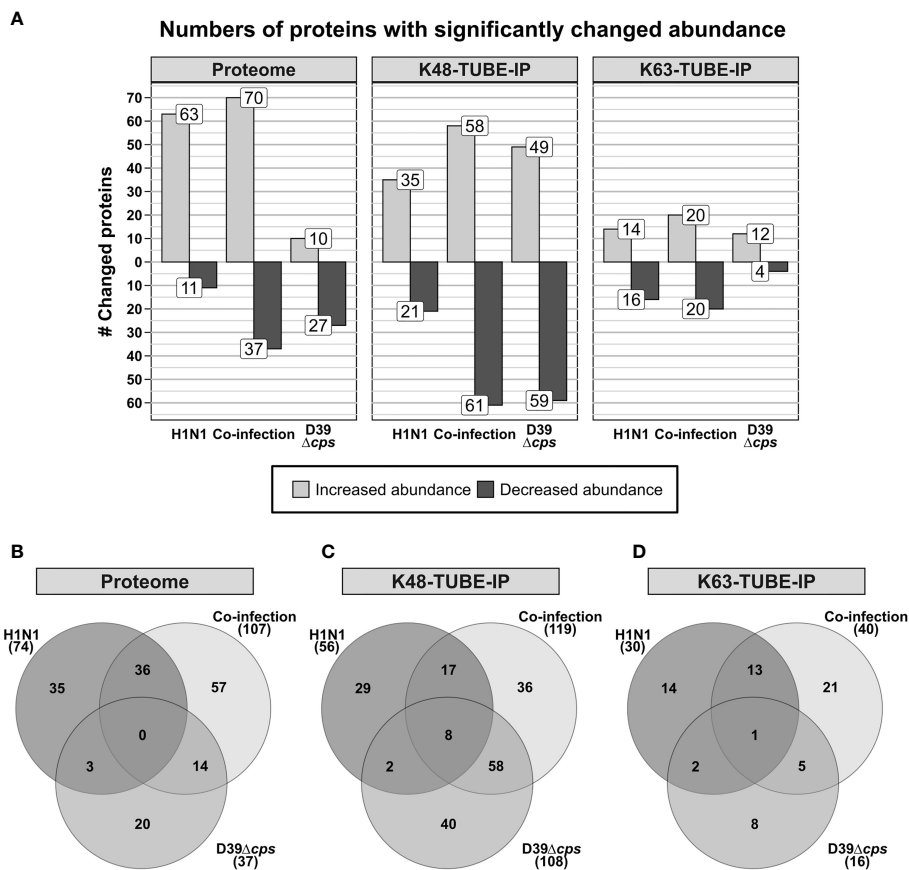


FIGURE 1 | Analysis of differentially abundant proteins and differential abundance in polyubiquitination of A549 cells in response to single and co-infections with influenza A virus H1N1 and *Streptococcus pneumoniae* D39 Δcps . **(A)** Number of proteins that have been detected with differential abundance on protein or polyubiquitination level in the different data sets. **(B–D)** Venn diagrams displaying the overlap of proteins detected with differential abundance between the analyzed single infection and co-infection.

0.0055) were enriched from proteins with reduced abundance. In contrast to the H1N1 infection, no terms were enriched from proteins with increased abundance.

Viral and bacterial co-infections of A549 cells mainly affected Gene Ontology Biological Process-terms (GOBP-terms) similar to those enriched in single infections. Proteins with increased abundance were annotated for GOBP terms *defense to virus*, *type I interferon signaling pathway* and *ISG15-protein conjugation*. The term *oxidation-reduction process* was enriched from proteins with decreased abundance (**Figure 2B**). In general, there is a reasonable quantity of proteins detected with the same regulation between the single infection and the co-infection (**Figure 1B**). Additionally, several proteins were quantified in the H1N1 and co-infection, but were missing in uninfected and *S. pneumoniae* infected samples. These proteins are MX1, MX2, IFI44, IFIT1, IFIT2, IFIT3 and IFIH1, which are all involved in *type I interferon signaling* and viral defense.

Furthermore, 17 proteins that are included in the integrated annotations for Ubiquitin and Ubiquitin-like Conjugation Database (iUUCD 2.0) (Zhou et al., 2018) and 2 proteins that are catalytically active subunits of the immunoproteasome as well as

the proteasome activator subunit beta (PA28beta) were detected with altered protein abundance upon infection (**Table 1**).

Functional Analysis of Differentially Abundant Proteins in K48 Enriched Samples

As ubiquitination is involved in the regulation of nearly every cellular process, we selectively enriched for K48 and K63 polyubiquitinated proteins. It was demonstrated that K48 and K63 polyubiquitin chains are the most abundant chain types in murine primary macrophages and in murine lung tissue (Heunis et al., 2020). K48 ubiquitination has a variety of functions in the eukaryotic cell. Still, the primary function is to mark proteins for proteasomal degradation.

After 24 h of H1N1 infection, there were fewer changes in protein abundance detected in K48 enriched samples compared to total proteome samples. GOBP terms that were most significantly overrepresented from proteins with increased abundance in the K48 enriched samples were *defense response to virus*, *type I interferon signaling pathway* and *negative*

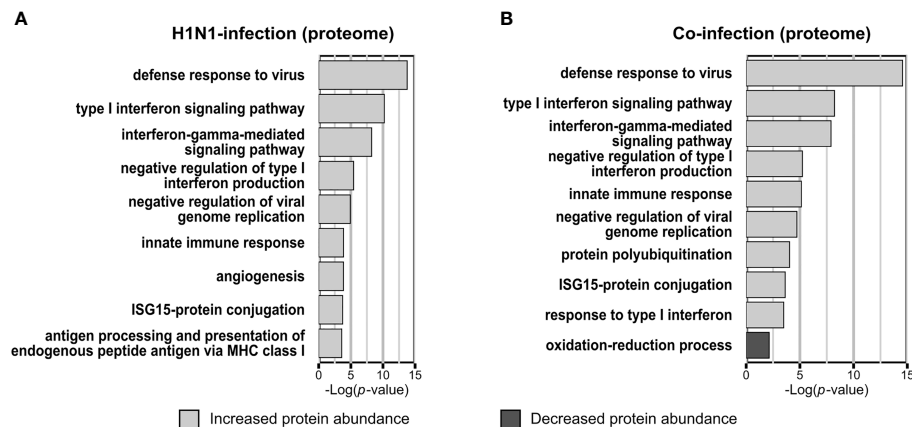


FIGURE 2 | Gene ontology biological process (GOBP) terms enriched from proteins with significantly changed abundance. Categorical annotation enrichment (p -value < 0.01) of GOBP terms from proteins with significantly altered abundance (p -value < 0.05 ; fold change > 1.5) in the proteome. Enrichment analysis of A549 cells infected with Influenza A virus **(A)** or co-infected with *Streptococcus pneumoniae* D39Δcps **(B)** [$n=3$]. **(A, B)** Displayed are the top hits of the enriched GOBP terms from proteins with increased and decreased abundance, ranked by the enrichment p -value.

regulation of viral genome replication, while RNA splicing was most significantly overrepresented from proteins with decreased abundance.

Upon *S. pneumoniae* infection we detected altered abundance of 108 putatively K48 polyubiquitinated proteins. Fifty-nine proteins were quantified with decreased abundance and 49 with increased abundance after infection. Only three out of 37 proteins detected with differential expression in the proteome samples were detected with altered abundance in the K48 polyubiquitin enrichment. Proteins with decreased abundance in K48 polyubiquitination mostly affected processes involved in

mRNA splicing and rRNA processing. Arp2/3 complex mediated actin nucleation and other processes related to actin filament organization were highly overrepresented by proteins with increased K48 polyubiquitination. In addition to actin filament related processes, FC-gamma receptor signaling pathway involved in phagocytosis was enriched from proteins with increased K48 polyubiquitination, as well.

In the viral and bacterial co-infection the pattern of proteins with significantly changed abundance after K48 enrichment is similar to both of the single infections. Moreover, the co-infection shares ~50% and ~15% of differentially expressed

TABLE 1 | List of proteins that were detected with differential abundance upon infection and are listed in the iUUCD 2.0 database or related to the immunoproteasome and proteasome regulation (highlighted with an asterisk).

Protein	iUUCD 2.0		fold change		
	family	ID	H1N1	Co-infection	D39
TMF1	E3 adaptor	IUUC-Hsa-046889	1.09	-1.81	-1.33
CIAO1	E3 adaptor	IUUC-Hsa-046528	—	-1.79	-1.43
CORO7	E3 adaptor	IUUC-Hsa-045847	1.43	1.93	1.94
MNAT1	E3	IUUC-Hsa-045876	1.58	1.34	1.19
RBCK1	E3	IUUC-Hsa-045738	1.66	1.77	-1.45
IRF2BP1	E3	IUUC-Hsa-046942	1.16	1.51	1.13
TRIM56	E3	IUUC-Hsa-046238	1.59	1.55	1.08
TRIM25	E3	IUUC-Hsa-045828	1.67	1.58	1.03
RNF213	E3	IUUC-Hsa-046140	1.64	1.99	-1.10
RNF121	E3	IUUC-Hsa-046468	—	1.53	1.57
PML	E3	IUUC-Hsa-045861	3.57	4.19	1.08
TRIM21	E3	IUUC-Hsa-046583	5.17	4.62	-1.44
DTX3L	E3	IUUC-Hsa-045921	19.49	18.17	-1.10
HERC5	E3	IUUC-Hsa-046342	12.21	28.65	—
UBE2T	E2	IUUC-Hsa-046513	1.31	-1.41	-1.54
UBE2E1	E2	IUUC-Hsa-046576	1.04	-1.95	-1.53
UBE2L6	E2	IUUC-Hsa-045943	5.23	7.72	1.33
PSME2*	—	—	1.27	1.53	1.15
PSMB9*	—	—	1.67	1.95	-1.11
PSMB8*	—	—	1.76	2.34	-1.02

The fold change upon each infection is given and highlighted in bold if the detected change is statistically significant (students t-test; p -value < 0.05 ; fold change > 1.5 ; $n=3$).

proteins with the bacterial and the viral infection, respectively (**Figure 1C**). Proteins that were shared between the single infections change their abundance into the same direction. Although the STRING network, which was generated from the co-infection (**Figure 3B**) data, has a high similarity to the network generated from the bacterial infection (**Figure 3A**), it also contains a cluster of proteins that has been detected upon viral infection (*response to virus*) (**Figure 3B**). Furthermore, eight proteins were found to be changed significantly in all infections and three of them are related to *RNA splicing* (**Figure 1C**). Ten proteins were only quantified in the viral and in co-infection samples. These proteins affect the processes of *response to virus*, *type I interferon signaling pathway* and *interferon-gamma-mediated signaling pathway*.

Functional Analysis of Differentially Abundant Proteins in K63 Enriched Samples

In contrast to K48 polyubiquitination, K63 polyubiquitin chains are thought to mediate non-proteasomal signals for endocytosis and immune responses. The K63 enriched data set displays the lowest number of quantified proteins within the three data sets obtained in this work. Accordingly, the K63 data set reveals fewer proteins detected with altered abundance. H1N1 infection induced variations in the K63 polyubiquitination level of 30 proteins. Proteins with reduced K63 ubiquitination affect *mRNA splicing* processes and proteins with increased K63 ubiquitination affect *redox* processes. Changes induced by the *S. pneumoniae* infection do not affect multiple pathways, only *negative regulation of mitochondrial outer membrane permeabilization involved in apoptotic signaling pathway* is affected by proteins with increased K63 polyubiquitination. Co-infection most significantly affected processes involved in *mRNA processing* from proteins with decreased polyubiquitination.

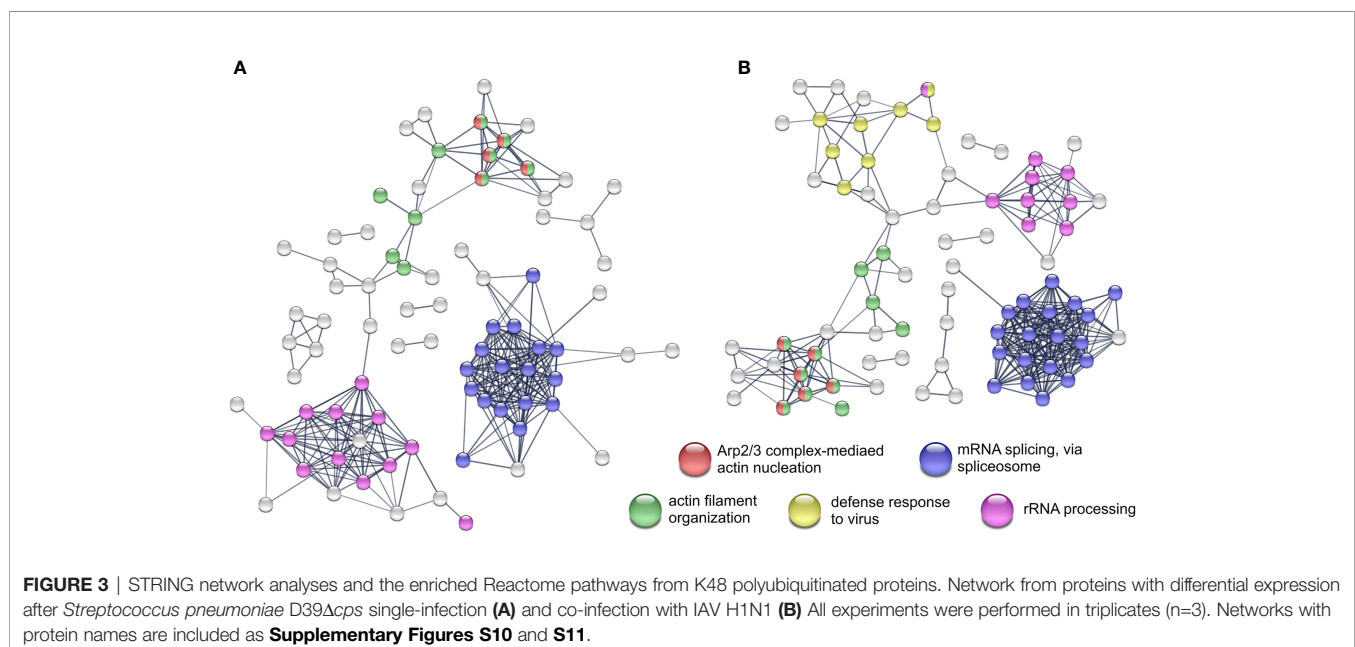
Proteins with increased polyubiquitination affected *redox* processes and *response to ER stress*.

DISCUSSION

In the work presented, we used *in vitro* cell culture based infection experiments to examine potential synergistic effects of the infecting pathogens in viral and bacterial co-infections on human lung epithelial cells. Therefore, we analyzed viral and bacterial mono-infections, along with bacto-viral co-infections of A549 cells, focusing on the proteome, as well as the selective enrichment of polyubiquitinated proteins. Infecting A549 cells with H1N1 for 24 h induced a pronounced immune response and viral defense of the host. The additional bacterial infection was performed at MOI 15 to be able to elaborate a potential synergisms of the pathogens.

Response to IAV H1N1 Infection

Influenza H1N1 infection induced a strong viral defense response of the A549 cells. This was established by the induction of the JAK-STAT cascade, type I interferon signaling, interferon γ signaling and induction of the ISG15 protein conjugation. Induction of the type I interferon production mediated by RIG-I and MAVS, which leads to the induction of a wide array of genes, can be assumed from increased protein abundance of interferon stimulated genes (Schoggins et al., 2011; Zhang et al., 2020). In addition, we detected a 25 fold increase in the abundance of DDX60 which was shown to be required for RIG-I mediated type I interferon expression after viral infection (Miyashita et al., 2011). From the proteins with higher abundance after viral infection, nine show E3 ligase activity and one protein is described as an E2 enzyme (Zhou et al., 2018) (**Table 1**). Among these proteins are HERC5 and TRIM25, both acting as E3 ligating enzymes for ISG15



(Wong et al., 2006; Mathieu et al., 2021), which increased twelve and five times in abundance in our experiments, respectively. UBE2L6, the ISG15 E2 transferring enzyme, was detected to be fivefold more abundant after viral infection. These results are in concordance with previously published data where an up-regulation of UPS genes in response to Interferon-stimulation was detected (Seifert et al., 2010). This, together with the increased abundance of the transcription factor IRF9, which induces the transcription of interferon stimulated genes (ISG) when forming a complex with STAT1 and STAT2, underpins the interferon mediated activation of the JAK-STAT pathway. OAS1-3 are degraders of viral RNA (Shim et al., 2017) and were also detected with increased abundance after viral infection. Moreover, increased protein abundance of the ubiquitin E3 ligase DTX3L and the interacting protein PARP9 as well as of PARP10, 12 and 14 was observed in IAV infected A549 cells. These results confirm the findings on increased protein abundances of PARP9 and PARP14 upon viral infection, first observed by Becker and colleagues (Becker et al., 2018). We were able to confirm these results using a different influenza strain, but the same cell line. It is reported by others that the outcome of the IAV infection depends not only on the MOI and the duration of the infection, but also on the cell line, as well as the employed viral stain (Becker et al., 2018; Wu et al., 2019). Influenza virus infection predispose the host cell to secondary bacterial infections, which was shown from mice and *in vitro* experiments (Sharma-Chawla et al., 2016; Bai et al., 2021). Bai and coworkers demonstrated that viral infection induced an increase in the abundance of PPIA, which interacts and mediates protection from proteasomal degradation of PTK2. Ultimately, this results in increased integrin $\alpha 5$ expression and actin rearrangement, which renders the host cell more susceptible for secondary bacterial infection (Bai et al., 2021). In contrast, we have not detected significant changes in the abundance of PPIA and integrin- $\alpha 5$ in the proteome nor in the abundance of PTK2 in the proteome and K48 enriched data set. These differences in the outcome of the viral infection can potentially be caused by several reasons. First, observed differences were caused by the use of different influenza strains. The second reason can be the infection duration and the MOI at which the experiments were conducted. Bai et al. showed that the mRNA level of PPIA reached its maximum at 12 hpi and decreased afterwards (Bai et al., 2021). The use of a higher MOI may result in a shifted maximal mRNA level and CypA expression. The reason causing the observed differences remains unclear. We can exclude the cell line as a cause, as we used A549, too. In addition, Becker et al. have not observed changes in the protein abundance of CypA or ITGA5 after IAV infection of A549 cells, as well (Becker et al., 2018).

Response to *Streptococcus pneumoniae* Infection

The pneumococcal infection induced differential abundance of 37 proteins. Furthermore, we detected 108 and 16 proteins with significantly altered abundance in K48 and K63 polyubiquitination, respectively.

The protein that showed the most prominent increase in abundance (about four fold) was PTGS2 or COX-2, being an inducible protein involved in the initial step of prostaglandin synthesis. In type II alveolar epithelial cells the induction of the COX-2 expression in response to pneumococci is controlled in a p38 MAPK and NF κ B dependent manner (N'Guessan et al., 2006; Szymanski et al., 2012). Bootsma and colleagues also observed an induction of COX-2 by the Δcps mutant of *S. pneumoniae* analyzing the transcriptional response of Detroit 562 pharyngeal epithelial cells to the adherence of different pneumococcal strains (Bootsma et al., 2007). They have shown that *S. pneumoniae* D39 and its isogenic Δcps mutant alter the expression of different gene sets. Infection with the Δcps mutant changed the expression of 156 genes (28 upregulated and 128 downregulated) (Bootsma et al., 2007). Given the fact that Detroit 562 cells are of pharyngeal origin and A549 cells are lung epithelial cells, the published results cannot be entirely transferred to our study. Nevertheless, Bootsma et al. also observed an increase in IL-6 and IL-8 levels upon *S. pneumoniae* D39 Δcps infection (Bootsma et al., 2007) (**Supplementary Figure S4**).

Bacterial pathogens such as *S. pneumoniae* use different strategies like transmigration or transcytosis to cross epithelial or endothelial barriers of the host. Pneumococcal uptake by A549 cells is low, however, A549 cells show increased uptake of *S. pneumoniae* D39 Δcps compared to the wild type strain (Talbot et al., 1996; Bootsma et al., 2007). Still, it was shown that pneumococcal phosphorylcholine mimics the natural ligand of PAFr initiating bacterial uptake in a β -arrestin dependent manner (Radin et al., 2005; Bertuzzi et al., 2019). Pneumococcal endocytosis is clathrin and caveolae mediated and the vast majority of endocytosed pneumococci is killed by lysosomal fusion of the endosome (Gradstedt et al., 2013). Pneumolysin, a cholesterol-dependent cytolysin expressed on the pneumococcal surface and released by autolysis, disables the acidification of the endosome by the formation of pores in the endosomal membrane (Barnett et al., 2015; Ogawa et al., 2018). The ubiquitin-proteasome system (UPS) is involved in the autophagosomal entrapment and killing of cytosolic pneumococci (Iovino et al., 2014; Ogawa et al., 2018). Additionally, pneumolysin directly interacts with actin and activates small GTPases leading to remodeling of the actin network (Hupp et al., 2013). Rho GTPases act upstream of the Arp2/3 complex, which facilitate actin nucleation and is involved in clathrin-mediated endocytosis and phagocytosis (Sirotkin, 2011; Sumida and Yamada, 2015; Jin et al., 2021). In our study, we observed increased abundance in K48 polyubiquitination of proteins belonging to the Arp2/3 complex and other actin and cytoskeleton organization related GO terms (**Figure 3A**). Moreover, the Reactome analysis revealed that Rho-GTPase signaling is affected by proteins with increased K48 polyubiquitination, as well. Thereby, polyubiquitination bridges the host proteome and ubiquitinome in response to pneumococcal infection. These results are not in contrast to the finding that *S. pneumoniae* D39 effectively overcomes the epithelial barrier by transmigration (Attali et al., 2008). We have not observed any changes in the abundance of junction proteins as it was described

by Peter and colleagues (Peter et al., 2017). This could be due to the use of a single cell line and no lung tissue.

In our K48 polyubiquitin analysis we detected reduced polyubiquitination in proteins involved in mRNA splicing and rRNA processing. Proteins involved in mRNA splicing mainly belong to the spliceosomal E complex. Changes in the spliceosome composition may indicate an early apoptotic state of the epithelial cells, linking the spliceosome and apoptosis (Schwerk and Schulze-Osthoff, 2005). It remains unclear what causes these effects upon pneumococcal infection and is a subject of future studies.

In addition to the K48 polyubiquitin analysis, Reactome analysis of proteins with altered abundance in K63 polyubiquitination also indicated involvement of the Rho-GTPase cycle, whereas the functional annotation enrichment analysis of K63 polyubiquitinated proteins showed only *negative regulation of mitochondrial outer membrane permeabilization involved in apoptotic signaling pathway* as an overrepresented GOBP term.

Viral and Bacterial Co-Infection

Bacterial and viral co-infections are related to increased severity of disease, increased morbidity and mortality (Siemens et al., 2017; Lim et al., 2019). Influenza A virus infection, caused by pandemic or seasonal strains, predispose the host to secondary bacterial infections (Sharma-Chawla et al., 2016; Siemens et al., 2017; LeMessurier et al., 2020). In our experiments we could not observe an increased cytotoxicity of the co-infection compared to bacterial or viral single infection (**Supplementary Figure S3**). Following the co-infection we observed similar IL6 and IL8 level compared to the bacterial single infection (**Supplementary Figure S4**). Unexpectedly, preceding viral infection reduced pneumococcal adherence to A549 epithelial cells in our experimental setup (**Supplementary Figure S9**). Still, viral and bacterial co-infection resulted in the highest number of proteins with significantly altered abundance on protein and polyubiquitination level. Interestingly, we did not detect over representation of pathways that have not been identified upon one of the two single infections. For all obtained data sets the pathways affected by co-infection resembles both of the single infections. This is in congruence with a previous study where we reported additive effects of IAV H1N1 and *Streptococcus pyogenes* co-infection of 16HBE cells (Sura et al., 2021). Nevertheless, here we have detected enhanced alteration of protein abundance and polyubiquitination incidence upon co-infection. This effect on protein abundance was also noticed for PSMB8, PSMB9 and for PSME2 (**Table 1**). These proteins are immunoproteasome subunits and proteasome activator PA28beta and are involved in altered generation of MHC I antigenic peptides presented to CD8 T-cells (Keller et al., 2015; McCarthy and Weinberg, 2015). The further increase in protein abundance upon co-infection might be induced by enhanced IFN- γ production caused by the bacterial superinfection as it was reported by Strehlitz and coworkers from mice experiments (Strehlitz et al., 2018). Upon co-infection higher numbers of proteins with significantly altered abundance were detected in all data sets when compared to the single infections. Still, these

observations are not reflected by an increased cytotoxicity of the viral bacterial co-infection.

In the presented study we used *S. pneumoniae* D39 Δ cps, an isogenic mutant that lacks the capsular polysaccharides. Thus, the outcome of the study and the observed alterations in the proteome and the ubiquitinome were potentially influenced by the absence of capsular polysaccharides. However, the interaction between A549 cells and the pneumococci is mainly based on bacterial adherence to the cell surface (Agarwal et al., 2010). It has been shown that the intimate contact of pneumococci with host cells is associated with a reduction of CPS (Hammerschmidt et al., 2005). While encapsulated wild-type pneumococci interact only moderately with non-professional host cells under *in vitro* conditions, binding can be enhanced using isogenic non-encapsulated mutants. Thereby, the induced signal transduction cascades can be elucidated and the host responses analyzed. Although this is not related to the pathophysiological conditions under *in vivo* conditions, important discoveries were made in the last decades using this combination of bacteria and host cells.

Importantly, we chose a MOI of only 15 bacteria per host cell to reduce the level of host cell damage caused by pneumolysin and hydrogen peroxide to a minimum in the bacterial single infections and co-infections. In *in vivo* studies higher bacterial infection doses are applied to study the effects in experimental acute pneumonia or septicemia infection models.

In *in vivo* experiments, co-infection appears to be adverse for the host, caused by the IAV induced expression of type I interferons suppressing the bacterial clearance by disturbed recruitment of immune cells (LeMessurier et al., 2020; Park et al., 2021). On the other hand, type I interferons increase the expression of tight junction proteins and decrease the expression of PAFr, reducing pneumococcal uptake and hindering transmigration (LeMessurier et al., 2013). The *in vitro* study presented here is based on A549 cells grown as a monolayer. Due to the lack of immune cells and their interaction with the epithelial barrier in our setup, this adverse effect was probably not observed. Furthermore, A549 cells grown as a monolayer do not form tight junctions (Carterson et al., 2005). The scarcity of tight junctions might explain the fact that we did not observe changes in the expression of tight junction proteins, whether induced by type I interferons, or by pneumococcal infection, as it was observed in lung tissue (LeMessurier et al., 2013; Peter et al., 2017).

It can be concluded that IAV and *S. pneumoniae* D39 Δ cps co-infection of monolayer grown A549 cells shows additive, but in the current setup no observable synergistic effects. It would be interesting to investigate whether this changes in polarized, 3D grown A549 cells and to determine the impact of the pneumococcal virulence factor pneumolysin.

DATA AVAILABILITY STATEMENT

The mass spectrometry proteomics data have been deposited to the ProteomeXchange Consortium (<http://proteomecentral.proteomexchange.org>) via the PRIDE (Perez-

Riverol et al., 2019) partner repository with the dataset identifier PXD028465.

AUTHOR CONTRIBUTIONS

Conceptualization: TS, US, and DB. Formal analysis: TS. Funding acquisition: SH, US and DB. Methodology: TS and VG. Data analysis: TS. Writing—first draft: TS. Writing—review and editing: TS, VG, CC, SM, SH, US, and DB. All authors contributed to the article and approved the submitted version.

FUNDING

This research was funded by the Mecklenburg-Pomerania Excellence Initiative (Germany), the European Social Fund (ESF) Grant KoInfekt (ESF/14-BM-A55-0008/16 and ESF/14-

BM-A55-0009/16), and the Helmholtz Institute (ZoonFlu). We acknowledge support for the Article Processing Charge from the German Research Foundation and the Open Access Publication Fund of the University of Greifswald.

ACKNOWLEDGMENTS

The authors want to acknowledge all partners of the collaborative project “KoInfekt”. Furthermore, the authors thank Claudia Hirschfeld for revising the manuscript.

SUPPLEMENTARY MATERIAL

The Supplementary Material for this article can be found online at: <https://www.frontiersin.org/articles/10.3389/fcimb.2022.817532/full#supplementary-material>

REFERENCES

- Agarwal, V., Asmat, T. M., Luo, S., Jensch, I., Zipfel, P. F., and Hammerschmidt, S. (2010). Complement Regulator Factor H Mediates a Two-Step Uptake of *Streptococcus Pneumoniae* by Human Cells. *J. Biol. Chem.* 285, 23486–23495. doi: 10.1074/jbc.M110.142703
- Aliberti, S., and Kaye, K. S. (2013). The Changing Microbiologic Epidemiology of Community-Acquired Pneumonia. *Postgrad. Med.* 125, 31–42. doi: 10.3810/pgm.2013.11.2710
- Attali, C., Durmort, C., Vernet, T., and Di Guilmi, A. M. (2008). The Interaction of *Streptococcus Pneumoniae* With Plasmin Mediates Transmigration Across Endothelial and Epithelial Monolayers by Intercellular Junction Cleavage. *Infect. Immun.* 76, 5350–5356. doi: 10.1128/IAI.00184-08
- Bai, X., Yang, W., Luan, X., Li, H., Li, H., Tian, D., et al. (2021). Induction of Cyclophilin A by Influenza A Virus Infection Facilitates Group A *Streptococcus* Coinfection. *Cell Rep.* 35, 109159. doi: 10.1016/j.celrep.2021.109159
- Barnett, T. C., Cole, J. N., Rivera-Hernandez, T., Henningham, A., Paton, J. C., Nizet, V., et al. (2015). Streptococcal Toxins: Role in Pathogenesis and Disease. *Cell Microbiol.* 17, 1721–1741. doi: 10.1111/cmi.12531
- Becker, A. C., Gannagé, M., Giese, S., Hu, Z., Abou-Eid, S., Roubaty, C., et al. (2018). Influenza A Virus Induces Autophagosomal Targeting of Ribosomal Proteins. *Mol. Cell Proteomics* 17, 1909–1921. doi: 10.1074/mcp.RA117.000364
- Bertuzzi, M., Hayes, G. E., and Bignell, E. M. (2019). Microbial Uptake by the Respiratory Epithelium: Outcomes for Host and Pathogen. *FEMS Microbiol. Rev.* 43, 145–161. doi: 10.1093/femsre/fuy045
- Bhat, K. P., and Greer, S. F. (2011). Proteolytic and non-Proteolytic Roles of Ubiquitin and the Ubiquitin Proteasome System in Transcriptional Regulation. *Biochim. Biophys. Acta* 1809, 150–155. doi: 10.1016/j.bbagr.2010.11.006
- Bootsma, H. J., Egmont-Petersen, M., and Hermans, P. W. M. (2007). Analysis of the *In Vitro* Transcriptional Response of Human Pharyngeal Epithelial Cells to Adherent *Streptococcus Pneumoniae*: Evidence for a Distinct Response to Encapsulated Strains. *Infect. Immun.* 75, 5489–5499. doi: 10.1128/IAI.01823-06
- Brundage, J. F. (2006). Interactions Between Influenza and Bacterial Respiratory Pathogens: Implications for Pandemic Preparedness. *Lancet Infect. Dis.* 6, 303–312. doi: 10.1016/S1473-3099(06)70466-2
- Carterson, A. J., Höner zu Bentrup, K., Ott, C. M., Clarke, M. S., Pierson, D. L., Vanderburg, C. R., et al. (2005). A549 Lung Epithelial Cells Grown as Three-Dimensional Aggregates: Alternative Tissue Culture Model for *Pseudomonas Aeruginosa* Pathogenesis. *Infect. Immun.* 73, 1129–1140. doi: 10.1128/IAI.73.2.1129-1140.2005
- Cawcutt, K., and Kalil, A. C. (2017). Pneumonia With Bacterial and Viral Coinfection. *Curr. Opin. Crit. Care* 23, 385–390. doi: 10.1097/MCC.0000000000000435
- Cox, J., Hein, M. Y., Lubner, C. A., Paron, I., Nagaraj, N., and Mann, M. (2014). Accurate Proteome-Wide Label-Free Quantification by Delayed Normalization and Maximal Peptide Ratio Extraction, Termed MaxLFQ. *Mol. Cell Proteomics* 13, 2513–2526. doi: 10.1074/mcp.M113.031591
- Cox, J., and Mann, M. (2008). MaxQuant Enables High Peptide Identification Rates, Individualized P.P.B.-Range Mass Accuracies and Proteome-Wide Protein Quantification. *Nat. Biotechnol.* 26, 1367–1372. doi: 10.1038/nbt.1511
- Da Huang, W., Sherman, B. T., and Lempicki, R. A. (2009a). Bioinformatics Enrichment Tools: Paths Toward the Comprehensive Functional Analysis of Large Gene Lists. *Nucleic Acids Res.* 37, 1–13. doi: 10.1093/nar/gkn923
- Da Huang, W., Sherman, B. T., and Lempicki, R. A. (2009b). Systematic and Integrative Analysis of Large Gene Lists Using DAVID Bioinformatics Resources. *Nat. Protoc.* 4, 44–57. doi: 10.1038/nprot.2008.211
- Gradstedt, H., Iovino, F., and Bijlsma, J. J. E. (2013). *Streptococcus Pneumoniae* Invades Endothelial Host Cells via Multiple Pathways and Is Killed in a Lysosome Dependent Manner. *PLoS One* 8, e65626. doi: 10.1371/journal.pone.0065626
- Hammerschmidt, S. (2016). Special Issue on ‘Microbe-Host Interactions’. *FEBS Lett.* 590, 3703–3704. doi: 10.1002/1873-3468.12466
- Hammerschmidt, S., Wolff, S., Hocke, A., Rosseau, S., Müller, E., and Rohde, M. (2005). Illustration of Pneumococcal Polysaccharide Capsule During Adherence and Invasion of Epithelial Cells. *Infect. Immun.* 73, 4653–4667. doi: 10.1128/IAI.73.8.4653-4667.2005
- Heunis, T., Lamoliatte, F., Marín-Rubio, J. L., Dannoura, A., and Trost, M. (2020). Technical Report: Targeted Proteomic Analysis Reveals Enrichment of Atypical Ubiquitin Chains in Contractile Murine Tissues. *J. Proteomics* 229, 103963. doi: 10.1016/j.jpro.2020.103963
- Hiemstra, P. S., McCray, P. B., and Bals, R. (2015). The Innate Immune Function of Airway Epithelial Cells in Inflammatory Lung Disease. *Eur. Respir. J.* 45, 1150–1162. doi: 10.1183/09031936.00141514
- Hupp, S., Förtsch, C., Wippel, C., Ma, J., Mitchell, T. J., and Iliev, A. I. (2013). Direct Transmembrane Interaction Between Actin and the Pore-Competent, Cholesterol-Dependent Cytolysin Pneumolysin. *J. Mol. Biol.* 425, 636–646. doi: 10.1016/j.jmb.2012.11.034
- Hu, H., and Sun, S.-C. (2016). Ubiquitin Signaling in Immune Responses. *Cell Res.* 26, 457–483. doi: 10.1038/cr.2016.40
- Iovino, F., Gradstedt, H., and Bijlsma, J. J. (2014). The Proteasome-Ubiquitin System is Required for Efficient Killing of Intracellular *Streptococcus Pneumoniae* by Brain Endothelial Cells. *mBio* 5, e00984–14. doi: 10.1128/mBio.00984-14
- Jassal, B., Matthews, L., Viteri, G., Gong, C., Lorente, P., Fabregat, A., et al. (2020). The Reactome Pathway Knowledgebase. *Nucleic Acids Res.* 48, D498–D503. doi: 10.1093/nar/gkz1031

- Jin, M., Shirazinejad, C., Wang, B., Yan, A., Schöneberg, J., Upadhyayula, S., et al. (2021). Asymmetric Arp2/3-Mediated Actin Assembly Facilitates Clathrin-Mediated Endocytosis at Stalled Sites in Genome-Edited Human Stem Cells. *bioRxiv*. doi: 10.1101/2021.07.16.452693
- Keller, I. E., Vosyka, O., Takenaka, S., Kloß, A., Dahlmann, B., Willems, L. I., et al. (2015). Regulation of Immunoproteasome Function in the Lung. *Sci. Rep.* 5, 10230. doi: 10.1038/srep10230
- LeMessurier, K. S., Hans, H., Liying, C., Elaine, T., and Vanessa, R. (2013). Type I Interferon Protects Against Pneumococcal Invasive Disease by Inhibiting Bacterial Transmigration Across the Lung. *PloS Pathog.* 9, e1003727. doi: 10.1371/journal.ppat.1003727
- LeMessurier, K. S., Tiwary, M., Morin, N. P., and Samarasinghe, A. E. (2020). Respiratory Barrier as a Safeguard and Regulator of Defense Against Influenza A Virus and *Streptococcus Pneumoniae*. *Front. Immunol.* 11. doi: 10.3389/fimmu.2020.00003
- Lim, Y. K., Kweon, O. J., Kim, H. R., Kim, T.-H., and Lee, M.-K. (2019). Impact of Bacterial and Viral Coinfection in Community-Acquired Pneumonia in Adults. *Diagn. Microbiol. Infect. Dis.* 94, 50–54. doi: 10.1016/j.diagmicrobio.2018.11.014
- Mathieu, N. A., Paparisto, E., Barr, S. D., and Spratt, D. E. (2021). HERC5 and the ISGylation Pathway: Critical Modulators of the Antiviral Immune Response. *Viruses* 13, 1102. doi: 10.3390/v13061102
- McCarthy, M. K., and Weinberg, J. B. (2015). The Immunoproteasome and Viral Infection: A Complex Regulator of Inflammation. *Front. Microbiol.* 6. doi: 10.3389/fmicb.2015.00021
- Miyashita, M., Oshiumi, H., Matsumoto, M., and Seya, T. (2011). DDX60, a DEXD/H Box Helicase, is a Novel Antiviral Factor Promoting RIG-I-Like Receptor-Mediated Signaling. *Mol. Cell Biol.* 31, 3802–3819. doi: 10.1128/MCB.01368-10
- Morens, D. M., Taubenberger, J. K., and Fauci, A. S. (2008). Predominant Role of Bacterial Pneumonia as a Cause of Death in Pandemic Influenza: Implications for Pandemic Influenza Preparedness. *J. Infect. Dis.* 198, 962–970. doi: 10.1086/591708
- N'Guessan, P. D., Hippenstiel, S., Etouem, M. O., Zahlten, J., Beermann, W., Lindner, D., et al. (2006). *Streptococcus Pneumoniae* Induced P38 MAPK- and NF-kappaB-Dependent COX-2 Expression in Human Lung Epithelium. *Am. J. Physiol. Lung Cell Mol. Physiol.* 290, L1131–L1138. doi: 10.1152/ajplung.00383.2005
- Ogawa, M., Matsuda, R., Takada, N., Tomokiyo, M., Yamamoto, S., Shizukuishi, S., et al. (2018). Molecular Mechanisms of *Streptococcus Pneumoniae*-Targeted Autophagy via Pneumolysin, Golgi-Resident Rab41, and Nedd4-1-Mediated K63-Linked Ubiquitination. *Cell Microbiol.* 20, e12846. doi: 10.1111/cmi.12846
- Palacios, G., Hornig, M., Cisterna, D., Savji, N., Bussetti, A. V., Kapoor, V., et al. (2009). *Streptococcus Pneumoniae* Coinfection is Correlated With the Severity of H1N1 Pandemic Influenza. *PloS One* 4, e8540. doi: 10.1371/journal.pone.0008540
- Park, S.-S., Gonzalez-Juarbe, N., Riegler, A. N., Im, H., Hale, Y., Platt, M. P., et al. (2021). *Streptococcus Pneumoniae* Binds to Host GAPDH on Dying Lung Epithelial Cells Worsening Secondary Infection Following Influenza. *Cell Rep.* 35, 109267. doi: 10.1016/j.celrep.2021.109267
- Perez-Riverol, Y., Csordas, A., Bai, J., Bernal-Llinares, M., Hewapathirana, S., Kundu, D. J., et al. (2019). The PRIDE Database and Related Tools and Resources in 2019: Improving Support for Quantification Data. *Nucleic Acids Res.* 47, D442–D450. doi: 10.1093/nar/gky1106
- Peter, A., Fatykhova, D., Kershaw, O., Gruber, A. D., Rueckert, J., Neudecker, J., et al. (2017). Localization and Pneumococcal Alteration of Junction Proteins in the Human Alveolar-Capillary Compartment. *Histochem Cell Biol.* 147, 707–719. doi: 10.1007/s00418-017-1551-y
- Radin, J. N., Orihuela, C. J., Murti, G., Guglielmo, C., Murray, P. J., and Tuomanen, E. I. (2005). Beta-Arrestin 1 Participates in Platelet-Activating Factor Receptor-Mediated Endocytosis of *Streptococcus Pneumoniae*. *Infect. Immun.* 73, 7827–7835. doi: 10.1128/IAI.73.12.7827-7835.2005
- Roth, G. A., Abate, D., Abate, K. H., Abay, S. M., Abbafati, C., Abbasi, N., et al. (2018). Global, Regional, and National Age-Sex-Specific Mortality for 282 Causes of Death in 195 Countries and Territories—2017: A Systematic Analysis for the Global Burden of Disease Study 2017. *Lancet* 392, 1736–1788. doi: 10.1016/S0140-6736(18)32203-7
- Rudnicka, A., and Yamauchi, Y. (2016). Ubiquitin in Influenza Virus Entry and Innate Immunity. *Viruses* 8, 293. doi: 10.3390/v8100293
- Ruuskanen, O., and Järvinen, A. (2014). What is the Real Role of Respiratory Viruses in Severe Community-Acquired Pneumonia? *Clin. Infect. Dis.* 59, 71–73. doi: 10.1093/cid/ciu242
- Saleh, M., Bartual, S. G., Abdullah, M. R., Jensch, I., Asmat, T. M., Petruschka, L., et al. (2013). Molecular Architecture of *Streptococcus Pneumoniae* Surface Thioredoxin-Fold Lipoproteins Crucial for Extracellular Oxidative Stress Resistance and Maintenance of Virulence. *EMBO Mol. Med.* 5, 1852–1870. doi: 10.1002/emmm.201202435
- Schoggins, J. W., Wilson, S. J., Panis, M., Murphy, M. Y., Jones, C. T., Bieniasz, P., et al. (2011). A Diverse Range of Gene Products Are Effectors of the Type I Interferon Antiviral Response. *Nature* 472, 481–485. doi: 10.1038/nature09907
- Schwerk, C., and Schulze-Osthoff, K. (2005). Regulation of Apoptosis by Alternative pre-mRNA Splicing. *Mol. Cell* 19, 1–13. doi: 10.1016/j.molcel.2005.05.026
- Seifert, U., Bialy, L. P., Ebstein, F., Bech-Otschir, D., Voigt, A., Schröter, F., et al. (2010). Immunoproteasomes Preserve Protein Homeostasis Upon Interferon-Induced Oxidative Stress. *Cell* 142, 613–624. doi: 10.1016/j.cell.2010.07.036
- Self, W. H., Balk, R. A., Grijalva, C. G., Williams, D. J., Zhu, Y., Anderson, E. J., et al. (2017). Procalcitonin as a Marker of Etiology in Adults Hospitalized With Community-Acquired Pneumonia. *Clin. Infect. Dis.* 65, 183–190. doi: 10.1093/cid/cix317
- Sharma-Chawla, N., Sender, V., Kershaw, O., Gruber, A. D., Volckmar, J., Henriques-Normark, B., et al. (2016). Influenza A Virus Infection Predisposes Hosts to Secondary Infection With Different *Streptococcus Pneumoniae* Serotypes With Similar Outcome But Serotype-Specific Manifestation. *Infect. Immun.* 84, 3445–3457. doi: 10.1128/IAI.00422-16
- Shim, J. M., Kim, J., Tenson, T., Min, J.-Y., and Kainov, D. E. (2017). Influenza Virus Infection, Interferon Response, Viral Counter-Response, and Apoptosis. *Viruses* 9, 223. doi: 10.3390/v9080223
- Siemens, N., Oehmcke-Hecht, S., Mettenleiter, T. C., Kreikemeyer, B., Valentin-Weigand, P., and Hammerschmidt, S. (2017). Port D'entrée for Respiratory Infections - Does the Influenza A Virus Pave the Way for Bacteria? *Front. Microbiol.* 8. doi: 10.3389/fmicb.2017.02602
- Sirotkin, V. (2011). Cell Biology: Actin Keeps Endocytosis on a Short Leash. *Curr. Biol.* 21, R552–R554. doi: 10.1016/j.cub.2011.06.029
- Strehlitz, A., Goldmann, O., Pils, M. C., Pessler, F., and Medina, E. (2018). An Interferon Signature Discriminates Pneumococcal From Staphylococcal Pneumonia. *Front. Immunol.* 9. doi: 10.3389/fimmu.2018.01424
- Sumida, G. M., and Yamada, S. (2015). Rho GTPases and the Downstream Effectors Actin-Related Protein 2/3 (Arp2/3) Complex and Myosin II Induce Membrane Fusion at Self-Contacts. *J. Biol. Chem.* 290, 3238–3247. doi: 10.1074/jbc.M114.612168
- Sura, T., Surabhi, S., Maaß, S., Hammerschmidt, S., Siemens, N., and Becher, D. (2021). The Global Proteome and Ubiquitinome of Bacterial and Viral Co-Infected Bronchial Epithelial Cells. *J. Proteomics* 250, 104387. doi: 10.1016/j.jpropt.2021.104387
- Szklarczyk, D., Gable, A. L., Lyon, D., Junge, A., Wyder, S., Huerta-Cepas, J., et al. (2019). STRING V11: Protein-Protein Association Networks With Increased Coverage, Supporting Functional Discovery in Genome-Wide Experimental Datasets. *Nucleic Acids Res.* 47, D607–D613. doi: 10.1093/nar/gky1131
- Szymanski, K. V., Toennies, M., Becher, A., Fatykhova, D., N'Guessan, P. D., Gutbier, B., et al. (2012). *Streptococcus Pneumoniae*-Induced Regulation of Cyclooxygenase-2 in Human Lung Tissue. *Eur. Respir. J.* 40, 1458–1467. doi: 10.1183/09031936.00186911
- Talbot, U. M., Paton, A. W., and Paton, J. C. (1996). Uptake of *Streptococcus Pneumoniae* by Respiratory Epithelial Cells. *Infect. Immun.* 64, 3772–3777. doi: 10.1128/iai.64.9.3772-3777.1996
- Troeger, C. E., Blacker, B. F., Khalil, I. A., Zimsen, S. R. M., Albertson, S. B., Abate, D., et al. (2019). Mortality, Morbidity, and Hospitalisations Due to Influenza Lower Respiratory Tract Infection: An Analysis for the Global Burden of Disease Study 2017. *Lancet Respir. Med.* 7, 69–89. doi: 10.1016/S2213-2600(18)30496-X
- Tyanova, S., and Cox, J. (2018). Perseus: A Bioinformatics Platform for Integrative Analysis of Proteomics Data in Cancer Research. *Methods Mol. Biol.* 1711, 133–148. doi: 10.1007/978-1-4939-7493-1_7

- Tyanova, S., Temu, T., Sinitcyn, P., Carlson, A., Hein, M. Y., Geiger, T., et al. (2016). The Perseus Computational Platform for Comprehensive Analysis of (Prote)Omics Data. *Nat. Methods* 13, 731–740. doi: 10.1038/nmeth.3901
- Vareille, M., Kieninger, E., Edwards, M. R., and Regamey, N. (2011). The Airway Epithelium: Soldier in the Fight Against Respiratory Viruses. *Clin. Microbiol. Rev.* 24, 210–229. doi: 10.1128/CMR.00014-10
- Wong, J. J. Y., Pung, Y. F., Sze, N. S.-K., and Chin, K.-C. (2006). HERC5 is an IFN-Induced HECT-Type E3 Protein Ligase That Mediates Type I IFN-Induced ISGylation of Protein Targets. *Proc. Natl. Acad. Sci. U. S. A.* 103, 10735–10740. doi: 10.1073/pnas.0600397103
- Wu, H., Zhang, S., Huo, C., Zou, S., Lian, Z., and Hu, Y. (2019). iTRAQ-Based Proteomic and Bioinformatic Characterization of Human Mast Cells Upon Infection by the Influenza A Virus Strains H1N1 and H5N1. *FEBS Lett.* 593, 2612–2627. doi: 10.1002/1873-3468.13523
- Yamauchi, Y. (2020). *Influenza A Virus Uncoating*, In: T. Mettenleiter, M. Kielian and M. Roossinck. *Advances in Virus Research* 106:1–38 (Advances in virus research). doi: 10.1016/bs.aivir.2020.01.001
- Zhang, Y., Xu, Z., and Cao, Y. (2020). Host-Virus Interaction: How Host Cells Defend Against Influenza A Virus Infection. *Viruses* 12, 376. doi: 10.3390/v12040376
- Zhou, J., Xu, Y., Lin, S., Guo, Y., Deng, W., Zhang, Y., et al. (2018). iUUCD 2.0: An Update With Rich Annotations for Ubiquitin and Ubiquitin-Like Conjugations. *Nucleic Acids Res.* 46, D447–D453. doi: 10.1093/nar/gkx1041
- Zinngrebe, J., Montinaro, A., Peltzer, N., and Walczak, H. (2014). Ubiquitin in the Immune System. *EMBO Rep.* 15, 322. doi: 10.1002/embr.201470030

Conflict of Interest: The authors declare that the research was conducted in the absence of any commercial or financial relationships that could be construed as a potential conflict of interest.

Publisher's Note: All claims expressed in this article are solely those of the authors and do not necessarily represent those of their affiliated organizations, or those of the publisher, the editors and the reviewers. Any product that may be evaluated in this article, or claim that may be made by its manufacturer, is not guaranteed or endorsed by the publisher.

Copyright © 2022 Sura, Gering, Cammann, Hammerschmidt, Maaß, Seifert and Becher. This is an open-access article distributed under the terms of the Creative Commons Attribution License (CC BY). The use, distribution or reproduction in other forums is permitted, provided the original author(s) and the copyright owner(s) are credited and that the original publication in this journal is cited, in accordance with accepted academic practice. No use, distribution or reproduction is permitted which does not comply with these terms.



Extensive/Multidrug-Resistant Pneumococci Detected in Clinical Respiratory Tract Samples in Southern Sweden Are Closely Related to International Multidrug-Resistant Lineages

Linda Yamba Yamba¹, Fabian Uddén¹, Kurt Fuursted², Jonas Ahl³, Hans-Christian Slotved² and Kristian Riesbeck^{1*}

OPEN ACCESS

Edited by:

Sven Hammerschmidt,
University of Greifswald, Germany

Reviewed by:

Catarina Silva Costa,
University of Lisbon, Portugal
Lesley McGee,
Centers for Disease Control and
Prevention (CDC), United States

*Correspondence:

Kristian Riesbeck
kristian.riesbeck@med.lu.se

Specialty section:

This article was submitted to
Molecular Bacterial Pathogenesis,
a section of the journal
Frontiers in Cellular and
Infection Microbiology

Received: 29 November 2021

Accepted: 21 February 2022

Published: 22 March 2022

Citation:

Yamba Yamba L, Uddén F, Fuursted K, Ahl J, Slotved H-C and Riesbeck K (2022) Extensive/Multidrug-Resistant Pneumococci Detected in Clinical Respiratory Tract Samples in Southern Sweden Are Closely Related to International Multidrug-Resistant Lineages. *Front. Cell. Infect. Microbiol.* 12:824449. doi: 10.3389/fcimb.2022.824449

¹ Clinical Microbiology, Department of Translational Medicine, Faculty of Medicine, Lund University, Malmö, Sweden, ² Department of Bacteria, Parasites and Fungi, Statens Serum Institut, Copenhagen, Denmark, ³ Infectious Diseases, Department of Translational Medicine, Faculty of Medicine, Lund University, Malmö, Sweden

Background/Objective: The frequencies of non-susceptibility against common antibiotics among pneumococci vary greatly across the globe. When compared to other European countries antibiotic resistance against penicillin and macrolides has been uncommon in Sweden in recent years. Multidrug resistance (MDR) is, however, of high importance since relevant treatment options are scarce. The purpose of this study was to characterize the molecular epidemiology, presence of resistance genes and selected virulence genes of extensively drug-resistant (XDR) ($n=15$) and MDR ($n=10$) *Streptococcus pneumoniae* detected in clinical respiratory tract samples isolated from patients in a southern Swedish county 2016-2018. With the aim of relating them to global MDR pneumococci.

Methods: Whole genome sequencing (WGS) was performed to determine molecular epidemiology, resistance genes and presence of selected virulence factors. Antimicrobial susceptibility profiles were determined using broth microdilution testing. Further analyses were performed on isolates from the study and from the European nucleotide archive belonging to global pneumococcal sequence cluster (GPSC) 1 ($n=86$), GPSC9 ($n=55$) and GPSC10 ($n=57$). Bacteria were analyzed regarding selected virulence determinants (pilus islet 1, pilus islet 2 and Zinc metalloproteinase C) and resistance genes.

Results: Nineteen of 25 isolates were related to dominant global MDR lineages. Seventeen belonged to GPSC1, GPSC9 or GPSC10 with MDR non-PCV serotypes in GPSC9 (serotype 15A and 15C) as well as GPSC10 (serotype 7B, 15B and serogroup 24). Pilus islet-1 and pilus islet-2 were present in most sequence types belonging to

GPSC1 and in two isolates within GPSC9 but were not detected in isolates belonging to GPSC10. Zinc metalloproteinase C was well conserved within all analyzed isolates belonging to GPSC9 but were not found in isolates from GPSC1 or GPSC10.

Conclusions: Although MDR *S. pneumoniae* is relatively uncommon in Sweden compared to other countries, virulent non-PCV serotypes that are MDR may become an increasing problem, particularly from clusters GPSC9 and GPSC10. Since the incidence of certain serotypes (3, 15A, and 19A) found among our MDR Swedish study isolates are persistent or increasing in invasive pneumococcal disease further surveillance is warranted.

Keywords: antimicrobial resistance (AMR), extensive drug resistance (XDR), multidrug-resistant (MDR), global pneumococcal sequence cluster, mucosal infection, respiratory tract, streptococcus pneumoniae, serotype

INTRODUCTION

Streptococcus pneumoniae is a commensal of the human respiratory tract and its primary niche is the nasopharynx. Dissemination from the nasopharynx can lead to different types of pneumococcal disease including pneumonia, acute otitis media and sinusitis, of which the bacterial species is considered the most common etiology (Weiser et al., 2018). *S. pneumoniae* also causes invasive pneumococcal disease (IPD), characterized as meningitis, sepsis, and bacteremic pneumonia that contributes to a high morbidity and mortality globally (Troeger et al., 2018). The most important virulence factor of the pneumococcus is the capsule and around 100 different serotypes have been identified (Ganaie et al., 2020). The first conjugated pneumococcal polysaccharide vaccine PCV7 was introduced in the year of 2000 in the US (covering serotypes 6B, 7F, 9V, 14, 18C, 19F and 23F). Serotype replacement then led to the development of higher valency vaccines, and PCV10 (PCV7 serotypes with addition of 1, 4 and 5) and PCV13 (PCV7 serotypes with addition of 1, 3, 4, 5, 6A and 19A) are mainly administrated. In southern Sweden, PCV7 was introduced in the child immunization program in 2009. PCV10 was implemented one year later with a shift to PCV13 in 2014, and a further change back to PCV10 in 2019.

In a meta-analysis performed by (Andrejko et al., 2021) on 312,783 pneumococci isolated from children, it was shown that the implementation of PCV in child immunization campaigns has resulted in an absolute significant decrease of penicillin non-susceptible pneumococci (PNSP). This reduction was mainly hypothesized to be attributed to reduction of non-susceptible vaccine serotypes (VT), suggesting the possibility to use vaccines also in control of antimicrobial resistance. Local changes with increased antimicrobial resistance due to serotype replacement is, however, a phenomenon to be aware of as has been observed in Sweden regarding IPD isolates in the post-PCV era. An increase of PNSP from 3.3% in 2007 to 5.6% in 2013-2016 has been observed, primarily due to the increase of non-vaccine types (NVT) PNSP (Naucle et al., 2017). Serotype switch events in already multidrug-resistant (MDR; nonsusceptibility to 3 or more different antimicrobial classes) VT lineages is another

way for new clones to expand after vaccine implementation. Examples of serotype switch events have been noted in the post PCV era but the general survival rate of the resulting strains in the population is to be followed through further studies (Savinova et al., 2020; Scherer et al., 2021).

In a study by Gladstone et al. (2019) global pneumococcal sequence clusters (GPSC) were defined as a new tool for epidemiological analysis of *S. pneumoniae* in the post PCV era. It was shown that some GPSCs have an increased accumulation of MDR isolates as for example GPSC1. Close surveillance of the GPSCs is of importance for the evaluation of effect of PCVs on the overall antimicrobial resistance (AMR) within different lineages.

The pattern of non-susceptibility to common antibiotics among pneumococci vary greatly across the globe (Andrejko et al., 2021). In Sweden, AMR to penicillin and macrolides has been low in later years compared to other European countries. The European center of disease control (ECDC) estimated that Sweden, in 2019, had 6.5% PNSP and 6.5% macrolide non-susceptible invasive *S. pneumoniae* compared to the EU average of 12.1 and 14.5% (ECDC, 2020a; ECDC, 2020b). During the years 2016-2018 *S. pneumoniae* detected in clinical respiratory tract samples in Skåne County, southern Sweden, were investigated regarding serotype distribution and antimicrobial susceptibility. Of the 2,131 included isolates, 11% were PNSP and 8% macrolide non-susceptible. Furthermore, 7% were MDR and 2% were extensively drug resistant (XDR; nonsusceptibility to 5 or more different antimicrobial classes) (Golden et al., 2015; Uddén et al., 2021). MDR and XDR isolates included both VT and NVT pneumococci (Uddén et al., 2021).

The purpose of this study was to do whole genome sequencing (WGS) on pneumococcal MDR isolates detected in Skåne County between 2016-2018 with the aim of studying their resistance genes and molecular epidemiology in a global context. We present data on GPSC, resistance genes and selected virulence genes. We also show data regarding the virulence factor zinc metalloproteinase C (ZmpC) and the presence of PI-1 and PI-2 islets among different MDR GPSC as possible contributors to virulence or increased transmission among pneumococci.

MATERIALS AND METHODS

Streptococcus pneumoniae Isolates

In our recent study, a total of 2,131 pneumococci were detected among clinical respiratory tract samples during 18 months in 2016–2018 (Uddén et al., 2021). Serotyping was performed as described in (Uddén et al., 2018). Briefly a multiplex polymerase chain reaction (PCR) scheme in combination with latex agglutination and the Quellung reaction was used. Of the 1,858 isolates that were available for further analyses, 26 isolates were classified as XDR based on non-susceptibility to ≥ 5 antimicrobial classes during screening with disk diffusion tests (oxacillin, erythromycin, clindamycin, tetracycline, trimethoprim-sulfamethoxazole and norfloxacin) and a gradient test for benzylpenicillin (Etest®; BioMérieux, Marcy-l'Étoile, FR), and were included in the current study. Minimum inhibitory concentrations (MIC) of the currently studied isolates were confirmed with broth microdilution (BMD) (Sensititre *Streptococcus* STP6F AST Plate; Thermo Fisher Scientific, Waltham, MA) and interpreted according to breakpoints provided by EUCAST 2021 to determine MDR ($n=10$) or XDR ($n=16$) phenotype (Uddén et al., 2021). One of 26 isolates was, however, excluded based on low quality of WGS, and not included in further analyses.

Whole Genome Sequencing

Illumina sequencing described by (Kavalari et al., 2019) was used for WGS. Species identification was performed using ribosomal multi locus sequence typing (rMLST) provided on PubMLST (<https://pubmlst.org>) (Jolley et al., 2018). Capsular loci were analyzed to determine capsular genotype using the PneumoCaT tool (Kapatai et al., 2016).

Molecular Epidemiology and Resistance Genes

Assembled genomes were uploaded to PathogenWatch (<https://pathogen.watch>) to assign MLST and GPSC (Jolley et al., 2018). Corresponding clonal complex (CC) of the detected sequence types, and additional epidemiological information regarding GPSC and MLST were acquired from the Global Pneumococcal Sequencing Project database (https://www.pneumogen.net/gps/GPSC_lineages.html, accessed 1-07-2021) and PubMLST. Clonal complexes were assigned by a single locus threshold (6/7) (Gladstone et al., 2019). PathogenWatch was additionally used to screen for antimicrobial resistance genes (*ermB*, *mefA*, *tetM*) and mutations (*folA/folP*, *gyrA/parC*) conferring resistance to commonly used antibiotics for pneumococcal disease and mosaic penicillin binding protein (PBP) profiles conferring resistance to β -lactam antibiotics in pneumococci (Li et al., 2017; Gladstone et al., 2019).

Determination of Virulence Factors

Genes encoding the virulome were screened for using NCBI Genome Workbench version 3.6.0 and BlastN was performed for comparison of nucleotide sequences. Selected sequences for virulence genes of interest related to *S. pneumoniae* were

collected from the Virulence finder database nucleotide dataset_B (downloaded 4/8-2021) (Weiser et al., 2018; Liu et al., 2019). Additional sequences were selected for detection of pilus islet 1 (PI-1) (GenBank accession numbers: EF560625–EF560637) and pilus islet 2 (PI-2) (GenBank accession number: EU311539.1) (Bagnoli et al., 2008; Moschioni et al., 2008). A 95% identity and 80% coverage were used for identification of a sequence (Kavalari et al., 2019).

Phylogeny, Resistance Determinants and Selected Virulome of Isolates Within GPSC1, GPSC9 and GPSC10

Three phylogenetic trees were constructed with the sequenced isolates belonging to GPSC1, GPSC9 and GPSC10 together with additional reference isolates described by Gladstone et al. (Gladstone et al., 2019) provided from ENA (<https://www.ebi.ac.uk/ena/browser/home>) (ENA run accessions in **Supplemental Material**). The isolates were selected to represent different sequence types within GPSC1 ($n=79$), GPSC9 ($n=50$) and GPSC10 ($n=52$). MinTyper 1.0 were used for the SNP distance matrices and creation of the phylogenetic trees (Hallgren et al., 2021). The trees were rooted to concatenated sequences of different reference strains, which are specified in each figure. The phylogenetic trees were visualized using Interactive tree of life (iTol v.5) (Letunic and Bork, 2021). Assembled genomes of the ENA isolates were downloaded from PathogenWatch together with metadata including PBP-profiles, resistance genes (*ermB*, *mefA*, *tetM*) and mutations (*folA/folP*) for the isolates (date 8/8-2021). The presence of selected virulence factors (ZmpC, PI-1 and PI-2) was analyzed as previously described.

RESULTS

Three Different Global Pneumococcal Sequence Clusters Dominated in the Catchment Area

Included isolates were serotyped and assigned to MLST, GPSC and CC by extraction from WGS data (**Table 1**). All isolates ($n=25$) were identified as *S. pneumoniae* using rMLST. Three different GPSC dominated among the samples, GPSC1 ($n=7$), GPSC9 ($n=5$) and GPSC10 ($n=5$). The dominating serotypes were 15A ($n=4$), 19A ($n=3$), 19F ($n=3$), 35B ($n=3$) and in total 10 different serotypes (3, 6B, 7B, 11A, 15A, 15B, 15C, 19A, 19F and 35B) and 1 serogroup (24) were identified and in general consistent with WGS. Isolates belonging to the same GPSC often carried identical resistance genes and closely related PBP profiles.

ZmpC and Pilus Islets Were Present Among Only a Fraction of Isolates

The isolates were analyzed for virulence factors known to be important for pneumococcal pathogenesis and colonization. Selected virulence factors, ZmpC and pilus islets, were present among only a selection of the isolates (**Table 1**). The virulence

TABLE 1 | XDR and MDR isolates were closely related to international MDR lineages.

Isolate	Year	Age	Sample type	Serotype	GPSC ^a	MLST	CC	Resistance	PCV coverage				Virulence		
ID	Years		Phenotype/Genotype					Profile	PCV10	PCV13	PCV15	PCV20	PI-1	PI-2	<i>zmpC</i>
1	2017	4	Nasopharynx	19F/19F	1	236 ^b	—	XDR	+	+	+	+	+	+	—
2	2017	34	Nasopharynx	3/3	1	271 ^b	CC320	XDR	—	+	+	+	+	+	—
3	2018	2	Nasopharynx	19A/19A	1	320	CC320	XDR	—	+	+	+	+	+	—
4	2018	0	Conjunctiva	19A/19A	1	320	CC320	XDR	—	+	+	+	+	+	—
5	2016	1	Nasopharynx	19F/19F	1	2920 ^b	—	XDR	+	+	+	+	+	+	—
6	2018	42	Nasopharynx	19A/19A	1	4768	CC320	XDR	—	+	+	+	+	+	—
7	2017	88	Nasopharynx	19F/19F	1	8359	—	XDR	+	+	+	+	+	+	—
8	2017	37	Nasopharynx	15A/15A	9	63 ^c	CC63	MDR-4	—	—	—	—	—	—	+
9	2017	3	Nasopharynx	15A/15A	9	63 ^c	CC63	MDR-4	—	—	—	—	—	—	+
10	2017	7	Sputum	15C/15C	9	782 ^c	CC63	XDR	—	—	—	—	—	—	+
11	2017	89	Sputum	15A/15A	9	3816 ^c	CC63	MDR-4	—	—	—	—	—	—	+
12	2017	32	Sputum	15A/15A	9	3816 ^c	CC63	MDR-3	—	—	—	—	—	—	+
13	2018	1	Nasopharynx	24/24	10	230 ^d	CC230	MDR-4	—	—	—	—	—	—	—
14	2017	2	Middle ear	15B/15B	10	4253 ^d	CC230	MDR-4	—	—	—	+	—	—	—
15	2017	9	Sputum	24/24	10	6227 ^d	CC230	MDR-4	—	—	—	—	—	—	—
16	2017	1	Nasopharynx	7B/7B	10	Novel1	—	MDR-4	—	—	—	—	—	—	—
17	2018	27	Nasopharynx	7B/7B	10	Novel1	—	MDR-4	—	—	—	—	—	—	—
18	2017	2	Nasopharynx	15C/15C	16	83 ^e	CC81	XDR	—	—	—	—	—	—	—
19	2017	1	Nasopharynx	11A/11A	43	8605	—	XDR	—	—	—	+	—	—	—
20	2017	68	Sputum	6B/6E	47	2040 ^f	CC315	MDR-3	+	+	+	+	+	+	—
21	2016	41	Conjunctiva	NT/NT	81	4149	—	XDR	—	—	—	—	—	—	—
22	2017	68	Sputum	35B/35B	91	373	—	XDR	—	—	—	—	—	—	—
23	2017	58	Bronchi	35B/35B	91	373	—	XDR	—	—	—	—	—	—	—
24	2017	0	Nasopharynx	35B/35B	91	373	—	XDR	—	—	—	—	—	—	—
25	2017	0	Nasopharynx	6B/6E	115	135	CC1348	XDR	+	+	+	+	+	—	—
									20%	36%	36%	44%	36%	28%	20%

The major GPSC identified were GPSC1 (*n*=7), GPSC9 (*n*=5) and GPSC10 (*n*=5) and 21/25 isolates belong to GPSC known to carry a high degree of resistance. Most of the isolates (13/25) were PMEN clones or single locus variants (SLV) of PMEN clones. Major clonal complexes identified were CC320 (*n*=4), CC230 (*n*=3) and CC63 (*n*=5). Some isolates were reclassified as MDR due to changes in resistance pattern upon BMD testing, and updated breakpoints by EUCAST in 2019, but 15/25 showed an XDR resistance profile. PCV coverage of the sequenced isolates was low; 20% for PCV10 and 36% for PCV13. Major non-PCV serotypes detected include MDR serotype 15A, 15C, serogroup 24, 7B and 35B. Additional coverage would not be increased with the use of PCV15 and only slightly with the use of PCV20, 44% with addition of serotype 11A and 15B. *Pilus islet 1* (PI-1) and *pilus islet-2* were present among 36% and 28% of the isolates respectively. PI-1 and PI-2 was carried by all isolates belonging to GPSC1. Zinc metalloproteinase C (*ZmpC*) was only present among isolates belonging to GPSC9 20% (*n*=5/25).

a- Bold - >2.5 in mean no of resistant classes in GPSC.

b- Identical or SLV of PMEN Taiwan19F-14 ST236.

c- Identical or SLV of PMEN Sweden15A-25 ST63.

d- Identical or SLV of PMEN Denmark14-32 ST230.

e- SLV of PMEN Spain23F-1 ST81.

f- SLV of PMEN Poland6B-20 ST315.

GPSC, Global pneumococcal sequence cluster; MLST, Multi locus sequence type; CC, Clonal complex (defined as 6/7 identical alleles); XDR, Extensively drug resistant; MDR, Multidrug resistant; PMEN, Pneumococcal molecular epidemiology network.

gene *zmpC* was only carried by the 5 isolates belonging to GPSC9. PI-1 was present in 36% (9/25) of the isolates and PI-2 in 28% (7/25) of the isolates. All isolates belonging to GPSC1 carried both PI-1 and PI-2 (*n*=7). All isolates were equipped with *ply*, *lytA*, *lytC*, *cbpE*, *pavA*, *hysA*, *eno*, *piuA*, *psaA*, *cppA*, *htrA* and *tig/ropA* that are common virulence genes.

High Correlation Between Genotypic and Phenotypic Antimicrobial Susceptibility Among MDR Pneumococci

All the isolates (*n*=25) were selected for further investigation including MIC test using BMD and WGS (Table 2). All isolates harbored *ermB* and *tetM*, and a minority (*n*=7) also carried *mefA* belonging to GPSC1. Trimethoprim-sulfamethoxazole resistance was observed in 15/25 isolates, although 24/25 carried genes related to antibiotic resistance to sulfamethoxazole with an

amino acid insertion in *folP*. The genotype correspondence with phenotype regarding β -lactam resistance was high with 23/25 isolates, having a benzylpenicillin MIC corresponding within 1 dilution step to their predicted MIC in relation to their PBP profile. Two isolates harboring *ermB* were susceptible to clindamycin upon testing with BMD, and one isolate was susceptible to tetracycline although harboring *tetM*. Two isolates harbored *cat* with phenotypic resistance to chloramphenicol. None of the included isolates carried mutations within *gyrA*/*parC* and were all susceptible to levofloxacin (Supplemental Material). All included isolates were susceptible to linezolid, vancomycin and meropenem (Supplemental Material). Based upon MICs determined with BMD, 10/25 isolates did not exhibit XDR phenotypes, because they were reclassified as susceptible to trimethoprim-sulfamethoxazole following updated EUCAST breakpoints in 2019.

TABLE 2 | Phenotypic and genotypic antimicrobial susceptibility correspondence was high.

Isolate	β-lactam antibiotics					Macrolide/Lincosamide			Tetracycline		Trimethoprim		Chloramphenicol	
ID	PBP profile	Benzylpenicillin		Cefotaxime		Ery		Cli			Sulfamethoxazole			
	1a-2b-2x	Inferred MIC	BMD MIC	Inferred MIC	BMD MIC	<i>ermB/mefA</i>	BMD MIC	BMD MIC	<i>tetM</i>	BMD MIC	<i>folA/folP</i>	BMD MIC	<i>cat</i>	BMD MIC
1	13-16-47	2	1 I	1	0.25 S	+/+	>2 R	>1 R	+	>8 R	+/+	4 R	–	2 S
2	17-16-47	2	1 I	1	1 I	+/+	>2 R	>1 R	+	>8 R	+/+	>4 R	–	4 S
3	13-11-16	4	4 R	2	2 I	+/+	>2 R	>1 R	+	>8 R	+/+	4 R	–	4 S
4	13-11-16	4	4 R	2	2 I	+/+	>2 R	>1 R	+	>8 R	+/+	>4 R	–	4 S
5	13-16-New	4	4 R	8	2 I	+/+	>2 R	>1 R	+	>8 R	+/+	>4 R	–	8 S
6	13-11-16	4	4 R	2	2 I	+/+	>2 R	>1 R	+	>8 R	+/+	4 R	–	4 S
7	13-14-20	4	4 R	1	1 I	+/+	>2 R	>1 R	+	>8 R	+/+	>4 R	–	4 S
8	New-7-138	0.5	0.5 I	0.5	0.5 S	+/-	>2 R	>1 R	+	>8 R	-/+	1 S	–	4 S
9	24-27-28	0.25	0.12 I	0.12	0.12 S	+/-	>2 R	>1 R	+	>8 R	-/-	≤0.5 S	–	4 S
10	17-53-36	2	0.5 I	1	0.25 S	+/-	>2 R	>1 R	+	>8 R	-/+	4 R	–	4 S
11	24-27-13	0.25	0.25 I	0.25	0.12 S	+/-	>2 R	>1 R	+	>8 R	-/+	1 S	–	4 S
12	24-27-13	0.25	0.12 I	0.25	0.12 S	+/-	>2 R	>1 R	+	≤1 S	-/+	1 S	–	4 S
13	New-15-22	0.5	1 I	0.12	0.12 S	+/-	>2 R	>1 R	+	>8 R	-/+	≤0.5 S	–	8 S
14	New-15-367	0.25	0.25 I	0.12	0.12 S	+/-	>2 R	>1 R	+	>8 R	-/+	1 S	–	≤1 S
15	17-15-22	0.5	0.5 I	0.12	0.12 S	+/-	>2 R	>1 R	+	>8 R	-/+	≤0.5 S	–	2 S
16	17-144-8	2	2 I	0.5	1 I	+/-	>2 R	>1 R	+	>8 R	-/+	1 S	–	4 S
17	17-144-8	2	0.25 I	0.5	1 I	+/-	>2 R	>1 R	+	>8 R	-/+	1 S	–	4 S
18	15-12-18	2	4 R	1	1 I	+/-	>2 R	>1 R	+	>8 R	+/+	>4 R	+	16 R
19	7-12-135	0.25	0.25 I	0.12	0.12 S	+/-	>2 R	>1 R	+	>8 R	+/+	4 R	–	4 S
20	New-53-35	0.5	0.25 I	0.25	0.25 S	+/-	>2 R	0.25 S	+	>8 R	-/+	1 S	–	4 S
21	25-7-56	2	2 I	1	1 I	+/-	>2 R	>1 R	+	>8 R	+/+	4 R	–	4 S
22	7-1-New	0.25	0.25 I	0.12	0.12 S	+/-	>2 R	>1 R	+	>8 R	+/+	2 I	–	2 S
23	7-1-242	0.25	0.5 I	0.12	0.12 S	+/-	>2 R	>1 R	+	>8 R	+/+	4 R	–	4 S
24	7-1-242	0.25	0.25 I	0.12	0.12 S	+/-	>2 R	>1 R	+	>8 R	+/+	4 R	–	4 S
25	8-67-103	0.25	0.25 I	0.25	0.25 S	+/-	>2 R	>1 R	+	>8 R	+/+	>4 R	+	16 R

Similar patterns of resistance were observed based on the GPSC. GPSC1 isolates (ID 1-7) showed a higher penicillin MIC (1-4 mg/ml), carriage of *ermB/mefA/tetM* as well as mutations conferring resistance to co-trimoxazole. GPSC9 isolates (ID 8-12) had a lower grade of penicillin nonsusceptibility (MIC 0.12-0.5 mg/ml) and carried *ermB* and *tetM*. One isolate (ID 10) was also resistant to co-trimoxazole with the *folA* I100L mutation and amino acid insertions in *folP* 57-70. Isolates belonging to GPSC10 (ID 13-17) had a low to high grade of penicillin nonsusceptibility (MIC 0.25-2 mg/ml) and carried *ermB* and *tetM*. Remaining isolates were of varied resistance patterns but were all non-susceptible to penicillin and macrolides.

Related Resistance Genes and Presence of Selected Virulence Genes Among Closely Associated Clones Within GPSC1, GPSC9 and GPSC10

To study selected virulence factors of interest and resistance genes, GPSC specific phylogenetic trees were constructed together with metadata. PI-1 and/or PI-2 was present among all the included isolates belonging to GPSC1 (**Figure 1**) but was only found in two isolates (PI-1) belonging to GPSC9 (**Figure 2**). No isolates belonging to GPSC10 carried PI-1 or PI-2 (**Figure 3**). All isolates belonging to GPSC9 carried *zmpC* but none of the GPSC1 or GPSC10 isolates carried the gene. Isolates that were closely related in the SNP tree carried similar PBP profiles, serotypes, and resistance genes in all the GPSC.

DISCUSSION

WGS was performed on clinical MDR isolates detected in Skåne County, southern Sweden during 18 months in 2016-2018. They belonged to dominant GPSCs that carry high frequencies of

antibiotic resistance, namely GPSC1, GPSC9 and GPSC10 (Gladstone et al., 2019).

GPSC1 is globally dominated by serotype 19A and 19F (Gladstone et al., 2019). After the introduction of PCV7/PCV10, including serotype 19F, in child immunization programs, an increased incidence of IPD caused by MDR serotype 19A CC320, GPSC1, was observed (Schroeder et al., 2017; Cassiolato et al., 2018). In contrast, introduction of PCV13 has decreased the incidence of IPD related to serotype 19A CC320 (Isturiz et al., 2017; Schroeder et al., 2017). Serotype 19A is, however, persisting both in Skåne County and among IPD cases in Sweden, 11% in 2020 (Public Health Agency of Sweden, 2021; Uddén et al., 2021). Of note is also that a variant of serotype 19A CC320 have been associated with PCV13 failures and breakthroughs in Ireland (Corcoran et al., 2021).

Serotypes 19A and 19F were the most common serotypes in GPSC1 in our study with one exception: a serotype 3 ST271 isolate. In 2015-2017, three serotype 3 ST271 MDR isolates were detected in two different states in the US and the serotype switch within the ST271 was described by Scherer et al. (Scherer et al., 2021). Two additional serotype 3 ST271 pneumococci are also described in PathogenWatch, isolated in South Africa 2013.

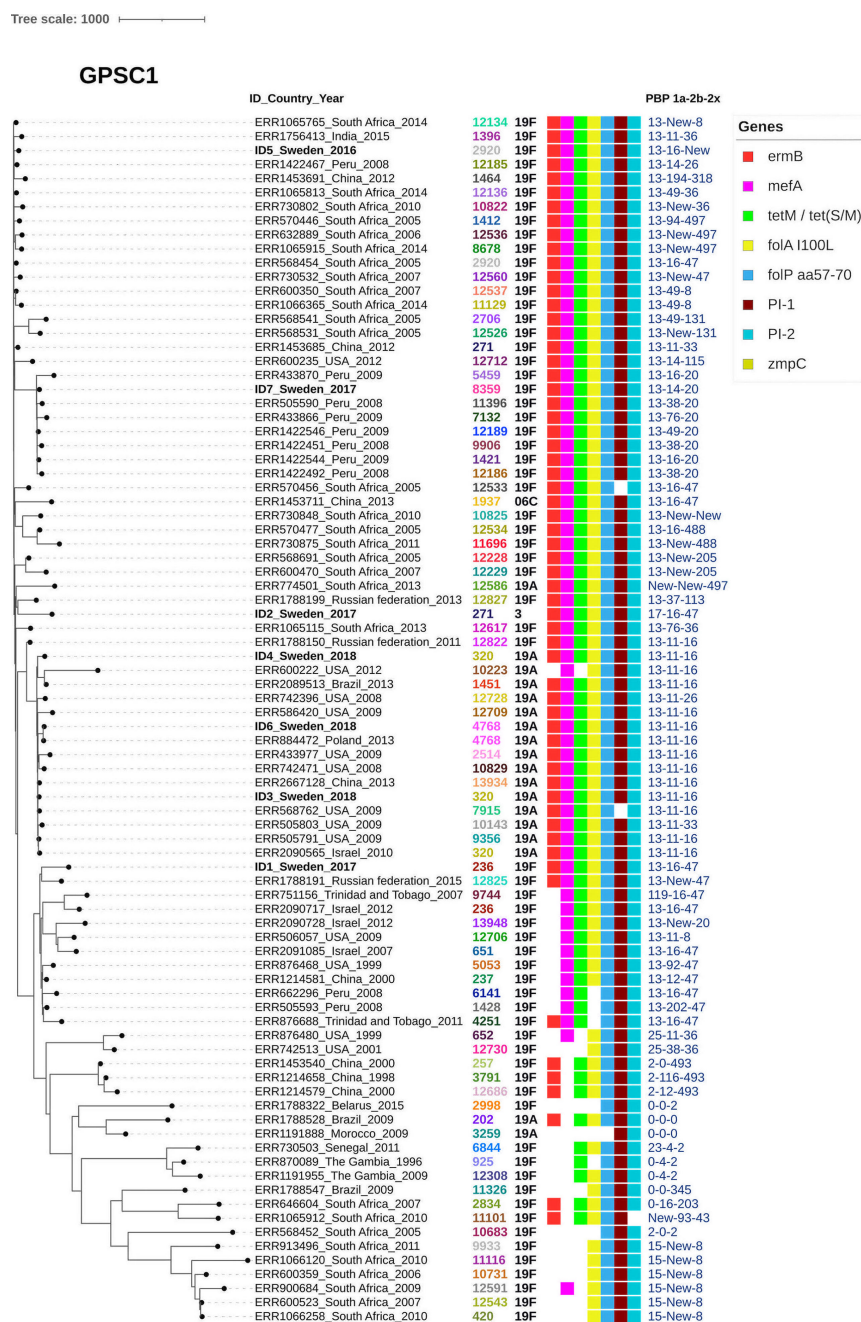


FIGURE 1 | Dual presence of both Pilus islet 1 and 2 is common within GPSC1. GPSC1 tree including 86 isolates showing ID number, country and year followed by serotype, MLST, gene presence and PBP-profile (1a-2b-2x). As a reference isolate ID 1 was used. Almost all isolates (83/86) carry both Pilus islet 1 (PI-1) and Pilus islet 2 (PI-2). The three isolates that were negative for PI-1 or PI-2 however contained larger fragments of the corresponding pilus islets. All the Swedish isolates and many of the included (55/86) carry dual macrolide resistance mechanisms with both *ermB* and *mefA*. Regarding the PBP profile PBP-1a allele 13 is common as well as the profile 13-11-16. Zinc metalloproteinase C (ZmpC) was not found among either of the isolates included.

The presence of an additional similar isolate in Sweden 2017, carrying identical resistance genes and PBP profile, may indicate global spread of the clone. The finding of this isolate, that is closely related to the widely distributed 19F ST271 clone, is of concern since the use of PCV13 has not reduced serotype 3 IPD

incidence in Sweden (Naucler et al., 2017; Public Health Agency of Sweden, 2021). Post PCV13 introduction in many Swedish counties, *S. pneumoniae* serotype 3 has remained the most common serotype causing IPD in Sweden, accounting for 15% of cases in 2020 (Public Health Agency of Sweden, 2021).

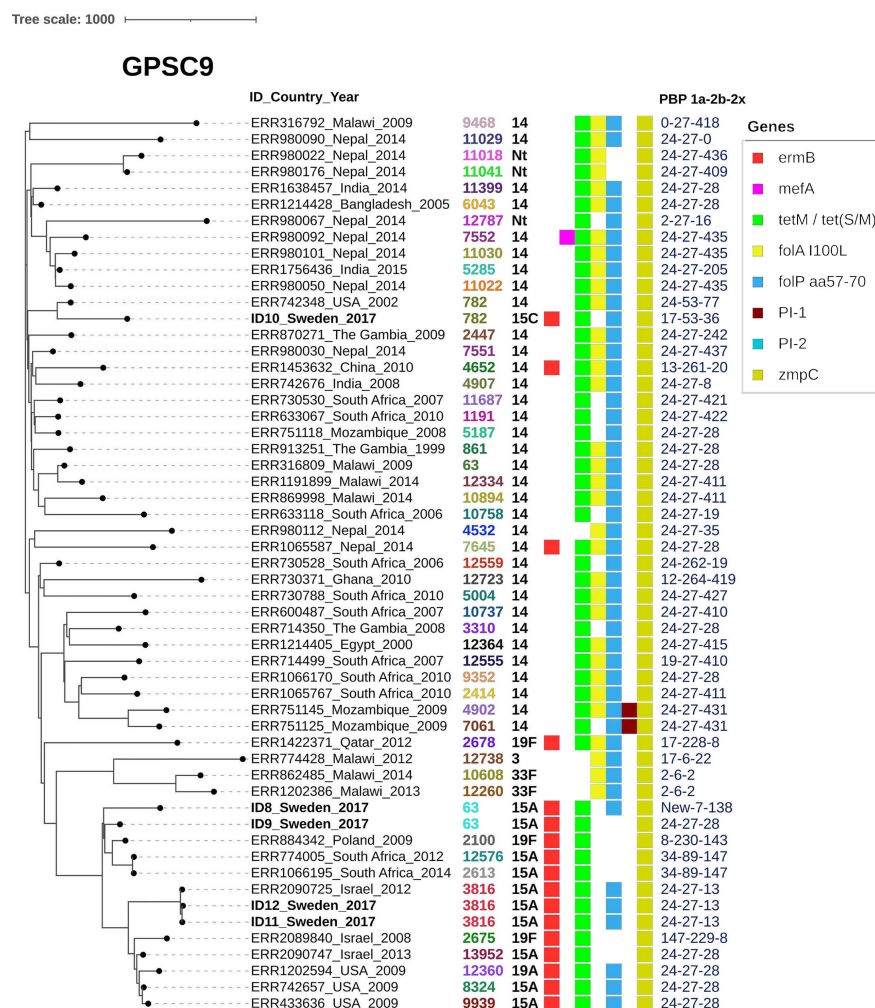


FIGURE 2 | Zinc metalloproteinase C is highly preserved among isolates belonging to GPSC9. GPSC9 tree including 55 isolates showing ID number, Country and Year followed by serotype, MLST, gene presence and PBP-profile (1a-2b-2x). As a reference isolate ID 9 was used. All the Swedish isolates and all the included 100% harbor the gene for zinc metalloproteinase C (*zmpC*). Macrolide resistance gene *ermB* was mostly present in a subclade with serotype 19A, 19F and 15A isolates. Most of the Swedish isolates (4/5), belonged to this subclade with one exception being the ST782 serotype 15C isolate more closely related to other pneumococci within GPSC9. This 15C isolate diverged in both serotype and PBP profile from other closely related pneumococci. Regarding the PBP profile PBP-1a allele 24 is common within the GPSC among our included isolates. Only two isolates carried Pilus islet 1 (PI-1) that are closely related from Mozambique. Pilus islet-2 was not found among either of the isolates included.

All currently studied GPSC1 isolates carried both PI-1 and PI-2, conferring increased adherence to host cells (Barocchi et al., 2006; Bagnoli et al., 2008). Our findings are in concordance with other studies in which the presence of PI-1 has been linked to MDR lineages with penicillin resistance, exemplified by CC320 that was also present among our MDR isolates (Dzaraly et al., 2020). In addition, GPSC1 and, specifically, CC320 have been shown to carry both PI-1 and PI-2 (Dzaraly et al., 2020; Nagaraj et al., 2021). Taken together the presence of MDR GPSC1 still warrants surveillance to follow serotype switch variants and expansion of MDR following PCV10 reintroduction in 2019 as previously discussed (Uddén et al., 2021).

GPSC10 has been described to be of concern regarding both multidrug resistance and serotype replacement in the post-PCV

era (Nagaraj et al., 2021). Several isolates in our study belonged to GPSC10, including some NVTs including 7B, 15B and serogroup 24. None of these serotypes are included in currently available PCVs, and to the best of our knowledge only 15B will be included in a future multivalent PCV (Greenberg et al., 2018; Essink et al., 2020).

GPSC9 has mostly been dominated by VT 14 but serotype 15A was the most common serotype found in our study. Serotype 15A has also increased in several parts of the world following the implementation of PCV13 (van der Linden et al., 2015; Nakano et al., 2016; Wu et al., 2020), and it is not targeted by any PCV currently in development to our knowledge (Greenberg et al., 2018; Essink et al., 2020). In both Norway and the US serotype 15A has increased in the post PCV era or been related to MDR

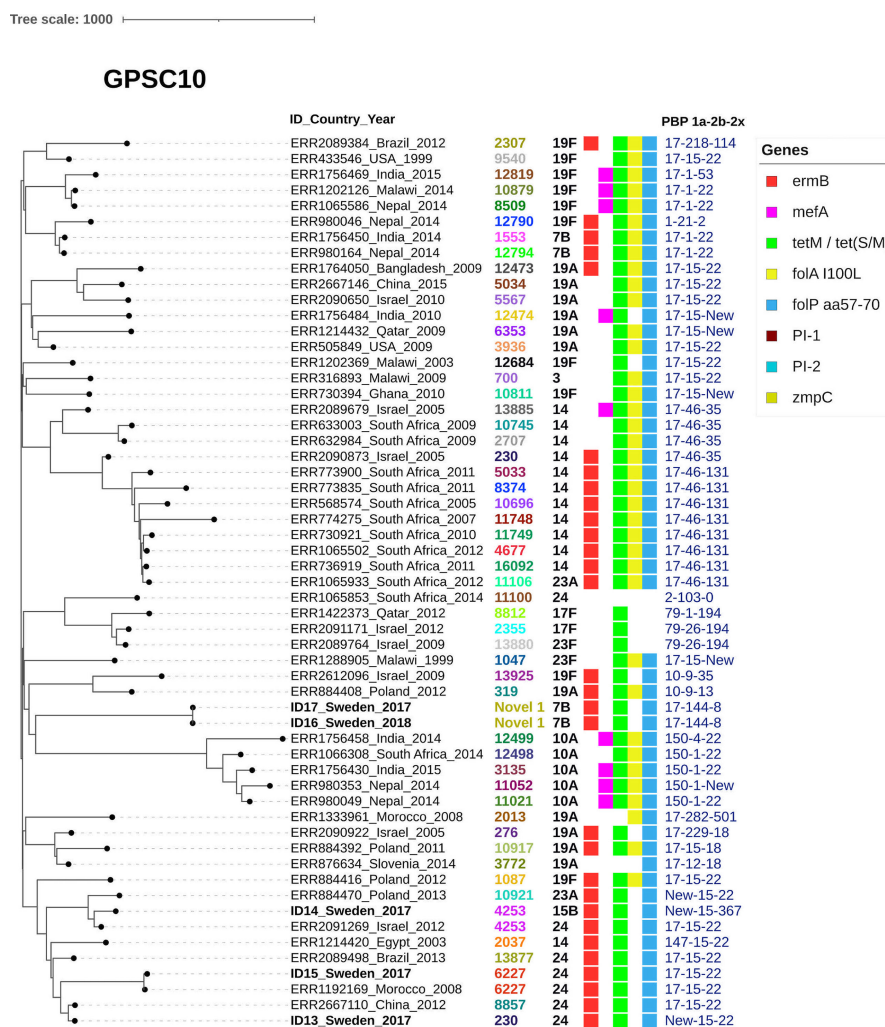


FIGURE 3 | GPSC10 lack both pilus islets and ZmpC. GPSC10 tree including 57 isolates showing ID number, Country and Year followed by serotype, MLST, gene presence and PBP-profile (1a-2b-2x). As a reference isolate ID 13 was used. All the Swedish isolates and all the included 100% harbored the zink metalloproteinase C gene (*zmpC*). Macrolide resistance mechanism *ermB* was mostly present in different sub-clades with serogroup 24, serotype 14 or 7B isolates. Regarding the PBP profile PBP-1a allele 17 was common within the GPSC among our included isolates. None of the isolates carried either Pilus islet 1, Pilus islet 2 or *zmpC*.

IPD cases (Beall et al., 2018; Siira et al., 2020). In the US CC63, belonging to GPSC9, was also found to be the main contributor to MDR invasive 15A isolates in 2015-2016 (Beall et al., 2018). In 2020, serotype 15A was one of the more common serotypes (7%) among IPD cases in Sweden and in 2016 serotype 15A together with 23B were the main contributors to MDR IPD (Nauler et al., 2017; Public Health Agency of Sweden, 2021). This NVT was also common among respiratory tract isolates and frequently MDR in Skåne County 2016-2018 (Uddén et al., 2021). Although the currently studied isolates are not from IPD cases, our results indicate that serotype 15A, GPSC9 MDR pneumococci are present in the population and is likely of importance regarding invasive pneumococcal disease also in Sweden.

Of the isolates detected in Skåne County, the *zmpC* gene was only present in GPSC9 ($n=5/25$). The gene was also present

among all GPSC9 isolates included from ENA. The protease encoded by *zmpC* cleaves human matrix metalloproteinase 9 and has, in mouse pneumonia models, been correlated to increased virulence in comparison to knockout strains (Oggioni et al., 2003) and inhibit neutrophil influx to the lung by cleavage of P-Selectin Glycoprotein 1 (Surewaard et al., 2013). Other targets of the protease include syndecan-1 and membrane-associated mucin MUC16 that are shed from the epithelium by the protease, increasing virulence (Chen et al., 2007; Govindarajan et al., 2012). ZmpC has in an observational study also been associated to a more severe clinical presentation among IPD patients with increased rates of ICU admission (Cremers et al., 2014). Previously ZmpC has been linked to serotypes 11A, 8 and 33F of ST53 and ST62, both belonging to GPSC3 (Camilli et al., 2006; Gladstone et al., 2019; Hansen et al., 2021).

In our study, the conservation within GPSC9 is presented. The protease importance for the success in dissemination and virulence of different GPSCs is something that can be of further interest to study due to its conservation in certain lineages recurring in pneumococcal disease like GPSC9 and most likely also GPSC3.

Irregularities between genotypic and phenotypic resistance were present although the concordance in general was high. One isolate carried *tetM* while still being sensitive, this has previously been noted and might be due to mutations within *tetM* not addressed in our study (Grohs et al., 2012). Overall β -lactam resistance showed a high correspondence pointing at the possibilities of using sequencing as a diagnostic tool for identifying resistance mechanisms in clinical isolates not detected by culture. Isolates included in the study were detected in routine clinical diagnostic testing. Isolated primarily from the nasopharynx (15/25) with an unknown indication for sampling. We thus cannot exclude that pneumococcus isolated might represent carriage strains rather than disease causing strains. However, they all represent highly resistant pneumococci that are present in the population of southern Sweden.

CONCLUSION

The majority of the sequenced XDR and MDR pneumococcal isolates detected in Skåne County belonged to a limited number of GPSCs, primarily GPSC1, GPSC9 and GPSC10. Many *S. pneumoniae* were NVTs belonging to internationally widespread pneumococcal lineages of which many also cause invasive pneumococcal disease. The prevalence of XDR and MDR clones causing disease that are not targeted by current PCVs is of concern, such as those detected within GPSC10 and GPSC9. The most prevalent serotypes found are also common or increasing among IPD cases in Sweden post PCV10/13. Further surveillance is of importance as this may affect both treatment and prophylactic measures regarding IPD and mucosal pneumococcal disease.

DATA AVAILABILITY STATEMENT

The data presented in the article will be made available by the authors upon request. The genomic sequence data for the 25

isolates are deposited in the European nucleotide archive (<https://www.ebi.ac.uk/ena>) (ENA project accession: PRJEB41999).

ETHICS STATEMENT

The study was approved by the local ethics committee (Regionala etikprövningsnämnden i Lund) 341 (approval no. 2012/286) and the ethical approval was updated (approval no. 2016/752) to include the current study period.

AUTHOR CONTRIBUTIONS

FU, JA, and KR contributed to conception of the study. LY, FU, H-CS, and KF developed methodology. LY and FU administered the project. LY, FU, and H-CS performed the bioinformatic analysis. LY wrote the first draft of the manuscript. All authors contributed to manuscript revision, read, and approved the submitted version.

FUNDING

This study was financially supported by an unrestrained grant from Pfizer, the Anna and Edwin Berger Foundation (KR), Swedish Heart Lung Foundation (KR, #20180401), the Royal Physiographical Society (FU, Forssman's Foundation), the Skåne County Council's research and development foundation (KR), and Swedish Research Council (KR, #2019-01053).

ACKNOWLEDGMENTS

We are grateful to Birgitta Andersson for excellent technical assistance. We thank the Clinical Microbiology laboratory at Laboratory Medicine Skåne (Lund, Sweden) for collecting all strains studied.

SUPPLEMENTARY MATERIAL

The Supplementary Material for this article can be found online at: <https://www.frontiersin.org/articles/10.3389/fcimb.2022.824449/full#supplementary-material>

REFERENCES

- Andrejko, K., Ratnasiri, B., Hausdorff, W. P., Laxminarayan, R., and Lewnard, J. A. (2021). Antimicrobial Resistance in Paediatric Streptococcus Pneumoniae Isolates Amid Global Implementation of Pneumococcal Conjugate Vaccines: A Systematic Review and Meta-Regression Analysis. *Lancet Microbe* 2 (9), e450–e460. doi: 10.1016/S2666-5247(21)00064-1
- Bagnoli, F., Moschioni, M., Donati, C., Dimitrovska, V., Ferlenghi, I., Facciotti, C., et al. (2008). A Second Pilus Type in Streptococcus Pneumoniae Is Prevalent in Emerging Serotypes and Mediates Adhesion to Host Cells. *J. Bacteriol.* 190 (15), 5480–5492. doi: 10.1128/jb.00384-08
- Barocchi, M. A., Ries, J., Zogaj, X., Hemsley, C., Albiger, B., Kanth, A., et al. (2006). A Pneumococcal Pilus Influences Virulence and Host Inflammatory Responses. *Proc. Natl. Acad. Sci. U. S. A.* 103 (8), 2857–2862. doi: 10.1073/pnas.0511017103
- Beall, B., Chochua, S., Gertz, R. E., Li, Y., Li, Z., McGee, L., et al. (2018). A Population-Based Descriptive Atlas of Invasive Pneumococcal Strains Recovered Within the U.S. During 2015–2016. *Front. Microbiol.* 9, 2670. doi: 10.3389/fmicb.2018.02670

- Camilli, R., Pettini, E., Grosso, M. D., Pozzi, G., Pantosti, A., and Oggioni, M. R. (2006). Zinc Metalloproteinase Genes in Clinical Isolates of Streptococcus Pneumoniae: Association of the Full Array With a Clonal Cluster Comprising Serotypes 8 and 11A. *Microbiology* 152 (2), 313–321. doi: 10.1099/mic.0.28417-0
- Cassiolato, A. P., Almeida, S. C. G., Andrade, A. L., Minamisava, R., and Brandileone, M. C. D. C. (2018). Expansion of the Multidrug-Resistant Clonal Complex 320 Among Invasive Streptococcus Pneumoniae Serotype 19a After the Introduction of a Ten-Valent Pneumococcal Conjugate Vaccine in Brazil. *PLoS One* 13 (11), e0208211. doi: 10.1371/journal.pone.0208211
- Chen, Y., Hayashida, A., Bennett, A. E., Hollingshead, S. K., and Park, P. W. (2007). Streptococcus Pneumoniae Sheds Syndecan-1 Ectodomains Through ZmpC, a Metalloproteinase Virulence Factor. *J. Biol. Chem.* 282 (1), 159–167. doi: 10.1074/jbc.M608542200
- Corcoran, M., Mreckiene, J., Cotter, S., Murchan, S., Lo, S. W., McGee, L., et al. (2021). Using Genomics to Examine the Persistence of Streptococcus Pneumoniae Serotype 19A in Ireland and the Emergence of a Sub-Clade Associated With Vaccine Failures. *Vaccine* 39 (35), 5064–5073. doi: 10.1016/j.vaccine.2021.06.017
- Cremers, A. J., Kokmeijer, I., Groh, L., de Jonge, M. I., and Ferwerda, G. (2014). The Role of ZmpC in the Clinical Manifestation of Invasive Pneumococcal Disease. *Int. J. Med. Microbiol.* 304 (8), 984–989. doi: 10.1016/j.ijmm.2014.06.005
- Dzarily, N. D., Muthanna, A., Mohd Desa, M. N., Taib, N. M., Masri, S. N., Rahman, N. I. A., et al. (2020). Pilus Islets and the Clonal Spread of Piliated Streptococcus Pneumoniae: A Review. *Int. J. Med. Microbiol.* 310 (7), 151449. doi: 10.1016/j.ijmm.2020.151449
- Essink, B., Sabharwal, C., Xu, X., Sundaraiyer, V., Peng, Y., Moyer, L., et al. (2020). 3. Phase 3 Pivotal Evaluation of 20-Valent Pneumococcal Conjugate Vaccine (PCV20) Safety, Tolerability, and Immunologic Noninferiority in Participants 18 Years and Older. *Open Forum Infect. Dis.* 7 (Supplement_1), S2–S2. doi: 10.1093/ofid/ofaa417.002
- European Centre for Disease Prevention and Control. (2020a). *Antimicrobial Resistance in the EU/EEA (EARS-Net) - Annual Epidemiological Report 2019*. Available at: <https://www.ecdc.europa.eu/sites/default/files/documents/surveillance-antimicrobial-resistance-Europe-2019.pdf> (Accessed July 7, 2021).
- European Centre for Disease Prevention and Control. (2020b). *Country Summaries - Antimicrobial Resistance in the EU/EEA 2019*. Available at: <https://www.ecdc.europa.eu/sites/default/files/documents/Country%20summaries-AER-EARS-Net%20202019.pdf> (Accessed July 7, 2021).
- Ganaie, F., Saad, J. S., McGee, L., Tonder, A. J. V., Bentley, S. D., Lo, S. W., et al. (2020). A New Pneumococcal Capsule Type, 10D, is the 100th Serotype and Has a Large Cps Fragment From an Oral Streptococcus. *mBio* 11 (3), e00937–e00920. doi: 10.1128/mBio.00937-20
- Gladstone, R. A., Lo, S. W., Lees, J. A., Croucher, N. J., van Tonder, A. J., Corander, J., et al. (2019). International Genomic Definition of Pneumococcal Lineages, to Contextualise Disease, Antibiotic Resistance and Vaccine Impact. *EBioMedicine* 43, 338–346. doi: 10.1016/j.ebiom.2019.04.021
- Golden, A. R., Rosenthal, M., Fultz, B., Nichol, K. A., Adam, H. J., Gilmour, M. W., et al. (2015). Characterization of MDR and XDR Streptococcus Pneumoniae in Canada–13. *J. Antimicrob. Chemother.* 70 (8), 2199–2202. doi: 10.1093/jac/dkv107
- Govindarajan, B., Menon, B. B., Spurr-Michaud, S., Rastogi, K., Gilmore, M. S., Argüeso, P., et al. (2012). A Metalloproteinase Secreted by Streptococcus Pneumoniae Removes Membrane Mucin MUC16 From the Epithelial Glycocalyx Barrier. *PLoS One* 7 (3), e32418. doi: 10.1371/journal.pone.0032418
- Greenberg, D., Hoover, P. A., Vesikari, T., Peltier, C., Hurley, D. C., McFetridge, R. D., et al. (2018). Safety and Immunogenicity of 15-Valent Pneumococcal Conjugate Vaccine (PCV15) in Healthy Infants. *Vaccine* 36 (45), 6883–6891. doi: 10.1016/j.vaccine.2018.02.113
- Grohs, P., Trieu-Cuot, P., Podglajen, I., Grondin, S., Firon, A., Poyart, C., et al. (2012). Molecular Basis for Different Levels of Tet(M) Expression in Streptococcus Pneumoniae Clinical Isolates. *Antimicrob. Agents Chemother.* 56 (10), 5040–5045. doi: 10.1128/aac.00939-12
- Hallgren, M. B., Overballe-Petersen, S., Lund, O., Hasman, H., and Clausen, P. T. L. C. (2021). MINTyper: An Outbreak-Detection Method for Accurate and Rapid SNP Typing of Clonal Clusters With Noisy Long Reads. *Biol. Methods Protoc.* 6 (1). doi: 10.1093/biomet/bpab008
- Hansen, C. B., Fuursted, K., Valentiner-Branth, P., Dalby, T., Jørgensen, C. S., and Slotved, H. C. (2021). Molecular Characterization and Epidemiology of Streptococcus Pneumoniae Serotype 8 in Denmark. *BMC Infect. Dis.* 21 (1), 421. doi: 10.1186/s12879-021-06103-w
- Isturiz, R., Sings, H. L., Hilton, B., Arguedas, A., Reinert, R. R., and Jodar, L. (2017). Streptococcus Pneumoniae Serotype 19A: Worldwide Epidemiology. *Expert Rev. Vaccines* 16 (10), 1007–1027. doi: 10.1080/14760584.2017.1362339
- Jolley, K. A., Bray, J. E., and Maiden, M. C. J. (2018). Open-Access Bacterial Population Genomics: BIGSdb Software, the PubMLST.org Website and Their Applications. *Wellcome Open Res.* 3, 124. doi: 10.12688/wellcomeopenres.14826.1
- Kapatai, G., Sheppard, C. L., Al-Shahib, A., Litt, D. J., Underwood, A. P., Harrison, T. G., et al. (2016). Whole Genome Sequencing of Streptococcus Pneumoniae: Development, Evaluation and Verification of Targets for Serogroup and Serotype Prediction Using an Automated Pipeline. *PeerJ* 4, e2477. doi: 10.7717/peerj.2477
- Kavalari, I. D., Fuursted, K., Krogfelt, K. A., and Slotved, H. C. (2019). Molecular Characterization and Epidemiology of Streptococcus Pneumoniae Serotype 24F in Denmark. *Sci. Rep.* 9 (1), 5481. doi: 10.1038/s41598-019-41983-8
- Letunic, I., and Bork, P. (2021). Interactive Tree Of Life (iTOL) V5: An Online Tool for Phylogenetic Tree Display and Annotation. *Nucleic Acids Res.* 49 (W1), W293–W296. doi: 10.1093/nar/gkab301
- Li, Y., Metcalf, B. J., Chochua, S., Li, Z., Gertz, R. E. Jr., Walker, H., et al. (2017). Validation of Beta-Lactam Minimum Inhibitory Concentration Predictions for Pneumococcal Isolates With Newly Encountered Penicillin Binding Protein (PBP) Sequences. *BMC Genomics* 18 (1), 621. doi: 10.1186/s12864-017-4017-7
- Liu, B., Zheng, D., Jin, Q., Chen, L., and Yang, J. (2019). VFDB 2019: A Comparative Pathogenomic Platform With an Interactive Web Interface. *Nucleic Acids Res.* 47 (D1), D687–d692. doi: 10.1093/nar/gky1080
- Moschioni, M., Donati, C., Muzzi, A., Massignani, V., Censini, S., Hanage, W. P., et al. (2008). Streptococcus Pneumoniae Contains 3 rlrA Pilus Variants That are Clonally Related. *J. Infect. Dis.* 197 (6), 888–896. doi: 10.1086/528375
- Nagaraj, G., Govindan, V., Ganaie, F., Venkatesha, V. T., Hawkins, P. A., Gladstone, R. A., et al. (2021). Streptococcus Pneumoniae Genomic Datasets From an Indian Population Describing Pre-Vaccine Evolutionary Epidemiology Using a Whole Genome Sequencing Approach. *Microb. Genomics* 7 (9). doi: 10.1099/mgen.0.000645
- Nakano, S., Fujisawa, T., Ito, Y., Chang, B., Suga, S., Noguchi, T., et al. (2016). Serotypes, Antimicrobial Susceptibility, and Molecular Epidemiology of Invasive and non-Invasive Streptococcus Pneumoniae Isolates in Paediatric Patients After the Introduction of 13-Valent Conjugate Vaccine in a Nationwide Surveillance Study Conducted in Japan in 2012–2014. *Vaccine* 34 (1), 67–76. doi: 10.1016/j.vaccine.2015.11.015
- Naucler, P., Galanis, I., Morfeldt, E., Darenberg, J., Örtqvist, Å., and Henriques-Normark, B. (2017). Comparison of the Impact of Pneumococcal Conjugate Vaccine 10 or Pneumococcal Conjugate Vaccine 13 on Invasive Pneumococcal Disease in Equivalent Populations. *Clin. Infect. Dis.* 65 (11), 1780–1790. doi: 10.1093/cid/cix685
- Oggioni, M. R., Memmi, G., Maggi, T., Chiavolini, D., Iannelli, F., and Pozzi, G. (2003). Pneumococcal Zinc Metalloproteinase ZmpC Cleaves Human Matrix Metalloproteinase 9 and is a Virulence Factor in Experimental Pneumonia. *Mol. Microbiol.* 49 (3), 795–805. doi: 10.1046/j.1365-2958.2003.03596.x
- Public Health Agency of Sweden. (2021). *Pneumokockinfektion Invasiv*. Available at: <https://www.folkhalsomyndigheten.se/folkhalsorapportering-statistik/statistik-a-o/sjukdomsstatistik/pneumokockinfektion-invasiv/?p=93938#statistics-nav> (Accessed October 15, 2021).
- Savinova, T., Brzhozovskaya, E., Shagin, D., Mikhaylova, Y., Shelenkov, A., Yanushevich, Y., et al. (2020). A Multiple Drug-Resistant Streptococcus Pneumoniae of Serotype 15a Occurring From Serotype 19A by Capsular Switching. *Vaccine* 38 (33), 5114–5118. doi: 10.1016/j.vaccine.2020.05.075
- Scherer, E. M., Beall, B., and Metcalf, B. (2021). Serotype-Switch Variant of Multidrug-Resistant Streptococcus Pneumoniae Sequence Type 271. *Emerg. Infect. Dis.* 27 (6), 1689–1692. doi: 10.3201/eid2706.203629
- Schroeder, M. R., Chancey, S. T., Thomas, S., Kuo, W. H., Satola, S. W., Farley, M. M., et al. (2017). A Population-Based Assessment of the Impact of 7- and 13-Valent Pneumococcal Conjugate Vaccines on Macrolide-Resistant Invasive Pneumococcal Disease: Emergence and Decline of Streptococcus Pneumoniae Serotype 19A (CC320) With Dual Macrolide Resistance Mechanisms. *Clin. Infect. Dis.* 65 (6), 990–998. doi: 10.1093/cid/cix446

- Siira, L., Vestheim, D. F., Winje, B. A., Caugant, D. A., and Steens, A. (2020). Antimicrobial Susceptibility and Clonality of *Streptococcus Pneumoniae* Isolates Recovered From Invasive Disease Cases During a Period With Changes in Pneumococcal Childhood Vaccination, Norway–2016. *Vaccine* 38 (34), 5454–5463. doi: 10.1016/j.vaccine.2020.06.040
- Surewaard, B. G., Trzciński, K., Jacobino, S. R., Hansen, I. S., Vughs, M. M., Sanders, E. A., et al. (2013). Pneumococcal Immune Evasion: ZmpC Inhibits Neutrophil Influx. *Cell Microbiol.* 15 (10), 1753–1765. doi: 10.1111/cmi.12147
- Troeger, C., Blacker, B., Khalil, I. A., Rao, P. C., Cao, J., Zimsen, S. R. M., et al. (2018). Estimates of the Global, Regional, and National Morbidity, Mortality, and Aetiologies of Lower Respiratory Infections in 195 Countries–2016: A Systematic Analysis for the Global Burden of Disease Study 2016. *Lancet Infect. Dis.* 18 (11), 1191–1210. doi: 10.1016/S1473-3099(18)30310-4
- Uddén, F., Filipe, M., Reimer, Å., Paul, M., Matuschek, E., Thegerström, J., et al. (2018). Aerobic Bacteria Associated With Chronic Suppurative Otitis Media in Angola. *Infect. Dis. Poverty* 7 (1), 42. doi: 10.1186/s40249-018-0422-7
- Uddén, F., Rünöw, E., Slotved, H. C., Fuursted, K., Ahl, J., and Riesbeck, K. (2021). Characterization of *Streptococcus Pneumoniae* Detected in Clinical Respiratory Tract Samples in Southern Sweden 2 to 4 Years After Introduction of PCV13. *J. Infect.* 83 (2), 190–196. doi: 10.1016/j.jinf.2021.05.031
- van der Linden, M., Perniciaro, S., and Imöhl, M. (2015). Increase of Serotypes 15A and 23B in IPD in Germany in the PCV13 Vaccination Era. *BMC Infect. Dis.* 15, 207. doi: 10.1186/s12879-015-0941-9
- Weiser, J. N., Ferreira, D. M., and Paton, J. C. (2018). *Streptococcus Pneumoniae*: Transmission, Colonization and Invasion. *Nat. Rev. Microbiol.* 16 (6), 355–367. doi: 10.1038/s41579-018-0001-8
- Wu, C. J., Lai, J. F., Huang, I. W., Shiao, Y. R., Wang, H. Y., and Lauderdale, T. L. (2020). Serotype Distribution and Antimicrobial Susceptibility of *Streptococcus Pneumoniae* in Pre- and Post- PCV7/13 Eras, Taiwan–2018. *Front. Microbiol.* 11, 557404. doi: 10.3389/fmicb.2020.557404

Conflict of Interest: JA and KR are participating in projects supported by Pfizer. KR is collaborating with Moderna and has been collaborating with GSK and been a scientific advisor to MSD and GSK. JA has received payments for lectures from AstraZeneca, GSK, MEDA and Pfizer. H-CS is involved with projects supported by Pfizer and has received payments for lecture from GSK.

The remaining authors declare that the research was conducted in the absence of any commercial or financial relationships that could be construed as a potential conflict of interest.

Publisher's Note: All claims expressed in this article are solely those of the authors and do not necessarily represent those of their affiliated organizations, or those of the publisher, the editors and the reviewers. Any product that may be evaluated in this article, or claim that may be made by its manufacturer, is not guaranteed or endorsed by the publisher.

Copyright © 2022 Yamba Yamba, Uddén, Fuursted, Ahl, Slotved and Riesbeck. This is an open-access article distributed under the terms of the Creative Commons Attribution License (CC BY). The use, distribution or reproduction in other forums is permitted, provided the original author(s) and the copyright owner(s) are credited and that the original publication in this journal is cited, in accordance with accepted academic practice. No use, distribution or reproduction is permitted which does not comply with these terms.



Streptococcus pneumoniae Strains Isolated From a Single Pediatric Patient Display Distinct Phenotypes

Hannah N. Agnew¹, Erin B. Brazel¹, Alexandra Tikhomirova¹, Mark van der Linden², Kimberley T. McLean¹, James C. Paton^{1*} and Claudia Trappetti^{1*}

¹ Research Centre for Infectious Diseases, Department of Molecular and Biomedical Science, The University of Adelaide, Adelaide, SA Australia, ² German National Reference Center for Streptococci, University Hospital Rheinisch-Westfälische Technische Hochschule (RWTH) Aachen, Aachen, Germany

OPEN ACCESS

Edited by:

Sven Hammerschmidt,
University of Greifswald, Germany

Reviewed by:

Krzysztof Trzcinski,
University Medical Center Utrecht,
Netherlands
Gustavo Gamez,
University of Antioquia, Colombia
Elissavet Nikolaou,
Royal Children's Hospital, Australia

*Correspondence:

Claudia Trappetti
claudia.trappetti@adelaide.edu.au
James C. Paton
james.paton@adelaide.edu.au

Specialty section:

This article was submitted to
Molecular Bacterial Pathogenesis,
a section of the journal
Frontiers in Cellular and
Infection Microbiology

Received: 31 January 2022

Accepted: 08 March 2022

Published: 31 March 2022

Citation:

Agnew HN, Brazel EB, Tikhomirova A,
van der Linden M, McLean KT,
Paton JC and Trappetti C (2022)
Streptococcus pneumoniae Strains
Isolated From a Single Pediatric
Patient Display Distinct Phenotypes.
Front. Cell. Infect. Microbiol. 12:866259.
doi: 10.3389/fcimb.2022.866259

Streptococcus pneumoniae is the leading cause of bacterial paediatric meningitis after the neonatal period worldwide, but the bacterial factors and pathophysiology that drive pneumococcal meningitis are not fully understood. In this work, we have identified differences in raffinose utilization by *S. pneumoniae* isolates of identical serotype and sequence type from the blood and cerebrospinal fluid (CSF) of a single pediatric patient with meningitis. The blood isolate displayed defective raffinose metabolism, reduced transcription of the raffinose utilization pathway genes, and an inability to grow *in vitro* when raffinose was the sole carbon source. The fitness of these strains was then assessed using a murine intranasal infection model. Compared with the CSF isolate, mice infected with the blood isolate displayed higher bacterial numbers in the nose, but this strain was unable to invade the ears of infected mice. A premature stop codon was identified in the *aga* gene in the raffinose locus, suggesting that this protein likely displays impaired alpha-galactosidase activity. These closely related strains were assessed by Illumina sequencing, which did not identify any single nucleotide polymorphisms (SNPs) between the two strains. However, these wider genomic analyses identified the presence of an alternative alpha-galactosidase gene that appeared to display altered sequence coverage between the strains, which may account for the observed differences in raffinose metabolic capacity. Together, these studies support previous findings that raffinose utilization capacity contributes to disease progression, and provide insight into a possible alternative means by which perturbation of this pathway may influence the behavior of pneumococci in the host environment, particularly in meningitis.

Keywords: *Streptococcus pneumoniae*, virulence, raffinose, clinical isolates, carbohydrate metabolism, meningitis, bacteremia

INTRODUCTION

Streptococcus pneumoniae (the pneumococcus) is the world's foremost bacterial pathogen, causing approximately 1.2 million deaths each year with over 190 million infections (Lavelle and Ward, 2021). This Gram-positive bacterium can asymptotically colonize the nasopharynx of humans at a very high rate of up to 95% of infants and 25% of adults (Trimble et al., 2020). However, in a

number of these carriers, pneumococci can disseminate from this niche to deeper mucosal sites within the body, such as the middle ear, to cause otitis media or they can invade sterile sites such as the lungs, blood, and brain, leading to invasive pneumococcal diseases (IPDs), such as pneumonia, bacteremia, and meningitis, respectively. Of the IPDs, meningitis has a high case fatality rate with 30% of cases in higher-income countries resulting in fatality and lower-income countries having a case fatality rate of 50% (Brouwer et al., 2010). Meningitis is caused by inflammation of the brain and spinal cord following bacterial infection. *S. pneumoniae* can disperse from the nasopharynx during colonization into the bloodstream, resulting in bacteremia. The bacteria carried in the blood cross the endothelial cell layer of the blood-brain barrier to invade the brain by receptor-mediated transcytosis, in which the bacterium binds a specific receptor on endothelial cells, facilitating the translocation through the barrier (Iovino et al., 2016). Replication of the pneumococci results in high levels of inflammation that damages the brain. Complications include cerebrospinal fluid pleocytosis, cochlear damage, hydrocephalus, and cerebrovascular complications. If left untreated, meningitis can result in severe health problems, including hearing loss, brain damage and death (Mook-Kanamori et al., 2011).

S. pneumoniae is a highly diverse and genetically plastic species, with at least 100 capsular serotypes superimposed on at least 16,000 sequence types (STs) (<https://pubmlst.org/>), identified by multilocus sequence typing (MLST) (Enright and Spratt, 1998; Kim and Weiser, 1998). The core genome is composed of approximately 1500 genes, accounting for ~70% of the genome, with the remaining ~30% made up of accessory regions (ARs), leading to increased diversity between STs (Obert et al., 2006). Capsule switching experiments have displayed that both serotype and genetic background (i.e. ST) affect virulence (Kelly et al., 1994; Mcallister et al., 2011), but strain complexity has made it difficult to determine if there is a link between ST/serotype and predisposition to cause invasive rather than localized disease, and the mechanisms by which pneumococci switch from commensalism to cause localized or invasive disease remain poorly understood.

Previous studies undertaken in our laboratory have demonstrated that *S. pneumoniae* clinical isolates of the same serotype and ST displayed different virulence phenotypes in mice, that correlated with their site of isolation in humans. Intranasal (i.n.) challenge in mice with clinical isolates of serotype 3 ST180, ST232 and ST233 showed that blood isolates preferentially spread to the blood, whilst ear isolates spread to the ear in a significant proportion of mice (Trappetti et al., 2013). Further studies using clinical isolates of serotype 14 ST15 showed that ear isolates were able to spread to the ear, whilst the blood isolates spread to the lungs of mice (Trappetti et al., 2013; Amin et al., 2015). Subsequent studies uncovered single nucleotide polymorphisms (SNPs) in matched blood and ear isolates of serotype 3 ST180 and serotype 14 ST15, including in genes within the raffinose uptake and utilization pathway for both STs, *rafK* and *rafR*, respectively. These SNPs affected growth when raffinose was the sole carbon source and influenced the

expression of the raffinose utilization genes *aga*, *rafG* and *rafK* (Minhas et al., 2019). Exchanging these mutations between the serotype 14 strains showed that these phenotypes were attributable to the SNPs, uncovering novel and clinically relevant molecular features that favour distinct lifestyles of pneumococcal disease.

We have now sought to investigate the bacterial drivers of meningitis, using clinically relevant serotype 15C *S. pneumoniae* isolates obtained at the same time from a single patient, provided to us by the German National Reference Center for Streptococci (Aachen). Pneumococci serotype 15C blood and CSF isolates (designated 60B and 60CSF, respectively) were isolated in 2015 from a child, aged 2, admitted to hospital with meningitis. We have performed *in vitro* and *in vivo* phenotypic characterization and genome comparisons of these clinical isolates and found differences in carbohydrate metabolism and gene expression *in vitro*, and distinct pathogenic phenotype differences between the isolates *in vivo*.

MATERIALS AND METHODS

Bacterial Strains and Growth Conditions

The *S. pneumoniae* strains used in this study are serotype 15C clinical isolates 60B (SN69534) and 60CSF (SN69531) (isolated from blood and CSF, respectively), D39 (serotype 2 ST595), and Rx1 (unencapsulated). Cells were routinely grown on Columbia agar supplemented with 5% (vol/vol) horse blood (BA), with or without gentamicin (40 µg/mL), at 37°C in 5% CO₂ overnight (McLean et al., 2020). Growth assays were performed with pneumococci grown in a chemically defined medium (CDM) (Kloosterman et al., 2006) comprising SILAC RPMI 1640 Flex Media, no glucose, no phenol red (Sigma), supplemented with amino acids (Table 1A), vitamins (Table 1B), uracil (0.01 mg/mL), adenine (0.01 mg/mL), choline chloride (0.005 mg/mL) and catalase (10 U/mL), and either 0.5% glucose, galactose, lactose, raffinose or melibiose.

MLST

To conduct MLST analysis, the *aroE*, *gdh*, *gki*, *recP*, *spi*, *xpt* and *ddl* genes of the blood strains were PCR amplified, purified using the QiaQuick Purification Kit (Qiagen), and sequenced as described previously (Enright and Spratt, 1998). Sanger sequencing was conducted by the Australian Genome Research Facility (AGRF). The sequence types (ST) of the pneumococci strains were determined by searching the MLST database (<https://pubmlst.org/>) for matching allelic profiles.

Growth Assays

Strains were grown in flat-bottom 96-well microtiter plates (Costar) with a final volume of 200 µL as previously described (Minhas et al., 2019). Strains were inoculated at a starting optical density at 600 nm (OD₆₀₀) of 0.05 in CDM supplemented with either 0.5% glucose, galactose, lactose, raffinose or melibiose, before being incubated at 37°C with 5% CO₂. The OD₆₀₀ was measured every 30 min for a total of 24 h in a SpectroSTAR

TABLE 1 | Components for the CDM.

	Components	Concentration in final media (mg/mL)
A) Amino acids	Alanine	0.24
	Glutamine	0.39
	Asparagine	0.35
	Arginine	0.125
	Lysine	0.44
	Isoleucine	0.215
	Methionine	0.125
	Phenylalanine	0.275
	Serine	0.34
	Threonine	0.225
	Tryptophan	0.05
	Valine	0.325
	Glycine	0.175
	Histidine	0.15
	Leucine	0.475
	Proline	0.675
	Cysteine hydrochloride	0.3
	Aspartic acid	0.3
B) Vitamins	Pyridoxal HCl	0.0028
	Thiamine	0.0014
	Pantothenic acid (Ca)	0.0014
	Biotin	0.00014
	Niacinamide	0.0014
	Riboflavin	0.0014
	Folic acid	0.0014

Omega spectrophotometer (BMG Labtech). Assays were conducted in triplicate with at least three repeated independent experiments.

Phenotypic Microarrays

Carbon phenotype microarray (PM) analysis using the PM microplates PM1 and PM2a (Biolog Inc.) was performed on the strains to test for the catabolism of 190 different carbon sources as previously described (Minhas et al., 2019). Every well of the microarrays contained a different carbon source. Briefly, cells were inoculated to a final OD₅₉₀ of 0.06 in the buffer provided, according to the manufacturer's instructions. This suspension was added in 100 µL aliquots to the wells, and the plate was incubated at 37°C, 5% CO₂. The OD₅₉₀ was measured every 15 min for 24 h. Catabolic activity was measured through colorimetric analysis. During catabolism, NADH is produced which subsequently reduces a colorless tetrazolium dye, resulting in a color change. The level of metabolism for each carbon source was arbitrarily determined by comparison with the negative value.

Biofilm Assays

The formation of biofilms was measured in real time using the real time cell analyzer (RTCA) xCELLigence (Agilent Technologies Inc.) instrument, as described previously for *Streptococcus mutans* and *Staphylococcus* spp. (Gutierrez et al., 2016). This instrument detects variation in the impedance signal (expressed as the arbitrary cell index, CI) as bacterial cells attach and form biofilms on the gold-microelectrodes present in the bottom of the E-plates (Agilent Technologies Inc.). Briefly, strains were grown overnight on BA plates at 37°C with 5% CO₂. Cells

were harvested and resuspended in 200 µL of CDM + 0.5% glucose or galactose a final OD₆₀₀ of 0.2. To the wells of the E-plate, 150 µL CDM + 0.5% glucose or 0.5% galactose was added before placing the plate in the cradle of the RTCA-DP system, within a 37°C incubator without CO₂ supplementation. An initial baseline impedance reading was taken before the E-plates were removed and 50 µL of bacterial suspension was added to wells for a 1 in 4 dilution, bringing the starting OD₆₀₀ to 0.05. For control wells, an additional 50 µL of CDM + 0.5% glucose or 0.5% galactose was added. E-plates were locked into the cradles of the RTCA-DP platform within the incubator and biofilm formation was monitored for 24 h by recording the impedance signal (CI) every 15 min. Assays were conducted in triplicate with at least two repeated independent experiments. Statistical analysis was performed using two-tailed Student's *t* test; *P* values < 0.05 were deemed statistically significant.

Adherence Assays

Adherence assays were carried out on the Detroit 562 human pharyngeal cell line as previously described (Trappetti et al., 2011). Briefly, cells were grown in Dulbecco's modified Eagle's medium (DMEM) supplemented with 10% fetal calf serum (FCS), 100 U/mL penicillin and 100 µg/mL streptomycin at 37°C in 5% CO₂. Wells of 24-well tissue culture trays were seeded with 2×10^5 Detroit cells in DMEM with 10% FCS and grown for 24 h before inoculation with pneumococci. These strains were grown overnight on BA plates, before being resuspended in CDM + 0.5% glucose or CDM + 0.5% galactose at a final OD₆₀₀ of 0.2. 500 µL of each bacterial suspension was added to the washed Detroit cell monolayers. As a control, each bacterial suspension was added in the same volume to empty wells. After

incubation for 2 h at 37°C, wells were washed 3 times with PBS before cells were detached from the plate by treatment with 100 μ L 0.25% trypsin-0.02% EDTA and 400 μ L of 0.1% Triton X-100 (Sigma). Samples were plated on BA to determine the number of adherent bacteria. Assays were conducted in triplicate with at least two repeated independent experiments. Statistical analysis was performed using two-tailed Student's *t* test; *P* values < 0.05 were deemed statistically significant. Data are presented as percentage of adherent bacteria, calculated using the colony forming units per mL (CFU/mL) of adherent bacteria and the CFU/mL of bacteria from the control wells that underwent the 2 h incubation. Control wells were also used to monitor the growth of bacteria during the incubation time, ensuring that each strain had similar rates of growth.

Capsule Assay

A FITC-dextran exclusion assay was used to determine the capsule thickness of strains based on previous methods (Hathaway et al., 2012), using FITC-Dextran 2000 kDa (Sigma). Briefly, pneumococci were grown overnight on BA plates in 37°C at 5% CO₂. Cells were washed in PBS, before being resuspended to a final OD₆₀₀ of 0.6 in 1 mL. A volume of 80 μ L bacterial suspension was mixed with 20 μ L FITC-dextran (10 mg/ml in MilliQ water). Each bacterial suspension was pipetted at a volume of 10 μ L onto a microscope slide and a coverslip applied securely. Imaging was conducted on 3 separate days with freshly prepared bacterial suspensions each time. The slides were viewed and imaged using an Olympus FV3000 Laser Scanning microscope with a 60 \times objective (Adelaide Microscopy). The images were analyzed using Zeiss Zen imaging software. Statistical analysis was performed using the Kruskal-Wallis test; *P* values < 0.05 were deemed statistically significant.

Targeted Gene Sequencing (Sanger Sequencing)

Selected genes of the raffinose operon from the strains underwent Sanger sequencing through AGRF (Adelaide, Australia). Briefly, samples were prepared for sequencing by PCR amplification of the region of interest using the primers listed in **Table 2**. PCR products were analyzed by gel electrophoresis, and successfully amplified products were purified using the QIAquick PCR Purification Kit (Qiagen) as per the manufacturer's instructions. Purified PCR products were evaluated for DNA quantity and quality using a Nanodrop (ThermoFisher). Samples were diluted in ultrapure nuclease-free water to a final concentration of either 18 ng/ μ L or 60 ng/ μ L depending on the size of the product, according to the Australian Genome Research Facility (AGRF) guidelines.

Genome Sequencing

S. pneumoniae strains were grown to mid-exponential phase in HI broth. Genomic DNA (gDNA) was extracted using the Promega Wizard® Genomic DNA Purification Kit according to the manufacturer's instructions, except the DNA pellet was rehydrated in ultrapure nuclease-free water. The lytic enzymes used were lysosome (30 mg/mL), 10 units mutanolysin and 0.1%

sodium deoxycholate (DOC). The gDNA was sequenced at the South Australian Genomics Centre (South Australian Health & Medical Research Institute, Adelaide, South Australia) on an Illumina MiSeq (250-bp paired-end reads). Genome assemblies were generated using shovill v1.1.0 (Seemann, 2020a), a bacterial isolate *de novo* genome assembly pipeline based on SPAdes (Prjibelski et al., 2020). The resulting genome assemblies were annotated using Prokka v1.14.6 (Seemann, 2014). Variant analysis was conducted using Snippy v4.6.0 (Seemann, 2020b) by performing all pairwise combination of aligning reads from one sample to the genome assembly of another sample. Gene presence/absence analysis was determined with a reciprocal-best-hit approach applied to the Prokka-derived amino acid sequences using mmseqs2 v13.45111 (Steinegger and Söding, 2017). A 3-step iterative searching strategy was applied using the easy-rbh workflow of mmseqs2 using sensitivities of 1, 3 and 7 (command line arguments: -start-sens 1 -sens-steps 3 -s 7) using a k-mer length of 6 (command line argument: -k 6).

RNA Extraction and qRT-PCR

Strains were initially grown overnight on BA plates at 37°C with 5% CO₂. Cells were harvested, washed, and resuspended in 1 mL of CDM + 0.5% glucose or raffinose to a final OD₆₀₀ of 0.2. Suspensions were incubated at 37°C with 5% CO₂ for 30 min. RNA was extracted using a Qiagen RNeasy Minikit as per the manufacturer's instructions. Differences in levels of gene expression were determined using one-step relative real-time qRT-PCR in a Roche LC480 real-time cycler, as previously described (Minhas et al., 2019). The specific primers used for the different genes are listed in **Table 2** and were used at a final concentration of 200 nM per reaction. Primers specific for *gyrA* mRNA were used as an internal control. Amplification data were analyzed using the comparative critical threshold ($2^{-\Delta\Delta CT}$) method (Livak and Schmittgen, 2001). Assays were performed in triplicate with a minimum of two independent experiments. Statistical analyses were performed using two-tailed Student's *t* test; *P* values < 0.05 were defined as statistically significant.

Murine Infection Model

Animal experiments were approved by the University of Adelaide Animal Ethics Committee. Female outbred 4- to 6-week-old CD-1 (Swiss) mice were anaesthetized by intraperitoneal injection of ketamine (8 mg/mL) and xylazine (0.8 mg/mL), and were challenged intranasally with 50 μ L of bacterial suspension containing 1×10^8 CFU in SB as previously described (Minhas et al., 2019). The challenge dose was retrospectively confirmed by serial dilution and plating on BA. At 24 h and 48 h, groups of 6 or 8 mice were euthanized by CO₂ asphyxiation before harvesting the blood, lungs, nasal tissue, ears, and brain. Tissues were homogenized and pneumococci enumerated as previously described by serial dilution and plating on BA plates containing 5 μ g/mL gentamicin (Trappetti et al., 2011). Statistical analyses of log-transformed CFU data were performed using two-tailed Student's *t* test; *P* values < 0.05 were deemed statistically significant.

TABLE 2 | Oligonucleotide primers used in this study for PCRs.

OLIGO NAME	SEQUENCE (5' → 3')	Reference
<i>seq_rafK_F</i>	AGAATCCAGTCAAATGTAGTGGAG	This study
<i>seq_rafK_R</i>	AAGTCAGTAATCATACGTACGGC	This study
<i>rafK_F</i>	AACGACGTAGCTCCAAAAGA	Minhas et al., 2019
<i>rafK_R</i>	GCTGGTTTACGTTCCAAGAA	Minhas et al., 2019
<i>seq_rafR_F</i>	TGTTTCAAAAGTAAGTAGCCATTTTCG	This study
<i>seq_rafR_R</i>	TTCTTCTAGAATCTCTGGAAGAATAAGG	This study
<i>seq_rafEFG_F1</i>	GGCGAAGTTTACTCAGGTGC	This study
<i>seq_rafEFG_R1</i>	GCTGAACTCTTCCTCTGTGC	This study
<i>seq_rafEFG_F2</i>	CACCATTTGGAATTGCAGGTG	This study
<i>seq_rafEFG_F3</i>	GAAAGCGGATGTGGATTAGGAG	This study
<i>seq_rafEFG_F4</i>	GCCTTTGACCAAGTCTTTTCG	This study
<i>seq_rafEFG_F5</i>	ATTCCAGAAAGTCTGGATGAAGC	This study
<i>seq_rafK_F2</i>	TCAAATGTAGTGGAGAATCAGCG	This study
<i>seq_rafK_R2</i>	CGAAGAGTATTAAGAGCATCACAATATAG	This study
<i>aga_F1</i>	TTCTATTTTGGAAAGCGATTTCAGG	This study
<i>aga_F2</i>	CTTTAGTGACTCATTAGATCAGGG	This study
<i>aga_F3</i>	CCGCAATATCACTAAGCTAGGG	This study
<i>aga_F4</i>	GAAGCAGCTGTACAATTTAATTACGG	This study
<i>rafF_R</i>	AGAAGGTTTGGCCTTTGATT	This study
<i>aga_F_RT</i>	GTCAGACTAAGTTGAGCCTTAG	Minhas et al., 2019
<i>aga_R_RT</i>	CCAACTATACAGGTTTCAGCA	Minhas et al., 2019
<i>rafG_F</i>	CCTATGGCAGCCTACTCCATC	Minhas et al., 2019
<i>rafG_R</i>	GGGTCTGTGGAATCGCATAGG	Minhas et al., 2019
<i>rafR_F</i>	CCAGCCATTCTGTATACATA	This study
<i>rafR_R</i>	CCTCCAGTGATTCTTAACCA	This study
<i>gyrA RT F</i>	ACTGGTATCGCGGTTGGGAT	McLean et al., 2020
<i>gyrA RT R</i>	ACCTGATTTCCTCATGCAA	McLean et al., 2020

RESULTS

Initial Characterization of Serotype 15C Blood and CSF Clinical Isolates

We began characterization of serotype 15C blood and CSF isolates from the same patient, denoted 60B and 60CSF, by performing multi-locus sequence typing (MLST) to determine the sequence type (ST). Both 60B and 60CSF have the sequence type 8711 (ST8711). Additional information provided by the German National Reference Center for Streptococci included the antibiotic sensitivity of the isolates. Both isolates, 60B and 60CSF had the same MIC values for all the antibiotics tested, with all MICs falling below the clinical breakpoint (European Committee on Antimicrobial Susceptibility Testing; EUCAST), indicating full sensitivity for both the isolates (data not shown).

Blood and CSF Isolates Metabolize Carbohydrate Sources Differently

As previous research undertaken in our lab has shown that isolates of the same serotype/ST potentially metabolize the carbohydrate raffinose differentially, we investigated the carbohydrate metabolism capabilities of 60B and 60CSF. Two types of phenotypic microarray plates, PM1 and PM2a, with a total of 190 carbon sources were used to test the isolates' metabolic ability. A total of 29 of the carbon sources are metabolized by both 60B and 60CSF, 10 carbon sources were metabolized by just 60CSF and the remaining 151 carbon sources were unable to be metabolized (Table 3). In line with prior research implicating an role for raffinose metabolism in tissue tropism, raffinose, and one of its derivatives, melibiose, were metabolized by 60CSF but not 60B. Of the carbon sources that

were differentially metabolized by 60B and 60CSF, we analysed the growth of these strains in chemically defined medium (CDM) with the clinically relevant sugars: raffinose, melibiose, lactose and galactose. The growth of 60B and 60CSF were comparable in CDM + glucose (Figure 1), and the growth pattern was consistent in CDM + galactose and CDM + lactose (data not shown). Although the phenotypic microarray showed that 60CSF was able to metabolize melibiose, there was no growth for either strain in CDM + melibiose, implying that melibiose may not be able to support growth of pneumococci as the sole carbon source in the present conditions (data not shown). Despite this, 60CSF was able to grow in CDM + raffinose, whilst 60B displayed an inability to grow in this medium (Figure 1). This indicates that despite the strains coming from the same patient and being closely related, there is a marked difference in their capacity to utilize raffinose as a carbon source.

Targeted Sequencing of the Raffinose Operon Reveals That *aga* Has a Premature Stop Codon in Both Isolates

Considering that raffinose was only metabolized by and capable of supporting the growth of 60CSF, and not 60B, we performed Sanger sequencing targeting the genes, that are part of the core genome, that are critical for raffinose metabolism to investigate whether they were functional in both strains (Figure 2). The raffinose uptake and utilization operon consists of eight main genes encoding an α -galactosidase (*aga*), transcriptional regulators (*rafS* and *rafR*), an ABC transporter with solute-binding protein and two cognate permeases (*rafE*, *rafF* and *rafG*), a sucrose phosphorylase (*gtfA*), and a protein of unknown function (*rafX*). Additionally, further

TABLE 3 | Phenotype microarray results for 60B and 60CSF in Biolog PM1 and PM2a plates.

CARBON SOURCE	60B	60CSF
L-Arabinose	+	+
N-Acetyl-D-Glucosamine	+	+
D-Galactose	+	+
D-Trehalose	+	+
D-Mannose	+	+
Glycerol	+	+
D-Xylose	+	+
D-Ribose	+	+
L-Rhamnose	-	+
D-Fructose	+	+
α -D-Glucose	+	+
Maltose	+	+
D-Melibiose	-	+
α -D-Lactose	+	+
Lactulose	+	+
Sucrose	+	+
β -Methyl-D- Glucoside	+	+
Maltotriose	+	+
D-Cellobiose	+	+
N-Acetyl- β -D-Mannosamine	+	+
D-Psicose	+	+
L-Lyxose	+	+
Chondroitin sulfate c	-	+
Dextrin	+	+
Inulin	+	+
Pectin	+	+
N-Acetyl-D Galactosamine	+	+
N-Acetyl Neuraminic Acid	+	+
D-Arabinose	-	+
2-Deoxy-DRibose	-	+
3-0-B-D-Galactopyranosyl-D-Arabinose	-	+
Palatinose	+	+
D-Raffinose	-	+
Salicin	+	+
D-Tagatose	-	+
Turanose	-	+
D-Glucosamine	+	+
5-Keto-DGluconic Acid	+	+
Dihydroxy Acetone	-	+

Catabolism was measured through a colorless tetrazolium dye being reduced by NADH produced during catabolism. +, metabolism occurred; -, no metabolism occurred. Metabolism was determined by calculating the change in OD₅₉₀ from the initial to final measurements. These values were then compared with the change in the negative control and an arbitrary value based on the change in negative control was used to determine if metabolism occurred. Carbon sources which neither strain metabolized are not shown. Bold font indicates carbon sources that were differentially metabolized by the strains.

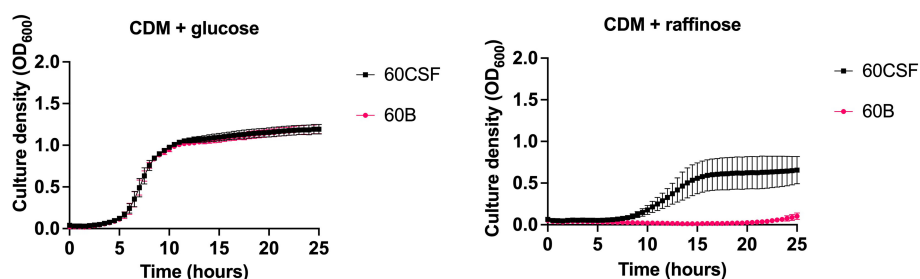


FIGURE 1 | Growth of 60B and 60CSF in CDM + glucose and CDM + raffinose. *S. pneumoniae* serotype 15C ST8711 blood isolate (60B) and CSF isolate (60CSF) were grown in 200 μ L CDM supplemented with 0.5% glucose (CDM + glucose) or 0.5% raffinose (CDM + raffinose). OD₆₀₀ was measured every 30 min for 24 h. Data are mean OD₆₀₀ \pm standard error mean (SEM) from three independent assays, each performed in triplicate.

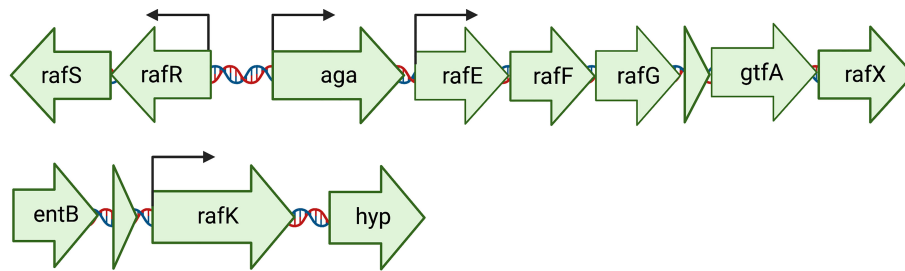


FIGURE 2 | Arrangement of the genetic loci required for the import and utilization of raffinose by *S. pneumoniae*. The main locus contains 8 genes: an ABC transporter with solute-binding protein and two cognate permeases (*rafE*, *rafF* and *rafG*); two transcriptional regulators, *rafS* (repressor) and *rafR* (activator), which control the expression of the gene encoding an α -galactosidase (*aga*); a sucrose phosphorylase (*gtfA*), and *rafX*, encoding a gene of unknown function. Further upstream is *rafK*, encoding an ATP-binding protein, essential for raffinose import into the cell (Rosenow et al., 1999). Arrows above the genes indicate locations of promoters. Created with BioRender.com.

upstream there is a gene encoding an ATP-binding protein (*rafK*), which is essential for import of raffinose into the bacteria (Rosenow et al., 1999) (Figure 2). The *aga*, *rafR*, *rafE*, *rafF*, *rafG* and *rafK* were sequenced. Each of these genes encode proteins with a critical role in raffinose uptake and utilization (Figure 3). The sequences of all the genes investigated were the identical between the 60B and 60CSF strains. However, for both 60B and 60CSF, there was a SNP in *aga* relative to the published D39 and TIGR4 genome sequences that resulted in an early stop codon, truncating the Aga protein at 213 a.a., compared with 721 a.a. for native Aga (Supplementary Figure 1). As the gene sequences involved in raffinose uptake and

metabolism were the same between 60B and 60CSF, we investigated if the expression of these genes correlated with the capacity to utilize raffinose by performing quantitative real-time reverse transcription-PCR (qRT-PCR).

The Blood and CSF Isolates Display Differences in the Transcription of Raffinose Utilization Genes

To determine if the difference in ability to utilize raffinose between the blood and CSF isolates corresponded with raffinose operon gene expression, 60B and 60CSF strains were grown to the same OD₆₀₀

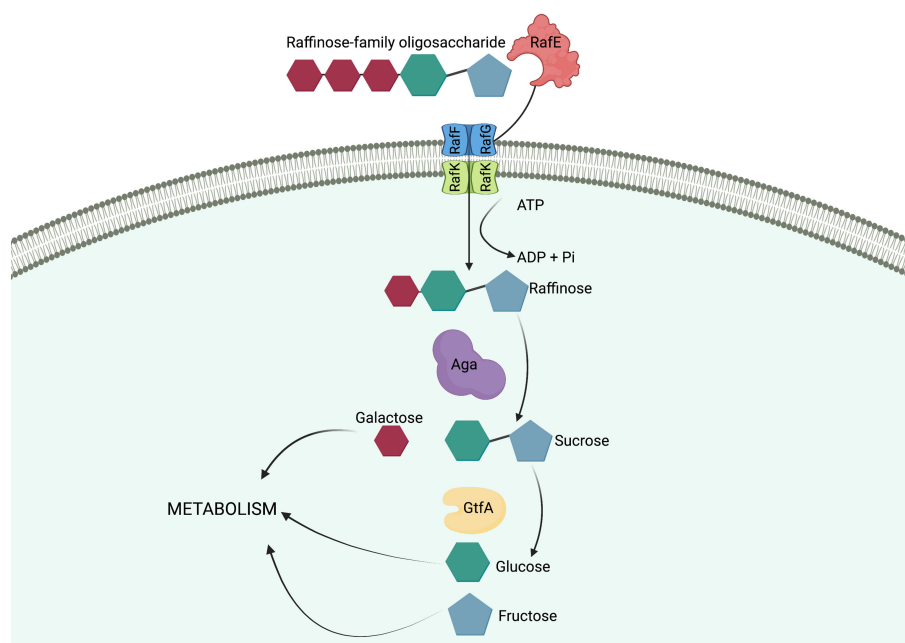


FIGURE 3 | Import and breakdown of raffinose in *S. pneumoniae*. A raffinose-family oligosaccharide (RFO) is delivered to the ABC transporter cell membrane components, RafF and RafG, by the solute-binding protein, RafE. The RFO is imported into the cell using the energy produced from the ATP-binding protein, RafK, with concomitant ATP hydrolysis. In the cytoplasm of the cell raffinose is sequentially degalactosylated by an α -galactosidase, Aga, releasing galactose, which can enter other metabolic pathways, and sucrose. A sucrose phosphorylase, GtfA, cleaves sucrose into glucose and fructose, both of which can enter further metabolic pathways and be utilized by the cell. (Hobbs et al., 2019). Created with BioRender.com.

(0.2) in CDM + Glucose and then washed and resuspended in CDM + Raffinose and incubated for a further 30 min. RNA was then extracted, and levels of *rafR*, *aga*, *rafK*, and *rafG* mRNA, representative of each of the three *RafR*-regulated transcriptional units, were then measured relative to *gyrA* mRNA by qRT-PCR. Although *rafR* was not expressed at detectable levels in either strain (data not shown), the expression levels of the α -galactosidase (*aga*) and the ATP binding protein component of the transporter (*rafK*) were significantly up-regulated in the CSF isolate compared to the blood isolate ($P < 0.05$), while the expression level of the putative permease (*rafG*) was comparable in both strains (Figure 4). These results indicate that, while the component of the raffinose ABC transporter gene (*rafG*) was equally expressed in both strains, the uptake of raffinose may be limited by the reduced transcription of the gene encoding the ATP binding protein *rafK* required to energize this transporter.

The Blood and CSF Isolates Display Altered Tissue Tropism

We next explored whether the two clinical isolates displayed any differences in disease phenotype using a mouse model of infection. Mice were intranasally challenged with 10^8 CFU of each strain and the bacterial burden in the blood, brain, ears, lungs, and nose were assessed at 24 and 48 h post challenge. Mice challenged with either strain showed no detectable bacteria present in the blood at either time point (data not shown). At 24 h post challenge, there was no significant difference in the relative bacterial burden between the mice infected with the 60B or 60CSF isolates in the brain or lungs (Figure 5). No bacteria for the 60B isolate were detected in the ears at 24 h post challenge (Figure 5), while bacteria were present in the ears of over 85% of the mice for the 60CSF strain (Figure 5; $P < 0.0001$). Conversely, the bacterial burden in the nose was higher for the 60B strain compared with the 60CSF strain (Figure 5; $P < 0.0001$). At 48 h post challenge, there were no observed significant differences between the two strains in any niche (data not shown).

Given the observed niche preferences for the strains at the 24 h time point, where the 60B strain was higher in the nose, while 60CSF higher in the ear, we investigated whether these strains produced varied amounts of capsule that may account for these differences. We analyzed the relative capsule abundance by

measuring the FITC-Dextran exclusion area of the two isolates, as well as D39 and Rx1 as encapsulated and unencapsulated control strains, respectively. No significant difference in the mean FITC-Dextran exclusion area was observed between the 60B and 60CSF strains (Figure 6). The unencapsulated control strain Rx1 displayed a significantly lower mean capsule area compared with the D39 strain ($P < 0.01$), which showed a mean area comparable to that of the 60B strain, while there was a minor but significant difference compared with the 60CSF strain (Figure 6; $P < 0.01$). We next considered whether the difference in tissue tropism could be due to an altered capacity of the bacterial strains to adhere to the nasopharyngeal epithelium. The *in vitro* adherence of each strain to Detroit 562 pharyngeal cells was explored in the presence of glucose or galactose as the sole carbon source, the latter representing the prevalent sugar present in the nasopharynx (Paixão et al., 2015). No significant difference in the total number of adherent cells was observed between the strains in either carbon source (Figure 7). Together, these data suggest that the differences in tissue tropism are not merely a consequence of altered capsule expression or nasopharyngeal adherence capabilities between the strains. To determine whether the 60B and 60CSF strains displayed a difference in biofilm formation capacity, we performed an assessment of their biofilm formation with the xCELLigence instrument. An analysis of biofilm formation was performed in glucose, the preferred carbon source, and galactose, a carbon source accessible during nasopharyngeal colonization, where biofilm formation is thought to occur. No significant difference in the rate of biofilm formation over a 24h period was observed between the strains (data not shown). Furthermore, although the maximum biofilm formation in 60CSF appeared higher than in 60B, with higher biofilm levels in the galactose medium, this difference was not statistically significant (Figure 8).

Genomic Analyses Identify a Putative Alpha-Galactosidase That May Contribute to Phenotypic Differences Between the Blood and CSF Strains

As we have previously shown niche-adaptation differences between closely related isolates (Minhas et al., 2019) and isolates from the same patient (Tikhomirova et al., 2021) to be driven by a SNPs in

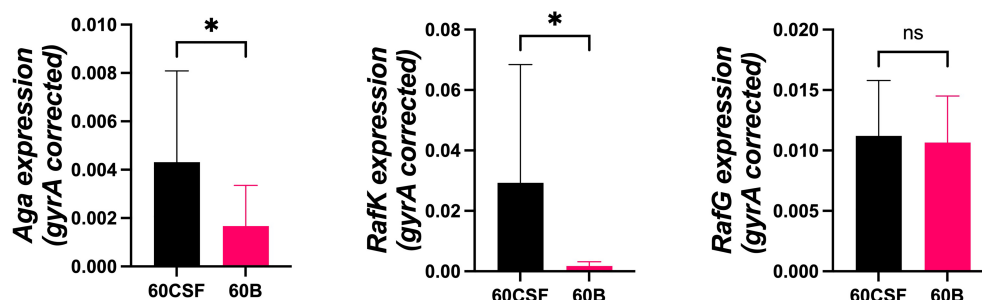


FIGURE 4 | Expression of *RafR*-regulated raffinose pathway genes by 60B and 60CSF isolates. Strains were grown to OD₆₀₀ 0.2 in CDM + glucose and then washed and resuspended in CDM + raffinose and incubated at 37°C for a further 30 min. RNA was then extracted, and levels of *aga*, *rafK*, and *rafG* mRNA were analyzed by qRT-PCR using *gyrA* rRNA as an internal control (see Materials and Methods). Data are mean OD₆₀₀ ± standard deviation (SD) from two independent assays. Significance of differences in gene expression between isolates was determined using two-tailed Student's *t* test; * $P < 0.05$. ns, not significant.

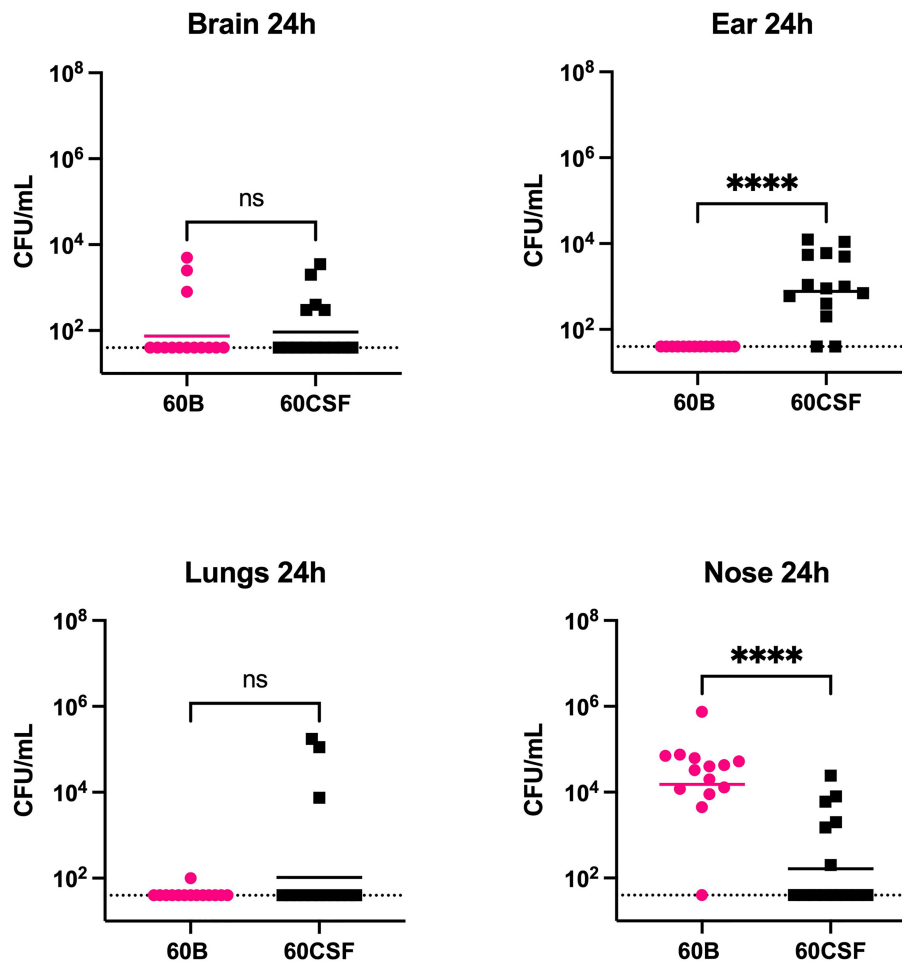


FIGURE 5 | Virulence phenotypes of blood and CSF isolates. In 2 separate experiments groups of 6 or 8 mice were infected intranasally with 10^8 CFU of the indicated strain. At 24 h, mice from each group were humanely euthanized and pneumococci in the brain, ear, lungs and nasal tissue were enumerated. Viable bacterial counts are displayed for each mouse in each niche; horizontal bars indicate the geometric mean (GM) CFU for each group; the dotted line indicates the detection threshold. Significance of differences in bacterial load between groups was determined using two-tailed Student's t test; **** $P < 0.0001$. ns, not significant.

loci responsible for uptake and utilization of raffinose, we performed whole genome sequencing of 60B and 60CSF on the Illumina platform, to determine whether the phenotypic differences observed here were a product of similar genomic events. SNP analysis comparing 60B and 60CSF sequences revealed that no SNPs were present in the well characterized raffinose locus or in any other coding regions. However, reciprocal best hit-based analysis revealed that there may be different fragments of a gene, encoding a putative glycosyl hydrolase family 36 (GH36) alpha-galactosidase, present between the blood and CSF isolates. The nucleotide and amino acid sequences shared no sequence similarity with the *aga* gene sequenced at the *raf* locus of these strains. We performed a BLASTn search using the nucleotide sequence for the largest fragment from the CSF isolate. This region showed 100% sequence identity to the latter 75% of an alpha-galactosidase gene that was present as part of the accessory genome in 68 out of 9029 other pneumococcal strains (0.75%), including the *S. pneumoniae* 4559, EF3030, and 947 strains (Junges et al., 2019; Minhas et al.,

2019). Based on the short-read sequencing, obtained with the Illumina platform, the blood isolate appeared to possess two fragments spanning a 594 bp and 967 bp region of the alpha-galactosidase (Supplementary Figure 2), while the CSF isolate possessed one larger gene fragment encompassing 1680 bp in total (Figure 9). The sequencing did not identify regions with similarity to the first 537 bp of this full-length gene in either isolate. However, the fragments in the CSF isolate encompassed the remainder of the gene, while the contigs from the Illumina sequencing did not yield sequences that correspond to the final 132 bp of this gene for the 60B strain. We conducted further analyses of the alpha-galactosidase gene in the *S. pneumoniae* 4559 blood isolate. The alpha-galactosidase gene, depicted as a pink arrow (Protein ID WP_000158269.1; Figure 10), was present in a ~13 kb region of DNA that possessed a relatively low GC content (33% GC) to that of the upstream and downstream DNA (40.4% GC and 40% GC, respectively), suggesting a possible horizontal gene transfer event may have occurred. However, there were no other genes or features

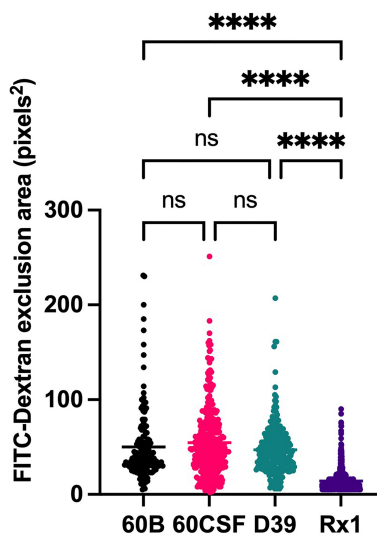


FIGURE 6 | Capsule area of blood and CSF isolates, measured using FITC-dextran exclusion assay. *S. pneumoniae* D39, Rx1, serotype 15C ST8711 blood isolate (60B) and CSF isolate (60CSF) were grown overnight before being resuspended to an OD₆₀₀ of 0.6 in 1 mL PBS. 80 μ L of bacterial suspension was added to 20 μ L FITC-dextran (10mg/mL in MilliQ water). A volume of 10 μ L of the bacterial FITC-dextran suspension was pipetted onto microscope slides, fixed with a coverslip, and imaged using a laser scanning microscope. Statistical analysis was performed using Kruskal-Wallis test; **** P < 0.0001. Imaging was conducted on 3 separate days with fresh bacterial suspensions prepared each time. ns, not significant.

identified nearby that would indicate that this region was a mobile genetic element. This ~13 kb region of *S. pneumoniae* 4559 contained nine genes in total, including genes with putative functions such as a NPCBM/NEW2 domain-containing glycoside hydrolase family 27 protein (WP_001813616.1), an additional alpha-galactosidase (WP_000687798.1), an alpha-L-fucosidase (WP_000683280.1), two carbohydrate ABC transporter permeases, (WP_001812774.1 and WP_000057512.1), an ABC

transporter substrate binding protein (WP_001036442.1), and a rhamnulokinase (WP_000388563.1) (**Figure 10**). In *S. pneumoniae* 4559, this region was situated adjacent to the zinc acquisition pathway genes, *adcCBA*. We then examined whether either the 60B or 60CSF contigs contained the adjacent gene sequences. Both isolates contained contigs with sequence identity to the glycoside hydrolase family 27 and alpha-galactosidase genes.

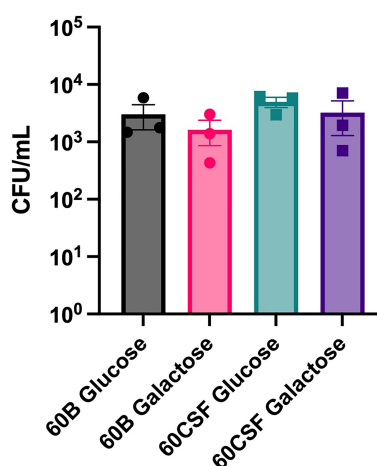


FIGURE 7 | Adherence of 60B and 60CSF to Detroit 562 cells. *S. pneumoniae* strains 60B and 60CSF at OD₆₀₀ 0.2 were inoculated onto monolayers of Detroit 562 cells in CDM + glucose or CDM + galactose, and incubated for 2 h before being tested for adherent bacteria. Data are mean adherent bacteria \pm standard error mean (SEM) from three independent assays, each performed in triplicate. Statistical analysis was performed using two-tailed Student's *t* test. No significant differences were detected between the adherence of the strains in different conditions.

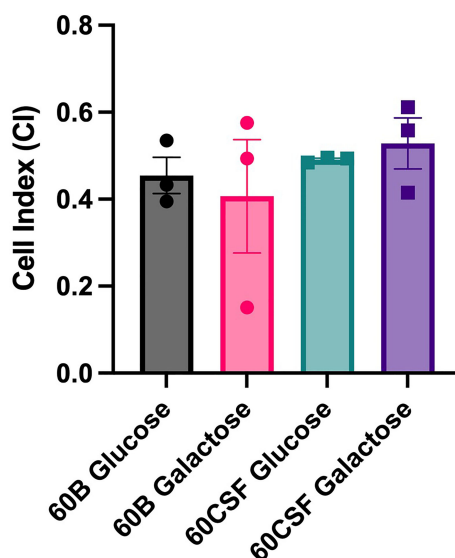


FIGURE 8 | Maximum biofilm formation by 60B and 60CSF. 60B and 60CSF were cultured overnight on BA plates before being diluted to a final OD₆₀₀ of 0.05 in CDM + 0.5% glucose or CDM + 0.5% galactose. 200 μ L of each bacterial strain in each sugar was placed into wells of a xCELLigence E-plate, with the plate being placed in the cradles of the RTCA-DP platform, and incubated at 37°C. Biofilm formation was determined by measuring cell index (CI) every 15 min over 24 h using real-time cell analysis (RTCA) xCELLigence technology. Data are mean maximum CI \pm standard error mean (SEM) from three independent assays, each performed in triplicate. Statistical analysis was performed using two-tailed Student's *t* test. No significant differences were detected between the biofilm formation of the strains in different carbon sources.

DISCUSSION

Over the past 20 years marked reductions in total death rates were achieved for many of the world's most important communicable diseases including malaria, tuberculosis and diarrhea, but the mortality due to lower respiratory infections

and meningitis remained fairly constant (GBD 2015 Child Mortality Collaborators, 2016). Notably, the decrease in pneumococcal isolates with serotypes covered by currently available conjugate vaccines, which often cause bacteremic disease, was counterbalanced by an increase in cases of meningitis associated with strains less likely to cause

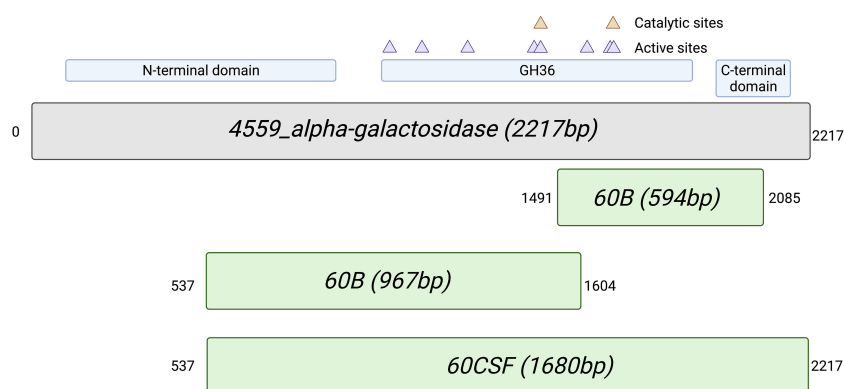


FIGURE 9 | Alignment of the alternative alpha-galactosidase gene with putative gene fragments. Gene fragments of 60B and 60CSF that correspond to an alternative alpha-galactosidase (protein ID: WP_000158269.1; locus tag: FJH52_RS10440; gene ID: Gl:446080414) found in *S. pneumoniae* strain 4559. The blood isolate, 60B, contained fragments that were 594bp and 967bp in length, whilst the CSF isolate, 60CSF, contained a single fragment of 1680bp. Numbers outside of gene fragments correspond to nucleotide position within strain 4559 alpha-galactosidase. A conserved domain search was performed on using NCBI conserved domain search (Lu et al., 2020). A glycosyl hydrolase family 36 (GH36) motif was found in strain 4559 alternative alpha-galactosidase. Two aspartic acid residues have been identified as the catalytic nucleophile and the acid/base, respectively, as indicated by the orange triangles. Active sites within the GH36 motif are indicated by purple triangles. A glycosyl hydrolase family 36 N-terminal domain, with a beta-supersandwich fold, and a glycosyl hydrolase family 36 C-terminal domain, with a beta-sandwich structure with a Greek key motif, were also located within the strain 4559 alternative alpha-galactosidase.

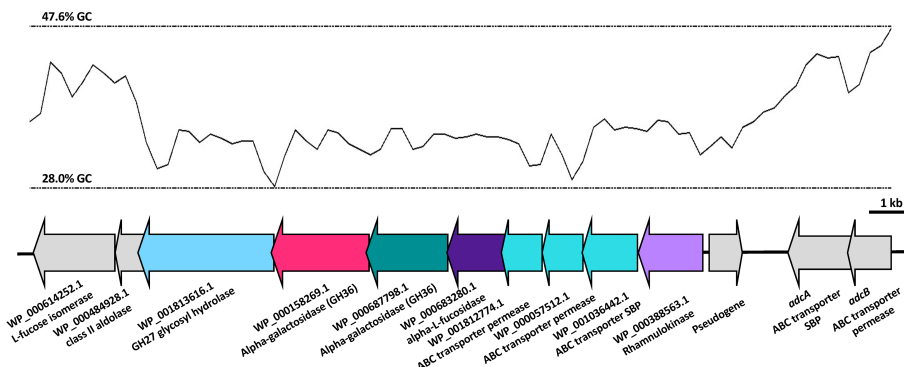


FIGURE 10 | Organisation of the *S. pneumoniae* 4559 alpha-galactosidase region. The GC content of the DNA is shown as a black line, with the upper and lower limits for this region as dotted lines. Open reading frames of genes are depicted in the direction of transcription, with genes in the lower GC region shown as colored arrows and genes adjacent to this region as grey arrows. The protein identification (ID) or name (if known), and putative function are indicated below the genes. Genes have been drawn to scale.

bacteremia (Mukerji and Briles, 2020). The lack of reduction in death rates of the diseases caused by the pneumococcus, despite the availability of an effective vaccine and suitable antimicrobial therapy, indicates that invasive pneumococcal disease is less well understood than we thought.

Understanding the bacterial features that dictate disease progression and phenotype is complicated by the high genetic diversity of *S. pneumoniae*. Certain serotypes have been associated with specific disease types, but non-capsular differences also contribute to disease progression. We have previously identified genetic and metabolic differences between clinical isolates of the same sequence type that were derived from the blood and ear of different patients. While these isolates exhibited related genetic backbones, these strains were isolated from distinct patients and possessed many additional gene alterations. In this study, we explored two clinical strains, possessing identical serotype, sequence type, and antibiotic sensitivity profiles, isolated at the same time from the blood and CSF of a single pediatric patient presenting with meningitis. These strains provided a unique opportunity to investigate whether differences may have arisen during the course of disease that could contribute to a change in lifestyle, such as permitting transfer across the blood-brain barrier or altered survival in the brain and CSF environment.

In vitro phenotypic characterization of these strains identified major differences in the metabolic capacity of the blood and CSF isolates. Compared with the isolate from the CSF, the blood isolate was unable to metabolize a range of carbohydrates, including L-rhamnose, 2-deoxy-D-ribose, D-arabinose, chondroitin sulfate c, D-tagatose, turanose and dihydroxy acetone and the two alpha-galactoside sugars, raffinose and melibiose. Importantly, we found that the blood isolate was unable to grow when raffinose was the sole carbon source.

This is distinct from our previous findings for serotype 14 ST15 strains, in which a pneumococcal blood isolate was able to grow in raffinose, while an ear isolate displayed perturbed growth (Minhas et al., 2019). In the current study, the CSF and blood

isolates appeared to possess extensive genomic similarity, with short-read genomic analyses identifying no SNPs in the coding regions of genes between these two strains. However, we found that despite the observed capacity for raffinose to be metabolized and sustain growth of the CSF isolate, both of the strains possessed a premature stop codon in the *aga* gene. The impact of the premature stop codon on the stability of the *aga* mRNA is unclear, but a truncated protein lacking the C-terminal region that harbors the catalytic and active sites suggest this protein would lack functionality. While the nucleotide sequence of this *aga* gene at the *raf* locus most closely resembled the D39 (SPD_1678) and TIGR4 (SP_1898) sequences, we also identified fragments of an alternative alpha-galactosidase gene region that was differentially present in the two strains. These fragments shared 100% identity with a portion of a gene encoding an alternative alpha-galactosidase that was present in strains including *S. pneumoniae* strain 4559, EF3030, 947, and 70585.

We performed a conserved domain search to determine whether the C-terminal region of this protein, which was not detected in the blood isolate, might be of functional significance. The region missing from the larger fragment of the blood isolate corresponded to a putative glycosyl hydrolase family 36 (GH36) motif, which contains three out of the eight putative active site residues, including one of the catalytic aspartic acid residues. By comparison, the first 538 bp region (~179 N-terminal amino acids) that were not detected in either isolate did not contain any of the putative active site residues. The gene regions identified did not possess significant similarity to any other related Streptococcal species, but the identification of similarity in other pneumococcal isolates points to the acquisition of this gene through a recombination event with another pneumococcal strain, possibly during nasopharyngeal colonization. In *S. pneumoniae* 4559, the sequence of DNA including the adjacent genes possesses a lower GC content, which suggests that it may have originally been acquired from another species with a relatively lower GC%. Despite the absence of features

consistent with a mobile genetic element, the pneumococcus is naturally transformable and will readily incorporate DNA from the environment. However, both the 60B and 60CSF appear to possess sequences that align with the genes upstream and downstream of this alpha-galactosidase. As a result, these findings must be validated by long-read sequencing to have confidence in the sequence and precise location of this region in both strains. Nevertheless, as these isolates were obtained from different sites of the same patient, it is possible that after transition to the brain, the 60B strain lost the C-terminal region of this additional alpha-galactosidase gene, resulting in abolished raffinose utilization capacity.

Notwithstanding the above differences in the *aga* gene sequences, the blood isolate also showed reduced transcription of *aga* at the *raf* locus, as well as *rafK*, which encodes the ATP-binding component of the raffinose importer. No difference in expression was observed for the permease component (*rafG*), but as RafK is required to energize the transport of raffinose by this pathway, these data point to a likely reduction in the import of raffinose in the isolate from the blood compared with the CSF isolate, which may further compound growth defect and reduced transcription of the *rafK* gene observed. Unexpectedly, we found that the expression of the gene encoding the transcriptional activator of these operons, *rafR*, was undetectable in both isolates. The *rafR* gene is co-transcribed with *rafS*, and their gene products regulate the raffinose-dependent stimulation of a divergently transcribed second promoter (P_A) directing the expression of *aga* (Rosenow et al., 1999). As a result, the regulation of this operon may be largely dependent on the levels of raffinose in the cell. Thus, the observed reduced transcription of the raffinose uptake genes in the blood isolate may be a consequence of increased accumulation of raffinose due to the potential inactivity of the alpha-galactosidase, whereby excess uncleaved raffinose may directly interact with the regulatory protein, leading to repression of these genes in the blood isolate, compared with the CSF isolate.

In addition to the metabolic differences observed *in vitro*, these strains possessed markedly different virulence profiles in mice. No mice challenged with the blood isolate had detectable levels of pneumococci in the ears, while we recovered the CSF isolate from the ears of >85% of the infected mice. In this study, the blood isolate displayed an inability to transit to the ear after intranasal challenge. These data are consistent with previous findings in other serotypes and sequence types, in which bacteria isolated from the blood typically display lower bacterial loads in the ears of mice post-challenge, compared with bacteria from other isolation sites (Amin et al., 2015; Minhas et al., 2019). In our previous study, increased capacity to metabolize raffinose correlated with reduced ear titers, but the defect in raffinose utilization was attributed to SNPs present in the regulator RafR or the import protein component RafK (Minhas et al., 2019). Another distinction between this study and the previous is that the isolates were obtained from the same patient. Although it is not known whether the blood strain originated from the CSF isolate or vice versa, this approach resulted in substantially reduced background genetic differences, including an absence

of detectable SNPs. In this study, the inability of the blood strain to utilize raffinose is likely a consequence of impaired alpha-galactosidase activity and is correlated with reduced ear titers. Together, these data suggest that perturbation of this pathway at distinct stages may result in substantially different virulence phenotypes. The burden of bacteria in the nasopharynx was higher for the blood isolate than the CSF isolate, suggesting that a defect in alpha-galactosidase activity may favour survival in this niche, or perturb transit to alternate sites. Overall, these findings expand our understanding of the pneumococcal factors that may dictate disease types in humans, pointing to possible new features of clinical significance.

The basis for the involvement of a raffinose utilization pathway in pneumococcal virulence remains unclear, but there are two prevailing hypotheses. First, that pneumococci may be exposed to raffinose in the oropharynx from dietary sources (generally plants). Consistent with this, many other streptococcal species, including *Streptococcus mutans*, and lactic acid bacteria possess loci with similar genes and gene organization to the pneumococcal raffinose locus. Alternatively, this pathway may function to import and utilize structurally related human glycans. Aga has been shown to effectively cleave a galactose unit from a linear blood group antigen, suggesting a possible alternative physiological substrate of this pathway, but as recent studies showed that Aga is localized intracellularly, the role of this protein in host glycan processing is also dependent on the efficient uptake of the glycan from the environment (Hobbs et al., 2019). However, these studies were performed on the Aga protein from the TIGR4 strain, which possesses limited (44%) amino acid sequence identity to the alternative alpha-galactosidase discussed here. While humans lack the capacity to metabolize raffinose, there is evidence that pneumococci require this pathway during disease, as detectable expression of the *raf* genes was observed in bacteria isolated from the lungs of mice (Minhas et al., 2020). Further studies of the full-length and truncated variants of this alternative alpha-galactosidase enzyme are required to elucidate the potential substrates and possible role *in vivo*. It is possible that the alpha-galactosidase variant described herein displays an altered specificity for an as yet unidentified substrate that is crucial during disease.

In a previous study, we found that during infection of the host, *S. pneumoniae* display two main patterns of gene expression; one was characteristic of bacteria in blood and one of bacteria in tissue, such as lungs and brain (Oggioni et al., 2006). In the present study, two clinical strains originated from the blood (planktonic state) and the brain (biofilm state) of a 2-year-old child admitted to hospital with suspected meningitis, showed the same capability to form *in vitro* biofilm. Biofilm formation is one of the most important virulence traits for the bacteria. Biofilms act as a reservoir for organisms, enabling escape from the action of host antibodies or antibiotics, as well as facilitating production of toxins and generation of resistant organisms. Bacteria in biofilms may also detach and cause bloodstream infections. The biofilm state is often associated with solid-tissue related infections; in cystic fibrosis, chronic

lung infections are due to *P. aeruginosa*, *Staphylococcus aureus* and *Haemophilus influenzae*, which reside in the airway in biofilms (Smyth, 2006; Starner et al., 2006). Otitis media is caused by nontypeable *H. influenzae* and pneumococcus living within a biofilm (Murphy, 2003; Weimer et al., 2010; Cevizci et al., 2015) and finally, endocarditis is considered to be a biofilm-related infection caused by staphylococci or streptococci (Donlan and Costerton, 2002). However, recent clinical studies of purpura fulminans, a disease state associated with meningococcal sepsis, showed that bacteria are mostly grouped in microcolonies in these lesions (Harrison et al., 2002). Thus, a new aspect of biofilm formation that remains poorly characterized may explain the unexpected findings for biofilm capacity obtained with the blood isolate. Importantly, the CSF and blood strains used in this study, were collected from the same patient who was admitted to the hospital with suspected meningitis and it is unknown whether the blood stain originated from the CSF isolate or vice versa. While the hematogenous route was for many years believed to be the only mode for the bacteria to enter the CSF, clinical studies in adult and neonatal human meningitis have shown that *S. pneumoniae* can travel directly from the nasopharyngeal tissue to the brain without any bloodstream invasion (Garges et al., 2006). Experimental infections have confirmed that initial nasopharyngeal colonization could be followed by isolation of high number of bacteria from olfactory epithelium, brain, olfactory bulbs and trigeminal ganglia in the absence of bacteremia (Van Ginkel et al., 2003). *In vivo* imaging also showed that pneumococci were able to directly localize in mice to the olfactory bulb and the brain, in the absence of detectable bacteremia (Marra and Brigham, 2001).

S. pneumoniae is an important commensal resident of the human nasopharynx, and like other commensals in this niche, colonisation is dependent on the capacity to adhere to the epithelium and exist within the nasal mucus. In our murine model of infection, we found that the blood isolate was better able to survive in the nasopharynx of the mice compared to the CSF strain. However, when the adherence of each strain was explored using *in vitro* cultured human nasopharyngeal epithelial cells, no significant difference in the total number of adherent cells was observed between the strains. In the nasopharynx, bacteria are predominantly embedded in the mucin glycans and pneumococci possess several surface components, such as surface-located pneumococcal adherence and virulence protein A (PavA), PavB and enolase (Eno), that enable persistence in this niche for weeks or months. Thus, inconsistencies between *in vitro* and *in vivo* results are likely due to the difference in available carbohydrates and the lack of expression of key pneumococcal surface adhesins in the *in vitro* assays. These adhesive interactions with the epithelial surface may be needed not only for colonization, but also for the initial step in the invasion process.

The pathophysiology of pneumococcal meningitis is not fully understood. In this study, we found that strains isolated from the brain and the blood of a single paediatric patient with meningitis and bacteraemia, showed remarkable differences *in vitro* and *in*

vivo assays. Importantly, we found that the CSF strain could metabolize raffinose, while the blood isolate lacks this ability. Progression from carriage to invasive disease exposes the pneumococcus to markedly different micro-environments to which the organism must adapt, and this might explain the loss or the acquisition of one gene or another. The exact role of raffinose in disease progression, particularly in meningitis, is still unclear and further studies using comparative genomic and transcriptomic analyses of other *S. pneumoniae* serotypes and/or other meningitis-causing bacteria, are needed.

DATA AVAILABILITY STATEMENT

The datasets presented in this study can be found in online repositories. The name of the repository and accession number can be found below: NCBI; PRJNA803929.

ETHICS STATEMENT

Animal experiments were approved by the University of Adelaide Animal Ethics Committee.

AUTHOR CONTRIBUTIONS

Conceptualization, HA, EB, AT, JP, and CT. Methodology, HA, EB, KM, AT, and CT. Investigation, HA, EB, KM, AT, ML, and CT. Formal analysis, HA, EB, AT, JP, and CT. Data curation, HA, EB, AT, JP, and CT. Writing—original draft preparation, HA, EB, AT, JP, and CT. All authors have read and agreed to the published version of the manuscript.

FUNDING

This work was supported by the National Health and Medical Research Council (NHMRC) Investigator grant 1174876 to JP, and by the Australian Research Council (ARC) Discovery Project DP190102980 to CT and JP.

ACKNOWLEDGMENTS

We would like to acknowledge Jane Sibbons and Adelaide Microscopy for assistance with the microscopy.

SUPPLEMENTARY MATERIAL

The Supplementary Material for this article can be found online at: <https://www.frontiersin.org/articles/10.3389/fcimb.2022.866259/full#supplementary-material>

REFERENCES

- Amin, Z., Harvey, R. M., Wang, H., Hughes, C. E., Paton, A. W., Paton, J. C., et al. (2015). Isolation Site Influences Virulence Phenotype of Serotype 14 *Streptococcus Pneumoniae* Strains Belonging to Multilocus Sequence Type 15. *Infect. Immun.* 83, 4781–4790. doi: 10.1128/IAI.01081-15
- Brouwer, M. C., Tunkel, A. R., and Van De Beek, D. (2010). Epidemiology, Diagnosis, and Antimicrobial Treatment of Acute Bacterial Meningitis. *Clin. Microbiol. Rev.* 23, 467–492. doi: 10.1128/CMR.00070-09
- Cevizci, R., Duzlu, M., Dundar, Y., Noyanalan, N., Sultan, N., Tutar, H., et al. (2015). Preliminary Results of a Novel Quorum Sensing Inhibitor Against Pneumococcal Infection and Biofilm Formation With Special Interest to Otitis Media and Cochlear Implantation. *Eur. Arch. Otorhinolaryngol.* 272, 1389–1393. doi: 10.1007/s00405-014-2942-5
- GBD 2015 Child Mortality Collaborators (2016). Global, Regional, National, and Selected Subnational Levels of Stillbirths, Neonatal, Infant, and Under-5 Mortality 1980–2015: A Systematic Analysis for the Global Burden of Disease Study 2015. *Lancet* 388, 1725–1774. doi: 10.1016/S0140-6736(16)31575-6
- Donlan, R. M., and Costerton, J. W. (2002). Biofilms: Survival Mechanisms of Clinically Relevant Microorganisms. *Clin. Microbiol. Rev.* 15, 167–193. doi: 10.1128/CMR.15.2.167-193.2002
- Enright, M. C., and Spratt, B. G. (1998). A Multilocus Sequence Typing Scheme for *Streptococcus Pneumoniae*: Identification of Clones Associated With Serious Invasive Disease. *Microbiol. (Soc. Gen. Microbiol.)* 144, 3049–3060. doi: 10.1099/00221287-144-11-3049
- Garges, H. P., Moody, M. A., Cotten, C. M., Smith, P. B., Tiffany, K. F., Lenfestey, R., et al. (2006). Neonatal Meningitis: What is the Correlation Among Cerebrospinal Fluid Cultures, Blood Cultures, and Cerebrospinal Fluid Parameters? *Pediatrics* 117, 1094–1100. doi: 10.1542/peds.2005-1132
- Gutierrez, D., Hidalgo-Cantabrana, C., Rodriguez, A., Garcia, P., and Ruas-Madiedo, P. (2016). Monitoring in Real Time the Formation and Removal of Biofilms From Clinical Related Pathogens Using an Impedance-Based Technology. *PLoS One* 11, e0163966–e0163966. doi: 10.1371/journal.pone.0163966
- Harrison, O. B., Robertson, B. D., Faust, S. N., Jepson, M. A., Goldin, R. D., Levin, M., et al. (2002). Analysis of Pathogen-Host Cell Interactions in Purpura Fulminans: Expression of Capsule, Type IV Pili, and PorA by *Neisseria Meningitidis* In Vivo. *Infect. Immun.* 70, 5193–5201. doi: 10.1128/IAI.70.9.5193-5201.2002
- Hathaway, L. J., Brugger, S. D., Morand, B., Bangert, M., Rotzetter, J. U., Hauser, C., et al. (2012). Capsule Type of *Streptococcus Pneumoniae* Determines Growth Phenotype. *PLoS Pathog.* 8, e1002574–e1002574. doi: 10.1371/journal.ppat.1002574
- Hobbs, J. K., Meier, E. P. W., Pluvineau, B., Mey, M. A., and Boraston, A. B. (2019). Molecular Analysis of an Enigmatic *Streptococcus Pneumoniae* Virulence Factor: The Raffinose-Family Oligosaccharide Utilization System. *J. Biol. Chem.* 294, 17197–17208. doi: 10.1074/jbc.RA119.010280
- Iovino, F., Seinen, J., Henriques-Normark, B., and Van Dijk, J. M. (2016). How Does *Streptococcus Pneumoniae* Invade the Brain? *Trends Microbiol. (Regular ed.)* 24, 307–315. doi: 10.1016/j.tim.2015.12.012
- Junges, R., Maienschein-Cline, M., Morrison, D. A., and Petersen, F. C. (2019). Complete Genome Sequence of *Streptococcus Pneumoniae* Serotype 19F Strain EF3030. *Microbiol. Resour. Announc.* 8, doi: 10.1128/MRA.00198-19
- Kelly, T., Dillard, J. P., and Yother, J. (1994). Effect of Genetic Switching of Capsular Type on Virulence of *Streptococcus Pneumoniae*. *Infect. Immun.* 62, 1813–1819. doi: 10.1128/iai.62.5.1813-1819.1994
- Kim, J. O., and Weiser, J. N. (1998). Association of Intrastrain Phase Variation in Quantity of Capsular Polysaccharide and Teichoic Acid With the Virulence of *Streptococcus Pneumoniae*. *J. Infect. Dis.* 177, 368–377. doi: 10.1086/514205
- Kloosterman, T. G., Bijlsma, J. J. E., Kok, J., and Kuipers, O. P. (2006). To Have Neighbour's Fare: Extending the Molecular Toolbox for *Streptococcus Pneumoniae*. *Microbiol. (Soc. Gen. Microbiol.)* 152, 351–359. doi: 10.1099/mic.0.28521-0
- Lavelle, E. C., and Ward, R. W. (2021). Mucosal Vaccines — Fortifying the Frontiers. *Nat. Rev. Immunol.* doi: 10.1038/s41577-021-00583-2
- Livak, K. J., and Schmittgen, T. D. (2001). Analysis of Relative Gene Expression Data Using Real-Time Quantitative PCR and the 2- $\Delta\Delta$ CT Method. *Methods (San Diego Calif.)* 25, 402–408. doi: 10.1006/meth.2001.1262
- Lu, S., Wang, J., Chitsaz, F., Derbyshire, M. K., Geer, R. C., Gonzales, N. R., et al. (2020). CDD/SPARCLE: The Conserved Domain Database in 2020. *Nucleic Acids Res.* 48, D265–D268. doi: 10.1093/nar/gkz991
- Marra, A., and Brigham, D. (2001). *Streptococcus Pneumoniae* Causes Experimental Meningitis Following Intranasal and Otitis Media Infections via a Nonhematogenous Route. *Infect. Immun.* 69, 7318–7325. doi: 10.1128/IAI.69.12.7318-7325.2001
- Mcallister, L. J., Ogunniyi, A. D., Stroehner, U. H., Leach, A. J., and Paton, J. C. (2011). Contribution of Serotype and Genetic Background to Virulence of Serotype 3 and Serogroup 11 Pneumococcal Isolates. *Infect. Immun.* 79, 4839–4849. doi: 10.1128/IAI.05663-11
- Mclean, K. T., Tikhomirova, A., Brazel, E. B., Legendre, S., Haasbroek, G., Minhas, V., et al. (2020). Site-Specific Mutations of GalR Affect Galactose Metabolism in *Streptococcus Pneumoniae*. *J. Bacteriol.* 203, e00180-20. doi: 10.1128/JB.00180-20
- Minhas, V., Aprianto, R., Mcallister, L. J., Wang, H., David, S. C., Mclean, K. T., et al. (2020). In Vivo Dual RNA-Seq Reveals That Neutrophil Recruitment Underlies Differential Tissue Tropism of *Streptococcus Pneumoniae*. *Commun. Biol.* 3, 293–293. doi: 10.1038/s42003-020-1018-x
- Minhas, V., Harvey, R. M., Mcallister, L. J., Seemann, T., Syme, A. E., Baines, S. L., et al. (2019). Capacity to Utilize Raffinose Dictates Pneumococcal Disease Phenotype. *mBio* 10, e02596–e02518. doi: 10.1128/mBio.02596-18
- Mook-Kanamori, B. B., Geldhoff, M., van der Poll, T., and Van De Beek, D. (2011). Pathogenesis and Pathophysiology of Pneumococcal Meningitis. *Clin. Microbiol. Rev.* 24, 557–591. doi: 10.1128/CMR.00008-11
- Mukerji, R., and Briles, D. E. (2020). New Strategy is Needed to Prevent Pneumococcal Meningitis. *Pediatr. Infect. Dis. J.* 39, 298–304. doi: 10.1097/INF.0000000000002581
- Murphy, T. F. (2003). Respiratory Infections Caused by non-Typeable *Haemophilus Influenzae*. *Curr. Opin. Infect. Dis.* 16, 129–134. doi: 10.1097/00001432-200304000-00009
- Obert, C., Sublett, J., Kaushal, D., Hinojosa, E., Barton, T., Tuomanen, E. I., et al. (2006). Identification of a Candidate *Streptococcus Pneumoniae* Core Genome and Regions of Diversity Correlated With Invasive Pneumococcal Disease. *Infect. Immun.* 74, 4766–4777. doi: 10.1128/IAI.00316-06
- Oggioni, M. R., Trappetti, C., Kadioglu, A., Cassone, M., Iannelli, F., Ricci, S., et al. (2006). Switch From Planktonic to Sessile Life: A Major Event in Pneumococcal Pathogenesis. *Mol. Microbiol.* 61, 1196–1210. doi: 10.1111/j.1365-2958.2006.05310.x
- Paixão, L., Oliveira, J., Verissimo, A., Vinga, S., Lourenço, E. C., Ventura, M. R., et al. (2015). Host Glycan Sugar-Specific Pathways in *Streptococcus Pneumoniae*: Galactose as a Key Sugar in Colonisation and Infection. *PLoS One* 10, e0121042. doi: 10.1371/journal.pone.0121042
- Prijbelski, A., Antipov, D., Meleshko, D., Lapidus, A., and Korobeynikov, A. (2020). Using SPAdes De Novo Assembler. *Curr. Protoc. Bioinf.* 70, e102. doi: 10.1002/cpbi.102
- Rosenow, C., Maniar, M., and Trias, J. (1999). Regulation of the Alpha-Galactosidase Activity in *Streptococcus Pneumoniae*: Characterization of the Raffinose Utilization System. *Genome Res.* 9, 1189–1197. doi: 10.1101/gr.9.12.1189
- Seemann, T. (2014). Prokka: Rapid Prokaryotic Genome Annotation. *Bioinformatics* 30, 2068–2069. doi: 10.1093/bioinformatics/btu153
- Seemann, T. (2020a) Shovill. Available at: <https://github.com/tseemann/shovill> (Accessed 2021).
- Seemann, T. (2020b) Snippy. Available at: <https://github.com/tseemann/snippy> (Accessed 2021).
- Smyth, A. (2006). Update on Treatment of Pulmonary Exacerbations in Cystic Fibrosis. *Curr. Opin. Pulm Med.* 12, 440–444. doi: 10.1097/01.mcp.0000245711.43891.16
- Starner, T. D., Zhang, N., Kim, G., Apicella, M. A., and McCray, P. B. Jr. (2006). *Haemophilus Influenzae* Forms Biofilms on Airway Epithelia: Implications in Cystic Fibrosis. *Am. J. Respir. Crit. Care Med.* 174, 213–220. doi: 10.1164/rccm.200509-1459OC

- Steinegger, M., and Söding, J. (2017). MMseqs2 Enables Sensitive Protein Sequence Searching for the Analysis of Massive Data Sets. *Nat. Biotechnol.* 35, 1026–1028. doi: 10.1038/nbt.3988
- Tikhomirova, A., Trappetti, C., Paton, J. C., Watson-Haigh, N., Wabnitz, D., Jarvis-Bardy, J., et al. (2021). A Single Nucleotide Polymorphism in an IgA1 Protease Gene Determines *Streptococcus Pneumoniae* Adaptation to the Middle Ear During Otitis Media. *Pathog. Dis.* 79, 1–8. doi: 10.1093/femspd/ftaa077
- Trappetti, C., Ogunniyi, A. D., Oggioni, M. R., and Paton, J. C. (2011). Extracellular Matrix Formation Enhances the Ability of *Streptococcus Pneumoniae* to Cause Invasive Disease. *PloS One* 6, e19844–e19844. doi: 10.1371/journal.pone.0019844
- Trappetti, C., van der Maten, E., Amin, Z., Potter, A. J., Chen, A. Y., Van Mourik, P. M., et al. (2013). Site of Isolation Determines Biofilm Formation and Virulence Phenotypes of *Streptococcus Pneumoniae* Serotype 3 Clinical Isolates. *Infect. Immun.* 81, 505–513. doi: 10.1128/IAI.01033-12
- Trimble, A., Connor, V., Robinson, R. E., Mclenaghan, D., Hancock, C. A., Wang, D., et al. (2020). Pneumococcal Colonisation is an Asymptomatic Event in Healthy Adults Using an Experimental Human Colonisation Model. *PloS One* 15, 1–12. doi: 10.1371/journal.pone.0229558
- Van Ginkel, F. W., Mcghee, J. R., Watt, J. M., Campos-Torres, A., Parish, L. A., and Briles, D. E. (2003). Pneumococcal Carriage Results in Ganglioside-Mediated Olfactory Tissue Infection. *Proc. Natl. Acad. Sci. U.S.A.* 100, 14363–14367. doi: 10.1073/pnas.2235844100
- Weimer, K. E., Armbruster, C. E., Juneau, R. A., Hong, W., Pang, B., and Swords, W. E. (2010). Coinfection With *Haemophilus Influenzae* Promotes Pneumococcal Biofilm Formation During Experimental Otitis Media and Impedes the Progression of Pneumococcal Disease. *J. Infect. Dis.* 202, 1068–1075. doi: 10.1086/656046

Conflict of Interest: The authors declare that the research was conducted in the absence of any commercial or financial relationships that could be construed as a potential conflict of interest.

Publisher's Note: All claims expressed in this article are solely those of the authors and do not necessarily represent those of their affiliated organizations, or those of the publisher, the editors and the reviewers. Any product that may be evaluated in this article, or claim that may be made by its manufacturer, is not guaranteed or endorsed by the publisher.

Copyright © 2022 Agnew, Brazel, Tikhomirova, van der Linden, McLean, Paton and Trappetti. This is an open-access article distributed under the terms of the Creative Commons Attribution License (CC BY). The use, distribution or reproduction in other forums is permitted, provided the original author(s) and the copyright owner(s) are credited and that the original publication in this journal is cited, in accordance with accepted academic practice. No use, distribution or reproduction is permitted which does not comply with these terms.



Increase of Macrolide-Resistance in *Streptococcus pneumoniae* Strains After the Introduction of the 13-Valent Pneumococcal Conjugate Vaccine in Lima, Peru

Brayan E. Gonzales¹, Erik H. Mercado¹, Maria Pinedo-Bardales¹, Noemi Hinojosa¹, Francisco Campos², Eduardo Chaparro^{3,4}, Olguita Del Águila⁵, María E. Castillo^{4,6}, Andrés Saenz⁷, Isabel Reyes⁸ and Theresa J. Ochoa^{1,4*}

OPEN ACCESS

Edited by:

Elsa Bou Ghanem,
University at Buffalo, United States

Reviewed by:

Anusak Kerdsin,
Kasetsart University, Thailand
Manmeet Bhalla,
University at Buffalo, United States
Jose Yuste,
Instituto de Salud Carlos III (ISCIII),
Spain

*Correspondence:

Theresa J. Ochoa
theresa.ochoa@upch.pe

Specialty section:

This article was submitted to
Molecular Bacterial Pathogenesis,
a section of the journal
Frontiers in Cellular and
Infection Microbiology

Received: 30 January 2022

Accepted: 04 April 2022

Published: 09 May 2022

Citation:

Gonzales BE, Mercado EH, Pinedo-Bardales M, Hinojosa N, Campos F, Chaparro E, Del Águila O, Castillo ME, Saenz A, Reyes I and Ochoa TJ (2022) Increase of Macrolide-Resistance in *Streptococcus pneumoniae* Strains After the Introduction of the 13-Valent Pneumococcal Conjugate Vaccine in Lima, Peru. *Front. Cell. Infect. Microbiol.* 12:866186. doi: 10.3389/fcimb.2022.866186

¹ Instituto de Medicina Tropical Alexander von Humboldt, Universidad Peruana Cayetano Heredia, Lima, Peru,

² Departamento de Pediatría, Hospital Nacional Docente Madre-Niño San Bartolomé, Lima, Peru, ³ Departamento de Pediatría, Hospital Nacional Cayetano Heredia, Lima, Peru, ⁴ Facultad de Medicina, Universidad Peruana Cayetano Heredia, Lima, Peru, ⁵ Servicio de Pediatría de Especialidades Clínicas, Hospital Nacional Edgardo Rebagliati Martins, Lima, Peru,

⁶ Oficina de Epidemiología, Instituto Nacional de Salud del Niño, Lima, Peru, ⁷ Departamento de Pediatría, Hospital Nacional Daniel Alcides Carrión, Lima, Peru, ⁸ Servicio de Hospitalización, Hospital de Emergencias Pediátricas, Lima, Peru

Streptococcus pneumoniae upper respiratory infections and pneumonia are often treated with macrolides, but recently macrolide resistance is becoming an increasingly important problem. The 13-valent pneumococcal conjugate vaccine (PCV13) was introduced in the National Immunization Program of Peru in 2015. This study aimed to evaluate the temporal evolution of macrolide resistance in *S. pneumoniae* isolates collected in five cross-sectional studies conducted before and after this vaccine introduction, from 2006 to 2019 in Lima, Peru. A total of 521 and 242 *S. pneumoniae* isolates recovered from nasopharyngeal swabs from healthy carrier children < 2 years old (2 carriage studies) and samples from normally sterile body areas from pediatric patients with invasive pneumococcal disease (IPD) (3 IPD studies), respectively, were included in this study. Phenotypic macrolide resistance was detected using the Kirby-Bauer method and/or MIC test. We found a significant increase in macrolide resistance over time, from 33.5% to 50.0% in carriage studies, and from 24.8% to 37.5% and 70.8% in IPD studies. Macrolide resistance genes [*erm*(B) and *mef*(A/E)] were screened using PCR. In carriage studies, we detected a significant decrease in the frequency of *mef*(A/E) genes among macrolide-resistant *S. pneumoniae* strains (from 66.7% to 50.0%) after introduction of PCV13. The most common mechanism of macrolide-resistant among IPD strains was the presence of *erm*(B) (96.0%, 95.2% and 85.1% in the 3 IPD studies respectively). Macrolide resistance was more common in serotype 19A strains (80% and 90% among carriage and IPD strains, respectively) vs. non-serotype 19A (35.5% and 34.4% among carriage and IPD strains, respectively). In conclusion, *S. pneumoniae* macrolide resistance rates are very high among Peruvian children. Future studies are needed in order to evaluate macrolide

resistance trends among pneumococcal strains, especially now after the COVID-19 pandemic, since azithromycin was vastly used as empiric treatment of COVID-19 in Peru.

Keywords: *Streptococcus pneumoniae*, macrolide-resistance, invasive pneumococcal disease, pneumococcal conjugate vaccine, healthy carrier

INTRODUCTION

Streptococcus pneumoniae, also known as pneumococcus, is the major cause of bacterial pneumonia in young children and a common cause of other infections, including sepsis, meningitis, and otitis media (O'Brien et al., 2009; Wahl et al., 2018). Approximately 300,000 deaths were caused by invasive pneumococcus worldwide in children less than 5 years old in 2015 (Dadonaite and Roser, 2018). The treatment of pneumococcal infections has become problematic due to the increase in antibiotic resistance (Cherazard et al., 2017). Moreover, it is important to consider that pneumococcal disease is preceded by asymptomatic carriage, which is especially high in children (Bogaert et al., 2004).

The prevalence of *S. pneumoniae* carriage in healthy children less than 5 years old ranges from 20.0% to 93.4% in low-income countries and is generally higher than rates reported in lower-middle income countries (Adegbola et al., 2014). Furthermore, the incidence of invasive pneumococcal disease (IPD) varies depending on several factors, including vaccine uptake, stages of life (predominant in childhood and elderly), the geographic location, and local serotype prevalence (Dion et al., 2021; Narváez et al., 2021). In general, the prevalent serotypes recovered from IPD are also frequently identified in colonized healthy children (Apte et al., 2021; Kozakova et al., 2021).

The antibiotics of the macrolide family have long been considered drugs of potential utility in the management of infections caused by *S. pneumoniae*. However, with the emergence of macrolide resistance, their clinical value in pneumococcal infections is threatened (Doern, 2006). Recent reports show that macrolide resistance in *S. pneumoniae* is geographically variable, ranging from 30 to 50% globally (Sader et al., 2018; Wang et al., 2019; Sharew et al., 2021). The main macrolide resistance mechanisms in pneumococci are ribosomal dimethylation by an enzyme encoded by *erm*(B), and efflux by an efflux pump encoded by *mef*(A), *mef*(E) or *mef*(A/E) (Cheng and Jenney, 2016; Schroeder and Stephens, 2016; Varghese et al., 2021).

More than 28 000 cases of pneumonia have been reported each year in the Peruvian population, with a fatality rate of 1.04 deaths per 100 episodes of pneumonia, and a mortality rate of 10.5 per 100 000 inhabitants among which pneumococcus remains as the main etiological agent (Ministry of Health of Peru, 2019). Pneumococcal conjugate vaccines (PCVs) are an effective intervention in reducing the incidence of disease caused by macrolide-resistant pneumococcal serotypes covered by the vaccine (Rodgers and Klugman, 2011). In Peru, PCV was introduced to the National Immunization Program as PCV7 in

2009, and was replaced by PCV10 in 2012, and PCV13 in 2015 (Davalos et al., 2016).

The aim of this study was to evaluate the variation over time of macrolide resistance in *S. pneumoniae* strains isolated as part of 2 Carriage studies in children < 2 years old and 3 IPD studies in pediatric patients < 18 years old, conducted before and after the introduction of PCV13 in Peru.

MATERIAL AND METHODS

Study Design

A temporal evaluation of the increase in macrolide resistance was conducted using data collected in five periods. We analyzed isolates of *S. pneumoniae* from patients with IPD collected during the years 2006-2008 (IPD-1) (Ochoa et al., 2010), 2009-2011 (IPD-2) (Luna-Muschi et al., 2019), and 2016-2019 (IPD-3), and isolates from healthy children (Carriage studies) collected during the years 2007-2009 (Carriage-1) (Mercado et al., 2012) and 2018-2019 (Carriage-2). The introduction of the PCV13 into the National Immunization Program in Peru (2015) was an important milestone in prevention of IPD. In this analysis, we considered studies conducted before 2015 as “pre-vaccine studies” and studies conducted after 2015 as “post-vaccine studies”.

Studies of Invasive Pneumococcal Disease

The study population and case definition of patients with IPD from the pre-vaccine studies (IPD-1 and IPD-2) have been described by Luna-Muschi et al. (2019). In IPD-3, as in the pre-vaccine studies, we only included pediatric patients with positive cultures for *S. pneumoniae* from a normally sterile areas (blood, cerebrospinal fluid [CSF], pleural fluid, synovial fluid, or peritoneal fluid) or biopsy culture. Pediatric patients were enrolled from public hospitals and private clinical laboratories in Lima that participated in the pre-vaccine studies.

Suspected *S. pneumoniae* isolates were transported on blood agar plates (Tryptone Soy Agar with 5% sheep blood) to the Pediatric Infectious Diseases Laboratory (the central laboratory of the study) on the same day of isolation. Bacterial cultures were grown on blood agar and re-identified based on colony morphology, alpha hemolysis, Gram staining, bile solubility, and optochin susceptibility test (World Health Organization, 2003). Strains were stored in skim milk at -70°C for further analysis.

Studies of Healthy Carrier Children

Mercado et al. (2012) described the study population for the pre-vaccine study (Carriage-1) in detail. In this analysis, we only

included data from patients enrolled in public hospitals in Lima. In each study we enrolled 1,000 healthy children between 2 and 24 months of age who attended the pediatric outpatient clinics, or the vaccination clinics of five hospitals in Lima; and whose family member reported that at the time of enrollment, the child did not suffer from any important disease or infection. Although, the child could have had a mild respiratory infection (rhinorrhea, mild cough, sneezing, temperature up to 38.5°C). Nasopharyngeal swab samples were taken using Rayon® (Puritan, sterile rayon tipped applicators). One sample was taken per patient. Nasopharyngeal swabs were placed in the STGG-transport-medium (skim milk, tryptone, glucose, and glycerol) and transported to the central laboratory of the study and stored at -70°C until processing. Nasopharyngeal swabs were inoculated on Todd Hewitt enrichment broth with 0.5% yeast extract for six hours at 37°C with an atmosphere of 5% CO₂ (Vidal et al., 2011) and streaked on blood agar. Bacterial cultures and isolates were analyzed using the same conventional methods as in IPD studies. Strains were stored in skim milk at -70°C for further analysis.

Antibiotic Susceptibility Testing

Susceptibility to macrolides were determined using erythromycin in pre-vaccine studies (IPD-1, IPD-2, and Carriage-1). In post-vaccine studies (IPD-3 and Carriage-2), we determined macrolide resistance using azithromycin. The Kirby Bauer method using antibiotic disks (Oxoid Ltd, Basingstoke, Hans, UK) for Carriage studies and the MIC test using E-test® (AB Biodisk, Solna, Sweden) for IPD studies were performed on Mueller Hinton agar with 5% sheep blood and incubated for 24 hours at 37°C in an atmosphere of 5% CO₂. Interpretation was carried out according to the Clinical and Laboratory Standards Institute (CLSI) guidelines corresponding to the existing edition of the year in which each study was carried out (**Supplementary Table S1**) (Clinical and Laboratory Standards Institute (CLSI), 2008; CLSI, 2015; CLSI, 2019).

DNA Extraction and PCR Detection of Macrolide-Resistant Genes

DNA isolation was performed using to the Chelex extraction method reported by Walsh et al. (2011). Each pneumococcal strain was resuspended in a single tube containing 200 µl of 5%

Chelex-100® solution (Bio-rad, California, United States) supplemented with 2 µl proteinase K (20 mg/ml), and incubated them for 60 minutes at 56°C. The suspension was homogenized for 10 seconds and incubated for 15 minutes at 95°C. Tubes with pneumococcal strains were homogenized and centrifuged at 13 000 rpm for five minutes and stored them at -20°C for further analysis.

Presence of macrolide resistance genes *erm*(B) and *mef*(A/E) was evaluated by conventional PCR using primers previously reported by Sutcliffe et al. (1996). Amplified products were separated in 1.5% agarose gel stained with ethidium bromide.

Pneumococcal Serotyping

Pneumococcal isolates from IPD-1 were serotyped by Quellung reaction at a reference lab in Israel (Soroka University Medical Center, Beer-Sheva, Israel). Serotyping of *S. pneumoniae* isolates from Carriage-1 and IPD-2 was performed by Quellung reaction at the Center for Disease Control and Prevention (CDC), Atlanta, USA. Isolates from post-vaccine studies (Carriage-2 and IPD-3) were serotyped by while genomic sequencing (WGS) in the reference laboratory, CDC Streptococcus Laboratory, USA.

Statistical Analysis

Statistical analyses of frequency and comparison between the populations of IPD and Carriage studies were performed with chi-square test (χ^2) and Fisher's exact test in the statistical package Stata/SE v.17.0 program. The statistical significance level was set at $p < 0.05$.

Ethical Aspects

This study, as well as all studies included in our analysis, were approved by the Institutional Review Board of Universidad Peruana Cayetano Heredia (Lima, Peru).

RESULTS

Macrolide Resistance Phenotype

A total of 763 *S. pneumoniae* isolates were analyzed from the Carriage (521) and the IPD (242) studies. A significant increase in the macrolide resistance phenotype was found over time (**Table 1** and **Figure 1**). Among carriage studies, the percentage of macrolide resistance increased significantly from 33.5% in the pre-vaccine study to 50.0% in the post-vaccine study ($p < 0.001$). Furthermore, in IPD studies, the

TABLE 1 | Macrolide susceptibility in 5 studies conducted from 2006 to 2019 before and after the introduction of PCV13 in Peru.

Study	Study Period	Susceptibility		Number of strains	S		I		R		p
		Method	Antibiotic		n	(%)	n	(%)	n	(%)	
Carriage-1 ^a	2006-2008	Disk diffusion	Erythromycin	313	195	(62.3)	13	(4.2)	105	(33.5)	< 0.001
Carriage-2 ^b	2018-2019	Disk diffusion	Azithromycin	208	88	(42.3)	16	(7.7)	104	(50.0)	
IPD-1 ^a	2006-2008	MIC	Erythromycin	101	76	(75.2)	0	(0.0)	25	(24.8)	< 0.001
IPD-2 ^a	2009-2011	MIC	Erythromycin	56	34	(60.7)	1	(1.8)	21	(37.5)	
IPD-3 ^b	2016-2019	MIC	Azithromycin	85	12	(14.1)	6	(7.1)	67	(78.8)	

13-valent conjugate vaccine (PCV13) was inserted into the National Immunization Program in 2015.

^aPre-vaccine studies (Pre PCV13).

^bPost-vaccine studies (Post PCV13).

S, susceptible; I, intermediate; R, resistant.

Statistical significance among carriage studies and among IPD studies.

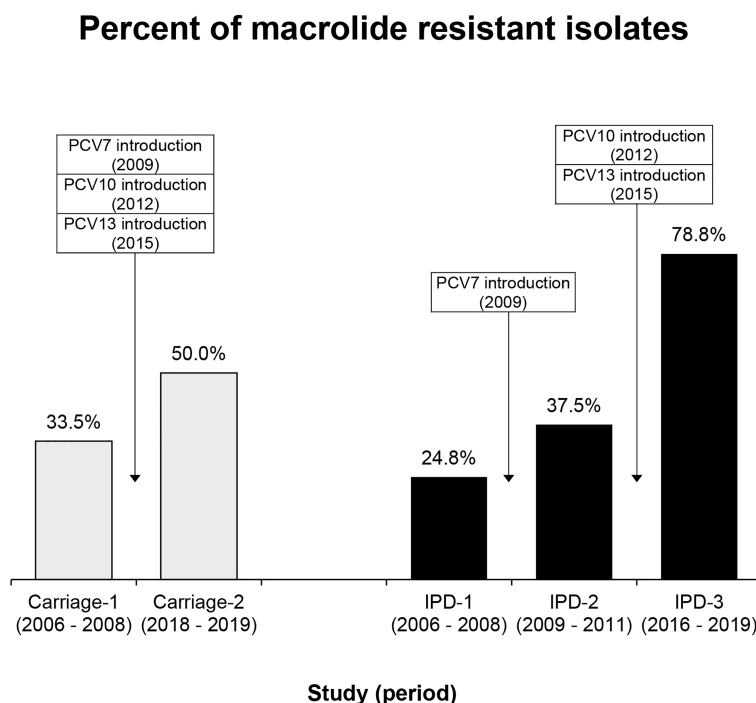


FIGURE 1 | Proportion of macrolide resistance in *S. pneumoniae* isolates in Carriage and IPD studies conducted from 2006 to 2019 in Peru. Carriage-1 (105/313), Carriage-2 (104/208), IPD-1 (25/101), IPD-2 (21/56) and IPD-3 (67/85). Statistical significance among carriage and among IPD studies is $p < 0.001$.

percentages of macrolide resistance increased significantly from 24.8% (IPD-1) and 37.5% (IPD-2) to 78.8% in IPD-3 ($p < 0.001$). Global macrolide resistance in pre-vaccine studies (including IPD-1 and IPD-2 pneumococcal isolates) was 29.3% (46/157).

Macrolide Resistance Genes

Among *S. pneumoniae* strains resistant to macrolides from carriage studies, a total of 80% (84/105) of the strains from the pre-vaccine period and 100% (104/104) of the strains from the post-vaccine period were analyzed to determine the presence of

macrolides resistance genes, *erm*(B) and *mef*(A/E). 21 strains from the Carriage pre-vaccine period were not recovered.

In Carriage studies, the most common macrolide resistance gene was *mef*(A/E), and its prevalence was significantly lower in the post-vaccine period than in the pre-vaccine period (Table 2). In Carriage post-vaccine study, *erm*(B) and *mef*(A/E) were present with similar frequency. There were 2 macrolide-resistant isolates without any of the evaluated genes in pre- and post-vaccine studies, respectively.

The *erm*(B) gene represents the most common mechanism of macrolide resistance among IPD strains. This gene was detected

TABLE 2 | Distribution of macrolide resistance genes.

Study	N	<i>erm</i> (B)		<i>mef</i> (A/E)		only <i>erm</i> (B)		only <i>mef</i> (A/E)		<i>erm</i> (B) + <i>mef</i> (A/E)	
		Positive n (%)	p	Positive n (%)	p	Positive n (%)	p	Positive n (%)	p	Positive n (%)	p
Healthy carrier children's			1.000		0.022		0.953		0.026		0.892
Carriage-1 ^a	84	42 (50.0)		56 (66.7)		26 (30.9)		40 (47.6)		16 (19.1)	
Carriage-2 ^b	104	52 (50.0)		52 (50.0)		33 (31.7)		33 (31.7)		19 (18.3)	
Invasive pneumococcal disease			0.296		0.070		0.103		0.435		0.134
IPD-1 ^a	25	24 (96.0)		12 (48.0)		12 (48.0)		0 (0.0)		12 (48.0)	
IPD-2 ^a	21	20 (95.2)		17 (80.9)		4 (19.1)		1 (4.8)		16 (76.2)	
IPD-3 ^b	67	57 (85.1)		42 (62.7)		20 (29.8)		5 (7.5)		37 (55.2)	

13-valent conjugate vaccine (PCV13) was inserted into the National Immunization Program in 2015.

^aPre-vaccine studies (Pre PCV13).

^bPost-vaccine studies (Post PCV13).

Statistical significance among carriage studies and among IPD studies.

in 96.0% of isolates from IPD-1, 95.2% in IPD-2, and 85.1% in IPD-3 (not statistically different) (Table 2). None of these genes were detected in one and five macrolide-resistant isolates from IPD-1 and IPD-3 respectively.

Macrolide Resistance of 19A Serotype Pneumococcal Isolates

We were able to serotype 472/521 pneumococcal isolates from Carriage and 236/242 pneumococcal isolates from IPD studies. Table 3 shows the 5 most prevalent serotypes from each study, with macrolide resistance rates and resistance genes. We found that the 19A serotype was significantly associated with macrolide resistance in comparison with non-19A serotypes, 80.0% vs. 35.5%, respectively, among carriage strains, and 90.0% vs. 34.4%, respectively, among IPD strains. Macrolide-resistant 19A isolates from carriers were associated with the presence of the *erm(B)* gene ($p=0.002$), while macrolide-resistant 19A

isolates from IPD patients were associated with *mef(A/E)* genes ($p<0.001$).

DISCUSSION

Our results show a significant increase in macrolide resistance through time in *S. pneumoniae* strains isolated in 2 Carriage studies in healthy carrier children, and 3 IPD studies in ill pediatric patients, conducted before and after the introduction of PCV13.

In the post-vaccine Carriage study, 50.0% of pneumococcal isolates were macrolide-resistant. A nasopharyngeal carriage study conducted in Cajamarca, an Andean region of Peru, reported that the frequency of erythromycin-resistant isolates before the introduction of PCV7 was 13.6% (among 125 pneumococcal strains in children < 3 years old) and 22.4% (among 125 pneumococcal strains in children < 3 years old)

TABLE 3 | Most prevalent pneumococcal serotypes, macrolide resistance and genes in carriage and IPD.

Most prevalent serotypes	n (%)	N	Susceptibility Resistant n (%)	N	<i>erm(B)</i> Positive n (%)	<i>mef(A/E)</i> Positive n (%)
Carriage-1 (N=280) ^a						
19F	59 (21.1)	59	30 (50.9)	30	17 (56.7)	28 (93.3)
6B	33 (11.8)	33	12 (36.4)	12	10 (83.3)	2 (16.7)
23F	24 (8.6)	24	7 (29.2)	7	2 (28.6)	5 (71.4)
14	13 (4.6)	13	0	—	—	—
19A ^d	9 (3.2)	9	4 (44.4)	4	4 (100.0)	0
Carriage-2 (N=208) ^c						
15C	24 (11.5)	24	9 (37.5)	9	1 (11.1)	7 (77.8)
19A	21 (10.1)	21	20 (95.2)	20	15 (75.0)	11 (55.0)
6C	21 (10.1)	21	15 (71.4)	15	3 (20.0)	12 (80.0)
23A	17 (8.2)	17	16 (94.1)	16	11 (68.8)	3 (18.8)
15B	15 (7.2)	15	0	—	—	—
IPD-1 (N=99) ^a						
14	26 (26.3)	26	3 (11.5)	3	3 (100.0)	2 (66.7)
6B	20 (20.2)	20	8 (40.0)	8	8 (100.0)	0
19F	11 (11.1)	11	7 (63.6)	7	7 (100.0)	6 (85.7)
23F	6 (6.1)	6	1 (16.7)	1	0	0
19A ^e	4 (4.0)	4	3 (75.0)	3	3 (100.0)	2 (66.7)
IPD-2 (N=58) ^b						
14	11 (19.0)	11	3 (27.3)	3	2 (66.7)	3 (100.0)
19F	9 (15.6)	9	8 (88.9)	8	8 (100.0)	8 (100.0)
23F	6 (10.3)	6	4 (66.7)	4	4 (100.0)	4 (100.0)
6B	6 (10.3)	6	3 (50.0)	3	3 (100.0)	0
19A	5 (8.6)	5	1 (25.0)	1	1 (100.0)	1 (100.0)
IPD-3 (N=81) ^c						
19A	42 (51.9)	42	41 (97.6)	41	36 (87.8)	38 (92.7)
24F	19 (23.5)	19	18 (94.7)	18	15 (83.3)	0
16F	2 (2.5)	2	0	—	—	—
23B	2 (2.5)	2	1 (50.0)	1	1 (100.0)	1 (100.0)
35B	2 (2.5)	2	0	—	—	—

13-valent conjugate vaccine (PCV13) was inserted into the National Immunization Program in 2015.

^aPre-PCV7 introduction.

^bPost-PCV7 introduction.

^cPost-PCV13 introduction.

^dSerotype 19A was number 9 among the most prevalent serotypes in Carriage-1.

^eSerotype 19A was number 6 among the most prevalent serotypes in IPD-1.

after the introduction of PCV7, a lower prevalence than our study (Hanke et al., 2016). In this vaccination period, the frequency of macrolide resistance was evaluated in 4 surveillance studies in Greece; they reported no significant change through time: 22.0% in 2005; 33.3% in 2006; 23.7% in 2007; and 20.5% in 2009 (Grivea et al., 2012). Furthermore, our prevalence is higher than the one reported in Cyprus after the introduction of PCV10 and PCV13, where 20.7% of all *S. pneumoniae* isolates were erythromycin-resistant (Hadjipanayis et al., 2016). A similar study conducted in carrier children Although our results show a significant increase, it is lower than the reported by Hashida et al. (2011) before PCV7 was introduced in the Japan's routine immunization program, with almost 69.4% macrolide-resistant pneumococcal isolates from children who attended daycare centers.

In IPD studies, the percentage of macrolide-resistant strains increased significantly and progressively: 24.8% in IPD-1, 37.5% in IPD-2, and 78.8% in IPD-3. There no other IPD studies in Peru to compare with our data. However, in other countries the results are different. For example, in the United States, the proportion of erythromycin-resistant isolates have not changed significantly after the introduction of PCV7: 19.4% in 1999, and 18.1% in 2004 (Kyaw et al., 2006). This prevalence is similar to the one described by Farrell et al. from American pediatric patients (< 14 years old) with IPD between 2000 and 2004. Additionally, they observed a decrease in the cases of IPD caused by vaccine serotypes and an increase in the cases of IPD by non-vaccine serotypes. In this study, the macrolide resistance did not change (from 40.6% to 38.7%), but the rate of resistance to macrolides in the non-vaccine serotypes increased from 21.0% to 27.0% (Farrell et al., 2007). In Brazil, before and after introduction of PCV10 the frequency of macrolide-resistant isolates was 12.0% and 21.0% respectively (Almeida et al., 2021). In Germany, the frequency of macrolide-resistant pneumococcus after the introduction of PCV7 decreased from 24.7% to 17.2%, and it continued decreasing after the introduction of PCV13 (8.2%) (Imöhl et al., 2015). However, it has been observed that the frequencies of macrolide-resistant *S. pneumoniae* from IPD patients changed temporally and geographically, before and after the introduction of PCVs. Probably the reason why macrolide resistance has not decreased in Peru after the introduction of PCVs is because some resistant serotypes, such as 19A, are still very common, especially among invasive diseases, mainly due to recent introduction of PCV13.

On the other hand, a current meta-analysis, conducted by Andrejko et al. in 2021, evaluated the impact of the introduction of PCVs on antibiotic resistance in more than 300,000 pneumococcal strains worldwide, isolated from carriers and IPDs, but they did not find a significant change in the proportion of non-susceptible isolates after the introduction of PCVs (Andrejko et al., 2021). This is different from our study, where we reported an increase in macrolide resistance in both groups.

In Carriage studies, *mef(A/E)* was the most common gene, and its frequency decreased significantly from 66.7% to 50.0%

after the introduction of PCV13. This frequency was comparable with the proportion found in Greece after the introduction of PCV7, where *mef(A/E)* genes were detected in 47.1% of total macrolide-resistant isolates from 2005 to 2009. Even though, in that country, unlike in Peru, the frequency of these genes increased after the introduction of PCV7 in the National Immunization Plan (41.6% one year before the introduction and 78.0% four years after the introduction) (Grivea et al., 2012). Other studies showed a decrease in the frequency of *mef(A/E)* in macrolide-resistant *S. pneumoniae* isolates in post-vaccine studies in countries with low immunization coverage, such as Russia, where PCV7 was marketed in 2009 but has never been offered for mass vaccination. In 2006, before the introduction of PCV7 in Russia, *mef(A)* was found in 43.8% of pneumococcal isolates (Vorobieva S Jensen et al., 2020), but after PCV7 the frequency of *mef* genes decreased to 13.0% (Mayanskiy et al., 2014). The decrease in the prevalence of *mef(A/E)* in *S. pneumoniae* from nasopharyngeal carrier children could be affected by other factors different than the introduction of PCVs.

In the post-vaccine Carriage study, *erm(B)* gene and, *erm(B)* + *mef(A/E)* were detected in 50.0% and 18.3%, respectively, but a statistically significant association was not found. In Jordan, after the introduction of PCV, *erm(B)* and [*erm(B)* + *mef(A/E)*] genes were detected in 50.0%, and 1.7% of macrolide-resistant *S. pneumoniae* (Al-Lahham et al., 2018). Furthermore, post-introduction of PCV7 in Jordan, Swedan et al. (2016) found that 43.8% of pneumococcal isolates in carrier children under 5 years, presented *erm(B)*, and 6.3% both genes. Even though the *erm(B)* + *mef(A/E)* prevalence is lower, the *erm(B)* frequencies are similar to ours, despite the fact that these studies were conducted in years of low vaccination rates in Jordan.

In pre and post vaccine IPD studies, *erm(B)* was the most frequent gene (85.0% - 96.0%) in macrolide-resistant isolates but, as well *mef(A/E)*, the presence of this gene was not found significantly associated with the introduction of PCVs. Our *erm(B)* frequency was similar that reported in Colombia before PCV13 (98.0%) (Ramos et al., 2014). On the other hand, in Brazil before the introduction of PCV13 *erm(B)* was detected in a lower frequency, 10.0% of intermediate or resistant erythromycin *S. pneumoniae* isolates and 7.0% of those isolates had both genes (Almeida et al., 2021). In the United States, after the introduction of PCV7, was found an increase in 18.0% the proportion of strains positive for both genes between the first and last year of surveillance study, with a corresponding decrease in the prevalence of positive isolates for only *mef(A)* (72.0% to 58.0%) and only *erm(B)* (15.8% to 11.2%) (Farrell et al., 2007). In Germany the *mef(A)* gene decreased in the post vaccine period (13.3% to 3.9% to 0.6%) but the presence of the *erm(B)* gene remained stable (between 3.9% and 5.4%); in addition, an increase in the prevalence of isolates with both genes *mef(A)* and *erm(B)* (0.0% to 0.8% to 1.7%) was observed (Imöhl et al., 2015). On the other hand, in Asia, their antibiotic resistance surveillance system reported that after PCV7 introduction, the macrolide-resistant pneumococcal isolates from IPD patients presented different genotype frequencies among the countries evaluated (Kim et al., 2012). This information support that the distribution of genotypes

among macrolide-resistant *S. pneumoniae* isolates is specific to each country and it is difficult to predict (Kim et al., 2012). We recommend the implementation of a specific surveillance plan to monitor the circulation of drug-resistant pathogens in each country and antimicrobial use.

Before the introduction of PCV13, *mef(A/E)*-encoded efflux pumps were the most common mechanism of macrolide resistance in North America, the United Kingdom, and some European countries (Schroeder and Stephens, 2016). However, in most countries in Europe, Asia and Latin America, *erm(B)* remained the most frequent mechanism. In 2012, the dual macrolide resistance genotype was reported with frequencies up to 52% (Bowers et al., 2012). Among isolates with this dual genotype, *Tn2010* was identified as the main mobile element containing *erm(B)* and *mef(E)/mel* (Del Grosso et al., 2007). Due to the pressure exerted by the first PCV (PCV7), the *Tn2010* “replacement” serotype 19A (ST320) emerged (Del Grosso et al., 2007; Schroeder and Stephens, 2016). ST320 is a multi-drug resistant strain that represents a “capsule switch” from serotype 19F; 19A (ST320) quickly became one of the most prevalent serotypes (Moore et al., 2008; Schroeder and Stephens, 2016; Agudelo et al., 2018). We believe that this replacement is related to the decreased presence of *mef(A/E)* genes and increased macrolide resistance. Further studies by WGS are need in our strains in order to confirm the presence of ST320 strains in Peru.

Serotype 19A was the predominant serotype in our IPD post-vaccine study and the second most common in healthy carrier children, the most common serotype was 15C (Abstract submitted to ISPPD 2022), and in both cases was associated with macrolide resistance. Additionally, the presence of only *erm(B)* and the presence of both genes were associated with this serotype (79.2% and 37.5%, respectively). In Jordan, a study in healthy carrier children reported that among serotype 19A isolates, 50.0% had *erm(B)* gene, 44.9% *mef(A)* and 1.7% both genes, in all cases, lower than the frequencies reported by us (Al-Lahham et al., 2018). In Spain, 71.5% of the serotype 19A strains presented resistance to erythromycin, similar to our findings (Alfayate Miguélez et al., 2020). However, there is still not enough evidence on the distribution of serotypes and their resistance patterns in isolates of pneumococcal carriage children.

S. pneumoniae serotype 19A has emerged as one of the leading causes of invasive disease in many countries, regardless

of whether conjugate pneumococcal vaccines are used (Isturiz et al., 2010). Among serotype 19A pneumococcal isolates from patients with IPD, 90.0% were resistant to macrolides (Table 4), higher than proportion detected in the United States (45.5%) (Farrell et al., 2007), and the average frequency in countries from Latin America (Bolivia, Brasil, Chile, Costa Rica, Republica Dominicana, Ecuador, El Salvador, Guatemala, Nicaragua, Panama, Paraguay y Uruguay) (43.3%) (Moreno et al., 2020). Additionally, our study reports that the presence of only *mef(A/E)* and both genes [*erm(B)* + *mef(A/E)*], was associated with serotype 19A (91.1% and 84.4% respectively). In Brazil, 44.0% of pneumococcal carriers presented the *mef(A)* gene, 36.0% *erm(B)* and both 20.0%, in contrast to our study, serotype 19A was not associated with erythromycin resistance (Caierão et al., 2014). In 2014, the results of the System of Surveillance Networks for Agents Responsible for Bacterial Pneumonia and Meningitis (SIREVA) revealed that serotype 19A prevalence varies from 0% in Nicaragua, Guatemala, and El Salvador to 36.7% in Peru (Pan American Health Organization, 2017). Due to the high prevalence of resistance to macrolides in this serotype, active surveillance is needed to evaluate its temporal and geographical evolution, which will allow better public health actions to control the spread of this serotype among healthy carrier children, who are vulnerable to developing pneumococcal disease (Løvlie et al., 2020).

Our study had some limitations. The focus of our study was on the most common macrolide-resistance mechanisms and we did not test the presence of the less common macrolide-resistance mechanisms, such as *erm(A)*, *erm(TR)*, *mef(I)*, *msr(D)*, *rpID* and *rpIV* (Schroeder and Stephens, 2016). Also, we used different methods of antibiotic susceptibility testing in the pre and post vaccine studies. Additional studies are needed to elucidate the potential impact of PCVs on the distribution of *mef(A/E)*. Despite these limitations, this is the first report of the increase in macrolide-resistance in *Streptococcus pneumoniae* strains after the introduction of the PCV13 vaccine in Lima, Peru. We strongly recommend a new study to evaluate the frequency of macrolide resistance among pneumococcal strains after the COVID-19 pandemic, since this family of antibiotics, especially azithromycin, was widely used for empiric treatment against SARS-CoV-2 in Peru, which could greatly affect the prevalence and mechanisms of macrolide resistance.

TABLE 4 | Macrolide resistance and genes among 19A pneumococcal isolates in carriage and IPD strains.

Serotype	Susceptibility			<i>erm(B)</i>		<i>mef(A/E)</i>		<i>erm(B) + mef(A/E)</i>	
	N	Resistant n (%)	p	N	Positive n (%)	p	Positive n (%)	p	Positive n (%)
Carriage studies									
19A	30	24 (80.0)	< 0.001	24	19 (79.2)	0.002	11 (45.8)	0.163	9 (37.5)
Another serotype	442	157 (35.5)		156	71 (45.5)		95 (60.9)		25 (16.0)
IPD studies									
19A	50	45 (90.0)	< 0.001	45	40 (88.9)	0.767	41 (91.1)	< 0.001	38 (84.4)
Another serotype	186	64 (34.4)		64	58 (90.6)		28 (43.8)		26 (40.6)

Statistical significance among carriage studies and among IPD studies.

DATA AVAILABILITY STATEMENT

The raw data supporting the conclusions of this article will be made available by the authors, without undue reservation.

ETHICS STATEMENT

The studies involving human participants were reviewed and approved by Comité Institucional de Ética en Investigación (CIEI) - Humanos Universidad Peruana Cayetano Heredia. Written informed consent to participate in this study was provided by the participants' legal guardian/next of kin.

AUTHOR CONTRIBUTIONS

BG and EM initiated and designed the macrolide research study. BG and MP-B wrote the first draft of the manuscript. BG, MP-B and NH performed the experiments (antibiotic susceptibility and PCRs) and analyzed and/or interpreted the results. FC, EC, OÁ, MC, AS, IR and TO were in charge of the design and conduct of all five surveillance studies, patient enrollment, sample collection and data acquisition. All authors contributed to the article and approved the submitted version.

FUNDING

The Carriage-1 study was funded by an institutional grant from of “Alberto Hurtado” School of Medicine at Universidad

Peruana Cayetano Heredia, awarded to Dr. Theresa Ochoa. The Carriage-2 study was funded by internal funds of the Pediatric Infectious Diseases Laboratory at the Universidad Peruana Cayetano Heredia. Finally, all IPD studies were supported by a research grant from Pfizer Laboratories to Grupo Peruano de Investigación en Neumococo (GPIN, Peruvian research group on pneumococcus). The external funders had no role in study design, data collection and interpretation, or the decision to submit the work for publication.

ACKNOWLEDGMENTS

We thank all members and study coordinators of Grupo Peruano de Investigación en Neumococo for providing us with the strains and databases of the previous healthy carrier children and IPD studies.

SUPPLEMENTARY MATERIAL

The Supplementary Material for this article can be found online at: <https://www.frontiersin.org/articles/10.3389/fcimb.2022.866186/full#supplementary-material>

REFERENCES

- Adegbola, R. A., DeAntonio, R., Hill, P. C., Roca, A., Usuf, E., Hoet, B., et al. (2014). Carriage of *Streptococcus pneumoniae* and Other Respiratory Bacterial Pathogens in Low and Lower-Middle Income Countries: A Systematic Review and Meta-Analysis. *PLoS One* 9 (8), e103293. doi: 10.1371/journal.pone.0103293
- Agudelo, C. I., DeAntonio, R., and Castañeda, E. (2018). *Streptococcus pneumoniae* Serotype 19A in Latin America and the Caribbean 2010-2015: A Systematic Review and a Time Series Analysis. *Vaccine* 36, 4861–4874. doi: 10.1016/j.vaccine.2018.06.068
- Alfayate Miguélez, S., Yague Guirao, G., Menasalvas Ruiz, A. I., Sanchez-Solis, M., Domenech Lucas, M., González Camacho, F., et al. (2020). Impact of Pneumococcal Vaccination in the Nasopharyngeal Carriage of *Streptococcus pneumoniae* in Healthy Children of the Murcia Region in Spain. *Vaccines* 9 (1), 14. doi: 10.3390/vaccines9010014
- Al-Lahham, A., Qayyas, J. A., and van der Linden, M. (2018). The Impact of the 7-Valent Pneumococcal Conjugate Vaccine on Nasopharyngeal Carriage of *Streptococcus pneumoniae* in Infants of Ajlun Governorate in Jordan. *Jordan J. Biol. Sci.* 11, 155–162.
- Almeida, S. C. G., Lo, S. W., Hawkins, P. A., Gladstone, R. A., Cassiolato, A. P., Klugman, K. P., et al. (2021). Genomic Surveillance of Invasive *Streptococcus pneumoniae* Isolates in the Period Pre-PCV10 and Post-PCV10 Introduction in Brazil. *Microb. Genomics* 7 (10), 635. doi: 10.1099/mgen.0.000635
- Andrejko, K., Ratnasiri, B., Hausdorff, W. P., Laxminarayan, R., and Lewnard, J. A. (2021). Antimicrobial Resistance in Pediatric *Streptococcus pneumoniae* Isolates Amid Global Implementation of Pneumococcal Conjugate Vaccines: A Systematic Review and Meta-Regression Analysis. *Lancet Microbe* 2 (9), e450–e460. doi: 10.1016/S2666-5247(21)00064-1
- Apte, A., Dayma, G., Naziat, H., Williams, L., Sanghavi, S., Uddin, J., et al. (2021). Nasopharyngeal Pneumococcal Carriage in South Asian Infants: Results of Observational Cohort Studies in Vaccinated and Unvaccinated Populations. *J. Glob. Health* 11, 4054. doi: 10.7189/jogh.11.04054
- Bogaert, D., van Belkum, A., Sluiter, M., Luijendijk, A., de Groot, R., Rümke, H. C., et al. (2004). Colonisation by *Streptococcus pneumoniae* and *Staphylococcus aureus* in Healthy Children. *Lancet Lond. Engl.* 363, 1871–1872. doi: 10.1016/S0140-6736(04)16357-5
- Bowers, J. R., Driebe, E. M., Nibecker, J. L., Wojack, B. R., Sarovich, D. S., Wong, A. H., et al. (2012). Dominance of Multidrug Resistant CC271 Clones in Macrolide-Resistant *Streptococcus pneumoniae* in Arizona. *BMC Microbiol.* 12, 12. doi: 10.1186/1471-2180-12-12
- Caierão, J., Hawkins, P., Sant'anna, F. H., da Cunha, G. R., d'Azevedo, P. A., McGee, L., et al. (2014). Serotypes and Genotypes of Invasive *Streptococcus pneumoniae* Before and After PCV10 Implementation in Southern Brazil. *PLoS One* 9 (10), e111129. doi: 10.1371/journal.pone.0111129
- Cheng, A. C., and Jenney, A. W. J. (2016). Macrolide Resistance in Pneumococci—Is It Relevant? *Pneumonia* 8, 10. doi: 10.1186/s41479-016-0010-1
- Cherazard, R., Epstein, M., Doan, T.-L., Salim, T., Bharti, S., and Smith, M. A. (2017). Antimicrobial Resistant *Streptococcus pneumoniae*: Prevalence, Mechanisms, and Clinical Implications. *Am. J. Ther.* 24 (3), e361–e369. doi: 10.1097/MJT.0000000000000551
- Clinical and Laboratory Standards Institute (CLSI) (2008). “Performance Standards for Antimicrobial Susceptibility Testing,” in *Eighteenth Information Supplement in M100-S18* (Wayne, PA: Clinical and Laboratory Standards Institute).
- CLSI (2015). “Performance Standards for Antimicrobial Susceptibility Testing,” in *Twenty-Fifth Information Supplement in M100-S25* (Wayne, PA: Clinical and Laboratory Standards Institute).
- CLSI (2019). “Performance Standards for Antimicrobial Susceptibility Testing,” in *Eighteenth Information Supplement. M100-S29* (Wayne, PA: Clinical and Laboratory Standards Institute).
- Dadonaite, B., and Roser, M. (2018) *Pneumonia* (Our World Data). Available at: <https://ourworldindata.org/pneumonia> (Accessed October 2, 2021).
- Davalos, L., Terrazas, Y., Quintana, A., Egoavil, M., Sedano, K., Castillo, M. E., et al. (2016). Características Epidemiológicas, Clínicas Y Bacteriológicas De

- Meningitis Neumocócica En Pacientes Pediátricos De Lima, Perú. *Rev. Peru. Med. Exp. Salud Publica* 33, 425–431. doi: 10.17843/rpmesp.2016.333.2349
- Del Grosso, M., Northwood, J. G. E., Farrell, D. J., and Pantosti, A. (2007). The Macrolide Resistance Genes *Erm*(B) and *Mef*(E) Are Carried by Tn2010 in Dual-Gene *Streptococcus pneumoniae* Isolates Belonging to Clonal Complex CC271. *Antimicrob. Agents Chemother.* 51 (11), 4184–4186. doi: 10.1128/AAC.00598-07
- Dion, S. B., Major, M., Gabriela Grajales, A., Nepal, R. M., Cane, A., Gessner, B., et al. (2021). Invasive Pneumococcal Disease in Canada 2010–2017: The Role of Current and Next-Generation Higher-Valent Pneumococcal Conjugate Vaccines. *Vaccine* 39 (22), 3007–3017. doi: 10.1016/j.vaccine.2021.02.069
- Doern, G. V. (2006). Macrolide and Ketolide Resistance With *Streptococcus pneumoniae*. *Med. Clin. North Am.* 90 (6), 1109–1124. doi: 10.1016/j.mcna.2006.07.010
- Farrell, D. J., Klugman, K. P., and Pichichero, M. (2007). Increased Antimicrobial Resistance Among Nonvaccine Serotypes of *Streptococcus pneumoniae* in the Pediatric Population After the Introduction of 7-Valent Pneumococcal Vaccine in the United States. *Pediatr Infect. Dis. J.* 26 (2), 123–128. doi: 10.1097/01.inf.0000253059.84602.c3
- Grivea, I. N., Sourla, A., Ntokou, E., Chrysanthopoulou, D. C., Tsantouli, A. G., and Syrogiannopoulos, G. A. (2012). Macrolide Resistance Determinants Among *Streptococcus pneumoniae* Isolates From Carriers in Central Greece. *BMC Infect. Dis.* 12, 255. doi: 10.1186/1471-2334-12-255
- Hadjipanayis, A., Efstathiou, E., Alexandrou, M., Panayiotou, L., Zachariadou, C., Petrou, P., et al. (2016). Nasopharyngeal Pneumococcal Carriage Among Healthy Children in Cyprus Post Widespread Simultaneous Implementation of PCV10 and PCV13 Vaccines. *PLoS One* 11 (10), e0163269. doi: 10.1371/journal.pone.0163269
- Hanke, C. R., Grijalva, C. G., Chochua, S., Pletz, M. W., Hornberg, C., Edwards, K. M., et al. (2016). Bacterial Density, Serotype Distribution and Antibiotic Resistance of Pneumococcal Strains From the Nasopharynx of Peruvian Children Before and After Pneumococcal Conjugate Vaccine 7. *Pediatr. Infect. Dis. J.* 35 (4), 432–439. doi: 10.1097/INF.0000000000001030
- Hashida, K., Shiomi, T., Hohchi, N., Ohkubo, N., Ohbuchi, T., Mori, T., et al. (2011). Nasopharyngeal *Streptococcus pneumoniae* Carriage in Japanese Children Attending Day-Care Centers. *Int. J. Pediatr. Otorhinolaryngol.* 75 (5), 664–669. doi: 10.1016/j.ijporl.2011.02.005
- Imöhl, M., Reinert, R. R., and van der Linden, M. (2015). Antibiotic Susceptibility Rates of Invasive Pneumococci Before and After the Introduction of Pneumococcal Conjugate Vaccination in Germany. *Int. J. Med. Microbiol.* 305 (7), 776–783. doi: 10.1016/j.ijmm.2015.08.031
- Isturiz, R. E., Luna, C. M., and Ramirez, J. (2010). Clinical and Economic Burden of Pneumonia Among Adults in Latin America. *Int. J. Infect. Dis.* 14 (10), e852–856. doi: 10.1016/j.ijid.2010.02.2262
- Kim, S. H., Song, J. H., Chung, D. R., Thamlikitkul, V., Yang, Y., Wang, H., et al. (2012). Changing Trends in Antimicrobial Resistance and Serotypes of *Streptococcus pneumoniae* Isolates in Asian Countries: An Asian Network for Surveillance of Resistant Pathogens (ANSORP) Study. *Antimicrob. Agents Chemother.* 56 (3), 1418–1426. doi: 10.1128/AAC.05658-11
- Kozakova, J., Krizova, P., and Maly, M. (2021). Impact of Pneumococcal Conjugate Vaccine on Invasive Pneumococcal Disease in Children Under 5 Years of Age in the Czech Republic. *PLoS One* 16 (2), e0247862. doi: 10.1371/journal.pone.0247862
- Kyaw, M. H., Lynfield, R., Schaffner, W., Craig, A. S., Hadler, J., Reingold, A., et al. (2006). Effect of Introduction of the Pneumococcal Conjugate Vaccine on Drug-Resistant *Streptococcus pneumoniae*. *N. Engl. J. Med.* 354 (14), 1455–1463. doi: 10.1056/NEJMoa051642
- Løvlie, A., Vestreim, D. F., Aaberge, I. S., and Steens, A. (2020). Changes in Pneumococcal Carriage Prevalence and Factors Associated With Carriage in Norwegian Children, Four Years After Introduction of PCV13. *BMC Infect. Dis.* 20 (1), 29. doi: 10.1186/s12879-019-4754-0
- Luna-Muschi, A., Castillo-Tokumori, F., Deza, M. P., Mercado, E. H., Egoavil, M., Sedano, K., et al. (2019). Invasive Pneumococcal Disease in Hospitalised Children From Lima, Peru Before and After Introduction of the 7-Valent Conjugated Vaccine. *Epidemiol. Infect.* 147, e91. doi: 10.1017/S0950268819000037
- Mayanskiy, N., Alyabieva, N., Ponomarenko, O., Lazareva, A., Katosova, L., Ivanenko, A., et al. (2014). Serotypes and Antibiotic Resistance of non-Invasive *Streptococcus pneumoniae* Circulating in Pediatric Hospitals in Moscow, Russia. *Int. J. Infect. Dis.* 20, 58–62. doi: 10.1016/j.ijid.2013.11.005
- Mercado, E. H., Egoavil, M., Horna, S. G., Torres, N., Velásquez, R., Castillo, M. E., et al. (2012). [Pneumococcal Serotypes in Carrier Children Prior to the Introduction of Anti-Pneumococcal Vaccines in Peru]. *Rev. Peru. Med. Exp. Salud Publica* 29, 53–60. doi: 10.1590/s1726-46342012000100008
- Ministry of Health of Peru (2019) *Clinical Practice Guide for Diagnosis and Treatment of Pneumonia in Children*. Available at: <http://bvs.minsa.gob.pe/local/MINSA/4931.pdf> (Accessed 10.18.21).
- Moore, M. R., Gertz, R. E., Woodbury, R. L., Barkocy-Gallagher, G. A., Schaffner, W., Lexau, C., et al. (2008). Population Snapshot of Emergent *Streptococcus pneumoniae* Serotype 19A in the United States 2005. *J. Infect. Dis.* 197 (7), 1016–1027. doi: 10.1086/528996
- Moreno, J., Duarte, C., Cassiolo, A. P., Chacón, G. C., Alarcon, P., Sánchez, J., et al. (2020). Molecular Characterization of Latin American Invasive *Streptococcus pneumoniae* Serotype 19A Isolates. *Vaccine* 38 (19), 3524–3530. doi: 10.1016/j.vaccine.2020.03.030
- Narváez, P. O., Gomez-Duque, S., Alarcon, J. E., Ramirez-Valbuena, P. C., Serrano-Mayorga, C. C., Lozada-Arcinegas, J., et al. (2021). Invasive Pneumococcal Disease Burden in Hospitalized Adults in Bogotá, Colombia. *BMC Infect. Dis.* 21 (1), 1059. doi: 10.1186/s12879-021-06769-2
- O'Brien, K. L., Wolfson, L. J., Watt, J. P., Henkle, E., Deloria-Knoll, M., McCall, N., et al. (2009). Burden of Disease Caused by *Streptococcus pneumoniae* in Children Younger Than 5 Years: Global Estimates. *Lancet Lond. Engl.* 374 (9693), 893–902. doi: 10.1016/S0140-6736(09)61204-6
- Ochoa, T. J., Egoavil, M., Castillo, M. E., Reyes, I., Chaparro, E., Silva, W., et al. (2010). Invasive Pneumococcal Diseases Among Hospitalized Children in Lima, Peru. *Rev. Panam. Salud Publica* 28(2), 121–127. doi: 10.1590/s1020-49892010000800008
- Pan American Health Organization (2017). *Regional Report of SIREVA II 2014. Data by Country and by Age Groups on the Characteristics of the Isolates of Streptococcus pneumoniae, Haemophilus influenzae and Neisseria meningitidis, in Bacterial Invasive Processes* (Washington D.C: Pan American Health Organization).
- Ramos, V., Duarte, C., Díaz, A., and Moreno, J. (2014). [Mobile Genetic Elements Associated With Erythromycin-Resistant Isolates of *Streptococcus pneumoniae* in Colombia]. *Biomedica* 34 (Suppl. 1), 209–216. doi: 10.7705/biomedica.v34i0.1684
- Rodgers, G. L., and Klugman, K. P. (2011). The Future of Pneumococcal Disease Prevention. *Vaccine* 29 (Suppl. 3), C43–C48. doi: 10.1016/j.vaccine.2011.07.047
- Sader, H. S., Flamm, R. K., Streit, J. M., Carvalhaes, C. G., and Mendes, R. E. (2018). Antimicrobial Activity of Ceftaroline and Comparator Agents Tested Against Organisms Isolated From Patients With Community-Acquired Bacterial Pneumonia in Europe, Asia, and Latin America. *Int. J. Infect. Dis.* 77, 82–86. doi: 10.1016/j.ijid.2018.10.004
- Schroeder, M. R., and Stephens, D. S. (2016). Macrolide Resistance in *Streptococcus pneumoniae*. *Front. Cell. Infect. Microbiol.* 6. doi: 10.3389/fcimb.2016.00098
- Sharew, B., Moges, F., Yismaw, G., Abebe, W., Fentaw, S., Vestreim, D., et al. (2021). Antimicrobial Resistance Profile and Multidrug Resistance Patterns of *Streptococcus pneumoniae* Isolates From Patients Suspected of Pneumococcal Infections in Ethiopia. *Ann. Clin. Microbiol. Antimicrob.* 20 (1), 26. doi: 10.1186/s12941-021-00432-z
- Sutcliffe, J., Grebe, T., Tait-Kamradt, A., and Wondrack, L. (1996). Detection of Erythromycin-Resistant Determinants by PCR. *Antimicrob. Agents Chemother.* 40 (11), 2562–2566. doi: 10.1128/AAC.40.11.2562
- Swedan, S. F., Hayajneh, W. A., and Bshara, G. N. (2016). Genotyping and Serotyping of Macrolide and Multidrug Resistant *Streptococcus pneumoniae* Isolated From Carrier Children. *Indian J. Med. Microbiol.* 34 (2), 159–165. doi: 10.4103/0255-0857.176840
- Varghese, R., Daniel, J. L., Neeravi, A., Baskar, P., Manoharan, A., Sundaram, B., et al. (2021). Multicentric Analysis of Erythromycin Resistance Determinants in Invasive *Streptococcus pneumoniae*; Associated Serotypes and Sequence Types in India. *Curr. Microbiol.* 78 (8), 3239–3245. doi: 10.1007/s00284-021-02594-7
- Vidal, J. E., Ludewick, H. P., Kunkel, R. M., Zähler, D., and Klugman, K. P. (2011). The LuxS-Dependent Quorum-Sensing System Regulates Early Biofilm Formation by *Streptococcus pneumoniae* Strain D39. *Infect. Immun.* 79 (10), 4050–4060. doi: 10.1128/IAI.05186-11
- Vorobieva S Jensen, V., Furberg, A.-S., Slotved, H.-C., Bazhukova, T., Haldorsen, B., Caugant, D. A., et al. (2020). Epidemiological and Molecular Characterization of *Streptococcus pneumoniae* Carriage Strains in Pre-School Children in Arkhangelsk, Northern European Russia, Prior to the Introduction

- of Conjugate Pneumococcal Vaccines. *BMC Infect. Dis.* 20 (1), 279. doi: 10.1186/s12879-020-04998-5
- Wahl, B., O'Brien, K. L., Greenbaum, A., Majumder, A., Liu, L., Chu, Y., et al. (2018). Burden of *Streptococcus pneumoniae* and *Haemophilus influenzae* Type B Disease in Children in the Era of Conjugate Vaccines: Global, Regional, and National Estimates for 2000–15. *Lancet Glob. Health* 6 (7), e744–e757. doi: 10.1016/S2214-109X(18)30247-X
- Walsh, T. R., Weeks, J., Livermore, D. M., and Toleman, M. A. (2011). Dissemination of NDM-1 Positive Bacteria in the New Delhi Environment and its Implications for Human Health: An Environmental Point Prevalence Study. *Lancet Infect. Dis.* 11 (5), 355–362. doi: 10.1016/S1473-3099(11)70059-7
- Wang, C. Y., Chen, Y. H., Fang, C., Zhou, M. M., Xu, H. M., Jing, C. M., et al. (2019). Antibiotic Resistance Profiles and Multidrug Resistance Patterns of *Streptococcus pneumoniae* in Pediatrics: A Multicenter Retrospective Study in Mainland China. *Medicine* 98, e15942. doi: 10.1097/MD.00000000000015942
- World Health Organization (2003) *Manual for the Laboratory Identification and Antimicrobial Susceptibility Testing of Bacterial Pathogens of Public Health Importance in the Developing World: Haemophilus influenzae, Neisseria meningitidis, Streptococcus pneumoniae, Neisseria gonorrhoea, Salmonella Serotype Typhi, Shigella, and Vibrio Cholerae* (Atlanta: World Health Organization). Available at: <https://apps.who.int/iris/handle/10665/68554> (Accessed August 16, 2021).
- Conflict of Interest:** The authors declare that the research was conducted in the absence of any commercial or financial relationships that could be construed as a potential conflict of interest.
- Publisher's Note:** All claims expressed in this article are solely those of the authors and do not necessarily represent those of their affiliated organizations, or those of the publisher, the editors and the reviewers. Any product that may be evaluated in this article, or claim that may be made by its manufacturer, is not guaranteed or endorsed by the publisher.

Copyright © 2022 Gonzales, Mercado, Pinedo-Bardales, Hinostroza, Campos, Chaparro, Del Águila, Castillo, Saenz, Reyes and Ochoa. This is an open-access article distributed under the terms of the Creative Commons Attribution License (CC BY). The use, distribution or reproduction in other forums is permitted, provided the original author(s) and the copyright owner(s) are credited and that the original publication in this journal is cited, in accordance with accepted academic practice. No use, distribution or reproduction is permitted which does not comply with these terms.



Pneumococcal Surface Proteins as Virulence Factors, Immunogens, and Conserved Vaccine Targets

Javid Aceil and Fikri Y. Avci*

Department of Biochemistry and Molecular Biology, Center for Molecular Medicine, The University of Georgia, Athens, GA, United States

Streptococcus pneumoniae is an opportunistic pathogen that causes over 1 million deaths annually despite the availability of several multivalent pneumococcal conjugate vaccines (PCVs). Due to the limitations surrounding PCVs along with an evolutionary rise in antibiotic-resistant and unencapsulated strains, conserved immunogenic proteins as vaccine targets continue to be an important field of study for pneumococcal disease prevention. In this review, we provide an overview of multiple classes of conserved surface proteins that have been studied for their contribution to pneumococcal virulence. Furthermore, we discuss the immune responses observed in response to these proteins and their promise as vaccine targets.

Keywords: *Streptococcus pneumoniae*, PspA, pneumolysin (PLY), PsrP, PhtD pneumococcal histidine triad protein D, conjugate vaccine, pneumococcal protein vaccine, CbpA

OPEN ACCESS

Edited by:

Elsa Bou Ghanem,
University at Buffalo, United States

Reviewed by:

Anders P. Hakansson,
Lund University, Sweden
Walter Adams,
San Jose State University,
United States

*Correspondence:

Fikri Y. Avci
avci@uga.edu

Specialty section:

This article was submitted to
Molecular Bacterial Pathogenesis,
a section of the journal
Frontiers in Cellular and
Infection Microbiology

Received: 09 December 2021

Accepted: 13 April 2022

Published: 12 May 2022

Citation:

Aceil J and Avci FY (2022)
Pneumococcal Surface Proteins as
Virulence Factors, Immunogens, and
Conserved Vaccine Targets.
Front. Cell. Infect. Microbiol. 12:832254.
doi: 10.3389/fcimb.2022.832254

INTRODUCTION

Streptococcus pneumoniae is a Gram-positive bacterial pathogen that lives as a commensal in the host upper respiratory tract but becomes invasive in the lung, ear, or blood (Bogaert et al., 2004; Weiser, 2010). Due to its high infectivity, *S. pneumoniae* (*Spn*) can commonly cause invasive pneumococcal diseases (IPDs) such as community-acquired pneumonia (CAP), and sepsis (Kumar et al., 2008; Weiser et al., 2018). Pneumococcal pneumonia is responsible for approximately 14% of all deaths of children under 5 years old worldwide, with the latest World Health Organization metrics reporting 740,180 deaths in 2019 (WHO, 2019; Cilloniz et al., 2016). Acute otitis media (AOM) remains the most common bacterial infection with high incidence rates and the possibility of re-infection for children <5 (Damoiseaux et al., 2006; Liese et al., 2014).

A major virulence factor of *Spn* is the capsular polysaccharide (CPS), which primarily acts as a shield for the bacterium against the host immune system (Geno et al., 2015). The structural identity of repeat units found within the capsular polysaccharide also distinguishes *Spn* into different serotypes, of which there are now over 100 identified (Ganaie et al., 2020; Ganaie et al., 2021). The pneumococcal conjugate vaccines that exist today have been generated utilizing the CPSs, as the immunogens, of the most prevalent serotypes globally associated with IPD and have been very successful at reducing the rates of IPDs for those included serotypes (Wantuch and Avci, 2018; Wantuch and Avci, 2019). However, factors such as geographic distribution of serotypes, serotype replacement or switching, and an increase in antibiotic-resistant strains all contribute to the persistence of IPD as one of the world's deadliest diseases (Wantuch and Avci, 2018). A first-of-its-

kind global assessment of bacterial antimicrobial resistance associated *Spn* with ~600,000 deaths (Murray et al., 2022). Antibiotic resistance is particularly augmented among serotypes included in the vaccines (Gladstone et al., 2019). Another factor to consider is that PCVs cannot protect against the emergence of non-encapsulated *S. pneumoniae* (NE*Spn*) strains found among non-typeable clinical isolates (Park et al., 2012; Park et al., 2014; Mohale et al., 2016). While NE*Spn*'s are yet to be significantly correlated with IPD, they can still result in infections through AOM (Hotomi et al., 2016) or conjunctivitis (Valentino et al., 2014).

In recent years, studies on molecular mechanisms of glycoconjugate vaccine-induced immune responses have shed light on the knowledge-based vaccine design (Avci et al., 2011; Avci et al., 2012; Middleton et al., 2017; Sun et al., 2019). Researchers have found new therapeutic approaches such as capsule-degrading enzymes (Middleton et al., 2018a; Middleton et al., 2018b; Paschall et al., 2020; Wantuch et al., 2021), capsule-specific protective antibodies (Babb et al., 2021; Ozdilek et al., 2021; Huang et al., 2021), or improved conjugation strategies (Duke et al., 2021). However, identifying and testing vaccine candidates employing conserved *Spn* surface protein immunogens remain an important area of research with the goal of serotype-independent coverage. Recognition of a conserved immunogen across pneumococcal isolates, commonly referred to as a serotype-independent vaccine, would allow for a wider breadth of coverage against pneumococcal pneumonia but would also provide better options for protection against AOM or meningitis. Herein, we describe an up-to-date view on four different classes of the well-studied pneumococcal surface proteins by their function and virulence mechanisms, procured immune response in the host as an immunogen, and potential as vaccine targets (**Table 1**).

CHOLESTEROL-DEPENDENT CYTOLYSIN (CDC)

The CDCs are a family of pore-forming toxins expressed by a multitude of bacterial species and have been shown to have additional and important effects besides their primary activity as beta-hemolytic toxins (Tweten, 2005). The only CDC expressed by *Spn* is pneumolysin (PLY).

PLY

Like other CDCs, PLY contains the threonine-leucine amino acid motif that mediates cholesterol recognition and membrane binding (Farrand et al., 2010). Multiple PLY monomers congregate at cholesterol lipid rafts of a cell to form the pre-pore complex before inserting themselves into the lipid bilayer (Nishimoto et al., 2020). PLY is unique among the CDCs because it has lost its signal peptide for the type II secretion pathway and it incorporates a domain that can activate the classical complement pathway and promote inflammation (Paton et al., 1984). PLY induces necroptosis (Gonzalez-Juarbe et al., 2015; Riegler et al., 2019), apoptosis, and direct cell toxicity (Nishimoto et al., 2020) acting on a plethora of cell types (Beurg et al., 2005; Braun et al., 2007). Another function of PLY is binding to the host receptor, mannose receptor C type-1 (MRC-1), to downregulate inflammation and enhance bacterial survival in the airways (Subramanian et al., 2019). A detailed discussion of PLY pathogenicity can be found here (Nishimoto et al., 2020).

PLY has been studied as a potential vaccine candidate going back decades (Paton et al., 1983; Anderson and Feldman, 2017), as it is present in practically all infectious strains (Kancierski and Mollby, 1987). In mice, monoclonal antibodies against PLY decreased bacterial burden in the lung and protected against invasive disease (Garcia-Suarez Mdel et al., 2004). There is

TABLE 1 | Major *Spn* surface protein immunogens.

Protein	Class	Major Virulence Mechanisms	Representative references
PLY	CDC	Cell Death, MRC-1 binding	(Gonzalez-Juarbe et al., 2015; Riegler et al., 2019; Subramanian et al., 2019; Nishimoto et al., 2020)
PspA	CBP	Inhibits complement, binds to lactoferrin, can bind lactate dehydrogenase	(Tu et al., 1999; Hammerschmidt et al., 1999; Hakansson et al., 2001; Senkovich et al., 2007; Mukerji et al., 2012; Park et al., 2021a)
CbpA	CBP	Inhibits complement, binds to secreted IgA, can bind lactate dehydrogenase	(Hammerschmidt et al., 1997; Haleem et al., 2019; Park et al., 2021a)
PcpA	CBP	Pneumococcal adhesion, biofilm formation	(Sanchez-Beato et al., 1998; Glover et al., 2008)
LytA	CBP	Facilitates release of PLY, inhibits complement	(Carvin et al., 1995; Ramos-Sevillano et al., 2015)
LytB	CBP	Biofilm formation, adherence	(Ramos-Sevillano et al., 2011; Bai et al., 2014)
LytC	CBP	Biofilm formation, adherence	(Ramos-Sevillano et al., 2011)
CbpD	CBP	Assists LytA in cell wall degradation	(Kausmally et al., 2005)
CbpE	CBP	Binds human plasminogen	(Attali et al., 2008a)
CbpF	CBP	Unclear, associated with cell wall hydrolases	(Molina et al., 2009)
CbpG	CBP	Pneumococcal adhesion, secreted form can cleave host extracellular matrix	(Mann et al., 2006)
CbpM	CBP	Binds fibronectin	(Afshar et al., 2016)
PhtA	PHT	Inhibits complement	(Ogunniyi et al., 2009)
PhtD	PHT	Inhibits complement	(Ogunniyi et al., 2009)
PhtE	PHT	Inhibits complement	(Ogunniyi et al., 2009)
PsrP	SRRP	Biofilm formation, lung cell adherence	(Rose et al., 2008; Sanchez et al., 2010)

evidence for anti-PLY antibodies helping delay pneumococcal carriage in high-risk infants (Francis et al., 2009) and protecting healthy individuals against pneumococcal infections (Huo et al., 2004). In mouse immunization experiments, PLY first showed promise when it protected against multiple *Spn* serotypes (Alexander et al., 1994). However, PLY still exhibited hemolytic activity in host cells, even when constructed to have a reduced cytotoxicity (Baba et al., 2001). Different derivatives of a detoxified PLY mutant (dPLY), a recombinant pneumolysoid with the intrinsic cytolytic functionality removed, have shown reactivity to IgGs against the crucial PLY epitopes and have been used successfully as an immunogen for specific serotypes in mice and rhesus macaques (Garcia-Suarez Mdel et al., 2004; Kirkham et al., 2006; Denoel et al., 2011; Salha et al., 2012). Further, chemically detoxified PLY is another derivative that induced anti-PLY IgG response with no sign of tissue damage in host histopathology exams and protected against intranasal challenge across three distinct serotypes (Hermand et al., 2017). More recently, multiple studies have successfully used dPLY or immunogenic regions of PLY as a standalone vaccine candidate to confer protection from *Spn* isolates (Thanawastien et al., 2021). dPLY has also been tested in conjunction with other immunogenic proteins as broadly protective vaccines that have made it up to phase II trials (Feldman and Anderson, 2014; Chen et al., 2015) (Clinical Trial Number, NCT01262872) (Table 2), or as a complementary immunogenic boost for the PCVs (Rowe et al., 2019).

In light of the past and current preclinical research and clinical phase trials, PLY—specifically the recombinant pneumolysoid—has shown significant promise as an important member of the multicomponent protein vaccine approach. PLY's multitudinous detrimental functions on the host (Figure 1A) indicate its potential value as a vaccine target.

CHOLINE-BINDING PROTEINS (CBPS)

CBPs are a major class of *Spn* surface proteins (Perez-Dorado et al., 2012). Phosphorylcholine residues in repeating units of teichoic and lipoteichoic acids on the cell wall allow CBPs to bind

and localize on the surface of *Spn* (Perez-Dorado et al., 2012). CBPs are especially interesting because many orthogonal approaches have unbiasedly reached the same conclusion: most CBPs contribute to bacterial virulence, and are immunogenic targets in human sera exposed to pneumococcal pneumonia (Giefing et al., 2008). Recent advances have been made toward CBPs as candidate antigens in vaccine design as well as expanded knowledge on pathogenicity and virulence mechanisms (Sempere et al., 2021). Here, we review CBPs that have shown contributions to *Spn* pathogenicity and are utilized in preclinical vaccine studies and clinical trial vaccine formulations.

PspA

Pneumococcal surface protein A, PspA, is one of the most well-studied CBPs. Its vaccine potential was initially identified over three decades ago as a protein expressed in all clinically relevant serotypes (Crain et al., 1990). PspA contains an N-terminal alpha-helical domain (α HD), a proline-rich domain (PRD), and the choline-binding domain at the C-terminus (Hollingshead et al., 2000). PspA is, however, highly variable between serotypes and strains in its α HD, being branched into six different clades based on sequence diversity and organized into three families due to sequence homology between clades (Hollingshead et al., 2000). Although there are two main families (Family 1 and Family 2) that encompass the majority of PspA variability, there is also a Family 3 of more uncommon PspAs as well as clinical isolates that do not express PspA. This has made it a challenge to resolve PspA as a conserved protein. PspA is known to bind to lactoferrin (Hammerschmidt et al., 1999; Hakansson et al., 2001; Senkovich et al., 2007) and has been implicated in both pneumococcal carriage as a colonization factor (McCool et al., 2002) and in invasive disease due to its ability to inhibit complement activation and opsonophagocytosis, the main clearance mechanism by the host immune system (Tu et al., 1999; Ren et al., 2003; Mukerji et al., 2012). However, in a serotype 3 strain and a serotype 19F strain, PspA had the added ability as an adhesin to bind GAPDH present on the surface of dying host cells (Park et al., 2021b). Similarly, PspA has recently demonstrated the ability to bind host lactate dehydrogenase (LDH) to enhance pneumococcal virulence through co-opted metabolic activity (Park et al., 2021a). These

TABLE 2 | Representative candidate protein-based vaccine formulations and trials.

Protein	Phase	Identifier	Status	Representative References
PhtD	Phase I	NCT01767402	Completed	(Leroux-Roels et al., 2015)
dPLY, PhtD-dPLY +/- PCV10	Phase I	NCT00707798	Completed	(Leroux-Roels et al., 2014)
PhtD-dPLY	Phase II	NCT00896064	Completed	—
PlyD1	Phase I	NCT01444352	Completed	(Kamtchoua et al., 2013)
PhtD	Phase I	NCT01444001	Completed	(Seiberling et al., 2012)
PcpA, PcpA + PhtD	Phase I	NCT01444339	Completed	(Bologa et al., 2012)
PhtD + PcpA + PlyD1	Phase I	NCT01764126	Completed	(Brooks et al., 2015)
		NCT01446926		
PcsB, StkP, PsaA	Phase I	NCT00873431	Completed	—
dPLY + PsaA + 24 CPS	Phase I/II	NCT03803202	Completed	—
	Phase I	NCT04525599	Active	—
PspA + PlyD	Phase Ia	NCT04087460	Active	—
PHID + dPLY + PhtD	Phase II	NCT01262872	Completed	(Odutola et al., 2016; Odutola et al., 2017; Odutola et al., 2019)

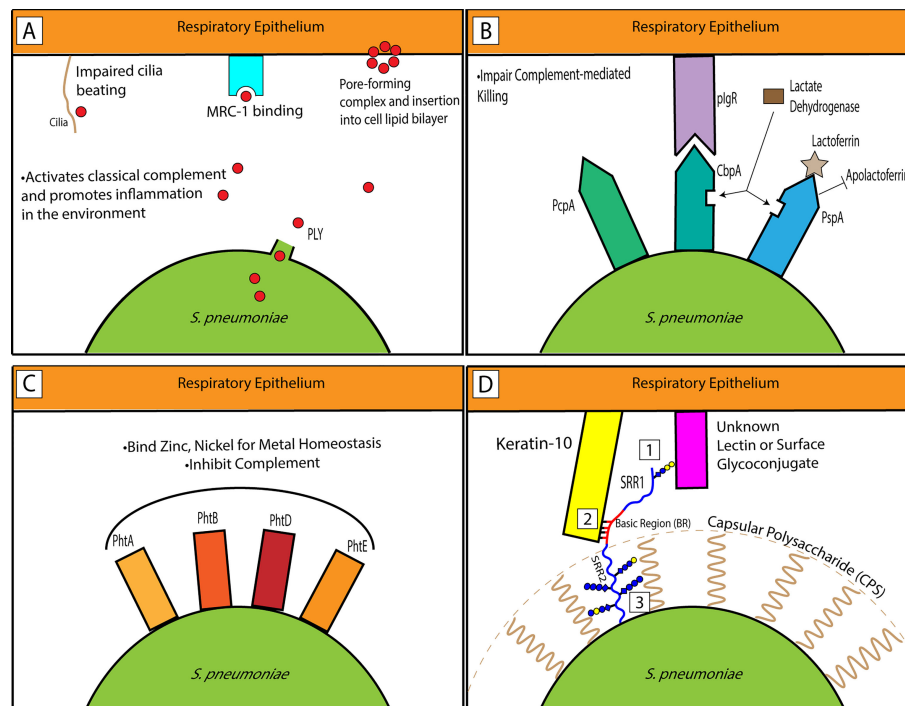


FIGURE 1 | Interactions of pneumococcal factors representative of classes within the host respiratory epithelium. **(A)** PLY is released from *Spn*. It is pro-inflammatory in the environment and PLY monomers aggregate to form ring complexes that can trigger host cell death. It can interact with MRC-1 to promote bacterial survival. **(B)** CBPs impair complement-mediated killing by the host. PcpA influences biofilm formation and pneumococcal adhesion. CbpA binds its main receptor, plgR, to promote adherence. PspA binds lactoferrin for critical iron uptake for the bacterium from the host and inhibits apolactoferrin. Both CbpA and PspA can bind lactate dehydrogenase to enhance virulence. **(C)** The PHTs are well-conserved surface proteins on the pneumococcus and maintain metal homeostasis through Zn and Ni binding. **(D)** A model showing PspR's SRR1-BR region extending past the CPS. While the SRR1 glycans potentially interact with another host ligand (1), the basic region binds Keratin-10 (2). Alternatively, as previously hypothesized, the glycans may be employed as important interactors with the CPS to hoist PspR up so that it can extend past the capsule (3).

findings have culminated in new forms of pathogenicity for PspA and unexplored potential as a vaccine candidate (Lane et al., 2022).

PspA has been investigated for more than three decades as an immunogen and potential vaccine candidate. In a phase I clinical trial, immunizations with a recombinant family 1 PspA produced in *E. coli* and administered to humans showed that PspA was immunogenic, and it passively protected mice against a pneumococcal challenge from serotypes 3, 6A, or 6B (Briles et al., 2000). Later on, a mouse monoclonal antibody specific for PspA induced a robust deposition of complement on the pneumococcal surface indicating a mechanism for PspA specific antibody responses (Ren et al., 2004). Because of its high variability, there was concern that many PspA variants would not be covered by a vaccine; however, recent research has elucidated the proline-rich domain (PRD) of PspA, which is far more conserved, could be used for uncommon strains outside of family 1 or family 2 (Mukerji et al., 2018). Thus, a strong collaboration between a subset of studies has culminated in a trivalent version of PspA that aims to redundantly cover all families and clades of PspA (Nakahashi-Ouchida et al., 2021). Macaques immunized with this trivalent PspA vaccine had high IgG titers towards family 1 or 2 strains and had reduced bacterial

load in the lungs compared to control macaques following an intratracheal challenge from a family 1 and a family 2 PspA strain. PspA is in an active clinical trial as a multicomponent vaccine with PlyD (Clinical Trial Number, NCT04087460) (Table 2). While the variability in PspA remains a challenge, it continues to be a strong candidate with decades of research behind it.

CbpA/PspC

Choline-binding protein A, CbpA, was first identified through its homology with PspA (McDaniel et al., 1992), but unconnectedly found as a pneumococcal protein that binds secretory IgA (SpsA) (Hammerschmidt et al., 1997) and as a novel CBP for its role in adherence and immunogenicity (Rosenow et al., 1997). Because of its unique set of roles, it is viewed as the major adhesin in the pneumococcus. It is also highly polymorphic, with 11 different group classifications based on homology and protein sequence among pneumococcal isolates (Brooks-Walter et al., 1999). This antigenic variation in the protein has recently been indicated as an immune evasion mechanism for the bacterium (Georgieva et al., 2018). CbpA has established roles in nasopharynx colonization and pneumococcal pneumonia (Balachandran

et al., 2002), but is more notably associated with meningitis (Orihuela et al., 2009). CbpA can bind polymeric immunoglobulin receptor (pIgR), which enables the bacterium to translocate across human nasopharyngeal epithelial cells (**Figure 1B**) (Zhang et al., 2000). The binding of CbpA to host protein factor H inhibits the alternative complement pathway (Weiser et al., 2018).

CbpA, similar to PspA, diminishes the effects of complement-mediated killing (Haleem et al., 2019), however, antibodies against CbpA have been shown to activate complement deposition and increase opsonophagocytosis (Ricci et al., 2011). CbpA and PspA have also recently been shown to have similar potential for binding lactate dehydrogenase released from dying host cells enhancing virulence of the bacterium in damaged tissues (Park et al., 2021a). As a vaccine candidate, CbpA has shown the ability to confer protection as the sole immunogen (Ogunniyi et al., 2007; Cao et al., 2009). Anti-CbpA antibodies are induced through help from CD4⁺ T lymphocytes following immunization with CbpA (Cao et al., 2009). However, CbpA has also been coupled with many other pneumococcal immunogens and the responses are additive and longer-lasting (Ogunniyi et al., 2007). One of the combinations involves the above-mentioned pneumolysin and CbpA combined as a fusion protein, which has shown promise as a vaccine with broad protection potential in mouse models of immunization, colonization, and infection (Mann et al., 2014).

PcpA

Pneumococcal choline-binding protein A, also sometimes referred to as CbpN, is another promising vaccine candidate that has emerged. First elucidated as a pneumococcal adhesion protein due to its leucine repeat regions (LRRs) (Sanchez-Beato et al., 1998), it was a hit in the genome-wide mutagenesis screen for lung virulence factors (Hava and Camilli, 2002) and subsequently shown to provide protection in lung infection and sepsis (Glover et al., 2008). Importantly, PcpA is present in all clinically relevant strains tested so far which encompassed 25 different strains (Glover et al., 2008). It has also been shown to be present in over 90 percent of pneumococcal clinical isolates ranging from non-complicated pneumonia to meningitis (Selva et al., 2012).

The virulence of PcpA is attributed to its pneumococcal adhesion and biofilm formation functionalities (Glover et al., 2008). Interestingly, while PcpA elicits protection in the lower respiratory tract, it does not impede colonization of the upper respiratory tract (Glover et al., 2008). PcpA-specific mAbs promote complement C3 deposition and are macrophage-dependent, as removal of either complement or macrophages compromised protection in mice (Visan et al., 2018). For these reasons, there have been multiple vaccination studies involving PcpA (Verhoeven et al., 2014; Verhoeven et al., 2014; Xu et al., 2015; Brooks et al., 2015; Ochs et al., 2016). In one study, PcpA was a component of a trivalent pneumococcal protein vaccine in a mouse model of immunization. PcpA-specific booster serum responses contributed to the clearance of pneumonia and reduced inflammation and tissue damage in the lungs (Xu et al., 2015). These IgG and IgA boosts from the trivalent

protein vaccine, specifically, have also shown a significant reduction in AOM in children (Xu et al., 2017). Due to its demonstrated safety and immunogenic potential against IPD and AOM, PcpA continues to be a mainstay in pneumococcal vaccine formulations in preclinical and clinical studies. PcpA is tested as a vaccine candidate in multiple clinical trials (**Table 2**).

LytA, LytB, LytC

N-acetylmuramoyl-L-alanine amidase (LytA), *N*-acetylglucosaminidase (LytB), and LytC, an autolytic lysozyme involved in polysaccharide cleavage on *N*-acetylmuramoyl-*N*-glucosaminyl residues, comprise a family of cell wall hydrolases (CWH) with established roles in virulence and observed potential for protection.

LytA is the more well-studied of the three enzymes due to its role in lysis being associated with the release of the cytotoxin PLY (Canvin et al., 1995). LytA, independent of its linkage to PLY, has shown an ability to inhibit activation of the alternative and classical pathways of the complement system (Ramos-Sevillano et al., 2015). The same study shows that LytA can cleave the C3b and iC3b components of complement-mediated opsonophagocytosis, indicating its role in evasion of the host immune response (Ramos-Sevillano et al., 2015). Following intranasal immunization with LytA, mice elicited both IgG and IgA antibodies that conferred protection against intranasal and intraperitoneal challenges from strains in serotypes 23F, 19F, 6A, 14, and 6B (Yuan et al., 2011).

LytB has been characterized as a CWH that positions itself at the polar regions on the surface of *Spn* and facilitates localized peptidoglycan hydrolysis and distinct cell separation after multiplying (De Las Rivas et al., 2002). It contributes toward biofilm formation and attachment to host epithelial cells, helps avoid complement-mediated immunity, and is well-conserved (Moscoso et al., 2005; Ramos-Sevillano et al., 2011; Bai et al., 2014). Immunizations with LytB in mice showed a strong IgG response in subclasses IgG1, IgG2b, and IgG3 (Corsini et al., 2016). This study also showed that antibodies against LytB increased recognition towards C1q and C3b to assist classical complement pathway activation and LytB-immunized mice were significantly better protected after challenge with strains in serotypes 23F and 3 (Corsini et al., 2016).

LytC was independently discovered through the same genome wide identification effort of proteins that protected mice from lethal sepsis challenge in which LytB was found (Wizemann et al., 2001). It has been established in similar roles to LytB for nasopharynx colonization and biofilm formation (Gosink et al., 2000; Ramos-Sevillano et al., 2011). However, direct immunization with LytC or antibodies directed against LytC have not as yet been published.

CbpD, CbpE, CbpF, CbpG, CbpM

CbpD has been previously described as a murein hydrolase that works with LytA to degrade the pneumococcal cell wall of cells during the competence (Kausmally et al., 2005). CbpE has been reported as an important receptor for human plasminogen, the precursor of plasmin, and this interaction is intrinsic for pneumococcal dissemination into host tissues

(Attali et al., 2008a; Attali et al., 2008b). CbpF is one of the more abundant proteins of the *Spn* surface, is associated with CWHs like LytA, LytB, and LytC, and has been successfully crystallized (Molina et al., 2007; Molina et al., 2009). These crystal structure studies have resulted in a molecular understanding of esters of bicyclic amines (EBAs) and how they may be used to compete with CBP binding to teichoic acid as a new generation of drugs aimed at limiting pneumococcal growth (Silva-Martin et al., 2014). CbpG was previously identified as a CBP involved in pneumococcal virulence with multifunction as a surface protein for adhesion and as a secreted form that can cleave host extracellular matrix (Gosink et al., 2000; Mann et al., 2006; Attali et al., 2008a). CbpG has been assessed as a protective antigen, where vaccinated mice developed antibodies against CbpG and showed resistance to pneumococcal colonization and statistically significant protection against bacteremia (Mann et al., 2006). CbpM has recently been shown to interact with fibronectin and was recognized in the sera acquired from ten patients with pneumococcal pneumonia (Afshar et al., 2016). CbpG and CbpM also worked well recently as immunogens to protect mice from a serotype 19F challenge (Kazemian et al., 2018).

To sum up, CBPs discussed above have shown vaccine potential in mouse immunization studies and/or human clinical trials. A diverse array of host interactions has been elucidated through pneumococcal adhesion properties associated with different CBPs (**Figure 1B**). PspA virulence has long been linked to its binding to lactoferrin. More recently, it has also been shown to bind host GAPDH and LDH. CbpA binds pIgR and sIgAs. PcpA is an important pneumococcal adhesion protein. Antibodies against any of these targets to neutralize these interactions can serve to weaken the virulence of the bacterium and allow the host immune response to take effect. Difficulties of CBPs as candidate vaccines may come from their sequence variability towards the N-termini, the region that is surface-exposed. While important for pneumococcal virulence, currently none of the proteins discussed in the 'Other CBPs' category have been included in any clinical trial (**Table 2**).

PNEUMOCOCCAL HISTIDINE TRIAD PROTEINS (PHTS)

The pneumococcal histidine triad proteins (PHTs) are a set of surface proteins in the *Streptococcus* genus with a role in metal ion homeostasis and a category-defining HxxHxH protein motif (Plumptre et al., 2012). They were first discovered based on their putative hydrophobic leader sequences, which indicate they were transported across the cytoplasmic membrane and thus were surface-exposed (Adamou et al., 2001). Large-scale mutagenesis screenings for *in vivo* lung infection also showed reduced fitness in bacteria with mutations in *phtA*, *phtB*, or *phtD* (Hava and Camilli, 2002). Including *phtE*, another member of this group, these four gene products redundantly bind and transport zinc (Plumptre et al., 2014). More recently, they have been observed to be highly upregulated in the presence of nickel (Manzoor et al., 2015) and a peptide-based approach revealed a strong binding

potential to nickel as well (Miller et al., 2018). All four PHTs are necessary components for pneumococcal survival and proliferation in the nasopharynx (Plumptre et al., 2014). Like PspA above, PHTs inhibit the complement pathway (**Figure 1C**) (Ogunniyi et al., 2009).

PhtA, PhtB

Pneumococcal histidine triad protein A (PhtA) was the first identified histidine repeat protein in *Spn*. Its sequence was then used to find homologous ORFs, which resulted in the characterization of the PHT family (Adamou et al., 2001). PhtA is highly conserved among the 23 serotypes tested that comprise the PPSV23 multivalent polysaccharide vaccine. Interestingly it was noted that for certain serotypes, PhtA and PhtB have gone through recombination events that have resulted in the resemblance of a fusion protein (Adamou et al., 2001). This has been observed again recently as a PhtA/PhtB fusion protein and a PhtA/PhtD fusion protein (Kawaguchiya et al., 2019). PhtB is also well conserved when it is on its own and not fused with PhtA, sharing 87% sequence homology with PhtD (Adamou et al., 2001). Immunizations with full-length PhtA or full-length PhtB have shown reactive mouse antisera to specific pneumococcal isolates. However, only full-length PhtA bound to all PPSV23 serotype bacterial isolates observed by flow cytometry and conferred protection in mice sepsis challenge with serotype 6A (Adamou et al., 2001). Furthermore, PhtA was present when tested in convalescent sera of 5 infants (Adamou et al., 2001). These findings convey the immunogenicity of this protein as natural to the host response. Immunization in mice with recombinant PhtB conferred protection against serotype 3 intranasal pneumococcal challenge (Zhang et al., 2001). Although they are well conserved and immunogenic, PhtA and PhtB or their fusion proteins have not yet been tested in clinical settings.

PhtD

Pneumococcal histidine triad protein D (PhtD) is the most studied of the PHTs. In one study, immunizations with PhtD protected mice against a serotype 6A sepsis challenge, as well as against a serotype 4 strain and the highly virulent serotype 3 strain, WU2 (Adamou et al., 2001). Purified human serum IgG antibodies recognizing PhtD have been further described, causing a significant reduction of pneumococcal adherence to human airway epithelial cells (Khan and Pichichero, 2012). Furthermore, intranasal immunization with PhtD generated robust antiserum and protected mice against pneumococcal colonization (Khan and Pichichero, 2013). PhtD has gone through phase I trials as a standalone immunogen or in combination with PcpA, showing efficacy at all dosages with no observed adverse reactions (**Table 2**) (Seiberling et al., 2012; Bologa et al., 2012). Recently, it was shown that antibodies against PhtD facilitated pneumococcal clearance through a complement- and macrophage-dependent opsonophagocytosis (Visan et al., 2018). In another study, immunizations of mice with PhtD and a C-terminal fragment of PhtD induced robust humoral immunity protecting mice against pneumococcal challenge (Andre et al., 2021). In sum, PhtD has emerged in

serotype-independent vaccine design due to its robust immune response and feasibility for inclusion in multicomponent vaccine trials.

PhtE

Pneumococcal histidine triad protein E (PhtE) differs from the other PHTs in the family because it has an extra histidine repeat region and it only shares 32% homology with its other family members (Adamou et al., 2001). Immunoblotting with antibody against recombinant PhtE recognized a full-length version as well as a potential mature, truncated version of PhtE in *Spn* whole cell lysates (Adamou et al., 2001). Further work has observed similar results to PhtD, with antibodies against PhtE reducing pneumococcal adherence and protecting mice against colonization (Khan and Pichichero, 2012; Khan and Pichichero, 2013). PhtE, also known as BVH-3, was used to immunize mice and confer protection against pneumococcal challenge (Hamel et al., 2004). PhtE has not yet been evaluated in clinical phase trials.

Of the PHTs, PhtD has shown high promise as a vaccine candidate with efficacy in preclinical animal studies and early human trials. Although immunizations of mice with PhtA, PhtB and PhtE have conferred variable degrees of protection against *Spn* challenge, PhtD had a significantly stronger and larger serotype coverage for the same protection, and it showed significantly higher reactivity against convalescent human sera collected from infants with culture-proven pneumococcal bacteremia (Adamou et al., 2001). Because the C-terminal region of PhtD is sufficient as a robust immunogen, it adds to its potential for inclusion in multicomponent vaccine design. This has been evident in multiple clinical trials (Table 2).

SERINE-RICH REPEAT PROTEINS (SRRPS)

SRRPs are a unique group of very large, glycosylated, surface-exposed proteins in Gram-positive bacteria and are commonly found within the *Streptococcus* genus (Lizcano et al., 2012). They fall in the category of LPXTG proteins, a motif that anchors the protein to the cell wall (Siegel et al., 2017). Because of their large size and abundant glycosylation, they require a dedicated accessory Sec system for transportation and export (Rigel et al., 2009). They are usually categorized as cell adhesins and have been strongly implicated in bacterial virulence from their functional binding (Wu et al., 1998; Siboo et al., 2005; Xiong et al., 2008; Sanchez et al., 2010).

PsrP

In *S. pneumoniae*, the Pneumococcal Serine-Rich Repeat Protein (PsrP) was first identified through large-scale mutagenesis screenings for lung infection (Hava and Camilli, 2002) and subsequently studied as a pathogenicity island (Obert et al., 2006). The PsrP locus is a 37 kB region that contains the protein itself as well as a multitude of specific glycosyltransferases and the

associated Sec transportation machinery (Obert et al., 2006). It has a basic region (BR) between two serine-rich repeat regions (SRR1 and SRR2) that binds to Keratin 10 on lung cells (Shivshankar et al., 2009). *S. pneumoniae* mutants deficient in PsrP are unable to establish lung infection in murine mouse models (Rose et al., 2008). Keratin-10 as a ligand is elevated in cellular senescence of lung cells and these keratin-10/PsrP interactions have been linked to increased susceptibility to pneumococcal pneumonia in the elderly (Shivshankar et al., 2011; Lizcano et al., 2012). Importantly, PsrP is also integral for biofilm formation (Sanchez et al., 2010; Schulte et al., 2016), a major factor in the bacterium's ability to colonize a host and aggregate (Sanchez et al., 2010; Blanchette-Cain et al., 2013).

The mature glycan of an SRRP has been discovered in a different *Streptococcus* species but has yet to be completely and directly elucidated for PsrP (Zhu et al., 2016). Like other SRRPs, PsrP is predicted to be heavily O-glycosylated due to the plethora of serine and threonine residues in the SRR1 and SRR2 regions. GtfA, the glycosyltransferase responsible for adding the first GlcNAc moiety in many SRRPs, was documented to function similarly for PsrP (Shi et al., 2014). GtfA deficient mutants also demonstrated an attenuation of biofilm formation, lung adhesion, and virulence in mice (Lizcano et al., 2017). The second, third, and fourth steps of the PsrP glycosylation pathway have also been elucidated and a proposed model of the complete glycosylation pathway was established (Zhou et al., 2010; Jiang et al., 2017). Recently, however, multiple glycosyltransferases (GTs), including some as-of-yet uncharacterized, were shown to significantly impact PsrP's biofilm formation and adhesion properties as well as lung infection in mice by intratracheal challenge (Middleton et al., 2021).

PsrP is predicted to be present in approximately 50% of all clinical isolates of *Spn* (Munoz-Almagro et al., 2010; Selva et al., 2012). Antibodies against a recombinant portion of PsrP containing the SRR1 and BR regions (rPsrP) were able to neutralize bacterial adhesion to lung cells *in vitro* and passive immunization with rPsrP rabbit antiserum provided protection *in vivo* to mice against challenge (Rose et al., 2008). Although antibodies and passive immunization have shown protection against bacterial lung infection, there isn't established work on PsrP as a vaccine for direct immunizations. It is possible that the glycosylation of PsrP in its native state is an important component of its antigenicity to be understood and harnessed (Figure 1D).

DISCUSSION

When discussing pneumococcal protein vaccine candidates, it is important to emphasize the success of the PCVs in drastically reducing mortality from pneumococcal disease. For a large amount of IPD associated with the serotypes included, the PCVs are a major success story (Avci et al., 2019). However, it is also important to recognize the challenges and complexity of continuing this empirical, serotype-specific approach for

emerging serotypes and unencapsulated isolates (Duke and Avci, 2018; Avci et al., 2019). As the diversity of *Spn* serotypes in clinical isolates continues to increase, higher valency of PCVs will be required. In addition, the possibility of carrier-induced epitope-specific suppression and the known variable humoral response elicited among serotypes included in multivalent preparations represent some of the challenges in the development of conjugate vaccine preparation (Di John et al., 1989; Avci et al., 2019). Thus, current research is exploring many forms of protein vaccine candidates as individual elements, together as multi-component protein vaccines, and a hand-in-hand complementary approach with the PCVs. A conserved pneumococcal vaccine or (to put it ambitiously) a universal pneumococcal vaccine goal has fueled protein-based vaccine research for many decades.

While this review focuses on surface protein candidates isolated from pneumococcus, there are two alternative approaches that have made considerable progress. The first is an inactivated whole-cell vaccine of a non-encapsulated pneumococcal strain that has progressed through pre-clinical trials, showing protection against nasopharyngeal carriage as well as IPD (Keech et al., 2020). Currently, forty-two human patients had safe responses and demonstrated antigen-specific antibodies and T-cell cytokine responses (Keech et al., 2020). The second approach uses a modified, live-attenuated *S. typhimurium* strain as a carrier to deliver the pneumococcal antigen PspA (Zhang et al., 2011). This vector system has shown significant protection in mice with high levels of sIgAs in the nasal mucosa, high IgG levels in serum, and is moving into phase I trials (Zhang et al., 2011; Liu et al., 2020).

Spn surface protein immunogens reviewed have shown variable degrees of protection capacity in preclinical and clinical studies making them candidates for next-generation pneumococcal vaccine formulations. Interestingly, the problems with serotype distribution based on geographical location can impact a protein-based vaccine too. A study using PCR detection of many of the discussed pneumococcal surface proteins observed non-uniform presence of multiple proteins originally expected to be conserved (Blumental et al., 2015), while another study showed downregulation of PcpA and PhtE and no changes in PLY, PspA, or PhtD when comparing serotypes 15A and 35B, two serotypes with increasing incidence rates and outside of PCV coverage (Fuji et al., 2021). Partly due to these reasons, a growing effort has developed for a multi-component approach as opposed to individual proteins in vaccine design (Table 2). A multi-component vaccine target comprised of PLY and PhtD together with 10 serotype-specific polysaccharide conjugates as an exciting prospect, is evaluated in phase II trials (Odutola et al., 2017). A trivalent version of three PspA variants has been generated to provide coverage across all families and clades (Nakahashi-Ouchida et al., 2021), while PspA has also been coupled with CbpA and PLY (Chen et al., 2015). Completed and ongoing trials of protein-based vaccines are listed in Table 2. Of note, most recently new formulations have shown success in mice, and/or macaques, indicating potential future clinical trials to be initiated. A recent study analyzed 100 pneumococcal proteins for

their predicted CD4⁺ T cell immunogenicity, and the prediction results were validated by stimulating human PBMCs (van de Garde et al., 2019). Based on the results of this study, PspA, PLY, and PhtD were indicated as vaccine candidates of interest. The study also noted pneumococcal surface adhesin A (PsaA) and PcsB, a peptidoglycan hydrolase, as potentially important immunogens (van de Garde et al., 2019). While these proteins do not fall into the classes discussed in this review, they are notably present in a unique clinical trial (Clinical Trial Number, NCT00873431). These constructs have all been shown to protect against many clinical isolates, and ongoing preclinical studies and clinical trials will shed light on whether they will reach a similar threshold of efficacy and coverage to PCV13 or the recently launched PCV15 and PCV20.

Considering the virulence mechanisms and current representation in clinical trial vaccine formulations (Table 2), dPLY and PhtD show high promise. Stimulating an antibody response against PLY can protect the host from tissue damage that would result in enhanced virulence and sensitive tissue access for the bacterium, specifically in the lung and heart. It also is present in all pneumococcal strains without variability that some of the other proteins display. Similarly, PhtD has a good prevalence among clinical pneumococcal isolates and has demonstrated strong immunogenic properties in convalescent human sera. Besides these two protein immunogens, PspA has shown to be highly immunogenic and protective albeit with its' high degree of sequence variability in clinical *Spn* isolates. PspA is moving into clinical trials in combination with PLY (Table 2) and has shown potential as a trivalent PspA vaccine in macaques.

PsaA—while not a member of any of the classes reviewed above—is a well-studied, conserved lipoprotein expressed by all *Spn* clinical isolates (Rajam et al., 2008). PsaA is highly immunogenic and it contributes to the pathogenicity of *Spn* (Rajam et al., 2008). It is a surface-exposed zinc binding member of an ABC-type transport system (Lawrence et al., 1998). It also exhibits adhesin properties and binds to human Annexin A2 on airway epithelial cells (Hu et al., 2021). As an immunogen, PsaA has shown vaccine potential, inducing robust immune responses (Johnson et al., 2002; Oliveira et al., 2006; Whaley et al., 2010). In a murine model of colonization with an *Spn* serotype 19A, concomitant administration of recombinant PsaA and PCV7 reduced colonization (Whaley et al., 2010). In a separate study, nasal inoculation of mice with recombinant lactic acid bacteria expressing PsaA induced a systemic and mucosal immune response and decrease in *Spn* colonization (Oliveira et al., 2006). Antibodies against PsaA showed a significant reduction in nasopharyngeal colonization in a mouse nasal colonization model (Johnson et al., 2002). PsaA was included in a promising clinical trial vaccine formulations with two other proteins, StkP and PcsB, that were prevalent in human sera of patients recovered from pneumococcal pneumonia (Giefing et al., 2008) (Clinical Trial Number, NCT00873431) (Table 2). PsaA is also a vaccine component in two other clinical trials (Clinical Trial Numbers, NCT03803202 and NCT04525599) (Table 2).

Sitting mostly on the outside of the pneumococcal protein vaccine conversation has been PsrP. While lung adhesion and biofilm formation are highly important functions for

pneumococcal infection and PsrP has a proven link to these functions, vaccination efforts have not been reported. This may be due to the lower overall prevalence of PsrP in clinical isolates compared to PLY and PspA or the molecular difficulties associated with the size and glycosylation state of the protein. The PCVs have brought significant attention to the possibilities involving glycosylation in vaccine design, but PsrP as a glycoprotein has yet to be considered. The potential role of PsrP glycans as part of B and T cell epitopes (Avci et al., 2011; Sun et al., 2016) may indicate PsrP as a protective vaccine target.

In conclusion, there are many attempts ongoing to achieve a serotype-independent, conserved pneumococcal protein vaccine while the serotype-dependent conjugate vaccines keep IPDs under control on a global scale. A serotype-independent protein vaccine has many potential advantages: a potentially lower-cost alternative for children in developing countries, higher coverage of geographical serotypes that can lead to IPD, or a new/alternative line of defense against AOM infection/recurrent infections. Cutting-edge approaches and innovative knowledge-based vaccine designs are making their way through preclinical research and clinical trials. These stepwise advancements from mice to macaques to humans highlight the

exciting potential for these different surface immunogens in becoming next-generation vaccines.

AUTHOR CONTRIBUTIONS

JA and FA wrote the manuscript. Both authors participated in the editorial process of the manuscript. Both authors have approved the manuscript.

FUNDING

This work was supported by National Institutes of Health grants R01AI123383, R01AI152766, and R41AI157287 (FA).

ACKNOWLEDGMENTS

We thank Drs. Jeremy Duke and Amy Paschall for their editorial assistance.

REFERENCES

- Adamou, J. E., Heinrichs, J. H., Erwin, A. L., Walsh, W., Gayle, T., Dormitzer, M., et al. (2001). Identification and Characterization of a Novel Family of Pneumococcal Proteins That are Protective Against Sepsis. *Infect. Immun.* doi: 10.1128/IAI69.2.949-958.2001
- Afshar, D., Pourmand, M. R., Jeddi-Tehrani, M., Saboor Yaraghi, A. A., Azarsa, M., and Shokri, F. (2016). Fibrinogen and Fibronectin Binding Activity and Immunogenic Nature of Choline Binding Protein M. *Iran J. Public Health* 45, 1610–1617.
- Alexander, J. E., Lock, R. A., Peeters, C. C., Poolman, J. T., Andrew, P. W., Mitchell, T. J., et al. (1994). Immunization of Mice With Pneumolysin Toxoid Confers a Significant Degree of Protection Against at Least Nine Serotypes of *Streptococcus Pneumoniae*. *Infect. Immun.* 62, 5683–5688. doi: 10.1128/iai.62.12.5683-5688.1994
- Anderson, R., and Feldman, C. (2017). Pneumolysin as a Potential Therapeutic Target in Severe Pneumococcal Disease. *J. Infect.* 74, 527–544. doi: 10.1016/j.jinf.2017.03.005
- Andre, G. O., Borges, M. T., Assoni, L., Ferraz, L. F. C., Sakshi, P., Adamson, P., et al. (2021). Protective Role of PhtD and its Amino and Carboxyl Fragments Against Pneumococcal Sepsis. *Vaccine* 39, 3626–3632. doi: 10.1016/j.vaccine.2021.04.068
- Attali, C., Durmort, C., Vernet, T., and Di Guilmi, A. M. (2008a). The Interaction of *Streptococcus Pneumoniae* With Plasmin Mediates Transmigration Across Endothelial and Epithelial Monolayers by Intercellular Junction Cleavage. *Infect. Immun.* 76, 5350–5356. doi: 10.1128/IAI00184-08
- Attali, C., Frolet, C., Durmort, C., Offant, J., Vernet, T., and Di Guilmi, A. M. (2008b). *Streptococcus Pneumoniae* Choline-Binding Protein E Interaction With Plasminogen/Plasmin Stimulates Migration Across the Extracellular Matrix. *Infect. Immun.* 76, 466–476. doi: 10.1128/IAI01261-07
- Avci, F., Berti, F., Dull, P., Hennessey, J., Pavliak, V., Prasad, A. K., et al. (2019). Glycoconjugates: What It Would Take To Master These Well-Known Yet Little-Understood Immunogens for Vaccine Development. *mSphere* 4, e00520-00519. doi: 10.1128/mSphere.00520-19
- Avci, F. Y., Li, X., Tsuji, M., and Kasper, D. L. (2011). A Mechanism for Glycoconjugate Vaccine Activation of the Adaptive Immune System and its Implications for Vaccine Design. *Nat. Med.* 17, 1602–1609. doi: 10.1038/nm.2535
- Avci, F. Y., Li, X., Tsuji, M., and Kasper, D. L. (2012). Isolation of Carbohydrate-Specific CD4(+) T Cell Clones From Mice After Stimulation by Two Model Glycoconjugate Vaccines. *Nat. Protoc.* 7, 2180–2192. doi: 10.1038/nprot.2012.138
- Baba, H., Kawamura, I., Kohda, C., Nomura, T., Ito, Y., Kimoto, T., et al. (2001). Essential Role of Domain 4 of Pneumolysin From *Streptococcus Pneumoniae* in Cytolytic Activity as Determined by Truncated Proteins. *Biochem. Biophys. Res. Commun.* 281, 37–44. doi: 10.1006/bbrc.2001.4297
- Babb, R., Doyle, C. R., Pirofski, L.-A., and Goldberg, J. B. (2021). Isolation and Characterization of Human Monoclonal Antibodies to Pneumococcal Capsular Polysaccharide 3. *Microbiol. Spectr.* 9, e01446-01421. doi: 10.1128/Spectrum.01446-21
- Bai, X. H., Chen, H. J., Jiang, Y. L., Wen, Z., Huang, Y., Cheng, W., et al. (2014). Structure of Pneumococcal Peptidoglycan Hydrolase LytB Reveals Insights Into the Bacterial Cell Wall Remodeling and Pathogenesis. *J. Biol. Chem.* 289, 23403–23416. doi: 10.1074/jbc.M114.579714
- Balachandran, P., Brooks-Walter, A., Virolainen-Julkunen, A., Hollingshead, S. K., and Briles, D. E. (2002). Role of Pneumococcal Surface Protein C in Nasopharyngeal Carriage and Pneumonia and its Ability to Elicit Protection Against Carriage of *Streptococcus Pneumoniae*. *Infect. Immun.* 70, 2526–2534. doi: 10.1128/IAI70.5.2526-2534.2002
- Beurg, M., Hafidi, A., Skinner, L., Cowan, G., Hondarrague, Y., Mitchell, T. J., et al. (2005). The Mechanism of Pneumolysin-Induced Cochlear Hair Cell Death in the Rat. *J. Physiol.* 568, 211–227. doi: 10.1113/jphysiol.2005.092478
- Blanchette-Cain, K., Hinojosa, C. A., Akula Suresh Babu, R., Lizcano, A., Gonzalez-Juarbe, N., Munoz-Almagro, C., et al. (2013). *Streptococcus Pneumoniae* Biofilm Formation is Strain Dependent Multifactorial and Associated With Reduced Invasiveness and Immunoreactivity During Colonization. *mBio* 4, e00745-00713. doi: 10.1128/mBio.00745-13
- Blumental, S., Granger-Farbos, A., Moisi, J. C., Soullie, B., Leroy, P., Njanpop-Lafourcade, B. M., et al. (2015). Virulence Factors of *Streptococcus Pneumoniae*. Comparison Between African and French Invasive Isolates and Implication for Future Vaccines. *PLoS One* 10, e0133885.
- Bogaert, D., De Groot, R., and Hermans, P. W. (2004). *Streptococcus Pneumoniae* Colonisation: The Key to Pneumococcal Disease. *Lancet Infect. Dis.* 4, 144–154. doi: 10.1016/S1473-3099(04)00938-7
- Bologa, M., Kamtchoua, T., Hopfer, R., Sheng, X., Hicks, B., Bixler, G., et al. (2012). Safety and Immunogenicity of Pneumococcal Protein Vaccine Candidates: Monovalent Choline-Binding Protein A (PcpA) Vaccine and Bivalent PcpA-Pneumococcal Histidine Triad Protein D Vaccine. *Vaccine* 30, 7461–7468. doi: 10.1016/j.vaccine.2012.10.076

- Braun, J. S., Hoffmann, O., Schickhaus, M., Freyer, D., Dagand, E., Bermpohl, D., et al. (2007). Pneumolysin Causes Neuronal Cell Death Through Mitochondrial Damage. *Infect. Immun.* 75, 4245–4254. doi: 10.1128/IAI.00031-07
- Briles, D. E., Hollingshead, S. K., King, J., Swift, A., Braun, P. A., Park, M. K., et al. (2000). Immunization of Humans With Recombinant Pneumococcal Surface Protein A (Rpspa) Elicits Antibodies That Passively Protect Mice From Fatal Infection With Streptococcus Pneumoniae Bearing Heterologous PspA. *J. Infect. Dis.* 182, 1694–1701. doi: 10.1086/317602
- Brooks, W. A., Chang, L. J., Sheng, X., Hopfer, R., and Team, P. P. R. S. (2015). Safety and Immunogenicity of a Trivalent Recombinant PcpA PhtD and PlyD1 Pneumococcal Protein Vaccine in Adults Toddlers and Infants: A Phase I Randomized Controlled Study. *Vaccine* 33, 4610–4617. doi: 10.1016/j.vaccine.2015.06.078
- Brooks-Walter, A., Briles, D. E., and Hollingshead, S. K. (1999). The pspC Gene of Streptococcus Pneumoniae Encodes a Polymorphic Protein PspC Which Elicits Cross-Reactive Antibodies to PspA and Provides Immunity to Pneumococcal Bacteremia. *Infect. Immun.* 67, 6533–6542. doi: 10.1128/IAI.67.12.6533-6542.1999
- Canvin, J. R., Marvin, A. P., Sivakumaran, M., Paton, J. C., Boulnois, G. J., Andrew, P. W., et al. (1995). The Role of Pneumolysin and Autolysin in the Pathology of Pneumonia and Septicemia in Mice Infected With a Type 2 Pneumococcus. *J. Infect. Dis.* 172, 119–123. doi: 10.1093/infdis/172.1.119
- Cao, J., Gong, Y., Li, D., Yin, N., Chen, T., Xu, W., et al. (2009). CD4(+) T Lymphocytes Mediated Protection Against Invasive Pneumococcal Infection Induced by Mucosal Immunization With ClpP and CbpA. *Vaccine* 27, 2838–2844. doi: 10.1016/j.vaccine.2009.02.093
- Chen, A., Mann, B., Gao, G., Heath, R., King, J., Maisonneuve, J., et al. (2015). Multivalent Pneumococcal Protein Vaccines Comprising Pneumolysinoid With Epitopes/Fragments of CbpA and/or PspA Elicit Strong and Broad Protection. *Clin. Vaccine Immunol.* 22, 1079–1089. doi: 10.1128/CI.00293-15
- Cilloniz, C., Martin-Loeches, I., Garcia-Vidal, C., San Jose, A., and Torres, A. (2016). Microbial Etiology of Pneumonia: Epidemiology Diagnosis and Resistance Patterns. *Int. J. Mol. Sci.* 17, 2120. doi: 10.3390/ijms17122120
- Corsini, B., Aguinalde, L., Ruiz, S., Domenech, M., Antequera, M. L., Fenoll, A., et al. (2016). Immunization With LytB Protein of Streptococcus Pneumoniae Activates Complement-Mediated Phagocytosis and Induces Protection Against Pneumonia and Sepsis. *Vaccine* 34, 6148–6157. doi: 10.1016/j.vaccine.2016.11.001
- Crain, M. J., Waltman, W. D., Turner, J. S., Yother, J., Talkington, D. F., Mcdaniel, L. S., et al. (1990). Pneumococcal Surface Protein A (PspA) is Serologically Highly Variable and is Expressed by All Clinically Important Capsular Serotypes of Streptococcus Pneumoniae. *Infect. Immun.* 58, 3293–3299. doi: 10.1128/iai.58.10.3293-3299.1990
- Damoiseaux, R. A., Rovers, M. M., Van Balen, F. A., Hoes, A. W., and De Melker, R. A. (2006). Long-Term Prognosis of Acute Otitis Media in Infancy: Determinants of Recurrent Acute Otitis Media and Persistent Middle Ear Effusion. *Fam Pract.* 23, 40–45. doi: 10.1093/fampra/cmi083
- De Las Rivas, B., Garcia, J. L., Lopez, R., and Garcia, P. (2002). Purification and Polar Localization of Pneumococcal LytB a Putative Endo-Beta-N-Acetylglucosaminidase: The Chain-Dispersing Murein Hydrolase. *J. Bacteriol.* 184, 4988–5000. doi: 10.1128/JB.184.18.4988-5000.2002
- Denoe, P., Philipp, M. T., Doyle, L., Martin, D., Carletti, G., and Poolman, J. T. (2011). A Protein-Based Pneumococcal Vaccine Protects Rhesus Macaques From Pneumonia After Experimental Infection With Streptococcus Pneumoniae. *Vaccine* 29, 5495–5501. doi: 10.1016/j.vaccine.2011.05.051
- Di John, D., Wasserman, S. S., Torres, J. R., Cortesia, M. J., Murillo, J., Losonsky, G. A., et al. (1989). Effect of Priming With Carrier on Response to Conjugate Vaccine. *Lancet* 2, 1415–1418. doi: 10.1016/S0140-6736(89)92033-3
- Duke, J. A., and Avci, F. Y. (2018). “Immunological Mechanisms of Glycoconjugate Vaccines,” in *Carbohydrate-Based Vaccines: From Concept to Clinic* (American Chemical Society Washington DC: American Chemical Society), 61–74.
- Duke, J. A., Paschall, A. V., Glushka, J., Lees, A., Moremen, K. W., and Avci, F. Y. (2021). Harnessing Galactose Oxidase in the Development of a Chemoenzymatic Platform for Glycoconjugate Vaccine Design. *J. Biol. Chem.* 101453.
- Farrand, A. J., Lachapelle, S., Hotze, E. M., Johnson, A. E., and Tweten, R. K. (2010). Only Two Amino Acids are Essential for Cytolytic Toxin Recognition of Cholesterol at the Membrane Surface. *Proc. Natl. Acad. Sci. U.S.A.* 107, 4341–4346. doi: 10.1073/pnas.0911581107
- Feldman, C., and Anderson, R. (2014). Review: Current and New Generation Pneumococcal Vaccines. *J. Infect.* 69, 309–325. doi: 10.1016/j.jinf.2014.06.006
- Francis, J. P., Richmond, P. C., Pomat, W. S., Michael, A., Keno, H., Phuanukoonnon, S., et al. (2009). Maternal Antibodies to Pneumolysin But Not to Pneumococcal Surface Protein A Delay Early Pneumococcal Carriage in High-Risk Papua New Guinean Infants. *Clin. Vaccine Immunol.* 16, 1633–1638. doi: 10.1128/CI.00247-09
- Fuji, N., Pichichero, M. E., and Kaur, R. (2021). Comparison of Specific in-Vitro Virulence Gene Expression and Innate Host Response in Locally Invasive vs Colonizer Strains of Streptococcus Pneumoniae. *Med. Microbiol. Immunol.* 210, 111–120. doi: 10.1007/s00430-021-00701-w
- Ganaie, F., Maruhn, K., Li, C., Porambo, R. J., Elverdal, P. L., Abeygunwardana, C., et al. (2021). Structural Genetic and Serological Elucidation of Streptococcus Pneumoniae Serogroup 24 Serotypes: Discovery of a New Serotype 24c With a Variable Capsule Structure. *J. Clin. Microbiol.* 59, e00540-00521. doi: 10.1128/JCM.00540-21
- Ganaie, F., Saad, J. S., Mcgee, L., Van Tonder, A. J., Bentley, S. D., Lo, S. W., et al. (2020). A New Pneumococcal Capsule Type 10D is the 100th Serotype and Has a Large Cps Fragment From an Oral Streptococcus. *mBio* 11. doi: 10.1128/mBio.00937-20
- Garcia-Suarez Mdel, M., Cima-Cabal, M. D., Florez, N., Garcia, P., Cernuda-Cernuda, R., Astudillo, A., et al. (2004). Protection Against Pneumococcal Pneumonia in Mice by Monoclonal Antibodies to Pneumolysin. *Infect. Immun.* 72, 4534–4540. doi: 10.1128/IAI.72.8.4534-4540.2004
- Geno, K. A., Gilbert, G. L., Song, J. Y., Skovsted, I. C., Klugman, K. P., Jones, C., et al. (2015). Pneumococcal Capsules and Their Types: Past Present and Future. *Clin. Microbiol. Rev.* 28, 871–899. doi: 10.1128/CMR.00024-15
- Georgieva, M., Kagedan, L., Lu, Y. J., Thompson, C. M., and Lipsitch, M. (2018). Antigenic Variation in Streptococcus Pneumoniae PspC Promotes Immune Escape in the Presence of Variant-Specific Immunity. *mBio* 9, e00264-00218. doi: 10.1128/mBio.00264-18
- Giefing, C., Meinke, A. L., Hanner, M., Henics, T., Bui, M. D., Gelbmann, D., et al. (2008). Discovery of a Novel Class of Highly Conserved Vaccine Antigens Using Genomic Scale Antigenic Fingerprinting of Pneumococcus With Human Antibodies. *J. Exp. Med.* 205, 117–131. doi: 10.1084/jem.20071168
- Gladstone, R. A., Lo, S. W., Lees, J. A., Croucher, N. J., Van Tonder, A. J., Corander, J., et al. (2019). International Genomic Definition of Pneumococcal Lineages to Contextualise Disease Antibiotic Resistance and Vaccine Impact. *EBioMedicine* 43, 338–346. doi: 10.1016/j.ebiom.2019.04.021
- Glover, D. T., Hollingshead, S. K., and Briles, D. E. (2008). Streptococcus Pneumoniae Surface Protein PcpA Elicits Protection Against Lung Infection and Fatal Sepsis. *Infect. Immun.* 76, 2767–2776. doi: 10.1128/IAI.01126-07
- Gonzalez-Juarbe, N., Gilley, R. P., Hinojosa, C. A., Bradley, K. M., Kamei, A., Gao, G., et al. (2015). Pore-Forming Toxins Induce Macrophage Necroptosis During Acute Bacterial Pneumonia. *PLoS Pathog.* 11, e1005337. doi: 10.1371/journal.ppat.1005337
- Gosink, K. K., Mann, E. R., Guglielmo, C., Tuomanen, E. I., and Masure, H. R. (2000). Role of Novel Choline Binding Proteins in Virulence of Streptococcus Pneumoniae. *Infect. Immun.* 68, 5690–5695. doi: 10.1128/IAI.68.10.5690-5695.2000
- Hakansson, A., Roche, H., Mirza, S., Mcdaniel, L. S., Brooks-Walter, A., and Briles, D. E. (2001). Characterization of Binding of Human Lactoferrin to Pneumococcal Surface Protein A. *Infect. Immun.* 69, 3372–3381. doi: 10.1128/IAI.69.5.3372-3381.2001
- Haleem, K. S., Ali, Y. M., Yesilkaya, H., Kohler, T., Hammerschmidt, S., Andrew, P. W., et al. (2019). The Pneumococcal Surface Proteins PspA and PspC Sequester Host C4-Binding Protein To Inactivate Complement C4b on the Bacterial Surface. *Infect. Immun.* 87, e00742-00718. doi: 10.1128/IAI.00742-18
- Hamel, J., Charland, N., Pineau, I., Ouellet, C., Rioux, S., Martin, D., et al. (2004). Prevention of Pneumococcal Disease in Mice Immunized With Conserved Surface-Accessible Proteins. *Infect. Immun.* 72, 2659–2670. doi: 10.1128/IAI.72.5.2659-2670.2004
- Hammerschmidt, S., Bethe, G., Remane, P. H., and Chhatwal, G. S. (1999). Identification of Pneumococcal Surface Protein A as a Lactoferrin-Binding Protein of Streptococcus Pneumoniae. *Infect. Immun.* 67, 1683–1687. doi: 10.1128/IAI.67.4.1683-1687.1999
- Hammerschmidt, S., Talay, S. R., Brandtzaeg, P., and Chhatwal, G. S. (1997). SpsA a Novel Pneumococcal Surface Protein With Specific Binding to Secretory

- Immunoglobulin A and Secretory Component. *Mol. Microbiol.* 25, 1113–1124. doi: 10.1046/j.1365-2958.1997.5391899.x
- Hava, D. L., and Camilli, A. (2002). Large-Scale Identification of Serotype 4 Streptococcus Pneumoniae Virulence Factors. *Mol. Microbiol.* 45, 1389–1406.
- Hermant, P., Vandercammen, A., Mertens, E., Di Paolo, E., Verlant, V., Denoel, P., et al. (2017). Preclinical Evaluation of a Chemically Detoxified Pneumolysin as Pneumococcal Vaccine Antigen. *Hum. Vaccin Immunother.* 13, 220–228. doi: 10.1080/21645515.2016.1234553
- Hollingshead, S. K., Becker, R., and Briles, D. E. (2000). Diversity of PspA: Mosaic Genes and Evidence for Past Recombination in Streptococcus Pneumoniae. *Infect. Immun.* 68, 5889–5900. doi: 10.1128/IAI.68.10.5889-5900.2000
- Hotomi, M., Nakajima, K., Hiraoka, M., Nahm, M. H., and Yamanaka, N. (2016). Molecular Epidemiology of Nonencapsulated Streptococcus Pneumoniae Among Japanese Children With Acute Otitis Media. *J. Infect. Chemother.* 22, 72–77. doi: 10.1016/j.jiac.2015.10.006
- Huang, J., Gingerich, A. D., Royer, F., Paschall, A. V., Pena-Briseno, A., Avci, F. Y., et al. (2021). Broadly Reactive Human Monoclonal Antibodies Targeting the Pneumococcal Histidine Triad Protein Protect Against Fatal Pneumococcal Infection. *Infect. Immun.* 89, e00747–00720. doi: 10.1128/IAI.00747-20
- Hu, Y., Park, N., Seo, K. S., Park, J. Y., Somarathne, R. P., Olivier, A. K., et al. (2021). Pneumococcal Surface Adhesion A Protein (PsaA) Interacts With Human Annexin A2 on Airway Epithelial Cells. *Virulence* 12, 1841–1854. doi: 10.1080/21505594.2021.1947176
- Huo, Z., Spencer, O., Miles, J., Johnson, J., Holliman, R., Sheldon, J., et al. (2004). Antibody Response to Pneumolysin and to Pneumococcal Capsular Polysaccharide in Healthy Individuals and Streptococcus Pneumoniae Infected Patients. *Vaccine* 22, 1157–1161. doi: 10.1016/j.vaccine.2003.09.025
- Jiang, Y. L., Jin, H., Yang, H. B., Zhao, R. L., Wang, S., Chen, Y., et al. (2017). Defining the Enzymatic Pathway for Polymorphic O-Glycosylation of the Pneumococcal Serine-Rich Repeat Protein PspP. *J. Biol. Chem.* 292, 6213–6224. doi: 10.1074/jbc.M116.770446
- Johnson, S. E., Dykes, J. K., Jue, D. L., Sampson, J. S., Carlone, G. M., and Ades, E. W. (2002). Inhibition of Pneumococcal Carriage in Mice by Subcutaneous Immunization With Peptides From the Common Surface Protein Pneumococcal Surface Adhesin A. *J. Infect. Dis.* 185, 489–496. doi: 10.1086/338928
- Kam Tchoua, T., Bologa, M., Hopfer, R., Neveu, D., Hu, B., Sheng, X., et al. (2013). Safety and Immunogenicity of the Pneumococcal Pneumolysin Derivative PlyD1 in a Single-Antigen Protein Vaccine Candidate in Adults. *Vaccine* 31, 327–333. doi: 10.1016/j.vaccine.2012.11.005
- Kancierski, K., and Molby, R. (1987). Production and Purification of Streptococcus Pneumoniae Hemolysin (Pneumolysin). *J. Clin. Microbiol.* 25, 222–225. doi: 10.1128/jcm.25.2.222-225.1987
- Kausmally, L., Johnsborg, O., Lunde, M., Knutsen, E., and Havarstein, L. S. (2005). Choline-Binding Protein D (CbpD) in Streptococcus Pneumoniae is Essential for Competence-Induced Cell Lysis. *J. Bacteriol.* 187, 4338–4345. doi: 10.1128/JB.187.13.4338-4345.2005
- Kawaguchiya, M., Urushibara, N., Aung, M. S., Shinagawa, M., Takahashi, S., and Kobayashi, N. (2019). Prevalence of Various Vaccine Candidate Proteins in Clinical Isolates of Streptococcus Pneumoniae: Characterization of the Novel Pht Fusion Proteins PhtA/B and PhtA/D. *Pathogens* 8, 162. doi: 10.3390/pathogens8040162
- Kazemian, H., Afshar, D., Garcia, E., Pourmand, M. R., Jeddi-Tehrani, M., Aminharati, F., et al. (2018). CbpM and CbpG of Streptococcus Pneumoniae Elicit a High Protection in Mice Challenged With a Serotype 19f Pneumococcus. *Iran J. Allergy Asthma Immunol.* 17, 574–585.
- Keech, C. A., Morrison, R., Anderson, P., Tate, A., Flores, J., Goldblatt, D., et al. (2020). A Phase 1 Randomized Placebo-Controlled Observer-Blinded Trial to Evaluate the Safety and Immunogenicity of Inactivated Streptococcus Pneumoniae Whole-Cell Vaccine in Adults. *Pediatr. Infect. Dis. J.* 39, 345–351. doi: 10.1097/INF.00000000000002567
- Khan, M. N., and Pichichero, M. E. (2012). Vaccine Candidates PhtD and PhtE of Streptococcus Pneumoniae are Adhesins That Elicit Functional Antibodies in Humans. *Vaccine* 30, 2900–2907. doi: 10.1016/j.vaccine.2012.02.023
- Khan, M. N., and Pichichero, M. E. (2013). CD4 T Cell Memory and Antibody Responses Directed Against the Pneumococcal Histidine Triad Proteins PhtD and PhtE Following Nasopharyngeal Colonization and Immunization and Their Role in Protection Against Pneumococcal Colonization in Mice. *Infect. Immun.* 81, 3781–3792. doi: 10.1128/IAI.00313-13
- Kirkham, L. A., Kerr, A. R., Douce, G. R., Paterson, G. K., Dilts, D. A., Liu, D. F., et al. (2006). Construction and Immunological Characterization of a Novel Nontoxic Protective Pneumolysin Mutant for Use in Future Pneumococcal Vaccines. *Infect. Immun.* 74, 586–593. doi: 10.1128/IAI.74.1.586-593.2006
- Kumar, S., Wang, L., Fan, J., Kraft, A., Bose, M. E., Tiwari, S., et al. (2008). Detection of 11 Common Viral and Bacterial Pathogens Causing Community-Acquired Pneumonia or Sepsis in Asymptomatic Patients by Using a Multiplex Reverse Transcription-PCR Assay With Manual (Enzyme Hybridization) or Automated (Electronic Microarray) Detection. *J. Clin. Microbiol.* 46, 3063–3072. doi: 10.1128/JCM.00625-08
- Lane, J. R., Tata, M., Briles, D. E., and Orihuela, C. J. (2022). A Jack of All Trades: The Role of Pneumococcal Surface Protein A in the Pathogenesis of Streptococcus Pneumoniae. *Front. Cell Infect. Microbiol.* 12, 826264. doi: 10.3389/fcimb.2022.826264
- Lawrence, M. C., Pilling, P. A., Epa, V. C., Berry, A. M., Ogunniyi, A. D., and Paton, J. C. (1998). The Crystal Structure of Pneumococcal Surface Antigen PsaA Reveals a Metal-Binding Site and a Novel Structure for a Putative ABC-Type Binding Protein. *Structure* 6, 1553–1561. doi: 10.1016/S0969-2126(98)00153-1
- Leroux-Roels, I., Devaster, J. M., Leroux-Roels, G., Verlant, V., Henckaerts, I., Moris, P., et al. (2015). Adjuvant System AS02V Enhances Humoral and Cellular Immune Responses to Pneumococcal Protein PhtD Vaccine in Healthy Young and Older Adults: Randomised Controlled Trials. *Vaccine* 33, 577–584. doi: 10.1016/j.vaccine.2013.10.052
- Leroux-Roels, G., Maes, C., De Boever, F., Traskine, M., Ruggeberg, J. U., and Borys, D. (2014). Safety Reactogenicity and Immunogenicity of a Novel Pneumococcal Protein-Based Vaccine in Adults: A Phase I/II Randomized Clinical Study. *Vaccine* 32, 6838–6846. doi: 10.1016/j.vaccine.2014.02.052
- Liese, J. G., Silfverdal, S. A., Giaquinto, C., Carmona, A., Larcombe, J. H., Garcia-Sicilia, J., et al. (2014). Incidence and Clinical Presentation of Acute Otitis Media in Children Aged <6 Years in European Medical Practices. *Epidemiol. Infect.* 142, 1778–1788. doi: 10.1017/S0950268813002744
- Liu, Q., Shen, X., Bian, X., and Kong, Q. (2020). Effect of Deletion of Gene Cluster Involved in Synthesis of Enterobacterial Common Antigen on Virulence and Immunogenicity of Live Attenuated Salmonella Vaccine When Delivering Heterologous Streptococcus Pneumoniae Antigen PspA. *BMC Microbiol.* 20, 150. doi: 10.1186/s12866-020-01837-0
- Lizcano, A., Akula Suresh Babu, R., Shenoy, A. T., Saville, A. M., Kumar, N., D'mello, A., et al. (2017). Transcriptional Organization of Pneumococcal pspP-Secy2a2 and Impact of GtfA and GtfB Deletion on PspP-Associated Virulence Properties. *Microbes Infect.* 19, 323–333. doi: 10.1016/j.micinf.2017.04.001
- Lizcano, A., Sanchez, C. J., and Orihuela, C. J. (2012). A Role for Glycosylated Serine-Rich Repeat Proteins in Gram-Positive Bacterial Pathogenesis. *Mol. Oral. Microbiol.* 27, 257–269. doi: 10.1111/j.2041-1014.2012.00653.x
- Mann, B., Orihuela, C., Antikainen, J., Gao, G., Sublett, J., Korhonen, T. K., et al. (2006). Multifunctional Role of Choline Binding Protein G in Pneumococcal Pathogenesis. *Infect. Immun.* 74, 821–829. doi: 10.1128/IAI.74.2.821-829.2006
- Mann, B., Thornton, J., Heath, R., Wade, K. R., Tweten, R. K., Gao, G., et al. (2014). Broadly Protective Protein-Based Pneumococcal Vaccine Composed of Pneumolysin Toxoid-CbpA Peptide Recombinant Fusion Protein. *J. Infect. Dis.* 209, 1116–1125. doi: 10.1093/infdis/jit502
- Manzoor, I., Shafeeq, S., Afzal, M., and Kuipers, O. P. (2015). The Regulation of the AdcR Regulon in Streptococcus Pneumoniae Depends Both on Zn(2+)- and Ni(2+)-Availability. *Front. Cell Infect. Microbiol.* 5, 91. doi: 10.3389/fcimb.2015.00091
- Mccool, T. L., Cate, T. R., Moy, G., and Weiser, J. N. (2002). The Immune Response to Pneumococcal Proteins During Experimental Human Carriage. *J. Exp. Med.* 195, 359–365. doi: 10.1084/jem.20011576
- Mcdaniel, L. S., Sheffield, J. S., Swiatlo, E., Yother, J., Crain, M. J., and Briles, D. E. (1992). Molecular Localization of Variable and Conserved Regions of pspA and Identification of Additional pspA Homologous Sequences in Streptococcus Pneumoniae. *Microb. Pathog.* 13, 261–269. doi: 10.1016/0882-4010(92)90036-N
- Middleton, D. R., Sun, L., Paschall, A. V., and Avci, F. Y. (2017). T Cell-Mediated Humoral Immune Responses to Type 3 Capsular Polysaccharide of Streptococcus Pneumoniae. *J. Immunol.* 199, 598–603. doi: 10.4049/jimmunol.1700026
- Middleton, D. R., Paschall, A. V., Duke, J. A., and Avci, F. Y. (2018a). Enzymatic Hydrolysis of Pneumococcal Capsular Polysaccharide Renders the Bacterium Vulnerable to Host Defense. *Infect. Immun.* 86, e00316–00318. doi: 10.1128/IAI.00316-18

- Middleton, D. R., Zhang, X., Wantuch, P. L., Ozdilek, A., Liu, X., Lopilato, R., et al. (2018b). Identification and Characterization of the Streptococcus Pneumoniae Type 3 Capsule-Specific Glycoside Hydrolase of Paenibacillus Species 32352. *Glycobiology* 28, 90–99. doi: 10.1093/glycob/cwx097
- Middleton, D. R., Aceil, J., Mustafa, S., Paschall, A. V., and Avci, F. Y. (2021). Glycosyltransferases Within the psrP Locus Facilitate Pneumococcal Virulence. *J. Bacteriol.* 203, e00389-00320. doi: 10.1128/JB.00389-20
- Miller, A., Dudek, D., Potocki, S., Czapor-Irzabek, H., Kozłowski, H., and Rowinska-Zyrek, M. (2018). Pneumococcal Histidine Triads - Involved Not Only in Zn(2+) But Also Ni(2+) Binding? *Metallomics* 10, 1631–1637. doi: 10.1039/C8MT00275D
- Mohale, T., Wolter, N., Allam, M., Ndlangisa, K., Crowther-Gibson, P., Du Plessis, M., et al. (2016). Genomic Analysis of Nontypeable Pneumococci Causing Invasive Pneumococcal Disease in South Africa 2003–2013. *BMC Genomics* 17, 470. doi: 10.1186/s12864-016-2808-x
- Molina, R., Gonzalez, A., Moscoso, M., Garcia, P., Stelter, M., Kahn, R., et al. (2007). Crystallization and Preliminary X-Ray Diffraction Studies of Choline-Binding Protein F From Streptococcus Pneumoniae. *Acta Crystallogr. Sect. F Struct. Biol. Cryst. Commun.* 63, 742–745. doi: 10.1107/S1744309107035865
- Molina, R., Gonzalez, A., Stelter, M., Perez-Dorado, I., Kahn, R., Morales, M., et al. (2009). Crystal Structure of CbpF a Bifunctional Choline-Binding Protein and Autolysis Regulator From Streptococcus Pneumoniae. *EMBO Rep.* 10, 246–251. doi: 10.1038/embor.2008.245
- Moscoso, M., Obregon, V., Lopez, R., Garcia, J. L., and Garcia, E. (2005). Allelic Variation of Polymorphic Locus lytB Encoding a Choline-Binding Protein From Streptococci of the Mitis Group. *Appl. Environ. Microbiol.* 71, 8706–8713. doi: 10.1128/AEM.71.12.8706-8713.2005
- Mukerji, R., Mirza, S., Roche, A. M., Widener, R. W., Croney, C. M., Rhee, D. K., et al. (2012). Pneumococcal Surface Protein A Inhibits Complement Deposition on the Pneumococcal Surface by Competing With the Binding of C-Reactive Protein to Cell-Surface Phosphocholine. *J. Immunol.* 189, 5327–5335. doi: 10.4049/jimmunol.1201967
- Mukerji, R., Hendrickson, C., Genschmer, K. R., Park, S. S., Bouchet, V., Goldstein, R., et al. (2018). The Diversity of the Proline-Rich Domain of Pneumococcal Surface Protein A (PspA): Potential Relevance to a Broad-Spectrum Vaccine. *Vaccine* 36, 6834–6843. doi: 10.1016/j.vaccine.2018.08.045
- Munoz-Almagro, C., Selva, L., Sanchez, C. J., Esteve, C., De Sevilla, M. F., Pallares, R., et al. (2010). PspA a Protective Pneumococcal Antigen is Highly Prevalent in Children With Pneumonia and is Strongly Associated With Clonal Type. *Clin. Vaccine Immunol.* 17, 1672–1678. doi: 10.1128/DOI.00271-10
- Murray, C. J. L., Ikuta, K. S., Sharara, F., Swetschinski, L., Robles Aguilar, G., Gray, A., et al. (2022). Global Burden of Bacterial Antimicrobial Resistance in 2019: A Systematic Analysis. *Lancet* 399, 606–607. doi: 10.1016/S0140-6736(21)02724-0
- Nakashishi-Ouchida, R., Uchida, Y., Yuki, Y., Katakai, Y., Yamanoue, T., Ogawa, H., et al. (2021). A Nanogel-Based Trivalent PspA Nasal Vaccine Protects Macaques From Intratracheal Challenge With Pneumococci. *Vaccine* 39, 3353–3364. doi: 10.1016/j.vaccine.2021.04.069
- Nishimoto, A. T., Rosch, J. W., and Tuomanen, E. I. (2020). Pneumolysin: Pathogenesis and Therapeutic Target. *Front. Microbiol.* 11, 1543. doi: 10.3389/fmicb.2020.01543
- Obert, C., Sublett, J., Kaushal, D., Hinojosa, E., Barton, T., Tuomanen, E. I., et al. (2006). Identification of a Candidate Streptococcus Pneumoniae Core Genome and Regions of Diversity Correlated With Invasive Pneumococcal Disease. *Infect. Immun.* 74, 4766–4777. doi: 10.1128/IAI.00316-06
- Ochs, M. M., Williams, K., Sheung, A., Lheritier, P., Visan, L., Rouleau, N., et al. (2016). A Bivalent Pneumococcal Histidine Triad Protein D-Choline-Binding Protein A Vaccine Elicits Functional Antibodies That Passively Protect Mice From Streptococcus Pneumoniae Challenge. *Hum. Vaccin Immunother.* 12, 2946–2952. doi: 10.1080/21645515.2016.1202389
- Odutola, A., Ota, M. O., Ogundare, E. O., Antonio, M., Owiafe, P., Worwui, A., et al. (2016). Reactogenicity Safety and Immunogenicity of a Protein-Based Pneumococcal Vaccine in Gambian Children Aged 2–4 Years: A Phase II Randomized Study. *Hum. Vaccin Immunother.* 12, 393–402. doi: 10.1080/21645515.2015.1111496
- Odutola, A., Ota, M. O. C., Antonio, M., Ogundare, E. O., Saidu, Y., Foster-Nyarko, E., et al. (2017). Efficacy of a Novel Protein-Based Pneumococcal Vaccine Against Nasopharyngeal Carriage of Streptococcus Pneumoniae in Infants: A Phase 2 Randomized Controlled Observer-Blind Study. *Vaccine* 35, 2531–2542. doi: 10.1016/j.vaccine.2017.03.071
- Odutola, A., Ota, M. O. C., Antonio, M., Ogundare, E. O., Saidu, Y., Owiafe, P. K., et al. (2019). Immunogenicity of Pneumococcal Conjugate Vaccine Formulations Containing Pneumococcal Proteins and Immunogenicity and Reactogenicity of Co-Administered Routine Vaccines - A Phase II Randomised Observer-Blind Study in Gambian Infants. *Vaccine* 37, 2586–2599. doi: 10.1016/j.vaccine.2019.03.033
- Ogunniyi, A. D., Grabowicz, M., Briles, D. E., Cook, J., and Paton, J. C. (2007). Development of a Vaccine Against Invasive Pneumococcal Disease Based on Combinations of Virulence Proteins of Streptococcus Pneumoniae. *Infect. Immun.* 75, 350–357. doi: 10.1128/IAI.01103-06
- Ogunniyi, A. D., Grabowicz, M., Mahdi, L. K., Cook, J., Gordon, D. L., Sadlon, T. A., et al. (2009). Pneumococcal Histidine Triad Proteins are Regulated by the Zn2+-Dependent Repressor AdcR and Inhibit Complement Deposition Through the Recruitment of Complement Factor H. *FASEB J.* 23, 731–738. doi: 10.1096/fj.08-119537
- Oliveira, M. L., Areas, A. P., Campos, I. B., Monedero, V., Perez-Martinez, G., Miyaji, E. N., et al. (2006). Induction of Systemic and Mucosal Immune Response and Decrease in Streptococcus Pneumoniae Colonization by Nasal Inoculation of Mice With Recombinant Lactic Acid Bacteria Expressing Pneumococcal Surface Antigen A. *Microbes Infect.* 8, 1016–1024. doi: 10.1016/j.micinf.2005.10.020
- Orihuela, C. J., Mahdavi, J., Thornton, J., Mann, B., Wooldridge, K. G., Abouseada, N., et al. (2009). Laminin Receptor Initiates Bacterial Contact With the Blood Brain Barrier in Experimental Meningitis Models. *J. Clin. Invest.* 119, 1638–1646. doi: 10.1172/JCI36759
- Ozdilek, A., Huang, J., Babb, R., Paschall, A. V., Middleton, D. R., Duke, J. A., et al. (2021). A Structural Model for the Ligand Binding of Pneumococcal Serotype 3 Capsular Polysaccharide-Specific Protective Antibodies. *mBio* 12, e0080021. doi: 10.1128/mBio.00800-21
- Park, I. H., Kim, K. H., Andrade, A. L., Briles, D. E., McDaniel, L. S., and Nahm, M. H. (2012). Nontypeable Pneumococci can be Divided Into Multiple Cps Types Including One Type Expressing the Novel Gene pspK. *mBio* 3, e000035-000012. doi: 10.1128/mBio.00035-12
- Park, I. H., Geno, K. A., Sherwood, L. K., Nahm, M. H., and Beall, B. (2014). Population-Based Analysis of Invasive Nontypeable Pneumococci Reveals That Most Have Defective Capsule Synthesis Genes. *PLoS One* 9, e97825. doi: 10.1371/journal.pone.0097825
- Park, S. S., Gonzalez-Juarbe, N., Martinez, E., Hale, J. Y., Lin, Y. H., Huffines, J. T., et al. (2021a). Streptococcus Pneumoniae Binds to Host Lactate Dehydrogenase via PspA and PspC To Enhance Virulence. *mBio* 12, e00673-00621. doi: 10.1128/mBio.00673-21
- Park, S. S., Gonzalez-Juarbe, N., Riegler, A. N., Im, H., Hale, Y., Platt, M. P., et al. (2021b). Streptococcus Pneumoniae Binds to Host GAPDH on Dying Lung Epithelial Cells Worsening Secondary Infection Following Influenza. *Cell Rep.* 35, 109267. doi: 10.1016/j.celrep.2021.109267
- Paschall, A. V., Middleton, D. R., Wantuch, P. L., and Avci, F. Y. (2020). Therapeutic Activity of Type 3 Streptococcus Pneumoniae Capsule Degrading Enzyme Pn3Pase. *Pharm. Res.* 37, 236. doi: 10.1007/s11095-020-02960-3
- Paton, J. C., Lock, R. A., and Hansman, D. J. (1983). Effect of Immunization With Pneumolysin on Survival Time of Mice Challenged With Streptococcus Pneumoniae. *Infect. Immun.* 40, 548–552. doi: 10.1128/iai.40.2.548-552.1983
- Paton, J. C., Rowan-Kelly, B., and Ferrante, A. (1984). Activation of Human Complement by the Pneumococcal Toxin Pneumolysin. *Infect. Immun.* 43, 1085–1087. doi: 10.1128/iai.43.3.1085-1087.1984
- Perez-Dorado, I., Galan-Bartual, S., and Hermoso, J. A. (2012). Pneumococcal Surface Proteins: When the Whole is Greater Than the Sum of its Parts. *Mol. Oral. Microbiol.* 27, 221–245. doi: 10.1111/j.2041-1014.2012.00655.x
- Plumtree, C. D., Hughes, C. E., Harvey, R. M., Eijkelkamp, B. A., Mcdevitt, C. A., and Paton, J. C. (2014). Overlapping Functionality of the Pht Proteins in Zinc Homeostasis of Streptococcus Pneumoniae. *Infect. Immun.* 82, 4315–4324. doi: 10.1128/IAI.02155-14
- Plumtree, C. D., Ogunniyi, A. D., and Paton, J. C. (2012). Polyhistidine Triad Proteins of Pathogenic Streptococci. *Trends Microbiol.* 20, 485–493. doi: 10.1016/j.tim.2012.06.004

- Rajam, G., Anderton, J. M., Carlone, G. M., Sampson, J. S., and Ades, E. W. (2008). Pneumococcal Surface Adhesin A (PsaA): A Review. *Crit. Rev. Microbiol.* 34, 163–173. doi: 10.1080/10408410802383610
- Ramos-Sevillano, E., Moscoso, M., Garcia, P., Garcia, E., and Yuste, J. (2011). Nasopharyngeal Colonization and Invasive Disease are Enhanced by the Cell Wall Hydrolases LytB and LytC of *Streptococcus Pneumoniae*. *PLoS One* 6, e23626. doi: 10.1371/journal.pone.0023626
- Ramos-Sevillano, E., Urzainqui, A., Campuzano, S., Moscoso, M., Gonzalez-Camacho, F., Domenech, M., et al. (2015). Pleiotropic Effects of Cell Wall Amidase LytA on *Streptococcus Pneumoniae* Sensitivity to the Host Immune Response. *Infect. Immun.* 83, 591–603. doi: 10.1128/IAI.02811-14
- Ren, B., Szalai, A. J., Thomas, O., Hollingshead, S. K., and Briles, D. E. (2003). Both Family 1 and Family 2 PspA Proteins can Inhibit Complement Deposition and Confer Virulence to a Capsular Serotype 3 Strain of *Streptococcus Pneumoniae*. *Infect. Immun.* 71, 75–85. doi: 10.1128/IAI.71.1.75-85.2003
- Ren, B., Szalai, A. J., Hollingshead, S. K., and Briles, D. E. (2004). Effects of PspA and Antibodies to PspA on Activation and Deposition of Complement on the Pneumococcal Surface. *Infect. Immun.* 72, 114–122. doi: 10.1128/IAI.72.1.114-122.2004
- Ricci, S., Janulczyk, R., Gerlini, A., Braione, V., Colomba, L., Iannelli, F., et al. (2011). The Factor H-Binding Fragment of PspC as a Vaccine Antigen for the Induction of Protective Humoral Immunity Against Experimental Pneumococcal Sepsis. *Vaccine* 29, 8241–8249. doi: 10.1016/j.vaccine.2011.08.119
- Riegler, A. N., Brissac, T., Gonzalez-Juarbe, N., and Orihuela, C. J. (2019). Necroptotic Cell Death Promotes Adaptive Immunity Against Colonizing Pneumococci. *Front. Immunol.* 10, 615. doi: 10.3389/fimmu.2019.00615
- Rigel, N. W., Gibbons, H. S., McCann, J. R., McDonough, J. A., Kurtz, S., and Braunstein, M. (2009). The Accessory SecA2 System of *Mycobacteria* Requires ATP Binding and the Canonical SecA1. *J. Biol. Chem.* 284, 9927–9936. doi: 10.1074/jbc.M900325200
- Rose, L., Shivshankar, P., Hinojosa, E., Rodriguez, A., Sanchez, C. J., and Orihuela, C. J. (2008). Antibodies Against PsrP a Novel *Streptococcus Pneumoniae* Adhesin Block Adhesion and Protect Mice Against Pneumococcal Challenge. *J. Infect. Dis.* 198, 375–383. doi: 10.1086/589775
- Rosenow, C., Ryan, P., Weiser, J. N., Johnson, S., Fontan, P., Ortqvist, A., et al. (1997). Contribution of Novel Choline-Binding Proteins to Adherence Colonization and Immunogenicity of *Streptococcus Pneumoniae*. *Mol. Microbiol.* 25, 819–829. doi: 10.1111/j.1365-2958.1997.mmi494.x
- Rowe, H. M., Mann, B., Iverson, A., Poole, A., Tuomanen, E., and Rosch, J. W. (2019). A Cross-Reactive Protein Vaccine Combined With PCV-13 Prevents *Streptococcus Pneumoniae*- and *Haemophilus Influenzae*-Mediated Acute Otitis Media. *Infect. Immun.* 87, e00253-00219. doi: 10.1128/IAI.00253-19
- Salha, D., Szeto, J., Myers, L., Claus, C., Sheung, A., Tang, M., et al. (2012). Neutralizing Antibodies Elicited by a Novel Detoxified Pneumolysin Derivative PlyD1 Provide Protection Against Both Pneumococcal Infection and Lung Injury. *Infect. Immun.* 80, 2212–2220. doi: 10.1128/IAI.06348-11
- Sanchez-Beato, A. R., Lopez, R., and Garcia, J. L. (1998). Molecular Characterization of PcpA: A Novel Choline-Binding Protein of *Streptococcus Pneumoniae*. *FEMS Microbiol. Lett.* 164, 207–214. doi: 10.1111/j.1574-6968.1998.tb13087.x
- Sanchez, C. J., Shivshankar, P., Stol, K., Trakhtenbroit, S., Sullam, P. M., Sauer, K., et al. (2010). The Pneumococcal Serine-Rich Repeat Protein is an Intra-Species Bacterial Adhesin That Promotes Bacterial Aggregation *In Vivo* and in Biofilms. *PLoS Pathog.* 6, e1001044. doi: 10.1371/journal.ppat.1001044
- Schulte, T., Mikaelsson, C., Beaussart, A., Kikhney, A., Deshmukh, M., Wolniak, S., et al. (2016). The BR Domain of PsrP Interacts With Extracellular DNA to Promote Bacterial Aggregation; Structural Insights Into Pneumococcal Biofilm Formation. *Sci. Rep.* 6, 32371. doi: 10.1038/srep32371
- Seiberling, M., Bologa, M., Brookes, R., Ochs, M., Go, K., Neveu, D., et al. (2012). Safety and Immunogenicity of a Pneumococcal Histidine Triad Protein D Vaccine Candidate in Adults. *Vaccine* 30, 7455–7460. doi: 10.1016/j.vaccine.2012.10.080
- Selva, L., Ciruela, P., Blanchette, K., Del Amo, E., Pallares, R., Orihuela, C. J., et al. (2012). Prevalence and Clonal Distribution of pcpA psrP and Pilus-1 Among Pediatric Isolates of *Streptococcus Pneumoniae*. *PLoS One* 7, e41587. doi: 10.1371/journal.pone.0041587
- Sempere, J., Llamasi, M., Del Rio Menendez, I., Lopez Ruiz, B., Domenech, M., and Gonzalez-Camacho, F. (2021). Pneumococcal Choline-Binding Proteins Involved in Virulence as Vaccine Candidates. *Vaccines (Basel)* 9, 181. doi: 10.3390/vaccines9020181
- Senkovich, O., Cook, W. J., Mirza, S., Hollingshead, S. K., Protasevich Ii Briles, D. E., et al. (2007). Structure of a Complex of Human Lactoferrin N-Lobe With Pneumococcal Surface Protein a Provides Insight Into Microbial Defense Mechanism. *J. Mol. Biol.* 370, 701–713. doi: 10.1016/j.jmb.2007.04.075
- Shi, W. W., Jiang, Y. L., Zhu, F., Yang, Y. H., Shao, Q. Y., Yang, H. B., et al. (2014). Structure of a Novel O-Linked N-Acetyl-D-Glucosamine (O-GlcNAc) Transferase GtfA Reveals Insights Into the Glycosylation of Pneumococcal Serine-Rich Repeat Adhesins. *J. Biol. Chem.* 289, 20898–20907. doi: 10.1074/jbc.M114.581934
- Shivshankar, P., Sanchez, C., Rose, L. F., and Orihuela, C. J. (2009). The *Streptococcus Pneumoniae* Adhesin PsrP Binds to Keratin 10 on Lung Cells. *Mol. Microbiol.* 73, 663–679. doi: 10.1111/j.1365-2958.2009.06796.x
- Shivshankar, P., Boyd, A. R., Le Saux, C. J., Yeh, I. T., and Orihuela, C. J. (2011). Cellular Senescence Increases Expression of Bacterial Ligands in the Lungs and is Positively Correlated With Increased Susceptibility to Pneumococcal Pneumonia. *Aging Cell* 10, 798–806. doi: 10.1111/j.1474-9726.2011.00720.x
- Siboo, I. R., Chambers, H. F., and Sullam, P. M. (2005). Role of SraP a Serine-Rich Surface Protein of *Staphylococcus Aureus* in Binding to Human Platelets. *Infect. Immun.* 73, 2273–2280. doi: 10.1128/IAI.73.4.2273-2280.2005
- Siegel, S. D., Reardon, M. E., and Ton-That, H. (2017). Anchoring of LPXTG-Like Proteins to the Gram-Positive Cell Wall Envelope. *Curr. Top. Microbiol. Immunol.* 404, 159–175.
- Silva-Martin, N., Retamosa, M. G., Maestro, B., Bartual, S. G., Rodes, M. J., Garcia, P., et al. (2014). Crystal Structures of CbpF Complexed With Atropine and Ipratropium Reveal Clues for the Design of Novel Antimicrobials Against *Streptococcus Pneumoniae*. *Biochim. Biophys. Acta* 1840, 129–135. doi: 10.1016/j.bbagen.2013.09.006
- Subramanian, K., Neill, D. R., Malak, H. A., Spelmink, L., Khandaker, S., Dalla Libera Marchiori, G., et al. (2019). Pneumolysin Binds to the Mannose Receptor C Type 1 (MRC-1) Leading to Anti-Inflammatory Responses and Enhanced Pneumococcal Survival. *Nat. Microbiol.* 4, 62–70. doi: 10.1038/s41564-018-0280-x
- Sun, L., Middleton, D. R., Wantuch, P. L., Ozdilek, A., and Avci, F. Y. (2016). Carbohydrates as T-Cell Antigens With Implications in Health and Disease. *Glycobiology* 26, 1029–1040. doi: 10.1093/glycob/cww062
- Sun, X., Stefanetti, G., Berti, F., and Kasper, D. L. (2019). Polysaccharide Structure Dictates Mechanism of Adaptive Immune Response to Glycoconjugate Vaccines. *Proc. Natl. Acad. Sci. U. S. A.* 116, 193–198. doi: 10.1073/pnas.1816401115
- Thanawastien, A., Joyce, K. E., Cartee, R. T., Haines, L. A., Pelton, S. I., Tweten, R. K., et al. (2021). Preclinical *In Vitro* and *In Vivo* Profile of a Highly-Attenuated Broadly Efficacious Pneumolysin Genetic Toxoid. *Vaccine* 39, 1652–1660. doi: 10.1016/j.vaccine.2020.04.064
- Tu, A. H., Fulgham, R. L., Mccrory, M. A., Briles, D. E., and Szalai, A. J. (1999). Pneumococcal Surface Protein A Inhibits Complement Activation by *Streptococcus Pneumoniae*. *Infect. Immun.* 67, 4720–4724. doi: 10.1128/IAI.67.9.4720-4724.1999
- Tweten, R. K. (2005). Cholesterol-Dependent Cytolysins, a Family of Versatile Pore-Forming Toxins. *Infect. Immun.* 73 (10), 6199–6209. doi: 10.1128/IAI.73.10.6199-6209.2005
- Valentino, M. D., McGuire, A. M., Rosch, J. W., Bispo, P. J., Burnham, C., Sanfilippo, C. M., et al. (2014). Unencapsulated *Streptococcus Pneumoniae* From Conjunctivitis Encode Variant Traits and Belong to a Distinct Phylogenetic Cluster. *Nat. Commun.* 5, 5411. doi: 10.1038/ncomms6411
- Van De Garde, M. D. B., Van Westen, E., Poelen, M. C. M., Rots, N. Y., and Van Els, C. (2019). Prediction and Validation of Immunogenic Domains of Pneumococcal Proteins Recognized by Human CD4(+) T Cells. *Infect. Immun.* 87, e00098-00019. doi: 10.1128/IAI.00098-19
- Verhoeven, D., Perry, S., and Pichichero, M. E. (2014a). Contributions to Protection From *Streptococcus Pneumoniae* Infection Using the Monovalent Recombinant Protein Vaccine Candidates PcpA PhtD and PlyD1 in an Infant Murine Model During Challenge. *Clin. Vaccine Immunol.* 21, 1037–1045. doi: 10.1128/CVI.00052-14

- Verhoeven, D., Xu, Q., and Pichichero, M. E. (2014b). Vaccination With a Streptococcus Pneumoniae Trivalent Recombinant PcpA PhtD and PlyD1 Protein Vaccine Candidate Protects Against Lethal Pneumonia in an Infant Murine Model. *Vaccine* 32, 3205–3210. doi: 10.1016/j.vaccine.2014.04.004
- Visan, L., Rouleau, N., Proust, E., Peyrot, L., Donadieu, A., and Ochs, M. (2018). Antibodies to PcpA and PhtD Protect Mice Against Streptococcus Pneumoniae by a Macrophage- and Complement-Dependent Mechanism. *Hum. Vaccin Immunother.* 14, 489–494. doi: 10.1080/21645515.2017.1403698
- Wantuch, P. L., and Avci, F. Y. (2018). Current Status and Future Directions of Invasive Pneumococcal Diseases and Prophylactic Approaches to Control Them. *Hum. Vaccin Immunother.* 14, 2303–2309. doi: 10.1080/21645515.2018.1470726
- Wantuch, P. L., and Avci, F. Y. (2019). Invasive Pneumococcal Disease in Relation to Vaccine Type Serotypes. *Hum. Vaccin Immunother.* 15, 874–875. doi: 10.1080/21645515.2018.1564444
- Wantuch, P. L., Jella, S., Duke, J. A., Mousa, J. J., Henrissat, B., Glushka, J., et al. (2021). Characterization of the Beta-Glucuronidase Pn3Pase as the Founding Member of Glycoside Hydrolase Family Gh169. *Glycobiology* 31, 266–274. doi: 10.1093/glycob/cwaa070
- Weiser, J. N. (2010). The Pneumococcus: Why a Commensal Misbehaves. *J. Mol. Med. (Berl)*. 88 (2), 97–102. doi: 10.1007/s00109-009-0557-x
- Weiser, J. N., Ferreira, D. M., and Paton, J. C. (2018). Streptococcus Pneumoniae: Transmission Colonization and Invasion. *Nat. Rev. Microbiol.* 16, 355–367. doi: 10.1038/s41579-018-0001-8
- Whaley, M. J., Sampson, J. S., Johnson, S. E., Rajam, G., Stinson-Parks, A., Holder, P., et al. (2010). Concomitant Administration of Recombinant PsaA and PCV7 Reduces Streptococcus Pneumoniae Serotype 19a Colonization in a Murine Model. *Vaccine* 28, 3071–3075. doi: 10.1016/j.vaccine.2010.02.086
- Wizemann, T. M., Heinrichs, J. H., Adamou, J. E., Erwin, A. L., Kunsch, C., Choi, G. H., et al. (2001). Use of a Whole Genome Approach to Identify Vaccine Molecules Affording Protection Against Streptococcus Pneumoniae Infection. *Infect. Immun.* 69, 1593–1598. doi: 10.1128/IAI.69.3.1593-1598.2001
- WHO (2019). “Pneumoniae Fact Sheet,” in *WHO Organization Report Geneva Switzerland*. Available at: <https://www.who.int/news-room/fact-sheets/detail/pneumonia>.
- Wu, H., Mintz, K. P., Ladha, M., and Fives-Taylor, P. M. (1998). Isolation and Characterization of Fap1 a Fimbriae-Associated Adhesin of Streptococcus Parasanguis Fw213. *Mol. Microbiol.* 28, 487–500. doi: 10.1046/j.1365-2958.1998.00805.x
- Xiong, Y. Q., Bensing, B. A., Bayer, A. S., Chambers, H. F., and Sullam, P. M. (2008). Role of the Serine-Rich Surface Glycoprotein GspB of Streptococcus Gordonii in the Pathogenesis of Infective Endocarditis. *Microb. Pathog.* 45, 297–301. doi: 10.1016/j.micpath.2008.06.004
- Xu, Q., Surendran, N., Verhoeven, D., Klapa, J., Ochs, M., and Pichichero, M. E. (2015). Trivalent Pneumococcal Protein Recombinant Vaccine Protects Against Lethal Streptococcus Pneumoniae Pneumonia and Correlates With Phagocytosis by Neutrophils During Early Pathogenesis. *Vaccine* 33, 993–1000. doi: 10.1016/j.vaccine.2015.01.014
- Xu, Q., Pryharski, K., and Pichichero, M. E. (2017). Trivalent Pneumococcal Protein Vaccine Protects Against Experimental Acute Otitis Media Caused by Streptococcus Pneumoniae in an Infant Murine Model. *Vaccine* 35, 337–344. doi: 10.1016/j.vaccine.2016.11.046
- Yuan, Z. Q., Lv, Z. Y., Gan, H. Q., Xian, M., Zhang, K. X., Mai, J. Y., et al. (2011). Intranasal Immunization With Autolysin (LytA) in Mice Model Induced Protection Against Five Prevalent Streptococcus Pneumoniae Serotypes in China. *Immunol. Res.* 51, 108–115. doi: 10.1007/s12026-011-8234-x
- Zhang, J. R., Mostov, K. E., Lamm, M. E., Nanno, M., Shimida, S., Ohwaki, M., et al. (2000). The Polymeric Immunoglobulin Receptor Translocates Pneumococci Across Human Nasopharyngeal Epithelial Cells. *Cell* 102, 827–837. doi: 10.1016/S0092-8674(00)00071-4
- Zhang, Y., Masi, A. W., Barniak, V., Mountzouris, K., Hostetter, M. K., and Green, B. A. (2001). Recombinant PcpA Protein a Unique Histidine Motif-Containing Protein From Streptococcus Pneumoniae Protects Mice Against Intranasal Pneumococcal Challenge. *Infect. Immun.* 69, 3827–3836. doi: 10.1128/IAI.69.6.3827-3836.2001
- Zhang, Q., Ma, Q., Li, Q., Yao, W., and Wang, C. (2011). Enhanced Protection Against Nasopharyngeal Carriage of Streptococcus Pneumoniae Elicited by Oral Multiantigen DNA Vaccines Delivered in Attenuated Salmonella Typhimurium. *Mol. Biol. Rep.* 38, 1209–1217. doi: 10.1007/s11033-010-0219-7
- Zhou, M., Zhu, F., Dong, S., Pritchard, D. G., and Wu, H. (2010). A Novel Glucosyltransferase is Required for Glycosylation of a Serine-Rich Adhesin and Biofilm Formation by Streptococcus Parasanguinis. *J. Biol. Chem.* 285, 12140–12148. doi: 10.1074/jbc.M109.066928
- Zhu, F., Zhang, H., Yang, T., Haslam, S. M., Dell, A., and Wu, H. (2016). Engineering and Dissecting the Glycosylation Pathway of a Streptococcal Serine-Rich Repeat Adhesin. *J. Biol. Chem.* 291, 27354–27363. doi: 10.1074/jbc.M116.752998

Conflict of Interest: The authors declare that the research was conducted in the absence of any commercial or financial relationships that could be construed as a potential conflict of interest.

Publisher’s Note: All claims expressed in this article are solely those of the authors and do not necessarily represent those of their affiliated organizations, or those of the publisher, the editors and the reviewers. Any product that may be evaluated in this article, or claim that may be made by its manufacturer, is not guaranteed or endorsed by the publisher.

Copyright © 2022 Aceil and Avci. This is an open-access article distributed under the terms of the Creative Commons Attribution License (CC BY). The use, distribution or reproduction in other forums is permitted, provided the original author(s) and the copyright owner(s) are credited and that the original publication in this journal is cited, in accordance with accepted academic practice. No use, distribution or reproduction is permitted which does not comply with these terms.



Dynamic Python-Based Method Provides Quantitative Analysis of Intercellular Junction Organization During *S. pneumoniae* Infection of the Respiratory Epithelium

OPEN ACCESS

Edited by:

Jorge Eugenio Vidal,
University of Mississippi Medical
Center, United States

Reviewed by:

Marc Chanson,
Université de Genève,
Switzerland
Bindu Nanduri,
Mississippi State University,
United States

*Correspondence:

Walter Adams
walter.adams@sjsu.edu

†Present addresses:

Shakir Hasan,
Department of Immunology, University
of Toronto, Toronto, ON, Canada

Specialty section:

This article was submitted to
Molecular Bacterial Pathogenesis,
a section of the journal
Frontiers in Cellular and
Infection Microbiology

Received: 30 January 2022

Accepted: 30 March 2022

Published: 10 June 2022

Citation:

Mo D, Xu S, Rosa JP, Hasan S and
Adams W (2022) Dynamic Python-
Based Method Provides Quantitative
Analysis of Intercellular Junction
Organization During *S. pneumoniae*
Infection of the Respiratory Epithelium.
Front. Cell. Infect. Microbiol. 12:865528.
doi: 10.3389/fcimb.2022.865528

Devons Mo¹, Shuying Xu^{2,3}, Juan P. Rosa^{2,3,4}, Shakir Hasan^{5†} and Walter Adams^{1*}

¹ Department of Biological Sciences, San Jose State University, San Jose, CA, United States, ² Department of Molecular Biology and Microbiology, Tufts University, Boston, MA, United States, ³ Graduate Program in Immunology, Tufts Graduate School of Biomedical Sciences, Boston, MA, United States, ⁴ Department of Biology, University of Puerto Rico, Cayey, PR, United States, ⁵ Institute of Microbiology of the CAS, Prague, Czechia

Many respiratory pathogens compromise epithelial barrier function during lung infection by disrupting intercellular junctions, such as adherens junctions and tight junctions, that maintain intercellular integrity. This includes *Streptococcus pneumoniae*, a leading cause of pneumonia, which can successfully breach the epithelial barrier and cause severe infections such as septicemia and meningitis. Fluorescence microscopy analysis on intercellular junction protein manipulation by respiratory pathogens has yielded major advances in our understanding of their pathogenesis. Unfortunately, a lack of automated image analysis tools that can tolerate variability in sample-sample staining has limited the accuracy in evaluating intercellular junction organization quantitatively. We have created an open source, automated Python computer script called “Intercellular Junction Organization Quantification” or IJOQ that can handle a high degree of sample-sample staining variability and robustly measure intercellular junction integrity. *In silico* validation of IJOQ was successful in analyzing computer generated images containing varying degrees of simulated intercellular junction disruption. Accurate IJOQ analysis was further confirmed using images generated from *in vitro* and *in vivo* bacterial infection models. When compared in parallel to a previously published, semi-automated script used to measure intercellular junction organization, IJOQ demonstrated superior analysis for all *in vitro* and *in vivo* experiments described herein. These data indicate that IJOQ is an unbiased, easy-to-use tool for fluorescence microscopy analysis and will serve as a valuable, automated resource to rapidly quantify intercellular junction disruption under diverse experimental conditions.

Keywords: adherens junctions, tight junctions, image analysis, brightness normalization, pneumonia

1 INTRODUCTION

A growing area of research has documented how pathogens damage the respiratory epithelium, an important physical barrier that prevents infectious microbes that enter the airways from disseminating into the bloodstream and gaining access to the deeper host tissues. Integral to the success of this barrier function are different intercellular junctions (IJs) such as adherens junctions (AJs) and tight junctions (TJs) (Campbell et al., 2017). An important feature shared by AJs and TJs is their distinct localization pattern between the borders of epithelial cells (Garcia et al., 2018). Both AJs and TJs form extracellular connections between adjacent cells and play important roles to maintain the structural and functional integrity of the respiratory epithelium (Ganesan et al., 2013). AJs mediate cell-cell adhesion and consist of several proteins, including E-cadherin, nectin, catenins, and afadin (Takeichi, 2014). Meanwhile, tight junctions regulate the passage of small molecules between cells, establish cell polarity, and are comprised of occludins, claudins, and junctional adhesion molecules (Zihni et al., 2016). Therefore, accurate and repeatable quantification of the integrity of AJs and TJs under various experimental conditions is an important aspect to many fields of study.

One area where the characterization of IJ integrity has had a large impact has been in understanding virulence strategies of respiratory bacterial pathogens that disrupt IJs as an important aspect of the disease process using fluorescence microscopy analysis. This is well documented by investigations of the Gram-positive pathogen, *Streptococcus pneumoniae*, which remains the leading cause of pneumonia mortality worldwide (Troeger et al., 2018). Investigation of IJ disruption during *S. pneumoniae* infection has revealed evidence of TJ disruption (Rayner et al., 1995), including fluorescence microscopy analysis of pneumococcal infection of human cells, which revealed reduced levels of the TJ proteins occludin, ZO-1, and claudin-5 (Peter et al., 2017; Jacques et al., 2020). Similar results were found after infection with the Gram-positive pathogen *Bordetella pertussis*, which led to decreased levels of ZO-1, occludin, and TJ organization, all of which were exacerbated by the production of adenylate cyclase toxin-hemolysin (Hasan et al., 2018). These studies demonstrate how qualitative and quantitative fluorescence microscopy analysis can provide important insights on how respiratory bacteria invade the host epithelium.

While qualitative assessments of IJ disruptions to the respiratory epithelium offer some insight into the pathogenesis of a disease, quantitative measurements of the arrangement of IJs can provide more comprehensive assessments of perturbations during infections. An image analysis metric commonly used to assess IJ disruption is mean fluorescence (McNeil et al., 2006; Hasan et al., 2018). While this metric can serve as a proxy measurement for IJ health, this analysis assumes that the expression of IJ proteins always has a strong linear correlation with the arrangement of IJs. However, depending on the context of the infection, IJ disruption can be observed as a rearrangement of IJ proteins rather than the destruction of these proteins. For instance, *Helicobacter pylori* infection of host cells recruits ZO-1

to extrajunctional sites of bacterial attachment (Amieva et al., 2003). Likewise, *Neisseria meningitidis* infection of brain endothelial cells recruited AJ and TJ proteins to bacterial attachment sites and induced what were termed “ectopic early junction-like domains” (Mathieu et al., 2009). In these cases, even though IJ disruption was qualitatively observed, this disruption is not captured by mean fluorescence, alone, thus limiting the application of this quantitative metric.

To circumvent the reliance on using mean fluorescence in image analysis, other methods have been developed which quantify the arrangement of IJs. Several methodologies utilize a semi-automated approach where the measurement and analysis protocols are augmented with computer scripts (Terryn et al., 2013; Brezovjakova et al., 2019; Gray et al., 2020). These methodologies usually require moderate human input for parameter set-up or data formatting, with the remainder of the analysis being completed by automation. Successful application of these methodologies requires proficiency in 1) using the automated scripts, 2) interpreting script readouts, and 3) adjusting script-specific parameters when quantitative and qualitative sample readouts do not match. Thus, semi-automated analysis methodologies are still relatively low-throughput and subject to human error and bias, especially if the user is inadequately trained.

Fully automated image analysis algorithms improve upon semi-automated methodologies as they dramatically increase the speed of analysis and minimize the opportunity for human bias. However, one major challenge that fully automated algorithms must overcome when analyzing microscopy images is how to successfully control for the variation in brightness for a signal of interest. These variations in brightness can occur when there are minor deviations in the optimal z-plane to detect a signal (i.e. a sample is not perfectly flat) and is particularly relevant when attempting to quantify IJs that are not present along the entire vertical border of lung epithelial cells. For example, TJs only occupy the most apical position along the vertical border between lung epithelial cells. Likewise, AJs are located immediately underneath the TJs in the basolateral direction of this vertical border. Because these IJs localize to specific vertical planes in a sample, the presence of even minor z-plane deviations can result in substantial variations in signal brightness. Therefore, finding a way to normalize this signal variability prior to quantifying IJ disruption is crucial for a fully automated image analysis algorithm to function reliably.

Here we describe a novel, fully automated, image analysis Python script for the quantification of IJ integrity. Notably, this script performs a normalization step prior to quantification, which facilitates the reliable analysis of IJ disruption. Due to this normalization step, the predetermined parameters for quantification are more consistently optimal, and artifacts are minimized. The Python script was designed to quantify the organization of AJs and TJs that form on polarized epithelial monolayers and as such we term this script “Intercellular Junction Organization Quantification” or IJOQ. In this study we will discuss the development process of this script and demonstrate its applications to *in vitro* and *in vivo* models of

S. pneumoniae infection and *B. pertussis* infection of human bronchial epithelial cells.

2 MATERIALS AND METHODS

2.1 Preparation of Epithelial Monolayers

Human pulmonary mucoepidermoid carcinoma-derived NCI-H292 (H292) cells were prepared as previously described (Adams et al., 2020). Briefly, H292s were grown on the underside of collagen-coated Transwell filters (0.33-cm², Corning Life Sciences) in RPMI 1640 medium (ATCC) with 2 mM L-glutamine, and 10% FBS.

2.2 Bacterial Strains and Growth Conditions

S. pneumoniae strain TIGR4 (serotype 4) was grown in Todd-Hewitt broth (BD Biosciences) supplemented with 0.5% yeast extract in 5% CO₂ and Oxyrase (Oxyrase, Mansfield, OH) and used at late log phase. For mice experiments, bacteria were grown to log phase and diluted in PBS to appropriate concentrations, as required. Bacterial number in stocks was confirmed by plating serial dilutions on blood agar.

2.3 Handling of Animals

Wild type BALB/cJ mice were purchased from The Jackson Laboratory (Bar Harbor, ME). Mice were matched for age and sex and maintained in a specific pathogen-free facility at Tufts University. All procedures were performed in accordance with Institutional Animal Care and Use Committee approved protocols.

2.4 Disruption of H292 Monolayer With Adherens Junction Inhibitor

H292 monolayers were treated with 10 mM 1,4-dithiothreitol (DTT) (Millipore Sigma) and incubated for 3 hours at 37°C. After incubation, monolayers were washed in PBS+Ca/Mg. To prepare samples for confocal imaging, monolayers were fixed in 4% paraformaldehyde and stored at 4°C. Monolayers were permeabilized with 0.1% Triton X-100 in PBS plus 3% BSA. Then, the monolayers were stained with DAPI, phalloidin, and primary anti-E-cadherin antibody (24E10, Cell Signaling), followed by a secondary α -rabbit-FITC antibody (Molecular Probes). The monolayers were then excised from the transwell inserts and mounted onto glass slides with ProLong Gold (ThermoFisher). Samples were visualized with confocal microscopy (Zeiss LSM 700).

2.5 H292 Monolayer Treatment and Sample Preparation

The apical surfaces of H292 monolayers were infected with 1×10^6 or 1×10^7 bacteria and incubated for 2.5 hours at 37°C. After incubation, monolayers were washed in PBS+Ca/Mg. Monolayers were fixed in 4% paraformaldehyde and stored at 4°C, then were permeabilized with 0.1% Triton X-100 in PBS plus 3% BSA. The monolayers were stained with DAPI, phalloidin, and primary anti-E-cadherin antibody (24E10, Cell

Signaling), followed by a secondary α -rabbit-FITC antibody (Molecular Probes). The monolayers were then excised from the transwell inserts and mounted onto glass slides with ProLong Gold (ThermoFisher). Samples were visualized with confocal microscopy (Leica SP8).

2.6 Mouse Treatment and Sample Preparation

Mice were challenged intratracheally with 1×10^7 bacteria or mock-infected with PBS. At 3- and 6-hours post-infection, mice were sacrificed, and their lungs were harvested. Lung tissues were fixed in 4% paraformaldehyde and sectioned to a thickness of 250 μ m with a Leica vibratome (0.145 mm/s, 70 Hz, blade angle 5°). Lung sections were permeabilized with 0.1% Triton X-100 in PBS plus 3% BSA, then stained with the primary anti-E-cadherin antibody (24E10, Cell Signaling) overnight. Following this, the lung sections were stained with DAPI, phalloidin, and secondary α -rabbit-FITC antibody. Samples were mounted with Vectashield Antifade Mounting Medium (Vector Laboratories) and visualized with confocal microscopy (Leica SP8).

2.7 Computer Simulation of Intercellular Junction Disruption

To assist in the *in silico* validation of the IJOQ Python script, a separate Python script, termed the “Simulator” script, was written to create simulations of IJ disruption. The script is open access, downloadable and has been deposited in the IJOQ project repository on GitHub (GNU General Public License version 3.0; <https://github.com/DevonsMo/IJOQ/blob/main/Simulator.py>) When executed, the simulator script produces simulated images of cell monolayers under various degrees of IJ disruption. To simulate IJ disruption, a probability is applied to each line to remove the line from the simulated image. Probabilities of 0, 0.1, 0.2, 0.3, 0.5, and 0.7 were used to simulate varying degrees of IJ disruption. Because a random number of lines are removed for each simulated image, the degree of removal is recorded as a sum of the lengths of the remaining lines, or the total junction length. The image is then saved as a completed simulated image.

2.8 Development of a Python Script to Measure Adherens Junction Health

A novel Python script called “Intercellular Junction Organization Quantification” or IJOQ was developed in order to automate the measurement of IJ disruption in epithelial cells. This script was designed to accept an image or a batch of images, process each image, measure the IJ organization, and then save the data in a.csv file. A flowchart summarizes the steps used by the script to analyze each image (Figure 1).

2.8.1 Importing the Image

After each image is imported, the image is resized such that the average of the height and width of the image is 512 pixels. This compression step reduces processing time in later steps, as well as ensures that the resulting IJOQ value is standardized. The aspect ratio of the image is conserved during compression.

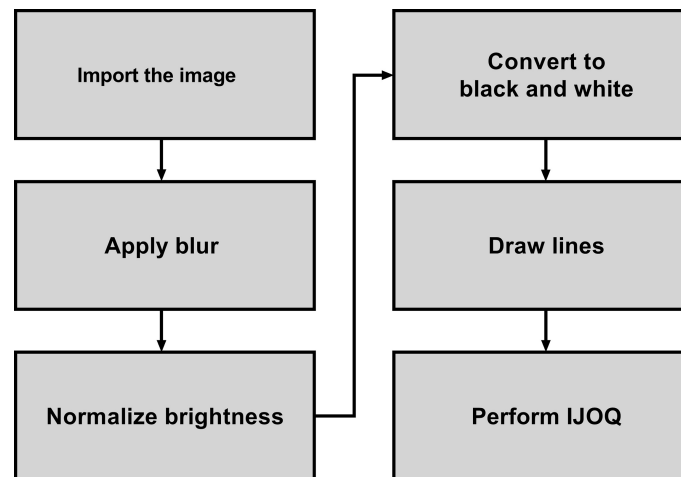


FIGURE 1 | Flowchart which depicts the steps used to analyze the image for AJ health.

Because there is a potential for the imported image to be a composite that contains multiple pseudo-colored fluorescent channels, the green color channel is extracted and used for further image processing. The script may be instructed to extract blue, red, or white color channels instead during calibration.

A mild Gaussian blur with a radius of 5 pixels is applied to the extracted channel in order to remove the effects of noise on later steps. The script may be instructed to use a different blur radius during calibration, depending on the extent of the noise present.

2.8.2 Normalizing the Brightness

To control for the substantial variations in brightness that exist in confocal microscopy images due to minor deviations in the z-plane, a normalization step was created to equalize the brightness within and across confocal microscopy images.

2.8.2.1 Measuring Background Brightness

To correct for within-image brightness variations, the image is first divided into equally sized sections. A larger section size, due to sampling a wider area, decreases the ability to normalize the within-image variation; however, a smaller section size, due to its limited coverage, decreases the ability to discriminate between the background and the IJs. Furthermore, smaller sections increase the computational time, as more pixels must be sampled overall. Dividing the image (**Figure 2A**) into 4 x 4 sections (**Figure 2B**) was qualitatively determined to be most optimal.

For a given section (i.e. **Figure 2B**, the upper leftmost square, highlighted in blue) the brightness values of 8 x 8 equally spaced pixels are recorded (**Figure 2C**), then arranged in order of increasing brightness (**Figure 2D**). The 35th pixel was determined to be an adequate threshold of background brightness for H292 cell monolayers during calibration (See **2.10 Calibration of the IJOQ Script**), and the brightness value of this pixel is recorded as the normalization threshold value of

its section. Because there are 16 sections this results in a total of 16 normalization threshold values.

2.8.2.2 Removing Background Brightness

The 16 normalization threshold values can be used to estimate the brightness value of the background in each section. However, because normalization threshold values are not necessarily similar, when normalization threshold values are applied uniformly to all pixels in their sections, there will be noticeable discrepancy in brightness along the borders of adjacent sections, leading to artifacting. To remove the potential for artifacting, the expected background brightness value of each pixel is calculated individually by taking into consideration the normalization threshold values of all nearby sections.

First, because the sampled pixels are distributed uniformly across a section, it is assumed that the normalization threshold value of a given section best applies to the center pixel of that section. Therefore, the center pixel of each section is given the expected background brightness value equivalent to the normalization threshold value of its section.

Then, the remaining pixels are considered. For all pixels which do not lie at the center of their section, there can be up to four section centers which are both within a section's height vertically and a section's width horizontally from that pixel: to the upper left, upper right, lower left, and lower right (**Figure 2E**, See blue pixel connected to four red pixels). The estimated background brightness value of a given pixel is calculated by linearly scaling the normalization threshold values of the four sections, based on the pixel's horizontal and vertical distance to the centers of those four sections. The equations used to calculate the expected brightness value of a given pixel are shown below:

$$Displacement_x = Position_{pixel,x} - Position_{section\ center,\ top\ left,x}$$

$$Displacement_y = Position_{pixel,y} - Position_{section\ center,\ top\ left,y}$$

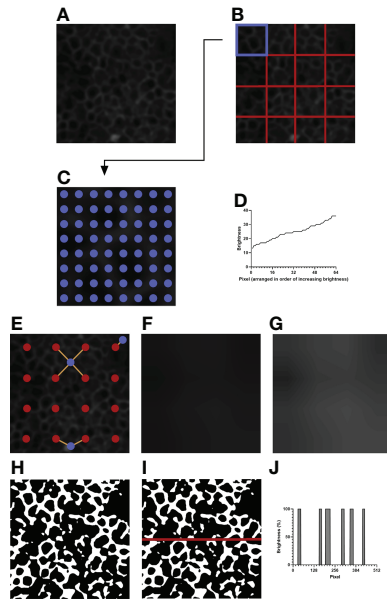


FIGURE 2 | An example of image processing. **(A)** The initial image after resizing and blurring. The green channel has been extracted. **(B)** The image is divided into 4 × 4 equally sized sections. **(C)** Depicted is the top left section of **(B)**, highlighted in blue. 8 × 8 evenly spaced pixels, highlighted in blue, are sampled for their brightness values. **(D)** The brightness values of the sampled pixels are arranged in increasing order. The brightness value of the 35th pixel is taken as the normalization threshold value of the section. **(E)** Example pixels are highlighted in blue. Orange lines are drawn between each example pixel and their nearby section centers, marked in red. **(F)** The expected brightness map is created by calculating the distance-based weighted average of the normalization threshold values of nearby sections for each pixel in the image. The map predicts the background brightness value of a given pixel. **(G)** The brightness map in **(F)** is enhanced in Adobe Photoshop CC 2021 to improve visibility. The enhanced version is not used for analysis and is shown to highlight the differences in brightness in the image. **(H)** Pixels that are brighter than their expected brightness values are set to white, while all other pixels are set to black. **(I)** IJOQ analysis generally traces 10 horizontal and 10 vertical lines through the prepared image. An example line is shown on the image. **(J)** The brightness values of the pixels traced through the example line in **(I)** are measured. Each color change (i.e. vertical line) increments the cell border frequency by 0.5.

$$Threshold_{average,top} = \left(\frac{Displacement_x}{Width} \times Threshold_{top\ left} \right) + \left(\left(1 - \frac{Displacement_x}{Width} \right) \times Threshold_{top\ right} \right)$$

$$Threshold_{average,bottom} = \left(\frac{Displacement_x}{Width} \times Threshold_{bottom\ left} \right) + \left(\left(1 - \frac{Displacement_x}{Width} \right) \times Threshold_{bottom\ right} \right)$$

$$Brightness_{expected}$$

$$= \left(\frac{Displacement_y}{Height} \times Threshold_{average,top} \right) + \left(\left(1 - \frac{Displacement_y}{Height} \right) \times Threshold_{average,bottom} \right)$$

This final calculated value, which effectively takes a horizontal displacement- and vertical displacement-based weighted average of the normalization threshold values of the nearest four sections, provides the expected brightness value of a pixel if that pixel does not contain an IJ.

Pixels which are near the border of the image will have fewer than four section centers that are near enough to be considered for calculation (**Figure 2E**, see blue pixels connected to one or two red pixels). Therefore, if fewer than four section sections are detected for a given pixel, the normalization threshold values of the missing sections are substituted by those of the sections nearest to the missing section centers.

Figure 2F depicts the brightness map, an image which shows the expected background brightness values when the process is repeated for every pixel in the image. Because the differences present in the brightness map are subtle to the human eye, **Figure 2G** depicts an equivalent brightness map enhanced with Adobe Photoshop CC 2021 using the Brightness/Contrast adjustment feature with a brightness setting of +150 and a contrast setting of +50. While this enhanced brightness map is not part of the normalization process, it highlights to the observer the areas in which brightness variations exist. To remove the background, the expected background brightness value of each pixel is subtracted from the brightness value of that pixel. To reduce noise, an extra value, calculated by taking 10% of the expected background brightness value, is further subtracted from the brightness value of the pixel. This value can be adjusted during calibration, depending on the extent of the noise present. An additional filtering step is then performed to increase the contrast of the resulting image. Pixels whose brightness values remained positive after normalization are set to white, while pixels whose brightness values became 0 or negative are set to black, resulting in the final prepared image that is now ready for analysis (**Figure 2H**).

2.8.3 Performing IJOQ

IJs are expected to lie at cell borders, so they should resemble a mesh-like structure when intact and healthy. Therefore, quantifying the organization of IJs should revolve around confirming this mesh-like appearance. To this end, the IJOQ is calculated by considering the number of color changes – from black to white and from white to black – that are detected when a path is traced through the image. For example, a single line traced horizontally through an image that has been prepared for analysis will encounter several color changes across the pixels present in the path (**Figure 2I**). Correspondingly, these color changes across pixels are represented as changes in percent brightness (**Figure 2J**). Any time there is a change in percent

brightness is detected, the IJOQ script assumes that the path is either entering a border or exiting a cell border. Therefore, the IJOQ script increments the “cell border frequency” value of the line by 0.5. As a result, should a line cross an entire intact cell border, which is detected as a color change from black to white to black, the value of the cell border frequency of the line will increase by 1. An organized network of IJs is expected to have a greater cell border frequency than a disorganized or disrupted network because any path traced through an image is expected to detect more cell borders in an intact network.

10 evenly spaced horizontal lines are traced across the width of the image and 10 evenly spaced vertical lines are traced across the height of the image. The cell border frequencies of all 20 paths are summed and divided by the total length of all lines. The resulting number, the IJOQ, expresses the number of expected intact cell borders that are crossed per pixel traced through the image. If a single image was imported, this value is then printed to the user; otherwise, if a batch of images was imported, the IJOQ values of all images are saved into a.csv file at the conclusion of analysis.

2.9 Installation and Setup of the IJOQ Script

The IJOQ script and all relevant scripts are open access, downloadable, and have been deposited in Github (GNU General Public License version 3.0; <https://github.com/DevonsMo/IJOQ/releases>). First, the latest version of Python 3 should be installed and the latest version of IJOQ should be downloaded. Following this, Python libraries required for the IJOQ computer script are installed by executing the “IJOQ Setup.py” script. Upon execution, the IJOQ setup script will update the Python package installer, pip, then install Pillow, NumPy, and Tkinter. The IJOQ script is compatible to run on Windows and Mac.

2.10 Calibration of the IJOQ Script

Before analysis, a calibration is performed to ensure that the parameters of the IJOQ script are adequate for the samples. Calibration is performed once, and the parameters derived during calibration can be re-used for later samples, given that the same cell type and imaging settings are used.

Calibration can be performed by executing the “IJOQ Calibration.py” script. The script will prompt for three negative control images, as well as for analysis settings. The calibration script applies a blur to the images, then uses Otsu’s Method to determine a valid threshold for background brightness. The settings can be saved to a.txt file for later usage.

2.11 Statistical Analysis

Statistical analysis was performed using GraphPad Prism (GraphPad Software, San Diego, CA). Pearson’s Correlation was calculated for the simulated image analysis. Comparison of the DTT treatment was performed using an unpaired t-test. All other comparisons between two groups were performed using ANOVA with Tukey’s *post-hoc*. P values < 0.05 were considered significant in all cases. Cohen’s d was calculated for the effect size

of the DTT treatment, while η^2 was calculated for the effect size of all other comparisons between groups.

3 RESULTS

3.1 IJOQ Robustly Analyzes *In Silico* Disruption of IJs

We first sought to determine whether IJOQ analysis is capable of accurately assessing IJ health under optimal, simulated conditions. Therefore, a separate Python script called the “Simulator” (See Materials and Methods) was developed to produce simulated images of IJs in a monolayer under varying degrees of disruption (**Figures 3A–F**). Because this script produces randomized simulations, precise IJ damage is not necessarily equal in all simulated images. As a result, the script records the total length of the IJs as a more precise measure of IJ health.

We produced 60 simulated images, with 10 images each corresponding to an IJ disruption value of approximately 0%, 10%, 20%, 30%, 50% and 70%. The IJOQ script was then used to analyze the simulated images. The IJOQ metric showed significant ($r^2 = 0.975$, $P < 0.0001$) correlation with the total junction length (**Figure 3K**). These findings demonstrate that IJOQ can precisely measure IJ health in a simulated monolayer across a broad range of IJ damage.

In the previous *in silico* experiment, IJOQ analysis was performed on individual simulated monolayers that had varying degrees of IJ disruption, but each monolayer was generated to mimic an ideal circumstance where there is no noise in the image (**Figure 3G**). Because most microscopy images contain various levels of noise we assessed the capacity for the IJOQ script to filter IJ signal from noise by applying IJOQ analysis to images containing suboptimal signal-to-noise ratios. To this end we applied an additive white Gaussian noise to the 60 simulated images and performed IJOQ on the resulting images. The IJOQ metric showed significant correlation ($r^2 = 0.989$, $p < 0.0001$) with the total junction length at a signal-to-noise ratio of 10, which is the approximate signal-to-noise ratio of our images based on preliminary data (**Figures 3H, L**). IJOQ continued to maintain a strong correlation ($r^2 = 0.963$, $p < 0.0001$) at a signal-to-noise ratio of 2 (**Figures 3I, M**), while the strength of the correlation began to decrease at signal-to-noise ratios of less than 0.5. Such signal-to-noise ratios may occur when examining tissues which exhibit high amounts of autofluorescence. For instance, murine renal tissues have previously been reported to display intense autofluorescence at a broad range of excitation wavelengths, including those for DAPI, FITC, and Texas Red (Sun et al., 2011; Zhang et al., 2018). Furthermore, fixatives such as aldehydes are known to increase autofluorescence of fixed tissues and impede histological observation (Baschong et al., 2001). Although IJOQ still exhibited a strong correlation ($r^2 = 0.579$, $p < 0.0001$) at a signal-to-noise ratio of 0.5 (**Figures 3J, N**), we recommend using images with a signal-to-noise ratio of at least 2 because a signal-to-noise ratio of 0.5 could require an impractical number of technical replicates. More crucially,

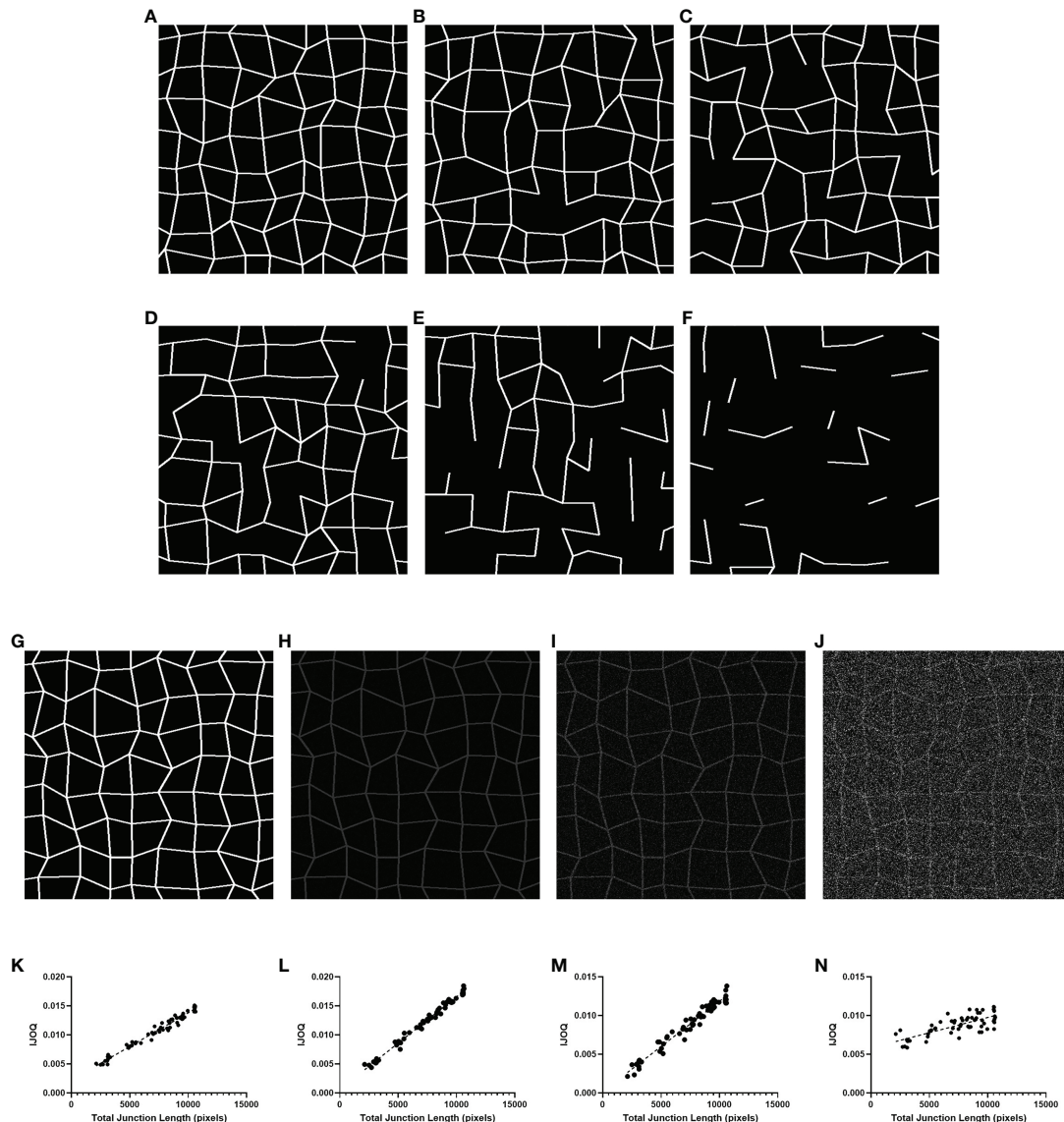


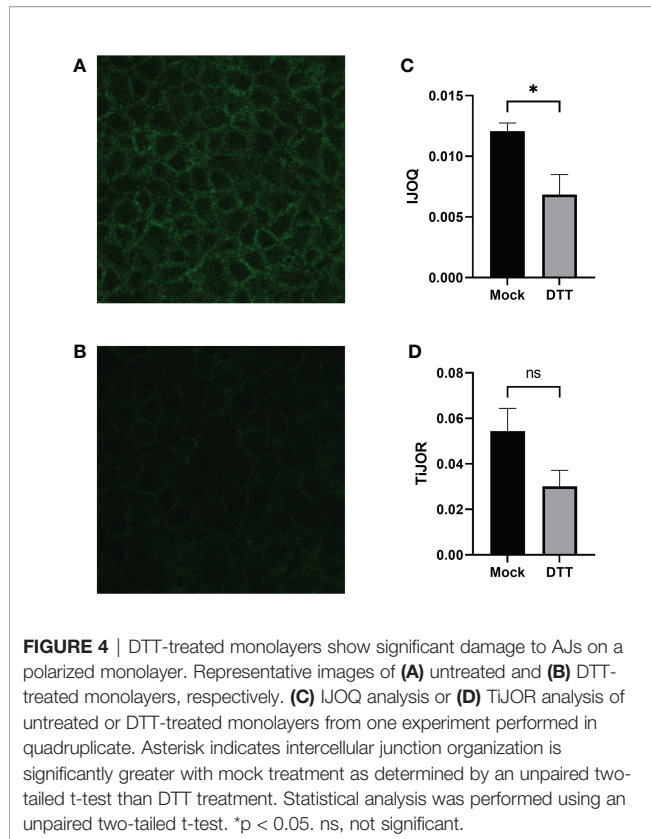
FIGURE 3 | IJOQ versus total junction length in simulated images. Examples of simulated cell monolayer images. IJ disruption was simulated at (A) 0%, (B) 10%, (C) 20%, (D) 30%, (E) 50%, and (F) 70%, respectively. (G) An example of the original simulated image with no noise applied. Additive noise was applied to reach (H) a signal-to-noise ratio of 10, (I) a signal-to-noise ratio of 2 and (J) a signal-to-noise ratio of 0.5. IJOQ shows a strong linear correlation under (K) ideal conditions ($r^2 = 0.975$), (L) a signal-to-noise ratio of 10 ($r^2 = 0.989$), (M) a signal-to-noise ratio of 2 ($r^2 = 0.963$) and (N) a signal-to-noise ratio of 0.5 ($r^2 = 0.579$) as determined by linear regression analysis.

however, because the extent of noise filtering required is determined during calibration, it is important to ensure that the signal-to-noise ratio remains consistent across images for successful application of the IJOQ script.

3.2 IJOQ Accurately Detects Chemically Disrupted AJs

We next asked whether the IJOQ script would be appropriate for measuring IJ disruption in an established *in vitro* system (Bhowmick et al., 2013; Adams et al., 2020). To address this question, we generated polarized H292 lung epithelial cell

monolayers, which express E-cadherin and form AJs (Heijink et al., 2010). The polarized H292 monolayers were then treated for 3 hours with 10 mM DTT, a reagent that has previously been shown to disrupt AJs in cell monolayers by interfering with E-cadherin cell-cell connections (Brückner and Janshoff, 2018). H292 monolayers were stained for E-cadherin and imaged by confocal microscopy to visualize the presence of AJs in the untreated and DTT treated samples (Figures 4A, B). Qualitatively we observed substantial disruption to E-cadherin localization and subsequent IJOQ analysis revealed that DTT-treated monolayers exhibited significantly lower AJ



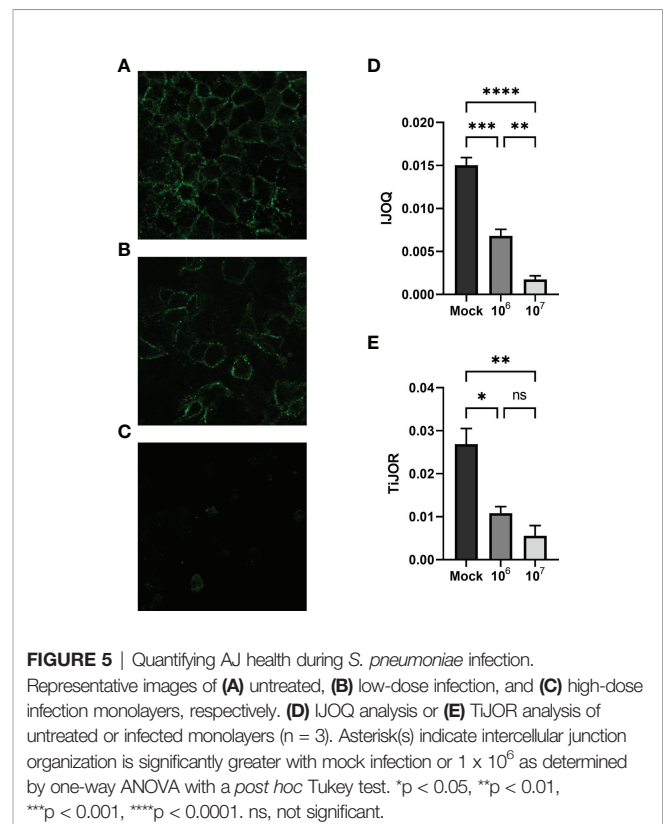
organization compared to untreated monolayers (Figure 4C, $d = 1.15$, $p < 0.05$). These data demonstrate that the IJOQ script successfully detects established chemical methods of AJ disruption.

To assess whether the IJOQ script improved upon semi-automated fluorescence microscopy analysis tools that are already available we reanalyzed our *in vitro* data with one such tool that is commonly used by the research community called Tight Junction Organization Ratio (TiJOR) (Terry et al., 2013). TiJOR was originally used to quantify TJ organization in response to *Pseudomonas aeruginosa* infection, but has since been used under a diverse range of experimental conditions (Terry et al., 2013; Putt et al., 2017; Hasan et al., 2018; Schilpp et al., 2021). Briefly, TiJOR operates by having a polygon arbitrarily drawn onto an image of a monolayer. The TiJOR script measures the number of brightness maxima when the drawn polygon is traced. Brightness maxima lower than an arbitrarily chosen threshold value are ignored to remove the effects of noise. Then, the TiJOR value of this polygon can be calculated by dividing the number of brightness maxima by the length of the perimeter of the polygon. The polygon can be expanded by an arbitrary step size, and the new polygon is analyzed similarly. This expansion can be arbitrarily repeated. The final TiJOR value is calculated by averaging the TiJOR values of all analyzed polygons. We performed TiJOR analysis on a set of identical images with a final polygon count of 100 and an expansion step size of 1. In contrast to our IJOQ, TiJOR failed to find a significant difference in AJ organization between the

untreated and DTT-treated samples and produced a smaller effect size (Figure 4D, IJOQ: $d = 1.15$ vs. TiJOR: $d = 0.91$), indicating that IJOQ provides a stronger and more sensitive assessment of chemically induced AJ disruption.

3.3 *S. pneumoniae* Infection Causes Dose-Dependent AJ Disruption in Lung Epithelial Cells When Assessed by IJOQ

Previous research has shown that *S. pneumoniae* infection of lung tissue compromises TJs in lung epithelial cells and AJs in lung endothelial cells; however *S. pneumoniae*-dependent disruption of AJs in lung epithelial cells has yet to be described (Rayner et al., 1995; Peter et al., 2017). To address this question we infected H292 monolayers with *S. pneumoniae* strain TIGR4, a capsular serotype 4 clinical isolate, at low (1×10^6 CFU) and high (1×10^7 CFU) doses. Upon visualizing the monolayers *via* fluorescence microscopy we observed moderate disruption of E-cadherin at the low dose infection and severe disruption of E-cadherin at the high dose infection (Figures 5A–C). We quantified these observations by analyzing the images using IJOQ and found that both low and high dose infections exhibited significant AJ disruption (Figure 5D, $p < 0.001$ and $p < 0.0001$, respectively). Furthermore, IJOQ discriminated between the two infectious doses as the analysis revealed that the high dose disrupted AJs significantly more than the low dose, accurately recapitulating our qualitative observations (Figure 5D, $p < 0.01$). These findings establish that *S. pneumoniae* infection disrupts AJs in lung epithelial cells *in vitro* and underscores the capacity for IJOQ to

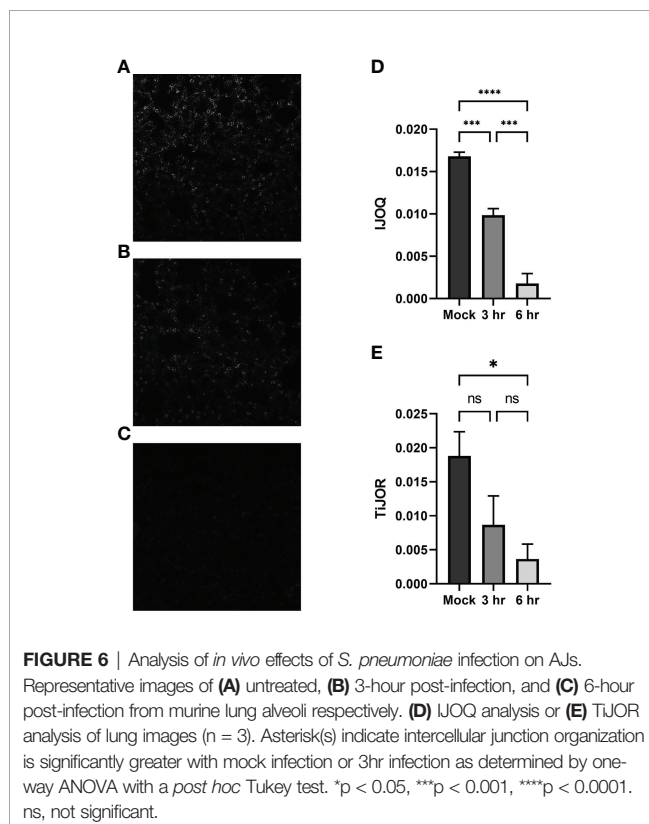


identify distinct levels of damage between different treatment conditions.

To determine if IJOQ offered greater quantitative resolution of *S. pneumoniae*-mediated AJ disruption than TiJOR analysis, the identical set of images was reanalyzed by TiJOR. Consistent with IJOQ, TiJOR found significant AJ disruption in the low-dose infection ($p < 0.05$) and high-dose infection ($p < 0.01$). Importantly, and in contrast to IJOQ, TiJOR failed to discover a significant difference between the low- and high-dose infections (Figure 5E, $p = 0.40$). Additionally, IJOQ analysis offered improved effect sizes when compared with TiJOR analysis (IJOQ: $\eta^2 = 0.97$ vs. TiJOR: $\eta^2 = 0.85$, respectively). These results highlight that compared to TiJOR, IJOQ analysis discriminates between more levels of *S. pneumoniae*-dependent AJ disruption and provides a more robust quantitative assessment of this damage.

3.4 *S. pneumoniae* Infection Causes Time-Dependent AJ disruption *In Vivo* by IJOQ Analysis

To determine if our *in vitro* findings of *S. pneumoniae*-dependent AJ disruption extend to an *in vivo* system BALB/cJ mice were challenged intratracheally with 1×10^7 CFU of TIGR4 and the mice were sacrificed 3 hours and 6 hours post-infection. Uninfected and infected lung sections were stained for E-cadherin and then visualized by fluorescence microscopy. Qualitatively, the mock-infected lungs exhibited well maintained AJ structure and were clearly defined (Figure 6A).



In contrast, partial disruption of AJs was observed at 3 hours post-infection and complete loss of AJ signal was observed at 6 hours post-infection (Figures 6B, C). To assess whether our IJOQ script was capable of identifying these qualitative degrees of AJ disruption in an *in vivo* setting, we calibrated the IJOQ script to the new sample parameters (See Materials and Methods) and then performed IJOQ analysis on the lung sections. IJOQ analysis was consistent with our qualitative observations, revealing significant disruption at both the 3 hour ($P < 0.001$) and 6 hour ($p < 0.0001$) time points. As with previous experiments, IJOQ analysis identified a significant difference between the two infection conditions with the 6 hour time point exhibiting a significant decrease in AJ organization compared to the 3 hour time point, a direct reflection of the qualitative observations (Figure 6D, $p < 0.001$).

To assess if IJOQ outperformed TiJOR analysis in an *in vivo* context, the lung sections were reanalyzed using the TiJOR program. Strikingly, while TiJOR was able to detect AJ disruption at the 6 hour time point ($p < 0.05$), it failed to detect AJ disruption at the 3 hour time point (Figure 6E, $p = 0.179$). Furthermore, TiJOR was unable to discriminate between the 3 hour and 6 hour time points (Figure 6E, $p = 0.670$) and compared to IJOQ, TiJOR had a smaller effect size (IJOQ: $\eta^2 = 0.96$ vs. TiJOR: $\eta^2 = 0.55$, respectively). Together, these findings indicate that IJOQ quantifies discrete levels of AJ disruption across *in vivo* samples and provides a stronger assessment of these differences compared to TiJOR.

3.5 IJOQ Outperforms TiJOR by Identifying CyaA-Dependent and Independent Disruption of TJs During *B. pertussis* Infection

While our previous experiments demonstrate that *S. pneumoniae*-dependent AJ disruption can accurately be assessed by IJOQ under *in vitro* and *in vivo* conditions, AJs are only one type of IJ. To explore the breadth of potential IJOQ applications we investigated whether IJOQ would be suitable for the analysis of a different type of IJ (i.e. TJs) in a different experimental system (i.e. *B. pertussis* infection). To this end, we obtained experimental data from a previously published study investigating *B. pertussis* infection of human bronchial epithelial cells cultured using an air-liquid interface model (Hasan et al., 2018). The authors observed that infection with wildtype (WT) *B. pertussis* or an adenylate cyclase toxin mutant ($\Delta cyaA$) disrupted ZO-1, a major component of TJs. Notably, after performing TiJOR analysis of entire images the authors demonstrated that while TJ organization was lower in both infectious conditions, only infection with WT bacteria resulted in a significant level of disruption (Hasan et al., 2018, See Figure 1C). We calibrated our IJOQ script to the new sample parameters (See Materials and Methods) and analyzed a subset of the original images (Supplemental Figure 1 and Table 1). In agreement with the original study we confirmed that WT *B. pertussis* infection causes significant TJ disruption (Figure 7A, $\eta^2 = 0.93$, $p < 0.05$). Surprisingly, our IJOQ analysis also revealed that the $\Delta cyaA$ infection causes a significant level of TJ disruption (Figure 7A, $\eta^2 = 0.93$, $p < 0.05$), a finding that is consistent with

TABLE 1 | IJOQ Calibration settings of a *B. pertussis* infection on bronchial epithelial cells.

Parameter Type	Parameter Compressed
image size	512
Channel	1
Blur radius	3
Section size	4
Pixels sampled	8
Normalization cutoff	56
Noise cutoff	0.1
Lines	10

the original qualitative observations from Hasan et al., but one that they were unable to detect quantitatively with TijOR. Because we only applied IJOQ to a subset of the original images, we wanted to determine if this subset was still representative of the full data set that was analyzed in the Hasan et al. paper by seeing if we could obtain similar results to the original study using TijOR. After reanalyzing the same subset of original images with TijOR we found that WT *B. pertussis* infection decreased TJ organization significantly ($p < 0.05$, ANOVA with Tukey's *post-hoc*), while a Δ cyaA mutant strain infection did not significantly decrease TJ organization ($p = 0.95$), recapitulating the original findings of the paper (Figure 7B, $\eta^2 = 0.89$, $p < 0.05$). Taken together, these findings indicate that IJOQ can accurately measure TJ organization in a different experimental system by confirming CyaA-dependent TJ disruption and identifying CyaA-independent TJ disruption during *B. pertussis* infection.

4 DISCUSSION

In this study we created an open-source, fully automated, image analysis Python script for the quantification of IJ health. Through a

combination of *in silico*, *in vitro*, and *in vivo* assays, IJOQ consistently identified discrete levels of IJ disruption across different experimental systems. This is in part a direct reflection of its core design features which enable it to handle a low signal-to-noise ratio and substantial variations in signal brightness.

The capacity for IJOQ to normalize signal brightness within and across samples through its extensive image pre-processing algorithm is one of the most important properties of the script. Many sources can give rise to variations in signal brightness including minor deviations in the optimal z-plane (e.g. the sample is not perfectly flat), subtle differences in staining protocol, and signal degradation during imaging, among others (Waters, 2009). To accurately account for these variations, IJOQ executes a normalization step to each image prior to quantification (Figure 2), which allows for the consistent optimization of thresholding parameters, a substantial reduction in false positive signals, and ultimately a high level of accuracy when assessing IJ disruption. This extensive image pre-processing step distinguishes IJOQ from several of the other semi-automated fluorescence microscopy tools currently available for junction analysis which either have a limited amount of image preprocessing or no preprocessing at all (Terryn et al., 2013; Brezovjakova et al., 2019; Gray et al., 2020). As a result, this could impact the capacity for these scripts to handle high levels of sample-sample variation and detect different levels of IJ disruption. For example, TijOR mostly refrains from image pre-processing beyond applying a mild Gaussian blur with a radius of 2 pixels (Terryn et al., 2013). Meanwhile, in our study's comparison between IJOQ and TijOR across *in vitro* and *in vivo* experiments we found that IJOQ and the corresponding statistical analysis revealed at least one to two discrete levels of IJ disruption in response to infection dose and time that were not detected by TijOR (Figures 4–7). Furthermore, IJOQ achieved larger effect sizes than TijOR in every direct comparison of statistical tests performed (Figures 4–7). Incorporation of more extensive pre-

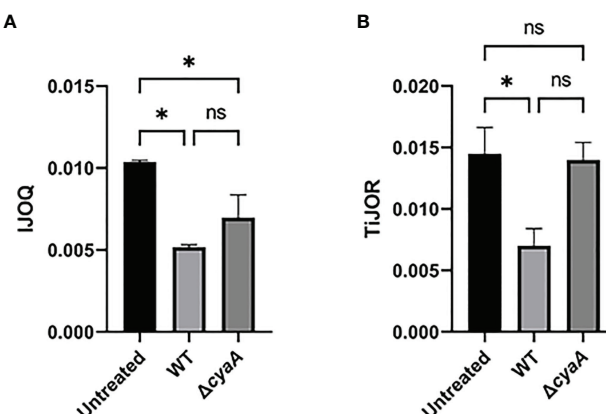


FIGURE 7 | IJOQ outperforms TijOR analysis of IJ disruption during *B. pertussis* infected bronchial cells. A subset ($n = 2$) of previously published data from (Hasan et al., 2018) of a *B. pertussis* infection on bronchial epithelial cells was analyzed with (A) IJOQ or (B) TijOR. Asterisk indicates intercellular junction organization is significantly greater with mock infection as determined by one-way ANOVA with a *post hoc* Tukey test. * $p < 0.05$. The original data and analysis can be found in Figure 1C from the following publication: Hasan et al. (2018). Bordetella pertussis Adenylate Cyclase Toxin Disrupts Functional Integrity of Bronchial Epithelial Layers. *Infect. Immun.* 86. ns, not significant.

processing steps into currently available semi-automated fluorescence microscopy tools may allow users to enhance their dataset analysis and have increased success with more technically challenging assays.

Because IJOQ was originally designed to assist in our analysis of *S. pneumoniae*-dependent disruption of AJs *in vitro*, we were unsure whether it would be able to handle a more challenging *in vivo* experimental system. While successful application of IJOQ to lung sections required the development of a calibration script, IJOQ accurately detected significant E-cadherin disruption *in vivo*, consistent with our *in vitro* results (**Figures 5, 6**). The finding that *S. pneumoniae* disrupts AJs in lung epithelial cells builds upon a growing body of literature documenting how *S. pneumoniae* infection of lung tissue results in the targeted disruption of IJs (Rayner et al., 1995; Peter et al., 2017; Jacques et al., 2020). Because IJ manipulation is a strategy that is prevalent across a variety of respiratory infections, we assessed whether IJOQ was capable of analyzing IJ disruption caused by a different airborne pathogen in a new experimental system (Hasan et al., 2018). We found that IJOQ analysis of the major TJ protein ZO-1 in bronchial epithelial cells grown using an air liquid interface model was successful in detecting CyaA-dependent and independent pathways of TJ disruption (**Figure 7**). Notably, this finding is consistent with the qualitative observations from the original paper and suggests that multiple *B. pertussis* virulence factors contribute to the disruption of TJs (Hasan et al., 2018). Furthermore, this demonstrates that IJOQ is not limited to the analysis of *S. pneumoniae*-dependent E-cadherin disruption, but rather that it can be broadly applied to assess the health of AJ and TJ components following infection by different respiratory pathogens.

Because IJOQ operates under the assumption that IJs should resemble a mesh-like structure, we expect that this script will accurately quantify the organization of AJ and TJ proteins that are consistent with this localization pattern. As such, we predict that IJOQ can successfully be applied to measure the organization of many AJ proteins (e.g. nectin, catenins, and afadin) and TJ proteins (e.g. occludins, claudins, and junctional adhesion molecules). By extension, IJOQ analysis should be robust across different cell types (e.g. epithelial and endothelial), different tissues (e.g. lung, gut, corneal), and after infection by different pathogens that disrupt this mesh-like pattern (e.g. *B. pertussis*, *S. aureus*, *P. aeruginosa*) (Inoshima et al., 2011; Reboud et al., 2017; Hasan et al., 2018). By the same token, we expect IJOQ to struggle quantifying IJs that violate this assumption. For example, gap junctions, another important IJ, are clusters of membrane channels that exhibit a localization pattern that is distinct from a mesh-like structure and thus, not appropriate for IJOQ analysis. Correspondingly, IJOQ does not attempt to measure IJ organization beyond confirming the presence of this mesh-like structure. As a result, it may not detect changes to the phenotype of individual junctions (e.g. continuous, punctate, perpendicular) or of individual gaps in the junctions (e.g. length). Furthermore, while IJOQ is capable of measuring changes to IJs across discrete timepoints (i.e. **Figure 6**), it was not designed to track very rapid dynamic changes of IJs over time (i.e. changes that might be observed across seconds in a video). Lastly, while

IJOQ can accept samples that have been co-stained with multiple fluorescent dyes, it is unable to analyze multiple fluorescent channels at once. Based on these design constraints, we do not envision IJOQ as an appropriate image analysis tool to accurately measure very rapid disruptions to IJ organization or to analyze colocalization patterns of IJ proteins. Fortunately, semi-automated fluorescence microscopy analysis programs such as Junction Mapper and Junction Analyzer Program (JAnaP) provide an excellent solution to execute these more detailed types of analysis (Brezovjakova et al., 2019; Gray et al., 2020). These programs provide users with a high level of accuracy for assessing a range of parameters that include individual junction phenotypes, as well as the length, area, and intensity of junction markers (Brezovjakova et al., 2019; Gray et al., 2020). Thus, these programs may offer additional insights into the nature of IJ localization. However, one important limitation of these programs is that they often have more stringent requirements with regard to image quality. For example, Junction Mapper recommends a signal-to-noise ratio above 22, a standard that would exclude many of the images analyzed in this study, which largely range between 10-12 (**Figure 3H**). In contrast, IJOQ efficiently processed all of our images and is capable of accurately analyzing data with a signal-to-noise ratio as low as 0.5 (**Figures 3J, N**). Other important considerations include the opportunity for user bias and speed of analysis. Semi-automated scripts require moderate levels of human input, which creates substantial opportunity for human bias as well as slower analysis speeds. For example, when we performed TjJOR analysis for this study, it could take up to several minutes per image. Conversely, because IJOQ is a fully automated script, human bias is greatly minimized, and it is capable of analyzing an image in 5-10 seconds. Furthermore, the user does not need to be present for the duration of the analysis, as the script automatically parses through the input folder, searches for images to analyze, and saves the measurements.

The steady increase in the use of fluorescence microscopy to describe biological phenomena has created an urgent demand for quantitative image analysis tools to help researchers rigorously assess their data. Our successful creation and application of a fully automated image analysis script to quantify IJ health has identified discrete levels of IJ disruption across different time points, inocula, cell types, and experimental systems. We envision IJOQ and other quantitative imaging methodologies as important resources that will help researchers uncover novel insights in the field of pathogenic microbiology and beyond.

DATA AVAILABILITY STATEMENT

The raw data supporting the conclusions of this article will be made available by the authors, without undue reservation.

ETHICS STATEMENT

The animal study was reviewed and approved by The Institutional Animal Care and Use Committee at Tufts University.

AUTHOR CONTRIBUTIONS

DM and WA contributed to the conception and design of the study. DM, SX, and WA performed experiments. DM, SX, and JR analyzed the data. DM performed the statistical analysis. DM and WA wrote the first draft of the manuscript. DM, SX, SH and WA contributed to manuscript revision, read, and approved the submitted version. All authors contributed to the article and approved the submitted version.

FUNDING

This work was supported by the National Institutes of General Medical Sciences Grant 1SC2GM141988-01 (to WA), by the California State University Program for Education and Research in Biotechnology Graduate Student COVID-19 Research Restart Program (to DM). SX was supported by the National Institute on Aging Grant 1 R21 AG071268 awarded to Joan Mecas and John Leong.

REFERENCES

- Adams, W., Bhowmick, R., Bou Ghanem, E. N., Wade, K., Shchepetov, M., Weiser, J. N., et al. (2020). Pneumolysin Induces 12-Lipoxygenase-Dependent Neutrophil Migration During Streptococcus Pneumoniae Infection. *J. Immunol.* 204, 101–111. doi: 10.4049/jimmunol.1800748
- Amieva, M. R., Vogelmann, R., Covacci, A., Tompkins, L. S., Nelson, W. J., and Falkow, S. (2003). Disruption of the Epithelial Apical-Junctional Complex by *Helicobacter Pylori* CagA. *Science*. (80-). 300, 1430–1434. doi: 10.1126/science.10811919.Disruption
- Baschong, W., Suetterlin, R., and Hubert Laeng, R. (2001). Control of Autofluorescence of Archival Formaldehyde-Fixed, Paraffin-Embedded Tissue in Confocal Laser Scanning Microscopy (CLSM). *J. Histochem. Cytochem.* 49, 1565–1571. doi: 10.1177/002215540104901210
- Bhowmick, R., Tin Maung, N. H., Hurley, B. P., Ghanem, E. B., Gronert, K., McCormick, B. A., et al. (2013). Systemic Disease During Streptococcus Pneumoniae Acute Lung Infection Requires 12-Lipoxygenase-Dependent Inflammation. *J. Immunol.* 191, 5115–5123. doi: 10.4049/jimmunol.1300522
- Brezovjakova, H., Tomlinson, C., Mohd-Naim, N., Swiatlowska, P., Erasmus, J. E., Huveneers, S., et al. (2019). Junction Mapper Is a Novel Computer Vision Tool to Decipher Cell-Cell Contact Phenotypes. *Elife* 8, e45413. doi: 10.7554/eLife.45413
- Brückner, B. R., and Janshoff, A. (2018). Importance of Integrity of Cell-Cell Junctions for the Mechanics of Confluent MDCK II Cells. *Sci. Rep.* 8, 1–11. doi: 10.1038/s41598-018-32421-2
- Campbell, H. K., Maiers, J. L., and DeMali, K. A. (2017). Interplay Between Tight Junctions & Adherens Junctions. *Exp. Cell Res.* 358, 39–44. doi: 10.1016/j.yexcr.2017.03.061
- Ganesan, S., Comstock, A. T., and Sajjan, U. S. (2013). Barrier function of airway tract epithelium. *Tissue Barriers* 1, e24997. doi: 10.4161/tisb.24997
- Garcia, M. A., Nelson, W. J., and Chavez, N. (2018). Cell – Cell Junctions Organize Structural and Signaling Networks. *Cold Spring Harb. Perspect. Biol.* 10, 1–28. Available at: <http://cshperspectives.cshlp.org/content/10/4/a029181>.
- Gray, K. M., Jung, J. W., Inglut, C. T., Huang, H. C., and Stroka, K. M. (2020). Quantitatively Relating Brain Endothelial Cell-Cell Junction Phenotype to Global and Local Barrier Properties Under Varied Culture Conditions via the Junction Analyzer Program. *Fluids Barriers CNS* 17, 1–20. doi: 10.1186/s12987-020-0177-y
- Hasan, S., Kulkarni, N., Asbjarnarson, A., Linhartova, I., Osicka, R., and Sebo, P. (2018). Bordetella Pertussis Adenylate Cyclase Toxin Disrupts Functional Integrity of Bronchial Epithelial Layers. *Infect. Immun.* 86, e00445–17. doi: 10.1128/IAI.00445-17

ACKNOWLEDGMENTS

We thank Dr. Hasan, Dr. Sebo, Dr. Guðmundsson, and Dr. Espinosa for kindly providing data from Hasan et al., (2018) to validate the IJOQ script. We thank Dr. Vance, Dr. Tweten, and Dr. Leong for helpful discussion and feedback on experimental design and manuscript revisions. We thank Elaine Nguyen, Tarek Jakoush, Vivian Nguyen, and Jasmin Do for technical assistance.

SUPPLEMENTARY MATERIAL

The Supplementary Material for this article can be found online at: <https://www.frontiersin.org/articles/10.3389/fcimb.2022.865528/full#supplementary-material>

Supplementary Figure 1 | *B. pertussis* infection of the bronchial epithelium. Shown are the images of (A) untreated, (B) WT, and (C) Δ cyaA infections from (Hasan et al., 2018) that were used for IJOQ and TJOQ analysis. The original data and analysis can be found in from the following publication: (Hasan et al. 2018). Bordetella pertussis Adenylate Cyclase Toxin Disrupts Functional Integrity of Bronchial Epithelial Layers. *Infect. Immun.* 86.

- Heijink, I. H., Brandenburg, S. M., Noordhoek, J. A., Postma, D. S., Slebos, D. J., and van Oosterhout, A. J. M. (2010). Characterisation of Cell Adhesion in Airway Epithelial Cell Types Using Electric Cell-Substrate Impedance Sensing. *Eur. Respir. J.* 35, 894–903. doi: 10.1183/09031936.00065809
- Inoshima, I., Inoshima, N., Wilke, G., Powers, M., Frank, K., Wang, Y., et al. (2011). A Staphylococcus Aureus Pore-Forming Toxin Subverts the Activity of ADAM10 to Cause Lethal Infection. *Nat. Med.* 17, 1310–1314. doi: 10.1038/nm.2451
- Jacques, L. C., Panagiotou, S., Baltazar, M., Senghore, M., Khandaker, S., Xu, R., et al. (2020). Increased Pathogenicity of Pneumococcal Serotype 1 Is Driven by Rapid Autolysis and Release of Pneumolysin. *Nat. Commun.* 11, 1–13. doi: 10.1038/s41467-020-15751-6
- Mathieu, C., Mikaty, G., Miller, F., Lecuyer, H., Bernard, C., Bourdoulous, S., et al. (2009). Meningococcal Type IV Pili Recruit the Polarity Complex to Cross the Brain Endothelium. *Science*. (80-). 325, 83–87. doi: 10.1126/science.1173196
- McNeil, E., Capaldo, C. T., and Macara, I. G. (2006). Zonula Occludens-1 Function in the Assembly of Tight Junctions in Madin-Darby Canine Kidney Epithelial Cells. *Mol. Biol. Cell* 17, 1922–1932. doi: 10.1091/mbc.E05
- Peter, A., Fatykhova, D., Kershaw, O., Gruber, A. D., Rueckert, J., Neudecker, J., et al. (2017). Localization and Pneumococcal Alteration of Junction Proteins in the Human Alveolar-Capillary Compartment. *Histochem. Cell Biol.* 147, 707–719. doi: 10.1007/s00418-017-1551-y
- Putt, K. K., Pei, R., White, H. M., and Bolling, B. W. (2017). Yogurt Inhibits Intestinal Barrier Dysfunction in Caco-2 Cells by Increasing Tight Junctions. *Food Funct.* 8, 406–414. doi: 10.1039/c6fo01592a
- Rayner, C. F. J., Jackson, A. D., Rutman, A., Dewar, A., Mitchell, T. J., Andrew, P. W., et al. (1995). Interaction of Pneumolysin-Sufficient and -Deficient Isogenic Variants of Streptococcus Pneumoniae With Human Respiratory Mucosa. *Infect. Immun.* 63, 442–447. doi: 10.1128/iai.63.2.442-447.1995
- Reboud, E., Bouillot, S., Patot, S., Béganton, B., Attrée, I., and Huber, P. (2017). Pseudomonas Aeruginosa ExlA and Serratia Marcescens ShlA Trigger Cadherin Cleavage by Promoting Calcium Influx and ADAM10 Activation. *PLoS Pathog.* 13, 1–20. doi: 10.1371/journal.ppat.1006579
- Schilpp, C., Lochbaum, R., Braubach, P., Jonigk, D., Frick, M., Dietl, P., et al. (2021). TGF- β 1 Increases Permeability of Ciliated Airway Epithelia via Redistribution of Claudin 3 From Tight Junction Into Cell Nuclei. *Pflugers Arch. Eur. J. Physiol.* 473, 287–311. doi: 10.1007/s00424-020-02501-2
- Sun, Y., Yu, H., Zheng, D., Cao, Q., Wang, Y., Harris, D., et al. (2011). Sudan Black B Reduces Autofluorescence in Murine Renal Tissue. *Arch. Pathol. Lab. Med.* 135, 1335–1342. doi: 10.5858/arpa.2010-0549-OA
- Takeichi, M. (2014). Dynamic contacts: Rearranging adherens junctions to drive epithelial remodelling. *Nat. Rev. Mol. Cell Biol.* 15, 397–410. doi: 10.1038/nrm3802

- Terry, C., Sellami, M., Fichel, C., Diebold, M. D., Gangloff, S., Le Naour, R., et al. (2013). Rapid Method of Quantification of Tight-Junction Organization Using Image Analysis. *Cytom Part A* 83 A, 235–241. doi: 10.1002/cyto.a.22239
- Troeger, C., Blacker, B., Khalil, I. A., Rao, P. C., Cao, J., Zimsen, S. R. M., et al. (2018). Estimates of the Global, Regional, and National Morbidity, Mortality, and Aetiologies of Lower Respiratory Infections in 195 Countries 1990–2016: A Systematic Analysis for the Global Burden of Disease Study 2016. *Lancet Infect. Dis.* 18, 1191–1210. doi: 10.1016/S1473-3099(18)30310-4
- Waters, J. C. (2009). Accuracy and Precision in Quantitative Fluorescence Microscopy. *J. Cell Biol.* 185, 1135–1148. doi: 10.1083/jcb.200903097
- Zhang, Y., Wang, Y., Cao, W. W., Ma, K. T., Ji, W., Han, Z. W., et al. (2018). Spectral Characteristics of Autofluorescence in Renal Tissue and Methods for Reducing Fluorescence Background in Confocal Laser Scanning Microscopy. *J. Fluoresc.* 28, 561–572. doi: 10.1007/s10895-018-2217-4
- Zihni, C., Mills, C., Matter, K., and Balda, M. S. (2016). Tight junctions: From simple barriers to multifunctional molecular gates. *Nat. Rev. Mol. Cell Biol.* 17, 564–580. doi: 10.1038/nrm.2016.80

Conflict of Interest: The authors declare that the research was conducted in the absence of any commercial or financial relationships that could be construed as a potential conflict of interest.

Publisher's Note: All claims expressed in this article are solely those of the authors and do not necessarily represent those of their affiliated organizations, or those of the publisher, the editors and the reviewers. Any product that may be evaluated in this article, or claim that may be made by its manufacturer, is not guaranteed or endorsed by the publisher.

Copyright © 2022 Mo, Xu, Rosa, Hasan and Adams. This is an open-access article distributed under the terms of the Creative Commons Attribution License (CC BY). The use, distribution or reproduction in other forums is permitted, provided the original author(s) and the copyright owner(s) are credited and that the original publication in this journal is cited, in accordance with accepted academic practice. No use, distribution or reproduction is permitted which does not comply with these terms.



Immune Memory After Respiratory Infection With *Streptococcus pneumoniae* Is Revealed by *in vitro* Stimulation of Murine Splenocytes With Inactivated Pneumococcal Whole Cells: Evidence of Early Recall Responses by Transcriptomic Analysis

OPEN ACCESS

Edited by:

Elsa Bou Ghanem,
University at Buffalo, United States

Reviewed by:

Sarah Clark,
University of Colorado, United States
Olanrewaju B. Morenikeji,
University of Pittsburgh at Bradford,
United States

*Correspondence:

Francesco Santoro
santorof@unisi.it

Specialty section:

This article was submitted to
Molecular Bacterial Pathogenesis,
a section of the journal
Frontiers in Cellular and
Infection Microbiology

Received: 05 February 2022

Accepted: 21 April 2022

Published: 20 June 2022

Citation:

Moscardini IF, Santoro F, Carraro M,
Gerlini A, Fiorino F, Germoni C,
Gholami S, Pettini E, Medaglini D,
Iannelli F and Pozzi G (2022) Immune
Memory After Respiratory Infection
With *Streptococcus pneumoniae* Is
Revealed by *in vitro* Stimulation of
Murine Splenocytes With Inactivated
Pneumococcal Whole Cells: Evidence
of Early Recall Responses by
Transcriptomic Analysis.
Front. Cell. Infect. Microbiol. 12:869763.
doi: 10.3389/fcimb.2022.869763

Isabelle Franco Moscardini¹, Francesco Santoro^{2*}, Monica Carraro², Alice Gerlini¹,
Fabio Fiorino², Chiara Germoni², Samaneh Gholami², Elena Pettini², Donata Medaglini²,
Francesco Iannelli² and Gianni Pozzi²

¹ Microbiotec srl, Siena, Italy, ² Laboratory of Molecular Microbiology and Biotechnology (LAMMB), Department of Medical
Biotechnologies, University of Siena, Siena, Italy

The *in vitro* stimulation of immune system cells with live or killed bacteria is essential for understanding the host response to pathogens. In the present study, we propose a model combining transcriptomic and cytokine assays on murine splenocytes to describe the immune recall in the days following pneumococcal lung infection. Mice were sacrificed at days 1, 2, 4, and 7 after *Streptococcus pneumoniae* (TIGR4 serotype 4) intranasal infection and splenocytes were cultured in the presence or absence of the same inactivated bacterial strain to access the transcriptomic and cytokine profiles. The stimulation of splenocytes from infected mice led to a higher number of differentially expressed genes than the infection or stimulation alone, resulting in the enrichment of 40 unique blood transcription modules, including many pathways related to adaptive immunity and cytokines. Together with transcriptomic data, cytokines levels suggested the presence of a recall immune response promoting both innate and adaptive immunity, stronger from the fourth day after infection. Dimensionality reduction and feature selection identified key variables of this recall response and the genes associated with the increase in cytokine concentrations. This model could study the immune responses involved in pneumococcal infection and possibly monitor vaccine immune response and experimental therapies efficacy in future studies.

Keywords: *Streptococcus pneumoniae*, *in vitro* stimulation, Transcriptomic Analysis, Recall immune responses, lung infection, cytokines/chemokines

1 INTRODUCTION

Streptococcus pneumoniae is a major human pathogen responsible for various diseases, including life-threatening conditions such as pneumonia, sepsis, and meningitis (Weiser et al., 2018). Current vaccines have been very efficient in reducing the death toll caused by this pathogen. However, strains not covered by the available vaccines represent a growing concern, demanding new serotype-independent strategies (Kaplan et al., 2013; Pichichero, 2017; Briles et al., 2019). Models to assess the response to new vaccine candidates would be of great use.

In vitro stimulation with live or killed bacteria has been used for decades for understanding the host's response to different pathogens, including *S. pneumoniae* (Zhan and Cheers, 1995; Schultz et al., 1998; Wu et al., 2011; de Stoppelaar et al., 2016). This technique has also been applied in vaccine studies, characterizing the immune response after a second stimulus (Paranavitana et al., 2010; Moffitt et al., 2011; Shao et al., 2015). Changes in gene expression and in cytokine concentration were metrics assessed by some of these works to study the immune profile of pneumococcal infection. In the present work, we propose the combination of transcriptomic and cytokine assays from murine splenocytes to assess the immune memory built in the days following pneumococcal infection.

The spleen plays a vital role in host defenses against encapsulated blood-borne pathogens due to its elevated perfusion and efficient immune surveillance of the circulatory system (Cerutti et al., 2013). In a pneumococcal bacteremia model, bacteria present a tropism to the spleen, and macrophages present in the splenic Red Pulp (RP) are responsible for an initial binding and subsequent clearance of *S. pneumoniae* mediated by mature neutrophils present on the RP (Deniset et al., 2017; Ercoli et al., 2018). Moreover, the splenic Marginal Zone (MZ) is a crucial area of antigen presentation to MZ B cells that are capable of rapidly differentiating into plasmablasts, secreting low-affinity IgM and IgG (Cerutti et al., 2013).

RNA sequencing technologies permit us to gain insights into the host's response due to the possibility of analyzing the changes in gene expression in different conditions. The transcriptomic information can be integrated with other biological layers or clinical data, permitting a more comprehensive understanding of biological processes in response to perturbations such as infection and vaccination.

In the current work, we propose the study of the host systemic responses to a pneumococcal lung infection by assessing gene expression and cytokine profiles of splenocytes, identifying biological pathways and the key features involved in this process.

2 METHODS

2.1 Animals and Animal Infection

Seven-week female C57BL/6 mice (Charles River Italia, Italy) were treated according to national guidelines (Decreto Legislativo 26/2014) utilizing the three R's principles. Animals

were maintained under specific pathogen-free conditions in the animal facility of the Laboratory of Molecular Microbiology and Biotechnology (L.A.M.M.B.), Department of Medical Biotechnologies at University of Siena, at 20–24°C, with 55 ± 10% of humidity, with food and water *ad libitum*. The study was approved by the Italian Ministry of Health with authorization n° 304/2018-PR. As previously described (Kadioglu et al., 2011) male and female mice respond differently to pneumococcal infection and, therefore the use of only female mice can be considered a limitation of this study.

Mouse-passaged TIGR4 strain of *S. pneumoniae* (Gerlini et al., 2014) was inoculated 1:50 in TSB (Tryptic-Soy Broth, Becton Dickinson, USA) supplemented with 0.1% of glucose (PanReac, Applichem, Italy), 1% of yeast extract (Oxoid, UK) and 0.016 M K₂HPO₄ (Sigma-Aldrich, USA) (TSB-GYP). The bacterial culture in mid-exponential phase (\approx OD₅₉₀ = 0.6), was centrifuged at 2,000 x g for 10 minutes and resuspended in an appropriate volume of saline. Before the centrifugation, the culture was Gram-stained and bacterial vital counts were performed using the multilayer plating method (Iannelli et al., 2021). Each mouse was anesthetized by intraperitoneal administration of 15 mg/kg tiletamine hydrochloride/zolazepam and 4 mg/kg xylazine and intranasally infected by instillation of 10⁷ CFU of TIGR4, prepared as described above, in the volume of 25 µl/nostril in TSB. Mice were euthanized at different time points with overdose of anesthesia and cervical dislocation, as shown in **Figure 1**. Non-infected mice composed the baseline group. Each group included 6 animals.

2.2 Sample Collection

After aseptic removal at different time points (days 0, 1, 2, 4, and 7 after infection), spleens were meshed onto 70 µm nylon screens (Sefar Italia, Italy) using a scalpel and scraper. Cells were washed two times in RPMI (Sigma-Aldrich) supplemented with 10% of fetal bovine serum (FBS, Gibco, USA) and 1% of penicillin-streptomycin (Sigma-Aldrich)(cRPMI), treated with red blood cells lysis buffer according to manufacturer instruction (eBioscience, USA), and resuspended in cRPMI for cell counting by an automatic cell counter (Bio-Rad, USA). Lungs were aseptically removed, meshed onto 40 µm nylon screens (Sefar Italia, Italy), suspended in 1 ml of TSB containing glycerol at a final concentration of 10% and frozen at -70°C.

2.3 Bacterial Cells Counts in Lungs

Bacterial colony forming units (CFUs) were determined by plating appropriate dilutions of frozen lungs using a multilayer plating procedure (Iannelli et al., 2021). The lower limit of detection was 10 CFU/ml. CFUs were counted at 1, 2, 4, and 7 days after intranasal infection and in the mock infected control group.

2.4 Preparation of Inactivated Whole Cells of *S. pneumoniae*

TIGR4 was inoculated 1:1000 (v:v) in 1 L of pre-heated (37°C) TSB-GYP in a GLS80 1 liter bottle (Duran, USA). Temperature was maintained constant at 37°C, the pH was continuously measured with a probe (InPro3030, Mettler Toledo) and kept

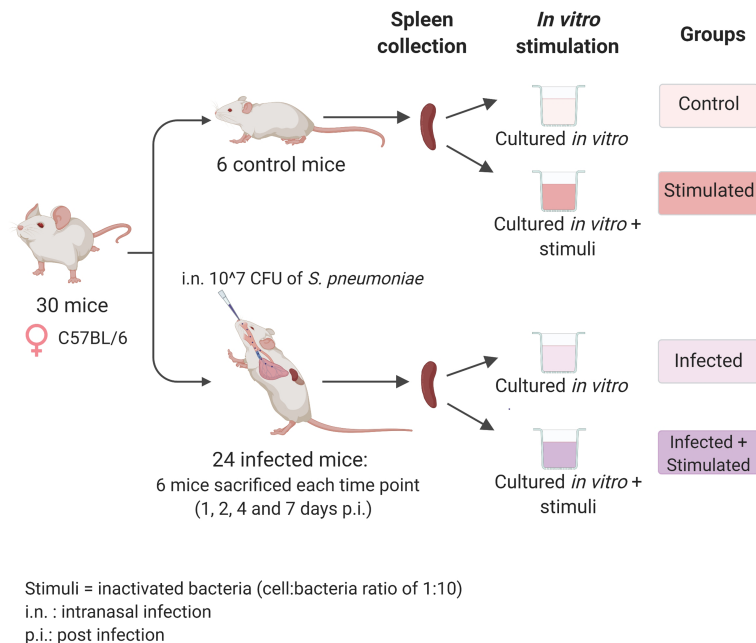


FIGURE 1 | Experimental design. Seven-weeks old C57BL/6 female mice were infected intranasally with a dose of 10^7 CFU/mouse of pneumococcal serotype 4, TIGR4 strain. After 1, 2, 4, and 7 days post-infection each group of mice ($n=6$) was euthanized and their spleens were collected for the isolation of splenocytes. Splenocytes from each single mouse were stimulated with formalin-inactivated TIGR4 (cell:bacteria 1:10), or maintained in cRPMI medium alone. The incubation was performed at 37°C in 5% CO_2 in a period of 6 hours for samples used in the RNA-sequencing experiment or 72 hours for samples used in the Bio-Plex Multiplex immunoassay. Non-infected mice were euthanized at day 0, splenocytes were collected and maintained in the same *in vitro* conditions of the unstimulated group and used as controls. Created with biorender.com.

at 6.9 by peristaltic pump controlled addition of 3M NaOH. Agitation was set at 100 rpm. Growth was monitored by aseptically drawing aliquots and measuring their OD_{590} in a Spectronic 200 spectrophotometer (ThermoFisher). At the peak OD_{590} (about 2.5, corresponding to 10^9 CFU/ml) bacteria were harvested by centrifugation, resuspended in PBS/10% glycerol and frozen at -70°C . TIGR4 bacteria were then thawed and inactivated by treatment with 1.5% formalin for 2 hours on a roller mixer at room temperature, then washed twice and resuspended in water.

2.5 Splenocyte Stimulation and Cytokine Secretion Assay

Splenocytes were cultured in a U-bottom 96-well plate in triplicate for 72 hours at 37°C with 5% CO_2 in cRPMI.

Splenocyte cultures were incubated in the presence or not of inactivated TIGR4, at a cell:bacteria ratio of 1:10. Unstimulated control splenocytes were cultured in cRPMI alone, and positive control splenocytes were stimulated with 50 ng/ml of phorbol 12-myristate 13-acetate (PMA) and 1 μM of Ionomycin (both from Sigma-Aldrich). After stimulation, cells were harvested and centrifuged at $500 \times g$ for 15 minutes at 4°C . The supernatant was recovered and frozen at -70°C for subsequent Luminex immunoassay.

A broad screening panel consisting of a biologically-relevant collection of adaptive immunity cytokines, pro-inflammatory cytokines, and anti-inflammatory cytokines was used. In

particular, IL-1 α , IL-1 β , IL-2, IL-3, IL-4, IL-5, IL-6, IL-9, IL-10, IL-12p40, IL-12p70, IL-13, IL-17, G-CSF, GM-CSF, IFN γ , and TNF- α , and of the chemokines Eotaxin, KC, MCP-1 (MCAF), MIP-1 α , MIP-1 β , and RANTES production by *in vitro* stimulated splenocytes was assessed with the BioPlex pro mouse cytokine group 1 - panel 23-plex immunoassay (Bio-Rad, USA) according to manufacturer guidelines, and analyzed by Bio-Plex Magpix Multiplex reader (Bio-Rad). Cytokine and chemokine concentration was expressed as picograms per milliliter (pg/ml) and were calculated using Bio-Plex Manager 6.1.

2.6 Splenocyte Stimulation for RNA-Sequencing

In a U-bottom plate, 1×10^6 splenocytes/well were seeded in quintuplicate and cultured for 6 hours at 37°C with 5% CO_2 in cRPMI in the presence of inactivated TIGR4 at a cell:bacteria ratio of 1:10. Unstimulated control splenocytes were cultured in cRPMI alone. Upon stimulation, cell replicates were centrifuged at $500 \times g$ for 10 minutes at 4°C . The supernatant was discarded, the pellet resuspended in 50 μl of lysis buffer RA1 (Macherey-Nagel, Germany), flash-frozen in liquid nitrogen, and stored at -70°C for subsequent RNA extraction.

2.7 RNA Extraction, Library Preparation, and Sequencing

The RNA purification was performed with the NucleoSpin[®] RNA kit (Macherey-Nagel) following manufacturer's

instructions, and, before DNase treatment, the extracted RNA was quantified by the Qubit[®] 2.0 Fluorometer (Invitrogen by Thermo Fisher Scientific, USA), using the Qubit RNA BR (Broad-Range) Assay Kit.

Contaminating DNA was removed from the extracted RNA by adding 10X TURBO DNase Buffer (TURBO DNase, Ambion by Thermo Fisher Scientific) and 1 µl of TURBO DNase (Ambion), and samples were incubated at 37°C for 30 minutes. After purification by the RNA Clean & Concentrator Kit (Zymo Research, USA), the obtained RNA was quantified using the Qubit[®] RNA BR Assay Kit.

Library preparation was performed as described in a previous publication (Santoro et al., 2021), using the Ion AmpliSeq[™] Transcriptome Mouse Gene Expression Kit from AmpliSeq (Thermo Fisher Scientific), allowing the amplification of 23,930 target genes. Libraries were diluted to 50 pM and pooled in equal volumes (7 µl), with eight individual samples per pool and loaded onto Ion PI[™] Chip v3 using the Ion Chef[™] Instrument. Sequencing was performed using Ion Proton[™] Sequencer.

All described steps were performed according to the manufacturer's instructions.

2.8 RNA-Sequencing Data Analysis

R software in version 3.6.3 was used for transcriptomic data analysis. The DESeq2 package (Love et al., 2014), performs differential expression analysis and multiple test correction, returning values of LogFC, and adjusted p values. Genes with an adjusted p-value smaller than 0.05 and an absolute value of log2 Fold Change greater than 0.5 were classified as differentially expressed and then used in the enrichment analysis performed by the hypergeometric test from the *tmod* package (Weiner 3rd and Domaszewska, 2016) using the Blood Transcription Modules (BTM) database (Li et al., 2014).

2.9 Cytokine Data Analysis

R software in version 3.6.3 and the software GraphPad Prism 8.0 were used to perform the statistical analysis. The cytokine concentrations between stimulated and unstimulated samples were compared using the Wilcoxon signed-rank test, a non-parametric test used to compare two related samples. Samples from different time points were analyzed using the Mann-Whitney test, a non-parametric test for non-matched samples. A p-value ≤ 0.05 was considered statistically significant.

2.10 Biomarker Analysis

The DaMiRseq (Chiesa et al., 2018) package was used to find possible biomarkers of the host response to the second stimulus, the inactivated bacteria. Stimulated samples were selected and divided into three groups: baseline, infected samples at days 1 and 2 (early time points), and infected samples at days 4 and 7 (late time points). Following a pipeline that permits normalization, data adjustment, and feature selection, the DaMiRseq package ranked the most important features to distinguish the three classes. The number of selected genes was chosen based on the importance established by the package;

genes with a scaled importance score higher than 0.5 were chosen (**Supplementary Image 1**).

2.11 Data Integration

To integrate RNA-sequencing results and the Cytokines Bioplex, we selected the concurrent samples from both experiments, and we performed the sparse version of Partial Least Squares (sPLS), provided by the MixOmics package. The PLS is a multivariate method to integrate two high dimensional matrices, maximizing the covariance between components from two data sets, in our case, the transcriptomic and cytokines assay data. The sparse version, sPLS, applies LASSO penalization in each pair of loading vectors from PLS, performing feature selection and providing the correlation values between the main features in each data set (Lê Cao et al., 2008).

According to the Q^2 criterion, two components would be sufficient to run the model (Q^2 of 0.33931900 and 0.08639437). As suggested by the *tune.spls* function, the optimal variable number was chosen in each component resulting in 16 genes for component 1 and 25 from component 2.

3 RESULTS

Groups of six C57BL/6 mice were intranasally inoculated with 10^7 CFUs of TIGR4 *S. pneumoniae* to generate lung infection. To study the systemic response induced at early time points after infection, we sacrificed animals after 1, 2, 4, and 7 days and isolated their splenocytes. We then stimulated splenocytes from each single mouse with formalin-inactivated whole pneumococcal cells and investigated the host responses by transcriptomic analysis and assessment of cytokine production (**Figure 1**).

3.1 Evidence of Pneumococcal Lung Infection in Mice

The weight loss of animals after infection is a critical clinical parameter of disease in the mouse model of infection, evaluated in different challenge murine models with different pathogens (Trammell and Toth, 2011; Pettini et al., 2015; Fiorino et al., 2021). Mouse body weight was measured every 24 hours for a period of seven days. Uninfected mice increased their body weight over time, which reflected their health status. Compared to naive mice, infected mice experienced a significant decrease in body weight soon after infection, and the average difference in the weight between the classes increased over time, being 1.07 grams at day 2 after infection and 1.52 grams at day 7 (**Figure 2A**).

The significance of these findings was assessed using the Mann-Whitney test, which showed significant differences in the weight from day 2 to day 7 after infection, indicating a long-lasting effect of the infection.

Pneumococcal cells were counted in the lungs of infected mice. Cell counts had a peak at day 4 after infection (**Figure 2B**). It is worth to note that, for each time point assayed, 2-5 mice had no detectable pneumococcal cells, suggesting that mice are able

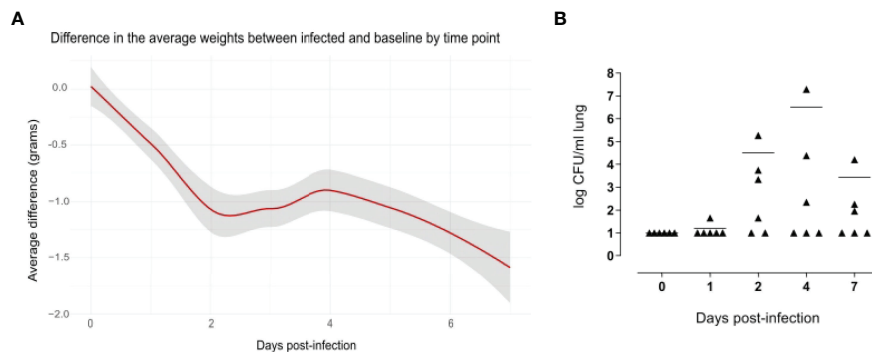


FIGURE 2 | Evidence of pneumococcal lung infection. Comparison of body weight variation of infected versus baseline **(A)**. Infected ($n=36$) and uninfected ($n=5$) mice were weighed every 24 hours for a period of 7 days. Values were obtained subtracting the pre-inoculum body weight from the body weight at each time-point, and then subtracting the mean in the control group from mean of the infected group in each time point. The average differences are expressed in grams and the gray shade represents the 0.95 confidence interval. From days 2 to 7 there were significant differences between the infected and baseline groups ($p < 0.05$, calculated using Mann-Whitney test). Pneumococcal cell counts in the lungs **(B)**. The lungs of mice sacrificed at 1, 2, 4 and 7 days after infection ($n=6$ per group) were collected, homogenized in a final volume of 1 ml and plated using a multilayer plating procedure. Pneumococcal cells were counted after 24 hours and 48 hours of incubation. Lungs of uninfected mice (0 days post-infection) were plated as a negative control. Data are expressed as CFUs/ml lung. The lower limit of detection was 10 CFU/ml lung. Average cell counts had a peak at day 4. For each time point, there were at least 2 mice without detectable pneumococci.

to spontaneously clear pneumococcal lung infection at an infectious dose of 1×10^7 CFUs of *S. pneumoniae* TIGR4. When setting up the mouse model, we also counted pneumococcal cells in the blood of six mice at 6 and 12 hours after intranasal infection, and in the blood of 12 mice at 24 and 96 hours after infection. Of those, only one animal had detectable pneumococcal cells in the blood (2.4×10^3 CFU/ml) at 24 hours after infection, suggesting that the infection is essentially limited to the mouse lungs without significant systemic spreading.

3.2 *In vitro* Splenocyte Stimulation With Pneumococcal Strain TIGR4 Activates Several Genes Related to Both Branches of the Immune System

Transcriptomic data from spleens of infected and uninfected mice with or without homologous *in vitro* stimulation were analyzed. We performed an Independent Principal Component Analysis (IPCA) and its sparse version, sIPCA, both proposed by MixOmics package (Yao et al., 2012), (i) to observe the distribution of our data, (ii) to understand how stimulation at different time points affects the clustering of samples, (iii) to identify the genes responsible for the main variance among samples, and (iv) to find possible outlier samples.

The IPCA approach (**Supplementary Image 2**) yielded a better clusterization among experimental groups and time points compared to PCA (data not shown). An outlier control sample was detected and removed. The sparse version of the IPCA (sIPCA, **Figure 3**) applies soft-thresholding in the independent loading vectors in IPCA, performing feature selection. The graph shows the presence of two well-defined groups in the sIPC1: the stimulated and unstimulated samples.

To better understand the genes that drive the formation of these clusters, the normalized expression values of the 50 genes selected by the first component of the sIPCA were divided into

two heatmaps (**Figure 3**). Genes positively correlated with the first component (driving the unstimulated cluster) included positive and negative regulators of the immune response, and they presented a decreased expression after stimulation. The genes negatively regulated with the first component (clustering the stimulated samples) were related to cytokines, chemokines, and inflammation, all of them presenting an increased expression compared to unstimulated samples.

3.3 Stimulation of Splenocytes From Infected Mice Highlights Biological Pathways of Pneumococcus Infection

We then proceeded with the differential expression analysis using the *DESeq2* package. To understand the biological alterations caused by the infection and the subsequent *in vitro* stimulation with inactivated pneumococcus, enrichment analysis was performed using three different comparisons. (i) Spleens from infected mice, (ii) stimulated spleens from non-infected mice, and (iii) stimulated spleens from infected mice, at different time points after infection, were all compared with control spleens.

The number of differentially expressed genes (DEGs) for each condition at each time point is presented in **Figure 4**. As expected, the stimulation of infected samples led to a higher number of DEGs compared to only infected samples, including specific genes that were not differentially expressed in the infection or stimulation alone. Days 4 and 7 presented the highest values of specific DEGs, in particular, new immune related genes and microRNAs were found, such as *Il2*, *Foxp3*, *Il16a*, *Ccr1* and *Mir155hg*.

The enrichment analysis was performed using the *Blood Transcription Modules (BTM)* database and the *tmod* package, the complete results of the different groups are reported in the **Supplementary Data Sheet 1**. **Figure 5** shows a summary of the

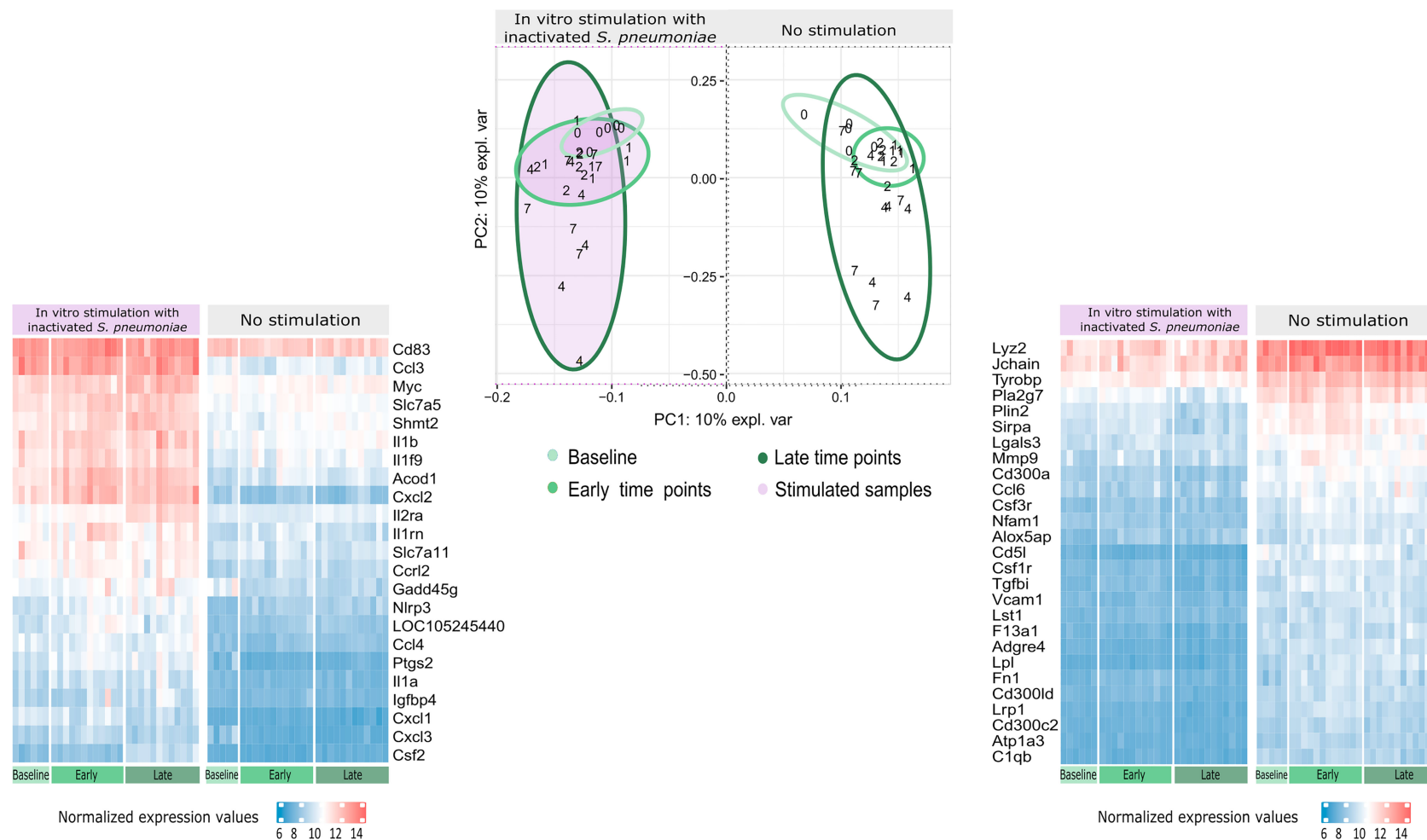


FIGURE 3 | Distribution of gene expression data and changes after stimulation. The sPCA proposed by MixOmics revealed two main clusters, one formed by stimulated samples (shaded in purple) and other formed by unstimulated samples. The IPC1 (x-axis) represents the variance between stimulated and unstimulated samples of infected and non-infected mice. IPC2 (y-axis) shows the variance between baseline samples with respect to the other groups in different study days (1, 2, 4, 7). After infection, samples from days 1 and 2 (early time points) form a smaller cluster closer to baseline samples (lighter green), while samples from days 4 and 7 (late time points) present a higher dispersion (darker green). The normalized expression values for the 50 most important genes selected by the sPCA in the first component were represented in heatmaps, with lower values represented in blue and higher values in red and time points represented in the bottom part, following the same green scale of the sPCA. The heatmap on the right, shows the 27 genes positively correlated with the first component, which include positive and negative regulators of the immune system and drive the formation of the cluster of unstimulated samples. The heatmap on the left shows the 23 genes negatively correlated with the first component, driving the stimulated samples to form a separate cluster. Most of these genes are related to cytokines and chemokines (Csf2, Ccl4, Il1a, Il1b, Il1rn, Il2ra, Cxcl1, Cxcl3, Cxcl2, Ccl3, Slc7a5) while others are related to immunity and inflammation (Cd83, Acod1, Slc7a11, Gadd45g, Nlrp3, Ptgs2 and Igfbp4).

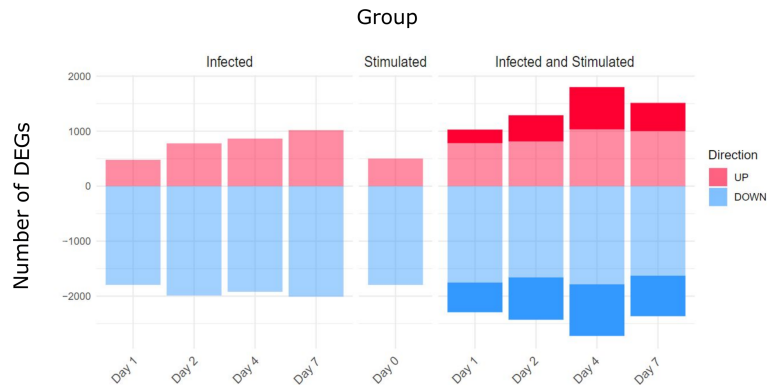


FIGURE 4 | Differentially Expressed genes (DEGs) for comparison and Time point. Three main comparisons against baseline controls were defined: infected samples, stimulated samples and infected and stimulated samples. Differentially Expressed Genes (DEGs) were obtained using the DESeq2 package and establishing thresholds of FDR < 0.05 and absolute logFC > 0.5. The stimulation of spleens from infected mice led to a higher number of DEGs compared to only infected or only stimulated spleens (number of specific genes highlighted in the figure).

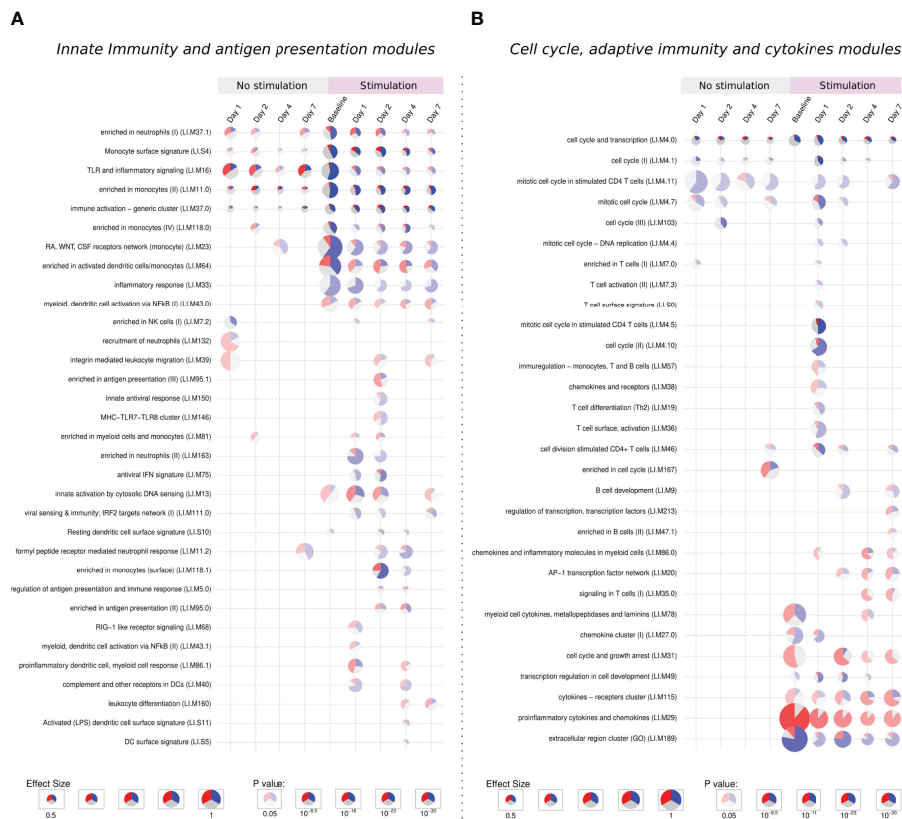


FIGURE 5 | Tmod enrichment analysis. From the list of genes provided by the DESeq2 package, genes were selected by their FDR value (< 0.05) and absolute log₂ Fold Change (> 0.5). The enriched blood transcription modules were obtained by the Hypergeometric test. **(A)** Modules related to innate immunity and antigen presentation, **(B)** modules related to cell cycle, adaptive immunity and cytokines modules. The effect size is proportional to the size of the pie, while the adjusted p-value is proportional to colour intensity. Within each pie, the proportion of significantly upregulated and downregulated genes is shown in red and blue, respectively. The gray portion of the pie represents genes that are not significantly differentially regulated.

main immune system modules activated for each comparison and time point. In total, 87 modules were significantly enriched, only 3 of them being specifically activated in infected samples, while 40 modules were only activated after stimulation of previously infected samples.

3.3.1 Activation of Extracellular Matrix, Cell Adhesion, and Innate Immune Response Modules

Five modules were consistently activated at almost all time points in both unstimulated and *in vitro* stimulated groups. Related to monocytes, immune activation, TLR signaling, and cell cycle, these modules showed a different pattern after stimulation, presenting more down-regulated genes. Following the same direction, modules related to the extracellular region, monocytes, and cell cycle are especially enriched in down-regulated genes after stimulation (Figures 5A, B).

The “extracellular region cluster” module shows the downregulation of genes involved in the interaction with extracellular components, growth control, and the vascular endothelium/angiogenesis (HSPG2, GH1, ENG). Moreover, the monocyte chemoattractant CCL2 is also down-regulated, while CCL18, important for the recruitment of T lymphocytes but not monocytes, is up-regulated.

The stimulation down-regulates genes responsible for the proliferation and differentiation of monocytes and macrophages like CSF2RA, CSF1R, and CSF3R, the latter one also important for adhesion. In monocytes modules, other genes linked to the extracellular matrix and cell adhesion followed the same behavior.

The downregulation of extracellular matrix genes could be due to the process of *in vitro* stimulation, decreasing the cell adhesion to the plate surface.

3.3.2 Activation of Cell Cycle, Cytokines, and Adaptive Immune Response Modules

The stimulation of infected samples led to the enrichment of many biological pathways not activated in the previous comparisons, including modules related to antiviral response, antigen presentation, T cells, B cells, and chemokines (Figures 5A, B).

On the first day, unstimulated samples presented the enrichment of T cell and cell cycle modules. After stimulation, these same modules are activated, together with many others related to T cells and cell cycle, in both cases enriched mainly by down-regulated genes.

In T cell modules we find down-regulated cell-cycle genes and genes linked to cell adhesion, like VCAM1 and SIR3PG, while ITGA4, another adhesion-related gene, was up-regulated in unstimulated samples but presented no change after stimulation. Negative regulators of the T cell activity (LILRB4, LILRB3, SIT1) were also downregulated, while the few up-regulated genes were mainly related to T cell activation (CD3E, GRAP2, CDCA7, and LAT).

On the other hand, the specific modules in late time points were mostly activated by up-regulated genes. We observe a stronger activation of the “cytokines – receptors cluster”

module and the specific enrichment of pathways like leukocyte differentiation, signaling in T cells, enriched in B cells, among other modules.

Cytokine modules are activated from the stimulation of baseline samples and looking inside these modules, indeed we see many up-regulated genes independently of the time point, especially those from the CCL family, IL1A, IL1RN, and TNF. Other genes such as CSF2, IL2RA, IL6, IL10 and IL1B present a modest increase in stimulation of baseline samples, but a major up-regulation at late time points.

Despite the high number of activated modules, the response to the stimuli after a previous infection does not show general up-regulation of the immune and inflammatory response. This second contact with the pathogen through the *in vitro* stimulation permitted us to appreciate biological processes which could not be detected in the primary infection, especially those related to antigen presentation, adaptive immunity, and cytokines. These processes are possibly related to a recall immune response starting within the first days after infection.

3.4 Cytokines Assay Suggests the Promotion of Innate and Adaptive Immune Responses From Day 4 After Infection

Regarding the concentration of cytokines in splenocyte culture supernatants, the infection without subsequent stimulation did not result in significant increases in the concentration of cytokines, with exception of IL-17a at day 7 after infection (data not shown).

The stimulation process induced a significant increase in KC and MIP-1a, compared to baseline samples (median of differences of 42.46 and 184.4 pg/ml, respectively). Despite cytokine changes between stimulated and control samples being noticeable in early stages, they increased considerably upon *in vitro* stimulation, at days 4 and 7 after the infection (Figure 6).

The comparison of stimulated samples from days 4 and 7 after infection with only infected samples showed a significant increase in all cytokine concentrations, with exception of MCP-1 and IL12p40 (Figure 6 and Supplementary Image 3), suggesting the involvement of both innate and adaptive branches of the immune system. This increase was more accentuated on day 7, in which the difference in the median between the stimulated and unstimulated groups was 2597 pg/ml for IL-17A, 769 pg/ml for GM-CSF and 374 pg/ml for IFN-gamma.

3.5 Gene Expression and Cytokines Data Integration Indicate Specific Patterns of Recall Immune Response After Stimulation

To identify the genes correlated with the increase in the concentration of cytokines, especially at late time points, data integration was performed using the sparse version of Partial Least Squares (sPLS), from MixOmics package. PLS can integrate two types of data measured on the same sample by maximizing the covariance between the components of each data set. The sparse version applies LASSO ℓ_1 penalizations in PLS analysis to perform feature selection.

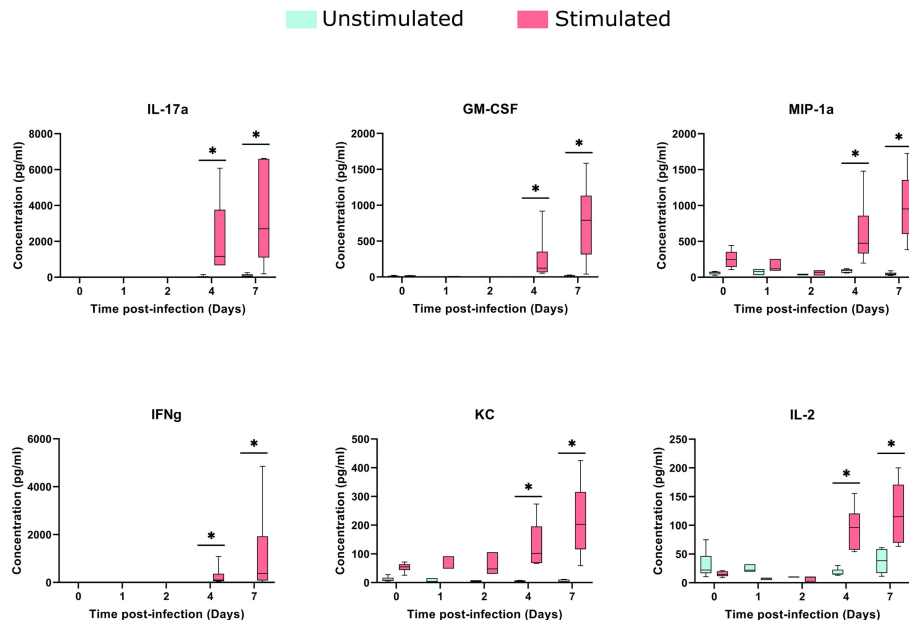


FIGURE 6 | Cytokines concentrations in the spleens after TIGR4 pneumococcal infection. The spleens were collected from infected mice at different time points and splenocytes were cultured for 72 hours in the presence or not of a stimulus (formalin-inactivated TIGR4 pneumococcal strain). The supernatants were collected and the concentration of 23 cytokines were assessed by Luminex immunoassay. Data was analyzed using GraphPad Prism software. To compare Stimulated to Unstimulated samples we used the Wilcoxon paired test. Concentrations from six of the cytokines are presented in the figure (for all the 23 cytokines see **Supplementary Image 3**). When compared to only infected samples, all the six cytokines presented a significant (*= $P < 0.05$) increase when stimulated in days 4 and 7 after infection.

As expected, the *in vitro* stimulated samples formed a different cluster compared to the non-stimulated samples, although there is a different behavior regarding time points in each cluster (**Figure 7A**). In the non-stimulated cluster there is a perturbation caused by infection, but some samples from day 7 cluster together with control samples from day 0. On the other hand, *in vitro* stimulated samples presented a different pattern, samples from days 4 and 7 form a new cluster, driven by the increase in cytokine concentration and the expression of certain genes (**Figure 7B**).

By performing data integration and feature selection, sPLS identifies the genes whose expression is strongly associated with the concentrations of cytokines, providing the correlation value for each variable. The genes with the highest values of correlation with the 23 cytokines were Cd69, Csf2, Il2ra, and Il2 (**Figure 7C**). Other genes related to the immune system (Foxp3, Tnfrsf4, Tnfrsf9, Il10, and Il6) were also found positively correlated with the cytokines.

3.6 Possible Biomarkers Elicited by *In Vitro* Stimulation

We aimed to understand if feature selection could summarize the impact of a previous infection on stimulated samples, indicating possible biomarkers of this infection. We applied the DaMiR-seq package, which provides data normalization, feature selection, and classification, based on different machine learning techniques. Three groups were established based on the transcriptomics and cytokine data distribution, focusing on the stimulation of uninfected samples, samples from early time

points after infection (days 1 and 2), and samples from late time points (days 4 and 7).

Eleven genes were chosen by applying a threshold of 0.5 to the scaled importance score identified by the DaMiR-seq package (**Supplementary Image 1**). These 11 genes allowed a clear clusterization of the three groups (**Figure 8**).

When compared to baseline stimulated samples, Fpr1, Nlrp3, and Slpi presented an increased expression in infected stimulated samples, independently of the time point. The stimulation of samples from early time points after the infection led to the increase in the expression of other inflammatory genes like Serpinb2 and Chil1 (Chitinase-3-like protein 1), and these values started to decrease in the subsequent days. At late time points, three other important genes, related to cytokine activity, had their expression increased when compared to the other groups: Ccr4, Csf2, and Il2.

Despite the small number of samples being a limitation for this type of analysis, the feature selection summarizes the new immunological processes that arise after the stimulation of infected samples and suggests the use of the *in vitro* stimulation model to detect the presence of a previous pneumococcal infection by measuring the expression of a few genes.

4 DISCUSSION

To characterize the host response to *S. pneumoniae* we proposed a murine model of intranasal infection followed by an *in vitro*

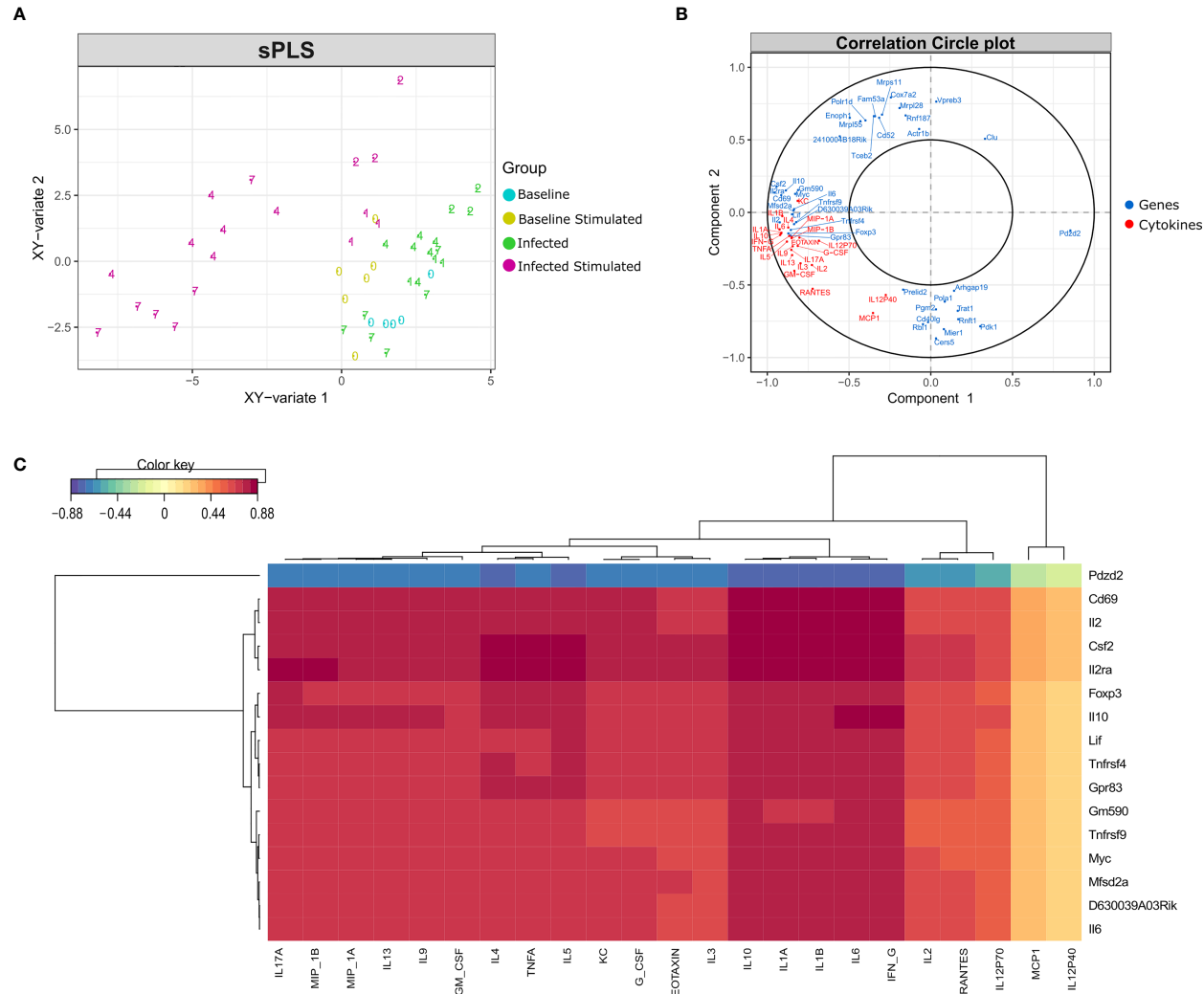


FIGURE 7 | Data integration using sPLS (Sparse Partial Least Squares). Data integration suggests a different pattern in stimulated samples from days 4 and 7 after infection, driven by the expression of a few genes and the concentration of most cytokines. **(A)** sPLS: Partial Least Squares regression applying the tune.spls function (MixOmics), 16 genes were selected for component 1 and 25 genes for component 2. Colors represent samples from different groups: infected or non-infected and with or without *in vitro* stimulation. Numbers indicate the study days. **(B)** Correlation Circle Plot: the selected genes (blue) and cytokines (red) are represented in a correlation circle plot. Variables positively associated are projected in the same direction from the origin, variables negatively correlated are projected in opposite directions. Variables displayed in a perpendicular angle are not correlated and the greater the distance from the origin the stronger the association. For example, the cytokine IL1B is positively correlated with the IL2 gene, but is negatively correlated with the gene Pdzd2. In general, cytokines and several genes related to cytokines are accumulated on the left side of the graph, indicating a high correlation among them. **(C)** Clustered Image Map (CIM): correlation between genes (mRNA), reported in vertical, and Cytokine production, in horizontal. The map highlights the correlation values for these variables for the genes selected on the first component of the sPLS. High positive correlations are represented by dark red, while high negative correlations by dark blue. Genes related to cytokines such as IL2ra, Csf2, IL10, IL6 and IL2 are positively correlated with most cytokines concentration. The select genes are strongly correlated with almost all cytokines, with exception of MCP1 and IL12p40.

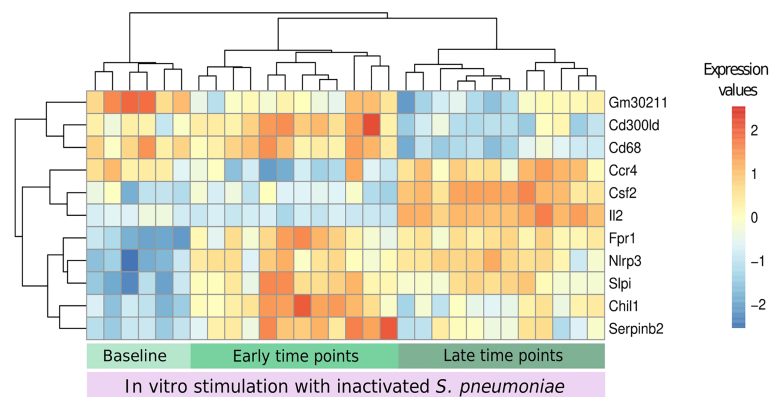


FIGURE 8 | Biomarkers of recall immune response. The DaMiR-seq package combines different classification methods to select possible biomarkers. After selecting the stimulated samples, this package was used to find genes involved in the differences between infected and uninfected samples after stimulation. Groups were established based on the results of data distribution (IPCA and sIPCA) and cytokines, where we observed a shared pattern between early time points (days 1 and 2) and another pattern at late time points (4 and 7). Eleven genes were selected based on the drop of the feature importance (**Supplementary Image 1**). The normalized expression values of the selected genes permitted to form three clear clusters.

stimulation of splenocytes with inactivated bacterial whole cells, at different time points after infection. Using a transcriptomic-based approach, our study has highlighted genes and biological pathways associated with the stimulation of baseline and previously infected samples, as well as the cytokines involved in the same processes.

In accordance with the genes selected by the sIPCA, the enrichment analysis has shown that the simple presence of inactivated bacteria leads to the activation of cytokines genes and different immune system pathways, mainly related to innate immunity. However, when this stimulation occurs in previously infected samples, there is a higher number of DEGs, revealing 40 new biological modules distributed across time points.

Stimulated samples presented downregulation of monocytes modules, together with the upregulation of antigen presentation and cytokine modules, which were also reported in gene expression data from alveolar macrophages (AM) in a pneumococcal colonization study, when comparing volunteers that developed carriage or not after experimental human pneumococcal challenge (Mitsi et al., 2020). In fact, the study did not suggest an increase in monocytes, but a higher monocyte-AM differentiation in people that developed carriage. On the other hand, monocytes seem to be recruited at the nose after the establishment of carriage (Jochems et al., 2018).

Recent vaccine studies have emphasized that innate immunity modules, including antigen presentation and dendritic cell activation, demonstrate stronger activation after a second contact with the antigen. Using an *in vivo* boost with the antigen alone following the priming with a chimeric vaccine against *Mycobacterium tuberculosis*, Santoro et al. have observed a faster and more robust response of dendritic cells and antigen presentation (Santoro et al., 2018). Similar results were recently observed in a different context, with an mRNA vaccine against SARS-CoV-2, in which the second dose activated new antigen presentation modules (Arunachalam et al., 2021).

Transcriptomics results have shown the presence of a particular response after a second contact with the pathogen and the concentrations of the cytokines suggested that this response is marked by different patterns of activation, with the stimulation allowing a better classification between early time points (1 and 2 days) and late time points (4 and 7) after infection. Moreover, the activated modules and the concentration of the soluble modulators suggested that both innate and adaptive branches of the immune system are promoted by the stimulation, suggesting cooperation between them.

In our model, cytokines secreted by macrophages, like MIP-1a (CCL3), KC (CXCL1), IL-1a, IL-1b, and IL-6 had a small, although significant, increase after stimulation of baseline samples. After stimulation of early time points, a small increase in the concentration of MIP-1b, RANTES, and TNF- α was observed, although not statistically significant. When the *in vitro* stimulus occurs at late time points after infection, the concentration of all these cytokines significantly increases, especially at day 7. In fact, innate immune responses to pneumococcus are known for polarization towards Th1 and Th17 responses through the release of cytokines (Bogaert et al., 2009).

Following this reasoning, it was expected that after the stimulation of baseline samples the cytokines linked to the adaptive immunity activation such as IL-17, IFN γ , and IL-2 did not present an increased concentration in comparison to unstimulated samples. G-CSF and GM-CSF presented a small increase, although not significant. Again, at early time points no important changes are seen, but at late time points, a significant increase in the concentration was observed for all these cytokines, suggesting the activation of a Th1 and Th17 response starting around day 4. A strong Th1 response characterized by high levels of IFN γ was also demonstrated in a murine model of bacterial meningitis by type 4 *S. pneumoniae*, already 48 hours after infection. (Pettini et al., 2015).

A previous study has highlighted the action of CD8 $^{+}$ T cells in helping AM to develop high MHC II expression after adenovirus

infection, a process that started coincidentally with the entry of T cells in the alveolar tissue, around 5 days after the infection (Yao et al., 2018). The activation of T cells in the spleen could follow a similar behavior in supporting macrophage activity and consequently increasing cytokine release.

Biomarker analysis and sPLS integration were employed to find genes that characterize the recall immune response and correlate with the increase in the concentration of the cytokines. Among the genes found positively correlated by the sPLS method, many were linked to the immune response. The TNF receptors *Tnfrsf9* and *Tnfrsf4*, are important for Th1 promotion and CD4 responses and, together with *Il2*, *Il2ra*, *Foxp3* and *Il10* participate in the “NF-kappaB signaling” biological pathway (Cho et al., 2021). Moreover, these genes are also associated with regulatory T cells, along with *Cd69* and *Il6*, two other features found correlated with cytokines in the same analysis (Maloy and Powrie, 2005; Kimura and Kishimoto, 2010; Chaudhry et al., 2011; Yu et al., 2018; Hinterbrandner et al., 2021).

The eleven genes selected as possible biomarkers are capable of correctly clustering the stimulated samples in the studied groups (baseline, early, and late time points, **Figure 8**). These genes could be cross validated in future studies using the same model of pneumococcal lung infection to study vaccine strategies and antimicrobial therapies. A link with pneumococcal infection, colonization, or vaccination was established in the literature for most of the selected genes. The *Il2* and *Csf2* genes were not only the first and third most important genes for the classification of samples regarding the presence of a previous infection but they were also among the genes with the highest correlation with the concentration of different cytokines, together with the *Il2ra* gene. This highlights the importance of the IL-2 signaling pathway to the described recall response. Indeed, different vaccine studies reported an increase in IL-2 cytokine after restimulation with pneumococcal proteins or peptides from these proteins (Kataoka et al., 2011; Singh et al., 2014; Elhaik Goldman et al., 2016; Converso et al., 2017).

Csf2 gene encodes for Granulocyte/Macrophage colony-stimulating factor (GM-CSF), a cytokine that presented one of the highest concentrations after stimulation of infected samples from late time points. Previous studies have described the increase in *Csf2* expression and GM-CSF concentration in the lungs from mice infected intranasally with *S. pneumoniae* (Steinwede et al., 2011). *In vitro* stimulation of PBMCs with *S. pneumoniae* has also increased the concentration of this cytokine. Furthermore, a protective role of GM-CSF in pneumococcal infection was described with intra-alveolar administration of this cytokine (Schmeck et al., 2004; Steinwede et al., 2011) and the resistance to lung infection attributed to the microbiota was found to be through GM-CSF signaling (Brown et al., 2017).

The lack of *Fpr1* and *Chil1* led to a higher mortality rate in murine models of pneumococcal meningitis and pneumonia, respectively (Dela Cruz et al., 2012; Oldekamp et al., 2014).

Slpi is involved in the innate immune response to bacterial infections, regulating the NF-kappa-B activation and inflammatory responses. This gene was up-regulated in the lungs of mice infected with pneumococcus, but the same was not observed in the spleen, suggesting that its expression is modulated at the site of

inflammation in the presence of inflammatory stimuli (Abe et al., 1997). Our data suggested a similar result, since *Slpi* expression did not change in the spleen of infected samples, but only increased after the *in vitro* stimulation.

Cd300ld presents no clear link with pneumococcal infection, but its encoded protein, an activating receptor in myeloid and mast cells, was downregulated in the blood of mice infected with *Streptococcus suis* (Dai et al., 2018).

The link of most of the selected genes with the physiopathology of pneumococcal infection supports the use of feature selection and machine learning techniques to unveil gene signatures, potentially finding new features and/or assigning new roles to genes involved in a process, such as recall responses. The changes in cytokines concentration and gene expression are two important ways to assess immunological information after infection or vaccination. Our findings suggest that *in vitro* stimulation is an important step to understanding the systemic response to pneumococcal lung infection and the immunological memory generated by this bacteria. The analysis of transcriptomic and cytokine data revealed a clustering of the samples based on the stage of infection (early vs late), with more intense signals at late time points. Integrative analysis identified few genes, related to the immune system, which could categorize the samples based on the infection stage and which may be useful in future studies to monitor vaccine immune response and experimental therapies efficacy.

DATA AVAILABILITY STATEMENT

The datasets generated for this study can be found in the GEO database under accession number: <https://www.ncbi.nlm.nih.gov/geo/query/acc.cgi?acc=GSE199605>. The bioinformatic analysis can be accessed at https://github.com/IsaMoscardini/Spleen_stimulation.

ETHICS STATEMENT

The animal study was reviewed and approved by the Italian Ministry of Health with authorization n° 304/2018-PR.

AUTHOR CONTRIBUTIONS

GP, FI and FS conceived and designed the experiments. FS and MC prepared the bacteria for animal infection and for *in vitro* stimulation. MC, FF, SG and EP performed animal experiments. MC and CG performed transcriptomic analysis. MC and FF analysed cytokines. DM secured funding. IM analysed data and drafted the paper with contributions from FS, AG and GP. All the authors reviewed, edited and approved the final version of the manuscript.

FUNDING

This study was carried out with financial support from the Commission of the European Communities, Seventh

Framework Programme, Innovative Medicines Initiative Joint Undertaking “Biomarkers for Enhanced Vaccine Safety” project BioVacSafe (IMI JU Grant No. 115308).

IM received a PhD fellowship under the Marie Skłodowska-Curie actions (MSCA) – Innovative Training Networks (ITN), Project VacPath (Novel vaccine vectors to resist pathogen challenge) grant agreement No 812915 funded by the European Union’s Horizon 2020 research and innovation programme.

SUPPLEMENTARY MATERIAL

The Supplementary Material for this article can be found online at: <https://www.frontiersin.org/articles/10.3389/fcimb.2022.869763/full#supplementary-material>

REFERENCES

- Abe, T., Tominaga, Y., Kikuchi, T., Watanabe, A., Satoh, K., Watanabe, Y., et al. (1997). Bacterial Pneumonia Causes Augmented Expression of the Secretory Leukoprotease Inhibitor Gene in the Murine Lung. *Am. J. Respir. Crit. Care Med.* 156, 1235–1240. doi: 10.1164/ajrccm.156.4.9701075
- Arunachalam, P. S., Scott, M. K. D., Hagan, T., Li, C., Feng, Y., Wimmers, F., et al. (2021). Systems Vaccinology of the BNT162b2 mRNA Vaccine in Humans. *Nature* 596, 410–416. doi: 10.1038/s41586-021-03791-x
- Bogaert, D., Weinberger, D., Thompson, C., Lipsitch, M., and Malley, R. (2009). Impaired Innate and Adaptive Immunity to Streptococcus Pneumoniae and its Effect on Colonization in an Infant Mouse Model. *Infect. Immun.* 77, 1613–1622. doi: 10.1128/IAI.00871-08
- Briles, D. E., Paton, J. C., Mukerji, R., Swiatlo, E., and Crain, M. J. (2019). Pneumococcal Vaccines. *Microbiol. Spectr.* 7(6). doi: 10.1128/microbiolspec.GPP3-0028-2018
- Brown, R. L., Sequeira, R. P., and Clarke, T. B. (2017). The Microbiota Protects Against Respiratory Infection via GM-CSF Signaling. *Nat. Commun.* 8, 1512. doi: 10.1038/s41467-017-01803-x
- Cerutti, A., Cols, M., and Puga, I. (2013). Marginal Zone B Cells: Virtues of Innate-Like Antibody-Producing Lymphocytes. *Nat. Rev. Immunol.* 13, 118–132. doi: 10.1038/nri3383
- Chaudhry, A., Samstein, R. M., Treuting, P., Liang, Y., Pils, M. C., Heinrich, J.-M., et al. (2011). Interleukin-10 Signaling in Regulatory T Cells is Required for Suppression of Th17 Cell-Mediated Inflammation. *Immunity* 34, 566–578. doi: 10.1016/j.immuni.2011.03.018
- Chiesa, M., Colombo, G. I., and Piacentini, L. (2018). DaMiRseq—an R/Bioconductor Package for Data Mining of RNA-Seq Data: Normalization, Feature Selection and Classification. *Bioinformatics* 34, 1416–1418. doi: 10.1093/bioinformatics/btx795
- Cho, J.-W., Son, J., Ha, S.-J., and Lee, I. (2021). Systems Biology Analysis Identifies TNFRSF9 as a Functional Marker of Tumor-Infiltrating Regulatory T-Cell Enabling Clinical Outcome Prediction in Lung Cancer. *Comput. Struct. Biotechnol. J.* 19, 860–868. doi: 10.1016/j.csbj.2021.01.025
- Converso, T. R., Goulart, C., Rodriguez, D., Darrieux, M., and Leite, L. C. C. (2017). Systemic Immunization With Rpotd Reduces Streptococcus Pneumoniae Nasopharyngeal Colonization in Mice. *Vaccine* 35, 149–155. doi: 10.1016/j.vaccine.2016.11.027
- Dai, J., Lai, L., Tang, H., Wang, W., Wang, S., Lu, C., et al. (2018). Streptococcus Suis Synthesizes Deoxyadenosine and Adenosine by 5'-Nucleotidase to Dampen Host Immune Responses. *Virulence* 9, 1509–1520. doi: 10.1080/21505594.2018.1520544
- Dela Cruz, C. S., Liu, W., He, C. H., Jacoby, A., Gornitzky, A., Ma, B., et al. (2012). Chitinase 3-Like-1 Promotes Streptococcus Pneumoniae Killing and Augments Host Tolerance to Lung Antibacterial Responses. *Cell Host Microbe* 12, 34–46. doi: 10.1016/j.chom.2012.05.017
- Deniset, J. F., Surewaard, B. G., Lee, W.-Y., and Kubes, P. (2017). Splenic Ly6Ghigh Mature and Ly6Gint Immature Neutrophils Contribute to
- Eradication of S. Pneumoniae. *J. Exp. Med.* 214, 1333–1350. doi: 10.1084/jem.20161621
- de Stoppelaar, S. F., Claushuis, T. A. M., Schaap, M. C. L., Hou, B., van der Poll, T., Nieuwland, R., et al. (2016). Toll-Like Receptor Signalling Is Not Involved in Platelet Response to Streptococcus Pneumoniae In Vitro or In Vivo. *PLoS One* 11, e0156977. doi: 10.1371/journal.pone.0156977
- Elhaik Goldman, S., Dotan, S., Talias, A., Lilo, A., Azriel, S., Malka, I., et al. (2016). Streptococcus Pneumoniae Fructose-1,6-Bisphosphate Aldolase, a Protein Vaccine Candidate, Elicits Th1/Th2/Th17-Type Cytokine Responses in Mice. *Int. J. Mol. Med.* 37, 1127–1138. doi: 10.3892/ijmm.2016.2512
- Ercoli, G., Fernandes, V. E., Chung, W. Y., Wanford, J. J., Thomson, S., Bayliss, C. D., et al. (2018). Intracellular Replication of Streptococcus Pneumoniae Inside Splenic Macrophages Serves as a Reservoir for Septicaemia. *Nat. Microbiol.* 3, 600–610. doi: 10.1038/s41564-018-0147-1
- Fiorino, F., Pettini, E., Koeberling, O., Ciabattini, A., Pozzi, G., Martin, L. B., et al. (2021). Long-Term Anti-Bacterial Immunity Against Systemic Infection by Salmonella Enterica Serovar Typhimurium Elicited by a GMMA-Based Vaccine. *Vaccines (Basel)* 9, 495. doi: 10.3390/vaccines9050495
- Gerlini, A., Colomba, L., Furi, L., Braccini, T., Manso, A. S., Pammolli, A., et al. (2014). The Role of Host and Microbial Factors in the Pathogenesis of Pneumococcal Bacteraemia Arising From a Single Bacterial Cell Bottleneck. *PLoS Pathog.* 10, e1004026. doi: 10.1371/journal.ppat.1004026
- Hinterbrandner, M., Rubino, V., Stoll, C., Forster, S., Schnüriger, N., Radpour, R., et al. (2021). Tnfrsf4-Expressing Regulatory T Cells Promote Immune Escape of Chronic Myeloid Leukemia Stem Cells. *JCI Insight* 6, e151797. doi: 10.1172/jci.insight.151797
- Iannelli, F., Santoro, F., Fox, V., and Pozzi, G. (2021). A Mating Procedure for Genetic Transfer of Integrative and Conjugative Elements (ICEs) of Streptococci and Enterococci. *Methods Protoc.* 4, 59. doi: 10.3390/mps4030059
- Jochems, S. P., Marcon, F., Carniel, B. F., Holloway, M., Mitsi, E., Smith, E., et al. (2018). Inflammation Induced by Influenza Virus Impairs Human Innate Immune Control of Pneumococcus. *Nat. Immunol.* 19, 1299–1308. doi: 10.1038/s41590-018-0231-y
- Kadioglu, A., Cuppone, A. M., Trappetti, C., List, T., Spreafico, A., Pozzi, G., et al. (2011). Sex-Based Differences in Susceptibility to Respiratory and Systemic Pneumococcal Disease in Mice. *J. Infect. Dis.* 204, 1971–1979. doi: 10.1093/infdis/jir657
- Kaplan, S. L., Barson, W. J., Lin, P. L., Romero, J. R., Bradley, J. S., Tan, T. Q., et al. (2013). Early Trends for Invasive Pneumococcal Infections in Children After the Introduction of the 13-Valent Pneumococcal Conjugate Vaccine. *Pediatr. Infect. Dis. J.* 32, 203–207. doi: 10.1097/INF.0b013e318275614b
- Kataoka, K., Fujihashi, K., Oma, K., Fukuyama, Y., Hollingshead, S. K., Sekine, S., et al. (2011). The Nasal Dendritic Cell-Targeting Flt3 Ligand as a Safe Adjuvant Elicits Effective Protection Against Fatal Pneumococcal Pneumonia. *Infect. Immun.* 79, 2819–2828. doi: 10.1128/IAI.01360-10
- Kimura, A., and Kishimoto, T. (2010). IL-6: Regulator of Treg/Th17 Balance. *Eur. J. Immunol.* 40, 1830–1835. doi: 10.1002/eji.201040391

- Lê Cao, K.-A., Rossouw, D., Robert-Granié, C., and Besse, P. (2008). A Sparse PLS for Variable Selection When Integrating Omics Data. *Stat. Appl. Genet. Mol. Biol.* 7. doi: 10.2202/1544-6115.1390
- Li, S., Roupahel, N., Duraisingham, S., Romero-Steiner, S., Presnell, S., Davis, C., et al. (2014). Molecular Signatures of Antibody Responses Derived From a Systems Biology Study of Five Human Vaccines. *Nat. Immunol.* 15, 195–204. doi: 10.1038/ni.2789
- Love, M. I., Huber, W., and Anders, S. (2014). Moderated Estimation of Fold Change and Dispersion for RNA-Seq Data With Deseq2. *Genome Biol.* 15, 550. doi: 10.1186/s13059-014-0550-8
- Maloy, K. J., and Powrie, F. (2005). Fueling Regulation: IL-2 Keeps CD4⁺ Treg Cells Fit. *Nat. Immunol.* 6, 1071–1072. doi: 10.1038/ni1105-1071
- Mitsi, E., Carniel, B., Reiné, J., Rylance, J., Zaidi, S., Soares-Schanoski, A., et al. (2020). Nasal Pneumococcal Density Is Associated With Microaspiration and Heightened Human Alveolar Macrophage Responsiveness to Bacterial Pathogens. *Am. J. Respir. Crit. Care Med.* 201, 335–347. doi: 10.1164/rccm.201903-0607OC
- Moffitt, K. L., Gierahn, T. M., Lu, Y., Gouveia, P., Alderson, M., Flechtner, J. B., et al. (2011). T(H)17-Based Vaccine Design for Prevention of Streptococcus Pneumoniae Colonization. *Cell Host Microbe* 9, 158–165. doi: 10.1016/j.chom.2011.01.007
- Oldekamp, S., Pscheidt, S., Kress, E., Soehnlein, O., Jansen, S., Pufe, T., et al. (2014). Lack of Formyl Peptide Receptor 1 and 2 Leads to More Severe Inflammation and Higher Mortality in Mice With of Pneumococcal Meningitis. *Immunology* 143, 447–461. doi: 10.1111/imm.12324
- Paranavithana, C., Zelazowska, E., DaSilva, L., Pittman, P. R., and Nikolich, M. (2010). Th17 Cytokines in Recall Responses Against Francisella Tularensis in Humans. *J. Interferon Cytokine Res.* 30, 471–476. doi: 10.1089/jir.2009.0108
- Pettini, E., Fiorino, F., Cuppone, A. M., Iannelli, F., Medagliani, D., and Pozzi, G. (2015). Interferon- γ From Brain Leukocytes Enhances Meningitis by Type 4 Streptococcus Pneumoniae. *Front. Microbiol.* 6. doi: 10.3389/fmicb.2015.01340
- Pichichero, M. E. (2017). Pneumococcal Whole-Cell and Protein-Based Vaccines: Changing the Paradigm. *Expert Rev. Vaccines* 16, 1181–1190. doi: 10.1080/14760584.2017.1393335
- Santoro, F., Donato, A., Lucchesi, S., Sorgi, S., Gerlini, A., Haks, M. C., et al. (2021). Human Transcriptomic Response to the VSV-Vectored Ebola Vaccine. *Vaccines (Basel)* 9, 67. doi: 10.3390/vaccines9020067
- Santoro, F., Pettini, E., Kazmin, D., Ciabattini, A., Fiorino, F., Gilfillan, G. D., et al. (2018). Transcriptomics of the Vaccine Immune Response: Priming With Adjuvant Modulates Recall Innate Responses After Boosting. *Front. Immunol.* 9. doi: 10.3389/fimmu.2018.01248
- Schmeck, B., Zahlten, J., Moog, K., van Laak, V., Huber, S., Hocke, A. C., et al. (2004). Streptococcus Pneumoniae-Induced P38 MAPK-Dependent Phosphorylation of RelA at the Interleukin-8 Promotor. *J. Biol. Chem.* 279, 53241–53247. doi: 10.1074/jbc.M313702200
- Schultz, M. J., Speelman, P., Zaat, S., van Deventer, S. J., and van der Poll, T. (1998). Erythromycin Inhibits Tumor Necrosis Factor Alpha and Interleukin 6 Production Induced by Heat-Killed Streptococcus Pneumoniae in Whole Blood. *Antimicrob. Agents Chemother.* 42, 1605–1609. doi: 10.1128/AAC.42.7.1605
- Shao, J., Zhang, J., Wu, X., Mao, Q., Chen, P., Zhu, F., et al. (2015). Comparing the Primary and Recall Immune Response Induced by a New EV71 Vaccine Using Systems Biology Approaches. *PloS One* 10, e0140515. doi: 10.1371/journal.pone.0140515
- Singh, R., Gupta, P., Sharma, P. K., Ades, E. W., Hollingshead, S. K., Singh, S., et al. (2014). Prediction and Characterization of Helper T-Cell Epitopes From Pneumococcal Surface Adhesin A. *Immunology* 141, 514–530. doi: 10.1111/imm.12194
- Steinwede, K., Tempelhof, O., Bolte, K., Maus, R., Bohling, J., Ueberberg, B., et al. (2011). Local Delivery of GM-CSF Protects Mice From Lethal Pneumococcal Pneumonia. *J. Immunol.* 187, 5346–5356. doi: 10.4049/jimmunol.1101413
- Trammell, R. A., and Toth, L. A. (2011). Markers for Predicting Death as an Outcome for Mice Used in Infectious Disease Research. *Comp. Med.* 61, 492–498.
- Weiner, J. N., Ferreira, D. M., and Paton, J. C. (2018). Streptococcus Pneumoniae: Transmission, Colonization and Invasion. *Nat. Rev. Microbiol.* 16, 355–367. doi: 10.1038/s41579-018-0001-8
- Wu, Y., Mao, H., Ling, M.-T., Chow, K.-H., Ho, P.-L., Tu, W., et al. (2011). Successive Influenza Virus Infection and Streptococcus Pneumoniae Stimulation Alter Human Dendritic Cell Function. *BMC Infect. Dis.* 11, 201. doi: 10.1186/1471-2334-11-201
- Yao, F., Coquery, J., and Lê Cao, K.-A. (2012). Independent Principal Component Analysis for Biologically Meaningful Dimension Reduction of Large Biological Data Sets. *BMC Bioinf.* 13, 24. doi: 10.1186/1471-2105-13-24
- Yao, Y., Jeyanthan, M., Haddadi, S., Barra, N. G., Vaseghi-Shanjani, M., Damjanovic, D., et al. (2018). Induction of Autonomous Memory Alveolar Macrophages Requires T Cell Help and Is Critical to Trained Immunity. *Cell* 175, 1634–1650.e17. doi: 10.1016/j.cell.2018.09.042
- Yu, L., Yang, F., Zhang, F., Guo, D., Li, L., Wang, X., et al. (2018). CD69 Enhances Immunosuppressive Function of Regulatory T-Cells and Attenuates Colitis by Prompting IL-10 Production. *Cell Death Dis.* 9, 905. doi: 10.1038/s41419-018-0927-9
- Zhan, Y., and Cheers, C. (1995). Differential Induction of Macrophage-Derived Cytokines by Live and Dead Intracellular Bacteria In Vitro. *Infect. Immun.* 63, 720–723. doi: 10.1128/iai.63.2.720-723.1995

Conflict of Interest: Authors IM and AG are employed by Microbiotec srl.

The remaining authors declare that the research was conducted in the absence of any commercial or financial relationships that could be construed as a potential conflict of interest.

Publisher's Note: All claims expressed in this article are solely those of the authors and do not necessarily represent those of their affiliated organizations, or those of the publisher, the editors and the reviewers. Any product that may be evaluated in this article, or claim that may be made by its manufacturer, is not guaranteed or endorsed by the publisher.

Copyright © 2022 Moscardini, Santoro, Carraro, Gerlini, Fiorino, Germoni, Gholami, Pettini, Medagliani, Iannelli and Pozzi. This is an open-access article distributed under the terms of the Creative Commons Attribution License (CC BY). The use, distribution or reproduction in other forums is permitted, provided the original author(s) and the copyright owner(s) are credited and that the original publication in this journal is cited, in accordance with accepted academic practice. No use, distribution or reproduction is permitted which does not comply with these terms.



Pneumococcal BgaA Promotes Host Organ Bleeding and Coagulation in a Mouse Sepsis Model

Moe Takemura^{1,2}, Masaya Yamaguchi^{1*}, Momoko Kobayashi¹, Tomoko Sumitomo¹, Yujiro Hirose¹, Daisuke Okuzaki³, Masayuki Ono¹, Daisuke Motooka³, Kana Goto^{1,4}, Masanobu Nakata^{1,5}, Narikazu Uzawa² and Shigetada Kawabata¹

OPEN ACCESS

Edited by:

Jorge Eugenio Vidal,
University of Mississippi Medical
Center, United States

Reviewed by:

Karthik Subramanian,
Rajiv Gandhi Centre for Biotechnology,
India

Anukul T. Shenoy,
Boston University, United States

*Correspondence:

Masaya Yamaguchi
yamaguchi.masaya.dent@osaka-
u.ac.jp

Specialty section:

This article was submitted to
Molecular Bacterial Pathogenesis,
a section of the journal
Frontiers in Cellular and
Infection Microbiology

Received: 27 December 2021

Accepted: 01 June 2022

Published: 01 July 2022

Citation:

Takemura M, Yamaguchi M,
Kobayashi M, Sumitomo T, Hirose Y,
Okuzaki D, Ono M, Motooka D,
Goto K, Nakata M, Uzawa N
and Kawabata S (2022)
Pneumococcal BgaA Promotes Host
Organ Bleeding and Coagulation
in a Mouse Sepsis Model.
Front. Cell. Infect. Microbiol. 12:844000.
doi: 10.3389/fcimb.2022.844000

¹ Department of Oral and Molecular Microbiology, Osaka University Graduate School of Dentistry, Suita, Osaka, Japan,

² Department of Oral and Maxillofacial Surgery II, Osaka University Graduate School of Dentistry, Suita, Osaka, Japan,

³ Genome Information Research Center, Research Institute for Microbial Diseases, Osaka University, Suita, Osaka, Japan,

⁴ Department of Pediatric Dentistry, Okayama University Graduate School of Medicine, Dentistry and Pharmaceutical Sciences, Okayama, Japan, ⁵ Department of Oral Microbiology, Kagoshima University Graduate School of Medical and Dental Sciences, Kagoshima, Japan

Streptococcus pneumoniae is a major cause of invasive diseases such as pneumonia, meningitis, and sepsis, with high associated mortality. Our previous molecular evolutionary analysis revealed that the *S. pneumoniae* gene *bgaA*, encoding the enzyme β -galactosidase (BgaA), had a high proportion of codons under negative selection among the examined pneumococcal genes and that deletion of *bgaA* significantly reduced host mortality in a mouse intravenous infection assay. BgaA is a multifunctional protein that plays a role in cleaving terminal galactose in *N*-linked glycans, resistance to human neutrophil-mediated opsonophagocytic killing, and bacterial adherence to human epithelial cells. In this study, we performed *in vitro* and *in vivo* assays to evaluate the precise role of *bgaA* as a virulence factor in sepsis. Our *in vitro* assays showed that the deletion of *bgaA* significantly reduced the bacterial association with human lung epithelial and vascular endothelial cells. The deletion of *bgaA* also reduced pneumococcal survival in human blood by promoting neutrophil-mediated killing, but did not affect pneumococcal survival in mouse blood. In a mouse sepsis model, mice infected with an *S. pneumoniae* *bgaA*-deleted mutant strain exhibited upregulated host innate immunity pathways, suppressed tissue damage, and blood coagulation compared with mice infected with the wild-type strain. These results suggest that BgaA functions as a multifunctional virulence factor whereby it induces host tissue damage and blood coagulation. Taken together, our results suggest that BgaA could be an attractive target for drug design and vaccine development to control pneumococcal infection.

Keywords: *Streptococcus pneumoniae*, BgaA, coagulation, virulence factor, neutrophil

INTRODUCTION

Streptococcus pneumoniae is an α -hemolytic gram-positive bacterium. Approximately 5%–10% of healthy adults and 20%–40% of healthy children carry *S. pneumoniae* asymptomatically in their oral and nasopharyngeal mucosa (Bogaert et al., 2004; Otsuka et al., 2013). Nonetheless, pneumococcal pneumonia is responsible for approximately 200 million cases and ~1.2 million deaths annually worldwide (GBD 2016 LowerRespiratory Infections Collaborators). In addition, *S. pneumoniae* can invade the host bloodstream, grow in blood and/or organs, and cause invasive pneumococcal diseases (IPD) such as meningitis and sepsis (CDC, 2019).

Currently, pneumococcal vaccines such as the 13-valent pneumococcal conjugate vaccine (PCV-13) and the 23-valent pneumococcal polysaccharide vaccine (PPV23) are licensed and used in many countries. Although pneumococcal vaccines have significantly reduced the incidence of pneumococcal infections globally (CDC, 2019), they also create a selective pressure that increases the emergence of non-vaccine serotypes of *S. pneumoniae*, causing the incidence of IPD to remain substantial (Flasche et al., 2011; Golubchik et al., 2012; Kim et al., 2016; Asner et al., 2019). In addition, *S. pneumoniae* is an antibiotic-resistant medium-priority pathogen, and antibiotic-resistant pneumococcal clones are emerging and expanding (WHO, 2017; CDC, 2019). Recently, we reported that pneumococcal strains isolated in Yangon, Myanmar, carried various antimicrobial resistance genes (Yamaguchi et al., 2021) that hinder the treatment of IPD. Thus, understanding the pneumococcal infectious process and the exacerbation mechanism is necessary to control IPD.

Previously, we performed molecular evolutionary analysis and laboratory-based analyses of streptococcal proteins (Yamaguchi et al., 2016; Yamaguchi, 2018; Yamaguchi et al., 2019a; Yamaguchi et al., 2019b). Negative selection plays an important role in maintaining the long-term stability of biological structures by removing deleterious mutations (Loewe, 2008). Mutations in nonessential but important genes promote the selection of bacterial lineages in the species. In other words, nonessential genes are under considerable negative selection, which would be important for the survival and/or evolutionary success of the species in the host and/or the environment. Our previous study focused on the evolutionary selective pressure on cell wall-anchoring proteins and demonstrated that *bgaA* was under remarkable negative selection pressure (Yamaguchi et al., 2020). The *bgaA* gene encodes the enzyme exo- β -galactosidase (BgaA), which hydrolyzes β 1-4 linkages between galactose and glucose or *N*-acetylglucosamine residues (Hobbs et al., 2018). Further bioinformatic and *in vitro* analyses indicated that the BgaA active site is evolutionarily conserved, and that the deletion of *bgaA* in *S. pneumoniae* significantly reduced mortality in a mouse model of blood infection (Yamaguchi et al., 2020). However, the precise role of BgaA in pneumococcal sepsis remains unknown.

S. pneumoniae expresses surface-associated exoglycosidases, including BgaA, the exo- α -neuraminidase NanN, and the exo- β -

N-acetylglucosaminidase StrH, which can degrade some host *N*-glycans (Robb et al., 2017). This results in the release of glycan molecules, which can be utilized by *S. pneumoniae* as a carbon source (Robb et al., 2017). In addition to its galactosidase activity, BgaA presents additional roles and is regarded as a multifunctional protein. For example, an adhesion assay using human epithelial cell lines showed that BgaA contributes to pneumococcal adherence to the cells in a glycosidase activity-independent manner (Limoli et al., 2011). BgaA also contributes to *in vivo* biofilm formation through the exposure of galactose (Blanchette et al., 2016). In addition, an opsonophagocytic killing assay indicated that BgaA plays an important role in the resistance to complement deposition and subsequent phagocytic killing (Dalia et al., 2010). In this study, we performed several *in vitro* and *in vivo* infection assays to further elucidate the role of BgaA in sepsis.

MATERIALS AND METHODS

Bacterial Strains and Cell Culture

S. pneumoniae strains were cultured as previously described elsewhere (Mori et al., 2012; Yamaguchi et al., 2019b; Yamaguchi et al., 2020). Briefly, the *S. pneumoniae* strain TIGR4 wild type (WT) and its isogenic *bgaA* mutant strain [$\Delta bgaA$, (Yamaguchi et al., 2020)] were cultured at 37°C in Todd-Hewitt broth (BD Biosciences, Franklin Lakes, NJ, USA) supplemented with 0.2% yeast extract (THY; BD Biosciences). For the following assays, *S. pneumoniae* strains were grown to exponential growth phase ($OD_{600} = \sim 0.40$) unless otherwise indicated and then resuspended in phosphate buffered saline (PBS) or the appropriate buffer.

Cell culture was performed as previously described (Sumitomo et al., 2012; Yamaguchi et al., 2016). Briefly, human alveolar A549 cells were maintained in Dulbecco's modified Eagle's medium (DMEM; Fujifilm Wako Pure Chemical Corporation, Osaka, Japan) supplemented with 10% fetal bovine serum (FBS), and human brain endothelial cells (hBMECs) were maintained in RPMI 1640 medium (Fujifilm Wako Pure Chemical Corporation) supplemented with 10% FBS, 10% NuSerum (BD Biosciences), and 1% MEM nonessential amino acids (Merck KGaA, Darmstadt, Germany). hBMECs were seeded and grown in collagen-coated plates. All cells were maintained at 37°C in a 5% CO₂ humidified environment.

S. pneumoniae Association Assays

Pneumococcal association with A549 cells and hBMECs was performed as previously described, with minor modifications (Yamaguchi et al., 2008; Yamaguchi et al., 2017). Briefly, human epithelial or endothelial cells were seeded at a density of 1×10^5 cells per well in 24-well plates 24 h before infection. In each well, $0.3\text{--}6.0 \times 10^7$ CFU of *S. pneumoniae* was added to infect cells. To determine the bacterial association, the infected cells were incubated for 1 h, washed twice with PBS, and then harvested with a solution containing 0.05% trypsin and 0.025%

Triton X-100. The associated *S. pneumoniae* was quantified using serial dilution plating on THY-blood agar.

Blood and Neutrophil Bactericidal Assays

Bactericidal assays were performed as previously described, with minor modifications (Mori et al., 2012; Yamaguchi et al., 2019a; Yamaguchi et al., 2019b). Briefly, heparinized human blood (190 μ L), mouse blood (180 μ L), or human neutrophils (2×10^5 cells in 180 μ L), and exponential phase bacteria (0.9 – 2.0×10^4 CFU, 1.5 – 13.3×10^4 CFU, and 1.8 – 8.3×10^4 CFU for human blood, mouse blood, and human neutrophils in 10, 20, or 20 μ L of PBS, respectively) were mixed in 96-well plates and incubated at 37°C in 5% CO₂ for 1, 2, or 3 h. Viable cell counts were determined by plating diluted samples on THY-blood agar. The growth index was calculated as the number of CFUs at the specified time point divided by the number of CFUs in the initial inoculum.

Human blood was collected *via* the median cubital vein from healthy donors who agreed to a protocol approved by the Institutional Review Board of Osaka University Graduate School of Dentistry (H26-E43). Human neutrophils were isolated from fresh human blood using Polymorphprep (Alere Technologies AS, Oslo, Norway) according to the manufacturer's instructions. Mouse blood was collected *via* cardiac puncture from healthy 6–7 weeks-old CD-1 female mice (Slc:ICR; Japan SLC, Hamamatsu, Japan). All mouse experiments were conducted following a protocol approved by the Animal Care and Use Committee of Osaka University Graduate School of Dentistry (28-002-0).

Mouse Infection Assays

Mouse infection assays were performed as previously described (Hirose et al., 2018; Yamaguchi et al., 2019a; Yamaguchi et al., 2019b; Yamaguchi et al., 2020). In the sepsis model, female CD-1 mice (Slc:ICR, 6–7-weeks-old) were intravenously infected with 0.4 – 7.1×10^6 CFU of *S. pneumoniae* TIGR4 WT or $\Delta bgaA$ strains *via* the tail vein. To assess bacterial burden, animals were euthanized by lethal intraperitoneal injection of sodium pentobarbital 24 and 36 h after intravenous infection, and blood, brain, lung, liver, spleen, and kidney samples were collected. Bacterial counts in blood or tissue homogenates were determined after plating serial dilutions, with those in the organ corrected for differences in tissue weight. To examine the histopathological features, each tissue specimen was fixed with 4% formaldehyde, embedded in paraffin, and cut into sections that were stained with hematoxylin and eosin solution. The stained tissues were observed using a BZ-X710 microscope (Keyence, Osaka, Japan).

RNA-Seq and Data Analysis

Murine blood was obtained at 12, 24, and 36 h after intravenous infection by cardiac puncture after lethal intraperitoneal injection of sodium pentobarbital. Heparin was added to the blood at a final concentration of 30 U/mL. Total RNA was extracted from leukocytes in the whole blood samples using the PureLink Total RNA Blood Purification Kit and DNase I, Amplification Grade (Thermo Fisher Scientific). RNA integrity was assessed using a 2100 Bioanalyzer (Agilent Technologies,

Santa Clara, CA, USA). Full-length cDNA was generated using a SMART-Seq HT Kit (Takara Bio, Shiga, Japan) according to the manufacturer's instructions. An Illumina library was prepared using a Nextera XT DNA Library Prep Kit (Illumina, San Diego, CA, USA) according to SMARTer kit instructions. Libraries were sequenced using the Illumina HiSeq 2500 system, with 75 bp single-end reads obtained. The obtained RNA-seq data were analyzed using iDEP ver 0.91, 0.92 or 0.951 (Ge et al., 2018; Ge, 2021). Pathway analysis was performed using the GAGE package and Kyoto Encyclopedia of Genes and Genomes (KEGG) or Reactome datasets on iDEP (Yu and He, 2016; Kanehisa et al., 2017). Raw data generated in this study was submitted to the Gene Expression Omnibus (GEO) dataset under the accession number GSE190418.

Measurement of Mouse Plasma Cytokines and Chemokines

Mouse plasma was collected at 24 and 36 h after pneumococcal intravenous infection. Cytokine and chemokine concentrations in mouse plasma were measured by MILLIPLEX MAP Mouse Cytokine/Chemokine Magnetic Bead Panel (catalogue number: MCYTOMAG-70K, Merck) and MAGPIX Dx instrument with xPONENT 4.2 (Luminex Japan, Tokyo, Japan) according to the manufacturers' instructions. Cytokine and chemokine concentrations were inferred from the standards by the acquisition software. We excluded several cytokines and chemokines for which the bead counts were insufficient or several values exceeded the measurement limits from the final data, which precluded accurate statistical analysis. Heatmap was generated using R software ver. 4.1.2 with gplots package.

Blood Coagulation Test and Platelet Aggregation Assay

Mice were euthanized by lethal intraperitoneal injection of sodium pentobarbital 36 h after intravenous infection, and blood aliquots were immediately collected. Blood was drawn from the vena cava of the heart into a syringe containing 3.2% (w/v) sodium citrate. Blood samples were centrifuged for 10 min at $845 \times g$ at room temperature, and the plasma was collected. Prothrombin time and fibrinogen levels were measured using a semi-automated coagulation analyzer KC1 Delta (Tcong Ireland Ltd., Wicklow, Ireland) and the reagents of prothrombin time and fibrinogen (Sysmex, Hyogo, Japan) according to manufacturer's guidelines (Nakahara et al., 2013).

For platelet aggregation assay, platelet-rich plasma (PRP) was prepared by centrifugation of anticoagulated whole blood at room temperature ($104 \times g$) for 10 min. The blood remaining after removing the PRP was centrifuged at $845 \times g$ for 10 min at room temperature to collect platelet-poor plasma (PPP). To measure platelet aggregation of infected mice, the plasmas were collected at 36 h after intravenous infection. For platelet aggregation assay *in vitro*, the plasmas were collected from uninfected mice. Obtained PRP was incubated for 30 min at room temperature with *S. pneumoniae* TIGR4 strains (1.5 – 2.5×10^6 CFU) WT, $\Delta bgaA$, or $\Delta bgaA$ with 40 units of commercial recombinant BgaA (rBgaA; β 1–4 Galactosidase S, New England

Biolabs Japan Inc., Tokyo, Japan). Platelet aggregation was assessed by light transmission at 37°C using a PRP3000S device (TAIYO Instruments, Inc., Osaka, Japan) according to the manufacturer's instructions. Platelets were tested for normal responses to collagen (10 µg/mL). The change in light transmission was recorded and compared with that of autologous PPP, which was considered 100% of light transmission.

Statistical Analysis

Statistical analysis of the data obtained from the experiments was performed using the Mann–Whitney *U*-test or Kruskal–Wallis test with Dunn's multiple comparisons test. Differences were considered statistically significant at $P < 0.05$. The tests were carried out using Graph Pad Prism version 7.0d or 8.4.2 (GraphPad Software, Inc., San Diego, CA, USA).

RESULTS

BgaA Contributes to Pneumococcal Association of Human Epithelial Cells and Vascular Endothelial Cells

The interaction between *S. pneumoniae* and the epithelial cells of its host is a prerequisite for pneumococcal disease development. Previous reports have demonstrated that BgaA contributes to the adherence of pneumococcal strains to human epithelial cells. The *bgaA* mutants in R6 and D39 presented reduced adherence to several epithelial cell lines, such as the human pharyngeal carcinoma cell line Detroit-562 and the human lung carcinoma cell line A549 cells (Limoli et al., 2011; Singh et al., 2014). However, the interaction between pneumococcal BgaA and human endothelial cells has not been previously reported. We confirmed the role of BgaA in pneumococcal association with A549 cells and investigated whether BgaA contributes to pneumococcal association with hBMECs. The $\Delta bgaA$ strain showed significantly lower rates of association with A549 and hBMECs compared with the WT strains (Figure 1A). These results suggest that BgaA contributes to pneumococcal association with endothelial cells and epithelial cells *in vitro*.

BgaA Promotes Pneumococcal Resistance to Human Neutrophil Killing

BgaA inhibits complement-mediated opsonophagocytosis (Dalia et al., 2010). To investigate whether BgaA contributes to pneumococcal survival in blood, we performed bactericidal assays using human blood. After one and two hours of incubation in human blood, there was no significant difference between the survival rates of the WT and $\Delta bgaA$ strains. However, after three hours of incubation, the survival rate of $\Delta bgaA$ strains was significantly decreased compared with that of WT strains (Figure 1B). In addition, we determined the pneumococcal survival rate after incubation for three hours with human neutrophils. The $\Delta bgaA$ strain had a significantly lower survival rate than that of the WT after three hours of incubation with human neutrophils, in line with the results of the human blood bactericidal assay (Figure 1C). Next, we performed

a mouse blood bactericidal assay. In contrast to the effect observed after incubation with human blood, there were no significant differences between the survival of WT and $\Delta bgaA$ strains after incubation with mouse blood (Figure 1D). Previously, we have shown no large difference in the growth curve of WT and $\Delta bgaA$ strains in the THY medium (Yamaguchi et al., 2020). Altogether, these data indicate that BgaA contributes to pneumococcal human-specific resistance to neutrophil killing under a condition without serum components as well as to the evasion from complement-mediated opsonophagocytosis (Dalia et al., 2010).

BgaA Deficiency Decreases Tissue Damages in a Mouse Sepsis Model

Our previous study indicated that the virulence of the $\Delta bgaA$ strain was significantly lower than that of the WT strain in a mouse sepsis model (Yamaguchi et al., 2020). To elucidate the precise role of BgaA in sepsis, we intravenously infected mice with pneumococcal strains and compared the bacterial burden in the blood, brain, lung, liver, spleen, and kidney 24 and 36 h after infection. In line with the results of previous studies, some of the mice infected with WT *S. pneumoniae* showed signs of imminent death 36 h after infection (Yamaguchi et al., 2020). At 24 h and 36 h after infection, the amount of CFUs in the blood, lung, liver, spleen, and kidney samples of the WT and $\Delta bgaA$ strains were similar (Figure 2). We also examined the histopathological features of the lungs and kidneys, as sepsis often leads to impaired function of these key organs (Fink and Warren, 2014). Histopathological analysis was performed in a blinded fashion by an independent pathologist. Microscopic observation of lungs and kidney samples stained with hematoxylin and eosin revealed that WT-infected mice exhibited more bleeding than PBS-treated or $\Delta bgaA$ -infected mice (Figure 3). Moreover, WT-infected mice showed bleeding in the renal bodies in the kidney, and microthrombi in the lungs and kidney, in addition to bleeding. Taken together, these results indicate that the deletion of *bgaA* reduces tissue damage in infected mice and decreases pneumococcal pathogenicity in a mouse sepsis model.

To investigate the effect of BgaA on the transcriptional response of host cells, leukocyte RNA was obtained from the blood of mice 12, 24, and 36 h after intravenous administration of WT or $\Delta bgaA$ pneumococcal strains, or PBS. The transcriptional responses of the murine leukocytes were visualized using a heat map, scatter plots, and principal component analysis (Figures 4A, B, and Supplementary Figure 1). The WT- and $\Delta bgaA$ -infected mice showed larger differences at later time points, while all mock mice showed similar tendencies. Venn diagrams showed that WT and $\Delta bgaA$ -infected mice shared 22 upregulated and 258 downregulated genes compared with PBS-treated mice at 12 h after infection (Supplementary Figure 1). At 24 h after infection, WT and $\Delta bgaA$ -infected mice shared 74 upregulated and 84 downregulated genes compared with PBS-treated mice. Moreover, WT-infected mice presented 15 additional upregulated genes and 53 additional downregulated genes compared with $\Delta bgaA$ -infected mice (Figure 4B and

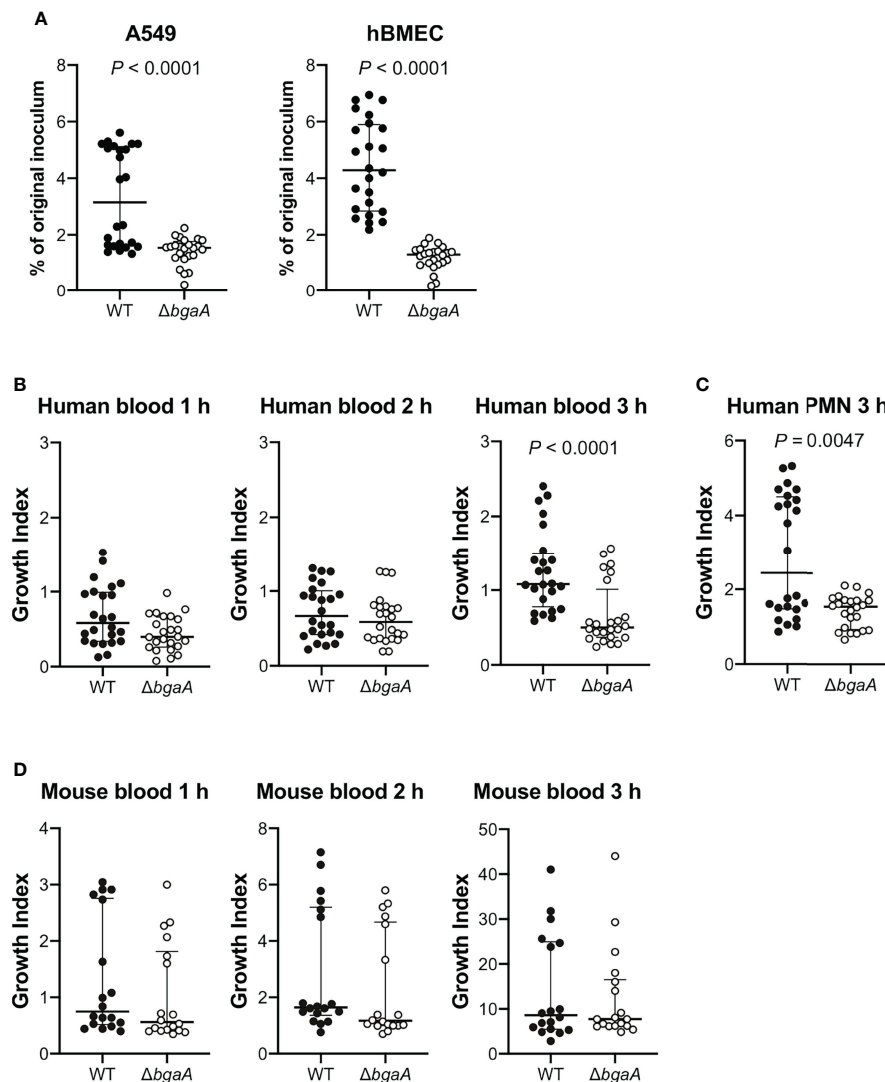


FIGURE 1 | Deficiency of *bgaA* decreases pneumococcal association with human epithelial and endothelial cells and survival after incubation with human neutrophils. **(A)** Rate of association with A549 cells and hBMECs by *S. pneumoniae* TIGR4 wild type and $\Delta bgaA$ strains. Association rates were calculated by dividing the CFU value obtained at one hour after infection by the value for the original inoculum. **(B)** Growth index of *S. pneumoniae* WT and $\Delta bgaA$ strains in human blood. Bacterial cells were incubated in human blood for one, two, and three hours at 37°C. **(C)** Growth index of *S. pneumoniae* WT and $\Delta bgaA$ strains with human neutrophils. Bacterial cells were incubated with human neutrophils for 3 h at 37°C. **(D)** Growth index of *S. pneumoniae* WT and $\Delta bgaA$ strains in mouse blood. Bacterial cells were incubated in mouse blood for one, two, and three hours at 37°C. **(B–D)** After incubation, samples were serially diluted and plated on TS blood agar. The number of CFUs was determined following incubation. Growth index was calculated by dividing the CFU after incubation by the CFU of the original inoculum. The median and interquartile range (IQR) are represented using horizontal and vertical lines. Differences between groups were analyzed using Mann–Whitney *U*-test. The data were pooled from three or four independent experiments. Individual values are provided in **Supplementary Data 1**.

Supplementary Figure 1). At 36 h after infection, WT and $\Delta bgaA$ -infected mice shared 165 upregulated and 6 downregulated genes compared with PBS-treated mice. WT-infected mice presented upregulated 234 genes and downregulated 382 genes compared with $\Delta bgaA$ -infected mice (**Figure 4B** and **Supplementary Figure 1**). Pathway analysis of the differentially expressed genes revealed that several signaling pathways associated with host innate immunity were significantly downregulated in WT-infected mice compared with $\Delta bgaA$ -infected mice at 24 h and 36 h, whereas there

were no significant up- or down-regulated pathways at 12 h post-infection (**Figure 4C**). Expression profiles of TNF- α signaling-related genes at 24 and 36 h after infection were visualized on a KEGG pathway diagram (**Supplementary Figure 2**). Genes encoding cytokines and chemokines, including TNF- α , CCL-2/MCP-1, and so on, were down-regulated in WT-infected mice compared with $\Delta bgaA$ -infected mice, while the expression of TNF- α signaling-related genes was not so largely changed. In addition, Reactome pathway analysis indicated that WT-infected mice presented significantly

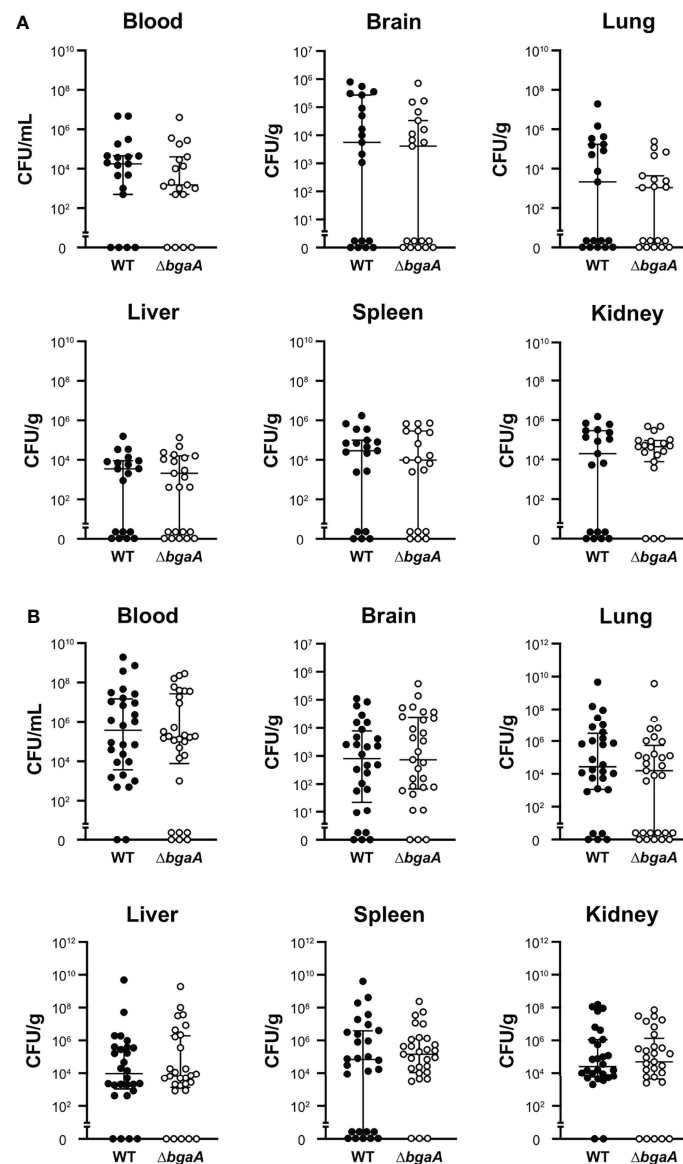


FIGURE 2 | Deficiency of *bgaA* did not affect the bacterial burden in mice. Mice were infected by intravenous injection of *S. pneumoniae* TIGR4 wild type or $\Delta bgaA$. The bacterial burden in the blood, brain, lung, liver, spleen, and kidney was assessed after 24 h (A) or 36 h (B) of infection. The median and IQR values are represented using vertical lines. All mice were perfused with PBS after blood collection, and organ samples were collected. Statistical differences between groups were analyzed using the Mann–Whitney U test. The bacterial burden values obtained from the four independent experiments were pooled. Individual values are provided in **Supplementary Data 2**.

upregulated platelet activation pathways compared with $\Delta bgaA$ -infected mice at 36 h (**Supplementary Table 1**). Expression profiles of complement and coagulation cascade at 36 h after infection were also visualized on a KEGG pathway diagram (**Figure 5**). Although the complement and coagulation cascades were not significantly upregulated in WT-infected mice compared with $\Delta bgaA$ -infected mice, many genes were upregulated in the coagulation cascade. These results indicate that BgaA inhibits host innate immunity activation and induces coagulation cascades at the RNA level.

BgaA Contributes to Blood Coagulation in a Mouse Sepsis Model

Figure 6A shows a heatmap of the data of measured mouse cytokines and chemokines in plasmas obtained using the MAGPIX multiplexing system. The graphs of each cytokine or chemokine are shown in **Figure 6B** and **Supplementary Figure 3**. Although genes encoding TNF- α , IL-1 β , IL-15, LIF, CCL-2/MCP-1, CXCL2/MIP-2, M-CSF/CSF-1, and GM-CSF/CSF-2 were down-regulated in RNA-seq analysis

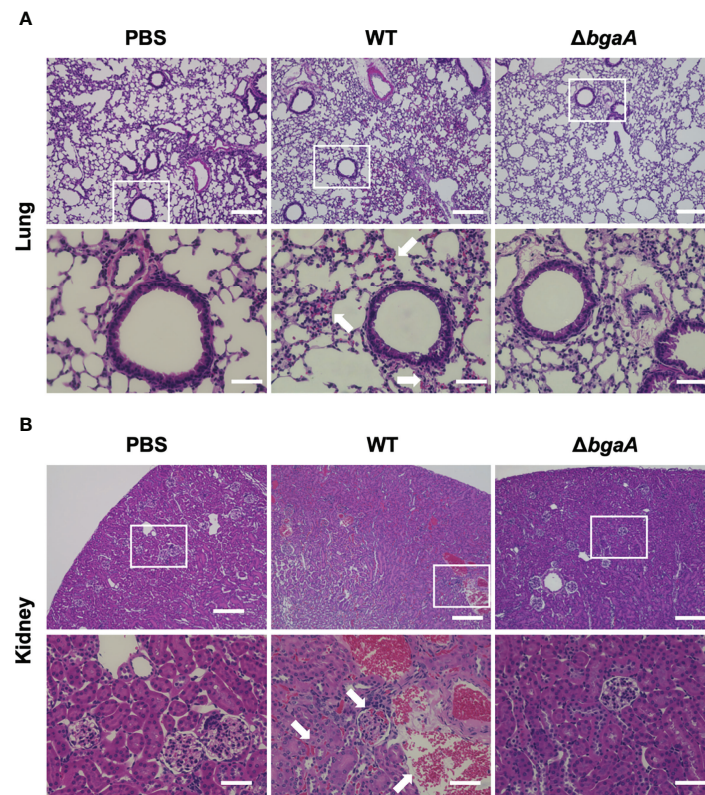


FIGURE 3 | Deficiency of *bgaA* decreases bleeding and microthrombus formation in mouse organs. Haematoxylin and eosin staining of infected mouse lungs (**A**) and kidneys (**B**) collected at 36 h after intravenous infection with PBS or *S. pneumoniae* TIGR4 WT or $\Delta bgaA$ strains. Arrows indicate bleedings and/or microthrombus formations. Scale bars are 200 μm (upper panels) and 40 μm (lower panels).

(**Supplementary Figure 2**), no significantly different cytokines and chemokines were observed between WT- and $\Delta bgaA$ -infected mice at 24 h and 36 h. These results indicate that BgaA deficiency activates host innate immunity pathways at the RNA level but not the protein level.

Generally, bacterial infections increase the blood concentration of fibrinogen and activate coagulation pathways (Davalos and Akassoglou, 2012). To compare blood coagulation, we measured fibrinogen levels and prothrombin time in mouse blood samples obtained 36 h after infection. WT-infected mice showed higher fibrinogen levels than the $\Delta bgaA$ -infected and PBS-treated mice; however, no significant differences were observed in prothrombin time among the groups of mice (**Figure 7A**). Next, we performed a platelet aggregation assay using mouse PRP and PPP 36 h after infection. As shown in **Figure 7B**, we assessed platelet aggregation rates using pooled PRP and PPP from six mice from each group. WT-infected mice showed reduced platelet aggregation rates compared with those in the other groups, while the level of platelet aggregation of PBS-treated and $\Delta bgaA$ -infected mice was comparable. In addition, we assessed platelet aggregation rates using individual PRPs and PPPs from six mice (**Supplementary Figure 4**). The individual data showed a tendency similar to that of pooled plasmas. To determine whether BgaA affects platelets directly, we performed

an *in vitro* platelet aggregation assay using uninfected mouse PRPs and *S. pneumoniae* WT, $\Delta bgaA$, and $\Delta bgaA$ with rBgaA (**Supplementary Figure 5**). The assay showed *S. pneumoniae* strains and rBgaA did not affect platelet aggregation in the PRP. These results indicate a possibility that BgaA does not act directly on platelets but inhibits the aggregation ability *via* host endothelial cells or other reactions in pneumococcal sepsis.

DISCUSSION

In a previous study, we demonstrated that BgaA is an evolutionarily conserved pneumococcal cell surface protein that functions as a virulence factor after mouse intravenous infection (Yamaguchi et al., 2020). In this study, we investigated the role of BgaA in pneumococcal sepsis. The deletion of *bgaA* significantly reduced pneumococcal association with human epithelial cells, in agreement with previous studies (King et al., 2006; Limoli et al., 2011; Singh et al., 2014). We also showed that the deletion of *bgaA* significantly reduced pneumococcal association with human endothelial cells and survival in human blood and human neutrophils. On the contrary, the deletion of *bgaA* did not affect pneumococcal survival in mouse blood, as demonstrated

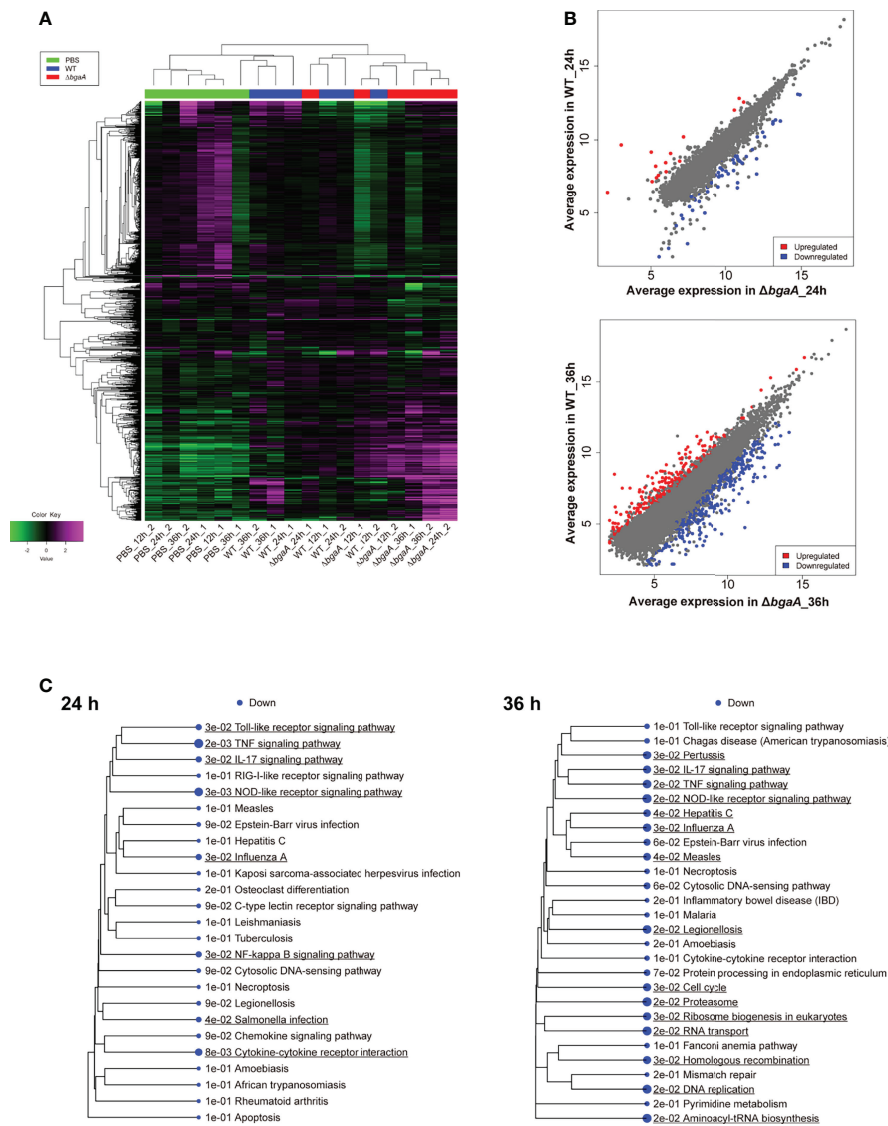


FIGURE 4 | Mouse blood RNA-seq analysis revealed that deficiency of *bgaA* up-regulated several innate immune pathways. RNA-seq analysis was performed using mouse blood at 12, 24 and 36 h after infection. All analysis and visualizations were performed using the iDEP package. **(A)** Heatmap with hierarchical clustering of most variable 1,000 genes. The data is centered by subtracting the average expression level for each gene. **(B)** Scatter plots illustrating host genes consistently altered among WT-infected and $\Delta bgaA$ -infected mice 24 and 36 h after infection. Differentially expressed genes were calculated using DESeq2. FDR cutoff value was 0.1 and Min fold change was 2. **(C)** Pathway trees. Enrichment pathway analyses were performed by GAGE using KEGG pathways. Circle sizes represent FDR values. FDR cutoff value was 0.2.

using an *ex vivo* model and evaluating the pneumococcal burden in the blood and organs of intravenously infected mice. RNA-seq enrichment pathway analysis indicated that the presence of BgaA significantly downregulated several host innate immunity pathways. However, there were no differences in cytokines and chemokines in plasma between WT- and $\Delta bgaA$ -infected mice. Furthermore, histopathological analysis and blood coagulation assays showed increased bleeding and microthrombus formation in the lungs and kidneys, as well as blood coagulation in WT-infected mice compared with those in PBS-treated or $\Delta bgaA$ -infected mice. Taken together, these results indicate that BgaA

functions as a virulence factor by increasing bleeding and blood coagulation in a mouse sepsis model.

BgaA inhibits complement component C3 deposition and, consequently, opsonophagocytosis by cleaving *N*-glycans on host glycoproteins that are involved in the complement cascade (Dalia et al., 2010). In this study, we confirmed that the deletion of *bgaA* reduced pneumococcal survival in human blood and non-opsonized human neutrophils. However, no significant difference was observed in the survival of the WT and $\Delta bgaA$ strains in mouse blood. Interestingly, it has been reported that in the *S. pneumoniae* strain C06_18, BgaA

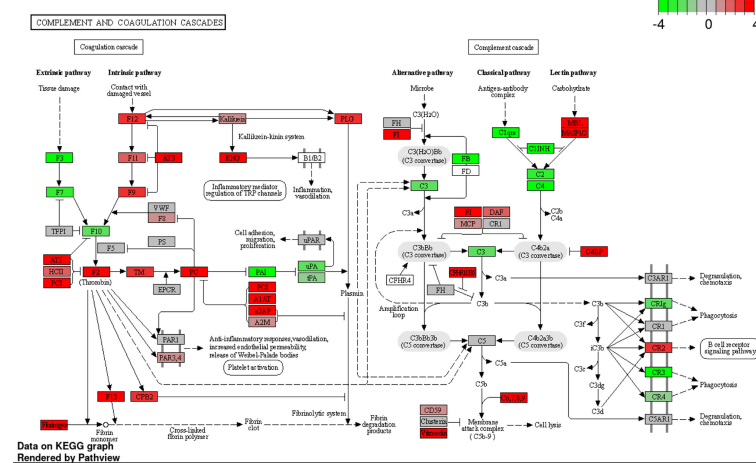


FIGURE 5 | Expression profiles of complement and coagulation cascades-related genes at 36 h after infection were visualized on a KEGG pathway diagram using RNA-seq data and the iDEP Pathview package. Red and green indicate genes induced or suppressed by $\Delta bgaA$ -infection compared with those by WT-infection, respectively. Fold-change (\log_2) cutoff in color code is 4.

contributes to pneumococcal association with several human epithelial cells, but not with mouse LA-4 epithelial cells (Limoli et al., 2011). BgaA mediates adherence to human epithelial cells through the interaction between its carbohydrate-binding modules and lactose or *N*-acetylglucosamine present in the cell surface of the host (Singh et al., 2014). The discrepancy between *in vitro* assays using human cells and *in vivo* mouse models could be attributed to differences in receptors between species. Thus, in a mouse model, BgaA has only a limited effect on pneumococcal association with host epithelial cells and evasion from host neutrophil killing. Moreover, BgaA induced bleeding and microthrombus formation in organs and blood coagulation in a mouse sepsis model. Furthermore, BgaA may contribute to the pneumococcal burden *via* its ability to associate with host epithelial and endothelial cells and evade opsonophagocytic killing in human sepsis.

Recently, increasing attention has been drawn to immunothrombosis, as severe acute respiratory syndrome coronavirus 2 (SARS-CoV-2) is believed to induce this process (Bonaventura et al., 2021; Loo et al., 2021). Generally, immunothrombosis is triggered by fibrin, monocytes, neutrophils, and platelets to reduce the dissemination and survival of pathogens (Engelmann and Massberg, 2013). However, uncontrolled immunothrombosis can cause thrombo-inflammation and disseminated intravascular coagulation (DIC) through a dysregulated coagulation system, leading to microthrombosis formation. Coronavirus disease 2019 (COVID-19)-associated coagulopathy is characterized by elevated levels of fibrinogen, mildly prolonged or no change in prothrombin time, and decreased or no change in platelet counts (Bonaventura et al., 2021; Loo et al., 2021). Hence, there are some similarities in the coagulopathy between our results in the mouse infection model and COVID-19, suggesting that the control of immunothrombosis may be important in various infectious diseases.

In our platelet aggregation assay, WT-infected mice showed increased fibrinogen levels in plasma, bleeding in organs, and reduced platelet aggregation rates compared with PBS-treated and $\Delta bgaA$ -infected mice. These results indicate that the presence of BgaA induces uncontrolled coagulation through microthrombosis and platelet consumption. The host coagulation system activates the complement pathway *via* the classical or alternative pathway, which plays a role in fibrin formation (de Bont et al., 2019). In addition, activated complement proteins can induce NETosis, a process during which neutrophils release neutrophil extracellular traps (NETs), which can serve as a direct scaffold for both thrombus formation and complement activation (de Bont et al., 2019). Since BgaA inhibits complement deposition to pneumococcal cells (Dalia et al., 2010), infection-induced excess complement might contribute to thrombus formation.

Pneumococcal NanA induces thrombocytopenia through platelet desialylation and haptic Ashwell receptor recognition (Grewal et al., 2008). In addition, NanA increases complement- and pneumolysin-mediated hemolysis and platelet aggregation (Syed et al., 2019). In vertebrates, sialic acid molecules are commonly found to be linked to galactose, *N*-acetylglucosamine, or another sialic acid through α -glycosidic bonds (Varki et al., 2015). BgaA inhibits complement deposition by cleaving *N*-glycans on host glycoproteins involved in the complement cascade, as well as NanA and StrH (Dalia et al., 2010). Further studies are needed to determine whether BgaA can enhance thrombocytopenia by cleaving galactose residues exposed by NanA-desialylation.

This study has several limitations. First, we could not construct and use the BgaA-complemented strain. Thus, we could not exclude the possibility that some phenotypes were independent of BgaA. However, the phenotype, association with human epithelial cells, is consistent with previous studies using several strains (King et al., 2006; Dalia et al., 2010; Limoli et al.,

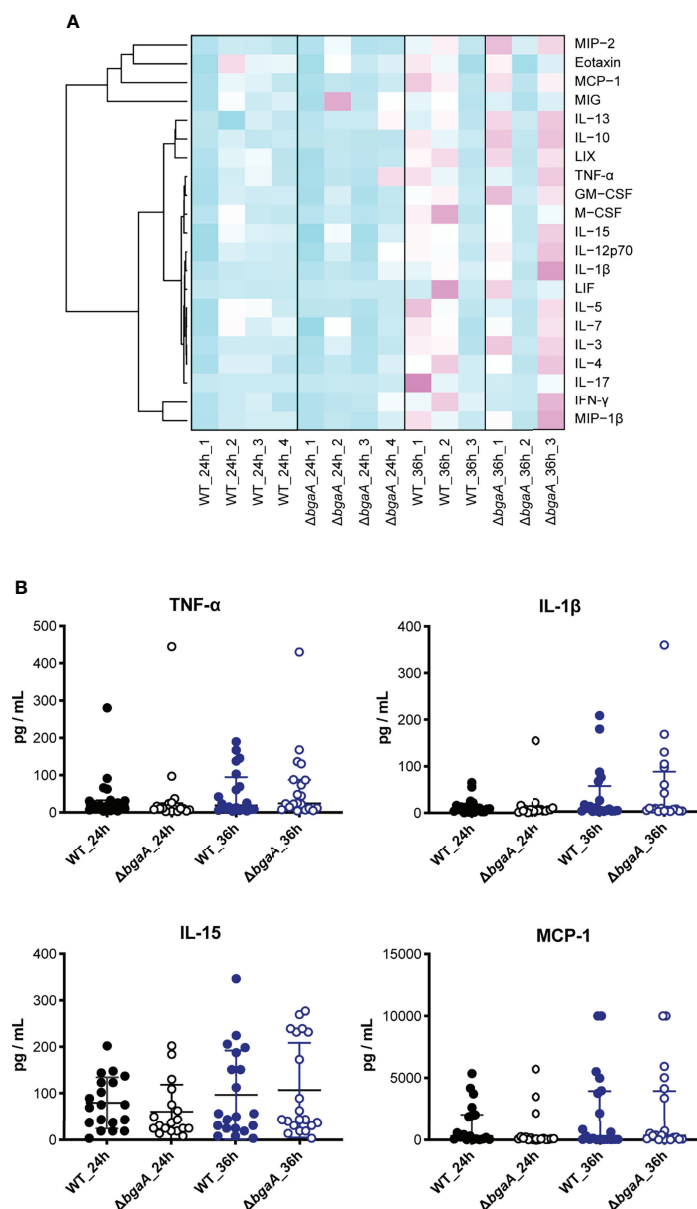


FIGURE 6 | Dendrogram and heatmap of cytokine and chemokine amounts in plasma from TIGR4-infected mice 24 and 36 h after intravenous infections.

(A) C57BL/6 mice were infected with *S. pneumoniae* TIGR4 intravenously, and the plasma was isolated 24 and 36 h after the infection. Cytokine and chemokine amounts in plasma were measured using MAGPIX. Light blue: low cytokine values; white: average values; magenta: high values. The data shown are the mean values for mice under each experimental condition ($n = 3$: 24h_1, 24h_2 and 36h_1, $n = 6-7$: 24h_3 and 24h_4, and $n = 8-9$: 36h_2 and 36h_3). **(B)** Actual amounts of TNF- α , IL-1 β , IL-15, and MCP-1 in **(A)** All individual values were plotted. The median and IQR values were represented using vertical lines. Statistical differences between groups were analyzed using a Kruskal-Wallis test followed by Dunn's multiple comparisons test. The data were pooled from three or four independent experiments. Other actual amounts are shown in **Supplementary Figure 3**.

2011). In addition, BgaA deficiency did not affect bacterial survival in *ex vivo* mouse blood and bacterial burdens in infected mouse organs. These results indirectly support the reliability of the results. Another limitation is that the precise molecular mechanism of BgaA in evasion from non-opsonic killing and the promotion of host coagulation was not elucidated. At least in PRP alone, *S. pneumoniae* and rBgaA do not affect platelet aggregation. Thus, it is possible that they affect other

complex cell-mediated mechanisms to alter the coagulation response. Moreover, RNA-seq analysis of leukocytes showed that a group of genes related to the coagulation cascade was upregulated in the presence of BgaA. Although clarification of these points requires comprehensive analysis, including host ligand or receptor identification, the investigation would be able to contribute to the control of pneumococcal sepsis-induced DIC.

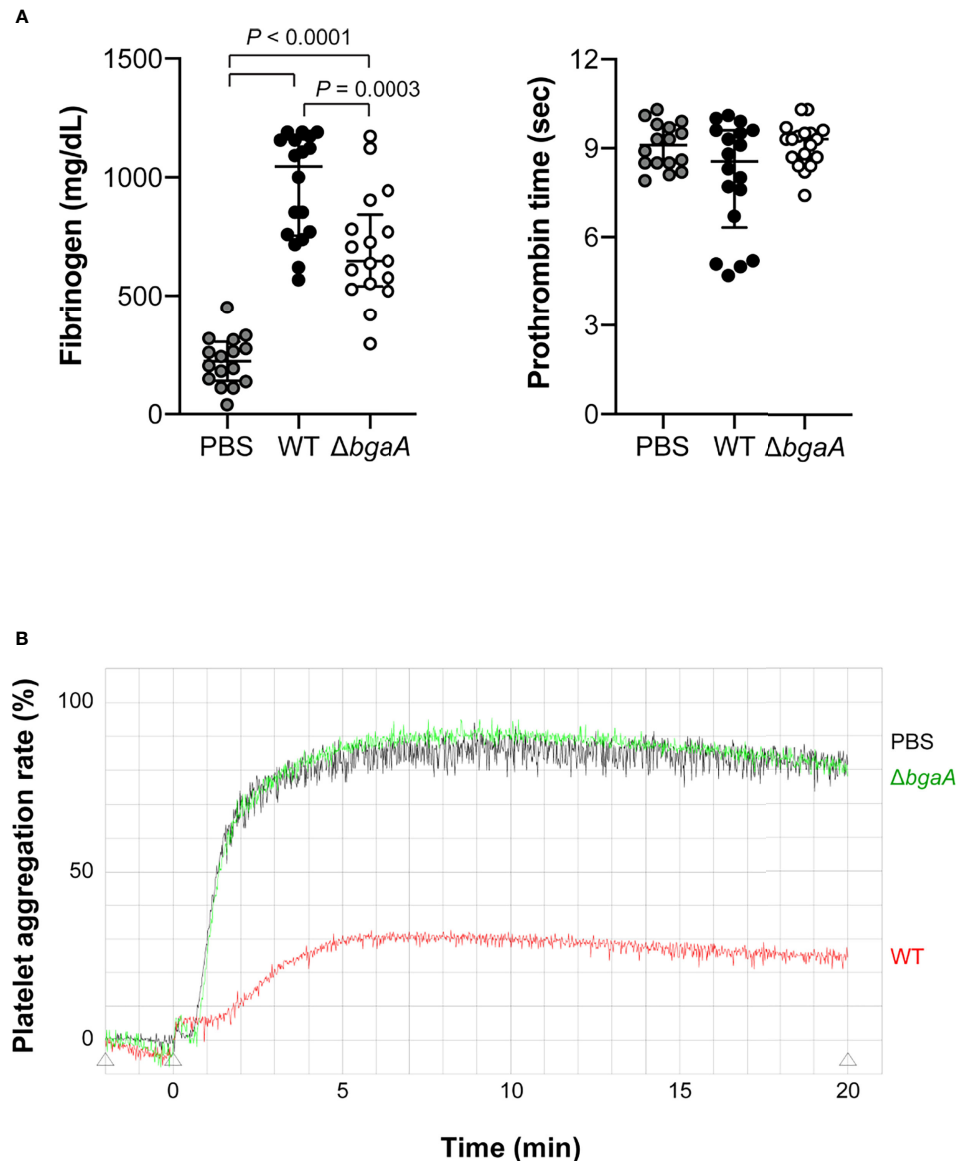


FIGURE 7 | Deficiency of *bgaA* decreases fibrinogen amount in plasma and suppresses platelet aggregation rate in a mouse model of sepsis. **(A)** Fibrinogen amount in mouse plasma and prothrombin time measured by semi-automated coagulation analyzer KC1 Delta. The median and IQR values are represented using vertical lines. Statistical differences between groups were analyzed using a Kruskal–Wallis test followed by Dunn’s multiple comparisons test. The data were pooled from three independent experiments. Individual values are shown in **Supplementary Data 3**. **(B)** Platelet aggregation assessed by light transmission. The data was obtained from pooled plasma from 6 mice in each group. Data from individual plasma are shown in **Supplementary Figure 4**. Mouse blood was collected at 36 h after intravenous infection with *S. pneumoniae* TIGR4 WT and $\Delta bgaA$ strains **(A, B)**.

Our previous evolutionary analysis indicated that *bgaA*, among other cell wall-anchoring proteins, was conserved in pneumococcal species and had a high percentage of codons that were under negative selection pressure. In addition, evolutionarily conserved residues contribute to the conformation of the BgaA active site (Yamaguchi et al., 2020), and additional bioinformatic analyses also support the importance of BgaA. Prasasty *et al.* predicted host-pathogen protein-protein interactions (HP-PPIs) using a logistic

regression model with HP-PPIs of three different pathogens as training data. In the predicted HP-PPI networks, network topology analysis revealed BgaA to be the most central among the *S. pneumoniae* proteins (Prasasty et al., 2021). In this study, we demonstrated that BgaA contributes to thrombus formation in a mouse sepsis model, in addition to adherence to host epithelial and endothelial cells and evasion from neutrophil-killing in humans. Our previous BLAST search indicated that BgaA does not have a high similarity with human proteins

(Yamaguchi et al., 2020). Thus, BgaA could be an attractive target for new drug and vaccine development. As BgaA is a large protein containing multiple domains, it is necessary to identify the functional domain and verify its effectiveness as a drug target in further studies.

DATA AVAILABILITY STATEMENT

The datasets presented in this study can be found in online repositories. The names of the repository/repositories and accession number(s) can be found below: <https://www.ncbi.nlm.nih.gov/geo/>, GSE190418.

ETHICS STATEMENT

The studies involving human participants were reviewed and approved by the institutional review board of Osaka University Graduate School of Dentistry (H26-E43). The patients/participants provided their written informed consent to participate in this study. The animal study was reviewed and approved by the Animal Care and Use Committee of Osaka University Graduate School of Dentistry (28-002-0).

AUTHOR CONTRIBUTIONS

MY and SK designed the study. MT and MK performed the experiments. DO and DM performed the next-generation sequencing. MY, MK, MO, and DO performed the bioinformatics analyses. MY, TS, YH, KG, MN, and SK

contributed to the experimental setup. MT drafted the original manuscript. MY substantially revised the text and figures. MK, TS, YH, DO, MO, DM, KG, MN, NU, and SK contributed to the writing of the manuscript. All authors contributed to the article and approved the submitted version.

FUNDING

This study was partly supported by AMED (JP20wm0325001), the Japan Society for the Promotion of Science KAKENHI (grant numbers 17H05103, 19H03825, 19K22710, 20KK0210, 20K23053, and 20K21675), SECOM Science and Technology Foundation, MSD Life Science Foundation, Public Interest Incorporated Foundation, Takeda Science Foundation, Naito Foundation, Kobayashi International Scholarship Foundation, and the Drug Discovery Science Division, Open and Transdisciplinary Research Initiatives, Osaka University. The funders had no role in the study design, data collection or analysis, decision to publish, or preparation of the manuscript.

ACKNOWLEDGMENTS

We appreciate Sunao Sato for his kind help with the pathological analysis. We also thank Hikaru Kodama for her technical assistance.

SUPPLEMENTARY MATERIAL

The Supplementary Material for this article can be found online at: <https://www.frontiersin.org/articles/10.3389/fcimb.2022.844000/full#supplementary-material>

REFERENCES

- Asner, S. A., Agyeman, P. K. A., Gradoux, E., Posfay-Barbe, K. M., Heininger, U., Giannoni, E., et al. (2019). Burden of Streptococcus Pneumoniae Sepsis in Children After Introduction of Pneumococcal Conjugate Vaccines: A Prospective Population-Based Cohort Study. *Clin. Infect. Dis.* 69 (9), 1574–1580. doi: 10.1093/cid/ciy1139
- Blanchette, K. A., Shenoy, A. T., Milner, J. 2nd, Gilley, R. P., McClure, E., Hinojosa, C. A., et al. (2016). Neuraminidase A-Exposed Galactose Promotes *Streptococcus Pneumoniae* Biofilm Formation During Colonization. *Infect. Immun.* 84 (10), 2922–2932. doi: 10.1128/IAI.00277-16
- Bogaert, D., van Belkum, A., Sluijter, M., Luijendijk, A., de Groot, R., Rumke, H. C., et al. (2004). Colonisation by *Streptococcus Pneumoniae* and *Staphylococcus Aureus* in Healthy Children. *Lancet* 363 (9424), 1871–1872. doi: 10.1016/S0140-6736(04)16357-5
- Bonaventura, A., Vecchie, A., Dagna, L., Martinod, K., Dixon, D. L., Van Tassel, B. W., et al. (2021). Endothelial Dysfunction and Immunothrombosis as Key Pathogenic Mechanisms in COVID-19. *Nat. Rev. Immunol.* 21 (5), 319–329. doi: 10.1038/s41577-021-00536-9
- CDC (2019). "Antibiotic Resistance Threats in the United States 2019" (Atlanta, GA: U.S. Department of Health and Human Services, CDC).
- Dalia, A. B., Standish, A. J., and Weiser, J. N. (2010). Three Surface Exoglycosidases From *Streptococcus Pneumoniae*, NanA, BgaA, and StrH, Promote Resistance to Opsonophagocytic Killing by Human Neutrophils. *Infect. Immun.* 78 (5), 2108–2116. doi: 10.1128/IAI.01125-09
- Davalos, D., and Akassoglou, K. (2012). Fibrinogen as a Key Regulator of Inflammation in Disease. *Semin. Immunopathol.* 34 (1), 43–62. doi: 10.1007/s00281-011-0290-8
- de Bont, C. M., Boelens, W. C., and Puij, G. J. M. (2019). NETosis, Complement, and Coagulation: A Triangular Relationship. *Cell Mol. Immunol.* 16 (1), 19–27. doi: 10.1038/s41423-018-0024-0
- Engelmann, B., and Massberg, S. (2013). Thrombosis as an Intravascular Effector of Innate Immunity. *Nat. Rev. Immunol.* 13 (1), 34–45. doi: 10.1038/nri3345
- Fink, M. P., and Warren, H. S. (2014). Strategies to Improve Drug Development for Sepsis. *Nat. Rev. Drug Discov.* 13 (10), 741–758. doi: 10.1038/nrd4368
- Flasche, S., Van Hoek, A. J., Sheasby, E., Waight, P., Andrews, N., Sheppard, C., et al. (2011). Effect of Pneumococcal Conjugate Vaccination on Serotype-Specific Carriage and Invasive Disease in England: A Cross-Sectional Study. *PLoS Med.* 8 (4), e1001017. doi: 10.1371/journal.pmed.1001017
- GBD 2016 LowerRespiratory Infections Collaborators (2018). Estimates of the Global, Regional, and National Morbidity, Mortality, and Aetiologies of Lower Respiratory Infections in 195 Countries 1990–2016: A Systematic Analysis for the Global Burden of Disease Study 2016. *Lancet Infect. Dis.* 18 (11), 1191–1210. doi: 10.1016/S1473-3099(18)30310-4
- Ge, X. (2021). iDEP Web Application for RNA-Seq Data Analysis. *Methods Mol. Biol.* 2284, 417–443. doi: 10.1007/978-1-0716-1307-8_22
- Ge, S. X., Son, E. W., and Yao, R. (2018). iDEP: An Integrated Web Application for Differential Expression and Pathway Analysis of RNA-Seq Data. *BMC Bioinf.* 19 (1), 534. doi: 10.1186/s12859-018-2486-6

- Golubchik, T., Brueggemann, A. B., Street, T., Gertz, R. E. Jr., Spencer, C. C., Ho, T., et al. (2012). Pneumococcal Genome Sequencing Tracks a Vaccine Escape Variant Formed Through a Multi-Fragment Recombination Event. *Nat. Genet.* 44 (3), 352–355. doi: 10.1038/ng.1072
- Grewal, P. K., Uchiyama, S., Ditto, D., Varki, N., Le, D. T., Nizet, V., et al. (2008). The Ashwell Receptor Mitigates the Lethal Coagulopathy of Sepsis. *Nat. Med.* 14 (6), 648–655. doi: 10.1038/nm1760
- Hirose, Y., Yamaguchi, M., Goto, K., Sumitomo, T., Nakata, M., and Kawabata, S. (2018). Competence-Induced Protein Ccs4 Facilitates Pneumococcal Invasion Into Brain Tissue and Virulence in Meningitis. *Virulence* 9 (1), 1576–1587. doi: 10.1080/21505594.2018.1526530
- Hobbs, J. K., Pluvina, B., and Boraston, A. B. (2018). Glycan-Metabolizing Enzymes in Microbe-Host Interactions: The *Streptococcus Pneumoniae* Paradigm. *FEBS Lett.* 592 (23), 3865–3897. doi: 10.1002/1873-3468.13045
- Kanehisa, M., Furumichi, M., Tanabe, M., Sato, Y., and Morishima, K. (2017). KEGG: New Perspectives on Genomes, Pathways, Diseases and Drugs. *Nucleic Acids Res.* 45 (D1), D353–D361. doi: 10.1093/nar/gkw1092
- Kim, L., McGee, L., Tomczyk, S., and Beall, B. (2016). Biological and Epidemiological Features of Antibiotic-Resistant *Streptococcus Pneumoniae* in Pre- and Post-Conjugate Vaccine Eras: A United States Perspective. *Clin. Microbiol. Rev.* 29 (3), 525–552. doi: 10.1128/CMR.00058-15
- King, S. J., Hippe, K. R., and Weiser, J. N. (2006). Deglycosylation of Human Glycoconjugates by the Sequential Activities of Exoglycosidases Expressed by *Streptococcus Pneumoniae*. *Mol. Microbiol.* 59 (3), 961–974. doi: 10.1111/j.1365-2958.2005.04984.x
- Limoli, D. H., Sladek, J. A., Fuller, L. A., Singh, A. K., and King, S. J. (2011). BgaA Acts as an Adhesin to Mediate Attachment of Some Pneumococcal Strains to Human Epithelial Cells. *Microbiology* 157 (Pt 8), 2369–2381. doi: 10.1099/mic.0.045609-0
- Loewe, L. (2008). Negative Selection. *Nat. Educ.* 1, 59.
- Loo, J., Spittle, D. A., and Newnham, M. (2021). COVID-19, Immunothrombosis and Venous Thromboembolism: Biological Mechanisms. *Thorax* 76 (4), 412–420. doi: 10.1136/thoraxjnl-2020-216243
- Mori, Y., Yamaguchi, M., Terao, Y., Hamada, S., Ooshima, T., and Kawabata, S. (2012). α -Enolase of *Streptococcus Pneumoniae* Induces Formation of Neutrophil Extracellular Traps. *J. Biol. Chem.* 287 (13), 10472–10481. doi: 10.1074/jbc.M111.280321
- Nakahara, M., Ito, T., Kawahara, K., Yamamoto, M., Nagasato, T., Shrestha, B., et al. (2013). Recombinant Thrombomodulin Protects Mice Against Histone-Induced Lethal Thromboembolism. *PLoS One* 8 (9), e75961. doi: 10.1371/journal.pone.0075961
- Otsuka, T., Chang, B., Shirai, T., Iwaya, A., Wada, A., Yamanaka, N., et al. (2013). Individual Risk Factors Associated With Nasopharyngeal Colonization With *Streptococcus Pneumoniae* and *Haemophilus Influenzae*: A Japanese Birth Cohort Study. *Pediatr. Infect. Dis. J.* 32 (7), 709–714. doi: 10.1097/INF.0b013e31828701ea
- Prasasty, V. D., Hutagalung, R. A., Gunadi, R., Sofia, D. Y., Rosmalena, R., Yazid, F., et al. (2021). Prediction of Human-*Streptococcus Pneumoniae* Protein-Protein Interactions Using Logistic Regression. *Comput. Biol. Chem.* 92, 107492. doi: 10.1016/j.compbiolchem.2021.107492
- Robb, M., Hobbs, J. K., Woodiga, S. A., Shapiro-Ward, S., Suits, M. D., McGregor, N., et al. (2017). Molecular Characterization of N-Glycan Degradation and Transport in *Streptococcus Pneumoniae* and Its Contribution to Virulence. *PLoS Pathog.* 13 (1), e1006090. doi: 10.1371/journal.ppat.1006090
- Singh, A. K., Pluvina, B., Higgins, M. A., Dalia, A. B., Woodiga, S. A., Flynn, M., et al. (2014). Unravelling the Multiple Functions of the Architecturally Intricate *Streptococcus Pneumoniae* Beta-Galactosidase, BgaA. *PLoS Pathog.* 10 (9), e1004364. doi: 10.1371/journal.ppat.1004364
- Sumitomo, T., Nakata, M., Yamaguchi, M., Terao, Y., and Kawabata, S. (2012). S-Carboxymethylcysteine Inhibits Adherence of *Streptococcus Pneumoniae* to Human Alveolar Epithelial Cells. *J. Med. Microbiol.* 61 (Pt 1), 101–108. doi: 10.1099/jmm.0.033688-0
- Syed, S., Hakala, P., Singh, A. K., Lapatto, H. A. K., King, S. J., Meri, S., et al. (2019). Role of Pneumococcal NanA Neuraminidase Activity in Peripheral Blood. *Front. Cell Infect. Microbiol.* 9. doi: 10.3389/fcimb.2019.00218
- Varki, A., Schnaar, R. L., and Schauer, R. (2015). "Sialic Acids and Other Nonulosonic Acids," in *Essentials of Glycobiology*. Eds. A. Varki, R. D. Cummings, J. D. Esko, P. Stanley, G. W. Hart, M. Aebi, A. G. Darvill, T. Kinoshita, N. H. Packer, J. H. Prestegard, R. L. Schnaar and P. H. Seeberger (Cold Spring Harbor, New York: Cold Spring Harbor Laboratory Press), 179–195.
- WHO (2017). *WHO Priority Pathogens List for R&D of New Antibiotics*. Available at: <http://www.who.int/mediacentre/news/releases/2017/bacteria-antibiotics-needed/en/>.
- Yamaguchi, M. (2018). Synergistic Findings From Microbiological and Evolutionary Analyses of Virulence Factors Among Pathogenic *Streptococcal* Species. *J. Oral. Biosci.* 60 (2), 36–40. doi: 10.1016/j.job.2018.02.004
- Yamaguchi, M., Goto, K., Hirose, Y., Yamaguchi, Y., Sumitomo, T., Nakata, M., et al. (2019a). Identification of Evolutionarily Conserved Virulence Factor by Selective Pressure Analysis of *Streptococcus Pneumoniae*. *Commun. Biol.* 2, 96. doi: 10.1038/s42003-019-0340-7
- Yamaguchi, M., Hirose, Y., Nakata, M., Uchiyama, S., Yamaguchi, Y., Goto, K., et al. (2016). Evolutionary Inactivation of a Sialidase in Group B *Streptococcus*. *Sci. Rep.* 6, 28852. doi: 10.1038/srep28852
- Yamaguchi, M., Hirose, Y., Takemura, M., Ono, M., Sumitomo, T., Nakata, M., et al. (2019b). *Streptococcus Pneumoniae* Evades Host Cell Phagocytosis and Limits Host Mortality Through Its Cell Wall Anchoring Protein PfbA. *Front. Cell Infect. Microbiol.* 9. doi: 10.3389/fcimb.2019.00301
- Yamaguchi, M., Nakata, M., Sumioka, R., Hirose, Y., Wada, S., Akeda, Y., et al. (2017). Zinc Metalloproteinase ZmpC Suppresses Experimental Pneumococcal Meningitis by Inhibiting Bacterial Invasion of Central Nervous Systems. *Virulence* 8 (8), 1516–1524. doi: 10.1080/21505594.2017.1328333
- Yamaguchi, M., Takemura, M., Higashi, K., Goto, K., Hirose, Y., Sumitomo, T., et al. (2020). Role of BgaA as a Pneumococcal Virulence Factor Elucidated by Molecular Evolutionary Analysis. *Front. Microbiol.* 11. doi: 10.3389/fmicb.2020.582437
- Yamaguchi, M., Terao, Y., Mori, Y., Hamada, S., and Kawabata, S. (2008). PfbA, a Novel Plasmin- and Fibronectin-Binding Protein of *Streptococcus Pneumoniae*, Contributes to Fibronectin-Dependent Adhesion and Antiphagocytosis. *J. Biol. Chem.* 283 (52), 36272–36279. doi: 10.1074/jbc.M807087200
- Yamaguchi, M., Win, H. P. M., Higashi, K., Ono, M., Hirose, Y., Motooka, D., et al. (2021). Epidemiological Analysis of Pneumococcal Strains Isolated at Yangon Children's Hospital in Myanmar via Whole-Genome Sequencing-Based Methods. *Microb. Genom.* 7 (2), 000523. doi: 10.1099/mgen.0.000523
- Yu, G., and He, Q. Y. (2016). ReactomePA: An R/Bioconductor Package for Reactome Pathway Analysis and Visualization. *Mol. Biosyst.* 12 (2), 477–479. doi: 10.1039/c5mb00663e

Conflict of Interest: The authors declare that the research was conducted in the absence of any commercial or financial relationships that could be construed as a potential conflict of interest.

Publisher's Note: All claims expressed in this article are solely those of the authors and do not necessarily represent those of their affiliated organizations, or those of the publisher, the editors and the reviewers. Any product that may be evaluated in this article, or claim that may be made by its manufacturer, is not guaranteed or endorsed by the publisher.

Copyright © 2022 Takemura, Yamaguchi, Kobayashi, Sumitomo, Hirose, Okuzaki, Ono, Motooka, Goto, Nakata, Uzawa and Kawabata. This is an open-access article distributed under the terms of the Creative Commons Attribution License (CC BY). The use, distribution or reproduction in other forums is permitted, provided the original author(s) and the copyright owner(s) are credited and that the original publication in this journal is cited, in accordance with accepted academic practice. No use, distribution or reproduction is permitted which does not comply with these terms.

Advantages of publishing in Frontiers



OPEN ACCESS

Articles are free to read
for greatest visibility
and readership



FAST PUBLICATION

Around 90 days
from submission
to decision



HIGH QUALITY PEER-REVIEW

Rigorous, collaborative,
and constructive
peer-review



TRANSPARENT PEER-REVIEW

Editors and reviewers
acknowledged by name
on published articles

Frontiers

Avenue du Tribunal-Fédéral 34
1005 Lausanne | Switzerland

Visit us: www.frontiersin.org

Contact us: frontiersin.org/about/contact



REPRODUCIBILITY OF RESEARCH

Support open data
and methods to enhance
research reproducibility



DIGITAL PUBLISHING

Articles designed
for optimal readership
across devices



FOLLOW US

@frontiersin



IMPACT METRICS

Advanced article metrics
track visibility across
digital media



EXTENSIVE PROMOTION

Marketing
and promotion
of impactful research



LOOP RESEARCH NETWORK

Our network
increases your
article's readership